

**The Potential of a Selective Histone Deacetylase Inhibitor
MI192 for Bone Tissue Engineering**

Kein Lon Man

Submitted in accordance with the requirements for the degree of
Doctor of Philosophy

The University of Leeds
School of Mechanical Engineering

May 2019

The candidate confirms that the work submitted is his own and that appropriate credit has been given where reference has been made to the work of others.

This copy has been supplied on the understanding that it is copyright material and that no quotation from the thesis may be published without proper acknowledgement.

© 2019 The University of Leeds and Kein Lon Man

Acknowledgements

First and foremost, I would like to thank my supervisor Dr Xuebin Yang for his tremendous support, advice and encouragement throughout my PhD. You have been a fantastic mentor, from which I have learnt a great deal. I would also like to thank my secondary supervisors for their contribution.

I would like to acknowledge the EPSRC Centre of Doctoral Training in Tissue Engineering and Regenerative Medicine (CDT TERM) for providing me with the opportunity to pursue my research interests within this field. It is also thanks to the funding provided by the CDT TERM I could attend numerous international research conferences and partake in a collaborative research visit within the CReaTE group, at the University of Otago, New Zealand. I am grateful for Dr Tim Woodfield and Dr Khoon Lim for hosting me within the CReaTE group and for their continued support in my research.

I am thankful to my friends outside of work, who supported me throughout this journey and reminded me of life outside of the lab. Special thanks to Rina for the support and advice she provided daily and for keeping me sane in the lab. Additionally, I would like to thank Rasha, Fahad and Lizzie for their help and support during my research.

I am eternally grateful for the continuous love and support my family have provided me during my PhD. I would like to thank my parents for instilling me with the determination and drive to undertake this challenge.

Finally, to Vivi, I am forever grateful for the love, patience, encouragement, understanding and support you have given me every day, without which none of this would have been possible.

Abstract

For functional tissue engineering, it is key to effectively control the lineage-specific differentiation of mesenchymal stromal cells (MSCs). Epigenetic approaches such as the inhibition of histone deacetylase (HDAC) enzymes have been shown to control MSCs fate, with HDAC3 isoform closely linked to osteogenic differentiation. Therefore, the research presented in this thesis aims to investigate the effects of the novel selective HDAC2 and 3 inhibitor - MI192 on the behaviour and osteogenic capacity of clinically relevant MSCs (hDPSCs and hBMSCs), to enhance their efficacy for bone augmentation strategies. In monolayer culture, a time-dose dependent decrease in MSCs viability was observed following MI192 treatment. MI192 halted cell cycle progression of MSCs in the G₂/M phase. MSCs HDAC activity was inhibited upon MI192 treatment, resulting in an increase in H3K9 histone acetylation. Alkaline Phosphatase Specific Activity (ALPSA) was significantly increased in hDPSCs and hBMSCs following a pre-treatment strategy of 2 and 50 μ M MI192 for 48 hours, respectively. Using these conditions, it was demonstrated that MI192 pre-treatment increased MSCs osteoblast-related gene/protein expression throughout osteogenic culture (Runx2, ALP, BMP2, Col1a and OCN) and enhanced calcium deposition/extracellular matrix mineralisation. MI192 pre-treatment enhanced hDPSCs ALPSA, osteoblast-related gene expression (*RUNX2*, *ALP*, *BMP2*, *COL1A* and *OCN*), extracellular matrix protein deposition (ALP, Col1a, OCN) and calcium deposition/mineralisation within the lyophilised *Bombyx Mori* silk scaffold and the bioassembled microtissue (BMT) construct (microtissues and 3D printed PEGT/PBT scaffold). However, substantially increased bone-like tissue formation induced by MI192 was observed within the BMT model. Similarly, MI192 pre-treatment enhanced hBMSCs osteogenic capacity (ALPSA, extracellular matrix protein expression and calcium deposition/mineralisation) within the GelMA hydrogel (GelMA alone and GelMA-PEGT/PBT construct) and BMT model. However, the bone-like tissue formation induced by MI192 pre-treatment was substantially enhanced within the BMT construct. After intraperitoneal implantation within CD1 nude mice using diffusion chambers, the MI192 pre-treated MSCs within the BMT construct exhibited increased extracellular matrix protein expression and calcium deposition/mineralisation, while inhibited the expression of chondrogenic proteins. Together, the findings presented in this thesis demonstrated that the selective HDAC2 & 3 inhibitor - MI192 promotes the *in vitro* and *in vivo* osteogenic capacity of MSCs acquired from human bone marrow and dental pulp tissues, indicating the potential of using epigenetic approaches to enhance MSCs efficacy for bone augmentation strategies.

Table of Contents

Acknowledgements	ii
Abstract	iii
Table of Contents	iv
List of Figures	xv
List of Tables	xxxiii
Chapter 1 - Literature Review	1
1.1 - Background	1
1.2 - Basic bone structure and physiology.....	2
1.2.1 - Cellular constituents of bone.....	3
1.2.2 - Bone formation.....	4
1.3 - DNA structure: Organization of the genetic material into chromatin.....	5
1.4 - Epigenetic modifications	7
1.4.1 - Acetylation.....	8
1.4.2 - Histone acetyltransferase (HAT) and histone deacetylase (HDAC).....	9
1.4.3 - Acetylation of non-histone proteins	11
1.4.4 - HDAC isoforms.....	11
1.4.5 - HDAC structure and activity	13
1.5 - HDAC inhibitors.....	14
1.5.1 - Structure and activity	14
1.5.2 - Specificity of HDAC inhibitors	17
1.5.3 - The biological role of HDAC enzymes and the effects of HDACis	17
1.5.3.1 - Cell cycle.....	17
1.5.3.2 - DNA damage.....	19

1.5.3.3 - Apoptosis	19
1.5.3.4 - Redox pathways	20
1.5.4 - Bone-associated HDAC isoforms.....	21
1.6 - Bone tissue engineering	22
1.6.1 - Clinical need and current approaches.....	22
1.6.2 - Tissue engineering approaches	23
1.6.2.1 - Cellular component	24
1.6.2.2 - Scaffolds	26
1.6.2.3 - Growth factors	28
1.6.2.4 - Environmental stimulation.....	29
1.6.2.5 - Gene therapy and iPSCs	29
1.7 - Utilisation of HDACi for bone tissue engineering.....	30
1.8 - Project aims and objectives	33
Chapter 2 - Materials and Methods	34
2.1 - General reagents.....	34
2.2 - MI192.....	34
2.3 - Culturing of cells.....	34
2.3.1 - Extraction of human dental pulp stromal cells from sound molars.....	34
2.3.2 - Processing human bone marrow mononuclear cells.....	35
2.3.3 - Detachment of cells and seeding.....	35
2.3.4 - Cell Counting.....	35
2.3.5 - <i>In vitro</i> expansion of human dental pulp stromal cells (hDPSC).....	36
2.3.6 - <i>In vitro</i> expansion of human bone marrow stromal cells (hBMSC)	36

2.3.7 - Osteogenic induction culture	36
2.3.8 - Chondrogenic induction culture	36
2.3.9 - Adipogenic induction culture.....	36
2.3.10 - Microtissue culture	37
2.4 - Polymerase chain reaction (PCR)	37
2.4.1 - RNA isolation	37
2.4.2 - Reverse transcription	37
2.4.3 - RT-qPCR	38
2.5 - Biochemical assays	39
2.5.1 - PicoGreen DNA quantification assay.....	39
2.5.2 - Alkaline phosphatase (ALP) quantitative assay	39
2.5.3 - ALP specific activity (ALPSA)	40
2.5.4 - AlamarBlue metabolic activity quantification assay	40
2.5.5 - HDAC activity assay	40
2.5.6 - H3K9 acetylation assay.....	41
2.5.7 - In-Cell Western (ICW) assay	41
2.6 - Assessment of Cell Morphology.....	42
2.7 - Cell cycle analysis	42
2.8 - Live/dead fluorescent staining.....	42
2.9 - Histological staining.....	43
2.9.1 - Paraffin embedding and sectioning	43
2.9.2 - Haematoxylin and Eosin (H&E) staining	43
2.9.3 - Picrosirius red/Alcian blue staining.....	43
2.9.4 - Oil red O staining for lipid droplets.....	44
2.9.5 - Alizarin red staining for calcium accumulation.....	44

2.9.6 - Von Kossa staining for mineral nodule formation	44
2.9.7 - Immunohistochemistry	45
2.10 - 3D printed PEGT/PBT fabrication and preparation	46
2.11 - Diffusion chamber preparation	46
2.12 - Intraperitoneal implantation	46
2.13 - X-ray analysis.....	47
2.14 - Statistical analysis.....	47
Chapter 3 - The Effects of MI192 on the Behaviour and Osteogenic Capacity of Human Dental Pulp Stromal Cells <i>In vitro</i> and <i>In vivo</i>	48
3.1 - Background	48
3.2 - Materials and Methods	52
3.2.1 - Cytotoxic effect of MI192 on hDPSCs.....	52
3.2.2 - Effect of MI192 on ALPSA in hDPSCs.....	52
3.2.3 - Effect of MI192 on hDPSCs ALP staining	52
3.2.4 - Effect of MI192 on the expression of osteogenic genes in hDPSCs.....	53
3.2.5 - Silk fibroin extraction and biomaterial fabrication	53
3.2.6 - Characterisation of silk scaffold.....	53
3.2.7 - Characterisation of 3D printed PEGT/PBT.....	54
3.2.8 - Scanning electron microscopy (SEM).....	54
3.2.9 - Silk preparation before experiments	54
3.2.10 - Static seeding of cells on silk scaffolds.....	54
3.2.11 - Microtissue culture and BMT construct assembly.....	55
3.2.12 - RNA isolation of silk constructs.....	55
3.2.13 - 3D construct preparation for ALPSA assay	55
3.3 - Results	56

3.3.1 - The Effects of MI192 on the Behaviour and Osteogenic Capacity of hDPSCs in 2D Culture	56
3.3.1.1 - Effect of MI192 on hDPSCs morphology	56
3.3.1.2 - Effect of MI192 on hDPSCs metabolic activity	58
3.3.1.3 - Effect of MI192 on hDPSCs DNA quantity	59
3.3.1.4 - Cytotoxic effect of MI192 on hDPSCs	60
3.3.1.5 - Effect of MI192 on HDAC specific activity in hDPSCs.....	61
3.3.1.6 - Effect of MI192 on histone H3K9 specific acetylation in hDPSCs.....	63
3.3.1.7 - Effect of MI192 on hDPSCs cell cycle progression.....	64
3.3.1.8 - Effect of MI192 on ALPSA in hDPSCs	68
3.3.1.9 - Effect of MI192 on hDPSCs ALP staining.....	70
3.3.1.10 - Effect of MI192 on the expression of osteogenic genes in hDPSCs.....	71
3.3.1.11 - Effect of MI192 on the expression of osteogenic proteins in hDPSCs.....	74
3.3.1.12 - Effect of MI192 on hDPSCs calcium deposition and mineralisation.....	76
3.3.2 - The Effects of MI192 on hDPSCs Osteogenic Differentiation in the Lyophilised Silk Scaffolds	79
3.3.2.1 - Porosity and pore morphology of lyophilised silk scaffolds.....	79
3.3.2.2 - Effects of silk concentration on scaffold swelling and degradation properties	80
3.3.2.3 - Mechanical properties of lyophilised silk scaffolds	81
3.3.2.4 - Assessment of hDPSCs viability and distribution within the silk scaffolds	82
3.3.2.5 - The effect of MI192 pre-treatment on hDPSCs ALPSA within the 2 and 5 wt% silk scaffolds.....	84
3.3.2.6 - The effect of MI192 on hDPSCs osteogenic gene expression within the silk scaffold. 85	
3.3.2.7 - The effect of MI192 on hDPSCs tissue formation within the silk scaffold	88

3.3.2.8 - The effect of MI192 on hDPSCs osteogenic protein expression within the silk scaffold	90
3.3.2.9 - The effect of MI192 on hDPSCs calcium deposition and mineralisation within the silk scaffold	93
3.3.3 - The Effects of MI192 on hDPSCs Osteogenic Differentiation within the BMT construct... 79	
3.3.3.1 - Macroscopic analysis of 3D printed PEGT/PBT scaffold	96
3.3.3.2 - Surface topography and 3D architecture of 3D printed PEGT/PBT scaffold.....	97
3.3.3.3 - BMT construct assembly.....	98
3.3.3.4 - Assessment of BMT cellular viability	99
3.3.3.5 - The effect of MI192 on hDPSCs osteogenic gene expression in microtissue culture	100
3.3.3.6 - The effect of MI192 on hDPSCs ALPSA in BMT culture.....	102
3.3.3.7 - The effect of MI192 on hDPSCs tissue formation within the BMT construct	103
3.3.3.8 - The effect of MI192 on hDPSCs osteogenic protein expression within the BMT construct.....	105
3.3.3.9 - The effect of MI192 on hDPSCs mineralisation within the BMT construct.....	108
3.3.4 - The Effects of MI192 on hDPSC BMT <i>in vivo</i> bone formation	110
3.3.4.1 - Macroscopic and X-ray analysis of hDPSC BMT constructs	110
3.3.4.2 - The effect of MI192 on hDPSCs tissue formation during BMT <i>in vivo</i> implantation .	111
3.3.4.3 - The effect of MI192 on hDPSCs osteogenic protein expression during BMT <i>in vivo</i> implantation	113
3.3.4.4 - The effect of MI192 on hDPSCs chondrogenic protein expression during BMT <i>in vivo</i> implantation	115
3.3.4.5 - The effect of MI192 on hDPSCs calcium deposition and mineralisation during BMT <i>in vivo</i> implantation	118

3.4 - Discussion	120
3.4.1 - The effects of MI192 on hDPSCs general behaviour in 2D culture	120
3.4.2 - The effects of MI192 on hDPSCs osteogenic capacity in 2D culture	124
3.4.3 - The effects of MI192 on hDPSCs osteogenic differentiation in the lyophilised silk scaffold	130
3.4.4 - The effects of MI192 on hDPSCs osteogenic differentiation within the BMT construct .	137
3.4.5 - The effects of MI192 on hDPSCs BMT <i>in vivo</i> bone formation.....	146
Chapter 4 - The Effects of MI192 on the Behaviour and Osteogenic capacity of Human Bone Marrow-Derived Stromal Cells <i>in vitro</i> and <i>In vivo</i>.....	154
4.1 - Background	154
4.2 - Materials and Methods	159
4.2.1 - Effect of MI192 on ALPSA in hBMSCs.....	159
4.2.2 - Effect of MI192 on the expression of osteogenic genes in hBMSCs.....	159
4.2.3 - GelMA macromer preparation	159
4.2.4 - Production of GelMA microspheres using microfluidics.....	159
4.2.5 - Microfluidic device.....	160
4.2.6 - GelMA microsphere formation and characterisation	161
4.2.7 - Optimisation of cell encapsulation and BMT assembly using cell-laden GelMA microspheres.....	161
4.2.8 - Encapsulation of MI192 pre-treated hBMSCs within GelMA hydrogel.....	162
4.2.9 - Fabrication of hBMSCs encapsulated GelMA-PEBT/PBT constructs.....	162
4.2.10 - Microtissue culture and BMT assembly	163
4.2.11 - 3D construct preparation for ALPSA assay	163
4.3 - Results	164
4.3.1 - The Effects of MI192 on the Behaviour and Osteogenic capacity of hBMSCs in 2D culture	164

4.3.1.1 - Effect of MI192 on hBMSCs morphology	164
4.3.1.2 - Effect of MI192 on hBMSCs metabolic activity	166
4.3.1.3 - Effect of MI192 on hBMSCs DNA quantity	167
4.3.1.4 - Effect of MI192 on HDAC specific activity in hBMSCs	168
4.3.1.5 - Effect of MI192 on the histone H3K9 specific acetylation in hBMSCs.....	169
4.3.1.6 - Effect of MI192 on hBMSCs cell cycle progression.....	170
4.3.1.7 - Effect of MI192 on ALPSA in hBMSCs	174
4.3.1.8 - Effect of MI192 on the expression of osteogenic genes in hBMSCs	175
4.3.1.9 - Effect of MI192 on the expression of osteogenic proteins in hBMSCs.....	178
4.3.1.10 - Effect of MI192 on hBMSCs calcium deposition and mineralisation.....	180
4.3.2 - The Effects of MI192 on hBMSCs Osteogenic Differentiation within the GelMA hydrogel	182
4.3.2.1 - Effect of GelMA concentration on microsphere morphology and size	182
4.3.2.2 - Effect of GelMA concentration on L929 cell-laden GelMA microsphere size and viability	184
4.3.2.3 - Viability of MI192 pre-treated hBMSCs encapsulated within the GelMA hydrogel..	185
4.3.2.4 - The effect of MI192 on hBMSCs ALPSA within the GelMA hydrogel.....	187
4.3.2.5 - The effect of MI192 on hBMSCs tissue formation within the GelMA hydrogel.....	188
4.3.2.6 - The effect of MI192 on hBMSCs osteogenic protein expression within the GelMA hydrogel.....	190
4.3.2.7 - The effect of MI192 on hBMSCs calcium deposition and mineralisation within the GelMA hydrogel	193
4.3.2.8 - The effect of MI192 on hBMSCs tissue formation within the GelMA-PEBT/PBT construct.....	196

4.3.2.9 - The effect of MI192 on hBMSCs osteogenic protein expression within the GelMA-PEBT/PBT construct.....	198
4.3.2.10 - The effects of MI192 on hBMSCs calcium deposition and mineralisation within the GelMA-PEBT/PBT construct	201
4.3.3 - The Effects of MI192 on hBMSCs Osteogenic Differentiation within the BMT construct	204
4.3.3.1 - The effect of MI192 on hBMSCs osteogenic gene expression in microtissue culture	204
4.3.3.2 - The effect of MI192 on hBMSCs ALPSA in BMT culture.....	206
4.3.3.3 - The effect of MI192 on hBMSCs tissue formation within the BMT construct	207
4.3.3.4 - The effect of MI192 on hBMSCs osteogenic protein expression within the BMT construct.....	209
4.3.3.5 - The effect of MI192 on hBMSCs chondrogenic protein expression within the BMT construct.....	213
4.3.3.6 - The effect of MI192 on hBMSCs calcium deposition and mineralisation within the BMT construct.....	216
4.3.4 - The Effects of MI192 on hBMSC BMT <i>in vivo</i> bone formation	218
4.3.4.1 - Macroscopic and X-ray analysis of hBMSC BMT constructs	218
4.3.4.2 - The effect of MI192 on hBMSCs tissue formation during BMT <i>in vivo</i> implantation	219
4.3.4.3 - The effect of MI192 on hBMSCs osteogenic protein expression during BMT <i>in vivo</i> implantation	221
4.3.4.4 - The effect of MI192 on hBMSCs chondrogenic protein expression during BMT <i>in vivo</i> implantation	223
4.3.4.5 - The effect of MI192 on hBMSCs calcium deposition and mineralisation during BMT <i>in vivo</i> implantation	226
4.4 - Discussion	228

4.4.1 - The effects of MI192 on hBMSCs general behaviour in 2D culture	228
4.4.2 - The effects of MI192 on hBMSCs osteogenic capacity in 2D culture.....	232
4.4.3 - The effects of MI192 on hBMSCs osteogenic differentiation within the GelMA hydrogel	237
4.4.4 - The effects of MI192 on hBMSCs osteogenic differentiation within the BMT construct	247
4.4.5 - The effects of MI192 on hBMSCs BMT <i>in vivo</i> bone formation.....	258
Chapter 5 - General discussion	265
5.1 - General discussion.....	265
5.1.1 - The effects of MI192 on MSCs general behaviour in 2D culture	267
5.1.2 - The effects of MI192 on MSCs osteogenic capacity in 2D culture	268
5.1.3 - The effects of MI192 on MSCs osteogenic capacity in 3D culture.....	272
5.1.4 - The effects of MI192 on MSCs bone formation <i>in vivo</i>	276
5.2 - Conclusion.....	281
5.3 - Future work.....	282
References	I
List of Abbreviations	XXXV
Appendix A - Supplementary data	XL
A1 - Comparison of MI192 pre-treatment on hDPSCs ALPSA from three donors	XL
A2 - Comparison of MI192 pre-treatment on hBMSCs ALPSA from two donors	XLI
A3 - Confirmation of multi-lineage differentiation potential of hDPSCs.....	XLII
A4 - Confirmation of multi-lineage differentiation potential of hBMSCs.....	XLIV
A5 - Viability of floating cell/debris induced by MI192 treatment on hBMSCs	XLVI
Appendix B - List of conference presentations and publications.....	XLVII
B1 - Oral presentations.....	XLVII

B2 - Poster presentations XLVIII

B3 - Publications..... XLIX

Appendix C - Rights for reprinting permission..... L

List of Figures

- Figure 1.1 - Structure of long bone. The femur is a typical long bone in the body, possessing both the cortical and cancellous bone regions. Adapted from (30).3
- Figure 1.2 - Histological staining of osteoblast (A) and osteoclast (B) (PC3 luciferase 2) in mouse bone. (A) Alkaline phosphatase staining of osteoblasts (black arrows). (B) Tartrate-resistant acid phosphatase staining of osteoclasts (black arrows) induced by PC3 tumour cells (author generated these images/stained sections). Scale bar= 20 μm4
- Figure 1.3 - Bone formation processes. Intramembranous ossification is the process in which mesenchymal progenitor cells directly differentiate to osteoblasts to form bone tissue. Endochondral ossification is the more indirect process, where condensation of mesenchymal progenitors creates a cartilaginous template for future bone formation.....5
- Figure 1.4 - Chromatin Hierarchical Structure. Chromatin has three organizational levels: DNA wraps around the histone proteins to form nucleosomes; these in turn couple to become the 30 nm chromatin fibre; supercoiling of the chromatin fibre produced the chromosome. Adapted with permission (44).6
- Figure 1.5 - Representation of the nucleosome core. Each nucleosome core particle consists of the DNA (blue) which wraps around the four core histone proteins that form the histone octamer protein complex: H2A (turquoise), H2B (green), H3 (yellow) and H4 (pink). C-terminal tails of the H2A proteins protrude from the centre of the nucleosome core. Reprinted with permission (45, 48).7
- Figure 1.6 - The process of acetylation and deacetylation. The enzymatic reaction of acetylation and deacetylation is mediated by HAT and HDAC enzymes, respectively.9
- Figure 1.7 - Schematic representation of the dynamic effects of HDAC/HAT on the nucleosome and the conformation of the chromatin structure. The transference of acetyl groups onto the histone lysine tail via HAT causes the opening of the chromatin structure, with HDAC activity reversing this effect (71). 10
- Figure 1.8 - A 'space-filling' representation of the HDACi compound SAHA bound into the HDAC active site. The inhibitor SAHA binds into the catalytic pocket of a HDAC-like protein based from the homologue found in *Aquifex aeolicus*. Adapted with permission (93). 13

Figure 1.9 - The general HDACi structure and their HDAC targets. (A) Natural and synthetic HDACi and their HDAC targets. (B) Representation of the general structure of HDAC inhibitor. Adapted from (99-101). 15

Figure 1.10 - Schematic representations of zinc-dependent HDAC inhibitor interacting with the HDAC catalytic pocket. The HDAC enzyme possesses 3 highly conserved regions: an internal cavity, a zinc-binding site and a hydrophobic channel. The zinc-dependent HDACi possesses 3 complementary sections: zinc-binding group, hydrophobic linker and a hydrophobic cap. The HDACi inserts into the catalytic pocket, where the zinc-binding group blocks deacetylation activity of the enzyme, while the cap group of the HDACi prevents further competitive bindings..... 16

Figure 1.11 - Summary of the biological effects HDACis in both normal and transformed cells. HDAC enzymes are involved in numerous cellular processes critical to cell survival, migration, proliferation and differentiation, therefore their inhibition with HDACis will dysregulate these processes. 20

Figure 1.12 - The four key components of tissue engineering. These components include cells, scaffolds with the addition of growth factors and environmental/mechanical stimulation. 23

Figure 1.13 - Schematic representation of stem cell hierarchy. Totipotent cells such as zygotes possess the greatest differentiation potency, with the ability to give rise to all cell types in the body. Pluripotent cells such as ESCs can differentiate into all adult tissues in the body, except embryonic tissues. Multipotent cells such as MSCs are capable of lineage-specific differentiation into unipotent cells which are terminally differentiated..... 25

Figure 1.14 - The differing effects of monolayer and 3D culture on cellular behaviour. 2D culture infers an “artificial” environment which alters key cellular processes such as proper adhesion, growth and tissue-specific differentiation. Adapted from (181). 27

Figure 1.15 - Representation of MI192 mechanism of action in enhancing MSCs osteogenic differentiation. MI192 selectively inhibits HDAC2 and 3 isoforms, resulting in enhanced histone acetylation at the H3K9K14 regions. This increased acetylation opens the chromatin structure, leading to enhanced production and acetylation of Runx2 transcription factor, stimulating the downstream expression of osteoblast-related genes. Adapted from (71). 32

Figure 3.1 - Schematic representation of the bioassembled microtissue (BMT) construct. Pre-cultured microtissues within the pores of a 3D printed scaffold. Reprinted with permission (253).
..... 50

Figure 3.2 - Phase contrast images of hDPSCs treated with/without a range of MI192 dose (1, 10, 20, 50, 100 μ M) for 24, 48 and 72 hours. Scale bar = 100 μ m. 57

Figure 3.3 - AlamarBlue analysis of hDPSCs metabolic activity treated with/without a range of MI192 doses (1, 5, 10, 20, 50, 100 μ M) for 24, 48 and 72 hours. Data expressed as mean \pm SD (n=3). Significance levels shown are the test groups compared to the basal control for that time point. *P \leq 0.05. 58

Figure 3.4 - DNA quantification of hDPSCs treated with/without a range of MI192 doses (1, 5, 10, 20, 50, 100 μ M) for 24, 48 and 72 hours. Data expressed as mean \pm SD (n=3). Significance levels shown are the test groups compared to the basal control for that time point. ***P \leq 0.001. 59

Figure 3.5 - Cytotoxicity analysis of hDPSCs treated with/without a range of MI192 doses (1, 5, 10, 20, 50, 100 μ M) for 24, 48 and 72 hours. Data expressed as mean \pm SD (n=3). The significance levels shown are the test groups compared to the basal control for that time point. *P \leq 0.05 and ***P \leq 0.001. 60

Figure 3.6 - HDAC specific activity in hDPSCs following MI192 treatment. A) HDAC specific activity of hDPSCs immediately after 24 and 48 hours MI192 treatment. B) HDAC specific activity of MI192 pre-treated hDPSCs (24 and 48 hours) after 1 week of culture in basal medium. Data expressed as mean \pm SD (n=3). Significance levels shown are the test groups compared to the basal control or between adjacent MI192 concentrations at that time point. *P \leq 0.05, **P \leq 0.01 and ***P \leq 0.001. 62

Figure 3.7 - H3K9 histone-specific acetylation levels in hDPSCs after treatment with five doses of MI192 for 24 and 48 hours. Data expressed as mean \pm SD (n=3). Significance levels shown are the test groups compared to the basal control for that time point. *P \leq 0.05 and **P \leq 0.01. 63

Figure 3.8 - The percentage of hDPSCs in the G₀/G₁, G₂/M and S phases after treatment with/without 2 μ M MI192 over 24, 48 and 72 hours. Data expressed as mean \pm SD (n=3). The significance levels shown are the test group compared to the basal control for that time point. *P \leq 0.05, **P \leq 0.01 and ***P \leq 0.001. 66

Figure 3.9 - Representative histograms from the flow cytometry analysis of hDPSCs cell cycle distribution dosed with/without 2 μ M MI192 for 24, 48 and 72 hours. The first peak represents cells within the G₀/G₁ phase, the second peak represents cells in the G₂/M phase and the area between the peaks represents cells in the S phase. 67

Figure 3.10 - ALPSA of hDPSCs pre-treated with/without MI192 for 24 and 48 hours prior to osteogenic culture. Cells were pre-treated with MI192 for, A) 24 hours (5, 10 and 20 μ M), B) 48 hours (1, 2 and 5 μ M) prior to culture in osteogenic medium for 2 weeks. Untreated cells cultured in basal and osteogenic medium used as controls. Data expressed as mean \pm SD (n=3). Significance levels shown are the test groups compared to the controls or between adjacent MI192 concentrations at that time point. *P \leq 0.05, **P \leq 0.01 and ***P \leq 0.001. 69

Figure 3.11 - ALP staining of hDPSCs pre-treated with/without 2 μ M MI192 for 48 hours prior to osteogenic culture for 2 weeks. A) Macroscopic image of the entire field. B) Microscopic images in high magnification (x 100)..... 70

Figure 3.12 - Relative expression of osteoblast-related genes in untreated/MI192 pre-treated hDPSCs after culture in osteogenic medium. Gene expression analysed on day 0, 3, 5, 7, 14, 21 and 28. Data expressed as mean \pm SD (n=3). Significance levels shown are the test group compared to the untreated control at the same time point. *P \leq 0.05, **P \leq 0.01 and ***P \leq 0.001. 73

Figure 3.13 - Protein expression of osteoblast-related markers in untreated/MI192 pre-treated hDPSCs after culture in osteogenic medium. Protein expression levels analysed on day 7, 14, 21 and 28. Data expressed as mean \pm SD (n=3). Significance levels shown are the test group compared to the untreated control at the same time point. *P \leq 0.05, **P \leq 0.01 and ***P \leq 0.001. 75

Figure 3.14 - Effect of MI192 pre-treatment on hDPSCs calcium deposition. (A) Alizarin red staining. Nodule-like formations highlighted by black arrows. Microscopic images at x 100. (B) Semi-quantitative analysis of Alizarin red stained untreated/MI192 pre-treated hDPSCs after 28 days osteogenic culture. Data expressed as mean \pm SD (n=3). ***P \leq 0.001. 77

Figure 3.15 - Effect of MI192 pre-treatment on hDPSCs mineral nodule formation. Von Kossa staining (black) of untreated/MI192 pre-treated hDPSCs after culture in osteogenic medium for 28 days. Mineral nodule formation indicated by the red arrows. Van Gieson's counterstaining to identify collagen deposition (pink). Microscopic images at x 100 (top row) and x 200 (bottom row). 78

Figure 3.16 - Pore morphology and porosity of 2 and 5 wt% lyophilised silk scaffolds. SEM micrographs of lyophilised silk scaffolds showing an interconnected network of thin sheet-like lamellae. Scale bars = 500 (top row) and 250 μm (bottom row), respectively. 79

Figure 3.17 - Effect of silk concentration on scaffold swelling and degradation properties. A) Increasing silk concentration decreases scaffold swelling capacity in both H_2O and PBS conditions. Data expressed as mean \pm SD (n=5). Significance determined between difference wt% scaffolds in the same swelling conditions. B) Increasing silk concentration reduces *in vitro* degradation rate. Data expressed as mean \pm SD (n=5). Significance determined between the different wt% scaffolds at each time point. *P \leq 0.05 and ***P \leq 0.001..... 80

Figure 3.18 - Effect of silk concentration on scaffold compressive modulus. Increasing silk concentration enhanced the compressive modulus of silk scaffolds. Data expressed as mean \pm SD (n=6). ***P \leq 0.001. 81

Figure 3.19 - Fluorescent imaging of viable untreated/MI192 pre-treated hDPSCs (green colour) within the (A) 2 wt% and (B) 5 wt% silk scaffolds. Viable hDPSCs on 2 and 5 wt% silk constructs after 24 hours and 6 weeks in osteogenic culture. Scale bar = 250 μm 83

Figure 3.20 - ALPSA in untreated/MI192 pre-treated hDPSCs cultured within the 2 and 5 wt% silk constructs under osteogenic conditions for 2 weeks. Data expressed as mean \pm SD (n=4). The significance levels shown are the test group compared to the untreated control within each wt% scaffold and between the same cells in different wt% scaffolds. ***P \leq 0.001. 84

Figure 3.21 - Relative expression of osteoblast-related genes in untreated/MI192 pre-treated hDPSCs cultured within the 5 wt% silk scaffolds throughout osteogenic culture. Gene expression analysed on day 3, 7, 10 and 14. Data expressed as mean \pm SD (n=4). Significance levels shown are the test group compared to the untreated control at the same time point. *P \leq 0.05, **P \leq 0.01 and ***P \leq 0.001..... 87

Figure 3.22 - H&E staining of untreated/MI192 pre-treated hDPSCs within the 5 wt% silk scaffolds after 6 weeks osteogenic culture. Silk scaffold stained a pink colour and tissues stained a lighter purple colour. Scale bars = 200 (top row) and 25 μm (bottom row), respectively..... 88

Figure 3.23 - Picrosirius red/Alcian blue staining of untreated/MI192 pre-treated hDPSCs within the 5 wt% silk scaffold after 6 weeks osteogenic culture. Collagens and GAGs stained with

Picrosirius red and Alcian blue, respectively. Scale bars = 200 (top row) and 25 μm (bottom row), respectively.....89

Figure 3.24 - ALP immunohistochemical staining of untreated/MI192 pre-treated hDPSCs cultured within the 5 wt% silk scaffolds after 6 weeks osteogenic culture. Positive ALP immunohistochemical staining (brown), with a weak Harris haematoxylin counterstain (purple). Scale bars = 200 (top row) and 25 μm (bottom row), respectively.....90

Figure 3.25 - Col1a immunohistochemical staining of untreated/MI192 pre-treated hDPSCs cultured within the 5 wt% silk scaffolds after 6 weeks osteogenic culture. Positive Col1a immunohistochemical staining (brown), with a weak Harris haematoxylin counterstain (purple). Scale bars = 200 (top row) and 25 μm (bottom row), respectively.....91

Figure 3.26 - OCN immunohistochemical staining of untreated/MI192 pre-treated hDPSCs cultured within the 5 wt% silk scaffold after 6 weeks osteogenic culture. Positive OCN immunohistochemical staining (brown), with a weak Harris haematoxylin counterstain (purple). Scale bars = 200 (top row) and 25 μm (bottom row), respectively.....92

Figure 3.27 - Negative immunohistochemical staining of untreated/MI192 pre-treated hDPSCs cultured within the 5 wt% silk scaffold after 6 weeks osteogenic culture. Scale bar = 25 μm93

Figure 3.28 - Calcium deposition of untreated/MI192 pre-treated hDPSCs cultured within the 5 wt% silk scaffold after 6 weeks osteogenic culture observed by Alizarin red staining. A) Alizarin red staining of histological sections. Scale bars = 200 (top row) and 100 μm (bottom row), respectively. B) Semi-quantitative analysis of Alizarin red stained entire constructs. Data expressed as mean \pm SD (n=3). ***P \leq 0.001.94

Figure 3.29 - Mineral nodule formation of untreated/MI192 pre-treated hDPSCs cultured within the 5 wt% silk scaffolds after 6 weeks osteogenic culture observed by Von Kossa staining. Mineral nodule formation indicated by red arrows. Weak Harris haematoxylin counterstain (purple). Scale bars = 100 (top row) and 25 μm (bottom row), respectively.....95

Figure 3.30 - Characteristic parameters of PEGT/PBT scaffolds. A) The scaffold pore size in the x-y/z plane and the fibre diameter/spacing. Data expressed as mean \pm SD (n=4). B) Bright-field images of the top view and sectional view of the PEGT/PBT scaffold. The red dotted circles (1 mm diameter) indicate the position of incorporated microtissues within the scaffold. Scale bar = 200 μm96

Figure 3.31 - SEM images of 3D printed PEGT/PBT scaffolds. A) Top-down view of PEGT/PBT scaffold demonstrating a smooth topography with even fibre thickness throughout. B) Bottom view of scaffold showing roughened surface due to adhesion to the printing plate. C) & D) Tilted views demonstrating the printing configuration and pore height of scaffold. Scale bars = 1 (top row) and 2 mm (bottom row), respectively.97

Figure 3.32 - Macroscopic image of assembled BMT construct. *In situ* image showing BMT construct immediately after manual incorporation of hDPSC pre-cultured microtissues (black arrow) into the 3D printed PEGT/PBT scaffold framework (white arrow). Scale bar = 300 μ m. 98

Figure 3.33 - Merged Live/Dead fluorescent images of untreated/MI192 pre-treated hDPSC BMT constructs 24 hours post assembly (Live cells green, dead cells red). Scale bar = 300 μ m..... 99

Figure 3.34 - Relative expression of osteoblast-related genes in untreated/MI192 pre-treated hDPSC microtissues under osteogenic conditions. Gene expression analysed on day 7, 14 and 21. Data expressed as mean \pm SD (n=4). Significance levels shown are the test group compared to the untreated control at the same time point. *P \leq 0.05, **P \leq 0.01 and ***P \leq 0.001. 101

Figure 3.35 - ALPSA in untreated/MI192 pre-treated hDPSC BMT constructs. ALPSA assessed after BMT constructs cultured under osteogenic conditions for 2 weeks. Data expressed as mean \pm SD (n=4). *P \leq 0.05. 102

Figure 3.36 - H&E staining of untreated/MI192 pre-treated hDPSC BMT constructs after 6 weeks osteogenic culture. Scaffold fibres highlighted by the black arrow. Scale bars = 200 (top row) and 100 μ m (bottom row), respectively..... 103

Figure 3.37 - Picosirius red/Alcian blue staining of untreated/MI192 pre-treated hDPSC BMT constructs after 6 weeks osteogenic culture. Collagen and GAG staining with Picosirius red and Alcian blue, respectively. Strong Picosirius red staining located in circular nodules highlighted by the black arrows. Scale bars = 200 (top row) and 50 μ m (bottom row), respectively..... 104

Figure 3.38 - ALP immunohistochemical staining of untreated/MI192 pre-treated hDPSC BMT constructs after 6 weeks osteogenic culture. Positive ALP immunohistochemical staining (brown), with a weak Harris haematoxylin counterstain (purple). Strong ALP expression located at the nodule-like formations highlighted with the black arrows. Scale bars = 50 (top row) and 25 μ m (bottom row), respectively. 105

Figure 3.39 - Col1a immunohistochemical staining of untreated/MI192 pre-treated hDPSC BMT constructs after 6 weeks osteogenic culture. Positive Col1a immunohistochemical staining (brown), with a weak Harris haematoxylin counterstain (purple). Strong Col1a expression located at the nodule-like formations highlighted with the black arrows. Scale bars = 50 (top row) and 25 μm (bottom row), respectively. 106

Figure 3.40 - OCN immunohistochemical staining of untreated/MI192 pre-treated hDPSC BMT constructs after 6 weeks osteogenic culture. Positive OCN immunohistochemical staining (brown), with a weak Harris haematoxylin counterstain (purple). Strong OCN expression located at the nodule-like formations highlighted with the red arrows. Scale bars = 50 (top row) and 25 μm (bottom row), respectively. 107

Figure 3.41 - Negative immunohistochemical staining of untreated/MI192 pre-treated hDPSCs BMT constructs after 6 weeks osteogenic culture. Scale bar = 25 μm 108

Figure 3.42 - Mineral nodule formation of untreated/MI192 pre-treated hDPSC BMT constructs after 6 weeks osteogenic culture observed by Von Kossa staining. Red arrows indicate mineral nodules. Scale bars = 50 (top row) and 25 μm (bottom row), respectively. 109

Figure 3.43 - Macroscopic and X-ray images of untreated/MI192 pre-treated hDPSCs BMT constructs after 8 weeks *in vivo* implantation. A) Macroscopic images immediately post extraction. B) X-ray radiographs of BMTs following extraction..... 110

Figure 3.44 - H&E staining of untreated/MI192 pre-treated hDPSC BMT constructs after 8 weeks *in vivo* implantation. Scale bars = 200 (top row) and 100 μm (bottom row), respectively. 111

Figure 3.45 - Picosirius red/Alcian blue staining of untreated/MI192 pre-treated hDPSC BMT constructs after 8 weeks *in vivo* implantation. Collagens and GAGs stained with Picosirius red and Alcian blue, respectively. Scale bars = 200 (top row) and 25 μm (bottom row), respectively. 112

Figure 3.46 - Col1a immunohistochemical staining of untreated/MI192 pre-treated hDPSC BMT constructs after 8 weeks *in vivo* implantation. Positive Col1a immunohistochemical staining (brown), with a weak Harris haematoxylin counterstain (purple). Scale bars = 200 (top row) and 25 μm (bottom row), respectively. 113

Figure 3.47 - OCN immunohistochemical staining of untreated/MI192 pre-treated hDPSC BMT constructs after 8 weeks *in vivo* implantation. Positive OCN immunohistochemical staining

(brown), with a weak Harris haematoxylin counterstain (purple). Scale bars = 200 (top row) and 25 μm (bottom row), respectively.	114
Figure 3.48 - AGG immunohistochemical staining of untreated/MI192 pre-treated hDPSC BMT constructs after 8 weeks <i>in vivo</i> implantation. Positive AGG immunohistochemical staining (brown), with a weak Harris haematoxylin counterstain (purple). Scale bars = 200 (top row) and 25 μm (bottom row), respectively.	115
Figure 3.49 - Col2a immunohistochemical staining of untreated/MI192 pre-treated hDPSC BMTs after 8 weeks <i>in vivo</i> implantation. Positive Col2a immunohistochemical staining (brown), with a weak Harris haematoxylin counterstain (purple). Scale bars = 200 (top row) and 25 μm (bottom row), respectively.	116
Figure 3.50 - Negative immunohistochemical staining of untreated/MI192 pre-treated hDPSC BMTs after 8 weeks <i>in vivo</i> implantation. Scale bars = 200 (top row) and 25 μm (bottom row), respectively.....	117
Figure 3.51 - Calcium deposition of untreated/MI192 pre-treated hDPSC BMT constructs after 8 weeks <i>in vivo</i> implantation observed by Alizarin red staining. Scale bars = 200 (top row) and 100 μm (bottom row), respectively.	118
Figure 3.52 - Mineralisation of untreated/MI192 pre-treated hDPSC BMT constructs after 8 weeks <i>in vivo</i> implantation observed by Von Kossa staining. Scale bars = 200 (top row) and 100 μm (bottom row), respectively.	119
Figure 4.1 - Representation of methacrylate gelatin synthesis and crosslinking. Macromers of Gelatin containing amine groups were reacted with methacrylic anhydride which added methacrylate pendant groups. Methacrylate gelatin crosslinked with UV light in the presences of Irgacure 2959 initiator. Reprinted with permission (368).	157
Figure 4.2 - Schematic representation of the microfluidic apparatus to form hydrogel microspheres. The continuous phase and macromer phase are delivered into the T-junction by syringe pumps. The macromer is injected along the main axis of the T-junction via a capillary needle, while the continuous phase in injected into the chamber perpendicularly. Microspheres exiting the T-junction are photo-polymerised within the coil then deposited in the collector.....	160

Figure 4.3 - *In situ* representation of A) GelMA hydrogels and B) GelMA-PEBT/PBT constructs. Cell-laden GelMA hydrogels placed within silicone moulds with/without 3D printed PEGT/PBT scaffold (red arrow) prior to photo-polymerisation. 162

Figure 4.4 - Phase contrast images of hBMSCs treated with/without a range of MI192 dose (1, 10, 20, 50, 100 μ M) for 24, 48 and 72 hours. Scale bar = 100 μ m. 165

Figure 4.5 - AlamarBlue analysis of hBMSCs metabolic activity treated with/without a range of MI192 doses (1, 10, 20, 50, 100 μ M) for 24, 48 and 72 hours. Data expressed as mean \pm SD (n=3). Significance levels shown are the test groups compared to the basal control for that time point. **P \leq 0.01 and ***P \leq 0.001. 166

Figure 4.6 - DNA quantification of hBMSCs treated with/without a range of MI192 doses (1, 10, 20, 50, 100 μ M) for 24, 48 and 72 hours. Data expressed as mean \pm SD (n=3). Significance levels shown are the test groups compared to the basal control for that time point. *P 167

Figure 4.7 - HDAC specific activity in hBMSCs following MI192 treatment for 24 and 48 hours. Data expressed as mean \pm SD (n=3). Significance levels shown are the test groups compared to the basal control or between adjacent MI192 concentrations at that time point. *P 168

Figure 4.8 - H3K9 histone-specific acetylation levels in hBMSCs after treatment with five doses of MI192 for 24 and 48 hours. Data expressed as mean \pm SD (n=3). Significance levels shown are the test groups compared to the basal control or between adjacent MI192 concentrations at that time point. *P \leq 0.05, **P \leq 0.01 and ***P \leq 0.001. 169

Figure 4.9 - The percentage of hBMSCs in the G₀/G₁, G₂/M and S phase after treatment with/without 50 μ M MI192 for 24, 48 and 72 hours. Data expressed as mean \pm SD (n=3). Significance levels shown are the test group compared to the basal control for that time point. *P \leq 0.05 and **P \leq 0.01. 172

Figure 4.10 - Representative histograms from the flow cytometry analysis of hBMSCs cell cycle distribution dosed with/without 50 μ M MI192 for 24, 48 and 72 hours. The first peak represents cells within the G₀/G₁ phase, the second peak represents cells in the G₂/M phase and the area between the peaks represents cells in the S phase. 173

Figure 4.11 - ALPSA in hBMSCs pre-treated with/without MI192 for 24 and 48 hours then cultured in osteogenic medium. Cells were pre-treated with MI192 doses (10 - 70 μ M) for 24 or 48 hours,

following which cells were cultured in osteogenic medium for 2 weeks, with untreated cells cultured in basal and osteogenic medium used as the controls. Data expressed as mean \pm SD (n=3). Significance levels shown are the test groups compared to the basal/osteogenic control or between adjacent MI192 concentrations at that time point. *P \leq 0.05 and ***P \leq 0.001. 174

Figure 4.12 - Relative expression of osteoblast-related genes in untreated/MI192 pre-treated hBMSCs after culture in osteogenic conditions. Gene expression analysed on day 3, 7, 14 and 21. Data expressed as mean \pm SD (n=3). Significance levels shown are the test group compared to the untreated control at the same time point. *P \leq 0.05 and **P \leq 0.01. 177

Figure 4.13 - Protein expression of osteoblast-related markers in untreated/MI192 pre-treated hBMSCs after culture in osteogenic conditions. Protein expression levels assessed on day 7, 14, 21 and 28. Data expressed as mean \pm SD (n=3). Significance levels shown are the test group compared to the untreated control at the same time point. *P \leq 0.05, **P \leq 0.01 and ***P \leq 0.001. 179

Figure 4.14 - Effects of MI192 pre-treatment on hBMSCs calcium deposition. A) Alizarin Red stained images. Microscopic image x100. B) Semi-quantification analysis of Alizarin red staining in untreated/MI192 pre-treated hBMSCs after 28 days osteogenic culture. Data expressed as mean \pm SD (n=3). ***P \leq 0.001..... 180

Figure 4.15 - Effect of MI192 pre-treatment on hBMSCs mineral nodule formation. Von Kossa staining (black) for functional mineral nodules (red arrows) of untreated/MI192 pre-treated hBMSCs after 28 days osteogenic culture. Van Gieson's counter staining undertaken to identify collagen deposition (pink). Microscopic images at x200 (top row) and x400 (bottom row). 181

Figure 4.16 - Effect of GelMA concentration on the morphology and size of microspheres. A) Phase contrast microscopy images of 5, 10, 15 wt% GelMA microspheres. Scale bar = 200 μ m. B) The diameter of GelMA microspheres in different conditions: immediately after formation (before swelling), 24 hours swelling in PBS at room temperature, 24 hours swelling in PBS at 37°C and 24 hours swelling in DMEM at 37°C. Data expressed as mean \pm SD (n=3). 183

Figure 4.17 - Diameters of 5 and 10 wt% L929 cell-laden GelMA microspheres before and after 24 hours swelling in the medium. Data expressed as mean \pm SD (n=3). *P \leq 0.05. 184

Figure 4.18 - Merged Live/Dead fluorescent image of L929 cells encapsulated in 10 wt% GelMA microspheres (live cells green, dead cells red). A) Cell-laden GelMA microspheres 24 hours after

encapsulation. B) Cell-laden microspheres placed within a 3D PEGT/PBT scaffold using an automated assembly device 3 days after encapsulation. Scale bars = 500 (left column) and 200 μm (right column), respectively. 185

Figure 4.19 - Merged Live/Dead fluorescent image of untreated/MI192 pre-treated hBMSCs encapsulated in 5 wt% GelMA (live cells green, dead cells red). A) 24 hours after encapsulation. B) After 6 weeks osteogenic culture. Scale bars = 100 (top row) and 50 μm (bottom row), respectively..... 186

Figure 4.20 - ALPSA in untreated/MI192 pre-treated hBMSCs encapsulated in the GelMA hydrogel. ALPSA assessed after cell-laden GelMA hydrogels cultured in osteogenic conditions for 2 weeks. Data expressed as mean \pm SD (n=3). ***P \leq 0.001. 187

Figure 4.21 - H&E staining of untreated/MI192 pre-treated hBMSCs encapsulated within the GelMA hydrogel after 6 weeks osteogenic culture. Scale bars = 200 (top row) and 100 μm (bottom row), respectively. 188

Figure 4.22 - Picrosirius red/Alcian blue staining of untreated/MI192 pre-treated hBMSCs encapsulated within the GelMA hydrogel after 6 weeks osteogenic culture. Collagens and GAGs stained with Picrosirius red and Alcian blue, respectively. Scale bars = 200 (top row) and 100 μm (bottom row), respectively. 189

Figure 4.23 - ALP immunohistochemical staining of untreated/MI192 pre-treated hBMSCs encapsulated within the GelMA hydrogel after 6 weeks osteogenic culture. Positive ALP immunohistochemical staining (brown), with a weak Harris haematoxylin counterstain (purple). Scale bars = 200 (top row) and 20 μm (bottom row), respectively..... 190

Figure 4.24 - Col1a immunohistochemical staining of untreated/MI192 pre-treated hBMSCs encapsulated within the GelMA hydrogel after 6 weeks osteogenic culture. Positive Col1a immunohistochemical staining (brown), with a weak Harris haematoxylin counterstain (purple). Scale bars = 200 (top row) and 20 μm (bottom row), respectively..... 191

Figure 4.25 - OCN immunohistochemical staining of untreated/MI192 pre-treated hBMSCs encapsulated within the GelMA hydrogel after 6 weeks osteogenic culture. Positive OCN immunohistochemical staining (brown), with a weak Harris haematoxylin counterstain (purple). Scale bars = 200 (top row) and 20 μm (bottom row), respectively..... 192

Figure 4.26 - Negative immunohistochemical staining of untreated/MI192 pre-treated hBMSCs encapsulated within the GelMA hydrogel after 6 weeks osteogenic culture. Scale bars = 100 μ m. 193

Figure 4.27 - Calcium deposition of untreated/MI192 pre-treated hBMSCs encapsulated within the GelMA hydrogel after 6 weeks osteogenic culture observed by Alizarin red staining. A) Semi-quantitative analysis of Alizarin red staining in the entire constructs. Data expressed as mean \pm SD (n=3). ***P \leq 0.001. B) Alizarin red staining of histological sections. Nodule-like formations highlighted by black arrows. Scale bars = 200 (top row) and 100 μ m (bottom row), respectively. 194

Figure 4.28 - Mineral nodule formation of untreated/MI192 pre-treated hBMSCs encapsulated within the GelMA hydrogel after 6 weeks osteogenic culture observed by Von Kossa staining. Mineral nodule formation highlighted by red arrows. Scale bars = 200 (top row) and 100 μ m (bottom row), respectively. 195

Figure 4.29 - H&E staining of untreated/MI192 pre-treated hBMSCs encapsulated within the GelMA-PEBT/PBT construct after 6 weeks osteogenic culture. Scale bars = 200 (top row) and 100 μ m (bottom row), respectively. 196

Figure 4.30 - Picrosirius red/Alcian blue of untreated/MI192 pre-treated hBMSCs encapsulated within the GelMA-PEBT/PBT construct after 6 weeks osteogenic culture. Collagens and GAGs stained with Picrosirius red and Alcian blue, respectively. Scale bars = 200 (top row) and 100 μ m (bottom row), respectively. 197

Figure 4.31 - ALP immunohistochemical staining of untreated/MI192 pre-treated hBMSCs encapsulated within the GelMA-PEBT/PBT construct after 6 weeks osteogenic culture. Positive ALP immunohistochemical staining (brown), with a weak Harris haematoxylin counterstain (purple). Scale bars = 100 (top row) and 20 μ m (bottom row), respectively. 198

Figure 4.32 - Col1a immunohistochemical staining of untreated/MI192 pre-treated hBMSCs encapsulated within the GelMA-PEBT/PBT construct after 6 weeks osteogenic culture. Positive Col1a immunohistochemical staining (brown), with a weak Harris haematoxylin counterstain (purple). Scale bars = 100 (top row) and 20 μ m (bottom row), respectively. 199

Figure 4.33 - OCN immunohistochemical staining of untreated/MI192 pre-treated hBMSCs encapsulated within the GelMA-PEBT/PBT construct after 6 weeks osteogenic culture. Positive

OCN immunohistochemical staining (brown), with a weak Harris haematoxylin counterstain (purple). Scale bars = 100 (top row) and 20 μm (bottom row), respectively. 200

Figure 4.34 - Negative immunohistochemical staining of untreated/MI192 pre-treated hBMSCs encapsulated within the GelMA-PEBT/PBT construct after 6 weeks osteogenic culture. Scale bars = 100 μm 201

Figure 4.35 - Calcium deposition of untreated/MI192 pre-treated hBMSCs encapsulated within the GelMA-PEBT/PBT construct after 6 weeks osteogenic culture observed by Alizarin red staining. Scale bars = 200 (top row) and 100 μm (bottom row), respectively. 202

Figure 4.36 - Mineral nodule formation of untreated/MI192 pre-treated hBMSCs encapsulated within the GelMA-PEBT/PBT construct after 6 weeks osteogenic culture observed by Von Kossa staining. Sample counterstained with Van Gieson's solution (pink). Scale bars = 200 (top row) and 20 μm (bottom row), respectively. 203

Figure 4.37 - Relative expression of osteoblast-related genes in untreated/MI192 pre-treated hBMSC microtissues in osteogenic conditions. Gene expression assessed on day 7, 14 and 21. Data expressed as mean \pm SD (n=3). Significance levels shown are the test group compared to the untreated control at the same time point. *P \leq 0.05 and **P \leq 0.01. 205

Figure 4.38 - ALPSA of untreated/MI192 pre-treated hBMSCs BMTs. ALPSA of BMT constructs were assessed after 2 weeks in osteogenic conditions. Data expressed as mean \pm SD (n=3). ***P \leq 0.001. 206

Figure 4.39 - H&E staining of untreated/MI192 pre-treated hBMSC BMT constructs after 6 weeks osteogenic culture. Incorporated microtissues (stained pink/purple) fused with neighbouring tissue modules around internal scaffold fibres. Scale bars = 200 (top row) and 100 μm (bottom row), respectively. 207

Figure 4.40 - Picrosirius red/Alcian blue staining of untreated/MI192 pre-treated hBMSC BMT constructs after 6 weeks osteogenic culture. Collagens and GAGs stained with Picrosirius red and Alcian blue, respectively. Strong Picrosirius red staining located in circular nodules highlighted with black arrows. Strong Alcian blue staining highlighted with blue arrows. Scale bars = 50 (top row) and 25 μm (bottom row), respectively. 208

Figure 4.41 - ALP immunohistochemical staining of untreated/MI192 pre-treated hBMSC BMT constructs after 6 weeks osteogenic culture. Positive ALP immunohistochemical staining (brown), with a weak Harris haematoxylin counterstain (purple). Nodule-like formations highlighted with red arrows. Scale bars = 200 (top row) and 25 μ m (bottom row), respectively..... 209

Figure 4.42 - BMP2 immunohistochemical staining of untreated/MI192 pre-treated hBMSC BMT constructs after 6 weeks osteogenic culture. Positive BMP2 immunohistochemical staining (brown), with a weak Harris haematoxylin counterstain (purple). Scale bars = 200 (top row) and 25 μ m (bottom row), respectively. 210

Figure 4.43 - Col1a immunohistochemical staining of untreated/MI192 pre-treated hBMSC BMT constructs after 6 weeks osteogenic culture. Positive Col1a immunohistochemical staining (brown), with a weak Harris haematoxylin counterstain (purple). Nodule-like formations highlighted with black arrows. Scale bars = 200 (top row) and 25 μ m (bottom row), respectively. 211

Figure 4.44 - OCN immunohistochemical staining of untreated/MI192 pre-treated hBMSC BMT constructs after 6 weeks osteogenic culture. Positive OCN immunohistochemical staining (brown), with a weak Harris haematoxylin counterstain (purple). Nodule-like formations highlighted with red arrows. Scale bars = 200 (top row) and 25 μ m (bottom row), respectively..... 212

Figure 4.45 - AGG immunohistochemical staining of untreated/MI192 pre-treated hBMSC BMT constructs after 6 weeks osteogenic culture. Positive AGG immunohistochemical staining (brown), with a weak Harris haematoxylin counterstain (purple). Scale bars = 200 (top row) and 25 μ m (bottom row), respectively. 213

Figure 4.46 - Col2a immunohistochemical staining of untreated/MI192 pre-treated hBMSC BMT constructs after 6 weeks osteogenic culture. 214

Figure 4.47 - Negative immunohistochemical staining of untreated/MI192 pre-treated hBMSC BMT constructs after 6 weeks osteogenic culture. Scale bar = 50 (top row) and 25 μ m (bottom row), respectively..... 215

Figure 4.48 - Calcium deposition of untreated/MI192 pre-treated hBMSC BMT constructs after 6 weeks osteogenic culture observed by Alizarin red staining. Nodule-like formations highlighted with black arrows. Scale bars = 200 (top row) and 25 μ m (bottom row), respectively..... 216

Figure 4.49 - Mineral nodule formation of untreated/MI192 pre-treated hBMSC BMT constructs after 6 weeks osteogenic culture observed by Von Kossa staining. Scale bar = 50 (top row) and 25 μm (bottom row), respectively. 217

Figure 4.50 - Macroscopic and X-ray images of untreated/MI192 pre-treated hBMSC BMT constructs after 8 weeks *in vivo* implantation. A) Macroscopic images immediately post extraction. B) X-ray radiographs of BMT following extraction. 218

Figure 4.51 - H&E staining of untreated/MI192 pre-treated hBMSC BMT constructs after 8 weeks *in vivo* implantation. Scale bars = 200 (top row) and 100 μm (bottom row), respectively. 219

Figure 4.52 - Picosirius red/Alcian blue staining of untreated/MI192 pre-treated hBMSC BMT constructs after 8 weeks *in vivo* implantation. Collagens and GAGs stained with Picosirius red and Alcian blue, respectively. Strong Picosirius red staining located in circular nodules highlighted by black arrows Scale bars = 200 (top row) and 20 μm (bottom row), respectively..... 220

Figure 4.53 - Col1a immunohistochemical staining of untreated/MI192 pre-treated hBMSC BMT constructs after 8 weeks *in vivo* implantation. Positive Col1a immunohistochemical staining (brown), with a weak Harris haematoxylin counterstain (purple). Scale bars = 200 (top row) and 20 μm (bottom row), respectively. 221

Figure 4.54 - OCN immunohistochemical staining of untreated/MI192 pre-treated hBMSC BMT constructs after 8 weeks *in vivo* implantation. Positive OCN immunohistochemical staining (brown), with a weak Harris haematoxylin counterstain (purple). Scale bars = 200 (top row) and 20 μm (bottom row), respectively. 222

Figure 4.55 - AGG immunohistochemical staining of untreated/MI192 pre-treated hBMSC BMT constructs after 8 weeks *in vivo* implantation. Positive AGG immunohistochemical staining (brown), with a weak Harris haematoxylin counterstain (purple). Scale bars = 200 (top row) and 20 μm (bottom row), respectively..... 223

Figure 4.56 - Col2a immunohistochemical staining of untreated/MI192 pre-treated hBMSC BMT constructs after 8 weeks *in vivo* implantation. Positive Col2a immunohistochemical staining (brown), with a weak Harris haematoxylin counterstain (purple). Scale bars = 200 (top row) and 20 μm (bottom row), respectively..... 224

Figure 4.57 - Negative immunohistochemical staining of untreated/MI192 pre-treated hBMSC BMT constructs after 8 weeks *in vivo* implantation. Scale bars = 200 (top row) and 20 μm (bottom row), respectively..... 225

Figure 4.58 - Calcium deposition of untreated/MI192 pre-treated hBMSC BMT constructs after 8 weeks *in vivo* implantation observed by Alizarin red staining. Scale bars = 200 (top row) and 100 μm (bottom row), respectively. 226

Figure 4.59 - Mineralisation of untreated/MI192 pre-treated hBMSC BMT constructs after 8 weeks *in vivo* implantation observed by Von Kossa staining. Scale bars = 200 (top row) and 100 μm (bottom row), respectively. 227

Figure A1 - ALPSA of hDPSCs from three different donors pre-treated with/without MI192. Cells pre-treated with MI192 (1, 2 and 5 μM) for 48 hours, following culture in osteogenic medium for 2 weeks, with untreated cells cultured in basal and osteogenic medium used as the controls. Data expressed as mean \pm SD (n=3). Significance levels shown are the test groups compared to the basal/osteogenic control or between adjacent MI192 concentrations for that time point. **P \leq 0.01 and ***P \leq 0.001. XL

Figure A2 - ALPSA of hBMSCs from two different donors pre-treated with/without MI192. Cells pre-treated with MI192 (30, 50 and 70 μM) for 48 hours, following culture in osteogenic medium for 2 weeks, with untreated cells cultured in basal and osteogenic medium used as the controls. Data expressed as mean \pm SD (n=3). Significance levels shown are the test groups compared to the basal/osteogenic control or between adjacent MI192 concentrations for that time point. ***P \leq 0.001. XLI

Figure A3 - Multi-lineage potential of hDPSCs. Osteogenic differentiation: Positive calcium accumulation was observed after 28 days cultured in osteogenic medium confirmed by Alizarin Red staining (Scale bar = 75 μm); Adipogenic differentiation: lipid droplet formation was observed in hDPSCs after 14 days culture in adipogenic induction medium after Oil red O staining (Scale bar = 75 μm); Chondrogenic differentiation: hDPSCs were capable of forming cartilage like pellets after 21 days cultured as pellets in chondrogenic induction medium, stained blue for GAGs (Alcian blue staining) and red for collagen (Picosirius red staining). Scale bar = 20 μm XLIII

Figure A4 - Multi-lineage potential of hBMSCs. Osteogenic differentiation: Positive calcium accumulation was observed after 28 days cultured in osteogenic medium confirmed by Alizarin

Red staining; Adipogenic differentiation: lipid droplet formation was observed in hBMSCs after 14 days culture in adipogenic induction medium after Oil red O staining (Scale bar = 50 μ m); Chondrogenic differentiation: hBMSCs were capable of forming cartilage like pellets after 21 days cultured as pellets in chondrogenic induction medium, stained blue for GAGs (Alcian blue staining) and red for collagen (Picrosirius red staining). Scale bar = 20 μ m.XLV

Figure A5 - AlamarBlue analysis of supernatant acquired from hBMSCs treated with/without MI192 (1, 10, 20, 50, 100 μ M) for 24, 48 and 72 hours. Data expressed as mean \pm SD (n=3). Significance levels shown are the sample compared to the basal control for that time point. *P \leq 0.05 and **P \leq 0.01.XLVI

List of Tables

Table 1.1 - The localisation, tissue distribution and biological function of isoform-specific HDAC enzymes. Adapted from (90, 91)	12
Table 2.1 - TaqMan probes utilised in this thesis.	38
Table 2.2 - Antibodies utilised for ICW and immunohistochemistry staining	45
Table 3.1 - Table of data from the flow cytometry analysis of the cell cycle distribution for hDPSCs. Cells dosed with/without 2 μM MI192 for 24, 48 and 72 hours. The table shows the average percentage of cells in each phase of the cell cycle, with the standard deviation (SD).....	64
Table 4.1 - The effect of MI192 treatment on the distribution of hBMSCs at different phases of the cell cycle. Cells dosed with/without 50 μM MI192, for 24, 48 and 72 hours. The table shows the average percentage of cells in each phase of the cell cycle, with the standard deviation (SD).	170
Table 5.1 - Summary of the effects of MI192 on the general and osteogenic properties of DPSCs and BMSCs in this thesis.	280
Table A1 - Donor information for hDPSCs and hBMSCs utilised in this thesis.	XLII

Chapter 1 - Literature Review

This chapter aims to review the appropriate literature relevant to the research presented in this thesis. This review provides an introduction in the field of epigenetics and the role histone deacetylase enzymes have in the body. Manipulation of epigenetics through the use of HDAC inhibitor compounds are introduced, with their design, mechanism of action and current use discussed. Finally, the potential of using these compounds for bone tissue engineering applications is also evaluated.

1.1 - Background

The continuously growing ageing population suffers from bone damage caused by traumatic injury, tumour resection, congenital defects or common age-associated diseases such as osteoporosis. Bone tissue has the intrinsic ability to regenerate, however critical-sized bone defects, spanning in excess of 20% of the bones length, cannot self-repair and can result in permanent defects (1). These defects often lead to a loss of tissue functionality and therefore requires surgical intervention (2). Annually, the combined health and social care cost for hip fractures alone in the UK is £2.3 billion (3), representing an enormous socioeconomic burden on society. Thus, the ability to generate new bone is still a major unmet clinical need. Alarmingly, this is expected to rise in the future, due to increasing life expectancy with the demand for continued quality of life in the older years.

Current clinical therapies such as autografts have been seen as the "gold standard" for many years as they are osteoconductive, osteoinductive and osteogenic (4-6). However, these procedures are highly invasive, limited by tissue availability and possess an increased risk of donor site morbidity (7, 8). Allografts are also associated with various limitations such as a high risk of immunogenicity, disease transmission, lacking both vascularisation and osteogenicity and are associated with increased costs (9, 10). Due to these various limitations, new approaches to regenerate damaged or diseased tissues are greatly needed. Within the tissue engineering and regenerative medicine field, extensive research has looked to develop alternative methods of producing bone tissue to meet the ever-increasing clinical need.

Tissue engineering comprises of four key elements: cells, growth factors, scaffolds and environmental/mechanical stimulation (11, 12). Stem/stromal cells are the key cell source used in tissue engineering applications, where they are directed to differentiate into the lineage required to produce functional tissue. The key for bone tissue engineering strategies is to effectively control the lineage-specific differentiation of stem cells into bone-forming cells (13). In recent years, technologies such as induced pluripotent stem cells (iPSC) and gene therapy have been utilised to

enhance the osteogenic capacity of cells, fostering much excitement within the field (14). However, due to the risks of random integration of reprogramming transgenes, such as *Oct4*, *Sox2*, *Klf4* and *c-Myc* into the host genome, the low process efficacy and the potential risk of virally induced tumourigenicity, alternative methods have been developed to generate pluripotent cells using non-integrating systems, albeit with limited success (15). Due to these drawbacks, alternative safer methods of controlling stem cell osteogenic differentiation have been investigated, such as altering their epigenetics.

It has become increasingly apparent that epigenetics plays a significant role in regulating cellular fate. Specifically, researchers have discovered that post-translational modifications to histone proteins, such as the activity of histone deacetylase (HDAC) enzymes, result in alterations in chromatin structure and ultimately affect stem cells properties, such as potency and differentiation potential (16). The majority of research has focused on utilising compounds that modify histone proteins for the treatment of various cancers. The US Food and Drug Administration (FDA) has approved four histone deacetylase inhibitors, Vorinostat, Romidepsin, Belinostat and Panobinostat for cancer therapy (17-19).

Since then, the focus of research has extended from the cancer therapeutics arena as researchers are beginning to investigate the effects of these compounds in other areas such as in inflammatory diseases, HIV therapeutics and prevention of cardiac diseases (20-22). In recent years, researchers have combined these epigenetics-modifying compounds with stem cells to improve their efficacy for tissue engineering applications, with particular potential being demonstrated within the bone tissue engineering field (23).

1.2 - Basic bone structure and physiology

The primary functions of bone tissue are to - 1) provide protection and support in the body, via supporting surrounding soft tissues such as tendons, ligaments and muscles; 2) retain a deposit of minerals essential for bone tissue homeostatic roles; 3) support the movement of the body allowing articulation at the joints; and 4) store bone marrow which is involved in the repair and regeneration of other tissues (24, 25). In the human body, bone tissue is a type of dense mineralised connective tissue, which can be divided as cortical and cancellous bones according to their mechanical properties and structure.

In a typical long bone such as the femur (Fig 1.1), the exterior regions are composed of cortical bone, where approximately 80 - 90% is mineralised providing the majority of the mechanical strength (26). Cortical bone possesses a compressive stiffness and strength of 12 - 20 GPa and 100 - 230 MPa,

respectively. Cancellous bone is mainly located in the internal and epiphysis regions possessing stiffness and strength of 0.2 - 0.8 GPa and 2 - 12 MPa, respectively (27). The natural composition of bone consists largely of collagen (20%), hydroxycarbonate apatite/calcium phosphate (69%) and water (9%), with proteins, polysaccharides and lipids present in low quantities (28). The primary function of cortical bone is to provide mechanical support, while the cancellous regions are involved in the metabolic activity of bone tissue. In natural conditions, bone tissue has the intrinsic regenerative capacity in response to injury as well as in skeletal development and remodelling during adulthood (4, 29).

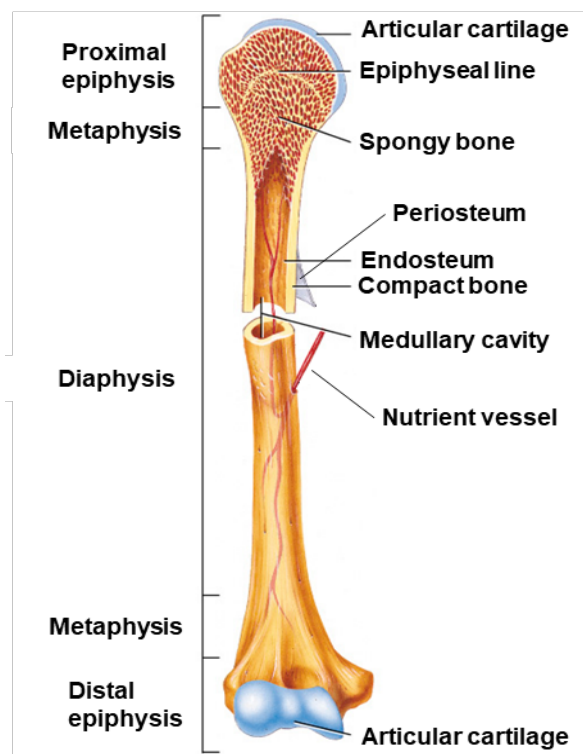


Figure 1.1 - Structure of long bone. The femur is a typical long bone in the body, possessing both the cortical and cancellous bone regions. Adapted from (30).

1.2.1 - Cellular constituents of bone

Mesenchymal stem/stromal cells (MSCs) are a subpopulation of stem cells that reside within the bone marrow and are responsible for giving rise to all cells of the mesoderm lineage (31). These MSCs are able to differentiate along the osteogenic lineage to generate cells responsible for modulating bone formation such as osteoblasts and osteocytes (32). The two key cells responsible for controlling bone remodelling are osteoblasts and osteoclasts (Fig 1.2). Osteoblasts are heavily involved in bone formation, where these cells produce a woven matrix called osteoid, consisting mainly of collagen type I and non-collagenous proteins such as osteonectin, osteopontin and

osteocalcin (OCN) which form the organic matrix (33). Following which the osteoid is mineralised by the nucleation of calcium and phosphate ions, forming the hydroxyapatite crystals within the matrix (34). On the other hand, osteoclasts are terminally differentiated multinucleated cell, responsible for resorbing the osteoid allowing bone tissue remodelling that is dictated by the direction of mechanical loading applied to bone (35). Dysregulation in the balance of bone remodelling can lead to bone diseases such as osteoporosis (36).

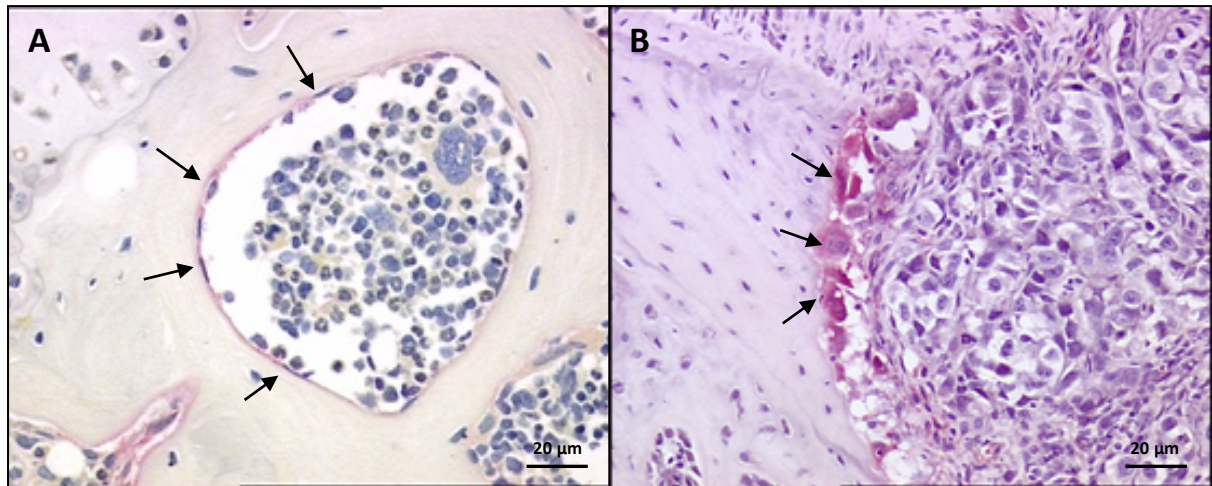


Figure 1.2 - Histological staining of osteoblast (A) and osteoclast (B) (PC3 luciferase 2) in mouse bone. (A) Alkaline phosphatase staining of osteoblasts (black arrows). (B) Tartrate-resistant acid phosphatase staining of osteoclasts (black arrows) induced by PC3 tumour cells (author generated these images/stained sections). Scale bar= 20 μm .

1.2.2 - Bone formation

Bone tissue forms via the process of endochondral and intramembrane ossification (Fig 1.3). Flat bones such as the Sternum form via the intramembrane ossification process, where mesenchymal progenitor cells differentiate directly into osteoblasts. This process is initiated by key osteogenic transcription factors, such as Runx2, and is influenced largely by the Wnt signalling pathway (37). Long bones form via the endochondral ossification, where there is an intermediary cartilage template phase before the formation of bone tissue (38). The cells vital in initiating this process are MSCs which have the potential to differentiate into the key cells involved in bone formation, such as chondrocytes and osteoblasts. These bone formation processes are tightly regulated by several growth factors and complex signalling pathways, such as transforming growth factor beta (TGF- β), bone morphogenetic protein (BMP) and the Wnt signalling pathway (38-40).

It is well known that many cellular processes maintain the homeostatic regulation of the intrinsic chemical reactions that produce collagens, growth factors, hormones, and other extracellular matrix

proteins that are characteristic of bone tissue (41); however, it is the underlying deoxyribonucleic acid (DNA) which provides the genomic information for all of these processes to occur.

Intramembranous Ossification

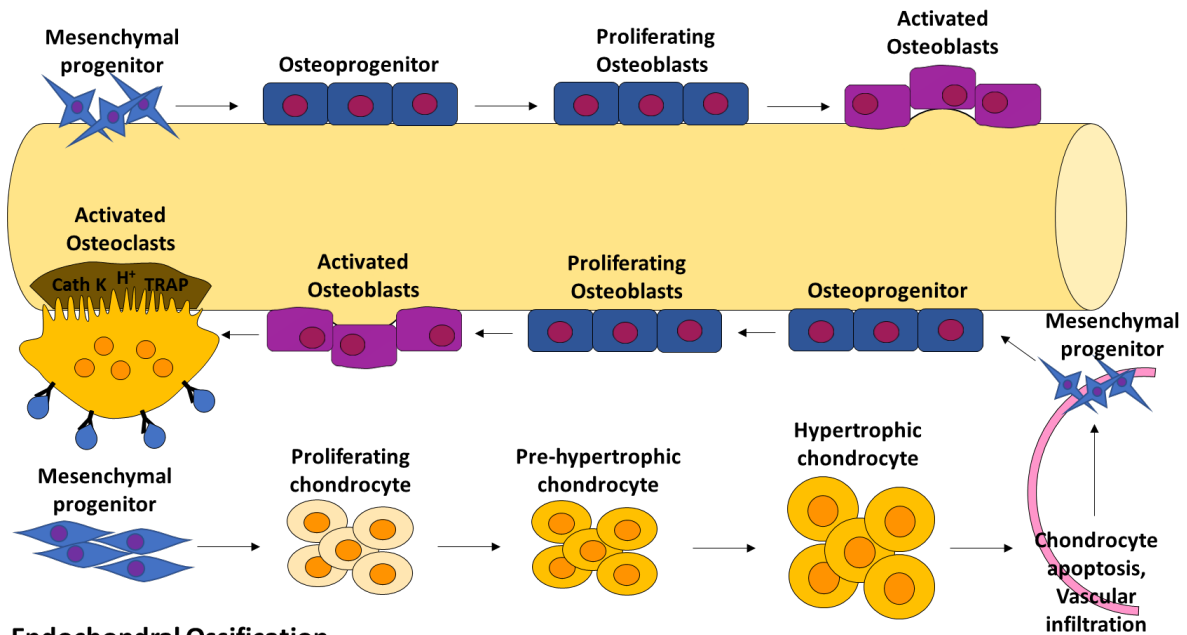


Figure 1.3 - Bone formation processes. Intramembranous ossification is the process in which mesenchymal progenitor cells directly differentiate to osteoblasts to form bone tissue. Endochondral ossification is the more indirect process, where condensation of mesenchymal progenitors creates a cartilaginous template for future bone formation.

1.3 - DNA structure: Organization of the genetic material into chromatin

The DNA molecule consists of two polynucleotide chains that are composed of four nucleotide subunits: adenine, guanine, cytosine and thymine (42). These nucleotides complementarily bind together to form the double helical 3D structure of the DNA. Due to the extensive size of the entire DNA molecule within each cell, DNA must be packaged with the use of specialised proteins called histones which bind and fold the DNA, packaging it into further assembly levels. This supercoiling of DNA allows for the processes such as DNA transcription, replication and damage repair to occur (43). These structures could be further packaged into chromatin, nucleosome-core particles, nucleosomes, and then chromosomes that are stored within the cell nucleus (Fig 1.4).

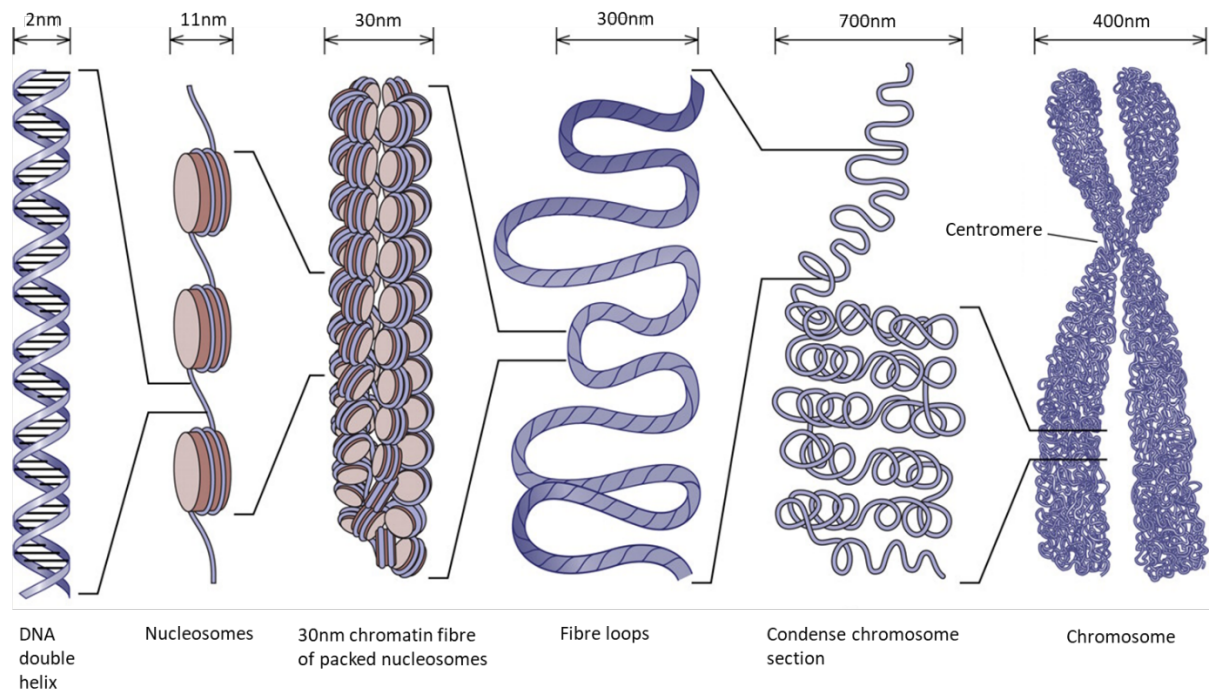


Figure 1.4 - Chromatin Hierarchical Structure. Chromatin has three organizational levels: DNA wraps around the histone proteins to form nucleosomes; these in turn couple to become the 30 nm chromatin fibre; supercoiling of the chromatin fibre produced the chromosome. Adapted with permission (44).

The nucleosome core particle consists of DNA of approximately 146 base pairs coiled 1.7 times around the histone complex containing an octamer of proteins, creating nucleosomes which are the fundamental molecular units of the chromatin (Fig 1.5) (45). The histone proteins form the octamer consisting of 2 copies of four highly conserved proteins: H2A, H2B, H3 and H4 (46). Each histone protein possesses a flexible amino-terminal tail domain that projects from the nucleosome core, and a histone fold domain which mediates histone-histone and DNA-histone interactions essential for nucleosome core assembly (47).

During the packaging process, histone proteins play a key role. This is due to the high abundance of positively charged amino acid residues on the histone protein tails, which allows for ionic interactions with the negatively charged regions of DNA, this accounts for the ease with which they are able to remodel the DNA structure. The underlying DNA sequence in all somatic cells are the same, however, the functionality of each cell differs drastically, due to the tightly regulated control of the expression of certain genes. A process which regulates the cells gene expression is the post-translational modification of the chromatin structure via epigenetics.

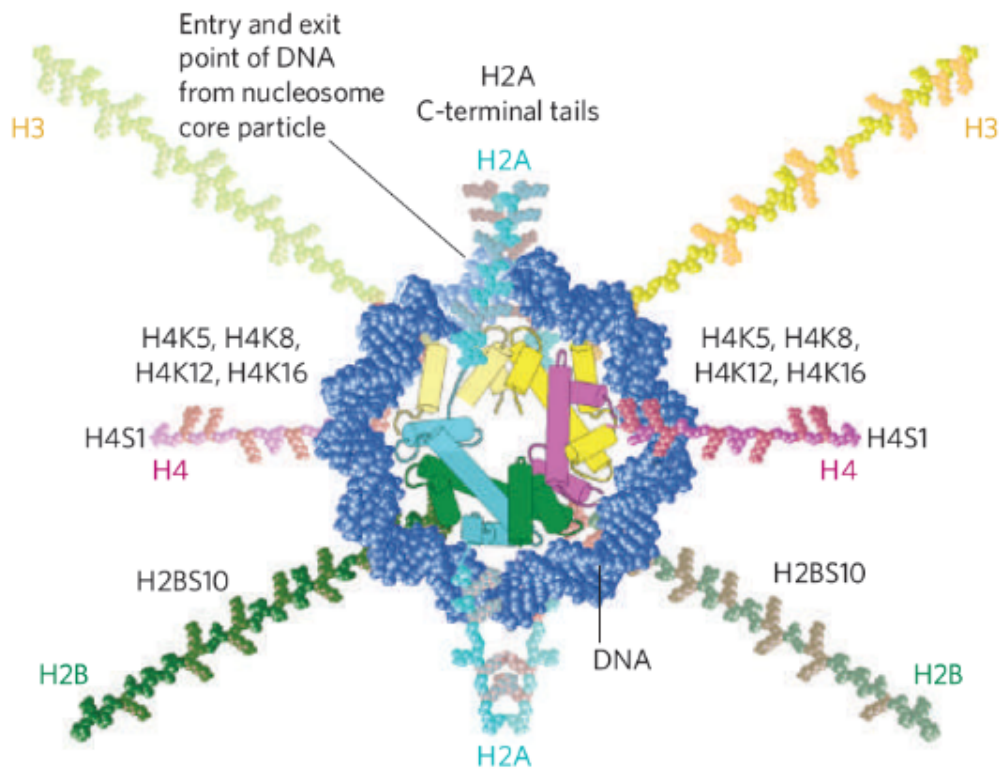


Figure 1.5 - Representation of the nucleosome core. Each nucleosome core particle consists of the DNA (blue) which wraps around the four core histone proteins that form the histone octamer protein complex: H2A (turquoise), H2B (green), H3 (yellow) and H4 (pink). C-terminal tails of the H2A proteins protrude from the centre of the nucleosome core. Reprinted with permission (45, 48).

1.4 - Epigenetic modifications

Epigenetics is the study of dynamic alterations in the transcriptional potential of the cell without altering the DNA sequence, via the process of post-translational modifications such as addition/removal of acetyl, methyl, and other chemical groups on DNA, histones and other DNA associated proteins. Other epigenetic modifications that occur to the DNA include ubiquitination, phosphorylation, sumoylation, citrullination and adenosine diphosphate ribosylation (49). Harnessing epigenetic approaches provides an alternative to the use of iPSCs or gene therapy for tissue engineering applications as it eliminates the increased risk of teratoma formation with those technologies (50). Various studies have demonstrated the influence of external environmental factors, such as infection, smoking, alcohol consumption and diet, in altering the extent of post-translational modifications, (51-54). However, the exact mechanisms by which they affect the DNA remains relatively unclear. Post-translational modifications are of particular interest to researchers in the medical field, as the cells' epigenome is the key influencer for human development and several disease states, including inflammatory diseases (55) and cancers (56). Acquiring a clearer

understanding of the effects of epigenetics may lead to the development of novel therapeutics. Researchers have identified a variety of post-translational modifications that occur to the DNA, with acetylation being one of the most abundant.

1.4.1 - Acetylation

An important epigenetic modification is the addition and removal of an acetyl group, a process called acetylation and deacetylation, respectively. These modifications occur at lysine residues on the chromatin's histone tail. Genome-wide analysis has shown that acetylation is one of the most abundant post-translational modifications that occur within the cell (57, 58). The addition of the acetyl groups neutralises the positive charge of the histone tail, which results in the weakening of the electrostatic interactions between the anionic DNA and nucleosomes, leading to much more open chromatin structure (59). Moreover, acetylation prevents further post-translational modifications, essentially blocking additional epigenetic modifications from occurring (60).

A number of important acetylation sites are involved in regulating the conformational change in the chromatin structure, such as Lys9, Lys14, Lys27 (histone 3) and Lys5, Lys8, Lys12 and Lys16 (histone 4) (61, 62). There are three mechanisms in which acetylation of the histones regulates transcriptional potential of the chromatin. Acetylation of the histone tail provides a docking site for the binding of additional regulatory proteins responsible for assessing the level of acetylation potentially mediating transcription, and therefore these enzymes act as co-activators and co-repressors (63, 64). In addition, epigenetic modifications to the histone amino-terminal domains by processes such as acetylation and methylation result in generating either synergistic or antagonistic interactions for chromatin-associated proteins to regulate the transition between the open and condensed chromatin structures (65). Finally, acetylation of certain lysine residues on the histone amino-terminal tails results in the neutralisation of its positive charge leading to the relaxation of the bonds between the DNA and the histone. The two enzymes responsible for controlling the acetylation state of histones proteins are histone acetyltransferase (HAT) and HDAC.

1.4.2 - Histone acetyltransferase (HAT) and histone deacetylase (HDAC)

The homeostatic balance between the condensed and unfolded chromatin is maintained by HAT and HDAC enzymes (66). Acetylation is mediated by HATs which transfers acetyl groups to the lysine residues, while HDACs are responsible for the removal of these acetyl groups (Fig 1.6).

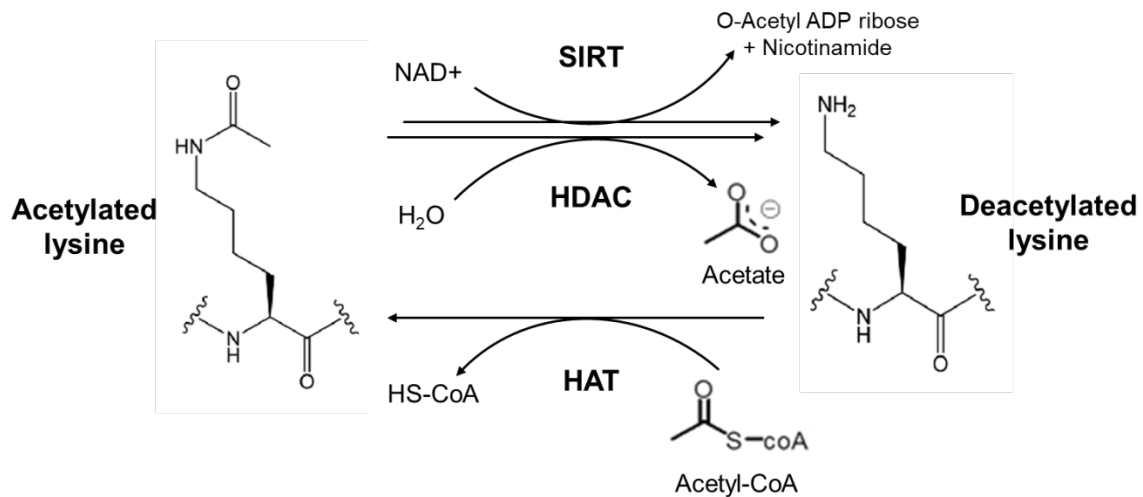


Figure 1.6 - The process of acetylation and deacetylation. The enzymatic reaction of acetylation and deacetylation is mediated by HAT and HDAC enzymes, respectively.

The HAT family are divided into two classes based on their cellular origin and function. Type A HATs are located within the nucleus, where they are involved in regulating the expression of genes through their acetylation activities to the histones, while type B HATs are found within the cytoplasm and function to acetylate newly synthesised histones before transportation into the nucleus (67). The overall acetylation state of histones is controlled by these enzymes via two mechanisms. They can act in a non-specific, un-regulated fashion, over a broad genomic area, or they can target specific sites of transcriptional activators/repressors which directly control the actions of HDACs and HATs (58). Acetylation results in relaxation of the condensed chromatin structure called heterochromatin, therefore reducing the DNAs affinity for the histones and creating a much more open, transcriptionally active chromatin called euchromatin (68-70)(Fig 1.7). The inhibitors of these HDAC enzymes, HDAC inhibitors (HDACis) target and block the active site, therefore, blocking the deacetylation action of the zinc ions found within the active sites of HDAC enzymes, leading to increased protein acetylation levels. The action of HDACis may affect the chromatin conformational structure, which has been linked to the differentiation potential of stem cells (58).

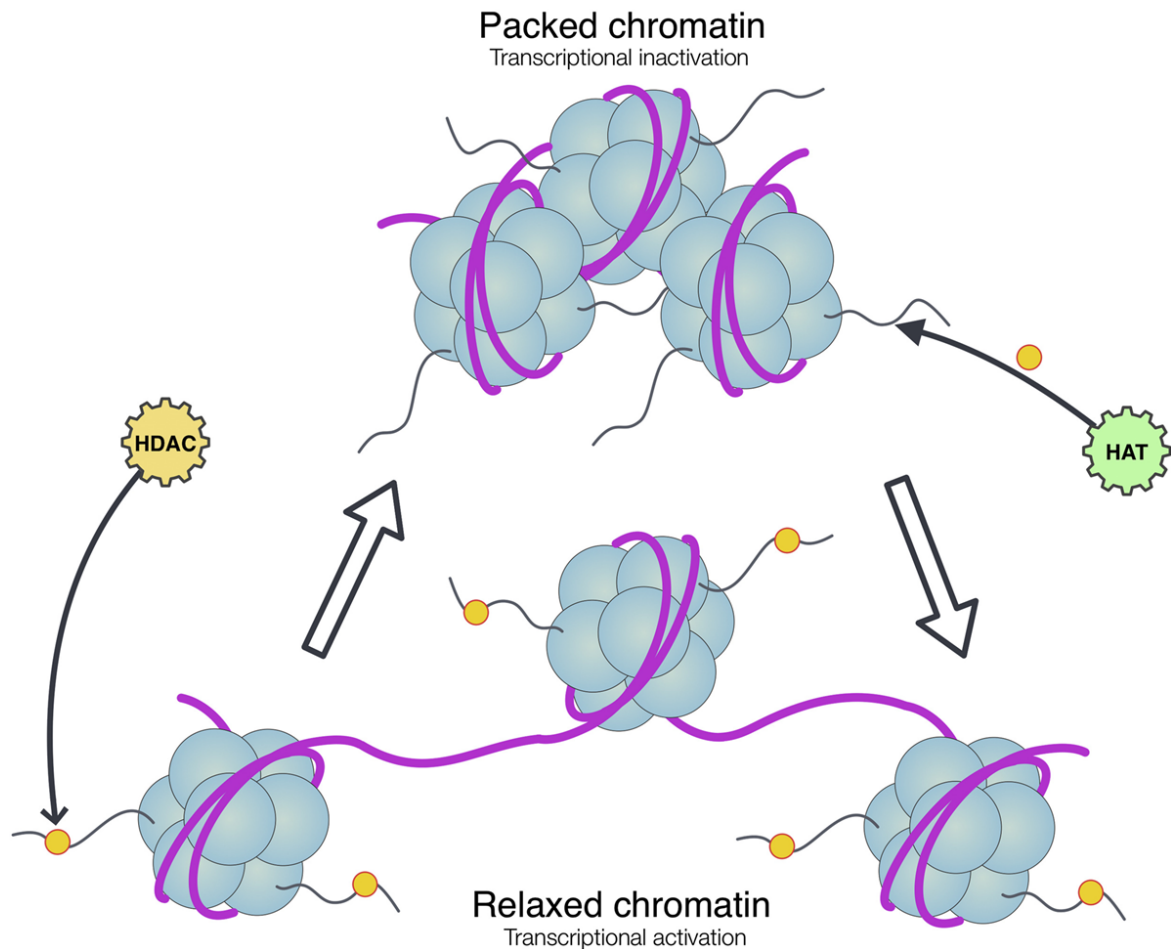


Figure 1.7 - Schematic representation of the dynamic effects of HDAC/HAT on the nucleosome and the conformation of the chromatin structure. The transference of acetyl groups onto the histone lysine tail via HAT causes the opening of the chromatin structure, with HDAC activity reversing this effect (71).

HDAC proteins play a key role in epigenetics and their inhibitor compounds have been explored in clinical trials for cancer treatments due to the ability to inhibit the deacetylation activity linked to tumour pathology, allowing the reactivation of tumour suppressor genes (72, 73). In addition, it has been demonstrated that HDACi compounds have the potential to control stem cells differentiation (66, 74), which could be a crucial component of tissue engineering approaches. Moreover, HDAC inhibition has been utilised to increase the generation efficiency of iPSCs (75), *in vitro* expansion methods of human hematopoietic stem cells (76), stem cell osteogenesis (74) and efficacy of cell-based therapies. The acetylation/deacetylation activity of HATs and HDACs is not solely isolated to histone proteins but also affects non-histone associated proteins.

1.4.3 - Acetylation of non-histone proteins

The amino acid lysine residues, the targets of HATs and HDACs, are not only found within histone proteins but also in a variety of cellular proteins, demonstrating these enzymes have multiples non-histone targets within the cell (77).

Numerous studies have shown that these enzymes have functions not related to histone proteins (78, 79), such as the effect of HDAC1 on the tumour suppressor p53 and interactions of HDAC6 with tubulin proteins (80). Deacetylation activity of non-histone proteins such as transcription factors and DNA repair/replication proteins affect a large proportion of every cellular process by preventing proper cellular function or by destabilising proteins (79, 81, 82). Choudhary *et al.* (2009) suggest that non-histone proteins may comprise the majority of the HATs and HDACs substrates (83); therefore, the large number of cellular targets will result in a wide range of cellular alterations via interactions with HATs and HDAC, indicating the importance of these enzymes (60, 66, 78, 84).

1.4.4 - HDAC isoforms

In the human body, 18 distinct HDAC genes encode for 18 enzymes, which differ in their structure and activity. These enzymes are grouped into four classes based on their molecular phylogenetic analysis of their primary structures and homology to yeast enzymes (85). These classes are further split into two categories; classical (classes I, II, IV) and sirtuins (class III) (72, 85). The activity of both categories of HDAC differs, where the classical HDAC are dependent on zinc ions, while the sirtuin class of HDAC utilises nicotinamide adenine dinucleotide. Notably, the tissue expression profiles of class I and II HDAC enzymes differ where class I isoforms are expressed ubiquitously (86), while class II isoforms have a differential expression distribution, with higher levels detected in tissues such as brains, heart, thymus, spleen, liver and kidney (87, 88). Different HDAC enzymes possess highly specific functions; often several enzymes can function together, and some have overlapping functions (89). While the physiological roles of each HDAC isoform are relatively unclear, studies inhibiting individual isoforms have started to provide some insight into their function (58) (Table 1.1). These insights can be acquired through the analysis of HDAC structure.

Table 1.1 - The localisation, tissue distribution and biological function of isoform-specific HDAC enzymes. Adapted from (90, 91)

HDAC	Localisation	Tissue distribution	Cellular functions
Class 1			
HDAC1	Nucleus	Ubiquitous	Transcription silencing, cell survival and proliferation, DNA damage response, involved in osteogenic, cartilage, adipogenic and epidermal development
HDAC2			Transcriptional silencing, regulation of cell cycle, DNA damage response, involved in neuronal cell development
HDAC3			Transcriptional silencing, cell survival and proliferation, suppress osteogenic differentiation
HDAC8			Involved in embryonic craniofacial and skull bone development, smooth muscle cell contractility
Class 2a			
HDAC4	Nucleus/ cytoplasm	Heart, skeletal muscle, brain	Transcriptional silencing, chondrocyte and osteocyte development, retinal protection, involved in neuronal activity
HDAC5			Transcriptional silencing, myocardium and endothelial functions
HDAC7			Transcriptional silencing, thymocyte differentiation, osteoclast activity
HDAC9			Transcriptional silencing, role in the myocardium and skeletal muscle
Class 2b			
HDAC6	Mainly cytoplasm	Heart, platelet, pancreas, kidney, spleen, liver	Tubulin-deacetylase regulates chaperones interactions, microtubule function and aggresome function
HDAC10			Involved in regulating melanin production
Class 4			
HDAC11	Nucleus/ cytoplasm	Heart, skeletal muscle, brain, kidney	Transcriptional silencing, immune regulation

1.4.5 - HDAC structure and activity

Each HDAC isoform exhibits slight variations in their structural composition. Full structural data of HDACs are limited as obtaining X-ray crystal structure are difficult. HDAC enzymes are typically isolated via co-crystallation with a signalling molecule or an inhibitor, which gives an indication into the function of these enzymes. At present, the structures of HDAC isoforms 1, 2, 3, 4, 7 and 8 have been well characterised (92). Figure 1.8 shows a representation of a HDAC structure with the HDACi, suberoylanilide hydroxamic acid (SAHA) bound to the zinc ions at the bottom of the catalytic pocket of the active site (93).

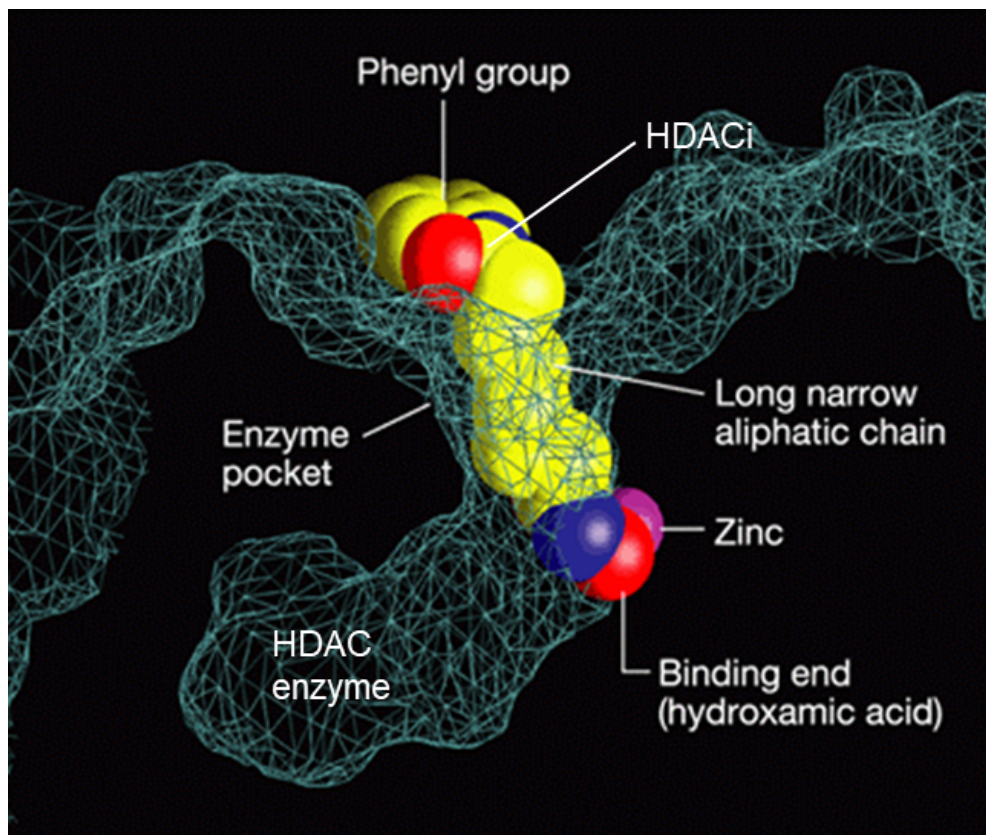


Figure 1.8 - A 'space-filling' representation of the HDACi compound SAHA bound into the HDAC active site. The inhibitor SAHA binds into the catalytic pocket of a HDAC-like protein based from the homologue found in *Aquifex aeolicus*. Adapted with permission (93).

As illustrated in Fig 1.8, the active site of HDAC enzymes possesses three highly conserved regions: an internal cavity, a zinc ion binding site and a long hydrophobic tunnel (88). The active site of the HDAC enzyme consists of a sock-shaped tunnel roughly 11 Å deep, which comprises approximately 390 amino acids. Within this cavity, the Zn²⁺ ion is situated at the bottom of this catalytic pocket (94). Lipophilic amino acids line the internal cavity of the active site giving a hydrophobic property. The internal cavity spans 14 Å long and is involved in accepting the cleaved acetate from the deacetylation activity of the zinc ion (95). There are differences between HDAC classes in terms of the pocket shape and residues; however, the catalytic zinc ion is common in all zinc-dependent HDAC proteins (38).

1.5 - HDAC inhibitors

1.5.1 - Structure and activity

The influence of epigenetics in contributing to a variety of different phenotypes and disease aetiologies has generated a growing interest in the mechanism by which HDACis can alter the activity of HDAC enzymes. HDACis are small molecular compounds isolated from natural sources such as Trichostatin A (TSA) or synthesised such as MS-275 (Fig 1.9A) (96). These inhibitors induce the accumulation of both acetylated histone and non-histone proteins, resulting in alterations of the histone structure. These alterations alter numerous key cellular functions, such as gene expression, proliferation, migration and cell death (71).

These inhibitors are generally classified as short-chain fatty acids, hydroxamic acids, cyclic peptides or benzamides. Zinc-dependent HDACis are divided into three segments which complement the HDAC enzyme: a cap region, hydrophobic linker and a functional zinc binding moiety (Fig 1.9B) (97). Hydroxamic acid-based HDACis contain the same linker and zinc bind region but possess differences in the cap region (98).

A

Natural HDACi	HDAC target	Synthetic HDACi	HDAC target
TSA	Pan Inhibitor (Class 1, 2a, 2b, 4)	MI192	HDAC 2 & 3 (Class 1)
NaB	Pan Inhibitor (Class 1, 2a, 2b)	MS275	HDAC 1, 2, 3 (Class 1)
Largazole	HDAC 1, 2, 3 (Class 1)	Vorinostat (SAHA)	Pan Inhibitor (Class 1, 2a, 2b, 4)
Romidepsin	HDAC 1 & 2 (Class 1)	Panobinostat	Pan Inhibitor (Class 1 & 2)
VPA	HDAC 1, 2, 3 (Class 1 & 2a)		

B

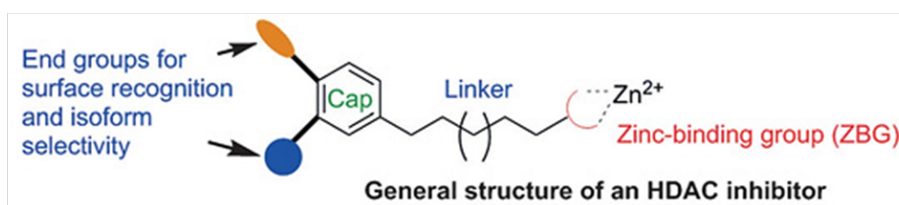


Figure 1.9 - The general HDACi structure and their HDAC targets. (A) Natural and synthetic HDACi and their HDAC targets. (B) Representation of the general structure of HDAC inhibitor. Adapted from (99-101).

High levels of deacetylation activity can be observed in tumour pathology, which can repress the expression of tumour suppressor genes, inhibit DNA repair, stimulate a halt in the cell cycle, and induce apoptosis (72). Due to this link, HDACis have been primarily used for cancer therapeutics (56). The FDA has approved four HDACis for cancer therapeutics: Romidepsin, Panobinostat, Belinostat and Vorinostat (17) (18, 102) (Fig 1.9). In recent years, research utilising these HDACis have expanded into other therapeutic areas, where HDACis have been identified as potential therapeutic tools for diabetes (103), inflammatory diseases (104), arthritis (21) and tissue engineering (23).

Inhibition of HDAC activity occurs when the HDACi inserts into the catalytic pocket, blocking the active site, via the interaction of the two atoms of the HDACis hydroxamic region with the zinc ion in the HDAC internal cavity, therefore preventing deacetylation (Fig 1.10). The aliphatic region of the HDACi occupies the enzyme cavity, while the hydrophobic interactions increase the strength of binding energy. The capping group of the inhibitor blocks access to the pocket, reducing the potential for competitive binding. The structural differences between different HDAC isoforms are

found within the entrance of the catalytic pocket. This is often the region of interest for researchers when designing specific HDACis (105), and therefore the selectivity of HDACis is defined by the cap region (106). The selectivity of HDACis is of great importance as it dictates how these compounds are utilised.

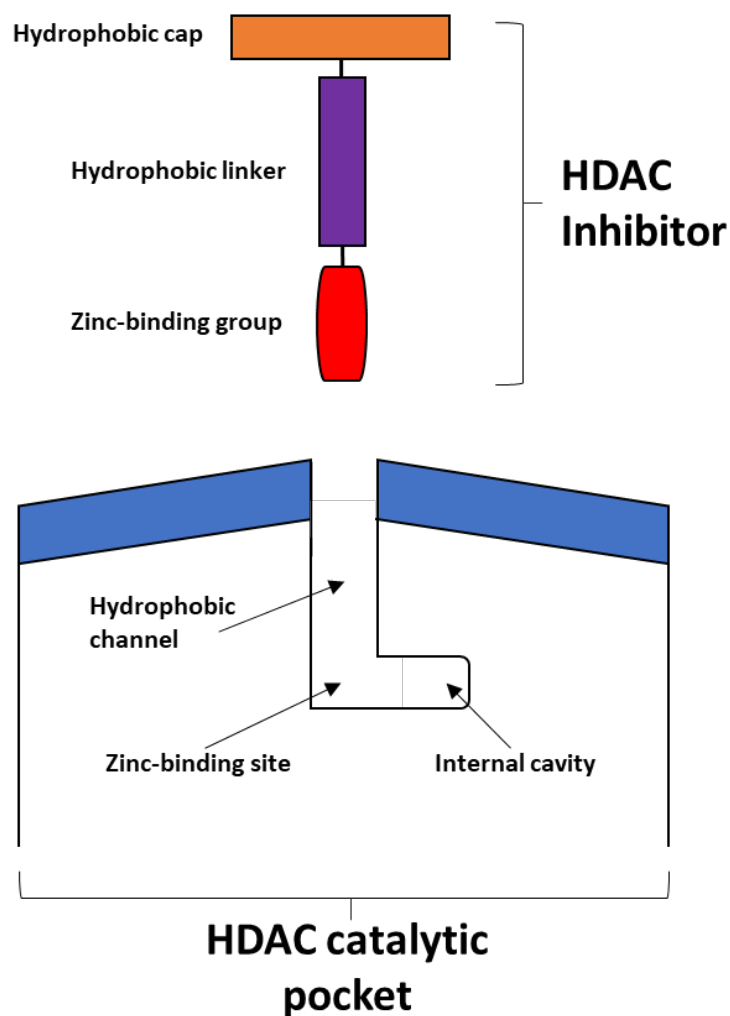


Figure 1.10 - Schematic representations of zinc-dependent HDAC inhibitor interacting with the HDAC catalytic pocket. The HDAC enzyme possesses 3 highly conserved regions: an internal cavity, a zinc-binding site and a hydrophobic channel. The zinc-dependent HDACi possesses 3 complementary sections: zinc-binding group, hydrophobic linker and a hydrophobic cap. The HDACi inserts into the catalytic pocket, where the zinc-binding group blocks deacetylation activity of the enzyme, while the cap group of the HDACi prevents further competitive bindings.

1.5.2 - Specificity of HDAC inhibitors

The majority of research has focused on non-specific (panHDACis) targeting a broad spectrum of HDAC isoforms (107). The first generation of HDACis such as SAHA and Romidepsin (17, 102), are relatively unselective, therefore resulting in reduced efficacy due to the inhibition of unwanted HDAC isoforms (108). The differences in the structure of HDAC isoforms allow for inhibitors to be specifically designed to target selective enzymes which could be the key to developing future HDAC-based therapeutics (107-109).

Several studies have shown that panHDACis are effective drugs (17, 102). However, research has started to shift away from this unselective approach and explore the use of isoform-specific HDACis. Due to the plethora of potential targets for panHDACis, it is difficult to elucidate their specific mechanism of action which leads to the increased potential side-effects. It has been suggested that the key to developing HDAC therapeutics is to target specific HDACs (107-109). The use of this selective approach is likely to increase the efficacy of HDACis and reduce unwanted side-effects from targeting unnecessary isoforms.

1.5.3 - The biological role of HDAC enzymes and the effects of HDACis

HDACi compounds were originally developed for cancer therapeutics, as these inhibitors target the abnormal epigenetics found within cancerous cells. The reason why HDACis are advantageous compared to conventional cancer therapies such as radio and chemotherapy is that these compounds possess certain selectivity in the targeted killing of cancer cells over normal non-transformed cells. HDACis have been shown to have a broad range of effects on both normal and cancerous cells, such as cell cycle progression, proliferation, differentiation, gene expression and cell death. To effectively utilise these epigenetic regulators for cell-based therapies, a greater understanding of the effects these compounds have on the cells must be evaluated.

1.5.3.1 - Cell cycle

The cell cycle is the process where cells prepare to divide prior to entering proliferation and differentiation. There are four main stages associated with this process: G₁, S, G₂ and M phase. The two gap phases, G₁ and G₂, are where the cells monitor internal and external environments to determine whether conditions are favourable to grow and divide and enter the S and M phases (110). During this process, normal cells must pass regulatory checkpoints between the phases, which when activated can halt cell cycle progression in cases such as if the DNA is damaged and requires repair, preventing cells from passing on the damaged or mutated DNA to daughter cells (111). Cell

cycle regulation is essential as if the checkpoint becomes damaged, this may lead to uncontrolled cell growth typical of cancerous cells. HDACi treatment on cancerous cells has been shown to halt cell cycle progression at either G₁ or G₂ stages, allowing for the activation of the cell's apoptotic mechanisms (112). The effects of HDACis on normal cells are less pronounced compared to cancerous cells, due to the intact cell cycle checkpoints (113). Numerous studies have shown that HDACi treatment on normal cells can halt cell cycle progression (114, 115). The differential halting of the cell cycle at certain stages may be due to the differential HDAC isoform inhibited.

The importance of specific HDAC isoforms on controlling cell cycle progression has been investigated. HDACs have been shown to affect the cell cycle by deacetylating non-histone proteins involved in regulating the cycle progression (114). HDAC1 has been shown to be heavily involved in cell cycle regulation, where it interacts with the E2F family of proteins, shown to modulate cell cycle progression, as this isoform deacetylates E2F1 which was previously acetylated by CBP and p300 HATs (77). HDAC1 knockout embryonic stem cells (ESCs) exhibited a reduced proliferation rate attributed to increased levels of p21, the cyclin-dependent kinase inhibitor 1 (CDK1). The repression of p21 is mediated by HDAC1 via deacetylating histones at the p21 promoter regions, resulting in the suppression of p21 gene expression (116). Enhanced p27 expression was also observed in HDAC1 knockdown cells, which further exacerbates the suppression of proliferation (116). Deletion of both HDAC1 and 2 led to enhanced G₁ cell cycle arrest, due to their regulation of both p21 and p57 genes, which are essential in regulating the transition from the G₁ to S phase. HDAC3 has also been shown to be involved in regulating cell cycle progression. This isoform has been reported to bind to the promoter region of CCND1, the gene which encodes for cyclin D, responsible for G₁/S phase transition (117). HDAC3 activity has been shown to suppress the expression of *CDKN1A* (p21), leading to the halting of the cell cycle (118).

The effects of HDACis on cell cycle progression have also been investigated. In adult neural stem cells, Jiang *et al.* (2014) showed that HDAC3 deletion caused defects in the progression through the G₂/M phase to the S phase of the cell cycle (119). Studies have demonstrated that HDAC enzymes have an integral role in regulating the cells cycle, which was discussed earlier in this chapter, therefore altering their activity with HDACis will result in inducing cell cycle arrest both in normal and cancerous cells (120). The inhibitor Vorinostat has been shown to cause cell cycle arrest at both G₁ and G₂/M phases at high concentrations in T24 bladder carcinoma cells (121).

1.5.3.2 - DNA damage

The acetylation of histone proteins induced by HDACi activity results in the opening of the chromatin structure which may result in increased exposure of the DNA to mutations (122, 123). In addition, it has been reported that HDACis have the ability to enhance the accumulation of reactive oxygen species (ROS), which can induce DNA damage (122, 124). These inhibitor compounds have been shown to inhibit numerous processes involved in the repair of DNA, such as down-regulating the gene expression of DNA repair proteins including *BRCA1*, *BRCA2*, *MRE11* and *RAN51* (125, 126). Also, HDACis have been shown to down-regulate the expression of the transcription factor E2F1, which is known to promote key DNA repair proteins, therefore impairing the recruitment of these proteins to repair foci (125, 126).

1.5.3.3 - Apoptosis

HDACi compounds were originally developed as an alternative cancer therapeutic approach due to their ability to target the abnormal epigenetic genome of transformed cells. These inhibitors induced cell death by stimulating both the intrinsic and extrinsic apoptotic pathways which both activate the caspase cascades (91). The intrinsic pathway is stimulated by the disruption of the mitochondrial membrane resulting in the release of several intermembrane proteins such as Smac, apoptosis-inducing factor and cytochrome c and the activation of caspases (127, 128). HDACis can stimulate the intrinsic apoptotic pathways by either activating pro-apoptotic factors or by suppressing anti-apoptotic proteins. HDACi compounds have been shown to upregulate pro-apoptotic proteins of the Bcl-2 family such as Bim, Bax and Bik, while inactivating anti-apoptotic proteins of the Bcl-2 family including Bcl-2, Bcl-w and Mcl-1 (129). These compounds have also been shown to suppress the pro-survival gene X-linked inhibitor of apoptosis expression (*XIAP*) (91).

The induction of apoptosis by the extrinsic route occurs via the binding of death receptors such as tumour necrosis factors (TNF) receptor-1, TNK-related apoptosis-inducing ligand receptor, Fas receptor, by their respective ligands which results in the downstream activation of caspase 8 and caspase 10 (130, 131). Both *in vitro* and *in vivo*, it has been demonstrated that HDACis are able to upregulate the expression of both the death receptors and their ligands in transformed cells, however, normal cells are unaffected (132, 133). The HDACi Romidepsin has been shown to down-regulate an inhibitor of the death receptor pathway, C-FLIP, and enhance the expression of TNF- α in both K562 and HL-60 cells (134). These reports demonstrate the efficacy of HDACi therapies in inducing the extrinsic apoptotic pathway in many transformed cells.

1.5.3.4 - Redox pathways

Numerous studies have reported that HDACi treatment results in the accumulation of ROS within transformed cells, but not in normal cells (127, 128, 135). HDACi selectivity is based on their interactions with the thioredoxin reduction-oxidation system, responsible for responding to the stress stimuli causing ROS to increase (135). During stress, the activity of thioredoxin increases leading to the stimulation of ribonucleotide reductase, which acts as a scavenger of ROS (136, 137). In normal cells upon HDACi treatment, thioredoxin levels increases, however, within transformed cells, thioredoxin levels remain unchanged (135). Figure 1.11 shows an overview of the biological effects HDACis can induce in both normal and transformed cells.

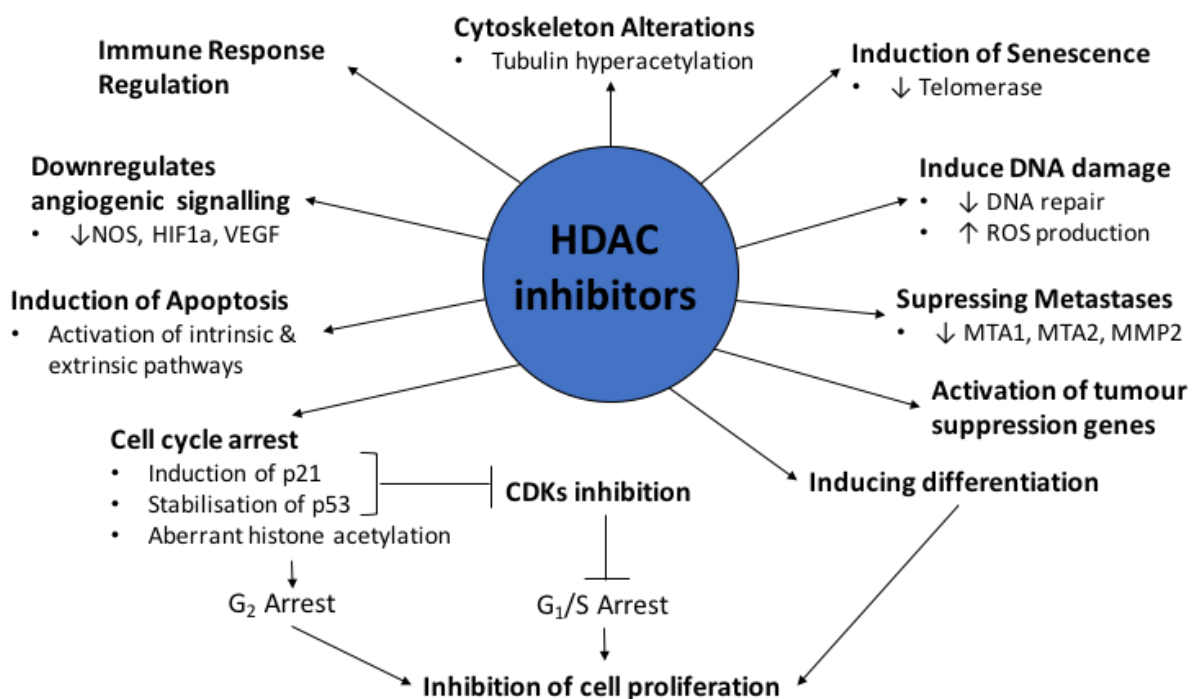


Figure 1.11 - Summary of the biological effects HDACis in both normal and transformed cells. HDAC enzymes are involved in numerous cellular processes critical to cell survival, migration, proliferation and differentiation, therefore their inhibition with HDACis will dysregulate these processes.

1.5.4 - Bone-associated HDAC isoforms

The roles of HDACs in osteoblast differentiation and maturation have been reported in the literature (138, 139). The ability of these compounds to enhance the osteogenic capacity of cells is not solely due to the effects on histone proteins, but also involves their interactions with non-histone proteins such as key osteogenic transcription factors. There are several HDAC isoforms which are proposed to be linked to osteoblast activity and HDAC3 is thought to be the most intimately linked to bone formation (113, 140, 141). HDAC3 isoform has been shown to act as a co-repressor for the transcription factor Runx2, which is thought to be the master transcription factor directing osteogenic differentiation (140). Numerous studies have shown HDAC3 binds to Runx2, T-cell factor, nuclear factor of activated T cells and zinc finger protein 521 (Zfp521), which results in modulation of osteoblastic differentiation by silencing the expression of key osteogenic genes (142, 143). This interaction leads to the suppression of OCN production, a late marker of osteogenesis, and the regulation of progenitors to differentiate into osteoblasts (140, 144, 145).

HDAC3 knockout studies *in vivo* have resulted in the reduction of osteoblast levels and an increase in the fatty deposit within the bone marrow which caused serious complications in the animal's health (141). Singh *et al.* (2013) showed that HDAC3 deletion in mouse neural crest cells leads to microcephaly, undetectable frontal bone formation and aberrant zygomatic arch formation (146). Similarly, HDAC3 conditional knockout mice possessed reduced calvarial density and bone thickness, where these calvarial cells expressed enhanced levels of cyclin-dependent kinase inhibitor p21 and numerous inhibitors of the Wnt signalling pathway (141). Likewise, during osteoblast differentiation HDAC1 is downregulated, suggesting its potential selective inhibition to stimulate osteogenesis (147). In addition to HDAC4, HDAC5 and HDAC6 have shown to play a role in osteogenesis (37).

HDAC enzymes have been shown to exert their functions on osteogenic differentiation independent from direct interaction with osteogenic transcription factors, via altering the transcriptional permissiveness of the chromatin structure. During the differentiation of osteoblasts, the activity of HDAC enzymes is reduced which results in the acetylation of both histone H3 and H4. Studies have reported that acetylation of histone H3 and H4, where the OCN promoter is located, increased the OCN production which is key for bone formation (148). These reports indicate that the process of acetylation in certain regions of the histone proteins results in tissue-specific transcriptional activation (148). Together, these studies suggest that HDACs play an essential role during osteoblast differentiation both by their effects at the chromatin structural level and at the transcriptional level, indicating that inhibition of these enzymes by HDACi compounds as a promising approach for modulating MSCs osteogenesis.

1.6 - Bone tissue engineering

1.6.1 - Clinical need and current approaches

Due to the ever-growing ageing population, there is an enormous clinical demand to regenerate or repair damaged bone tissue. Tissue engineering provides a potential solution to the increasing clinical demand and limitations of current “gold standard” treatments; however, to date, there has been limited success in developing clinically relevant bone tissue for bone augmentation strategies.

Bone engineered tissues should possess certain properties which will optimally direct cell growth into functional bone tissue. These properties must mimic those found naturally in the body, where these devices should promote new bone formation (osteoinduction) and allow the ingrowth of bone into the graft tissue (osteoconduction) (4, 149). In addition, the implanted device must degrade at a similar rate at which new bone is created and also the construct should mimic the surrounding bone tissue in terms of their mechanical properties (150, 151).

The current clinical therapies utilised to repair large bone defects are autografts and allografts and these have been seen as the “gold standard” treatment for many decades. The process of autografting occurs when bone tissue is taken from the patient and is then grafted into the defect site. This procedure is relatively successful as the graft used is osteoconductive, osteoinductive and highly vascularised, increasing the chances of effective integration into the host tissue (4). Also, there is a low risk of infection/disease transmission. However, this procedure is associated with limited tissue sourcing, substantial cost and accompanied by donor site morbidity complications (151, 152). Allografts have also been seen as an alternative tissue grafting source for bone tissue repair. These bone grafts are usually acquired from cadavers, though they are associated with poor integration (153). Additionally, the use of allografts are associated with an increased risk of infection, immune rejection, disease transmission and variable quality of harvested tissue (154). As with autografts, allografts also suffer from nutrient supply limitations. Xenografts are tissues acquired from another species and repurposed for human use (155). These tissues are usually extracted and undergo the rigorous decellularisation procedures to remove all xenogeneic cellular materials leaving the tissue extracellular matrix component intact. This decellularisation technology has seen success in the tissue engineering field for simple tissue grafts such as skin grafts (ALLODERM SELECT™); however, there has been difficulty in decellularising bone tissue for the repair of large bone defects, due to issues in removing sufficient amount of cellular and genomic material for safe xenogeneic implantation, while not affecting the tissue structure (156).

1.6.2 - Tissue engineering approaches

It has been proposed that tissue engineered constructs may have the potential to replace the need for autograft/allografts and meet the rising clinical demands for bone tissue. Within the tissue engineering field, there are four key components which require consideration in creating functional tissue: cells, scaffolds, growth factors and environmental/mechanical stimulation (Fig 1.12) (157, 158).

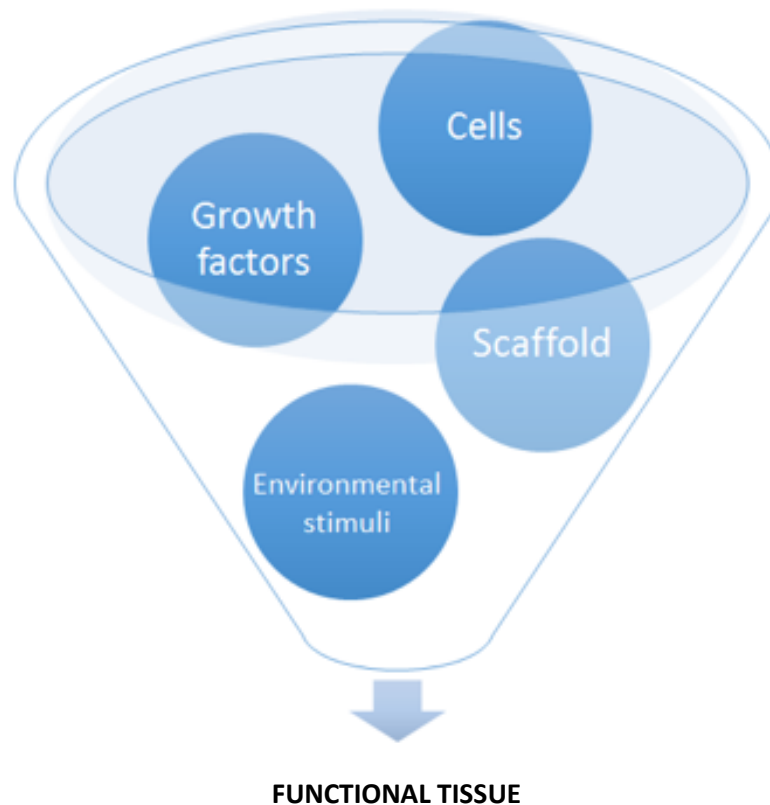


Figure 1.12 - The four key components of tissue engineering. These components include cells, scaffolds with the addition of growth factors and environmental/mechanical stimulation.

1.6.2.1 - Cellular component

Many of the bone engineering strategies utilise cellular components such as stem/stromal cells and tissue-specific cells (159). The limitations of using tissue-specific cells include their limited cell numbers, require an extensive *In vitro* expansion period and are difficult to isolate (160). While initially most research has been performed with tissue-specific cells, there has been a noticeable shift to the use of stem cells.

One of the key defining properties of stem cells is their self-renewal capacity. This is the process of asymmetric division of stem cells into two daughter cells, one of which maintains the undifferentiated state and self-renewal capacity of the parent cell, while the other cell is more differentiated (16, 75, 161). The advantages of utilising stem cells are they have the ability to differentiate into multiple cell lineages, are found in numerous sites around the body and exhibit a more rapid rate of proliferation compared to tissue-specific cells (162). These cells are classified in terms of their differentiation potential (163). Totipotent cells, such as zygotes, have the highest differentiation potential which are able to differentiate into all types of cells within an organism (Fig 1.13). Pluripotent cells, such as ESCs, are able to create cells from the embryo and therefore all adult tissues, however, are unable to form embryonic tissues. Additionally, iPSCs are generated from reprogramming somatic cells, therefore possesses a similar differentiation capacity to ESCs. Adult stem cells are classified as multipotent and can differentiate into tissue-specific cells. Lastly, unipotent cells are considered terminally differentiated and can only maintain one cell type or lineage (75).

Due to the pluripotency of ESCs, this stem cell source has been utilised for tissue engineering purposes, however, due to the ethical issue and regulatory requirements, this has limited the use of ESCs as a stem cell source. In addition, allogeneic rejection and teratoma formation have been observed upon implantation, furthering the drawbacks associated with using ESCs for clinical use (153). Therefore, the majority of research within the field has utilised multipotent cells. Post-natal or adult stem cells have been successfully isolated from numerous tissue locations such as dental pulp, skeletal muscle, synovium, bone marrow and adipose (153, 164-166).

Differentiation Potency

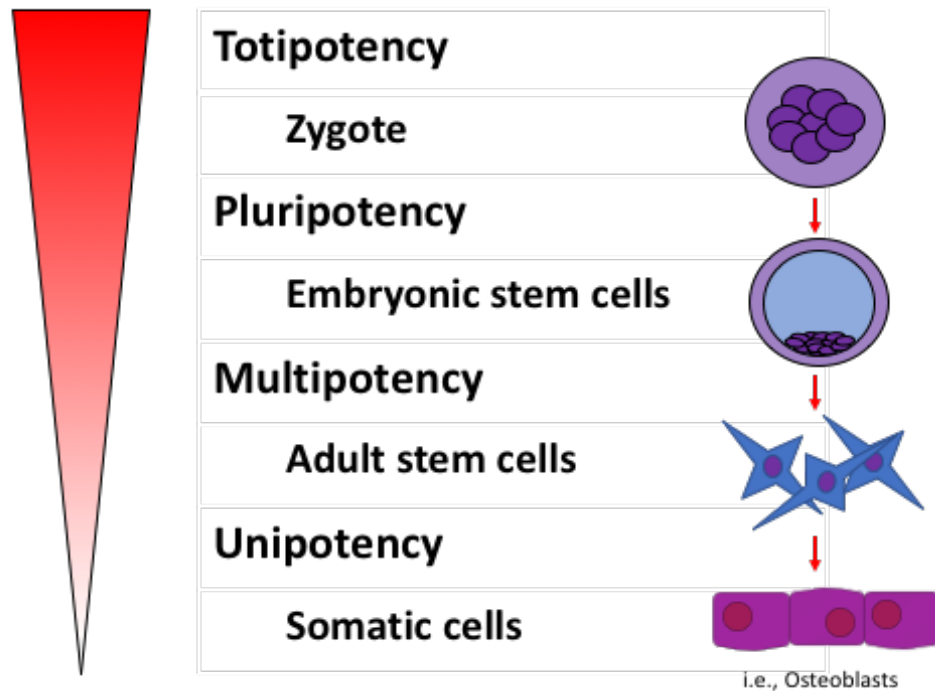


Figure 1.13 - Schematic representation of stem cell hierarchy. Totipotent cells such as zygotes possess the greatest differentiation potency, with the ability to give rise to all cell types in the body. Pluripotent cells such as ESCs can differentiate into all adult tissues in the body, except embryonic tissues. Multipotent cells such as MSCs are capable of lineage-specific differentiation into unipotent cells which are terminally differentiated.

Theoretically, stem cells are able to respond to any stimuli they are exposed to, such as the influence of growth factors, scaffolds or mechanical stimulation (167). MSCs are an example of these multipotent cells capable of differentiating into several cell types such as bone, cartilage and adipose tissues, defined by their mesoderm lineage. Cells collectively termed MSCs can adhere to tissue culture plastic, possess a fibroblastic morphology and self-renewal capacity, and differentiate into multiple cell lineages (31, 153).

The key for bone tissue engineering strategies is to effectively control the lineage-specific differentiation of MSCs. Controlling the key pathways involved in the differentiation of stem cells into bone cells, such as BMP and Wnt signalling pathways, could lead to the improved efficacy of bone tissue engineering strategies. To mimic the bone forming environment within the body, chemicals such as ascorbic acid, phosphate sources and dexamethasone have been utilised (168-170). In addition to these chemicals, growth factors such as BMPs have also been used to stimulate osteogenesis (58). However, current approaches to stimulate osteogenesis are associated with

various limitations, such as high cost, limited efficacy, ill-defined protocols or adverse side-effects. Due to these drawbacks, this has resulted in increasing investigations into alternative methods to enhance bone engineering strategies (16, 171, 172).

There are controversies within the field in regard to the use of the term mesenchymal “stem” cells. The discourse surrounding the use of this term is that it can be misleading referring to a heterogeneous cell population containing a combination of tissue-specific progenitor cells and non-stem cells (173). Additionally, within this heterogeneous population, cells possess varying levels of multipotency. Hence, there is a growing consensus to term these cells mesenchymal “stromal” cells

It should be noted that MSCs are now believed to play a wider role in regenerative therapies besides their direct differentiation into the cells of interests. A growing number of studies have demonstrated that MSCs trophic, immunomodulatory and paracrine functions are important in normal healing processes or tissue regeneration (174). MSCs trophic properties included the secretion of chemokines and growth factors to stimulate cell proliferation and angiogenesis. Inflammatory conditions at the sites of musculoskeletal trauma hinder the natural repair process (175). MSCs are able to modulate this environment via anti-inflammatory and immunomodulatory mechanisms. MSCs secrete anti-inflammatory proteins and growth factors such as nitrous oxide, IL-4 and TGF- β 1 that target complex feedback mechanisms that prevent the proliferation and function of key immune cells such as natural killer cells, macrophages and T cells. Numerous studies have demonstrated the immunomodulatory capacity of MSCs on key immune cells at the site of fracture repair (174, 176), therefore, it is possible the trophic properties of these MSCs could be integral in the success of tissue engineering constructs.

1.6.2.2 - Scaffolds

The majority of early research focused on culturing cells in monolayer due to the established protocols, ease of expansion and some degree of *in situ* replication, however growing cells on tissue culture plastic forces cells to behave in a manner which is foreign to their natural *in situ* microenvironment (177, 178) (Fig 1.14). In the body, cells are situated in a complex, three-dimensional (3D) microenvironment surrounded by other cells, extracellular matrix components and a variety of diffusible compounds such as growth factors and chemicals etc. In monolayer culture, cellular morphology is altered which has a substantial effect on inducing altered mechanobiological signals through the cells, such as altered adhesion occurring through the *x-y* plane, unrestricted spreading and migration of cells, forced apical-basal polarity and the cells are influenced by the high stiffness in contact with tissue culture plastic. In addition, when cells are cultured in monolayer, they

are situated within culture media which lacks the soluble factor gradients that exist *in vivo* (178, 179). Due to the acquired understanding of the limitations of 2D culture, there has been a shift towards the utilisation of 3D “scaffold” systems to more closely mimic the *in situ* conditions. MSCs require a 3D microenvironment which allows for proper adhesion, growth, aggregation and tissue-specific differentiation (180).

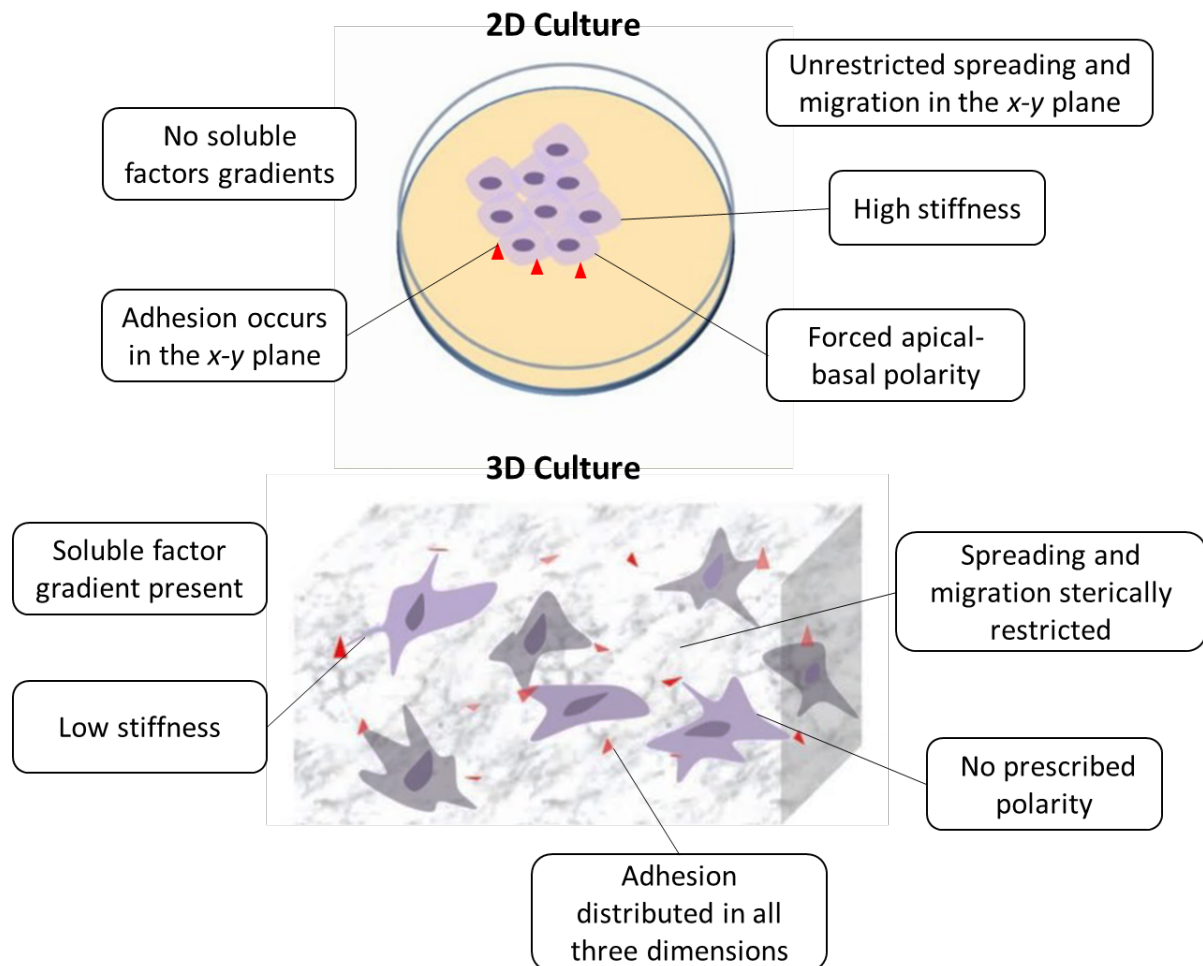


Figure 1.14 - The differing effects of monolayer and 3D culture on cellular behaviour. 2D culture infers an “artificial” environment which alters key cellular processes such as proper adhesion, growth and tissue-specific differentiation. Adapted from (181).

Scaffolds are vital for bone tissue engineering strategies as it provides a suitable platform for cells to migrate, proliferate, differentiate and promote new bone formation (182). The scaffold component is defined as a 3D solid biomaterial which is porous in structure and promotes biomaterial-cell interactions, cellular proliferation and differentiation, tissue ingrowth and vascularisation, nutrient/waste diffusion and is able to biodegrade with minimal *in vivo* toxicity (183). In addition, they must possess mechanical properties similar to the native bone. Ideally, scaffolds which are

osteoconductive, osteoinductive and osseointegrative would be beneficial. Various materials, both natural and synthetic, have been investigated for bone tissue engineering applications.

In general, natural scaffolds can compose of proteins such as silk, collagen and gelatin, or as polysaccharides such as glycosaminoglycans (GAGs), cellulose, and chitin (150). These materials are highly biocompatible providing an osteoinductive and osteogenic environment; however, they lack the mechanical properties for the tissue of interest (184). Synthetic materials in principle possess modifiable mechanical and biodegradative properties, however, they lack the intrinsic biocompatible properties which natural material possess such as the arginine-glycine-aspartic acid (RGD) binding motifs (185). In general, three groups of biomaterials have been used in the fabrication of scaffolds for tissue engineering applications: polymers, ceramics and composites. Natural polymers such as collagen provide excellent biocompatible properties but possess a low mechanical modulus compared to the native tissue (186). Synthetic polymers in principle can be modified to satisfy these requirements, however, are associated with reduced bioactivity when compared to natural polymers (187). Polymers in the form of hydrogels have been well researched for tissue engineering purposes due to their high biocompatibility, porosity and water content. Ceramic materials (bioceramics and bioglasses) possess good biocompatibility, a porous structure and suitable mechanical properties. Additionally these materials are resistant to corrosion and wear which has led to their use in total hip arthroplasty (188) However, the clinical application of ceramics for tissue engineering has been hindered due to their brittleness which has limited the use of these materials to non-load bearing applications such as in orthopaedic dentistry (189). Composite scaffolds can utilise the best aspects of certain materials and combine them to produce a composite which exhibits both of their properties. Therefore, a key challenge which remains for bone tissue engineering is the utilisation of an appropriate biomaterial that complements the other essential components for engineering function tissue (cells, growth factors, and environmental stimuli).

1.6.2.3 - Growth factors

For bone tissue engineering applications, growth factors have been utilised to stimulate MSCs differentiation into osteoprogenitors and osteoblasts. The growth factors currently utilised have been acquired from the improved understanding of the molecular mechanisms involved in the fracture healing process (190). Many of these key molecules which are involved within this complex physiological process have been identified and are clinically used. From the numerous osteogenic inducing growth factors identified, BMP2 has been most commonly used in either viral or non-viral delivery of genes into MSCs or in slow release systems (191). Numerous other growth factors have been identified besides BMPs during the bone healing process, with varying functions such as cell

proliferation, angiogenesis and chemotaxis. Numerous studies have investigated the ability of these factors to augment bone repair (190, 192, 193).

1.6.2.4 - Environmental stimulation

The environment in which cells exist in the body plays an essential part in the development of that tissue of interest. Mechanical stimulation has often been utilised to create tissue engineered constructs in the form of bioreactors, to replicate the mechanical forces in which that tissue would experience *in situ* (194). During bone fracture healing, numerous mechanical loads are exerted to the defect area such as external fixators and formation of intermediary tissue such as fibrous tissue. Also, high shear strain and fluid flows are thought to play a major role in the bone regeneration process (4). To date, there has been limited success for developing clinically relevant bone tissue. Numerous approaches have been developed to enhance the efficacy of bone tissue engineering strategies such as gene therapy and iPSCs.

1.6.2.5 - Gene therapy and iPSCs

Recent advancements in the knowledge of the genome and associated technologies have propelled research investigating the effects of altering the genome for numerous applications via gene therapy. This procedure involves the transference of genetic materials into the cell of interest's genome, allowing that cell to express the coded protein. These procedures can be performed via two methods: viral transfection or non-viral transduction of a vector either by the direct *in vivo* method or the *ex-vivo* gene transfer strategy (195). These procedures have shown promise in the tissue engineering field such as using gene therapy to enhance the expression of BMP2 in animal studies (196). However, there are numerous concerns with issues regarding the safety, efficacy and cost of this technology (4, 197).

With the advancements in gene therapy, the creating of iPSCs soon followed, where the retroviral ectopic transduction of *Oct4*, *Klf4*, *Sox2* and *c-Myc* genes into mouse fibroblast occurred in Shinya Yamanaka's Laboratory (198). Since their inception, these iPSCs have garnered great interest among researchers due to their ability to replicate the pluripotent potential of ESCs and also these cells are created from numerous different adult cells such as dermal fibroblasts by cellular programming to a pluripotent state (199). In addition to possessing the pluripotency of ESCs, iPSCs do not elicit an immune response, as they are derived from the patient (200). The use of these cells for bone tissue engineering applications has also shown promise in the preclinical setting both *in vitro* and *in vivo*. Kao *et al.* (2010) demonstrated that iPSCs were able to replicate the osteogenic capacity of ESCs (201), while Levi *et al.* (2012) showed that critical-sized bone defects were completely healed in mice

using these cells (202). Reports have demonstrated the potential of using iPSCs for bone tissue augmentation in the preclinical setting, however, as with ESCs, iPSCs have been reported to undergo teratoma formation if not fully differentiated before implantation (198, 203). In addition, the poor induction yields as low as <1% observed from murine adult somatic cells is a major limitation of this technology (153). These technologies aiming to enhance the efficacy of MSCs differentiation have shown promise; however, they are associated with limitations in relations to their clinical safety and cost-effectiveness. Due to these issues, researchers have started to investigate the potential of using epigenetic approaches as an alternative method to enhance the efficacy of osteogenic differentiation of MSCs.

1.7 - Utilisation of HDACi for bone tissue engineering

Several studies have examined the potential of using HDACi compounds for bone tissue engineering applications *in vitro*. Hu *et al.* (2014) and Kim *et al.* (2013) demonstrated that sodium butyrate (NaB) was capable of enhancing osteogenic differentiation of adipose-derived stem cells (ADSC) and periodontal ligament fibroblasts (204, 205). Valproic acid (VPA), MS-275 and TSA have also been shown to enhance the expression of osteogenic genes in preosteoblasts (46). However, various studies have suggested that TSA may not induce osteoblastic maturation (113). De Boer *et al.* (2006) utilised TSA to induce increased expression of alkaline phosphatase (ALP) and mineralisation of human bone marrow stromal cells (hBMSCs) (74). Kim *et al.* (2011, 2012) found that MS-275 stimulated bone regeneration *in vitro* and *in vivo* (206, 207). From the many studies utilising HDACi compounds for tissue engineering applications, it has become clear that the methods of delivery and the time in which the inhibitors are administered to cells are essential factors (208, 209) and this had often led to the development of pre-treatment strategies to induce lineage-specific differentiation (74, 210-212). Due to the broad spectrum of substrates panHDACis target, this leads to differential effects within the cells, therefore this may limit their therapeutic potential. Consequently, there is a great emphasis for researchers to look towards utilising specific HDACis to minimise side-effects and to maximise osteogenic differentiation.

The majority of studies investigating the efficacy of HDACis to stimulate osteogenesis have utilised non-selective panHDACis, which due to their broad inhibition of HDAC isoforms, results in reduced differentiation efficacy and potential side-effects (213). Therefore, the investigation into the selective targeting of bone-associated HDAC isoforms to stimulate osteogenesis is warranted. HDAC3 is known to act as a co-repressor for the key osteogenic transcription factor Runx2, responsible for modulating OCN production, an essential component for bone formation (140). A novel benzamide derivative compound MI192 has demonstrated its potential in the treatment of

leukaemia and rheumatoid arthritis (21, 100). Previously, it has been reported that MI192 enhanced the osteogenic capacity of ADSCs compared to the panHDACi TSA (214). While TSA targets a broad spectrum of HDAC isoforms, MI192 primarily inhibits HDAC2 and 3 (MI192 and TSA exerts >250- and >1.6-fold selectivity for HDAC2/3 isoform over other HDAC isoforms, respectively) (100, 141). Due to MI192 selective inhibition of the bone-associated HDAC3 isoform, this HDACi likely possesses a greater potency in enhancing MSCs osteogenic differentiation compared to panHDACis, as demonstrated previously (214). Therefore, the hyperacetylation induced by MI192 treatment will enhance the transcriptional permissiveness of the chromatin, leading to the increased production of key osteogenic factors such as Runx2. This chromatin modification mechanism is likely shared by all HDACis. However, due to the isoform selectivity of MI192, this will likely increase the transcriptional activity of the Runx2 transcription factor, due to inhibiting HDAC3 repression of Runx2. Consequently, the newly synthesised Runx2 protein, with enhanced transcriptional activity, likely stimulates the production of downstream bone-related markers (Fig 1.15). As the effects of MI192 on ADSCs osteogenic differentiation has been previously reported (214), the effects of this selective HDACi in promoting the osteogenic capacity of other clinically relevant MSCs, such as human dental pulp stromal cells (hDPSCs) and hBMSCs, should be investigated as these MSCs are extensively utilised for bone tissue engineering applications. The investigation of these MSCs could provide clinicians with a greater option in applying this epigenetic-based approach to stimulate MSCs for bone augmentation strategies.

In the literature, there have been few studies reporting the effects of these epigenetic-based approaches to stimulate bone formation in 3D culture (209, 215), with these studies using panHDACis. As previously mentioned, the 2D culture environment provides numerous artificial stimuli which detrimentally affects MSCs differentiation into the tissue of interest (177). With the rapid growth of the tissue engineering field, there are an overwhelming variety of scaffolds which differ in their material composition, biocompatibility, cost, ease of manufacture etc. Therefore, it is important to evaluate the effects of selective HDACis in stimulating clinically relevant MSCs bone formation in 3D culture, which has not been explored in the literature to date. Additionally, due to the wide-ranging effects of different 3D culture environments on MSCs behaviour, there is a precedence to investigate the effects of HDACi treated MSCs osteogenic capacity in different 3D scaffold systems, potentially providing clinicians with greater opportunities to apply this epigenetic-based strategy for the repair of critical-sized bone defects.

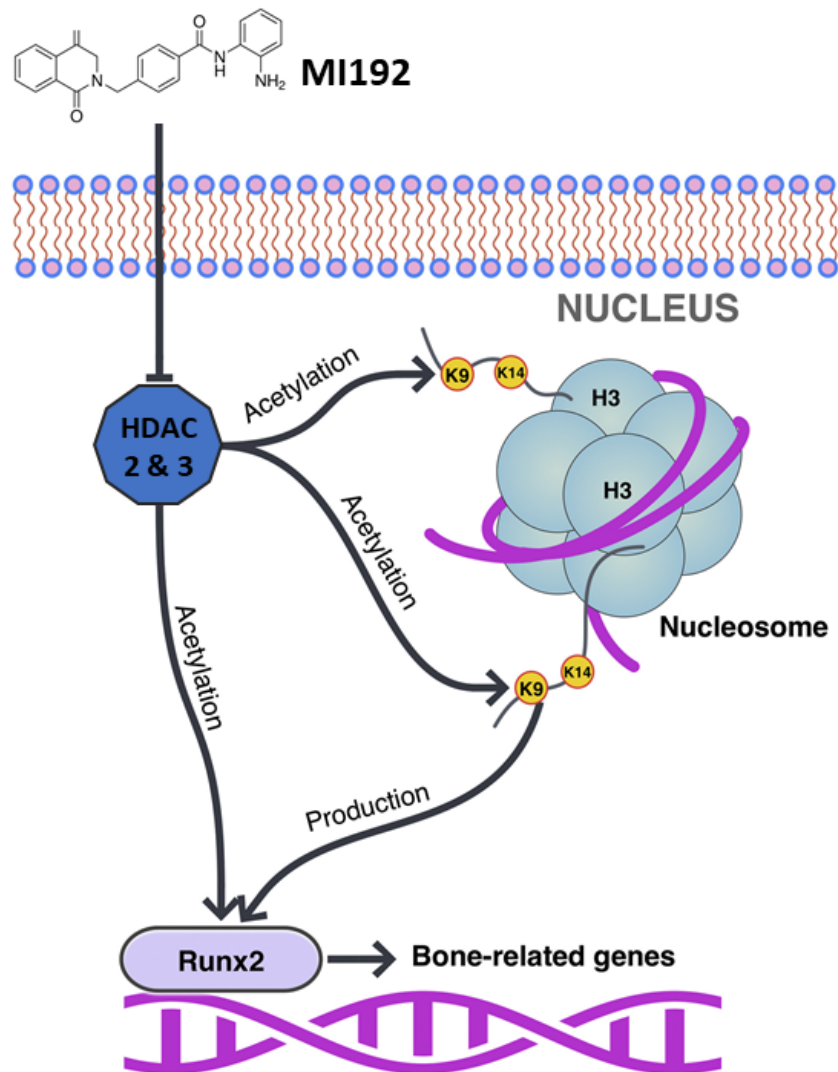


Figure 1.15 - Representation of MI192 mechanism of action in enhancing MSCs osteogenic differentiation. MI192 selectively inhibits HDAC2 and 3 isoforms, resulting in enhanced histone acetylation at the H3K9K14 regions. This increased acetylation opens the chromatin structure, leading to enhanced production and acetylation of Runx2 transcription factor, stimulating the downstream expression of osteoblast-related genes. Adapted from (71).

Compared to *in vitro* studies, there have been limited investigations into the efficacy of HDACis to stimulate bone formation *in vivo*. Cho *et al.* (2005) demonstrated that TSA and NaB increased osteogenic differentiation of MSCs both *in vitro* and *ex vivo*, however, these results could not be recapitulated *in vivo* (74, 212). Jung *et al.* (2010) observed an enhanced osteoblastic differentiation when HDACis NaB and TSA were loaded onto α -calcium scaffolds and placed within a critical-sized rat bone defect model (208). Lee *et al.* (2011) showed that pre-soaking collagen scaffolds with the HDACi Largazole were able to enhance bone formation in calvarial bone defect models (215). Similarly, Xu *et al.* (2009) demonstrated the use of both VPA and NaB in combination with ADSCs in a hypoxic environment resulted in the *in vivo* regeneration of bone tissue (211). However, studies

have reported HDACi treatment had a detrimental effect on bone formation *in vivo*. McGee-Lawrence and Westendorf (2011) reported SAHA had a negative effect on the trabecular skeleton in C57BL/6 mice, with a reduction in osteoblast numbers (216). Boluk *et al.* (2004) found that VPA treatment resulted in decreased bone mineral density within epileptic patients (217). From the limited *in vivo* studies investigating the efficacy of these epigenetic-based approaches, all have utilised panHDACis. Consequently, there is growing precedence to investigate the potential of selective HDACi compounds to stimulate bone formation within the *in vivo* environment, as this pre-clinical validation step would provide greater evidence for the potential use of selective HDACis to promote bone formation in the clinical setting.

1.8 - Project aims and objectives

The aim of this project was to investigate the effects of the novel selective HDAC2 and 3 inhibitor - MI192 on the behaviour and osteogenic capacity of clinically relevant MSCs, to enhance their efficacy for bone augmentation strategies.

The following objectives were identified in order to achieve this aim:

- To isolate and characterise clinically relevant MSCs (hDPSCs and hBMSCs).
- To investigate the effects of MI192 on the general behaviour of MSCs in 2D *in vitro* culture.
- To evaluate the effects of MI192 on MSCs osteogenic differentiation in 2D *in vitro* culture.
- To determine the effects of MI192 on MSCs bone formation in 3D *in vitro* models.
- To investigate the effects of MI192 on MSCs bone formation *in vivo*.

Chapter 2 - Materials and Methods

This chapter contains all the general materials and methods used in the subsequent chapters in this thesis. Chapter-specific methods will be described in the relevant chapters.

2.1 - General reagents

All reagents, including dimethyl sulfoxide (DMSO) and ethanol (EtOH), were purchased from Sigma-Aldrich unless stated otherwise. Tissue culture consumables including flasks, plates and falcon tubes were acquired from Corning. General reagents used for tissue culture include phosphate buffered saline (1x PBS, Lonza, BE17-516F), alpha minimal essential medium (α -MEM, Lonza, BE12-169F), penicillin-streptomycin (P/S, Sigma-Aldrich, P4333), L-glutamine (L-G, Sigma-Aldrich, G7513), foetal calf serum (FCS, Sigma-Aldrich, F9665) and 0.25% (w/v) trypsin-EDTA (ethylenediaminetetraacetic acid) solution (T/E, Sigma-Aldrich, T4049).

2.2 - MI192

MI192 was previously synthesised by a student within the research group, where the method of synthesis was stated in Chapter 3 of his thesis (214). MI192 was dissolved in filter-sterilised DMSO to make a 100 mM stock solution (3.81 mg in 100 μ l DMSO). The MI192 stock solution was added directly to the culture medium to generate the desired concentrations for use immediately.

2.3 - Culturing of cells

All cells were incubated at 37°C with 5% CO₂ and approximately 90% humidity within an incubator. Experimental work using cells were undertaken within a laminar flow hood (class II) using aseptic technique.

2.3.1 - Extraction of human dental pulp stromal cells from sound molars

Human dental pulp stromal cells (hDPSCs) were isolated from extracted impacted third molars obtained with the patient consent through the Leeds Dental Institute Research Tissue Bank (REC 07/H1306/93) and ethical approval (180615/km/173). Briefly, tooth surfaces were cleaned thoroughly with 70% EtOH-soaked tissue and any remaining soft tissue was removed with sterile forceps and a scalpel blade. Molars were cracked within sterile gloves using a clamp to reveal the pulp chamber. The pulp tissue was carefully removed and then digested in fresh medium containing 3 mg/ml collagenase type 1 (Sigma-Aldrich, SCR103) and 4 mg/ml dispase (Roche, 4942078001) for 1 hour at 37°C with agitation on a MACSmix tube rotator (Miltenyi Biotec). A single cell suspension was obtained by passing cells through a 70- μ m strainer (BD Biosciences, 352350). The cell

suspension was centrifuged at 200g for 5 minutes before re-suspended in basal medium and seeded into flasks at appropriate cell density.

2.3.2 - Processing human bone marrow mononuclear cells

Human bone marrow mononuclear cells were acquired from Lonza (2M-125C). Prior to the thawing of cells, DNase I (Sigma-Aldrich, D4513) was added at 20 U/ml to the medium containing 10% FBS. Cells were thawed and transferred to 50-ml falcon tube, where 1 ml prepared medium was added dropwise, and cells were gently swirled for 1 minute. 3 ml prepared medium was added dropwise to the cell suspension and gently rotated for 3 minutes. The remaining DNase I-containing medium was added dropwise, with the intermittent swirling of the cell suspension to reach a final total volume of 50 ml. The cell suspension was centrifuged at 200g for 15 minutes at room temperature. The supernatant was removed, leaving 2 ml of medium with the cell pellet, which was used for resuspension. The cell suspension was transferred to a 15-ml falcon tube, rinsing the original 50-ml tube with medium and then transferring this wash medium into the 15-ml falcon tube. Medium was added dropwise until a total volume of 15 ml was reached. The cell suspension was then centrifuged at 200g for 15 minutes at room temperature. The supernatant was removed leaving approximately 2 ml medium with the cell pellet, which was used to re-suspend and count cells. Cells were rested for 1 hour within the incubator and then seeded at appropriate cell seeding density.

2.3.3 - Detachment of cells and seeding

Culture medium was aspirated, and cells were washed twice with PBS, prior to incubation with T/E for 5 - 10 minutes until a complete detachment of cells from the tissue culture plastic. The cell suspension was then neutralised with equal volumes of basal media then centrifuged at 1200 RPM for 5 minutes. The resulting supernatant was then aspirated, and the cell pellet was re-suspended in an appropriate volume of culture media. Cells were then counted and seeded at densities depending on the experiment.

2.3.4 - Cell Counting

To count cells, a mixture containing 50 µl cell suspension with an equal volume of trypan blue solution (Sigma-Aldrich, T8154) was added to a haemocytometer and the cell number was counted under a light microscope. Cells stained dark blue were classed as dead/non-viable and were not counted. The total viable cells in 4 corner squares and the centre square were counted and the average cell number per square was determined. The total area of each square was 1 mm² and the depth of each square was 0.1 mm, therefore the final volume of each square was 100 nl. Total cell

number is determined by multiplying the average number of cells by the dilution factor of trypan blue, then by 10,000 and finally by cell suspension total volume:

Total number of cells =

Average cell count x Trypan blue dilution factor x Total volume of cell suspension

2.3.5 - *In vitro* expansion of human dental pulp stromal cells (hDPSC)

Cells were expanded in basal medium consisting of α -MEM, 10% FCS, P/S (100 units/ml, 100 μ g/ml) and 2 mM-L-G. The medium was changed every 3 - 4 days. Cells were passaged when approaching 80% confluence. Cells of up to passage 4 were used for experiments.

2.3.6 - *In vitro* expansion of human bone marrow stromal cells (hBMSC)

Cells were expanded in basal medium consisting of α -MEM, 10% FCS, P/S (100 units/ml, 100 μ g/ml) and 1 ng/ml recombinant human fibroblastic growth factor (FGF) basic (R&D systems, 233-FB-025). The medium was changed every 3 - 4 days. Cells were passaged when approaching 80% confluence. Cells of up to passage 4 were used for experiments.

2.3.7 - Osteogenic induction culture

To promote osteogenic differentiation, basal medium was supplemented with 50 μ M L-ascorbate 2-phosphate sesquimagnesium salt hydrate (Sigma-Aldrich, A8960), 10 mM β -glycerol phosphate (Sigma-Aldrich, G9422) and 100 nM dexamethasone (Sigma-Aldrich, D4902). The medium was changed every 3 - 4 days.

2.3.8 - Chondrogenic induction culture

For chondrogenic differentiation, cell pellets were created by centrifuging cells (2.5×10^5) in a 15-ml Falcon tube for 4 minutes at 300g. The supernatant was removed, and the resulting cell pellet was cultured in StemMACs ChondroDiff Media (Miltenyi Biotec, 130-091-691) supplemented with P/S (100 units/ml, 100 μ g/ml) for 21 days. The medium was changed every 3 - 4 days.

2.3.9 - Adipogenic induction culture

For adipogenic differentiation, 1×10^5 cells were seeded into 12-well plates and cultured in StemMACs AdipoDiff Media (Miltenyi Biotec, 130-091-677) supplemented with P/S (100 units/ml, 100 μ g/ml) for 14 days. The medium was changed every 3 - 4 days.

2.3.10 - Microtissue culture

Cells (250,000 cells per well) were seeded in a v-shaped bottom 96-well polypropylene plate (Greiner Bio-One, 651201), suspended in 250 μ l of osteogenic medium. Plates were centrifuged at 300g for 4 minutes. After 24 hours, cells had usually condensed into spheroid pellets (microtissues) which were then gently agitated. The medium was changed three times a week.

2.4 - Polymerase chain reaction (PCR)

Before real-time quantitative polymerase chain reaction (RT-qPCR), ribonucleic acid (RNA) was isolated from cells and reverse transcribed into complementary DNA (cDNA).

2.4.1 - RNA isolation

To extract RNA, cells in monolayer were lysed by incubation with RLT buffer and then stored at -80°C until required. Microtissues were lysed after 7, 14 and 21 days in osteogenic culture. The sample size was four per group (n=4). Samples were collected and placed in RLT buffer within an Eppendorf tube. Microtissues were homogenised by passing through a 20-gauge needle. Samples were then vortexed for 15 seconds and placed into a sonicator for 15 minutes. This process was repeated four times. The lysate solution was transferred into the QIAshredder (Qiagen, 79654) and centrifuged at 10000 RPM for 3 minutes. The lysate was then stored at -80°C until required.

RNA was extracted using the RNeasy mini kit (Qiagen, 74104) following the manufacturer's instructions. Briefly, the lysate containing the RNA is loaded onto the column, where it attaches to the membrane then undergoes multiple wash steps and the RNase-Free DNase kit (Qiagen, 79254) was utilised to digest any genomic DNA contaminants. RNase-free distilled water (dH₂O) was utilised to elute the purified RNA from the column. The concentration and quality of RNA was measured at 260 nm using the Thermo Scientific ND1000 Nanodrop spectrophotometer. The RNA purity determined by assessing the 260/280 nm ratio, where a ratio above 1.8 was considered of good purity. RNA was stored at -80°C until required.

2.4.2 - Reverse transcription

Reverse transcription was undertaken to generate a single-stranded cDNA from the isolated RNA. 200 ng of RNA was transcribed to cDNA using the high capacity RNA to cDNA Kit (Applied Biosystems, 4387406), following the manufacturer's instructions. Briefly, 200 ng of the RNA dissolved in water, 10 μ l of 10x buffer and 1 μ l enzyme were made to a final volume of 20 μ l with nuclease-free water. Reactions were then performed within a PTC-100 ThermoCycler (F. Hoffmann-

La Roche Ltd. MJ Research) at 37°C for 1 hour, then at 95°C for 5 minutes for the enzyme denaturing step. The cDNA stored at -20°C before use. From the manufacturer’s recommendations, it was presumed that the reverse transcription process was 100% efficient.

2.4.3 - RT-qPCR

The mRNA expression levels were determined by RT-qPCR using the TaqMan gene expression assay. Briefly, a 20 µl reaction volume composed of 10 µl TaqMan Gene Expression Master Mix (Life Technologies, 4369016), 8.5 µl RNase-Free dH₂O, 1 µl of the probe and 0.5 µl of cDNA. The 20 µl reaction mix was added into each well in 96-well PCR plates for use in the Roche LightCycler (Starlab, I1402-9909). Negative controls lacking probe or cDNA were included in each plate. The plates were sealed and centrifuged for 10 seconds before use in the LightCycler. Amplification curves were obtained using a LightCycler 480 real-time QPCR system. Samples went through a 10 min pre-incubation step at 95°C, 45 cycles of 10 seconds at 95°C, 30 seconds at 60°C and 60 seconds at 72°C. At the end of the 45 cycles, the samples were cooled to 40°C. For each sample, the cycle threshold (Ct) value was acquired and the comparative Ct method ($2^{-\Delta\Delta Ct}$) was utilised to quantify the levels of gene expression in relation to the housekeeping gene, GAPDH. Probes utilised for TaqMan PCR are shown in Table 2.1.

Table 2.1 - TaqMan probes utilised in this thesis.

Gene symbol	Description	TaqMan assay identification
<i>GAPDH</i>	Glyceraldehyde-3-phosphate dehydrogenase (Housekeeping gene)	Hs99999905_m1
<i>RUNX2</i>	Runt-related transcription factor 2	Hs00231692_m1
<i>ALPL</i>	Alkaline phosphatase	Hs01029144_m1
<i>COL1A1</i>	Collagen, type I	Hs00164004_m1
<i>BMP2</i>	Bone morphogenetic protein 2	Hs00154192_m1
<i>OCN/BGLAP</i>	Osteocalcin/PMF-bone gamma-carboxyglutamate (gla) protein	Hs00609452_g1

2.5 - Biochemical assays

For biochemical assays (PicoGreen and ALPSA), cells were washed twice with PBS and stored at -80°C in 200 µl of 0.1% Triton X-100 in PBS per well (Fisher Scientific, BPE151-500). Cells then underwent three freeze-thaw cycles between -80°C and 37°C, with scraping in-between to lyse the cells. Samples were checked microscopically to ensure full lysis.

2.5.1 - PicoGreen DNA quantification assay

Cells were seeded at 1×10^4 cells per well in three 96-well plates and incubated in basal medium. After 24 hours, the medium was replaced with fresh basal medium supplemented with MI192 at a range of concentrations (1, 5, 10, 20, 50, 100 µM) and incubated for 24, 48 and 72 hours. Untreated cells in basal medium were used as control. At each time point, cells were prepared for lysing as described in section 2.5. The sample size was three for each group (n=3). After lysing of cells, DNA quantification was determined by Quant-iT™ PicoGreen® DNA assay (Invitrogen, Life Technologies, P7581). The pre-prepared Lambda DNA standard was diluted to 2 µg/ml with 1x TE buffer (10 mM Tris-HCl, 1 mM EDTA, Sigma-Aldrich, 93302) to make a working standard solution. This was further diluted to five standard concentrations ranging from 1 ng/ml to 1 µg/ml.

10 µl of cell lysate solution was added to 90 µl of 1x TE buffer into a 96-well plate (Corning) in triplicate. 100 µl of PicoGreen reagent (1:200 dilution in 1x TE buffer) was added to all samples, standards and blanks (1 x TE alone) and then incubated at 37°C in the dark for 5 minutes. The fluorescence was then measured in a Varioskan Flash Multimode Microplate Reader (Thermo Scientific) at 480 nm excitation and 520 nm emission. The standard curve generated was used to determine the sample DNA concentration in ng. The total DNA (µg per well) was calculated from the ng DNA per ml calculated and the harvest volume of Triton X-100 from each well.

2.5.2 - Alkaline phosphatase (ALP) quantitative assay

The ALP activity was determined using the 4-nitrophenyl colourimetric phosphate liquid system (pNPP, Sigma-Aldrich, 4264-83-9). ALP standards (5 - 100 nM) were prepared by serial dilution of 4-nitrophenyl (10 mM solution, Sigma-Aldrich, N7660) in ALP assay buffer (60 µl 2% Tergitol type NP-40 in dH₂O (Sigma-Aldrich, NP40S), in 10 ml 1.5 M alkaline buffer solution (Sigma-Aldrich, A9226) and 20 ml dH₂O). 90 µl of pNPP was added to 10 µl of cell lysate and incubated with the standards and blank in a 96-well plate for 30 - 60 minutes at 37°C in darkness. To stop the reaction, 100 µl of 1 M NaOH was added to all wells and absorbance at 405 nm was read using the Varioskan Flash Multimode Microplate Reader (Thermo Scientific). The generated standard curve was used to

determine the ALP values of the samples in mM. To determine the net ALP activity (nM/hour/well): - Calculated ALP (mM) were multiplied by 1000, Triton X-100 harvest volume, then divided by the assay volume and the ALP reaction time.

$$\text{net ALP activity} = \frac{\left(\frac{(mM \text{ ALP} \times 1000) \times \text{Triton harvest volume}}{\text{incubation time}} \right)}{\text{Assay volume}}$$

2.5.3 - ALP specific activity (ALPSA)

ALPSA was calculated by dividing the total ALP concentration per well by the total DNA content of that sample determined by PicoGreen DNA assay (nM ALP/hour/μg of DNA).

$$\text{ALPSA} = \frac{\text{ALP per hour per well (nM)}}{\text{DNA content per well (}\mu\text{g)}}$$

2.5.4 - AlamarBlue metabolic activity quantification assay

AlamarBlue is a resazurin-based reagent that can measure the metabolic function of viable cells. The active compound of AlamarBlue (resazurin) is non-toxic, non-fluorescent and cell permeable (218). Upon entering the cells, resazurin is converted to its reduced form resorufin by mitochondrial enzymes, which is highly fluorescent (219). The conversion is proportional to the number of metabolically active cells and where the absorbance or fluorescence can be measured.

Cells were seeded at 1×10^4 cells per well in three 96-well plates and incubated in basal medium. After 24 hours, the medium was replaced with fresh basal media supplemented with MI192 at a range of concentrations (1, 5, 10, 20, 50, 100 μM) and incubated for 24, 48 and 72 hours. Untreated cells in basal medium were used as control. The sample size was three for each group (n=3). At each time point, 20 μl of AlamarBlue® reagent (Thermo Scientific, DAL1025) was added to each well and incubated for 4 hours at 37°C. Fluorescence readings were acquired using a Varioskan Flash Multimode Microplate Reader at an excitation wavelength of 540 - 570 nm and an emission wavelength of 580 - 610 nm.

2.5.5 - HDAC activity assay

Cells were cultured in two 96-well plates (1×10^4 cells per well) in basal medium. After 24 hours, the medium was replaced with fresh basal medium containing MI192 (1, 5, 10, 20, 50 μM). Basal medium alone was used as a control. The sample size was three for each group (n=3). At 24 and 48 hours, the HDAC activity of the cells was measured using an *in situ* HDAC activity fluorometric assay kit (Biovision, K339) following the manufacturer's instructions. Briefly, the medium was replaced

with 100 µl reaction mix containing HDAC substrate and incubated with cells for 3 hours at 37°C. Similarly, a series of standards from a provided deacetylated sample were also plated. 100 µl lysine developer was added to the plate which was incubated for a further 30 minutes at 37°C. Fluorescence readings were acquired using a Varioskan Flash Multimode Microplate Reader at an excitation wavelength of 368 nm and emission wavelength at 442 nm. Resulting HDAC activity was normalised with the DNA content of each group, determined by PicoGreen DNA assay to give HDAC specific activity.

2.5.6 - H3K9 acetylation assay

Detection of H3K9 acetylation was performed using the EpiQuik™ *In Situ* Histone H3-K9 Acetylation Assay Kit (Epigentek, P-4004). Cells were cultured in two 96-well plates (1 x 10⁴ cells per well) in basal medium. After 24 hours, the medium was replaced with fresh basal medium containing MI192 (1, 5, 10, 20, 50 µM). Basal medium alone was used as a control. The sample size was three for each group (n=3). After treatment, cells were incubated overnight in basal medium for 24 hours before performing the assay, according to the manufacturer's protocol. The absorbance was read on the Varioskan Flash Multimode Microplate Reader at 450 nm within 10 minutes. Resulting acetylation activity was normalised with the DNA content of each group, determined by PicoGreen DNA assay to give H3K9 specific acetylation.

2.5.7 - In-Cell Western (ICW) assay

This quantitative immunofluorescence method combined the specificity of Western blotting with the reproducibility and high throughput analysis of ELISA to assessed protein levels within cells (220, 221). Cells were cultured in four 96-well plates (1 x 10⁴ cells per well) in basal medium. After 24 hours, the medium was replaced with MI192 pre-treatment medium for 48 hours (2 or 50 µM for hDPSCs or hBMSCs, respectively). Basal medium alone was used as a control. The sample size was three for each group (n=3). Medium in all groups was replaced with osteogenic medium and plates were cultured for 7, 14, 21 and 28 days. At each time point, one of the plates was stopped for analysis. Following cell culture, 96-well plates were washed in PBS followed by fixation in 10% neutral buffered formalin (NBF, Cellpath, BAF-0010-01A) in PBS for 20 minutes immediately after treatment. Cells were permeabilised by washing five times in 0.1% Triton X-100 in PBS for 5 minutes per wash. Solutions from CellTag 700 staining ICW Kit I (Li-Cor Biosciences, 926-41091), was utilised for this protocol. Nonspecific binding was blocked using the Odyssey® blocking buffer for 1.5 hours at room temperature. The samples were incubated with antibodies (Table 2.2) in Odyssey® buffer at 4°C overnight with gentle shaking. Samples were then washed extensively in PBS containing 0.1%

Tween 20 (Sigma-Aldrich, P9416) five times for 5 minutes per wash. Samples were then incubated with the IRDye 800CW Goat-anti-Mouse secondary antibody (1:800) with the CellTag™ 700 stain (1:500) in the Odyssey® blocking buffer for 1 hour at room temperature with gentle shaking. Samples were extensively washed in PBS containing 0.1% Tween 20 for 5 minutes per wash. After a final wash, all liquid was removed, and the plate was scanned on the Odyssey SA Imaging System (Li-Cor Biosciences) using both 700 and 800 nm detection channels at a 200 nm resolution, medium quality with a focus offset of 3.0 mm. Quantitative In-cell Western analysis was performed using Image Studio version 5 (Li-Cor Biosciences).

2.6 - Assessment of Cell Morphology

Cells were seeded at 1×10^5 cells per well in two 12-well plates in basal medium. After 24 hours, medium was replaced with fresh basal medium supplemented with MI192 at a range of concentrations (1, 10, 20, 50, 100 μ M). Untreated cells in basal medium alone was used as the control. The sample size was three for all groups (n=3). Cells were observed under the Leica DM16000 B inverted microscope at 24, 48 and 72 hour time points.

2.7 - Cell cycle analysis

Cells were seeded within 6-well plates (1×10^5 cells/well) and cultured in basal medium for 48 hours to ensure normal cell cycle function. The medium in the test group was replaced with fresh basal medium containing MI192 (2 or 50 μ M for hDPSCs or hBMSCs, respectively), and the basal medium alone group was used as the control. The sample size was three for each group (n=3). At 24, 48 and 72 hours, the cells were trypsinised and re-suspended with 500 μ l ice-cold 70% (v/v) EtOH/PBS then stored in -80°C for assessment. For staining, the cell suspension was centrifuged at 800 RPM for 5 minutes and the pellet was washed with 500 μ l 4°C FACS buffer (PBS with addition of 0.1% (w/v) bovine serum albumin (Sigma-Aldrich, A9418) and 0.1% TWEEN-20 (Sigma-Aldrich, P9416)) and then centrifuged at 800 RPM for 5 minutes. The resulting cell pellet was re-suspended with 500 μ l of freshly made staining solution (20 μ g/ml propidium iodide (Sigma-Aldrich, P4170) and 200 μ g Ribonuclease A (Sigma-Aldrich, R6513)) and incubated for 20 minutes at room temperature. Cells were then placed on ice for assessment with Attune NxT Flow Cytometer (Life Technologies). Subsequent cell cycle analysis was undertaken using the ModFit LT™ software (LT v3, Verity).

2.8 - Live/dead fluorescent staining

CellTracker™ Green CMFDA (5-chloromethylfluorescein diacetate) dye (ThermoFisher Scientific, C7025) and Ethidium homodimer I (EthD-1, Sigma-Aldrich, E1903) were utilised to label live/dead

cells, respectively. CMFDA dye freely passes through the cell membrane, where it reacts with cellular components and is transformed into cell membrane-impermeant products. EthD-1 is a membrane impermeable dye, which can only enter cells with damaged cell membranes and binds to DNA in dead cells. Briefly, 10 µl of DMSO was added to 1 vial containing 50 µg CFMDA, which was further diluted in 5 ml prewarmed basal medium (10 µg/ml). EthD-1 (20 µl) was added to the 5 ml culture medium. Samples were incubated within this dye-containing medium for 30 minutes in the incubator protected from light. After incubation, samples were washed with fresh basal medium prior to imaging utilising the confocal laser scanning microscope (CLSM, Leica-TCS-SP8).

2.9 - Histological staining

2.9.1 - Paraffin embedding and sectioning

All samples for histological analysis were processed using the VIP Tissue processor (Sakura) where samples (fixed in 10% NBF) were passed through 70% EtOH, 90% EtOH, 4 changes of 100% EtOH, 3 changes of 100% xylene and 3 changes of wax, prior to paraffin embedding. Sections were then cut using a Leitz rotary microtome at 5 µm thickness and mounted on glass slides using a 40°C water bath. Superfrost™ Plus Microscope Slides (Fisherbrand, 12-550-15) were used to mount the sections. Slides were then placed on a plate heater to melt the section to the slide and then was placed in a 37°C oven overnight to dry. Prior to any histological staining, paraffin sections on slides were dewaxed by passing slides through 100% xylene (VWR, VWRC28975) for 5 minutes, two 100% EtOH baths for 5 minutes each and running tap water for 5 minutes.

2.9.2 - Haematoxylin and Eosin (H&E) staining

Slides were stained with Harris's Haematoxylin (Shandon, 6765002) for 3 minutes and then cleared in running tap water. Following which sections were immersed in Scott's tap water (Leica Microsystems, 02901) for 2 minutes, cleared in running tap water and then stained with 1% aq. Eosin (Leica Microsystems, 01592E) for 2 minutes. These samples were then cleared in running tap water and immersed in two 100% EtOH baths for 5 minutes each, and then in Xylene for 5 minutes before mounting in DPX (distyrene, plasticizer and xylene, Agar Scientific, R1340). The stains were then observed under an Olympus BX50 microscope.

2.9.3 - Picrosirius red/Alcian blue staining

Slides were stained with Weigert's Haematoxylin (equals parts Weigert's solution A and B, TCS Biosciences, HS375-500, HS380-500) for 10 minutes, then cleared in running tap water for 10 minutes. Sections were dipped in 1% HCl in absolute methanol and then wash in running tap water

for 5 minutes prior to staining with Alcian blue solution for 10 minutes (1% w/v in 3% acetic acid, TCS Biosciences, HS116-500). These were then washed in running water for 1 minute then stained with 1% Phosphomolybdic acid (Polysciences, Inc, 24901A) for 20 minutes, following which sections were washed in running tap water for 1 minute. Slides were then incubated with Picrosirius red (Polysciences, Inc, 24901B) for 60 minutes, following which samples were blotted dry, immersed in two 100% EtOH baths for 5 minutes each, and then in 100% Xylene for 5 minutes before mounting in DPX. The stains were then observed under an Olympus BX50 microscope.

2.9.4 - Oil red O staining for lipid droplets

Samples were washed twice with PBS and fixed with 10% NBF for 1 hour. Following which the samples were washed with dH₂O, and then incubated with 50% isopropanol (Sigma-Aldrich, 190764) for 5 minutes. Samples are then stained with Oil Red O solution (70- μ m pore filtered 0.6% in 50% isopropanol Oil Red solution (Sigma-Aldrich, O1391) for 15 minutes. Cells were briefly rinsed with 50% isopropanol then washed three times with dH₂O. Cells were air-dried and observed under the Leica DMI6000 B inverted microscope.

2.9.5 - Alizarin red staining for calcium accumulation

Monolayer samples were washed twice with PBS, fixed in 10% NBF for 1 hour, and then washed three times with dH₂O. Paraffin sections were dewaxed and taken to water. Samples were incubated with Alizarin Red solution (40 mM at pH 4.1 +/- 0.1, Millipore, TMS-008-C) for 15 minutes at room temperature, followed by three washes of dH₂O. Slides were dewaxed, cleared and mounted for observation under an Olympus BX50 microscope. Monolayer stained samples were air dried and observed under a Leica DMI6000 B inverted microscope. The Alizarin red stained samples were de-stained by the addition of 10% Cetylpyridinium chloride (Sigma-Aldrich, C0732) to each sample for 1 hour on a rocking device. Following this, 10 μ l of the de-stained extract was diluted with 90 μ l dH₂O and absorbance was read at 550 nm using the Varioskan Flash Multimode Microplate Reader.

2.9.6 - Von Kossa staining for mineral nodule formation

Monolayer samples were washed twice with PBS and fixed in 10% NBF for 1 hour and then washed with dH₂O three times. Paraffin section was dewaxed and taken to water. Solutions from the Von Kossa Staining Kit (Atom Scientific, RRSK39-100) were utilised in this protocol. Samples were then incubated with 10% (w/v) aqueous silver nitrate solution at room temperature in an ultraviolet (UV) light box for 10 minutes. This was followed by three washes in dH₂O and then incubated with 5% sodium thiosulfate for 5 minutes. Samples were then incubated with Van Gieson's solution for 5

minutes. Following incubations, sections were dewaxed, cleared and mounted in Xylene, then observed under an Olympus BX50 microscope. Monolayer samples were air-dried and observed under a Leica DMI6000 B inverted microscope.

2.9.7 - Immunohistochemistry

EnVision™ Detection Systems Peroxidase/DAB, Rabbit/Mouse (Dako, K406511) were utilised for this procedure. Sections were immersed in two Xylene and two 100% EtOH baths for 5 minutes each before taken to running tap water. Slides were placed in PBS bath before samples were incubated with 'Dual Endogenous Enzyme Block' from the EnVision™ kit for 10 minutes. Sections were washed in a PBS bath for 5 minutes and then samples were blocked in 20% Normal goat serum (Dako, X090710) in PBS for 30 minutes. Samples were washed in PBS bath for 5 minutes. Primary antibodies (Table 2.2) were added to samples at the desired concentration in 1% BSA (Sigma-Aldrich, A2058) in PBS, and then left to incubate overnight at 4°C. Negative controls were incubated in 1% BSA in the same conditions. The next day, sections were washed in a PBS bath for 10 minutes, before the addition of the secondary antibody HRP goat anti-rabbit to slides for 30 minutes. Slides were washed in a PBS bath for 5 minutes, following which Dako DAB developing solution was added to samples for 10 minutes. Sections were then washed in running tap water for 5 minutes before immersion in Harris Haematoxylin for 20 seconds and then cleared in running tap water. Samples were then dehydrated through two EtOH and two Xylene baths before mounting in DPX. The resulting staining was observed under an Olympus BX50 microscope.

Table 2.2 - Antibodies utilised for ICW and immunohistochemistry staining

Antibody	Catalogue number	Concentration
<i>In vitro studies</i>		
Alkaline Phosphatase (ALP)	ab126820 (Abcam)	1/500
Bone morphogenic protein 2 (BMP)	MA5-23763 (Invitrogen)	1/500
Collagen type I (Col1a)	ab6308 (Abcam)	1/100
Osteocalcin (OCN)	ab13420 (Abcam)	1/800
Aggrecan (AGG)	ab3778 (Abcam)	1/100
Collagen type II (Col2a)	ab185430 (Abcam)	1/500

<i>In vivo studies</i>		
Collagen type I (Col1a)	ab3778 (Abcam)	1/100
Osteocalcin (OCN)	ab185430 (Abcam)	1/200

2.10 - 3D printed PEGT/PBT fabrication and preparation

Bio-degradable poly (ethylene glycol)-terephthalate/poly (butylene terephthalate) (PEGT/PBT) block copolymers were provided by Dr Tim Woodfield in the Christchurch Regenerative Medicine and Tissue Engineering (CReaTE) research group at the University of Otago. PEGT/PBT copolymer composition was defined by a PEG molecular weight (MW) of 300 g/mol and a PEGT:PBT weight percent (wt%) ratio of 55:45. Briefly, PEGT/PBT scaffolds were fabricated in a layer by layer process using a 3D BioPlotter (EnvisionTec, Germany) with a 1 mm fibre spacing. Fibres were oriented in a 0 - 90° pattern in order to provide space for microtissue assembly in a bi-layered fashion. Scaffolds with dimensions of approximately 3.3 × 2.1 × 2.1 mm were then sterilised in 70% EtOH overnight. Following which scaffolds were washed in plain medium prior to the incorporation of microtissues.

2.11 - Diffusion chamber preparation

Diffusion chambers were assembled by attaching mixed cellulose ester membrane (0.22 µm pore size, Millipore, GSWP01300) to the bottom surface of the Plexiglas® Rings (Ø 14 mm x 2 mm) (Millipore, PR0001401) with cyanoacrylate glue. Once affixed, constructs were placed in the centre of the chamber and another membrane was affixed to the top of the chamber as described previously. When membranes have been fixed, basal medium was introduced into the chamber via the small hole within the side wall of the chamber ring with a sterile 1 ml syringe and needle. Care was taken to ensure no air bubbles remained within the chamber, after which a small plastic rod cut to the width of the chamber side wall was inserted into the hole, sealed with cyanoacrylate glue. Chambers were placed in basal medium within 24-well plates overnight to ensure chambers were properly sealed prior to implantation.

2.12 - Intraperitoneal implantation

Diffusion chambers (untreated/MI192 pre-treated groups, n=3 for each condition) were implanted within the intraperitoneal cavity of immunocompromised CD1 male nude mice (30 g). Mice were placed in a trifluorane chamber and anaesthetised for approximately 2-3 minutes (level 5 trifluorane and 2.5% oxygen). After induction, the mice were transferred onto a heated mat and anaesthesia

was maintained (level 2.5 trifluorane and 2.5% oxygen) via a nose cone. The abdominal region was sterilised with 70% EtOH, and a single incision through the skin and intraperitoneal membrane were made at the lower abdominal regions large enough to insert the chamber. Care was taken not to damage the underlying organs. Two chambers were placed into either side of the abdominal region. The intraperitoneal membrane and skin wound were closed using 5-0 coated VICRYL and 5-0 Ethilion sutures, respectively. Following closure, the area was cleaned with sterile injection water and Vetergesic injection (0.03 mg/ml) was given to each mouse. Then the trifluorane was switched off and the mice were transferred to a heated chamber until they were fully recovered. At 8 weeks post-surgery, the animals were sacrificed using schedule 1 (cervical dislocation) and chambers were extracted. Membranes were cut open and samples fixed in 10% NBF overnight at 4°C.

2.13 - X-ray analysis

The Omnicure 51500 Dental X-ray machine was used to acquire X-ray images of samples. Images were then analysed using the Corestream CS7600.

2.14 - Statistical analysis

All experiments were repeated at least three times. Data expressed as mean \pm standard deviation (SD). All statistical analysis was undertaken using one-way ANOVA with Tukey post-hoc modification using IBM SPSS software (IBM Analytics, version 21). P values equal to or lower than 0.05 was considered significant. For all graphs: * $P \leq 0.05$, ** $P \leq 0.01$ and *** $P \leq 0.001$.

Chapter 3 - The Effects of MI192 on the Behaviour and Osteogenic Capacity of Human Dental Pulp Stromal Cells *In vitro* and *In vivo*

The chapter aims to investigate the effects of MI192 on hDPSCs behaviour and osteogenic capacity in 2D and 3D *in vitro* and *in vivo*. Primarily, the general effects of MI192 on hDPSCs were evaluated by assessing morphology, viability, HDAC activity, H3K9 acetylation and cell cycle. The effects of MI192 on hDPSCs osteogenic capacity was assessed by ALPSA, ALP staining, osteogenic gene/protein expression and mineralisation. These parameters were examined in both 2D and 3D (lyophilised silk scaffold and BMT model) *in vitro* culture environments. Finally, the effects of MI192 on hDPSCs bone formation was investigated in a physiologically relevant *in vivo* model (diffusion chamber).

3.1 - Background

Within the bone tissue engineering field, BMSCs have been the gold standard MSCs source utilised due to their well-established characteristics and proven multi-lineage potential (153). However, in recent years, researchers have looked at alternative sources of MSCs due to limitations associated with BMSCs such as low yield volume, heterogeneity of differentiation potential, invasive acquisition and low proliferation rate (222). To date, five different types of stromal cells have been isolated and characterised from the dental tissues, including DPSCs (223), periodontal ligament stromal cells (PDLCS) (224), apical papilla stromal cells (225), dental follicle progenitor stromal cells (226) and stromal cells from exfoliated deciduous teeth (227). DPSCs have attracted increasing attention due to their ease of accessibility, high proliferation rate and their multi-lineage potential (228). These cells have been shown to co-express MSC markers, however, they are considered a heterogeneous population and lack specific markers for the consistent isolation and characterisation of the MSC population (229). Under sufficient conditions, these cells are able to differentiate into osteo/odontoblasts (230), indicating its potential utility for bone tissue engineering. In addition, cryopreservation of the extracted tooth prior to DPSCs isolation is an important advantage of this MSC source. A number of studies reported that cryopreservation does not affect the viability, MSC marker expression and differentiation capacity, therefore enhancing the potential therapeutic use of extracted teeth for future applications (231, 232), which may open a new avenue for the cryopreservation of extracted teeth prior to DPSCs isolation.

With the growing interest in DPSCs for bone tissue engineering, there are an increasing number of studies investigating the use of HDACis to enhance the differentiation capacity of these cells. For example, TSA and VPA have been shown to accelerate DPSCs osteogenic differentiation and mineralisation *in vitro* (233, 234). However, the majority of these studies were focused on

panHDACis. In recent years, research is shifting towards the use of isoform-selective HDACis to minimise potential side-effects and to enhance differentiation potential. Previously, it was demonstrated that the HDAC2 and 3 selective inhibitor - MI192 accelerated ADSCs osteogenic differentiation and mineralisation compared to the panHDACi TSA (214), therefore indicating the potential effectiveness of utilising selective HDACis for bone tissue engineering applications.

Another key challenge for tissue engineering is the choice of an appropriate biomaterial which can provide sufficient biological and mechanical properties to mimic natural bone matrix and direct new tissue growth. A variety of biomaterials have been utilised for bone tissue engineering applications (184, 235, 236). Silk is a natural polymer that can be found abundantly and easily acquired by silkworms and spiders. In general, there are two types of silk fibroin, mulberry silk and non-mulberry silk, acquired from *Bombyx mori* (BM) and *Antheraea mylitta* (AM) silkworms respectively (237). The silk material possesses valuable characteristics such as being biocompatible, biodegradable, highly porous and controllable mechanical properties (169, 238). Lyophilised silk sponges are highly tunable in terms of its degradative and mechanical properties, creating a versatile biomaterial for tissue engineering applications. This material is also favoured by researchers as they are easily processed via different methods such as electrospinning, hydrogels and cast into complex shapes to match the application of interest. To date, silk fibroin has been widely utilised for multiple tissue engineering applications such as cardiac (237), nervous (239), cartilage (169) and bone tissue engineering (240). Saha *et al.* (2013) incorporated silk scaffolds with BMP2 (169), while Zhao *et al.* (2009) coated their scaffolds with apatite to enhance the osteogenic potential of these constructs (241). Meinel *et al.* (2005) used silk scaffolds to repair critical-sized bone defects within mouse models (242). As this biomaterial has proven its potential for bone tissue engineering, the silk scaffolds could provide an ideal environment to investigate the effects on MI192 on stimulating hDPSCs osteogenic differentiation in 3D culture.

In recent years, increasing studies have utilising scaffolds created from additive manufacturing and biofabrication techniques. Advances in biofabrication technologies have allowed for the reproducible creation of biologically functional products with the structural organization of living cells, biomaterials, cell aggregates such as microtissues, or hybrid cell-material constructs, through bioprinting or bioassembly and subsequent tissue maturation processes (243, 244). In particular, modular assembly, where cellular components are combined with a structural scaffold possesses great potential for bone tissue engineering. An increasingly utilised 3D culture approach in organoid, cancer and tissue engineering research is the formation of cellular aggregates, termed microtissues (245-247). The high cell density approach of microtissues have been shown to be beneficial for

accelerating bone-like tissue formation when compared to 2D and lower density scaffold systems (245, 248-250). Moreover, it has been demonstrated that high-density culture plays a significant role in stimulating hDPSCs osteogenic capacity (251, 252). Although the use of microtissues for bone tissue engineering shows promise, their potential clinical application is limited due to being too small for large bone defects, lacking spatial organisation and insufficient mechanical properties. To overcome these limitations, the spatial assembly of these tissue modules by automated biofabrication processes could allow for the development of more complex constructs, such as to repair osteochondral defects (81). An example of a modular tissue assembly approach for tissue engineering applications is the bioassembled microtissue (BMT) construct (253).

The BMT model is a culture system which closely replicates the cell-cell and cell-matrix interactions that occurs *in vivo* (253). The CReaTE group at the University of Otago developed a high throughput process to fabricate pre-cultured microtissues (spheroidal pellets) of regular size and shape, which were combined with a 3D printed porous scaffold (Fig 3.1) (253). The 3D printed scaffold provides mechanical reinforcements to the microtissues while increasing the size of tissue formed for large bone defects. Moreover, this modular assembly method enhances the cell seeding efficiency within scaffolds, eliminating cell wash out that occurs in conventional 3D models, therefore resulting in a construct with a high cell load (254). Additionally, this approach allows for the spatial control of cellular components within a scaffold, avoiding unwanted cellular distribution. This 3D *in vitro* model has the potential to accelerate bone-like tissue formation and ultimately lead to enhanced bone defect repair. Therefore, in addition to assessing the effects of MI192 on hDPSCs osteogenic differentiation within the silk scaffold, the effects within this novel BMT model were investigated.

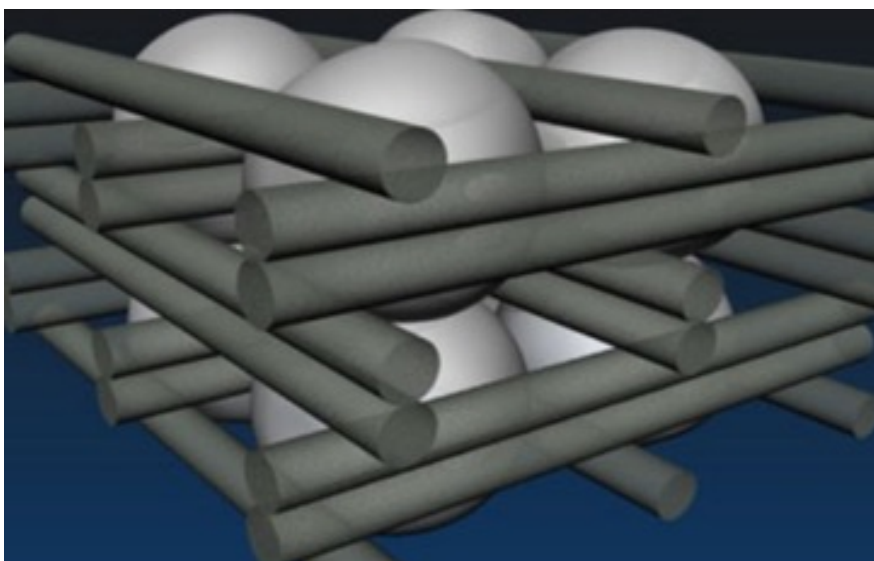


Figure 3.1 - Schematic representation of the bioassembled microtissue (BMT) construct. Pre-cultured microtissues within the pores of a 3D printed scaffold. Reprinted with permission (253).

To date, limited studies have investigated the effects of HDACis on bone tissue regeneration *in vivo* (208, 212); therefore, in the literature, there is a lack of knowledge regarding how these HDACi therapies behave in physiological conditions. The importance of evaluating the use of HDACis for bone tissue engineering *in vivo* was demonstrated by de Boer *et al.* (2006), where they could not replicate the enhancement in MSCs osteogenesis upon TSA and NaB treatment which was previously demonstrated *in vitro* (74). The diffusion chamber model provides an ideal environment for cell incubations where it separates the 3D construct from the host cells and tissues (255, 256); therefore, all new tissue formation within the chamber would be of donor origin. In addition, it minimises foreign material contamination and infection, providing a much more physiologically relevant model compared to *in vitro* culture. Numerous studies have shown the effectiveness of diffusion chambers for evaluating *in vivo* bone formation (257, 258). Consequently, this model was utilised to evaluate the effect of MI192 on hDPSCs bone formation within a 3D construct in a physiologically relevant environment.

Therefore, the aim of this chapter was to investigate the effects of the HDAC2 & 3 selective inhibitor - MI192 on the behaviour and osteogenic capacity of hDPSCs in 2D and 3D *in vitro* and *in vivo*.

The main objectives of this chapter:

- To evaluate the effects of MI192 on the behaviour and osteogenic capacity of hDPSCs in 2D *in vitro* culture (section 3.3.1).
- To determine the effects of MI192 on hDPSCs bone formation within 3D *in vitro* scaffold systems:
 - BM lyophilised silk scaffold (section 3.3.2).
 - Bioassembled microtissue model (section 3.3.3).
- To investigate the effects of MI192 on hDPSCs bone formation *in vivo* (section 3.3.4).

3.2 - Materials and Methods

3.2.1 - Cytotoxic effect of MI192 on hDPSCs

Cells were seeded at 1×10^4 cells per well in three 96-well plates in basal medium. After 24 hours, the medium was replaced with fresh basal medium supplemented with/without MI192 (1, 5, 10, 20, 50, 100 μM) and incubated for 24, 48 and 72 hours. The sample size was three for each group ($n=3$). At each time point, one of the plates were used for cytotoxicity assessment. The CytoTox 96® Non-Radioactive Cytotoxicity Assay (Promega, Cat. no: G9260) was used according to the manufacturer's instructions. Briefly, the prepared reagent (100 μl per well) was added directly to the medium of the plate. The plate was then incubated for 30 minutes at 37°C and the fluorescence was then measured in a Varioskan Flash Multimode Microplate Reader (Model 3001, Thermo Scientific) (excitation/emission wavelengths of 488/520 nm). The CytoTox-Fluor Assay is a single-reagent-addition assay that measures the relative number of dead cells in a cell population. A fluorogenic peptide substrate (bis-alanyl-alanyl-phenylalanyl-rhodamine 110) reacts with proteases that have been released from dead cells. The peptide cannot penetrate the membrane of live cells.

3.2.2 - Effect of MI192 on ALPSA in hDPSCs

Cells were seeded in two 24-well plates (5×10^4 cells per well) in basal medium. After 24 hours, the medium was replaced with MI192 pre-treatment medium (5, 10 and 20 μM MI192 for 24 hours or 1, 2 and 5 μM MI192 for 48 hours). Following pre-treatment, cells were cultured in osteogenic medium for 2 weeks. Untreated cells in basal or osteogenic medium were used as controls. The sample size was three for each group ($n=3$). After culture, cells were processed for ALPSA as described in Chapter 2.

3.2.3 - Effect of MI192 on hDPSCs ALP staining

Cells were seeded at 5×10^4 cells per well in a 24-well plate in basal medium. After 24 hours, the medium was replaced with fresh basal medium supplemented with MI192 (2 μM). Untreated cells in basal medium used as control. Following 48 hours pre-treatment, the medium in both groups was replaced with osteogenic medium and plates were cultured for 2 weeks. The sample size was three for each group ($n=3$). After 2 weeks culture, cells were washed twice in PBS, fixed in 98% EtOH for 15 minutes, and then washed with three washes of dH_2O . The samples were incubated with ALP staining solution (0.4 ml Naphthol AS-MX (Sigma-Aldrich, 855), 4.2 mg Fast Violet B salt (Sigma-Aldrich, F3381) and 9.6 ml dH_2O) for 30 - 60 minutes at 37°C in the dark. Cells were then washed with dH_2O , air dried and observed under a Leica DMI6000 B inverted microscope.

3.2.4 - Effect of MI192 on the expression of osteogenic genes in hDPSCs

Cells were seeded at 5×10^4 cells per well within 24-well plates in basal medium. After 24 hours, the medium was replaced with fresh basal medium supplemented with MI192 (2 μ M). Untreated cells in basal medium used as control. Following 48 hours pre-treatment, the medium in both groups was replaced with osteogenic medium and plates were cultured for 0, 3, 5, 7, 14, 21 and 28 days. The sample size was three for each group per time point ($n=3$). At each time point, one of the plates was stopped for RNA isolation, cDNA conversion and RT-qPCR as described in Chapter 2.

3.2.5 - Silk fibroin extraction and biomaterial fabrication

Silk scaffolds utilised in this chapter were provided by Dr Jelena Rnjak-Kovacinac at the University of New South Wales, Sydney. Briefly, silk fibroin was extracted from *BM* silk cocoons obtained from Tajima Shoji Co Ltd (Japan) as previously described (259). *BM* silk cocoons (5 g) were cut into small pieces and boiled in sodium carbonate solution for 30 minutes (2L, 0.02 M) (Sigma-Aldrich, 451614) to remove sericin. Pure silk fibroin was solubilised in aqueous lithium bromide (9.3 M, 25% in wt/v) for 4 hours at 60°C. Removal of trace solvents was undertaken by dialyzing the solution against dH₂O using SnakeSkin™ Dialysis tubing (3500MWCO, Thermo Fisher Scientific, 68035) for three days and centrifuged at 8700 RPM to remove debris. The concentration of silk fibroin was determined by drying and weighing a known volume of solution. Silk fibroin is referred to as silk in this thesis. Aqueous silk solutions (2 and 5 % in wt/v in dH₂O) were transferred into wells of a 24-well plate (3 ml/well). Silk was frozen overnight at -20°C and lyophilised at -80°C for 48 hours. Scaffolds were removed from moulds and rendered insoluble by autoclaving at 121°C for 20 minutes at 15 psi to induce beta-sheet formation (260). Samples were rehydrated in sterile deionized H₂O. Non-porous “skin” on top of the scaffolds was removed prior to further assessment.

3.2.6 - Characterisation of silk scaffold

Degradation was determined by placing scaffolds (2 and 5 wt%) ($\varnothing 8 \times 5$ mm) into 1.5-ml Eppendorf tubes and dried at 60°C, following which the mass of dry scaffolds was measured. The sample size was five for each group ($n=5$). In each tube, Protease XIV solution (2 U/ml in PBS) (Sigma-Aldrich, P5147) was added and incubated at 37°C. Every 2 days, the solution was removed, and scaffolds were washed with dH₂O, following which samples were dried at 60°C and dry mass was recorded. Fresh Protease XIV solution was added to samples and the procedure repeated until day 8. Degradation was calculated as a percentage of remaining mass compared to the mass of the original scaffold (260). The swelling capacity of the scaffolds (2 and 5 wt%) was assessed using H₂O and PBS. Briefly, dried scaffolds ($\varnothing 8 \times 5$ mm) were rehydrated in H₂O and PBS, following which hydrated

scaffold weight was recorded. Fold increase in mass was calculated by comparing the scaffold dry and hydrated mass (260). The sample size was five for each group for each condition (n=5). The scaffold compressive modulus was determined using an Instron 3365 universal testing machine with a 50N load cell. Scaffolds (2 and 5 wt%) ($\varnothing 8 \times 5$ mm) were compressed (10 mm/min) to 90% of original height and compressive modulus determined between 10 - 30% strain. The sample size was six for each group (n=6).

3.2.7 - Characterisation of 3D printed PEGT/PBT

The interconnecting pore size of the 3D printed PEGT/PBT scaffolds in the x-y plane and z plane, in addition to the fibre spacing and diameter was measured from calibrated bright-field images (n=4 for each parameter measured).

3.2.8 - Scanning electron microscopy (SEM)

Microscopic analysis of scaffold surface topography was undertaken by scanning electron microscopy (SEM). Samples were mounted on 26-mm stubs and gold sputter-coated (40 mA, 60 seconds) and placed in the specimen chamber of a Hitachi S-3400N VP-SEM. Images were acquired with a 5 kV electron beam and a working distance of 12 - 13 mm.

3.2.9 - Silk preparation before experiments

Lyophilised silk sponges (2 and 5 wt%) were cut with a sterile scalpel blade ($\varnothing 5 \times 2$ mm) and washed with PBS. Scaffolds were then incubated in α -MEM containing 10% FCS overnight at 37°C. Prior to the addition of cells, the scaffolds were washed with plain medium.

3.2.10 - Static seeding of cells on silk scaffolds

Briefly, excess media from scaffolds was removed using a 1-ml pipette and air dried. Cell pellets containing 2×10^5 cells were created using untreated and MI192 pre-treated hDPSCs (2 μ M MI192 for 48 hours). Subsequent pellets were re-suspended in 20 μ l of basal medium. A concentrated cell suspension (10 μ l) was placed in the bottom of an untreated 24-well plate (Corning, CLS3473-24EA). Scaffolds were placed on top of the solution for 10 minutes to allow absorption of cell suspension. After this period, the remaining cell suspension was pipetted on the top of the scaffold and cells were allowed to adhere for 4 hours within the incubator. 500 μ l of basal medium was added to each well and the scaffold/cells were left overnight to settle. After this period, the basal medium was removed and replaced with osteogenic medium. The medium was changed every 3 - 4 days. Silk

constructs were cultured for a subsequent 6 weeks for histological analysis. The sample size was three for both groups (n=3).

3.2.11 - Microtissue culture and BMT construct assembly

Untreated and MI192 pre-treated hDPSCs (2 μ M MI192 for 48 hours) were suspended in 250 μ l of osteogenic medium with 2.5×10^5 cells per well in a v-shaped bottom 96-well plate (Greiner Bio-One, 651201). Microtissues were formed utilising the procedure described in Chapter 2. After 1 week culture, microtissues were manually transferred into the scaffold (2 microtissues per pore) using a 1-ml pipette tip to form the BMT construct. A total of 16 microtissues were incorporated into the scaffold in a bi-layer configuration (8 microtissues per layer). BMTs were cultured in osteogenic conditions for a subsequent 6 weeks. The sample size was three for both groups (n=3).

3.2.12 - RNA isolation from cell-silk constructs

RNA isolation of cell-laden silk constructs was undertaken after 3, 7, 10 and 14 days in osteogenic culture. The sample size was four for each group per time point (n=4). Cell-laden silk constructs were sliced using a sterile scalpel into small pieces and placed into an Eppendorf tube containing 500 μ l RLT buffer. The silk samples were then vortexed for 15 seconds and placed into a sonicator for 15 minutes. This process was repeated four times. The lysate solution was then transferred into the QIAshredder (Qiagen, 79654) and centrifuged at 10000 RPM for 3 minutes. The lysate was used for RNA isolation, cDNA conversion and RT-qPCR as described in Chapter 2.

3.2.13 - 3D construct preparation for ALPSA assay

Following osteogenic culture for 2 weeks, cell-laden silk and BMT constructs were processed for ALPSA assay. Cell-laden silk constructs were washed twice with PBS, cut into thin slices using a sterile scalpel and then transferred into Eppendorf tubes. Similarly, BMT constructs were washed twice with PBS and placed in Eppendorf tubes. 500 μ l 0.1% Triton X-100 in PBS was added and tubes were vortexed and sonicated for 5 minutes. Samples were frozen at -80°C then thawed in a 37°C oven, and the freeze/thaw process was repeated 5 times. Microtissues were homogenised by passing through a 20-gauge needle between freeze/thaw steps. Following this, samples were centrifuged at $10000g$ for 10 minutes at 4°C , then lysate was collected and utilised for ALPSA assay described in Chapter 2. The sample size was four for each group (n=4).

3.3 - Results

3.3.1 - The Effects of MI192 on the Behaviour and Osteogenic Capacity of hDPSCs in 2D Culture

3.3.1.1 - Effect of MI192 on hDPSCs morphology

After 24 hours of culturing in basal medium with/without MI192, the images show that the hDPSCs in basal culture exhibited a typical fibroblast-like morphology (Fig 3.2). The cells after treatment with 1 μM MI192 possessed a more flattened/elongated morphology compared to those in the basal group, with a noticeable number of floating dead/detached cells. In the groups treated with 10 and 20 μM MI192, there was an increased quantity of floating cells/debris. Cells treated with 50 and 100 μM MI192 exhibited the lowest cellular density at this time point.

At the 48 hour time point, cells in the basal group possessed increased cell density compared to the previous time point with a continuation in the fibroblast-like morphology (Fig 3.2). The cells treated with 1 μM MI192 also demonstrated a fibroblast-like morphology similar to that in the basal group. In this group, there was an increase in cell density over the previous time point, although less than the basal group. In the groups treated with 10 and 20 μM MI192, there was a reduction in the cell density compared to cells treated with lower MI192 concentrations or under basal conditions. Following treatment with 50 μM MI192, there was a substantially reduced cell density compared to lower MI192 concentration groups with increased numbers of the small black dots, while cells treated with 100 μM MI192 displayed the highest quantity of floating dead/detached cells at this time point.

After 72 hours, cells in basal conditions reached confluence while still possessing the fibroblast-like shape observed in earlier time points (Fig 3.2). Following 1 μM MI192 treatment, an increased quantity of floating dead/detached cells was much more noticeable compared to previous time points. In the cells treated with 10 or 20 μM MI192, there was a reduction in the cell density with an increased number of floating dead/detached cells. Moreover, the cells treated with 50 or 100 μM MI192 exhibited very few attached cells, with the highest quantity of floating dead/detached cells at this time point.

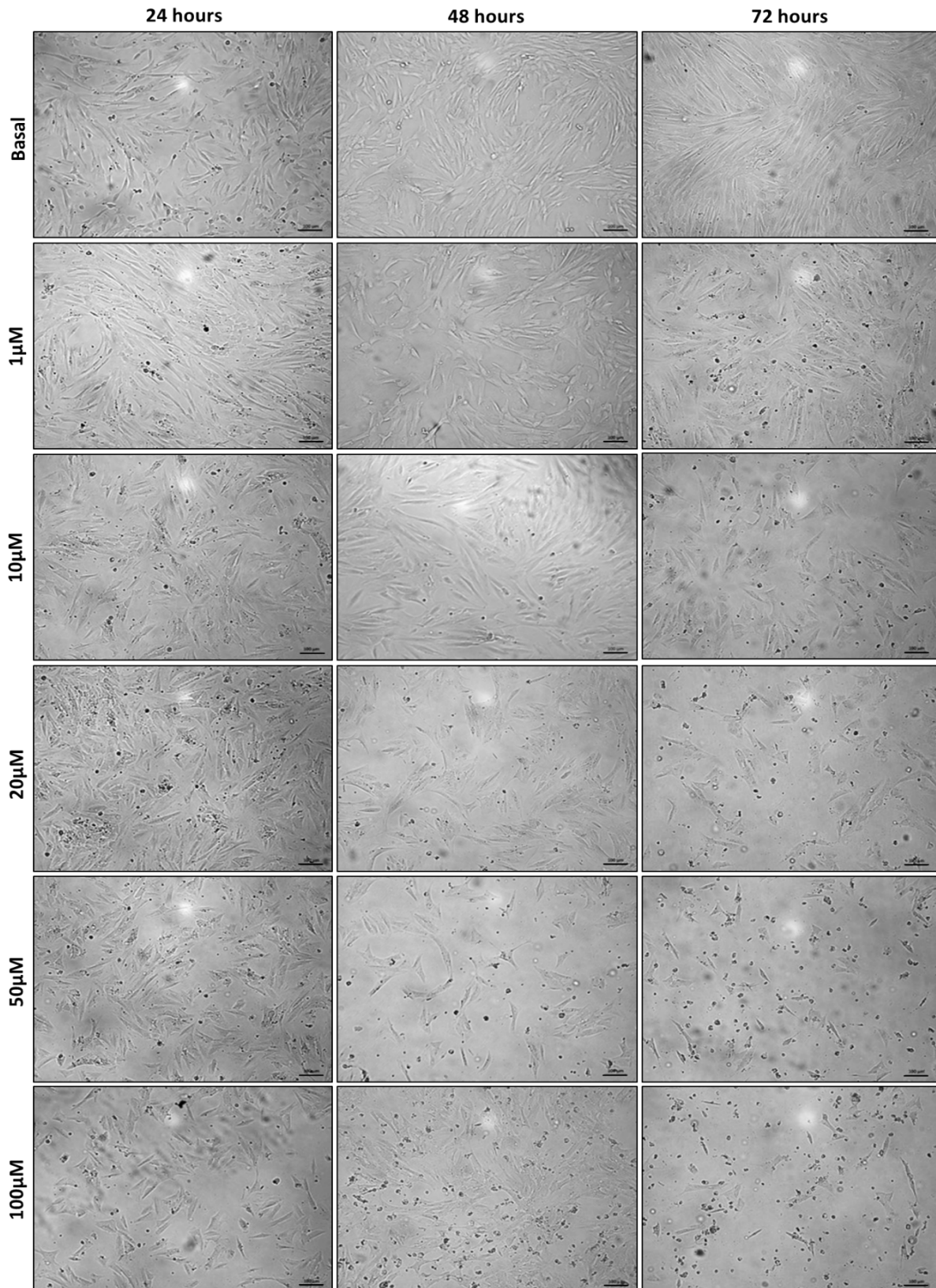


Figure 3.2 - Phase contrast images of hDPSCs treated with/without a range of MI192 dose (1, 10, 20, 50, 100 μM) for 24, 48 and 72 hours. Scale bar = 100 μm.

3.3.1.2 - Effect of MI192 on hDPSCs metabolic activity

After 24 hours of culturing in basal medium supplemented with/without MI192 (1 - 100 μM), AlamarBlue analysis showed a dose-dependent decrease in the metabolic activity of hDPSCs, where MI192 at 20 μM and higher concentrations significantly reduced the metabolic activity compared to the untreated group ($P \leq 0.05$) (Fig 3.3). MI192 treatment for 48 hours showed a similar dose-dependent reduction in metabolic activity, however, MI192 at 5 μM and greater concentrations significantly reduced the metabolic activity compared to the untreated group ($P \leq 0.05$). After 72 hours treatment, there was a severe reduction in the metabolic activity where treatment with MI192 at 1 μM and above concentrations led to a significant reduction compared to the untreated control group ($P \leq 0.05$).

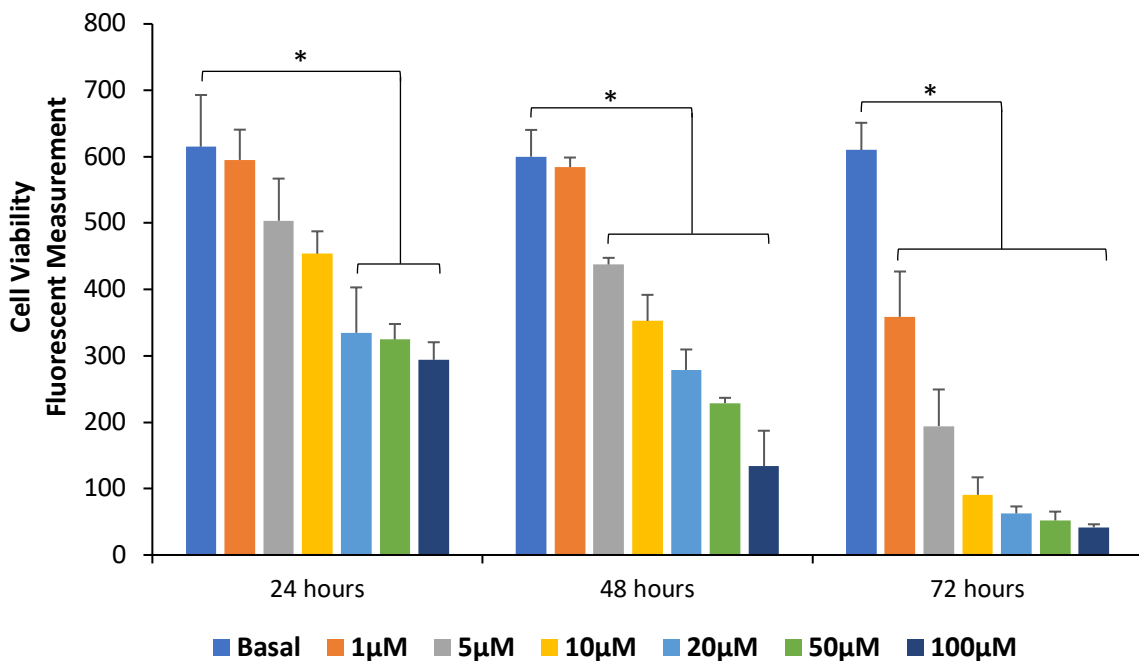


Figure 3.3 - AlamarBlue analysis of hDPSCs metabolic activity treated with/without a range of MI192 doses (1, 5, 10, 20, 50, 100 μM) for 24, 48 and 72 hours. Data expressed as mean \pm SD (n=3). Significance levels shown are the test groups compared to the basal control for that time point. * $P \leq 0.05$.

3.3.1.3 - Effect of MI192 on hDPSCs DNA quantity

Cells were treated with/without MI192 (1 - 100 μM) for up to 72 hours, and DNA content assessed via PicoGreen assay. At 24 hours, MI192 caused a dose-dependent reduction in the DNA content, where MI192 at 5 μM and greater concentrations significantly reduced the DNA quantity compared to that in the untreated cells ($P \leq 0.001$) (Fig 3.4). MI192 treatment for 48 and 72 hours also showed a similar dose-dependent decrease in DNA content, where MI192 at 1 μM and greater concentrations significantly decreased the DNA content compared to untreated cells for the same time points ($P \leq 0.001$). For each MI192 concentration, a time-dependent reduction in DNA content was observed.

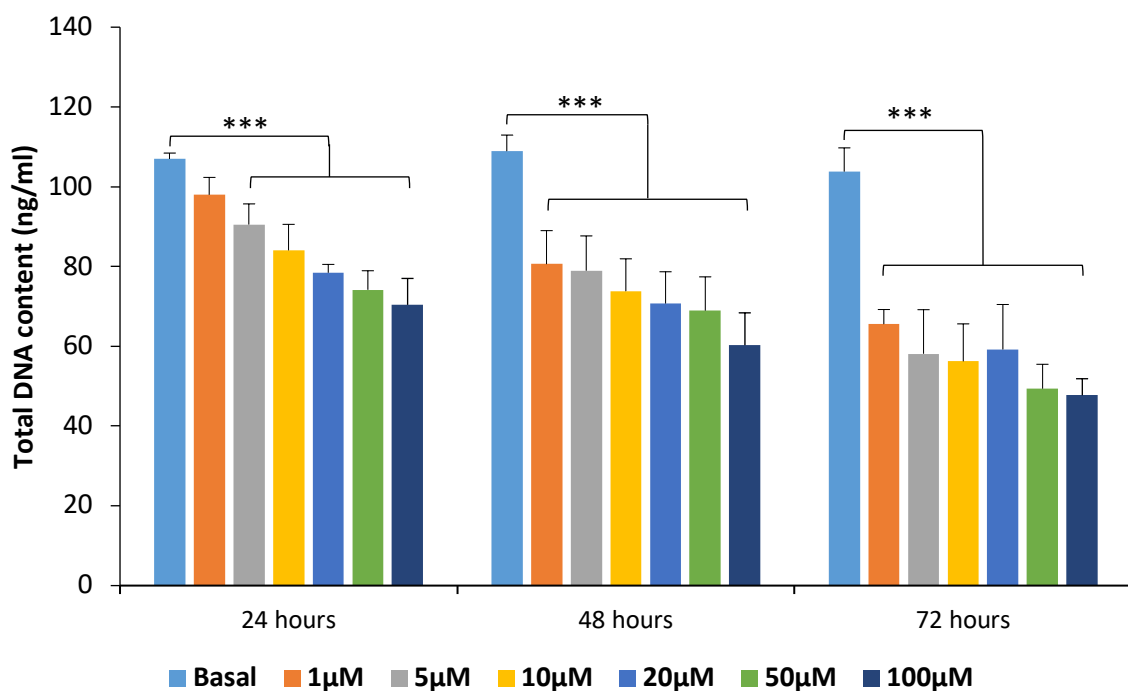


Figure 3.4 - DNA quantification of hDPSCs treated with/without a range of MI192 doses (1, 5, 10, 20, 50, 100 μM) for 24, 48 and 72 hours. Data expressed as mean \pm SD (n=3). Significance levels shown are the test groups compared to the basal control for that time point. * $P \leq 0.001$.**

3.3.1.4 - Cytotoxic effect of MI192 on hDPSCs

After 24 hours of culturing in basal medium supplement with/without MI192 concentrations (1 - 100 μM), MI192 at 10 μM and greater concentrations significantly increased the cytotoxicity marker levels ("dead cell" protease activity) compared to the untreated group ($P \leq 0.05$) (Fig 3.5). A similar dose-dependent increase in the cytotoxicity marker was observed at 48 hours, where MI192 treatment of 5 μM and above significantly enhanced the cytotoxicity levels ($P \leq 0.001$). Treatment with MI192 at 1 μM and greater concentrations for 72 hours significantly enhanced the cytotoxicity level in hDPSCs compared to the untreated cells ($P \leq 0.001$).

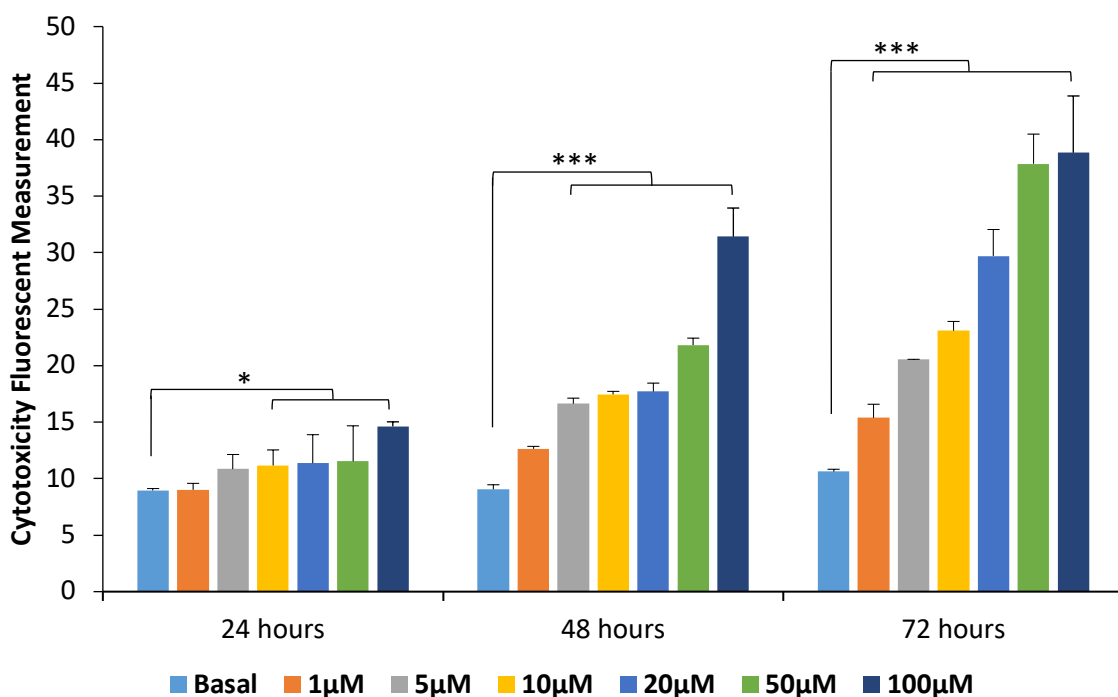


Figure 3.5 - Cytotoxicity analysis of hDPSCs treated with/without a range of MI192 doses (1, 5, 10, 20, 50, 100 μM) for 24, 48 and 72 hours. Data expressed as mean \pm SD ($n=3$). The significance levels shown are the test groups compared to the basal control for that time point. * $P \leq 0.05$ and *** $P \leq 0.001$.

3.3.1.5 - Effect of MI192 on HDAC specific activity in hDPSCs

Treatment of hDPSCs with different MI192 concentrations (1 - 50 μ M) for 24 and 48 hours, lead to a significant reduction in the HDAC specific activity (≥ 3.4 - and 4.1-fold respectively) compared to the untreated controls in a dose-dependent manner ($P \leq 0.001$) (Fig 3.6A). There was also a significant reduction in the HDAC specific activity between treatments with different MI192 doses for both 24 and 48 hours ($P \leq 0.05 - 0.001$).

The effects of MI192 pre-treatment for 24 and 48 hours on hDPSCs HDAC specific activity was assessed following 1 week culture in basal medium. Following MI192 pre-treatment for 24 and 48 hours, HDAC specific activity was significantly reduced (≥ 1.95 - and 2.25-fold, respectively) compared to the untreated cells, in a dose-dependent manner ($P \leq 0.001$) (Fig 3.6B). A significant reduction in the HDAC specific activity was also observed between MI192 doses of 1 and 5 μ M (24 and 48 hours) ($P \leq 0.05$ and $P \leq 0.01$) and between 20 and 50 μ M (48 hours) ($P \leq 0.01$).

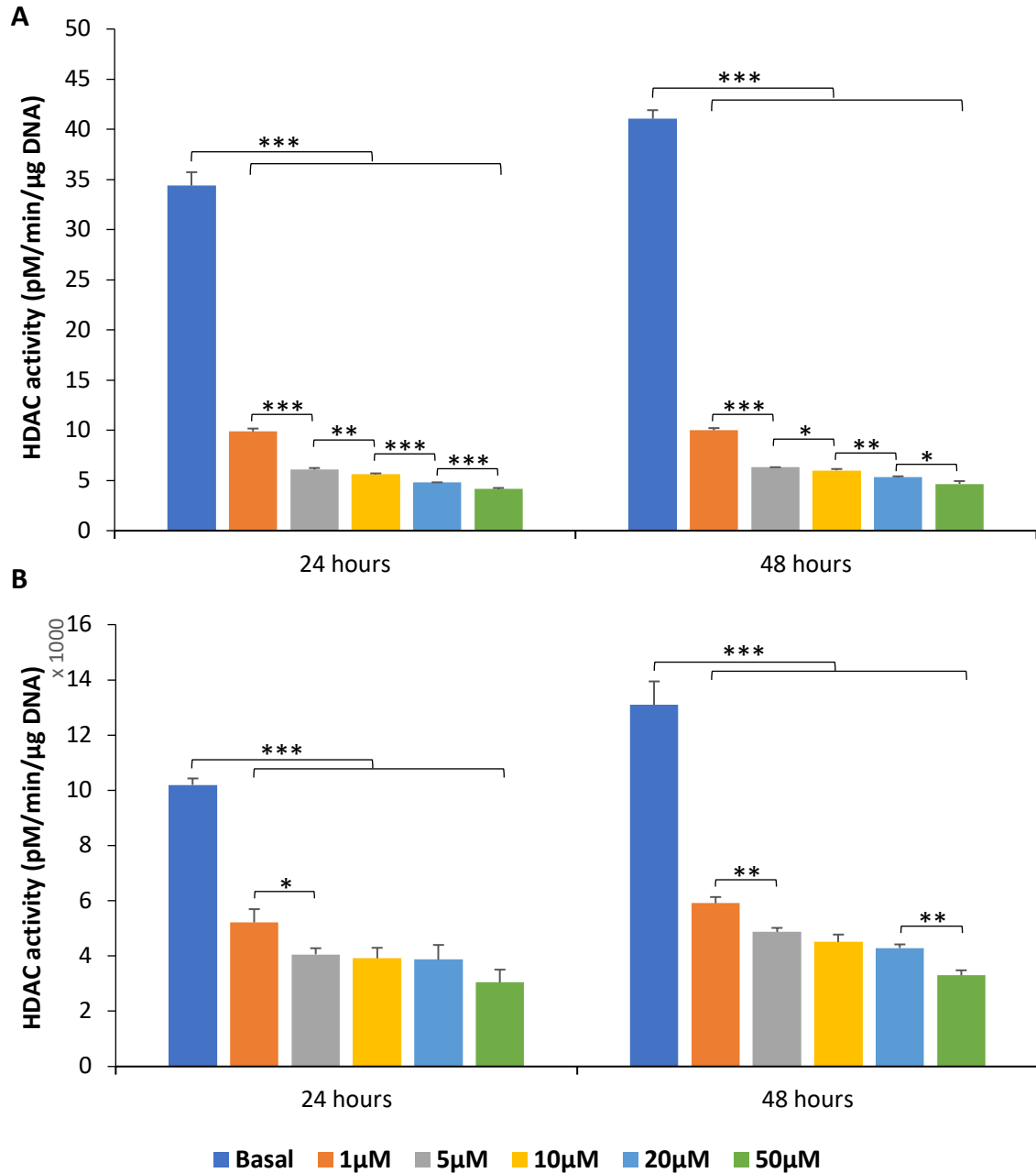


Figure 3.6 - HDAC specific activity in hDPSCs following MI192 treatment. A) HDAC specific activity of hDPSCs immediately after 24 and 48 hours MI192 treatment. B) HDAC specific activity of MI192 pre-treated hDPSCs (24 and 48 hours) after 1 week of culture in basal medium. Data expressed as mean \pm SD (n=3). Significance levels shown are the test groups compared to the basal control or between adjacent MI192 concentrations at that time point. *P \leq 0.05, **P \leq 0.01 and ***P \leq 0.001.

3.3.1.6 - Effect of MI192 on histone H3K9 specific acetylation in hDPSCs

Treatment of hDPSCs with different concentrations of MI192 (1 - 50 μ M) for 24 hours resulted in a dose-dependent reduction in the H3K9 specific acetylation levels, where MI192 of 20 μ M and greater concentrations significantly reduced the acetylation levels compared to the untreated group ($P \leq 0.05$). After 48 hours, MI192 treatment caused a dose-dependent increase in the acetylation level, where MI192 of 1 μ M and greater concentrations significantly enhanced the H3K9 specific acetylation level compared to the untreated control group (Fig 3.7) (1 - 10 μ M: $P \leq 0.05$, 20 - 50 μ M: $P \leq 0.01$).

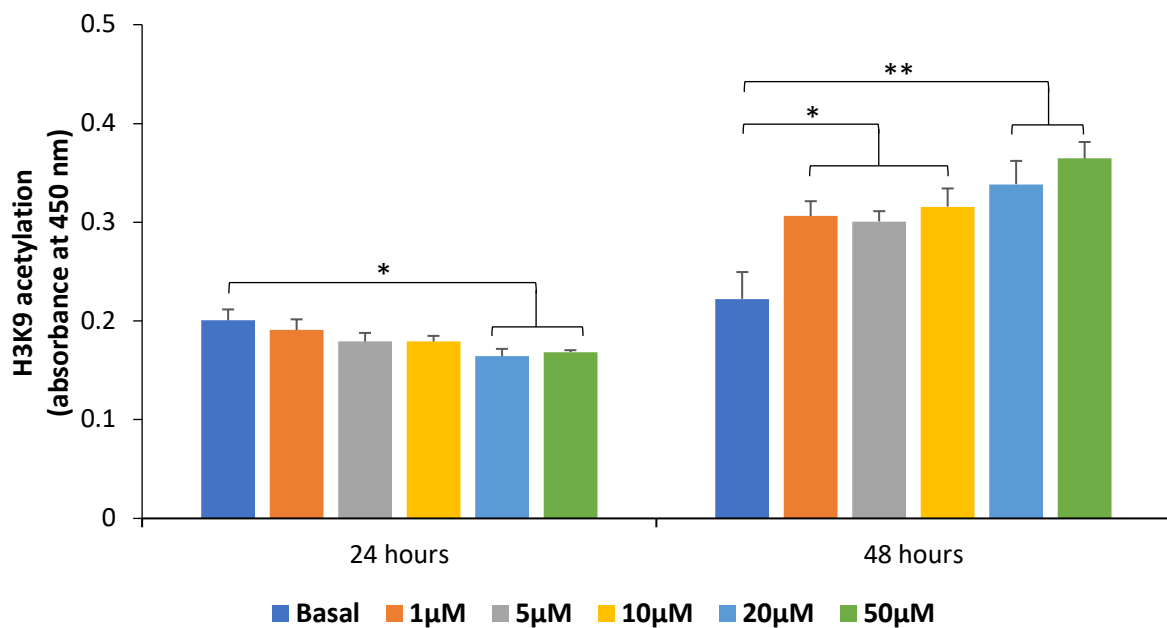


Figure 3.7 - H3K9 histone-specific acetylation levels in hDPSCs after treatment with five doses of MI192 for 24 and 48 hours. Data expressed as mean \pm SD (n=3). Significance levels shown are the test groups compared to the basal control for that time point. * $P \leq 0.05$ and ** $P \leq 0.01$.

3.3.1.7 - Effect of MI192 on hDPSCs cell cycle progression

HDPSCs were cultured with/without 2 μ M MI192 for 24, 48 and 72 hours. The percentage of cells distributed within the different phases of the cell cycle is shown in Table 3.1 and Figure 3.8. The representative histograms from the FACS analysis show the number of cells at different stages of the cell cycle (Fig 3.9).

Table 3.1 - Table of data from the flow cytometry analysis of the cell cycle distribution for hDPSCs. Cells dosed with/without 2 μ M MI192 for 24, 48 and 72 hours. The table shows the average percentage of cells in each phase of the cell cycle, with the standard deviation (SD).

		G₀/G₁		G₂/M		S Phase	
		Phase	SD	Phase	SD	Mean %	SD
		Mean %		Mean %			
24 hours	Untreated	58.96	2.71	15.14	0.87	25.90	2.81
	MI192	50.14	4.31	22.09	2.61	27.77	5.14
48 hours	Untreated	78.36	4.13	6.18	1.71	15.46	2.45
	MI192	52.13	7.49	19.00	0.47	28.88	1.17
72 hours	Untreated	82.05	1.45	6.06	0.52	11.90	1.93
	MI192	53.91	3.63	23.37	2.62	22.72	2.99

G₀/G₁ phase

At the 24 hour stage, the percentage of cells in the G₀/G₁ phase was reduced in the MI192 treated group (50.14%) compared to the untreated cells (58.96%), however not statistically significant ($P > 0.05$) (Fig 3.8). However, the percentage of cells significantly decreased in the MI192 treated group (52.13%) compared to the untreated cells after 48 hours treatment (78.36%) ($P \leq 0.01$). A similar pattern was observed at 72 hours, with MI192 treatment (53.91%) significantly reducing the percentage of cells in this phase compared to the untreated cells (82.05%) ($P \leq 0.05$).

G₂/M phase

The percentage of cells in the G₂/M phase within the MI192 treated group (22.09%) was significantly increased compared to the untreated cells (15.14%) at the 24 hours stage ($P \leq 0.05$) (Fig 3.8). At 48 hours, the MI192 treated group (19.00%) continued to exhibit a significantly enhanced G₂/M phase percentage compared to the untreated cells (6.18%) ($P \leq 0.001$). At 72 hours, a similar trend was observed where MI192 treatment (23.37%) substantially increased the number of cells in the G₂/M phase compared to untreated control at this time point (6.06%) ($P \leq 0.001$).

S phase

After 24 hours, MI192 treatment (27.77%) increased the percentage of cells in the S phase compared to the untreated group (25.90%), however not significantly ($P > 0.05$) (Fig 3.8). At 48 hours, a significant enhancement was observed in the MI192 treated group (28.88%) compared to the untreated cells (15.46%) ($P \leq 0.01$). After 72 hours treatment, the MI192 treated cells (22.72%) maintained a significant higher S phase percentage compared to the untreated group (11.90%) ($P \leq 0.001$).

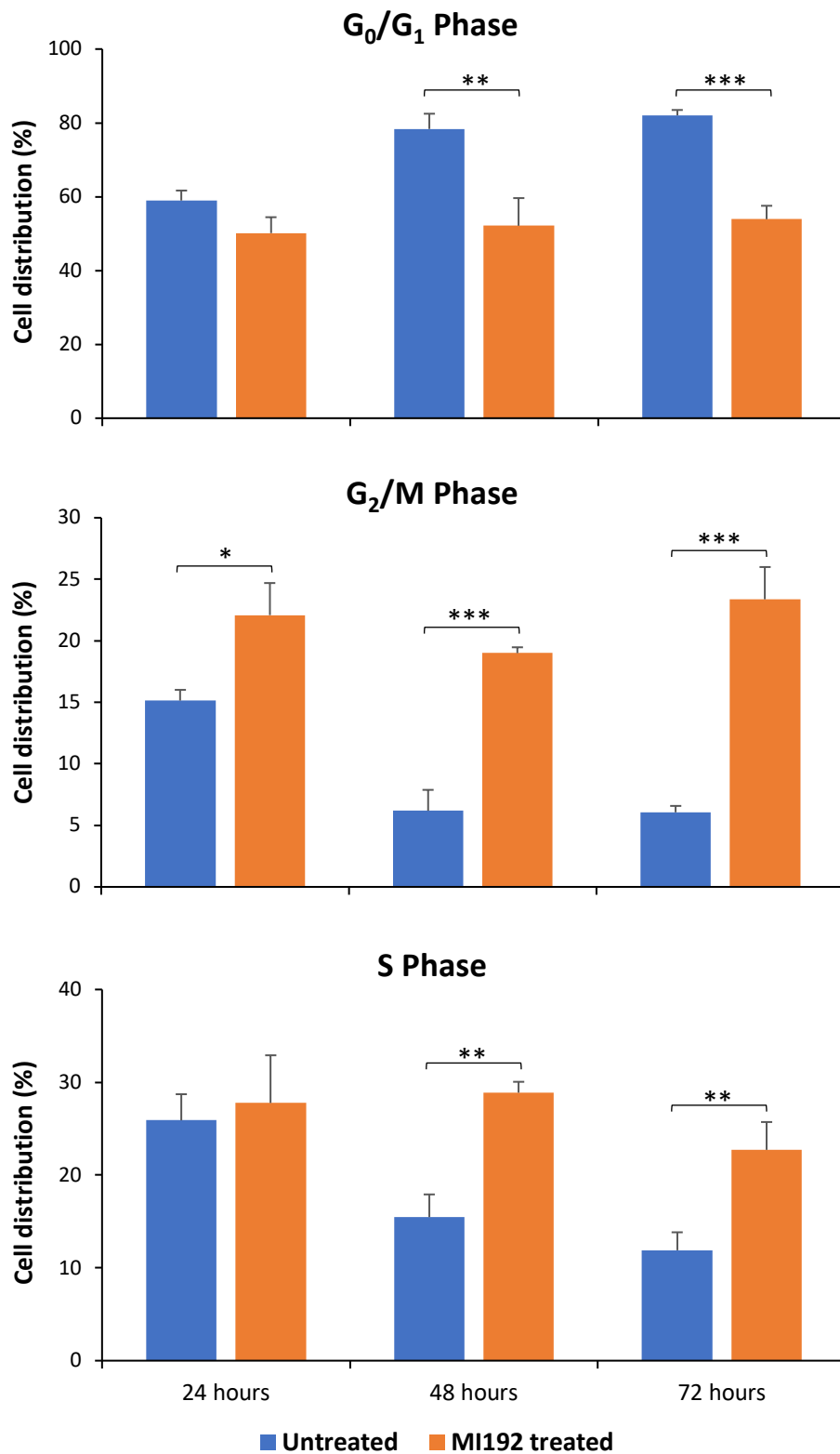


Figure 3.8 - The percentage of hDPSCs in the G₀/G₁, G₂/M and S phases after treatment with/without 2 μ M MI192 over 24, 48 and 72 hours. Data expressed as mean \pm SD (n=3). The significance levels shown are the test group compared to the basal control for that time point. *P \leq 0.05, **P \leq 0.01 and *P \leq 0.001.**

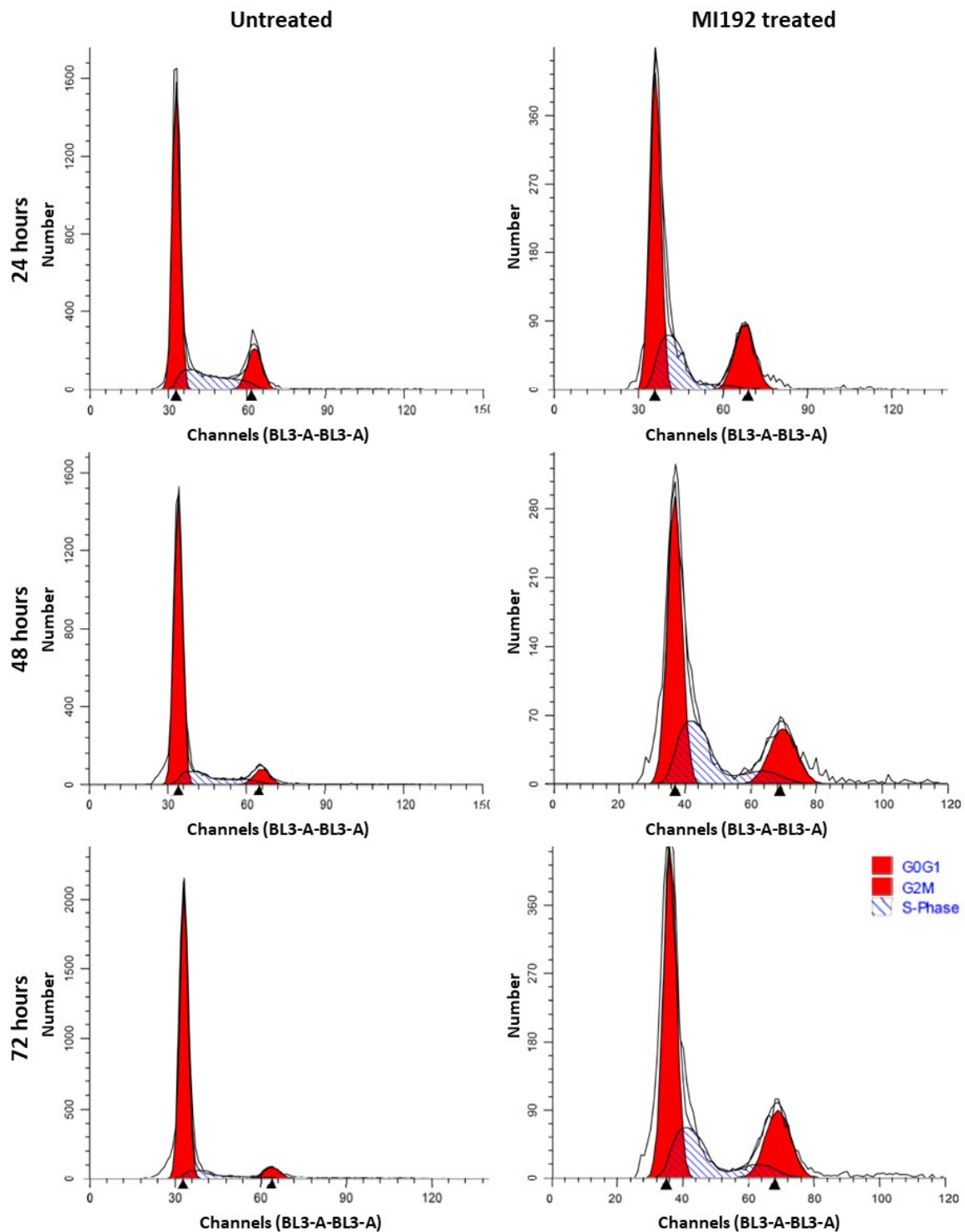


Figure 3.9 - Representative histograms from the flow cytometry analysis of hPSCs cell cycle distribution dosed with/without 2 μ M MI192 for 24, 48 and 72 hours. The first peak represents cells within the G_0/G_1 phase, the second peak represents cells in the G_2/M phase and the area between the peaks represents cells in the S phase.

3.3.1.8 - Effect of MI192 on ALPSA in hDPSCs

Cells were treated with a "safe" range of MI192 concentrations for 24 (5, 10, 20 μM) and 48 hours (1, 2, 5 μM) and then cultured in osteogenic conditions for 2 weeks, following which ALPSA was quantified. MI192 pre-treatment for 24 hours at concentrations up to 20 μM significantly reduced ALPSA (≥ 1.55 -fold) compared to that of the cells in the untreated osteogenic control group in a dose-dependent manner ($P \leq 0.001$) (Fig 3.10A). A significant reduction in ALPSA was also observed between 10 and 20 μM MI192 groups ($P \leq 0.05$).

After 48 hours pre-treatment, cells treated with 1, 2 and 5 μM MI192 showed significantly enhanced ALPSA (≥ 1.56 -fold) compared to the untreated cells cultured in osteogenic and basal medium (Fig 3.10B) ($P \leq 0.01$). Treatment with 2 and 5 μM MI192 elicited the highest ALPSA compared to the 1 μM MI192 group or the untreated controls ($P \leq 0.01$ and 0.001 respectively), although no significance was observed between 2 and 5 μM MI192 groups ($P > 0.05$). The osteogenic control group exhibited significantly increased ALPSA compared to the untreated cells cultured in basal conditions at both time points ($P \leq 0.01$). MI192 pre-treatment for 48 hours was shown to stimulate hDPSCs ALPSA in different donors shown in the Appendix (Fig A1). The optimised MI192 pre-treatment condition of 2 μM MI192 for 48 hours was used for the rest of this study.

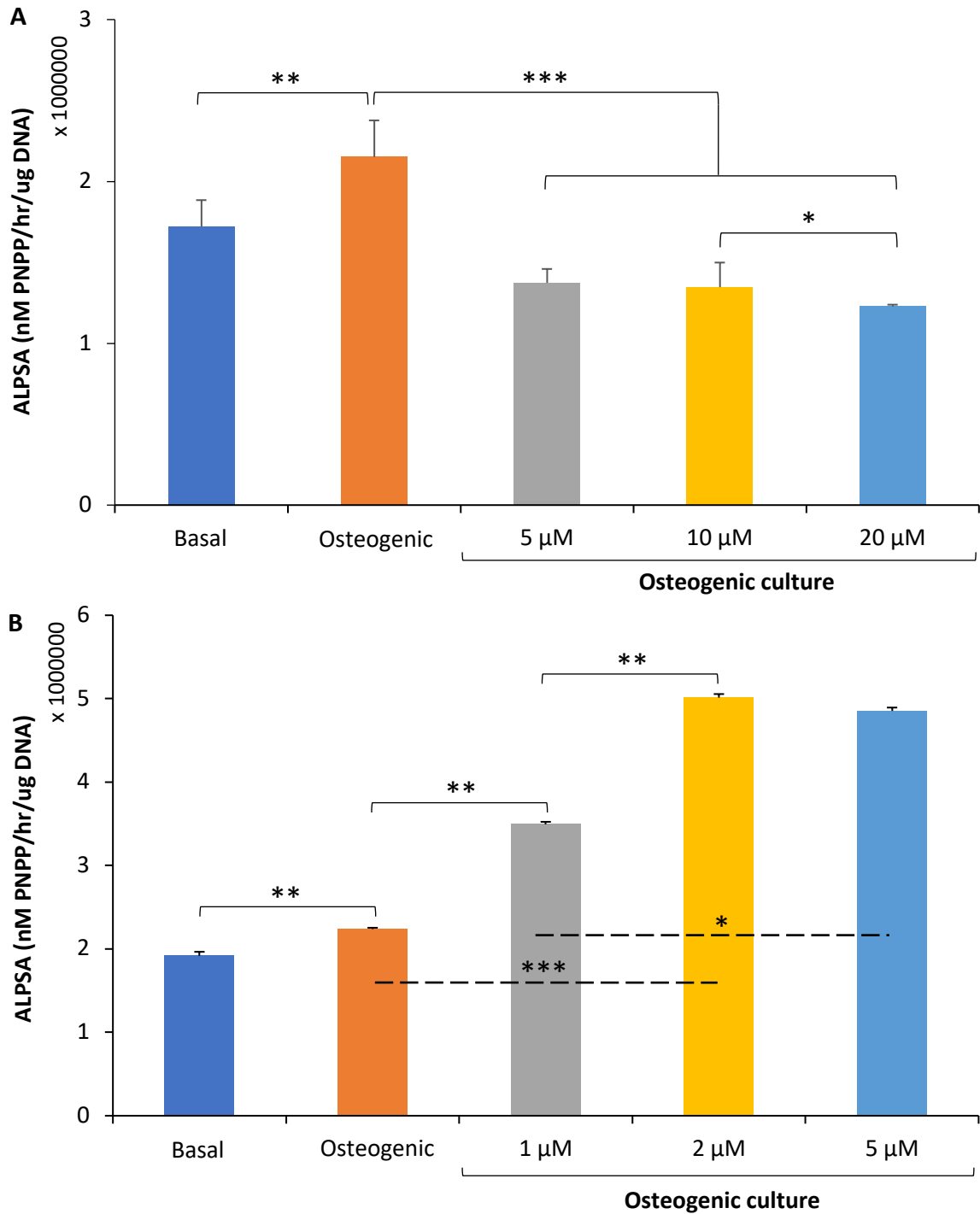


Figure 3.10 - ALPSA of hDPSCs pre-treated with/without MI192 for 24 and 48 hours prior to osteogenic culture. Cells were pre-treated with MI192 for, A) 24 hours (5, 10 and 20 μ M), B) 48 hours (1, 2 and 5 μ M) prior to culture in osteogenic medium for 2 weeks. Untreated cells cultured in basal and osteogenic medium used as controls. Data expressed as mean \pm SD (n=3). Significance levels shown are the test groups compared to the controls or between adjacent MI192 concentrations at that time point. *P \leq 0.05, **P \leq 0.01 and ***P \leq 0.001.

3.3.1.9 - Effect of MI192 on hDPSCs ALP staining

Figure 3.11 shows the ALP staining of hDPSCs pre-treated with/without 2 μ M MI192 for 48 hours, followed by 2 weeks culture in osteogenic conditions. Untreated cells cultured in osteogenic conditions were used as the control. Macroscopic image shows the MI192 pre-treated group exhibited slightly stronger global ALP staining intensity compared to the untreated control group (Fig 3.11A). The microscopic image shows MI192 pre-treated cells phenotype were much more flattened/elongated when compared to the control group with higher staining intensity located within the cells (Fig 3.11B).

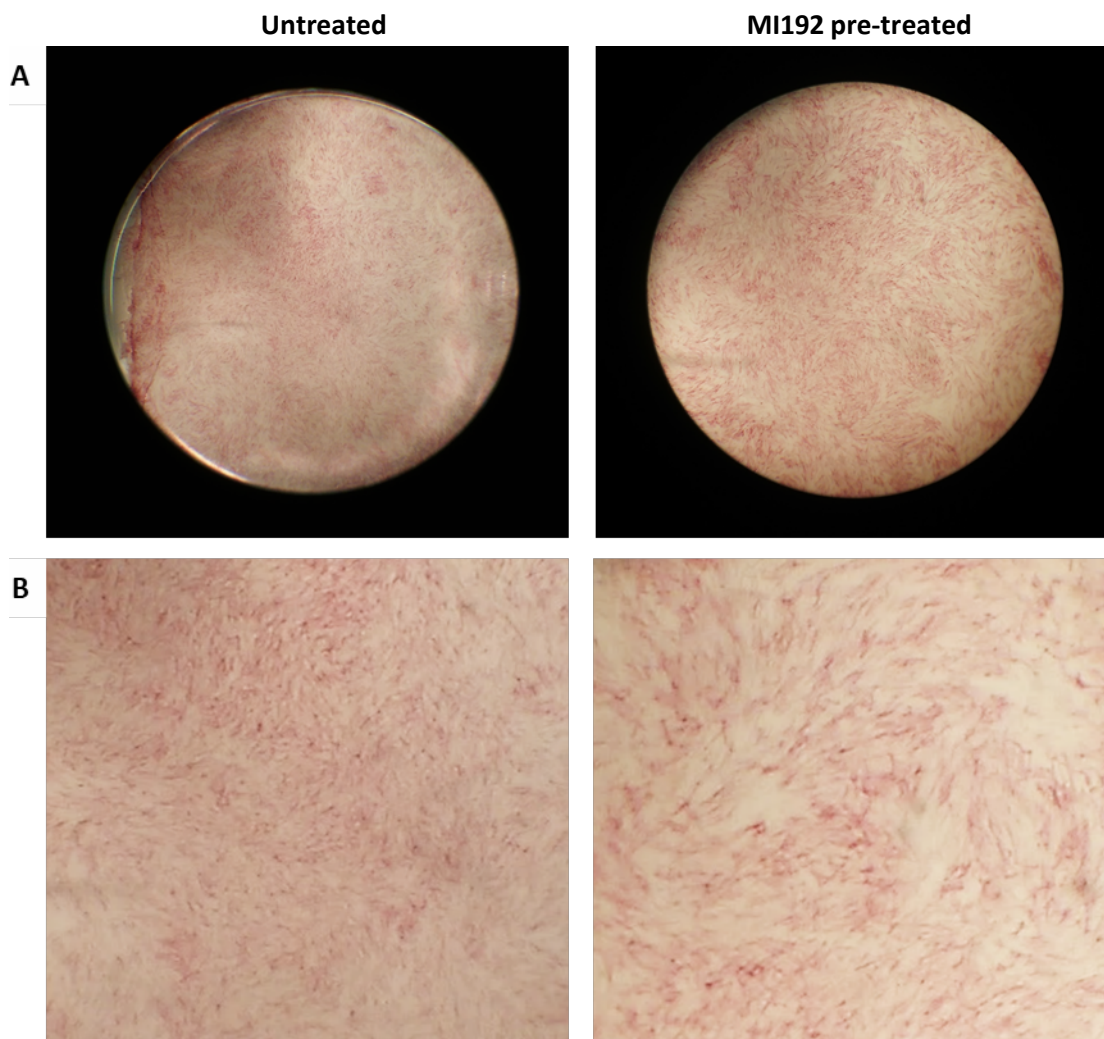


Figure 3.11 - ALP staining of hDPSCs pre-treated with/without 2 μ M MI192 for 48 hours prior to osteogenic culture for 2 weeks. A) Macroscopic image of the entire field. B) Microscopic images in high magnification (x 100).

3.3.1.10 - Effect of MI192 on the expression of osteogenic genes in hDPSCs

Cells were pre-treated with/without 2 μ M MI192 for 48 hours, following which cells were cultured in osteogenic conditions for up to 28 days. The effects of MI192 on the mRNA levels of key osteoblast-related genes (*RUNX2*, *ALP*, *BMP2*, *COL1A* and *OCN*) were assessed using RT-qPCR (Fig 3.12).

RUNX2

The *RUNX2* mRNA levels were significantly reduced in the MI192 pre-treated cells compared to that in the untreated group immediately post pre-treatment (1.24-fold) ($P \leq 0.05$). However, from day 3 to 14, the *RUNX2* mRNA levels were similar between both the untreated and MI192 pre-treated groups ($P > 0.05$). On day 21 and 28, MI192 pre-treatment significantly upregulated *RUNX2* mRNA expression (1.16- and 1.15-fold, respectively) when compared to that in the untreated cells ($P \leq 0.05$ and 0.01, respectively).

ALP

The *ALP* mRNA expression was significantly upregulated in the MI192 pre-treated cells compared to that in the untreated cells immediately after pre-treatment (1.24-fold) ($P \leq 0.05$). There was no significant difference in the expression between the test and control groups from days 3 to 14 ($P > 0.05$), where a time-dependent reduction in the *ALP* expression was observed in both groups. On day 21 and 28, the mRNA expression levels recovered, where *ALP* was significantly higher in the MI192 pre-treated cells compared to that in the control group ($P \leq 0.01$ and $P \leq 0.001$, respectively), with a time-dependent increase in the expression levels in both groups (1.17- and 1.19-fold, respectively).

BMP2

The *BMP2* mRNA expression levels were similar between the groups immediately post pre-treatment ($P > 0.05$), however following culture in osteogenic medium, the MI192 pre-treated cells exhibited a significant increase in the *BMP2* mRNA level from day 3 through day 28 (1.15-, 1.2-, 1.28-, 1.23-, 1.18- and 1.06-fold, respectively), although a time-dependent decrease in the expression level was observed from day 3 to day 14 in both groups ($P \leq 0.05$ - $P \leq 0.001$).

COL1A

The *COL1A* mRNA expression levels were significantly increased in the MI192 pre-treated cells immediately after treatment compared to that in the untreated group (3-fold) ($P \leq 0.01$). There was a significant enhancement in the *COL1A* mRNA levels in the test group compared to that in the untreated cells on day 5 and day 14 (1.1- and 1.14-fold) ($P \leq 0.05$ and $P \leq 0.01$, respectively). However, there was no significant difference between the groups at days 3, 7, 21 and 28 ($P > 0.05$). During the culture period, both groups exhibited a fluctuating expression profile.

OCN

The mRNA expression levels of *OCN* were similar between the groups on day 0 and day 3 ($P > 0.05$). However, the MI192 pre-treated group exhibited significantly enhanced *OCN* expression by approximately 1.5-fold on day 5 ($P \leq 0.05$), 1.95-fold on day 7 ($P \leq 0.001$), 1.81-fold on day 14 ($P \leq 0.001$) and 1.17-fold on day 21 ($P \leq 0.001$), compared to that in the untreated control at the same time points. A time-dependent decrease in the expression was observed in both groups from day 5 to day 14, however, the expression level increased in both groups on day 21 and declined again on day 28.

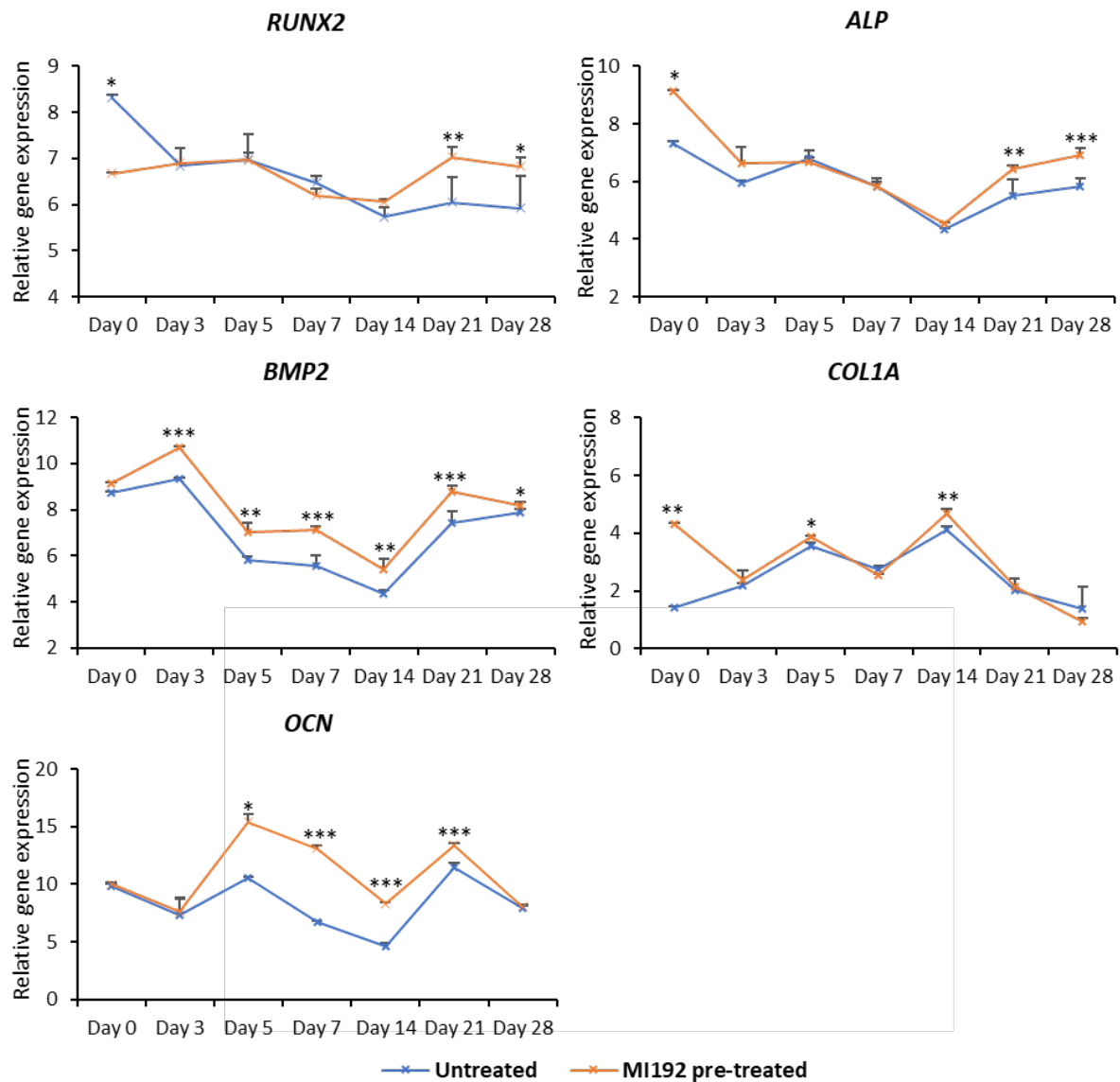


Figure 3.12 - Relative expression of osteoblast-related genes in untreated/MI192 pre-treated hDPSCs after culture in osteogenic medium. Gene expression analysed on day 0, 3, 5, 7, 14, 21 and 28. Data expressed as mean \pm SD (n=3). Significance levels shown are the test group compared to the untreated control at the same time point. *P \leq 0.05, **P \leq 0.01 and ***P \leq 0.001.

3.3.1.11 - Effect of MI192 on the expression of osteogenic proteins in hDPSCs

Cells were pre-treated with/without 2 μ M MI192 for 48 hours, following which cells were cultured in osteogenic conditions for up to 28 days. The expression of key osteoblast-related markers (Runx2, ALP, BMP2, Col1a and OCN) was also assessed at the protein level using ICW (Fig 3.13).

Runx2

MI192 pre-treatment significantly reduced the Runx2 protein levels on day 7 (1.57-fold) ($P \leq 0.01$), however, significant upregulation in the MI192 pre-treated group was observed on day 14 compared to that in the control group (1.14-fold) ($P \leq 0.05$). On day 21, the expression was reduced in the MI192 pre-treated group (1.17-fold), however, the reduction was not statistically significant ($P > 0.05$). On day 28, the expression was significantly enhanced in the MI192 pre-treated group compared to that in the untreated control (1.5-fold) ($P \leq 0.05$). A time-dependent increase in Runx2 protein expression was observed in both groups.

ALP

The ALP protein expression was significantly and consistently upregulated in the MI192 pre-treated cells on day 7, 14, 21 and 28 (1.35-, 1.21-, 1.48- and 1.51-fold, respectively) compared to that in the untreated group ($P \leq 0.01$ and $P \leq 0.001$). Both groups exhibited a time-dependent increase in ALP protein expression levels.

BMP2

The MI192 pre-treated groups exhibited significantly enhanced BMP2 protein expression compared to that in the untreated cells at each time point assessed (1.43-, 1.68-, 2.16- and 1.35-fold, respectively) ($P \leq 0.01$ for days 7 and 14, $P \leq 0.001$ for day 21 and $P \leq 0.01$ for day 28). A time-dependent increase in the BMP2 expression was observed in both groups, with the peak expression levels observed on day 21 and 28 for the MI192 pre-treated and untreated cells, respectively.

Col1a

The Col1a protein expression levels were significantly upregulated in the MI192 pre-treated cells on days 7, 14, 21 and 28 compared to the expression in the untreated group at each time point ($P \leq 0.01$, $P \leq 0.001$, $P \leq 0.01$, and $P \leq 0.01$, respectively). In both groups, cells exhibited a fluctuating protein expression profile throughout the culture period, with the MI192 pre-treated cells displaying increased expression levels at each time point compared to the control (2.24-, 1.71-, 3.15- and 2.17-fold, respectively).

OCN

The OCN protein expression levels were significantly elevated in the MI192 pre-treated group (2.12-, 1.15-, 1.26- and 1.4-fold, respectively) compared to that in the untreated cells on day 7, 14, 21 and 28 ($P \leq 0.01$ - $P \leq 0.001$). A time-dependent increase in the OCN protein expression levels was observed in both MI192 pre-treated and untreated hDPSCs.

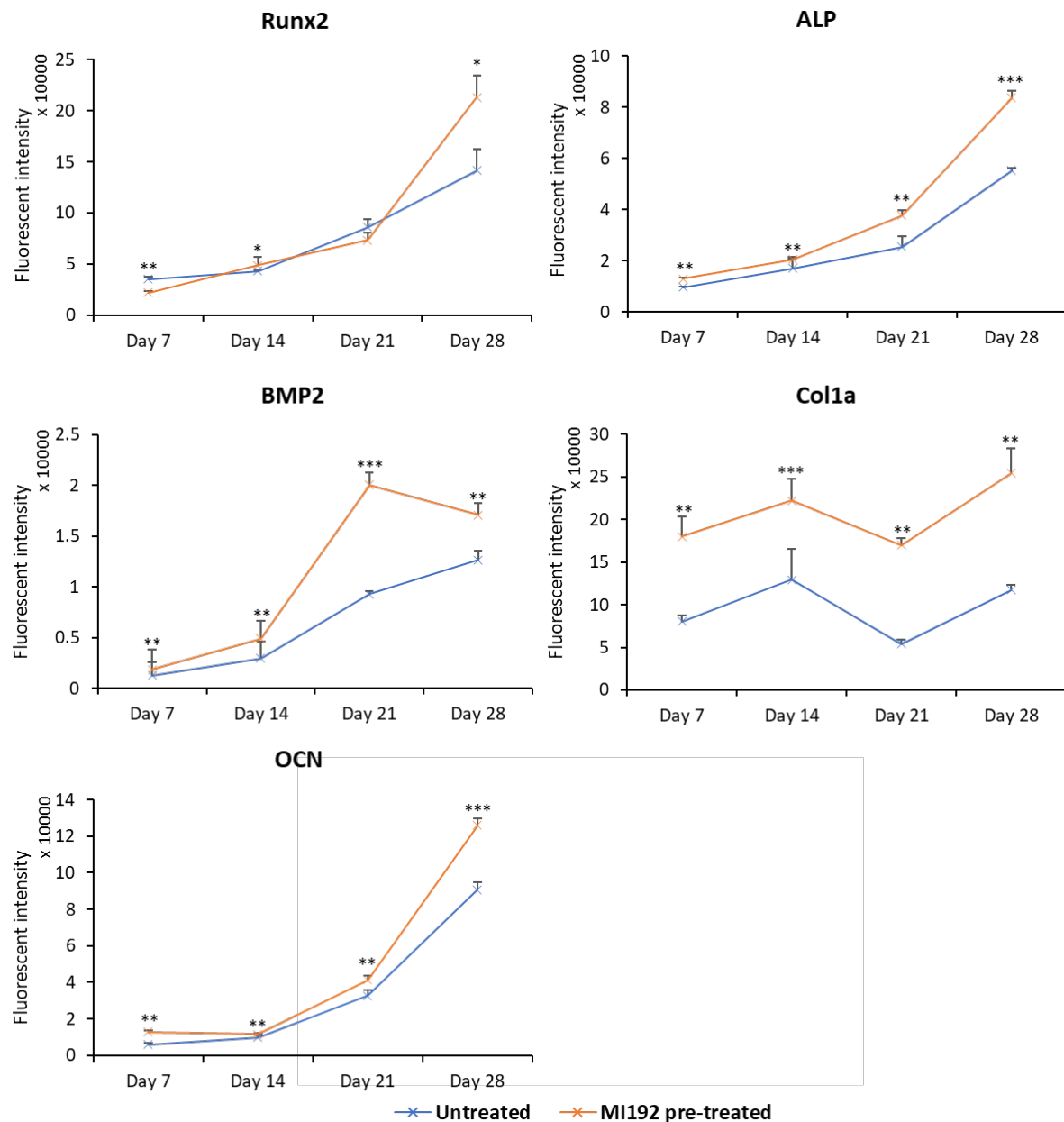


Figure 3.13 - Protein expression of osteoblast-related markers in untreated/MI192 pre-treated hDPSCs after culture in osteogenic medium. Protein expression levels analysed on day 7, 14, 21 and 28. Data expressed as mean \pm SD (n=3). Significance levels shown are the test group compared to the untreated control at the same time point. * $P \leq 0.05$, ** $P \leq 0.01$ and *** $P \leq 0.001$.

3.3.1.12 - Effect of MI192 on hDPSCs calcium deposition and mineralisation

After 48 hours pre-treatment with/without 2 μ M MI192 followed by 28 days in osteogenic conditions, calcium accumulation was identified via Alizarin red staining. Figure 3.14A shows the MI192 pre-treated hDPSCs possessed extensive red staining for calcium accumulation throughout when compared to the untreated cells after 28 days in osteogenic conditions. Numerous nodule-like formations (black arrow) was observed within the MI192 pre-treated group, while a fewer number of nodules are visible in the untreated cells.

The Alizarin red stained samples were de-stained, allowing for quantification of calcium accumulation. Following Alizarin red semi-quantification, the calcium accumulation within the MI192 pre-treated group was significantly enhanced when compared to the untreated group (4.75-fold) (Fig 3.14B) ($P \leq 0.001$).

Following Von Kossa staining for functional mineral nodules, more extensive black staining was observed in the MI192 pre-treated group compared to the untreated cells (Fig 3.15). The MI192 pre-treated group exhibited an increased number of mineral nodules (red arrows) compared to the untreated cells, distributed uniformly throughout. Moreover, the HDACi pre-treated group exhibited increased Van Gieson's staining (pink) intensity throughout for collagen deposition compared to the untreated control, particularly situated with increased intensity in close proximity to the mineral nodules.

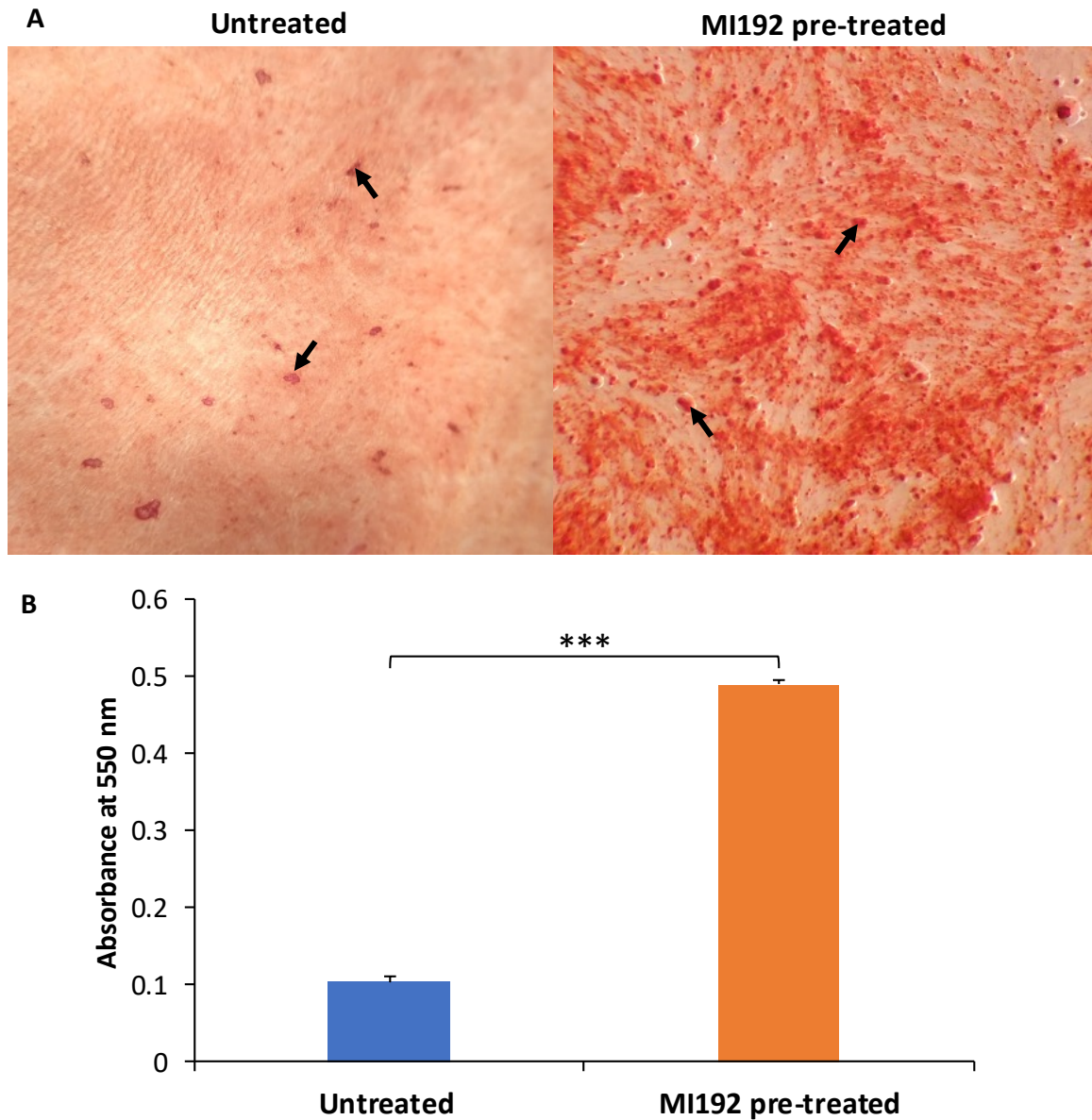


Figure 3.14 - Effect of MI192 pre-treatment on hDPSCs calcium deposition. (A) Alizarin red staining. Nodule-like formations highlighted by black arrows. Microscopic images at x 100. (B) Semi-quantitative analysis of Alizarin red stained untreated/MI192 pre-treated hDPSCs after 28 days osteogenic culture. Data expressed as mean \pm SD (n=3). ***P \leq 0.001.

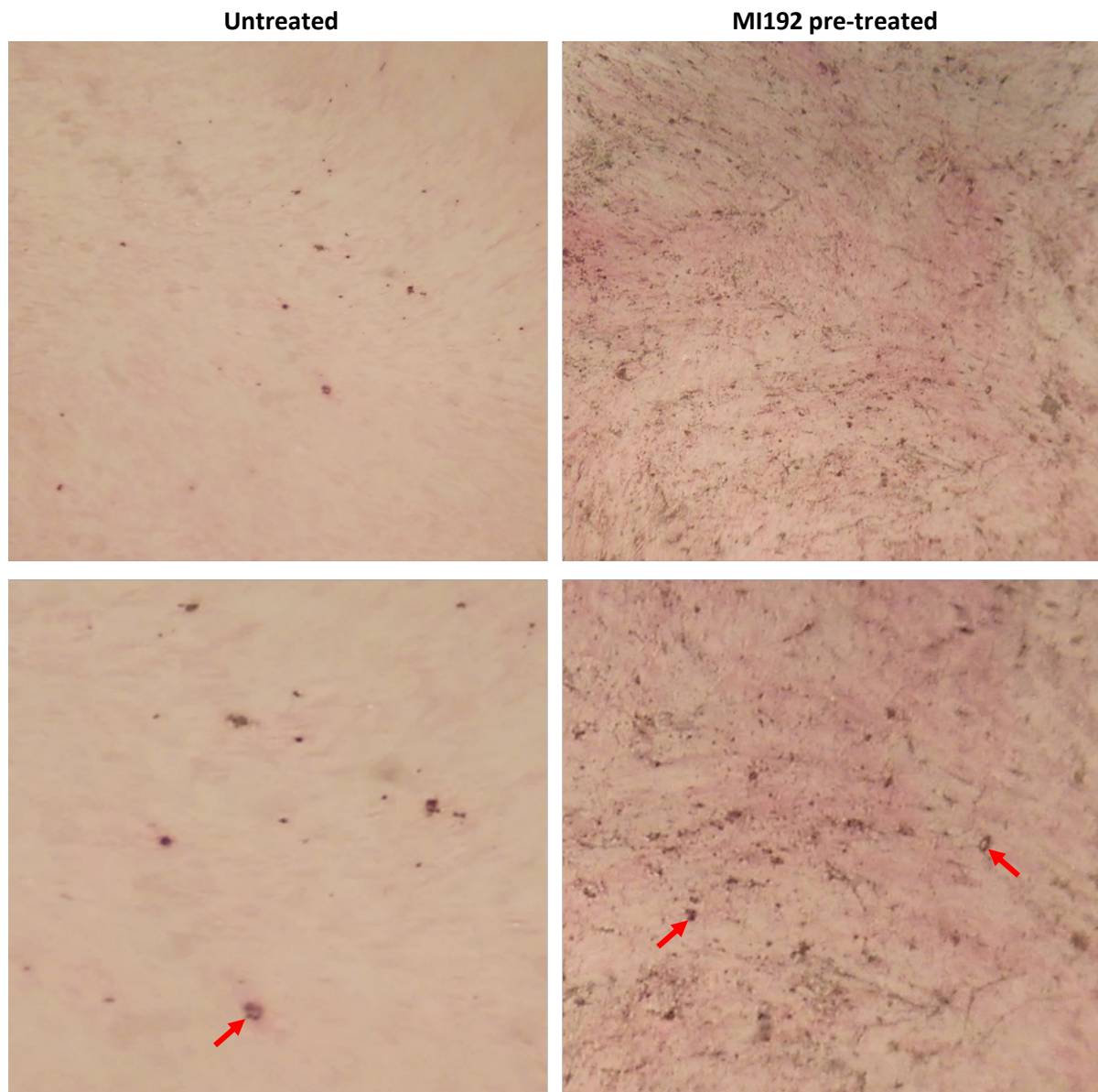


Figure 3.15 - Effect of MI192 pre-treatment on hDPSCs mineral nodule formation. Von Kossa staining (black) of untreated/MI192 pre-treated hDPSCs after culture in osteogenic medium for 28 days. Mineral nodule formation indicated by the red arrows. Van Gieson's counterstaining to identify collagen deposition (pink). Microscopic images at x 100 (top row) and x 200 (bottom row).

3.3.2 - The Effects of MI192 on hDPSCs Osteogenic Differentiation in the Lyophilised Silk Scaffolds

3.3.2.1 - Porosity and pore morphology of lyophilised silk scaffolds

SEM analysis of the silk scaffold revealed a highly porous structure, with a network of thin sheet-like lamellae (Fig 3.16). The thickness of the silk lamellae tended to decrease with silk concentration.

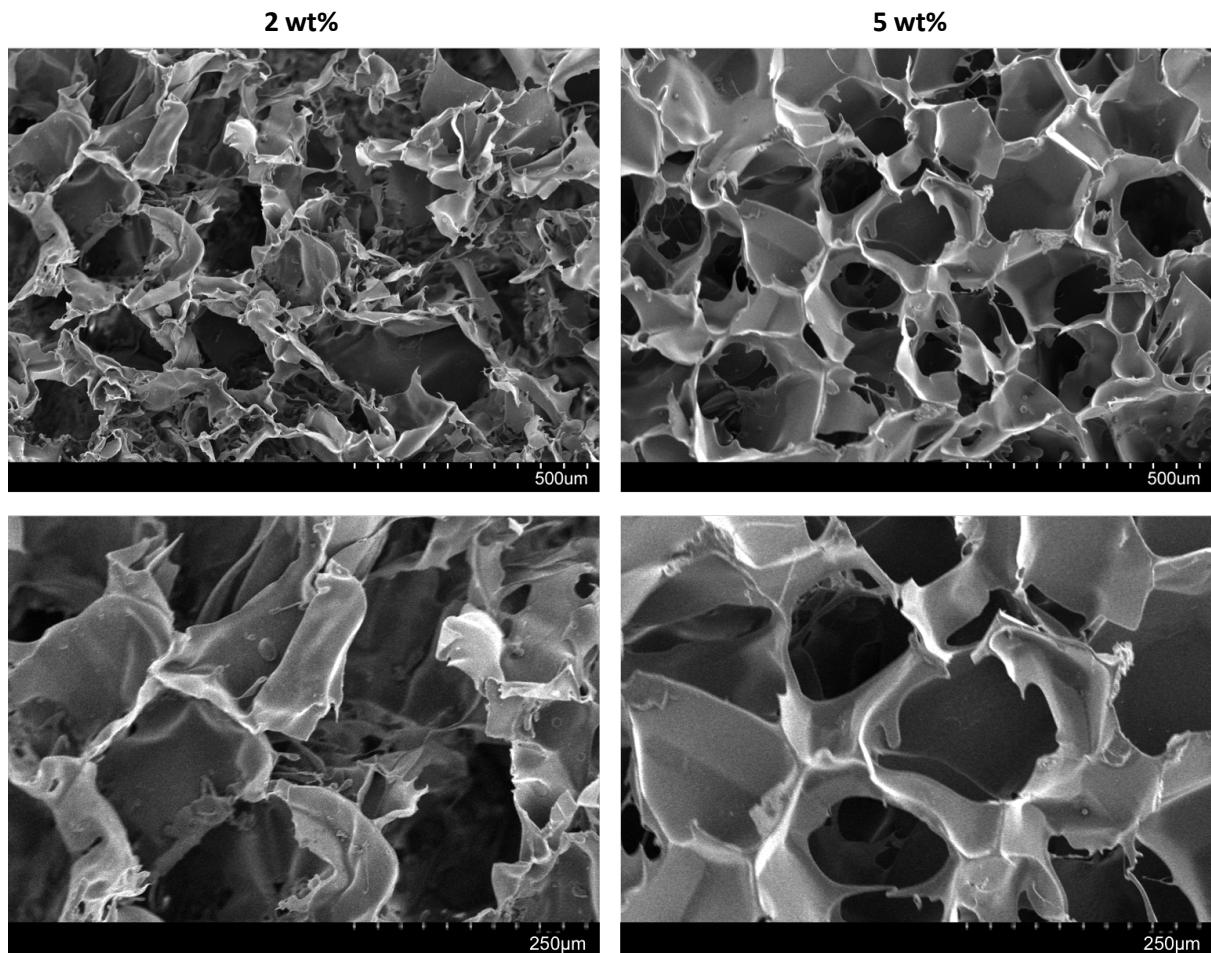


Figure 3.16 - Pore morphology and porosity of 2 and 5 wt% lyophilised silk scaffolds. SEM micrographs of lyophilised silk scaffolds showing an interconnected network of thin sheet-like lamellae. Scale bars = 500 (top row) and 250 μm (bottom row), respectively.

3.3.2.2 - Effects of silk concentration on scaffold swelling and degradation properties

Figure 3.17A shows the fold increase in mass following hydration of dry scaffolds in H₂O and PBS. The 5 wt% group exhibited a significant decrease in the mass of scaffolds following hydration in H₂O or PBS when compared to the 2 wt% scaffolds in the same conditions ($P \leq 0.001$). The 2 wt% silk scaffolds absorbed 31.1 ± 2.0 (mean \pm SD) and 31.76 ± 0.4 times their mass in H₂O and PBS, respectively. The 5 wt% scaffolds absorbed 17.2 ± 0.4 and 17.2 ± 0.5 times their mass in water and PBS, respectively.

To evaluate the effects of silk concentration on lyophilised scaffold degradation, *in vitro* degradation in the presence of Protease XIV was investigated (Fig 3.17B). Degradation of the silk sponges was assessed after exposure to Protease XIV for 2, 4, 6 or 8 days, showing the percent remaining mass. At each time point, the remaining mass of 2 wt% silk scaffolds was significantly lower than that of 5 wt% scaffolds ($P \leq 0.05 - 0.001$).

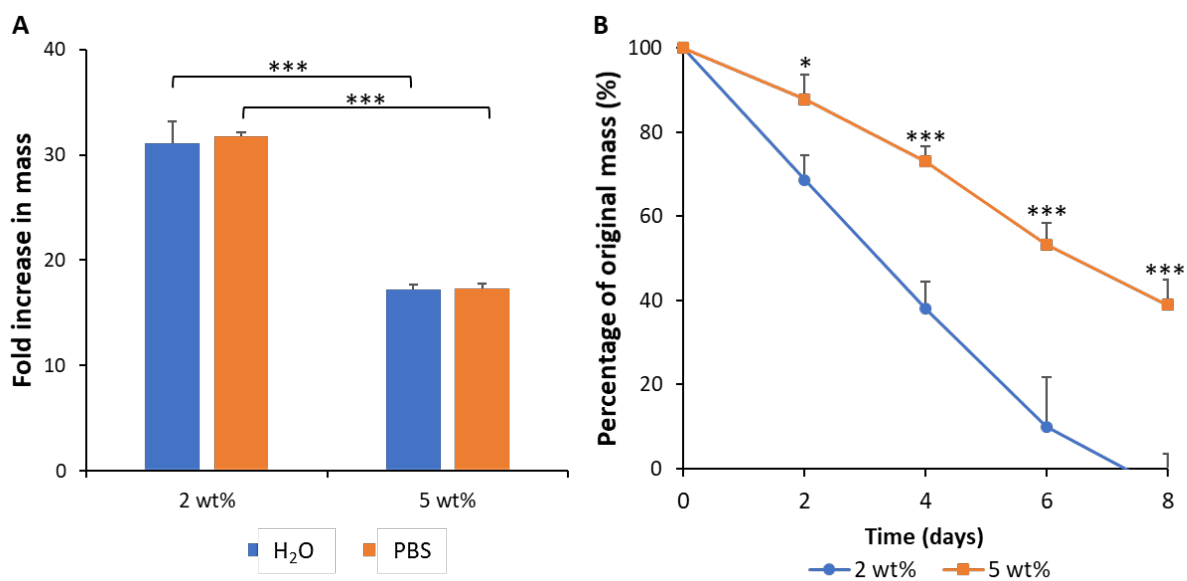


Figure 3.17 - Effect of silk concentration on scaffold swelling and degradation properties. A) Increasing silk concentration decreases scaffold swelling capacity in both H₂O and PBS conditions. Data expressed as mean \pm SD (n=5). Significance determined between difference wt% scaffolds in the same swelling conditions. B) Increasing silk concentration reduces *in vitro* degradation rate. Data expressed as mean \pm SD (n=5). Significance determined between the different wt% scaffolds at each time point. * $P \leq 0.05$ and *** $P \leq 0.001$.

3.3.2.3 - Mechanical properties of lyophilised silk scaffolds

When compressed to 90% of their original size, 5 wt% silk scaffolds were stronger and less elastic than 2 wt% group (Fig 2.8). The compression modulus of 5 wt% scaffolds was 34.52 ± 4.52 kPa (mean \pm SD) and was significantly higher than that of 2 wt% silk scaffolds which showed a modulus of 8.07 ± 0.71 kPa (4.3-fold) ($P \leq 0.001$).

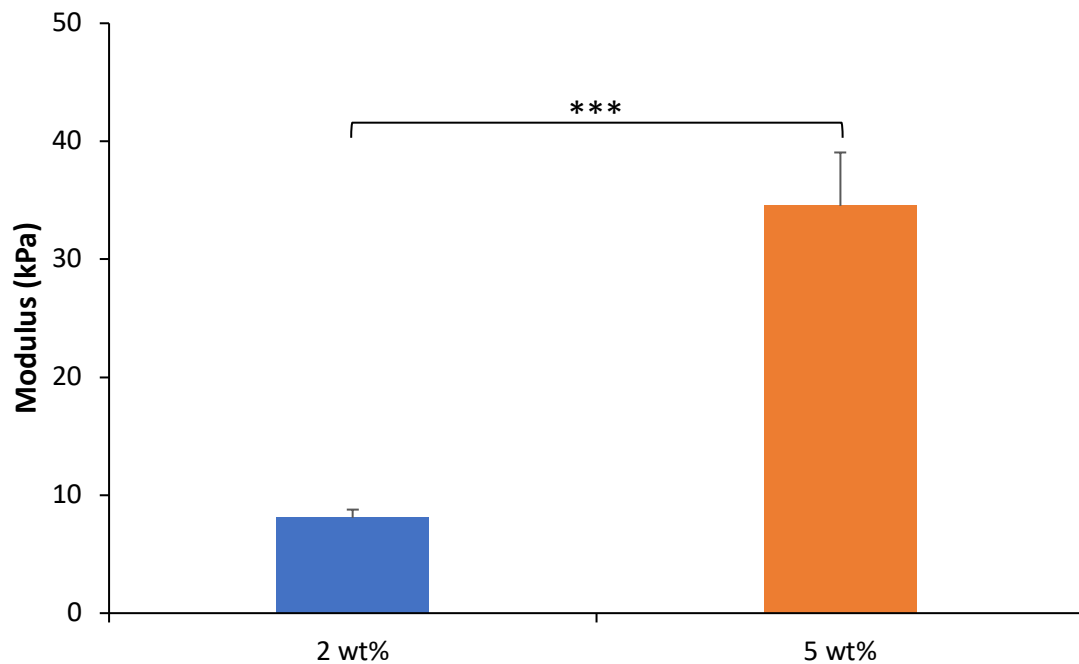


Figure 3.18 - Effect of silk concentration on scaffold compressive modulus. Increasing silk concentration enhanced the compressive modulus of silk scaffolds. Data expressed as mean \pm SD ($n=6$). *** $P \leq 0.001$.

3.3.2.4 - Assessment of hDPSCs viability and distribution within the silk scaffolds

MI192 pre-treated and untreated hDPSCs were seeded on both wt% scaffolds and labelled with CFMDA to visualise viable cells 24 hours post seeding and after 6 weeks in osteogenic culture (Fig 3.19). The interconnectivity of silk was confirmed by the ingrowth/penetration of fluorescently labelled cells attached to the internal lamellae network of the scaffold. Within the 2 wt% group, viable cells in both groups are well distributed throughout, with the majority of the cells exhibiting an elongated morphology after 24 hours, although a small number of cells possessed a circular morphology (Fig 3.19A). The cell density between the groups at this time point was similar. After 6 weeks osteogenic culture, cells exhibited a fibroblastic-like morphology and were more uniformly distributed throughout the scaffold compared to the previous time point. The MI192 pre-treated cells exhibited a slighter larger/elongated morphology compared to the untreated group at both time points.

Within the 5 wt% group, viable cells were observed in both groups distributed throughout the scaffold after 24 hours post seeding (Fig 3.19B). There were two distinct cellular morphologies at this time point, circular and fibroblastic. At this time point, a higher cell density was observed in the 2 wt% scaffold compared to the higher wt% group. After 6 weeks osteogenic culture, both cell groups exhibited a more fibroblastic-like morphology which was uniformly distributed throughout the scaffold, with an increased cell density compared to 24 hours post seeding. Within the 5 wt% group, cells appeared slightly larger when compared to the same cells in the 2 wt% scaffold after 6 weeks osteogenic culture. Moreover, MI192 pre-treated cells exhibited a slightly larger/elongated morphology when compared to untreated cells. Similar to the observations 24 hours post seeding, a lower cell density was observed in the 5 wt% scaffold compared to the 2 wt% group after 6 weeks osteogenic culture.

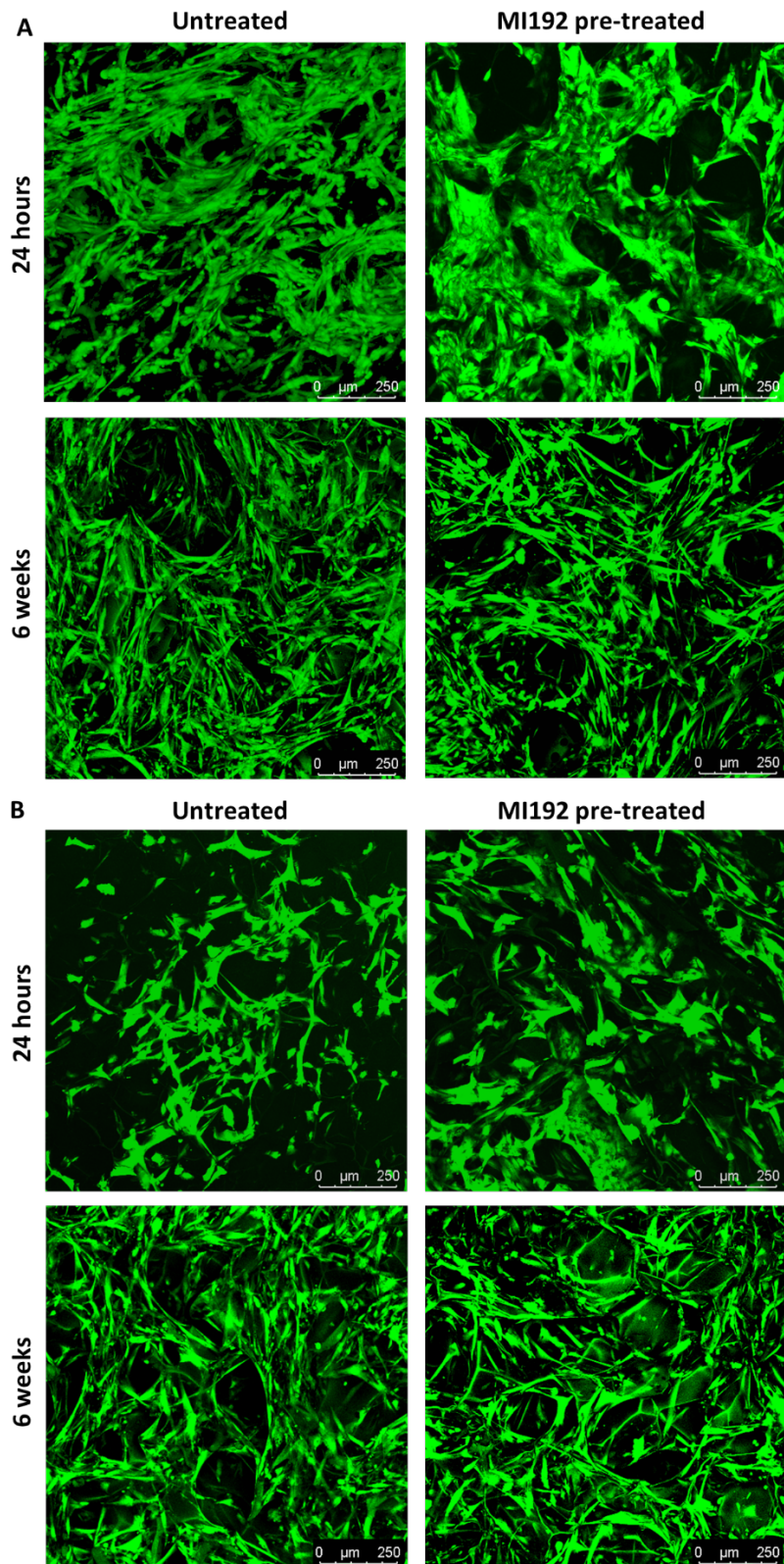


Figure 3.19 - Fluorescent imaging of viable untreated/MI192 pre-treated hDPSCs (green colour) within the (A) 2 wt% and (B) 5 wt% silk scaffolds. Viable hDPSCs on 2 and 5 wt% silk constructs after 24 hours and 6 weeks in osteogenic culture. Scale bar = 250 μm.

3.3.2.5 - The effect of MI192 pre-treatment on hDPSCs ALPSA within the 2 and 5 wt% silk scaffolds

Figure 3.20 shows the ALPSA of untreated/MI192 pre-treated hDPSCs cultured within 2 and 5 wt% silk sponges for 2 weeks in osteogenic culture. Within the 2 wt% group, MI192 pre-treated cells exhibited significantly enhanced ALPSA when compared to untreated cells (2.17-fold) ($P \leq 0.001$). A similar profile was observed in the 5 wt% scaffolds, where MI192 pre-treated cells possessed a significantly increased ALPSA (1.93-fold) compared to the untreated group ($P \leq 0.001$). The untreated and MI192 pre-treated cells on the 5 wt% scaffolds displayed significantly higher ALPSA when compared to the respective cells on the 2 wt% scaffolds (1.43- and 1.27-fold, respectively) ($P \leq 0.001$).

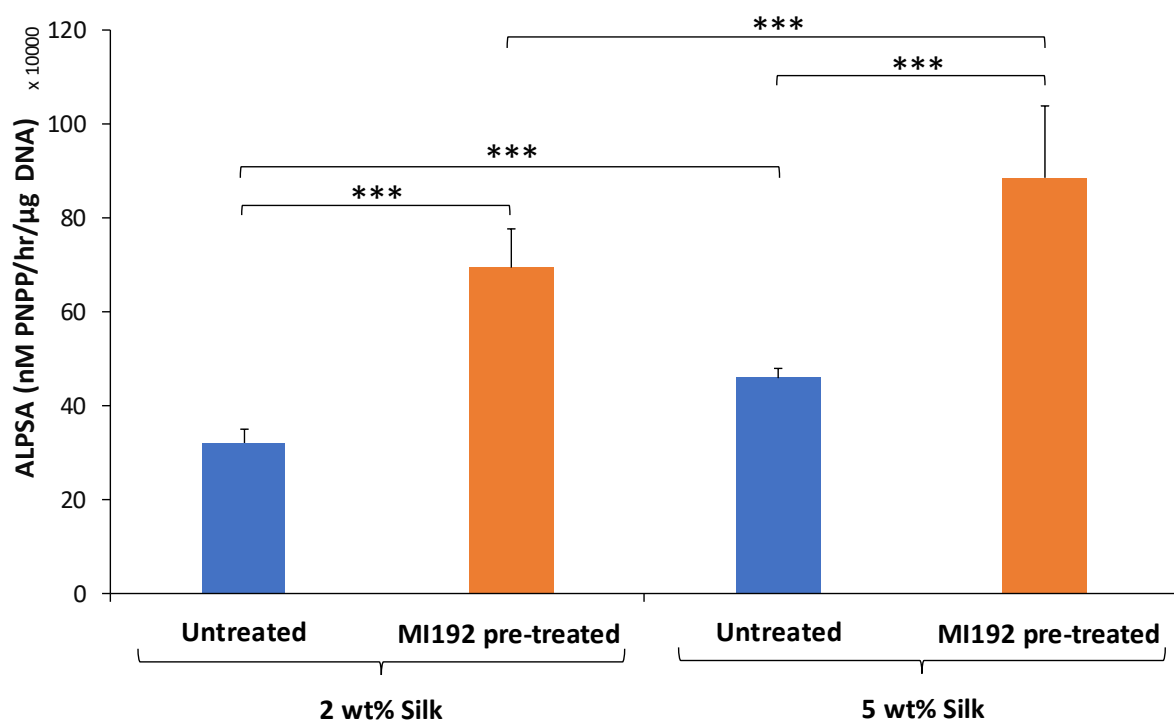


Figure 3.20 - ALPSA in untreated/MI192 pre-treated hDPSCs cultured within the 2 and 5 wt% silk constructs under osteogenic conditions for 2 weeks. Data expressed as mean \pm SD (n=4). The significance levels shown are the test group compared to the untreated control within each wt% scaffold and between the same cells in different wt% scaffolds. *** $P \leq 0.001$.

3.3.2.6 - The effect of MI192 on hDPSCs osteogenic gene expression within the silk scaffold

The mRNA levels of osteoblast-related genes (*RUNX2*, *ALP*, *BMP2*, *COL1A* and *OCN*) were assessed within untreated and MI192 pre-treated hDPSCs cultured within the 5 wt% silk scaffold throughout 14 days osteogenic culture (Fig 3.21).

RUNX2

The *RUNX2* mRNA expression levels were reduced in the MI192 pre-treated group compared to that in the untreated cells after 3 days of osteogenic culture, however not significantly ($P > 0.05$). On day 7, the MI192 pre-treated cells showed significantly upregulated *RUNX2* mRNA expression compared to that in the untreated cells (1.18-fold) ($P \leq 0.001$). The expression levels were significantly reduced in the MI192 pre-treated cells compared to that in the untreated group on day 10 (1.14-fold) and 14 (1.11-fold) ($P \leq 0.001$ in both cases). The peak *RUNX2* expression was observed on day 7 and day 10 in the MI192 pre-treated and untreated cells, respectively.

ALP

The *ALP* mRNA expression levels were significantly downregulated in the MI192 pre-treated group compared to that in the untreated cells after 3 days of osteogenic culture (1.26-fold) ($P \leq 0.001$). After 7 days culture, the MI192 pre-treated cells exhibited a significant upregulation in *ALP* expression compared to that in the untreated group (1.49-fold) ($P \leq 0.001$). A significant reduction in *ALP* mRNA expression was observed in the MI192 pre-treated cells compared to the expression observed within the untreated cells on day 10 (1.22-fold) ($P \leq 0.001$), while no significant difference in expression was observed on day 14 ($P > 0.05$). The peak *ALP* expression was observed in the MI192 pre-treated and untreated groups on day 7 and day 3, respectively.

BMP2

After 3 days osteogenic culture, the *BMP2* mRNA levels were significantly reduced in the MI192 pre-treated cells (1.24-fold) ($P \leq 0.001$), however, on day 7, *BMP2* expression was significantly increased in the MI192 pre-treated group compared to that in the untreated cells (1.23-fold) ($P \leq 0.001$). On day 10, *BMP2* mRNA levels were significantly reduced in the MI192 pre-treated cells compared to that in the untreated group (1.15-fold) ($P \leq 0.05$), however, no significance was observed on day 14 ($P > 0.05$). The *BMP2* peak mRNA expression levels were observed on day 7 and day 10 for the MI192 pre-treated and untreated cells, respectively.

COL1A

The *COL1A* mRNA expression levels were increased in the MI192 pre-treated group after 3 days osteogenic culture, however not significantly compared to that in the untreated cells ($P > 0.05$). On day 7 and 10, mRNA expression levels were significantly upregulated in the MI192 pre-treated group compared to that in the untreated control (1.85- and 1.66-fold) ($P \leq 0.01$ - 0.001), while on day 14 expression levels were similar between the groups ($P > 0.05$). Within both groups, the *COL1A* mRNA expression peaked at day 10.

OCN

The *OCN* mRNA expression levels were similar between the groups on day 3 ($P > 0.05$), however, on day 7 the MI192 pre-treated cells exhibited a significantly upregulated mRNA level when compared to that in the untreated group (1.13-fold) ($P \leq 0.01$). On day 10 and 14, *OCN* mRNA levels were significantly increased in the MI192 pre-treated cells compared to that in the untreated group (1.11- and 1.18-fold) ($P \leq 0.05$). A time-dependent increase in *OCN* mRNA expression was observed in both groups, with peak expression observed on day 10.

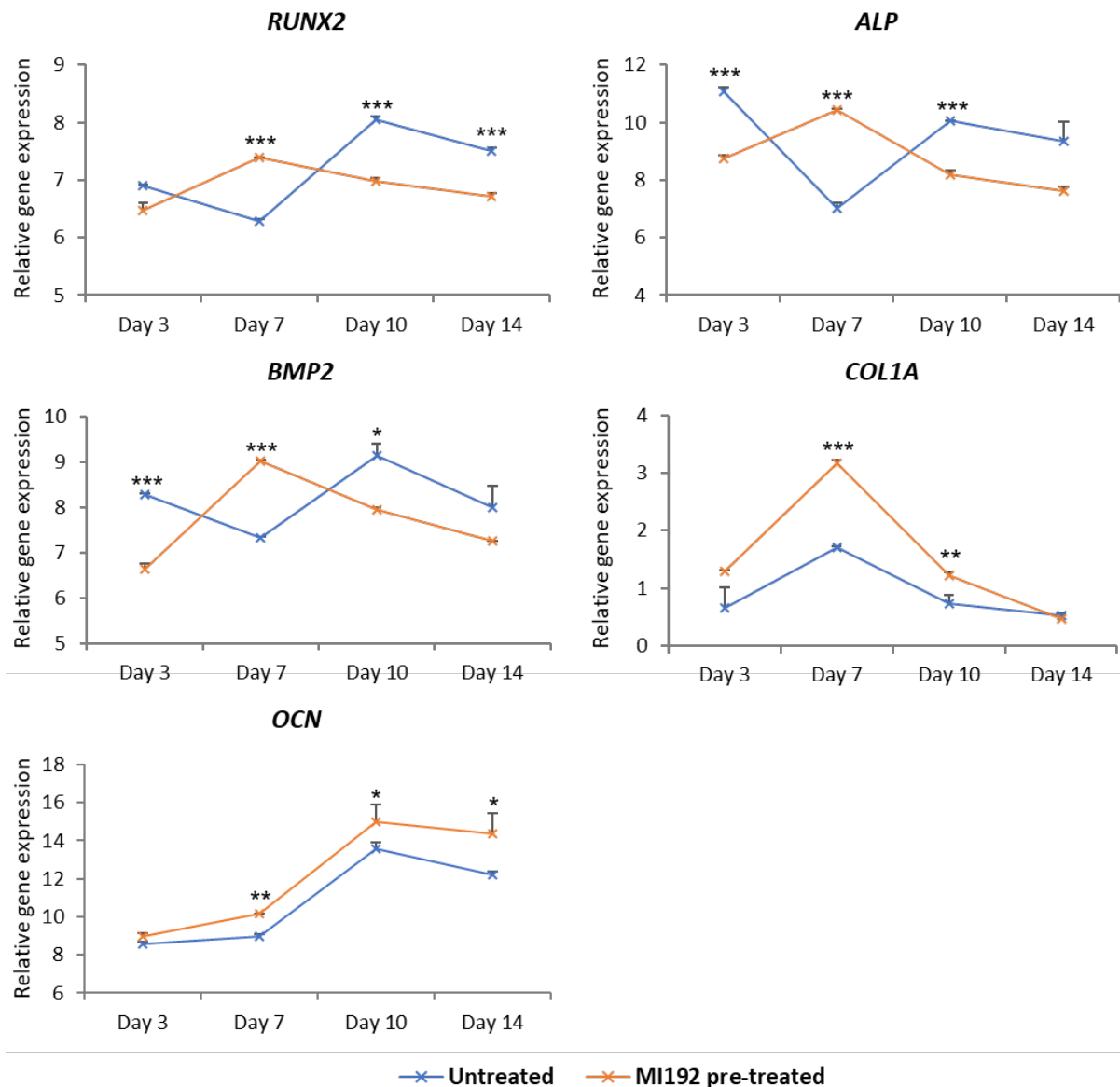


Figure 3.21 - Relative expression of osteoblast-related genes in untreated/MI192 pre-treated hDPSCs cultured within the 5 wt% silk scaffolds throughout osteogenic culture. Gene expression analysed on day 3, 7, 10 and 14. Data expressed as mean \pm SD (n=4). Significance levels shown are the test group compared to the untreated control at the same time point. * $P \leq 0.05$, ** $P \leq 0.01$ and *** $P \leq 0.001$.

3.3.2.7 - The effect of MI192 on hDPSCs tissue formation within the silk scaffold

H&E staining showed that both the MI192 pre-treated and untreated hDPSCs were able to penetrate the 5 wt% scaffolds completely after 6 weeks osteogenic culture (Fig 3.22). Cells within the scaffolds were able to attach to the internal porous structure and migrate through the pores. The cell densities between the groups were similar.

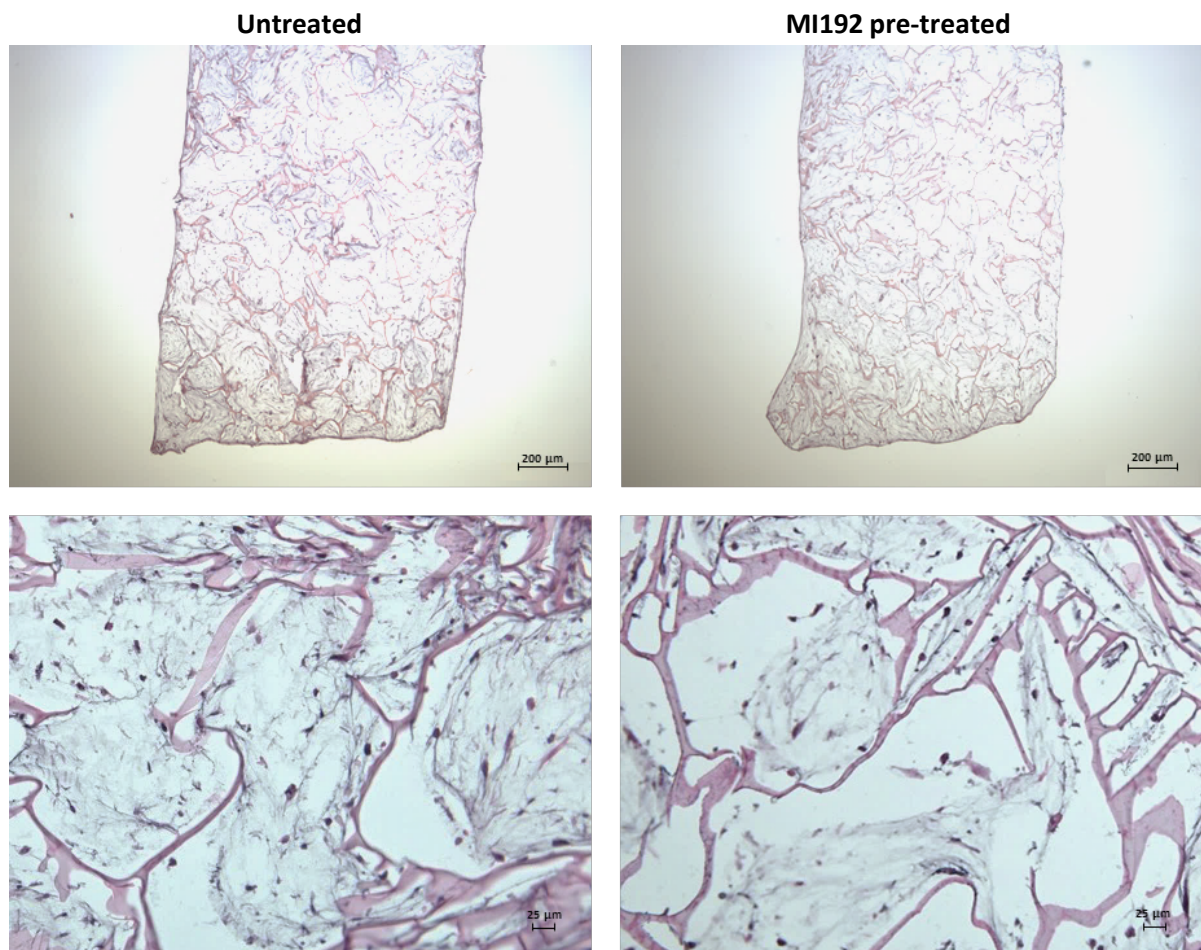


Figure 3.22 - H&E staining of untreated/MI192 pre-treated hDPSCs within the 5 wt% silk scaffolds after 6 weeks osteogenic culture. Silk scaffold stained a pink colour and tissues stained a lighter purple colour. Scale bars = 200 (top row) and 25 μm (bottom row), respectively.

Picrosirius red/Alcian blue staining was performed to assess the effects of MI192 pre-treatment on the expression of collagens and GAGs in hDPSCs within 5 wt% silk scaffolds after 6 weeks osteogenic culture (Fig 3.23). Both groups displayed strong Picrosirius red staining for collagens throughout the scaffold, with particularly strong staining intensity located at the periphery of the construct. The MI192 pre-treated group exhibited more uniform Picrosirius red staining throughout the construct compared to the untreated control. There was little Alcian blue staining for GAG expression in both groups.

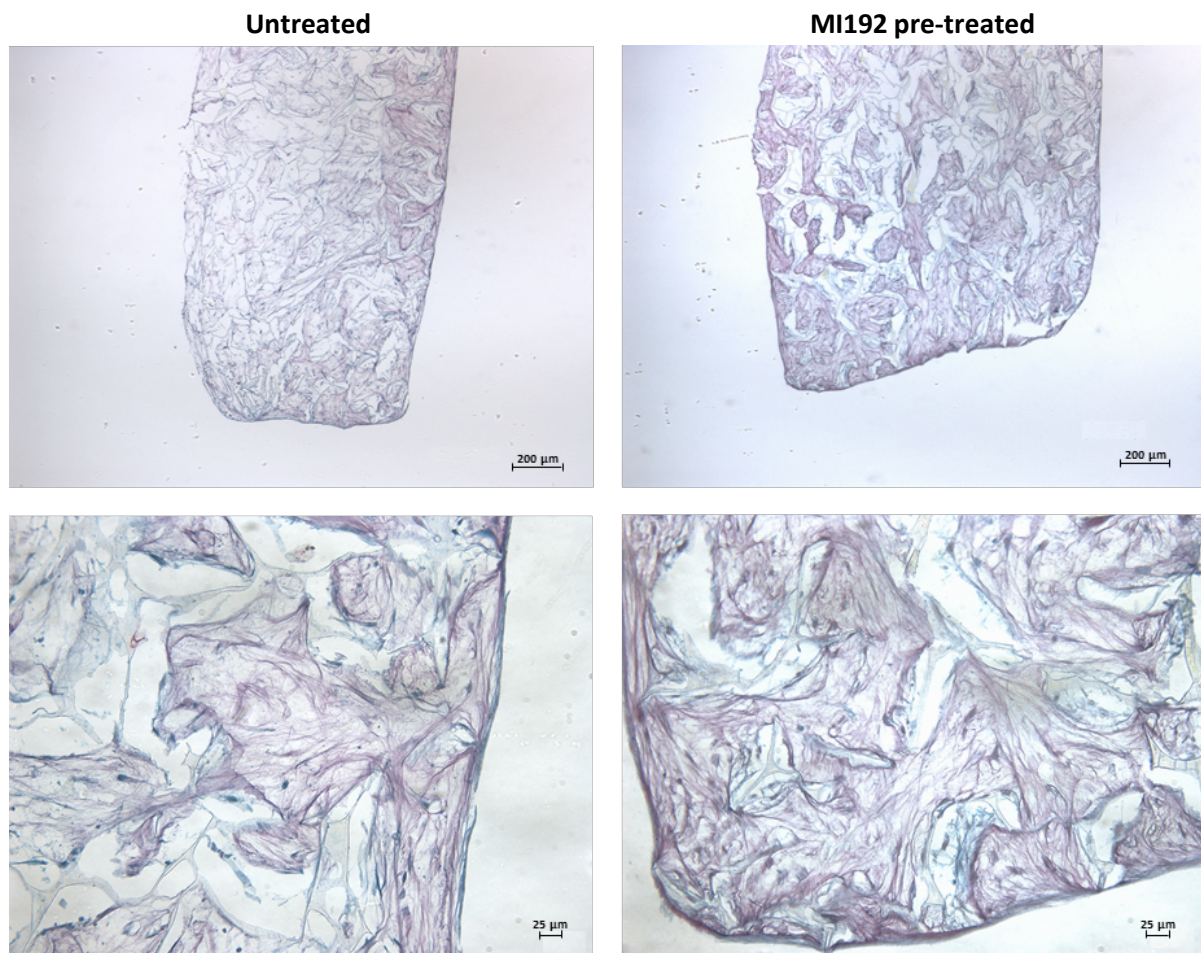


Figure 3.23 - Picrosirius red/Alcian blue staining of untreated/MI192 pre-treated hDPSCs within the 5 wt% silk scaffold after 6 weeks osteogenic culture. Collagens and GAGs stained with Picrosirius red and Alcian blue, respectively. Scale bars = 200 (top row) and 25 μm (bottom row), respectively.

3.3.2.8 - The effect of MI192 on hDPSCs osteogenic protein expression within the silk scaffold

ALP

Within the 5 wt% scaffolds, both the MI192 pre-treated and untreated groups exhibited positive ALP expression throughout the scaffolds, with the strongest staining intensity located at the periphery of the construct (Fig 3.24). Between the groups, the MI192 pre-treated construct exhibited a stronger global ALP staining intensity when compared to the untreated control.

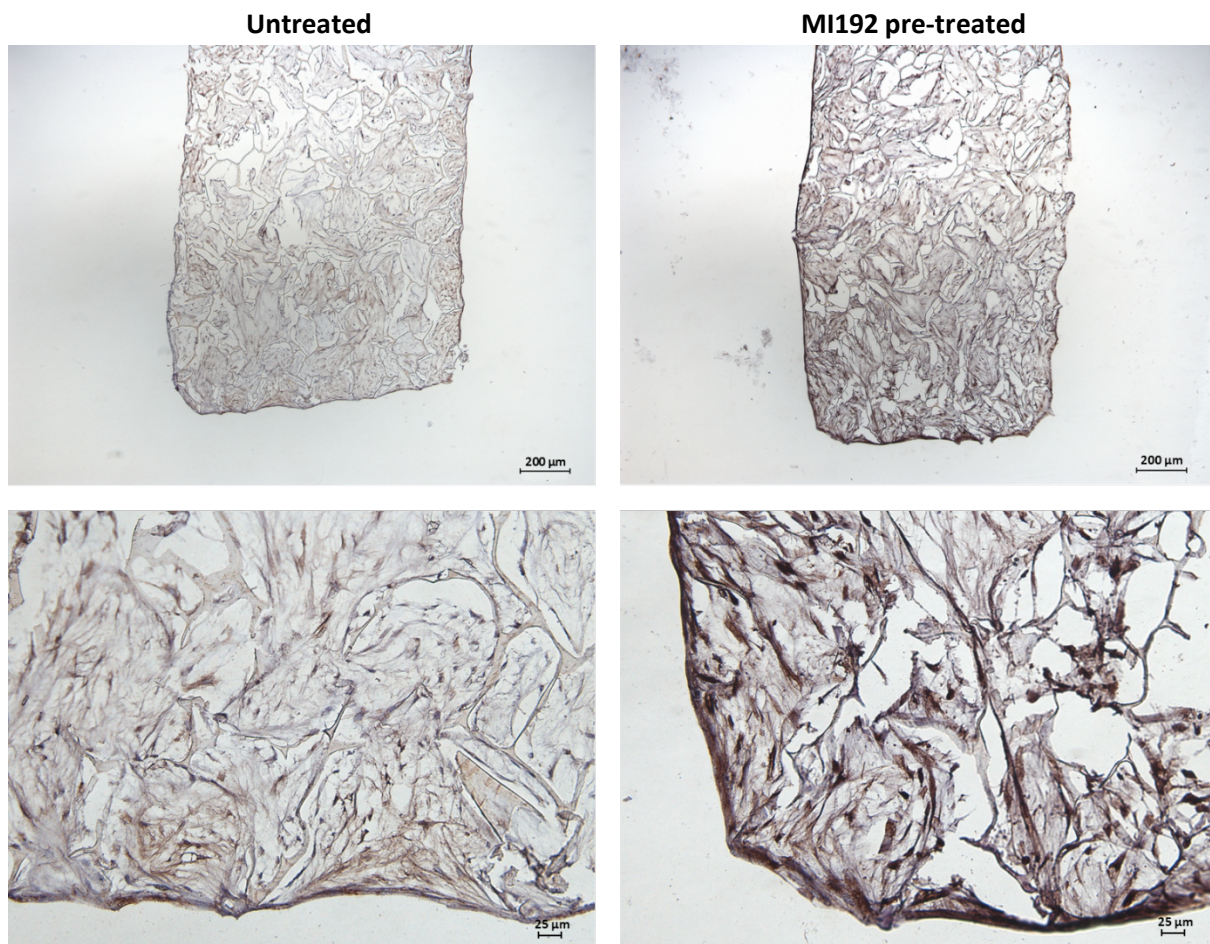


Figure 3.24 - ALP immunohistochemical staining of untreated/MI192 pre-treated hDPSCs cultured within the 5 wt% silk scaffolds after 6 weeks osteogenic culture. Positive ALP immunohistochemical staining (brown), with a weak Harris haematoxylin counterstain (purple). Scale bars = 200 (top row) and 25 μm (bottom row), respectively.

Col1a

The MI192 pre-treated group displayed much stronger Col1a protein expression throughout the scaffold when compared to the untreated group, with the strongest staining intensity situated at the periphery of the construct in both groups (Fig 3.25).

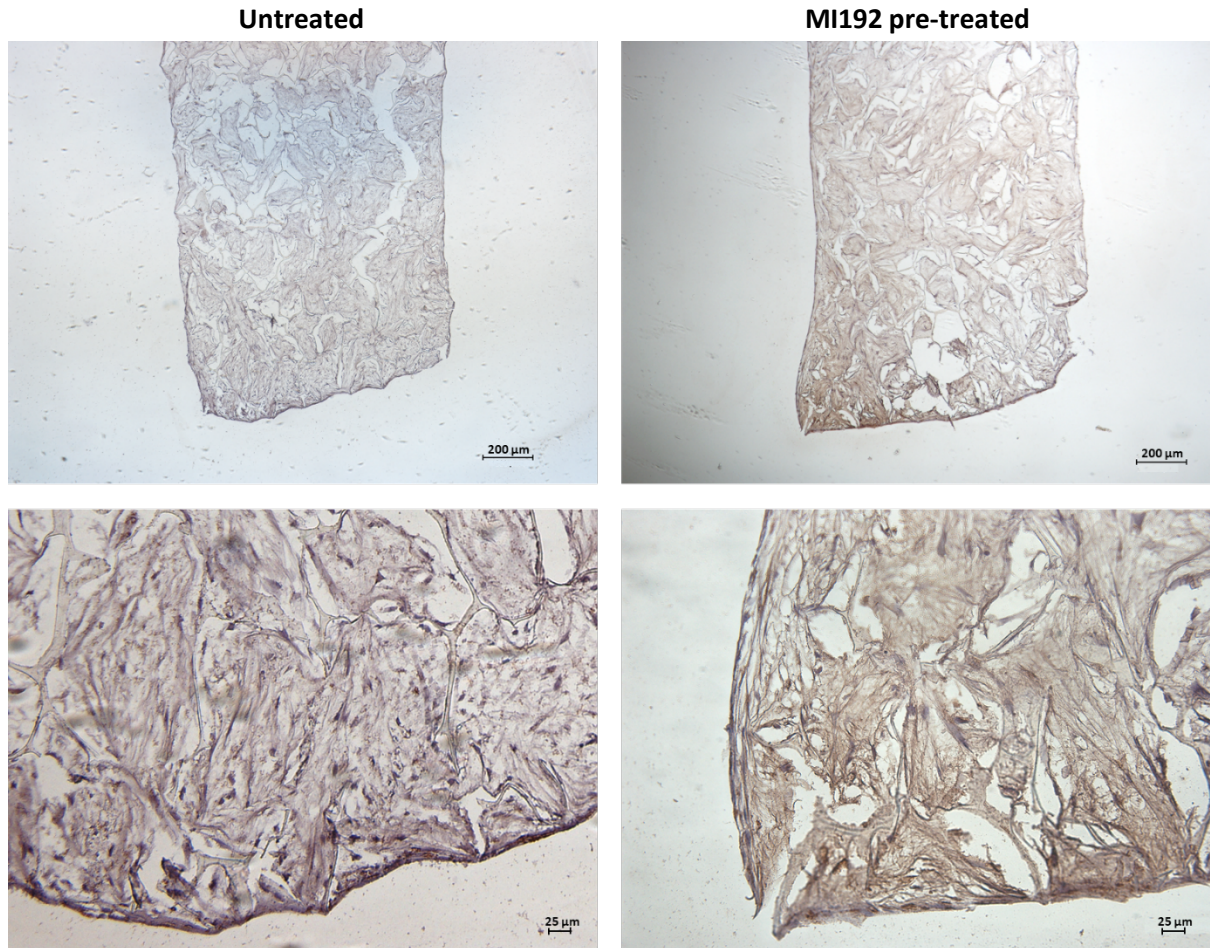


Figure 3.25 - Col1a immunohistochemical staining of untreated/MI192 pre-treated hDPSCs cultured within the 5 wt% silk scaffolds after 6 weeks osteogenic culture. Positive Col1a immunohistochemical staining (brown), with a weak Harris haematoxylin counterstain (purple). Scale bars = 200 (top row) and 25 µm (bottom row), respectively.

OCN

Positive OCN expression was observed in both the MI192 pre-treated and untreated cells within the 5 wt% silk scaffolds, with particular strong staining situated at the periphery of the construct (Fig 3.26). The MI192 pre-treated group exhibited much stronger global staining for OCN throughout the scaffold compared to the untreated group. Negative immunostaining of untreated and MI192 pre-treated silk constructs is shown in Figure 3.27.

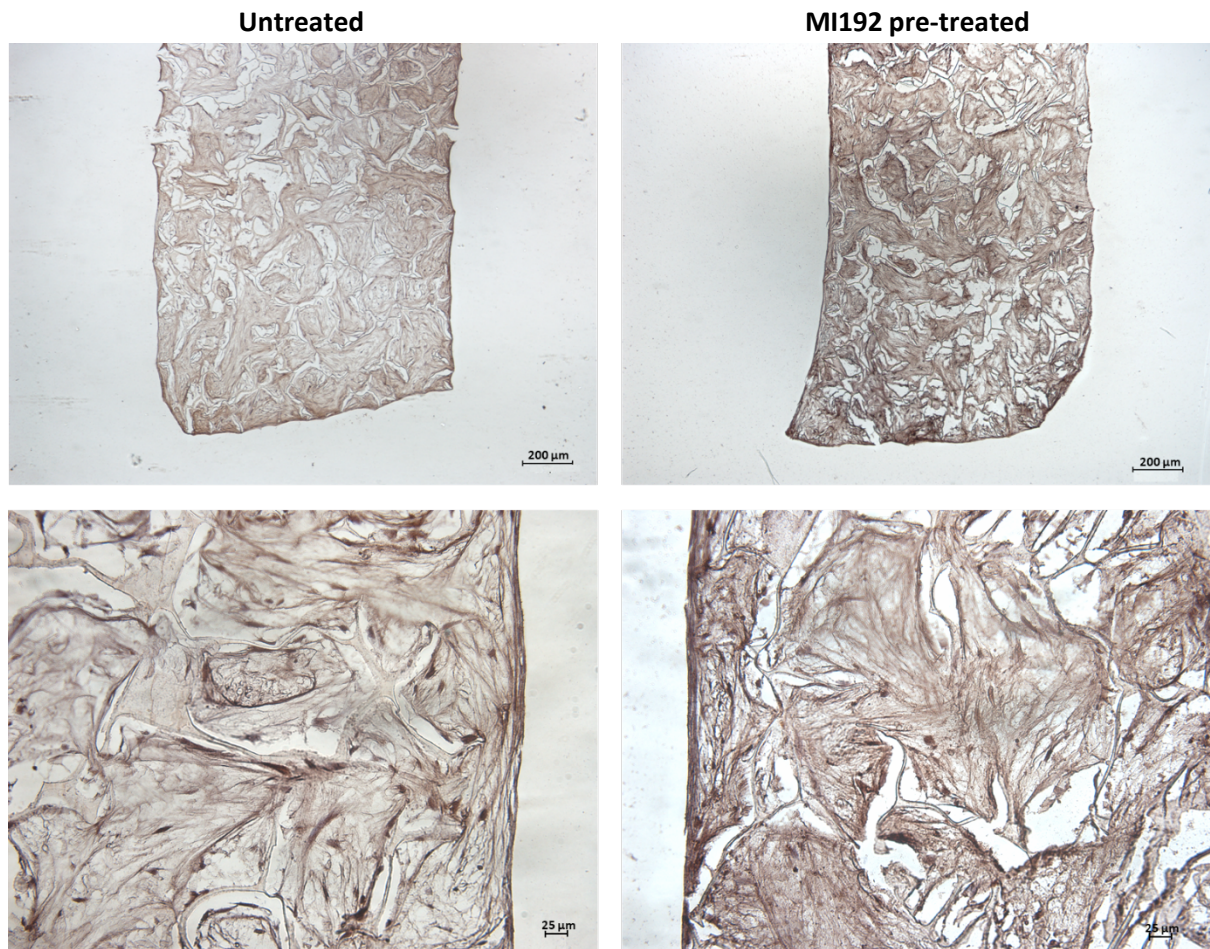


Figure 3.26 - OCN immunohistochemical staining of untreated/MI192 pre-treated hDPSCs cultured within the 5 wt% silk scaffold after 6 weeks osteogenic culture. Positive OCN immunohistochemical staining (brown), with a weak Harris haematoxylin counterstain (purple). Scale bars = 200 (top row) and 25 μm (bottom row), respectively.

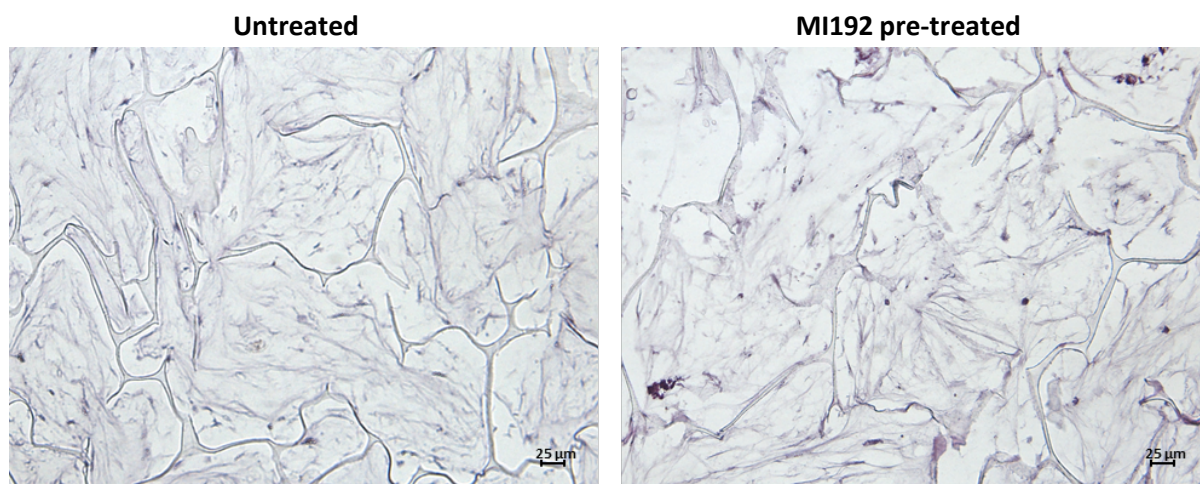


Figure 3.27 - Negative immunohistochemical staining of untreated/MI192 pre-treated hDPSCs cultured within the 5 wt% silk scaffold after 6 weeks osteogenic culture. Scale bar = 25 µm.

3.3.2.9 - The effect of MI192 on hDPSCs calcium deposition and mineralisation within the silk scaffold

Alizarin red staining was performed to assess the effects of MI192 pre-treatment on hDPSCs calcium deposition within the 5 wt% silk scaffold after 6 weeks osteogenic culture. Following histological analysis, calcium deposition was observed in both groups, with the strongest intensity staining located towards the outer regions of the construct (Fig 3.28A). The MI192 pre-treated group showed the strongest Alizarin red staining intensity compared to the untreated group. Semi-quantitative analysis of Alizarin red staining of the entire silk constructs showed that MI192 pre-treatment significantly increased calcium deposition compared to that of the untreated group (1.73-fold) (Fig 3.28B).

Von Kossa staining was utilised to assess mineralisation with the silk scaffolds. Mineral nodule formation was observed throughout the scaffolds, with an increased mineral density situated at the outer regions of both untreated and MI192 pre-treated constructs (Fig 3.29). A larger quantity of mineral nodules (red arrows) was observed throughout the scaffolds in the MI192 pre-treated group when compared to the untreated group.

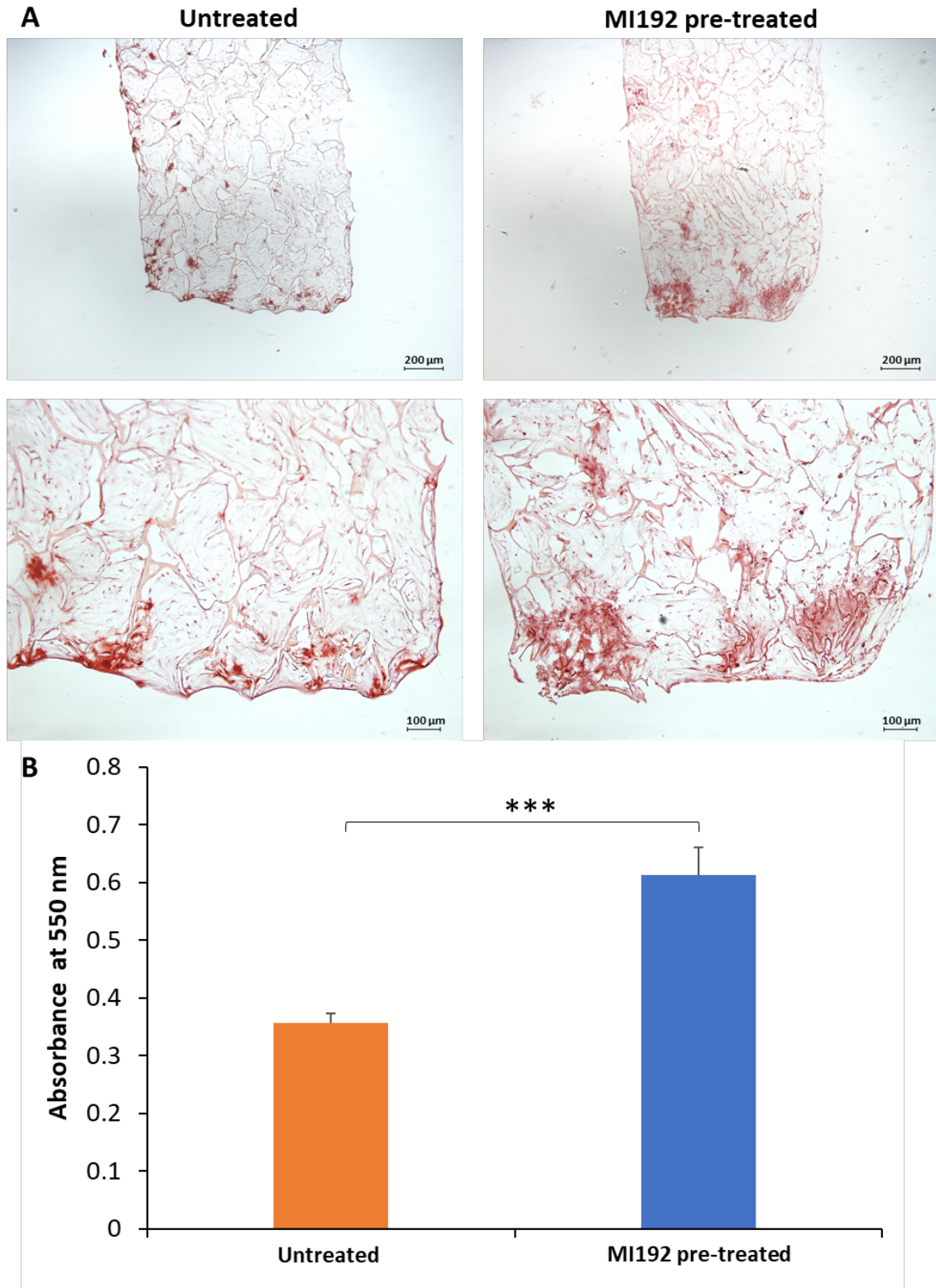


Figure 3.28 - Calcium deposition of untreated/MI192 pre-treated hDPSCs cultured within the 5 wt% silk scaffold after 6 weeks osteogenic culture observed by Alizarin red staining. A) Alizarin red staining of histological sections. Scale bars = 200 (top row) and 100 μm (bottom row), respectively. B) Semi-quantitative analysis of Alizarin red stained entire constructs. Data expressed as mean \pm SD (n=3). *P \leq 0.001.**

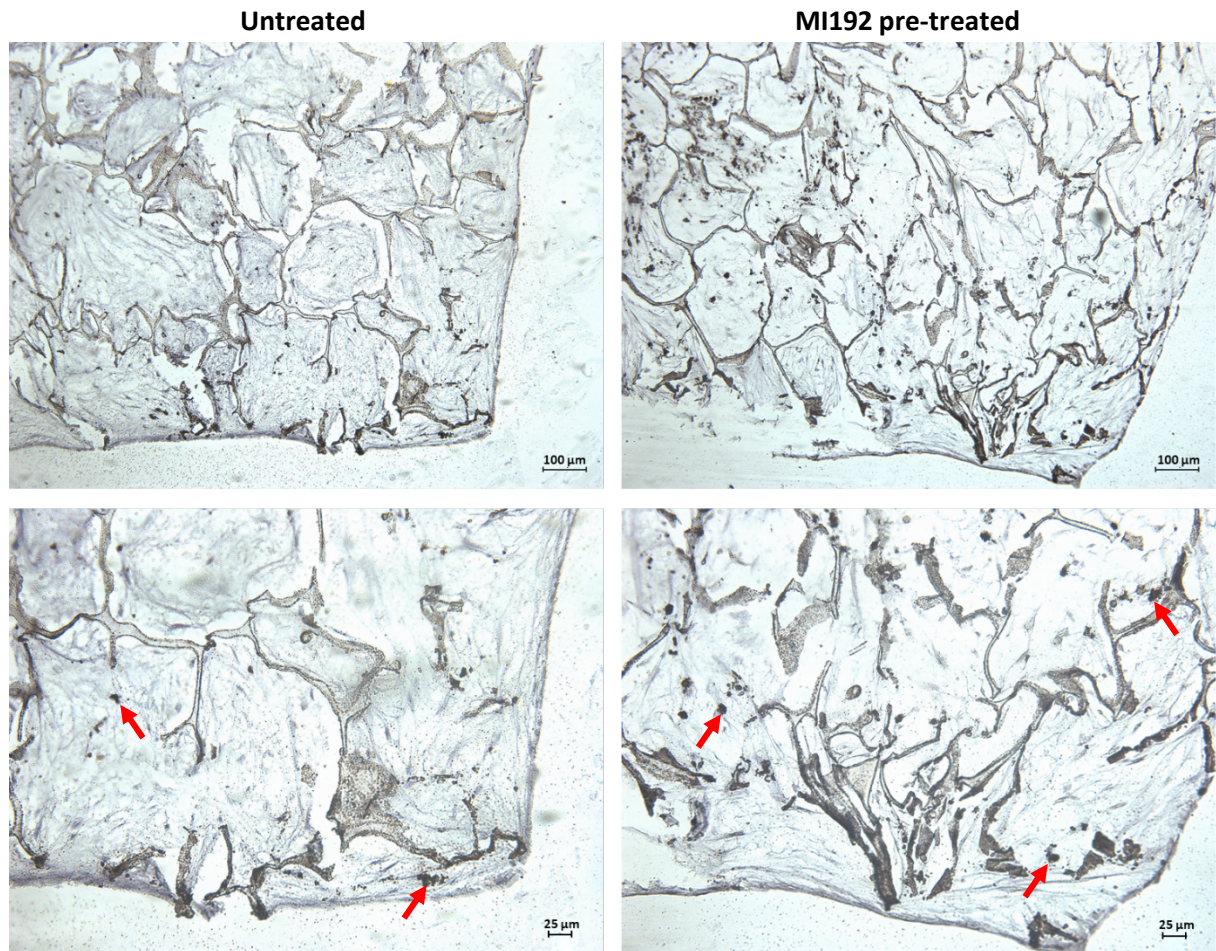


Figure 3.29 - Mineral nodule formation of untreated/MI192 pre-treated hDPSCs cultured within the 5 wt% silk scaffolds after 6 weeks osteogenic culture observed by Von Kossa staining. Mineral nodule formation indicated by red arrows. Weak Harris haematoxylin counterstain (purple). Scale bars = 100 (top row) and 25 μm (bottom row), respectively.

3.3.3 - The Effects of MI192 on hDPSCs Osteogenic Differentiation within the BMT construct

3.3.3.1 - Macroscopic analysis of 3D printed PEGT/PBT scaffold

The 3D printed PEGT/PBT scaffolds possessed a fibre spacing of $958.7 \pm 29.1 \mu\text{m}$, a pore size of $748.6 \pm 23.1 \mu\text{m}$, and fibres width of $241.2.7 \pm 19.9 \mu\text{m}$ (mean \pm SD) (Fig 3.30A). The double stacking of printed fibres in the 0, 0, 90, 90° conformation, allowed for the creation of a pore height of $764.8 \pm 24.7 \mu\text{m}$. Representative bright-field images of the 3D printed plotted scaffold (top and sectional view) are shown in figure 3.30B.

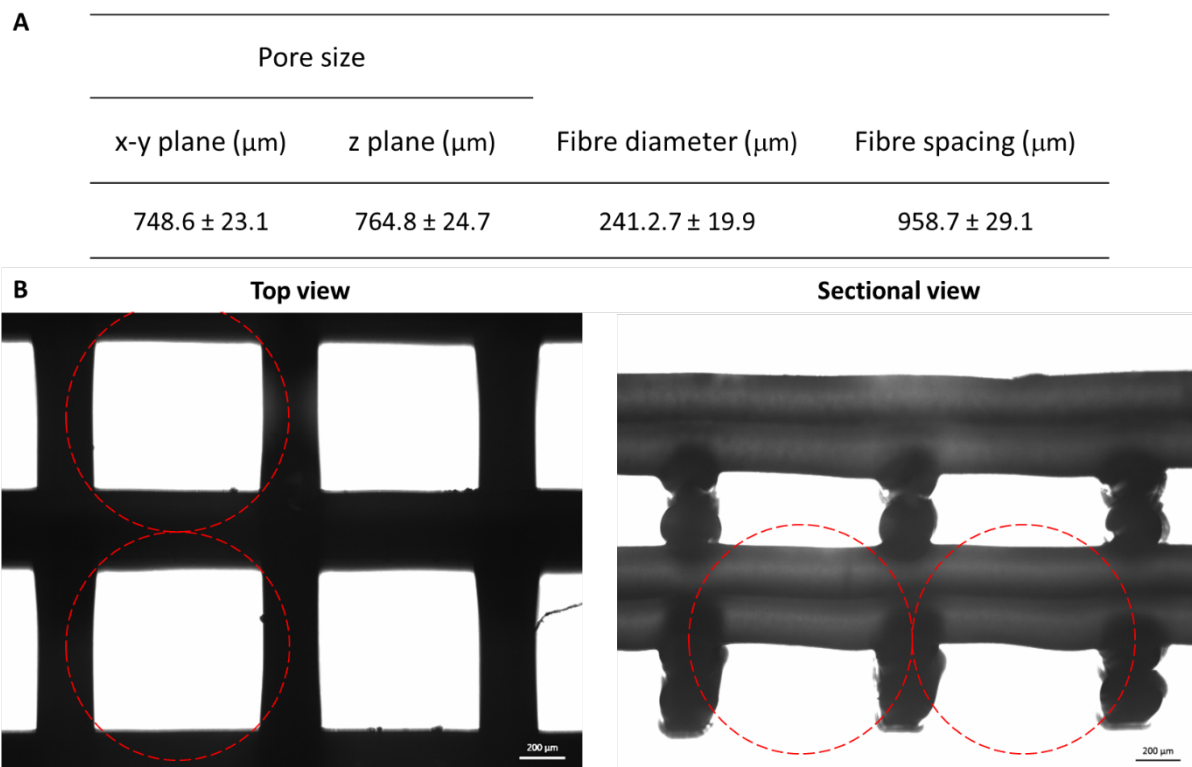


Figure 3.30 - Characteristic parameters of PEGT/PBT scaffolds. A) The scaffold pore size in the x-y/z plane and the fibre diameter/spacing. Data expressed as mean \pm SD (n=4). B) Bright-field images of the top view and sectional view of the PEGT/PBT scaffold. The red dotted circles (1 mm diameter) indicate the position of incorporated microtissues within the scaffold. Scale bar = 200 μm .

3.3.3.2 - Surface topography and 3D architecture of 3D printed PEGT/PBT scaffold

Figure 3.31A and B show the surface topography of the top and bottom layers of the 3D printed PEGT/PBT scaffold. From the top-down view, a smooth surface topography was observed. The bottom-up view of the construct showed a roughened surface due to the contact with the cold plate while printing. Figures 3.31C and D show a lower magnification tilted image of these scaffolds demonstrating their unique fibre stacking conformation.

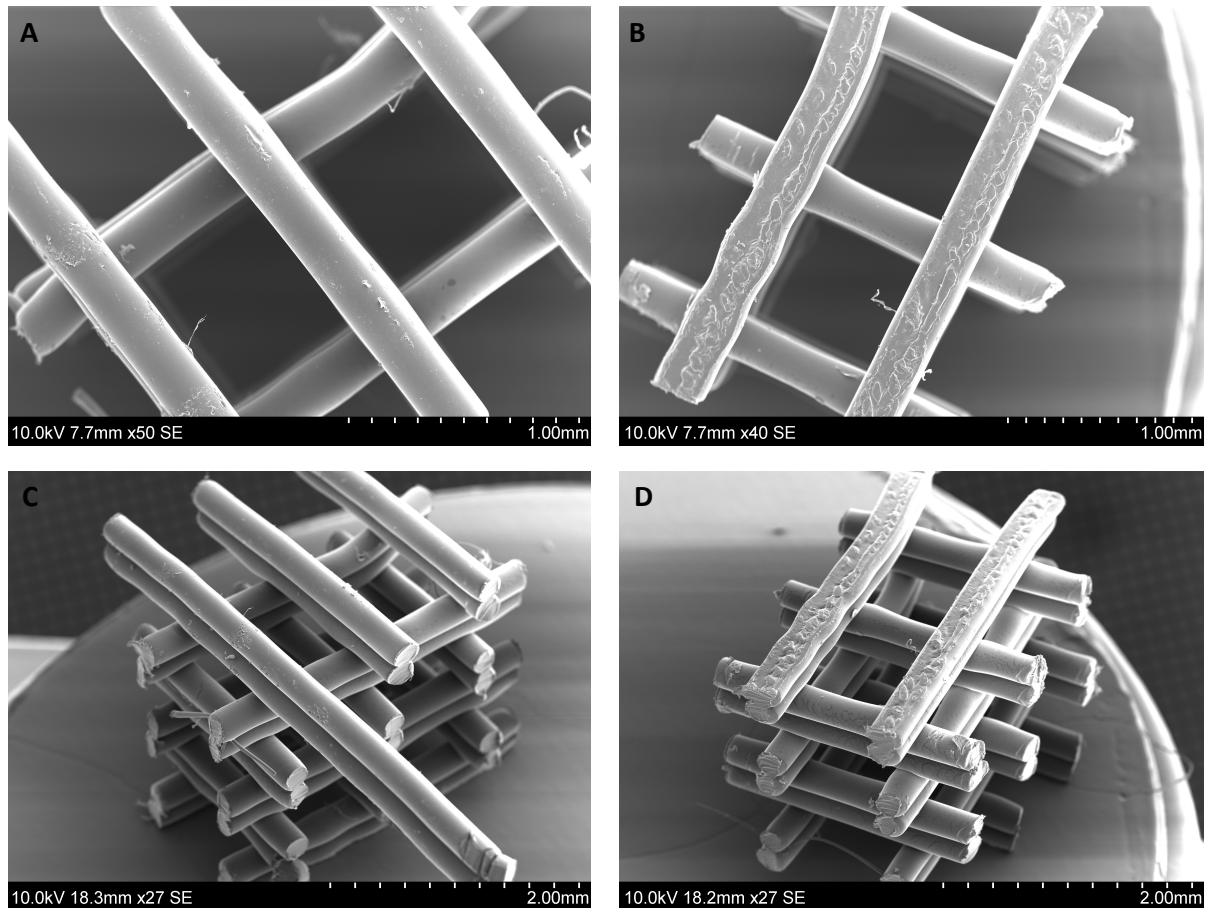


Figure 3.31 - SEM images of 3D printed PEGT/PBT scaffolds. A) Top-down view of PEGT/PBT scaffold demonstrating a smooth topography with even fibre thickness throughout. B) Bottom view of scaffold showing roughened surface due to adhesion to the printing plate. C) & D) Tilted views demonstrating the printing configuration and pore height of scaffold. Scale bars = 1 (top row) and 2 mm (bottom row), respectively.

3.3.3.3 - BMT construct assembly

After 7 days pre-culture in v-shaped bottom 96-well plates, hDPSC microtissues were manually transferred into the pores of the 3D printed PEGT/PBT scaffold using 1-ml pipette tips. The 3D printed scaffolds were designed with a 1-mm fibre spacing, which allowed for the press-fit of two hDPSC microtissues per pore. Therefore, a total of 16 microtissues were incorporated per scaffold in a bi-layered configuration, with 8 microtissues per layer. Figure 3.32 shows a macroscopic image of the BMT immediately after formation *in situ*. The black/white arrows show the location of the incorporated microtissues/3D printed scaffold, respectively.

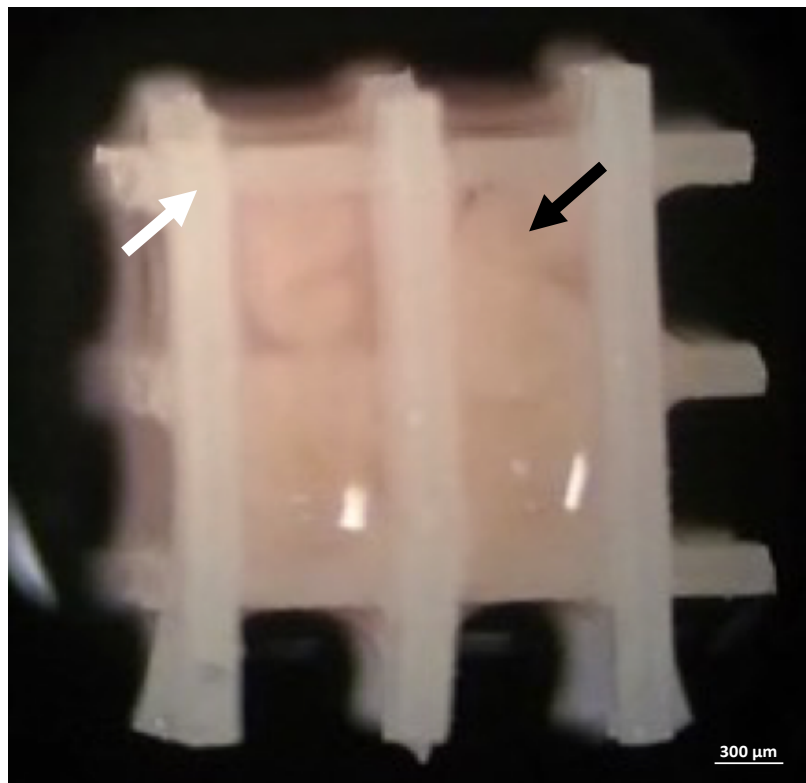


Figure 3.32 - Macroscopic image of assembled BMT construct. *In situ* image showing BMT construct immediately after manual incorporation of hDPSC pre-cultured microtissues (black arrow) into the 3D printed PEGT/PBT scaffold framework (white arrow). Scale bar = 300 μm.

3.3.3.4 - Assessment of BMT cellular viability

The MI192 pre-treated and untreated hDPSC BMTs were labelled with CFMDA/EthD-1 to visualise the viable/dead cells 24 hours after BMT assembly via CLSM (Fig 3.33). The scaffold absorbed the EthD-1 dye in both groups. The scaffold possessed a generally smooth topography with no cells attached after 24 hours. The rough scaffold surface topography observed in the untreated group was due to contact with the cold stage during printing. Within the microtissues, a large majority of cells were viable in both groups, with a low number of dead cells visible.

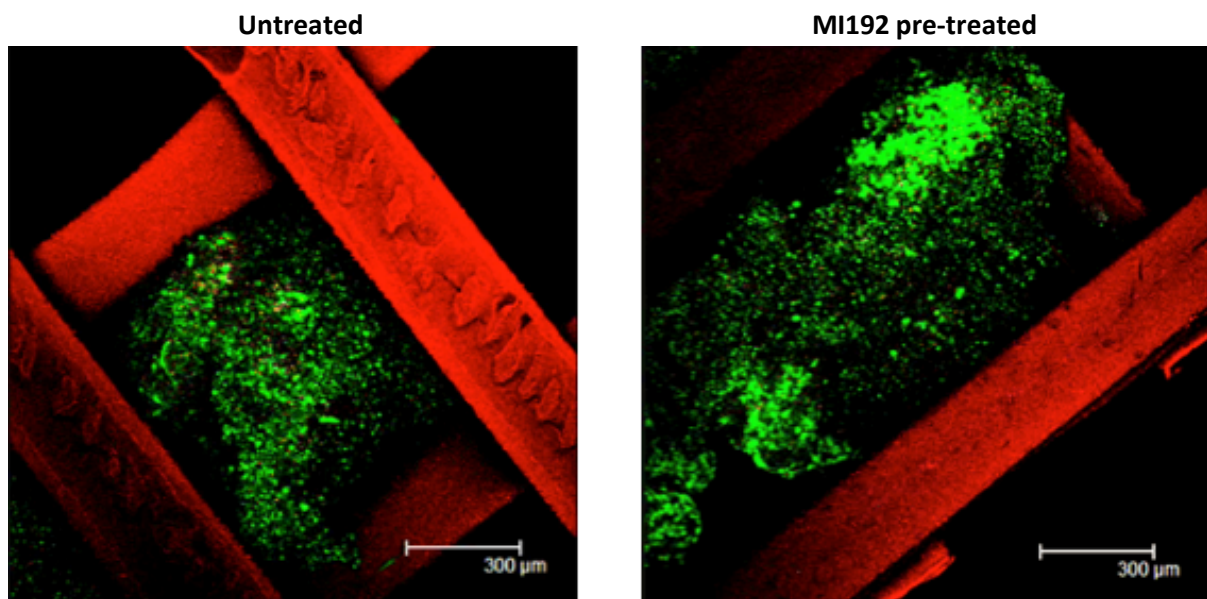


Figure 3.33 - Merged Live/Dead fluorescent images of untreated/MI192 pre-treated hDPSC BMT constructs 24 hours post assembly (Live cells green, dead cells red). Scale bar = 300 µm.

3.3.3.5 - The effect of MI192 on hDPSCs osteogenic gene expression in microtissue culture

The mRNA expression levels of osteoblast-related genes (*RUNX2*, *ALP*, *BMP2*, *COL1A* and *OCN*) within untreated and MI192 pre-treated hDPSC microtissues were assessed throughout 21 days osteogenic culture (Fig 3.34).

RUNX2

After 7 days osteogenic culture, the *RUNX2* mRNA levels within the MI192 pre-treated cells were upregulated compared to that in the untreated group, however not significantly ($P > 0.05$). A similar increase in the *RUNX2* expression was observed in the MI192 pre-treated cells compared to that in the control cells on days 14 and 21, although not significant ($P > 0.05$).

ALP

The *ALP* mRNA expression levels were significantly increased in the MI192 pre-treated group compared to that in the untreated cells on day 7 (1.10-fold) ($P \leq 0.05$). After 14 days osteogenic culture, mRNA expression levels remained significantly enhanced within the MI192 pre-treated group compared to that in the untreated cells (1.25-fold) ($P \leq 0.01$), however, expression levels were similar between the groups on day 21 ($P > 0.05$).

BMP2

The *BMP2* mRNA expression levels were significantly upregulated in the MI192 pre-treated cells compared to the expression within the untreated control on day 7 (1.04-fold) ($P \leq 0.05$). A similar significant enhancement in *BMP2* mRNA levels was observed in the MI192 pre-treated cells compared to that in the control cells on day 14 (1.19-fold) ($P \leq 0.001$) and 21 (1.03-fold) ($P \leq 0.05$).

COL1A

In the MI192 pre-treated group, *COL1A* mRNA expression levels were significantly upregulated on day 7 (3.81-fold) ($P \leq 0.001$) and 14 (1.24-fold) ($P \leq 0.01$) compared to that in the untreated cells, however, expression levels were similar between the groups on day 21 ($P > 0.05$).

OCN

OCN mRNA expression levels were significantly increased in the MI192 pre-treated cells on day 7 compared to that in the untreated group (1.24-fold) ($P \leq 0.001$). On day 14 and 21, expression remained significantly upregulated in the MI192 pre-treated cells compared to that in the untreated group (1.09- and 1.02-fold) ($P \leq 0.05$ and $P \leq 0.001$).

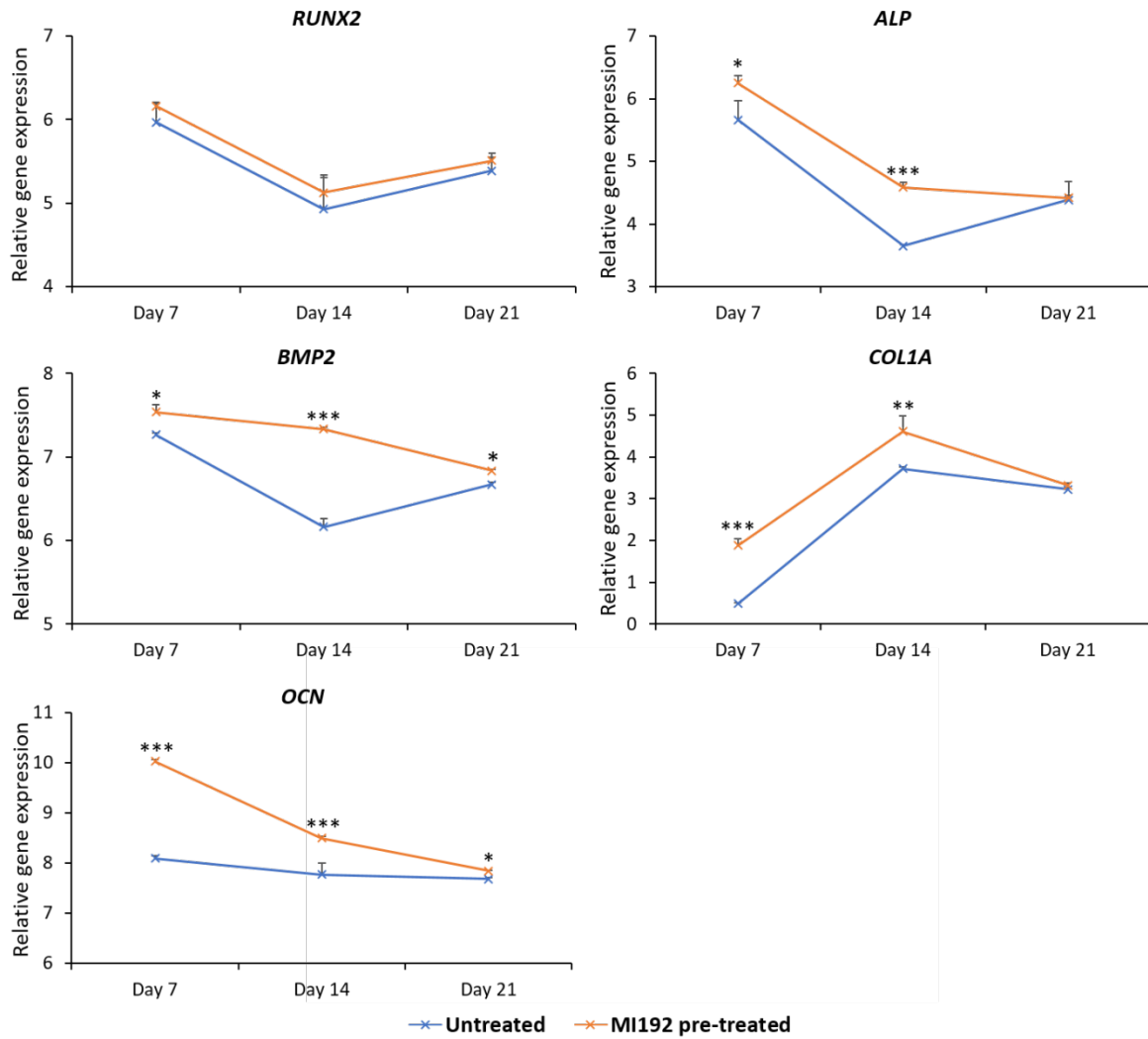


Figure 3.34 - Relative expression of osteoblast-related genes in untreated/MI192 pre-treated hDPSC microtissues under osteogenic conditions. Gene expression analysed on day 7, 14 and 21. Data expressed as mean \pm SD (n=4). Significance levels shown are the test group compared to the untreated control at the same time point. * $P \leq 0.05$, ** $P \leq 0.01$ and *** $P \leq 0.001$.

3.3.3.6 - The effect of MI192 on hDPSCs ALPSA in BMT culture

ALPSA in MI192 pre-treated and untreated hDPSC BMT constructs cultured under osteogenic conditions was assessed (Fig 3.35). The MI192 pre-treated group exhibited a substantially enhanced ALPSA (2.35-fold) when compared to the untreated group after 2 weeks in osteogenic culture ($P \leq 0.05$).

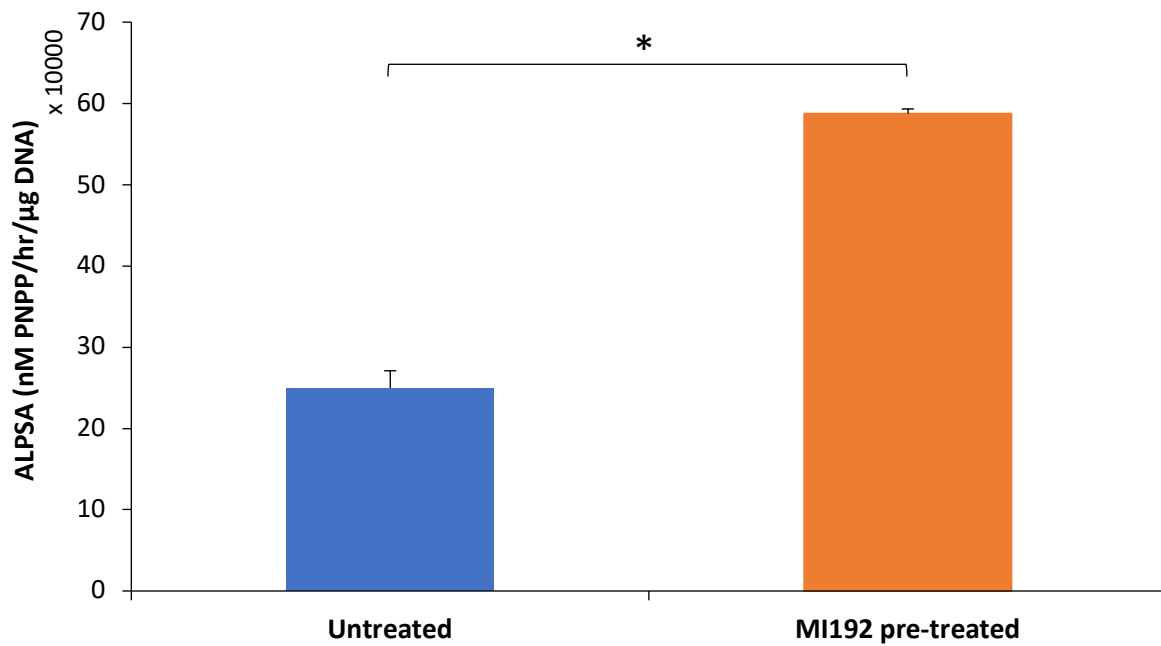


Figure 3.35 - ALPSA in untreated/MI192 pre-treated hDPSC BMT constructs. ALPSA assessed after BMT constructs cultured under osteogenic conditions for 2 weeks. Data expressed as mean \pm SD (n=4). * $P \leq 0.05$.

3.3.3.7 - The effect of MI192 on hDPSCs tissue formation within the BMT construct

Histological analysis was undertaken to assess the effect of MI192 pre-treatment on hDPSC tissue formation within the BMT construct after 6 weeks osteogenic culture. H&E staining showed that within the untreated and MI192 pre-treated groups, the incorporated tissue modules occupied the entire void volume of the 3D printed scaffolds, where microtissues fusion was observed within the constructs (Fig 3.36). Additionally, microtissues in both groups formed around the internal scaffold fibres (black arrows) (scaffold fibres dislodge during histological analysis).

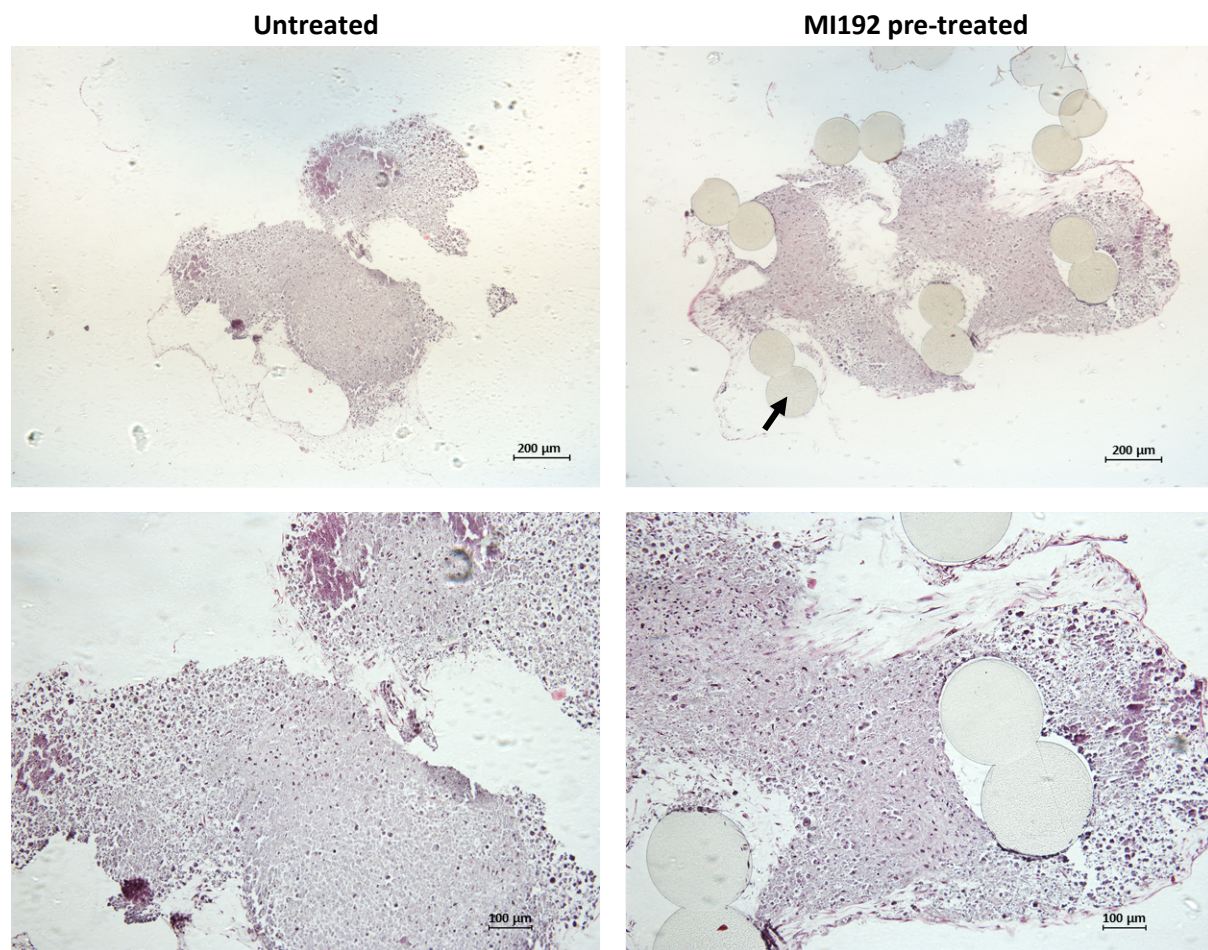


Figure 3.36 - H&E staining of untreated/MI192 pre-treated hDPSC BMT constructs after 6 weeks osteogenic culture. Scaffold fibres highlighted by the black arrow. Scale bars = 200 (top row) and 100 µm (bottom row), respectively.

Picrosirius red/Alcian blue staining was also utilised to evaluate the effects of MI192 pre-treatment on hDPSCs collagen and GAG expression within the BMT construct after 6 weeks osteogenic culture (Fig 3.37). Within the untreated group, strong Picrosirius red staining was located at the periphery of the individual microtissues with weaker staining situated within the core of each tissue module. The MI192 pre-treated group also displayed strong staining for Picrosirius red; however, the collagen expression was distributed more uniformly throughout the construct when compared to the untreated BMT. Additionally, the MI192 pre-treated group possessed an increased number of circular nodules (black arrows), which exhibited the strongest Picrosirius red intensity within the construct, when compared to the untreated BMT. Moreover, the untreated construct exhibited an increased GAG accumulation when compared to the MI192 pre-treated group, particularly located within the core of the microtissues.

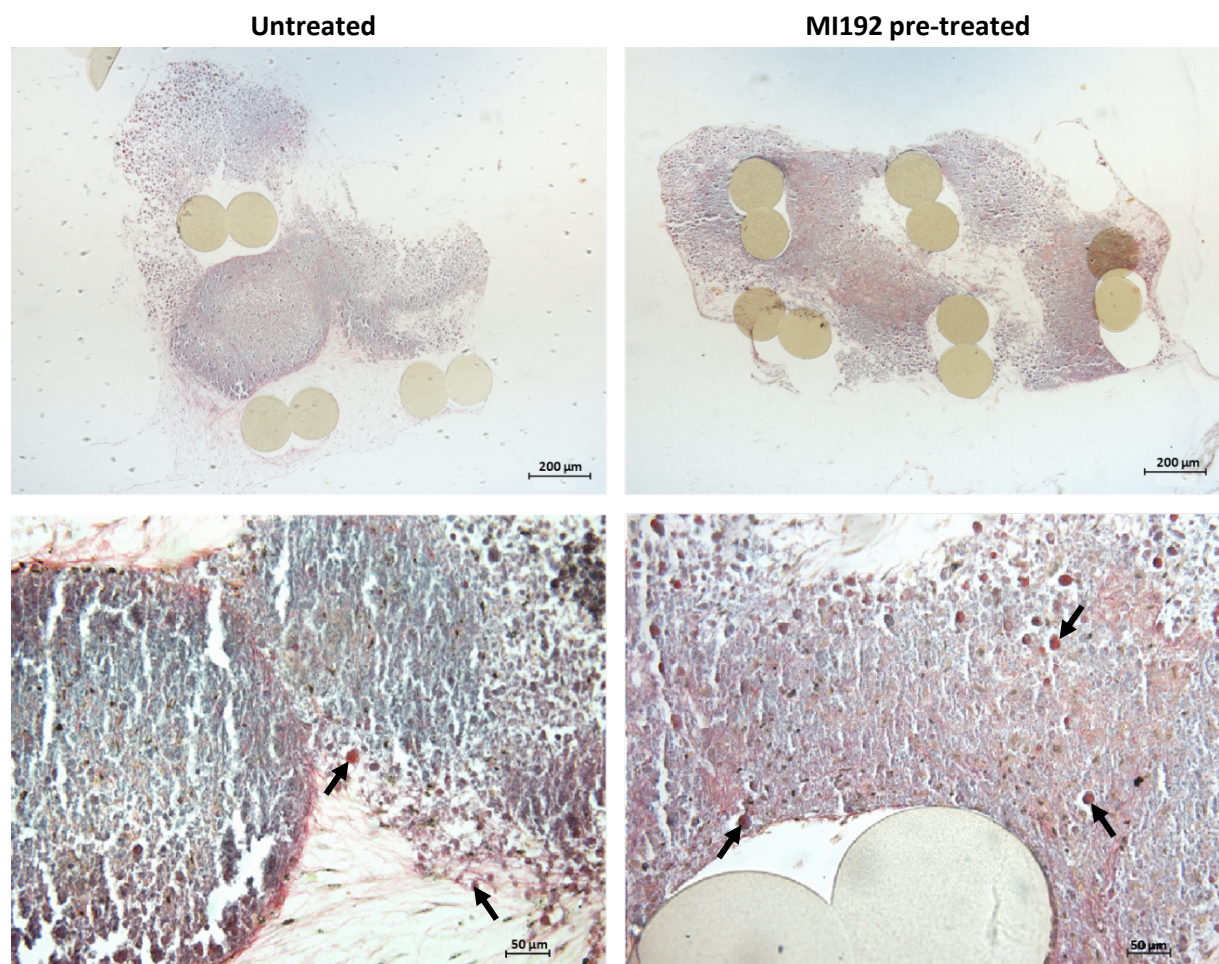


Figure 3.37 - Picrosirius red/Alcian blue staining of untreated/MI192 pre-treated hDPSC BMT constructs after 6 weeks osteogenic culture. Collagen and GAG staining with Picrosirius red and Alcian blue, respectively. Strong Picrosirius red staining located in circular nodules highlighted by the black arrows. Scale bars = 200 (top row) and 50 µm (bottom row), respectively.

3.3.3.8 - The effect of MI192 on hDPSCs osteogenic protein expression within the BMT construct

ALP

Both BMTs formed by MI192 pre-treated and untreated hDPSCs displayed strong ALP staining throughout the construct after 6 weeks of osteogenic culture, however, the MI192 pre-treated group exhibited slightly stronger global ALP staining when compared to the untreated control group (Fig 3.38). Additionally, the MI192 pre-treated group possessed a higher quantity of circular nodules (black arrows) which expressed the strongest ALP staining intensity within the construct, when compared to the untreated group.

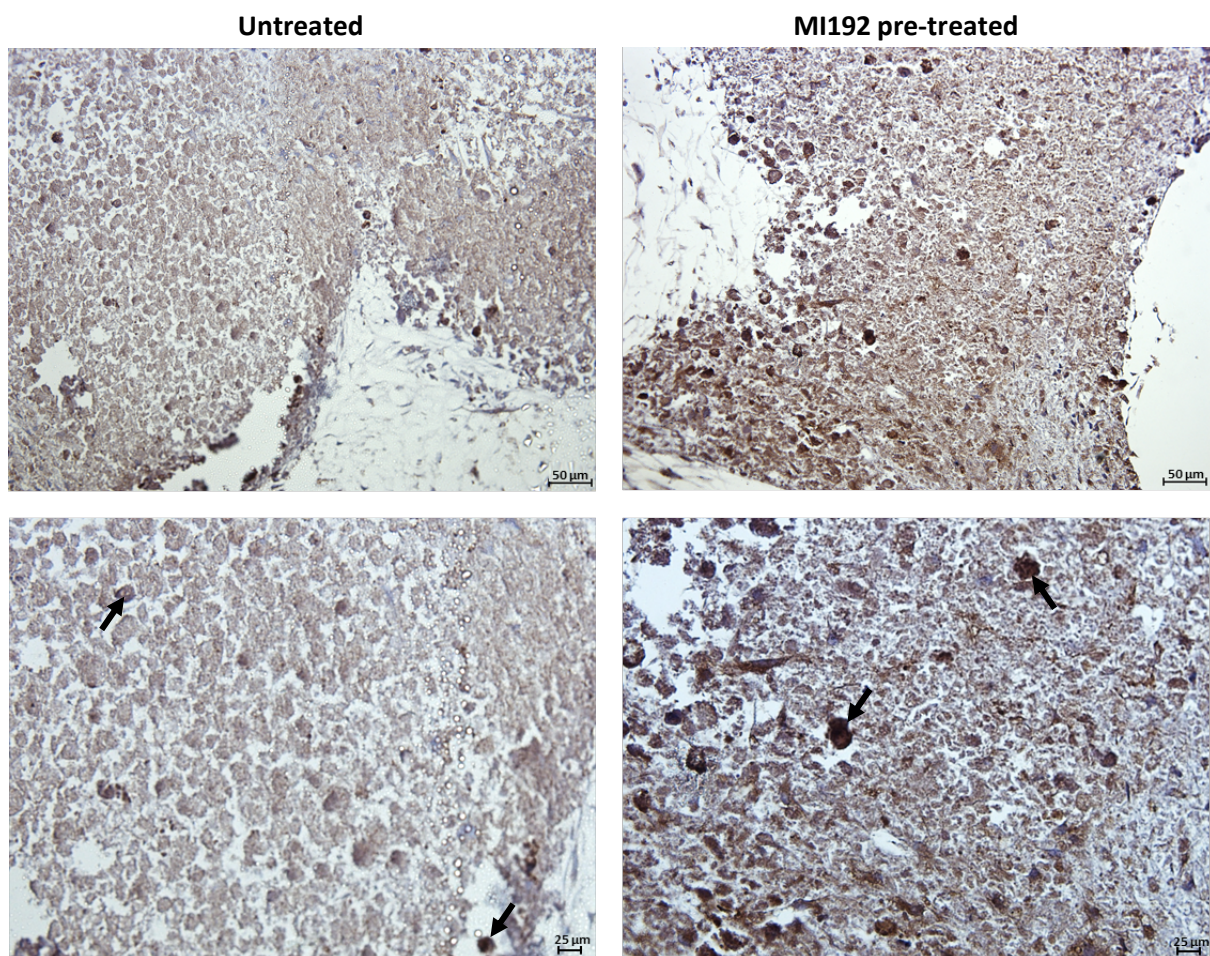


Figure 3.38 - ALP immunohistochemical staining of untreated/MI192 pre-treated hDPSC BMT constructs after 6 weeks osteogenic culture. Positive ALP immunohistochemical staining (brown), with a weak Harris haematoxylin counterstain (purple). Strong ALP expression located at the nodule-like formations highlighted with the black arrows. Scale bars = 50 (top row) and 25 µm (bottom row), respectively.

Col1a

The MI192 pre-treated group exhibited strong Col1a protein staining within the core and periphery of each microtissue (Fig 3.39). In comparison, the untreated group expressed much weaker Col1a staining throughout the construct, with slightly stronger staining situated at the outer regions of the microtissue. The strongest Col1a expression was located in close proximity to the nodule-like formations (black arrows) within the constructs, which was at an increased density within the MI192 pre-treated group.

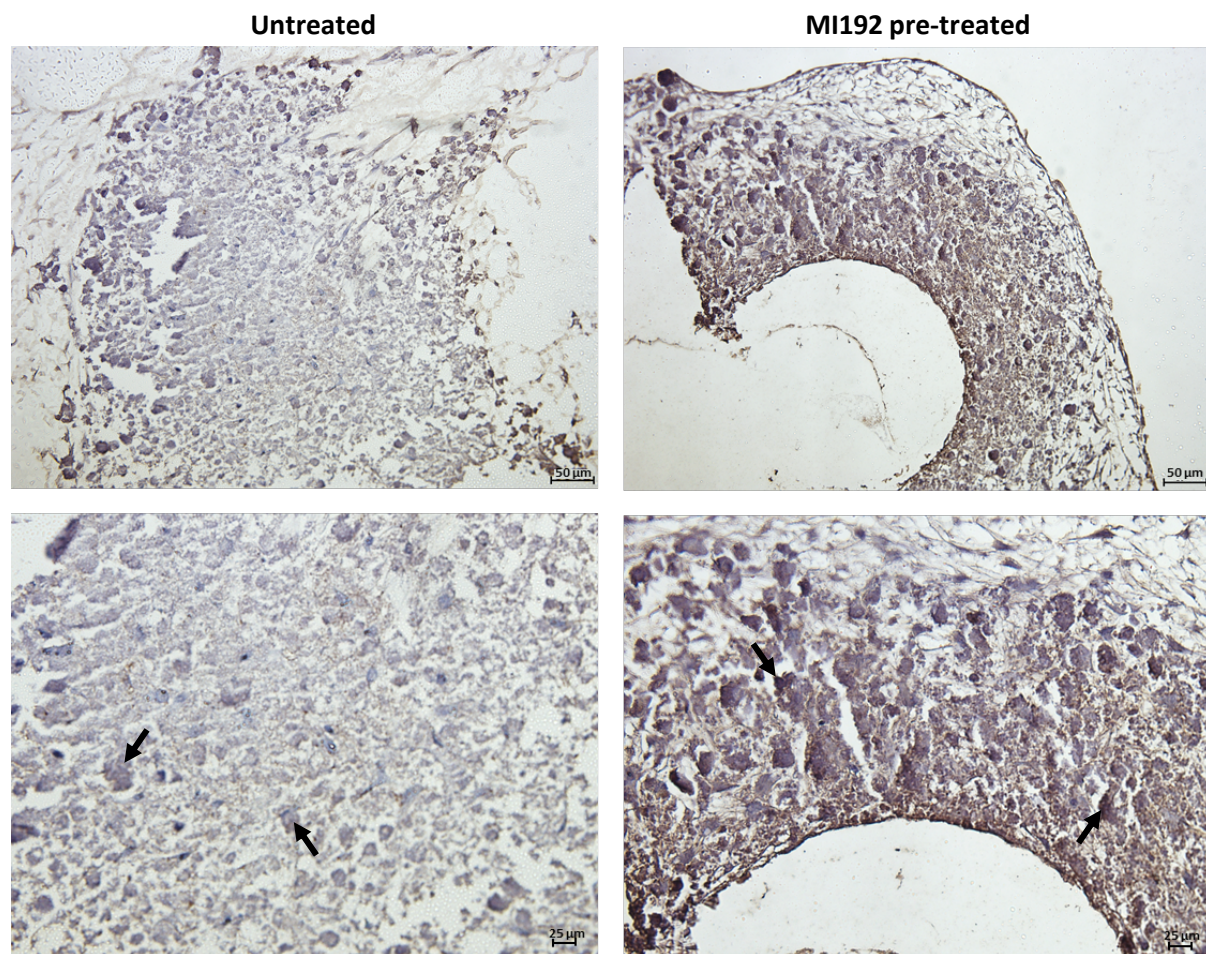


Figure 3.39 - Col1a immunohistochemical staining of untreated/MI192 pre-treated hDPSC BMT constructs after 6 weeks osteogenic culture. Positive Col1a immunohistochemical staining (brown), with a weak Harris haematoxylin counterstain (purple). Strong Col1a expression located at the nodule-like formations highlighted with the black arrows. Scale bars = 50 (top row) and 25 µm (bottom row), respectively.

OCN

Positive OCN protein expression was present in both MI192 pre-treated and untreated BMTs with strong staining located throughout the construct (Fig 3.40). The MI192 pre-treated constructs exhibited strong OCN staining intensity distributed uniformly throughout the microtissues. Within the untreated group, similar OCN staining intensity was observed at the periphery of each microtissue, with weaker staining situated at the core of each incorporated tissue module. The strongest OCN protein staining is situated in the nodule-like formations (red arrows) observed within the microtissues, which were at a higher quantity within the MI192 pre-treated group.

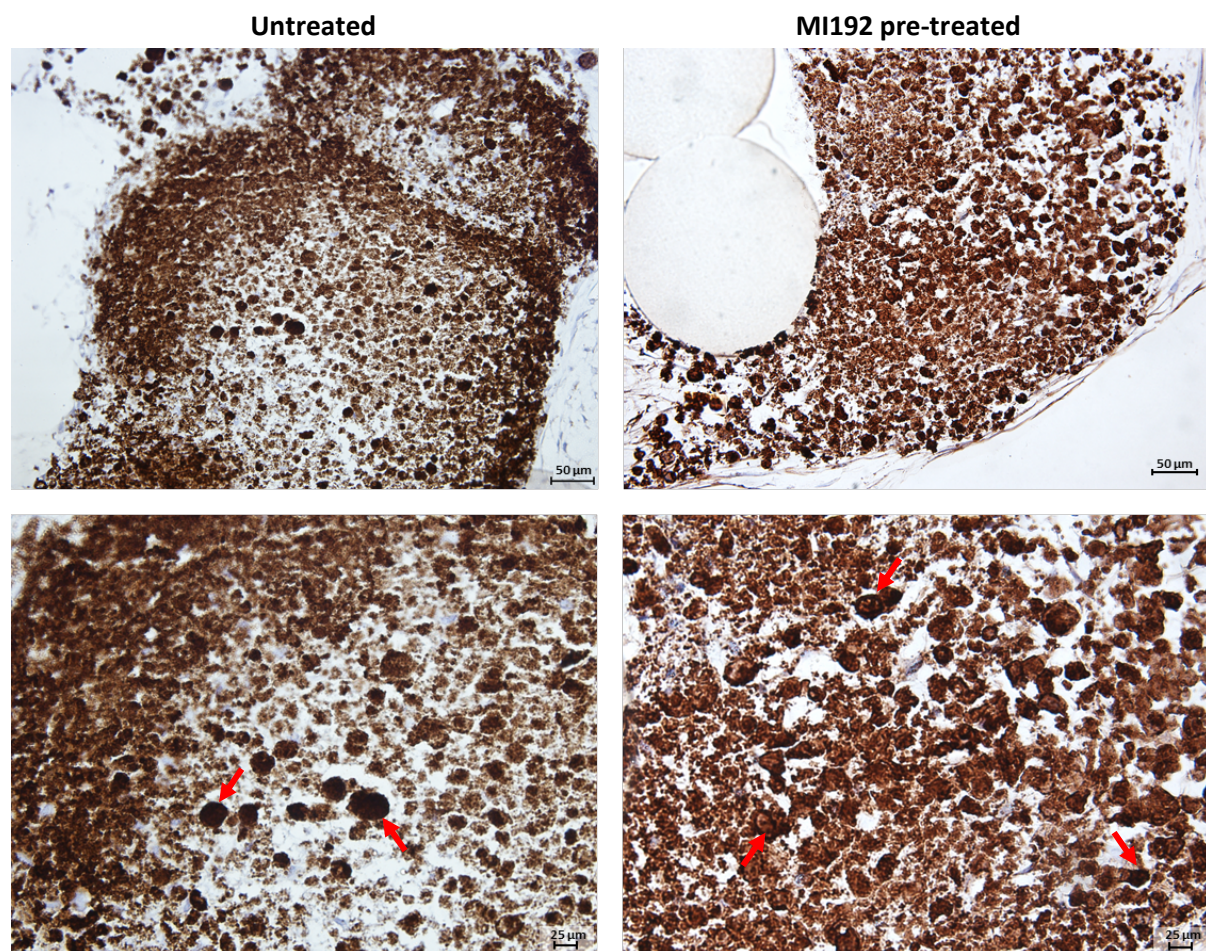


Figure 3.40 - OCN immunohistochemical staining of untreated/MI192 pre-treated hDPSC BMT constructs after 6 weeks osteogenic culture. Positive OCN immunohistochemical staining (brown), with a weak Harris haematoxylin counterstain (purple). Strong OCN expression located at the nodule-like formations highlighted with the red arrows. Scale bars = 50 (top row) and 25 μm (bottom row), respectively.

Negative immunostaining of MI192 pre-treated and untreated BMT constructs after 6 weeks osteogenic culture is shown observed in Figure 3.41.

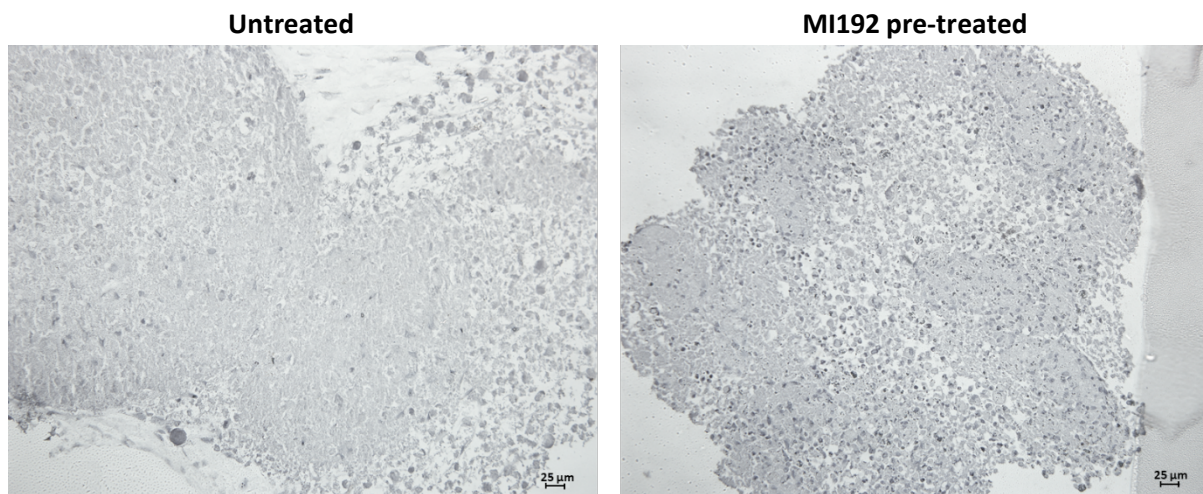


Figure 3.41 - Negative immunohistochemical staining of untreated/MI192 pre-treated hDPSCs BMT constructs after 6 weeks osteogenic culture. Scale bar = 25 µm.

3.3.3.9 - The effect of MI192 on hDPSCs mineralisation within the BMT construct

Following Von Kossa staining, functional mineral nodules were observed in both BMT groups. The MI192 pre-treated BMT possessed substantially stronger black staining intensity throughout the construct when compared to the untreated group (Fig 3.42). Moreover, the MI192 pre-treated BMT exhibited enhanced quantity and size of functional mineral nodules compared to the untreated construct, with these nodule-like formations displaying the strongest Von Kossa staining intensity within the BMT constructs (red arrows).

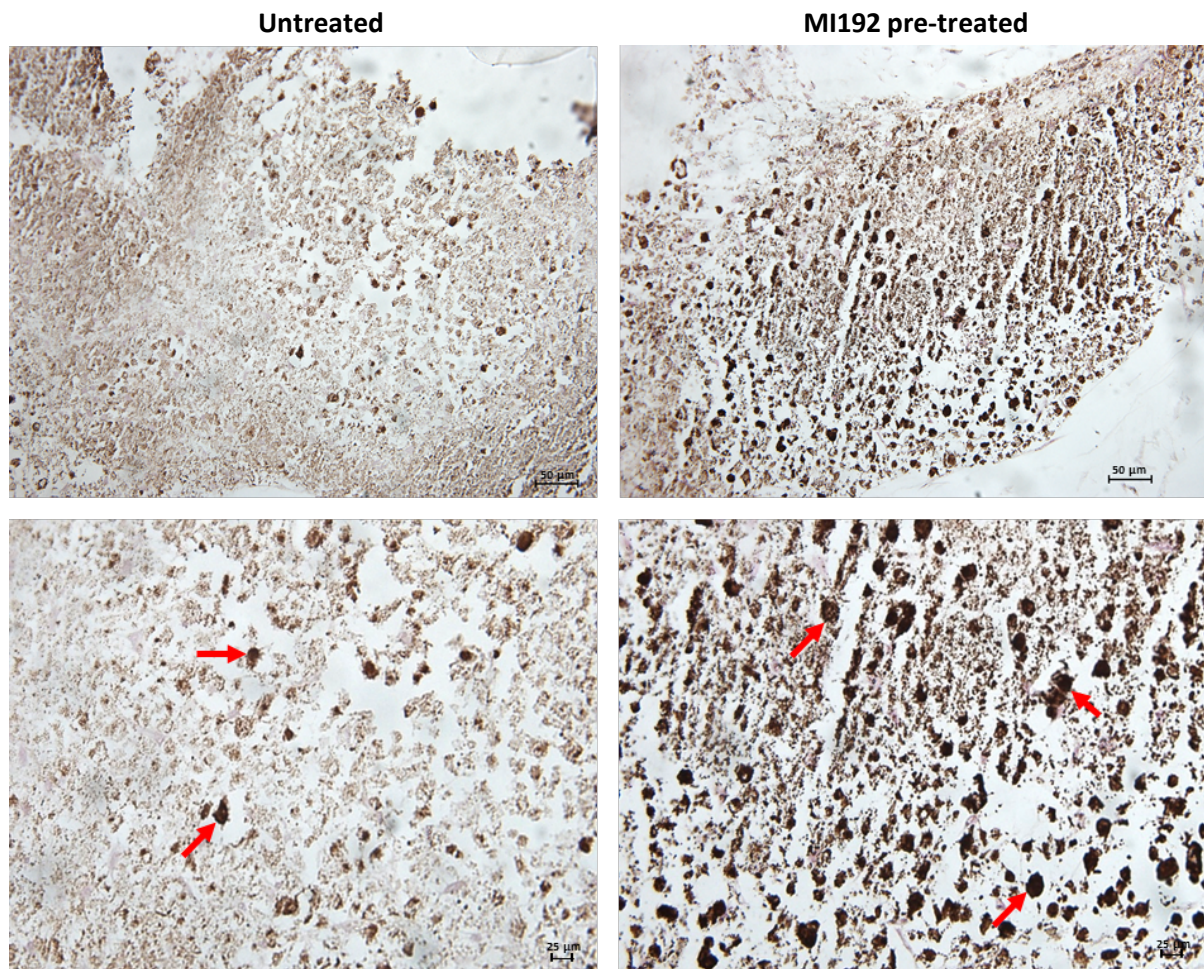


Figure 3.42 - Mineral nodule formation of untreated/MI192 pre-treated hDPSC BMT constructs after 6 weeks osteogenic culture observed by Von Kossa staining. Red arrows indicate mineral nodules. Scale bars = 50 (top row) and 25 μm (bottom row), respectively.

3.3.4 - The Effects of MI192 on hDPSC BMT *in vivo* bone formation

3.3.4.1 - Macroscopic and X-ray analysis of hDPSC BMT constructs

Within the diffusion chambers, the 3D printed PEGT/PBT scaffold in both groups remained intact after 8 weeks intraperitoneal implantation. Within each group, microtissues which were incorporated prior to placement within the chambers remained within the scaffold framework (Fig 3.43A). No tissue formation was observed in the regions surrounding the BMT construct in the chamber. The X-ray images show strong radio-opacity within the construct particularly in regions where the microtissues were incorporated within the scaffolds (Fig 3.43B). The scaffolds framework possessed a much-reduced radio-opacity compared to the microtissue regions. From the images, no clear difference in radio-opacity was observed between the MI192 pre-treated and untreated groups.

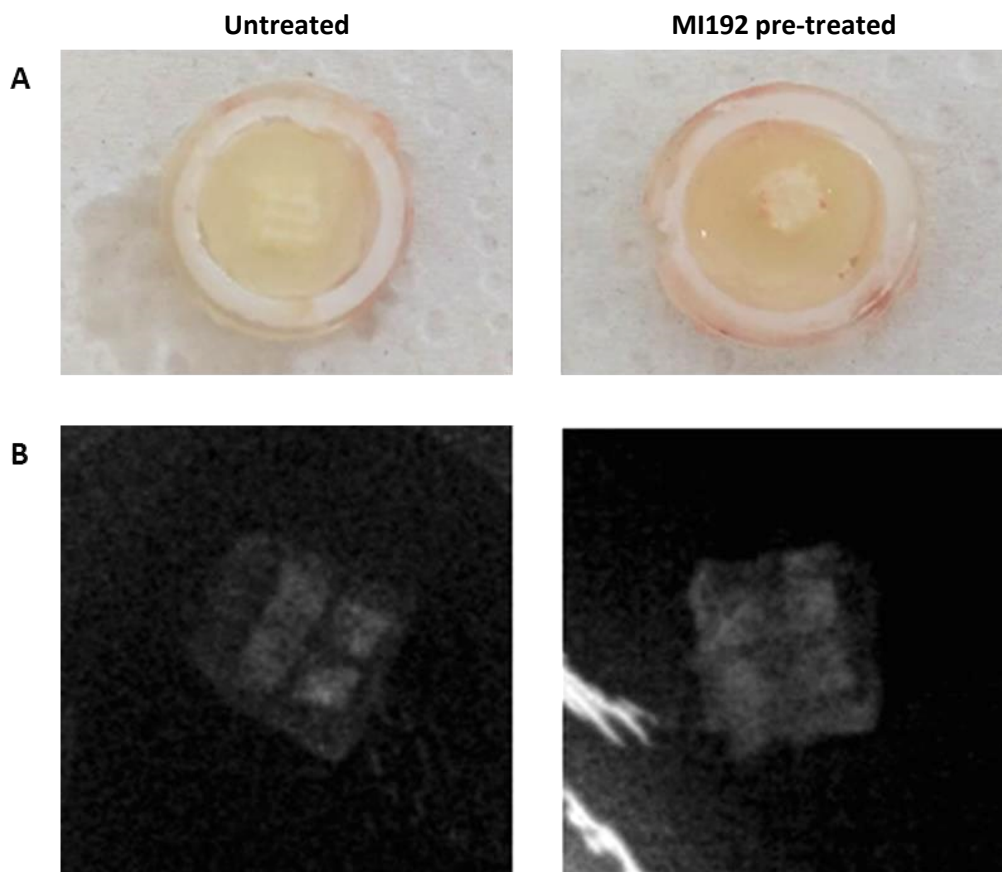


Figure 3.43 - Macroscopic and X-ray images of untreated/MI192 pre-treated hDPSCs BMT constructs after 8 weeks *in vivo* implantation. A) Macroscopic images immediately post extraction. B) X-ray radiographs of BMTs following extraction.

3.3.4.2 - The effect of MI192 on hDPSCs tissue formation during BMT *in vivo* implantation

Histological analysis was undertaken to investigate the effects of MI192 pre-treatment on hDPSCs tissue formation within the BMT construct following 8 weeks *in vivo* implantation (Fig 3.44). Following H&E staining, within both groups incorporated microtissues were seen occupying the internal volume of the 3D printed scaffold, where the fusion of microtissues within the scaffold framework and around the internal scaffold fibres was observed (scaffold fibres dislodged during histological analysis). The MI192 pre-treated group displayed much denser tissue formation which was uniformly distributed throughout the construct when compared to the untreated control. Moreover, within the MI192 pre-treated group, a greater degree of tissue organisation was observed, with each microtissue exhibiting a unidirectional stratified tissue distribution.

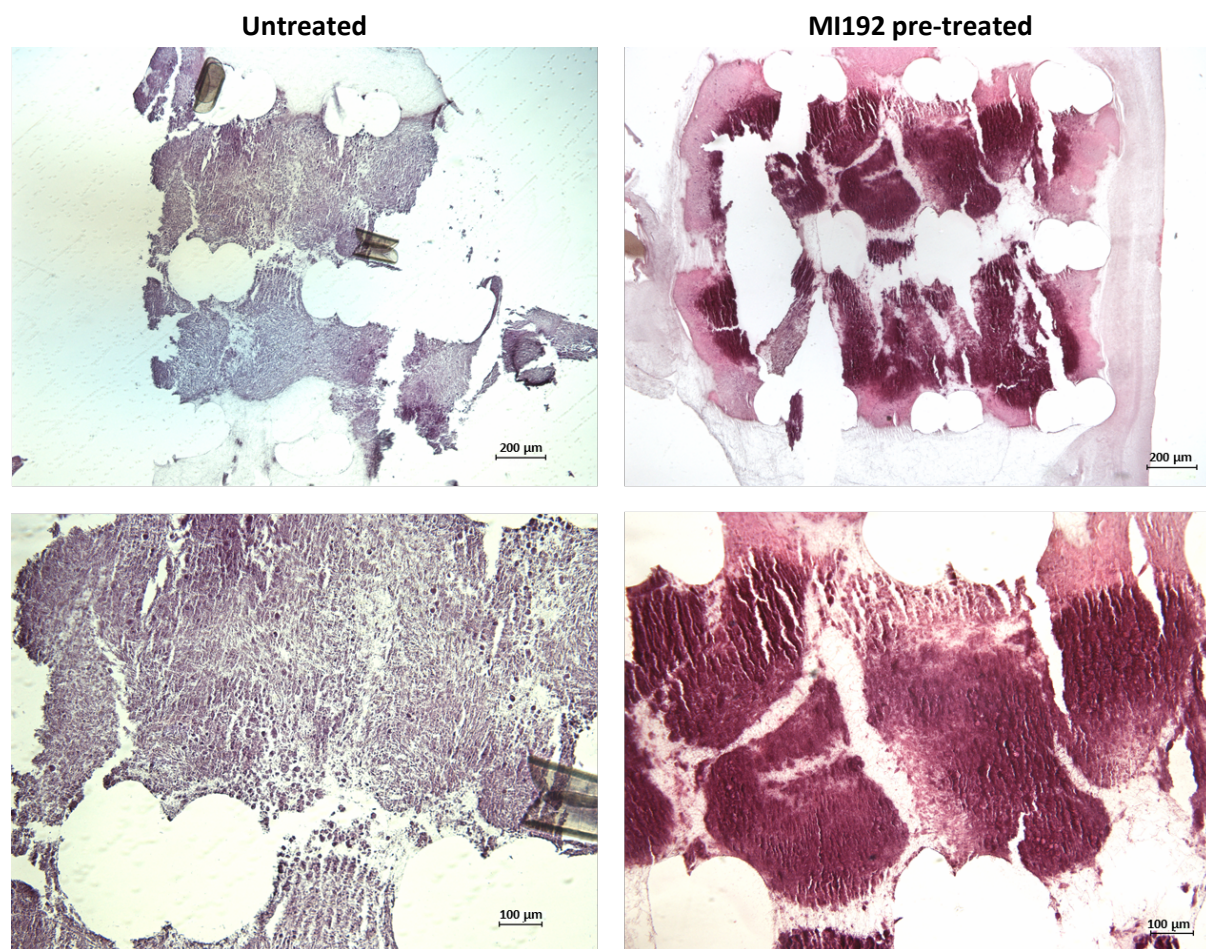


Figure 3.44 - H&E staining of untreated/MI192 pre-treated hDPSC BMT constructs after 8 weeks *in vivo* implantation. Scale bars = 200 (top row) and 100 µm (bottom row), respectively.

Figure 3.45 shows Picosirius red/Alcian blue staining for collagens and GAGs within MI192 pre-treated and untreated hDPSC BMTs following 8 weeks *in vivo* implantation. The MI192 pre-treated BMT exhibited positive collagen expression throughout, with increased expression intensity located at the outer regions of the microtissues and at the periphery of the construct. In comparison, the untreated group exhibited weaker Picosirius red staining which was expressed at a similar staining intensity throughout the BMT. Collagen deposition followed the uniform direction of tissue formation in the MI192 pre-treated group, while the expression in the untreated group was more aberrant in nature. Additionally, the untreated group exhibited positive Alcian blue staining for GAG accumulation which was distributed uniformly throughout the construct. Much weaker underlying Alcian blue staining was observed in the MI192 pre-treated BMT construct.

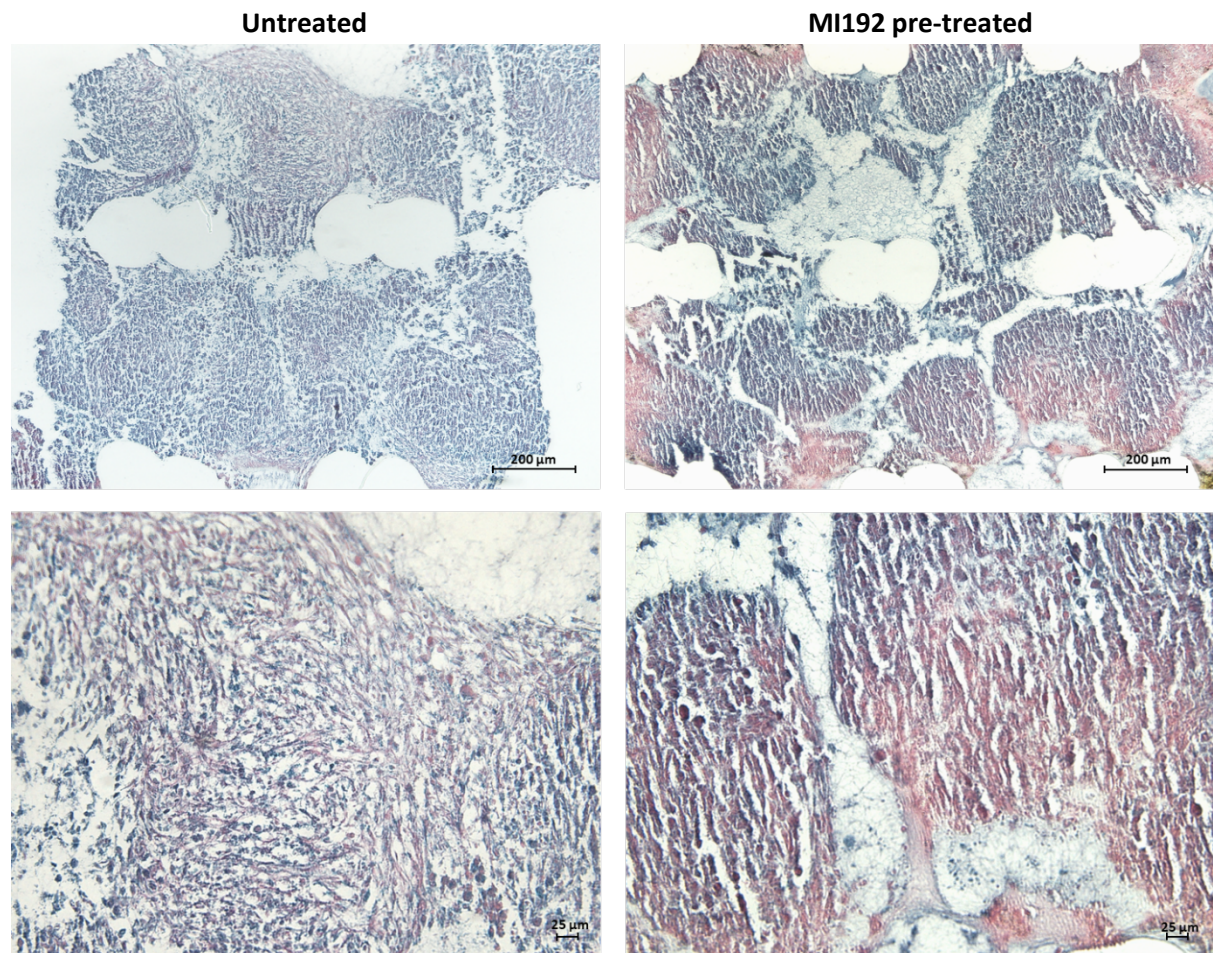


Figure 3.45 - Picosirius red/Alcian blue staining of untreated/MI192 pre-treated hDPSC BMT constructs after 8 weeks *in vivo* implantation. Collagens and GAGs stained with Picosirius red and Alcian blue, respectively. Scale bars = 200 (top row) and 25 μm (bottom row), respectively.

3.3.4.3 - The effect of MI192 on hDPSCs osteogenic protein expression during BMT *in vivo* implantation

Col1a

Positive Col1a expression was observed in the untreated BMT group primarily located at the edges of individual microtissues within the construct (Fig 3.46). The MI192 pre-treated group exhibited much stronger Col1a staining intensity throughout the construct, with the strongest staining located at the edges of individual microtissues.

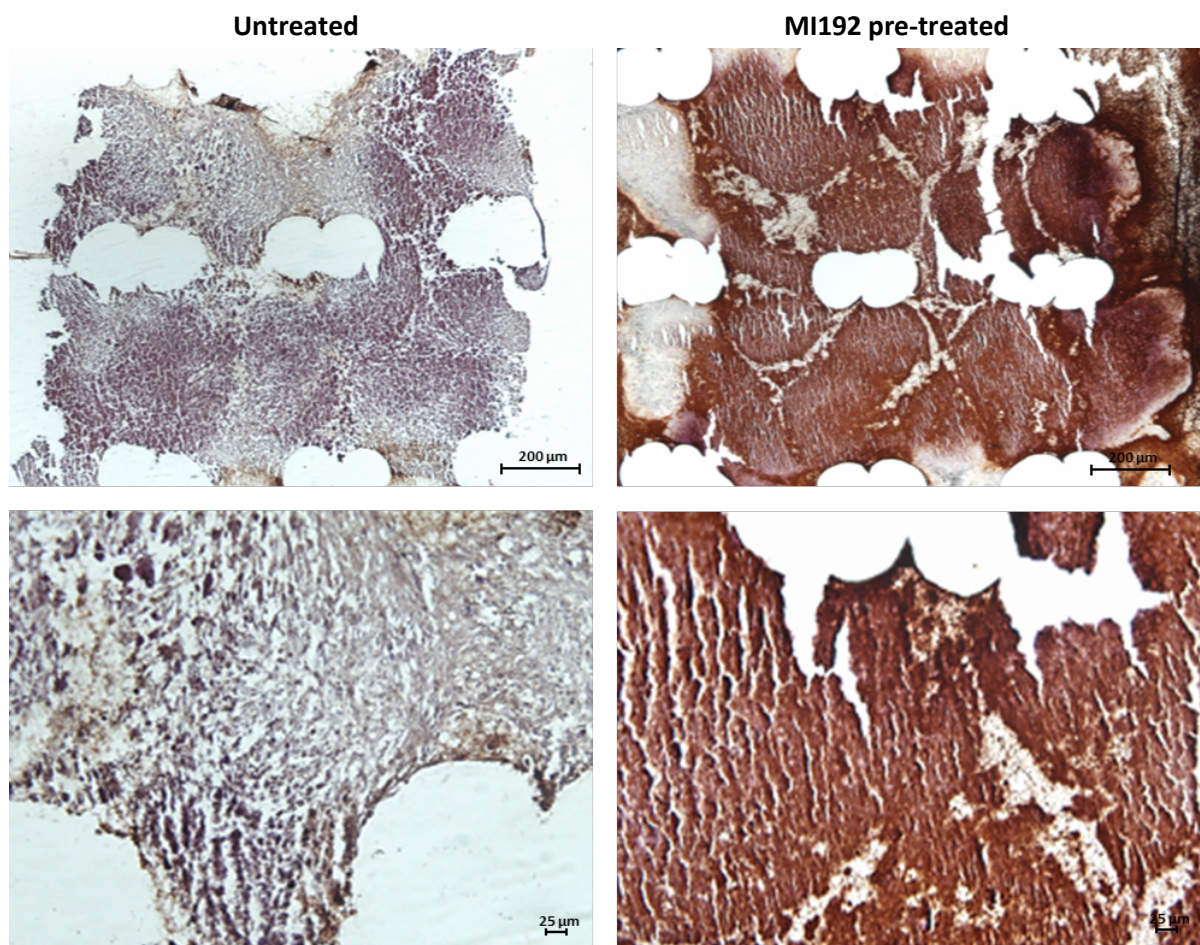


Figure 3.46 - Col1a immunohistochemical staining of untreated/MI192 pre-treated hDPSC BMT constructs after 8 weeks *in vivo* implantation. Positive Col1a immunohistochemical staining (brown), with a weak Harris haematoxylin counterstain (purple). Scale bars = 200 (top row) and 25 μm (bottom row), respectively.

OCN

Figure 3.47 shows OCN protein immunostaining of MI192 pre-treated and untreated hDPSC BMTs. The untreated group exhibited positive OCN staining which was expressed aberrantly throughout the construct. Within the MI192 pre-treated group, positive OCN staining was observed at a much stronger staining intensity compared to the untreated group. Additionally, protein staining was distributed more uniformly throughout the construct when compared to the untreated group, with a slight increase in expression intensity observed at the outer regions of the individual microtissues.

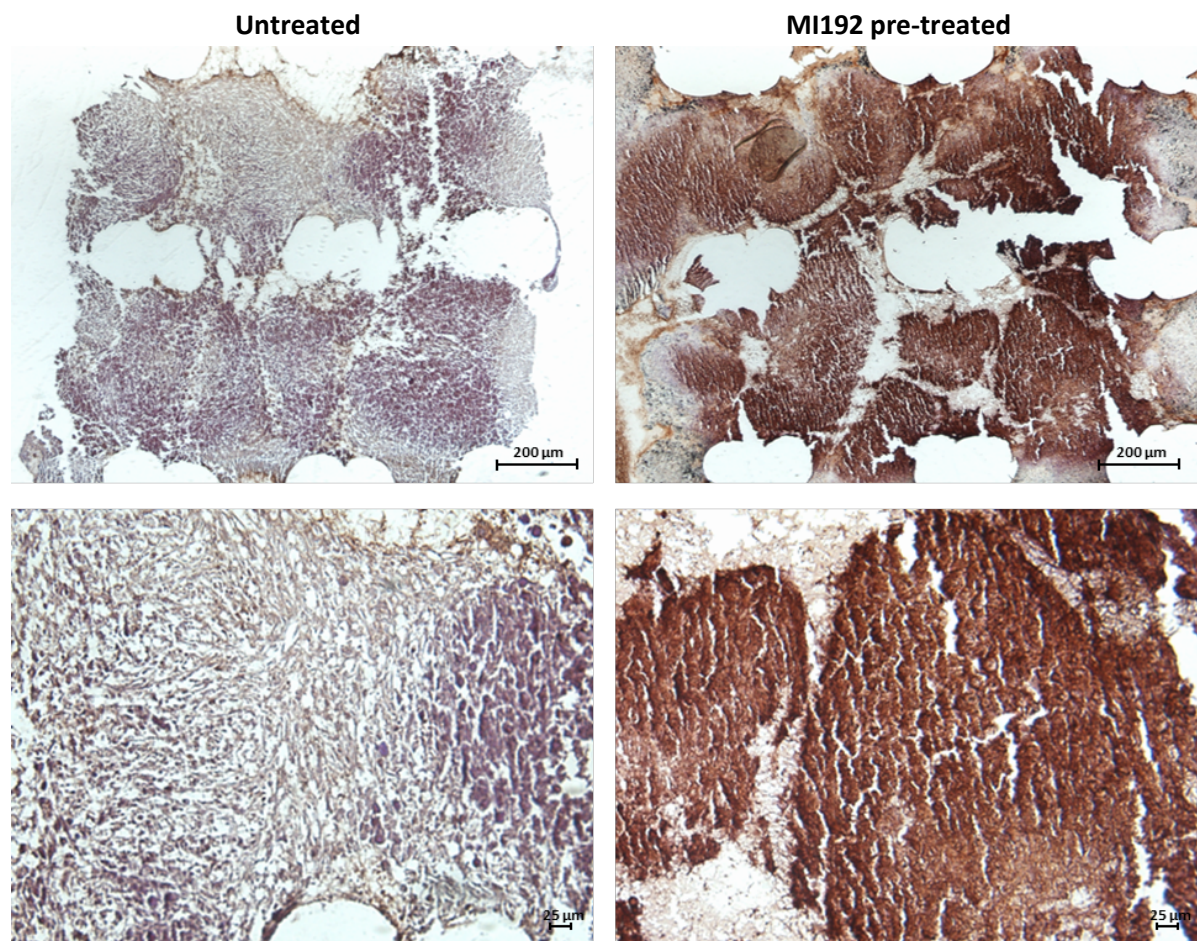


Figure 3.47 - OCN immunohistochemical staining of untreated/MI192 pre-treated hDPSC BMT constructs after 8 weeks *in vivo* implantation. Positive OCN immunohistochemical staining (brown), with a weak Harris haematoxylin counterstain (purple). Scale bars = 200 (top row) and 25 μm (bottom row), respectively.

3.3.4.4 - The effect of MI192 on hDPSCs chondrogenic protein expression during BMT *in vivo* implantation

AGG

Positive AGG expression was observed in the untreated group throughout the construct, with increased intensity observed at the periphery of the construct (Fig 3.48). The MI192 pre-treated group exhibited much-reduced staining intensity for AGG within the BMT construct.

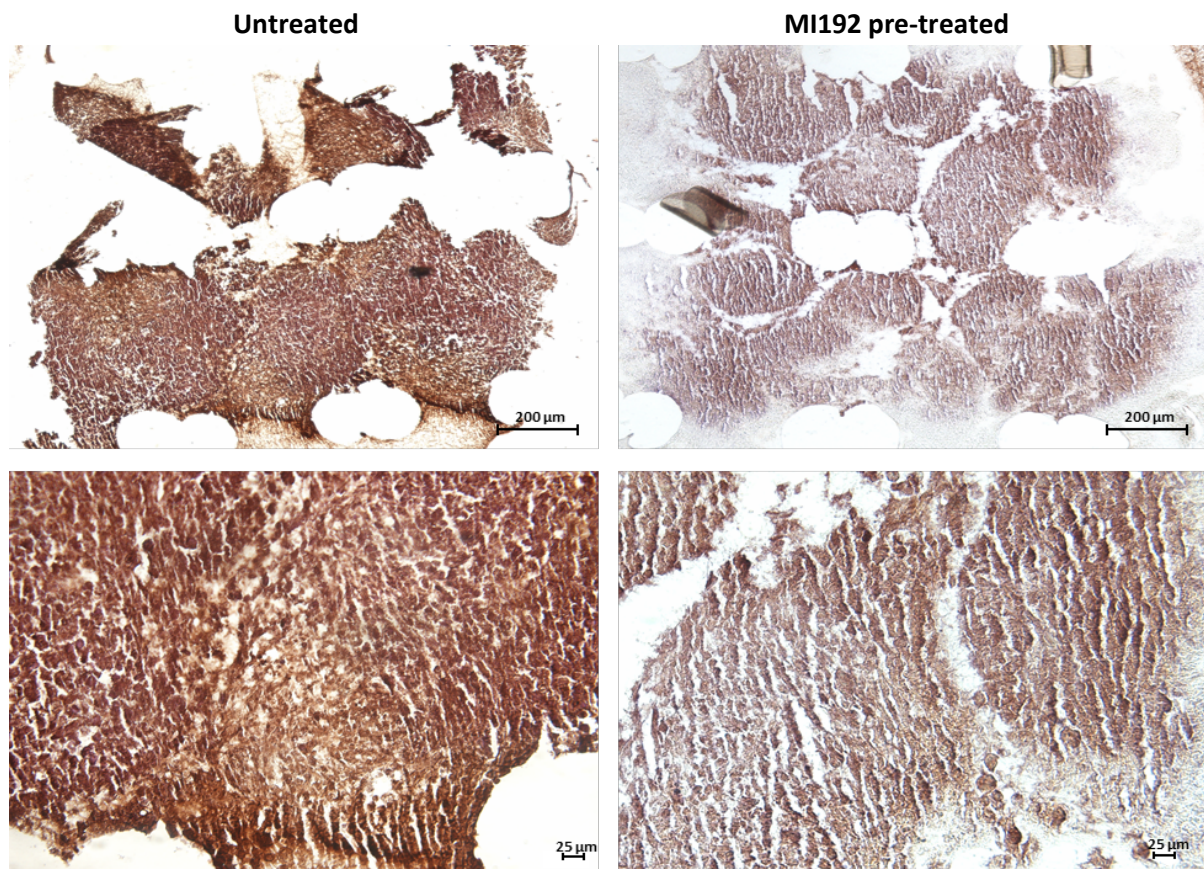


Figure 3.48 - AGG immunohistochemical staining of untreated/MI192 pre-treated hDPSC BMT constructs after 8 weeks *in vivo* implantation. Positive AGG immunohistochemical staining (brown), with a weak Harris haematoxylin counterstain (purple). Scale bars = 200 (top row) and 25 μm (bottom row), respectively.

Col2a

Positive expression of Col2a was observed in both the MI192 pre-treated and untreated hDPSCs BMTs (Fig 3.49), however, the untreated group exhibited much stronger staining intensity for this protein, particularly located in one quadrant in the construct. Negative immunostaining of untreated and MI192 pre-treated hDPSC BMT constructs after 8 weeks *in vivo* implantation is shown in figure 3.50.

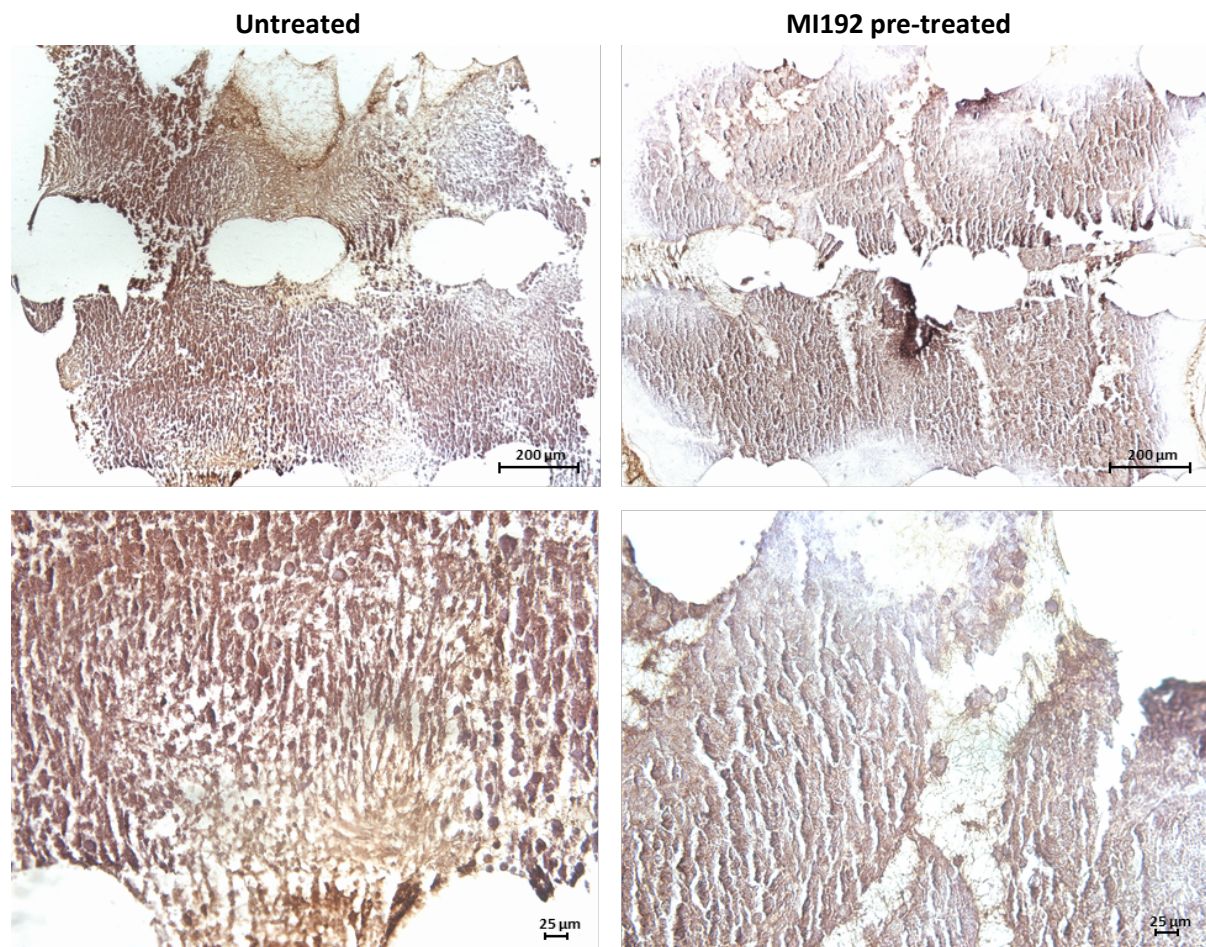


Figure 3.49 - Col2a immunohistochemical staining of untreated/MI192 pre-treated hDPSC BMTs after 8 weeks *in vivo* implantation. Positive Col2a immunohistochemical staining (brown), with a weak Harris haematoxylin counterstain (purple). Scale bars = 200 (top row) and 25 μm (bottom row), respectively.

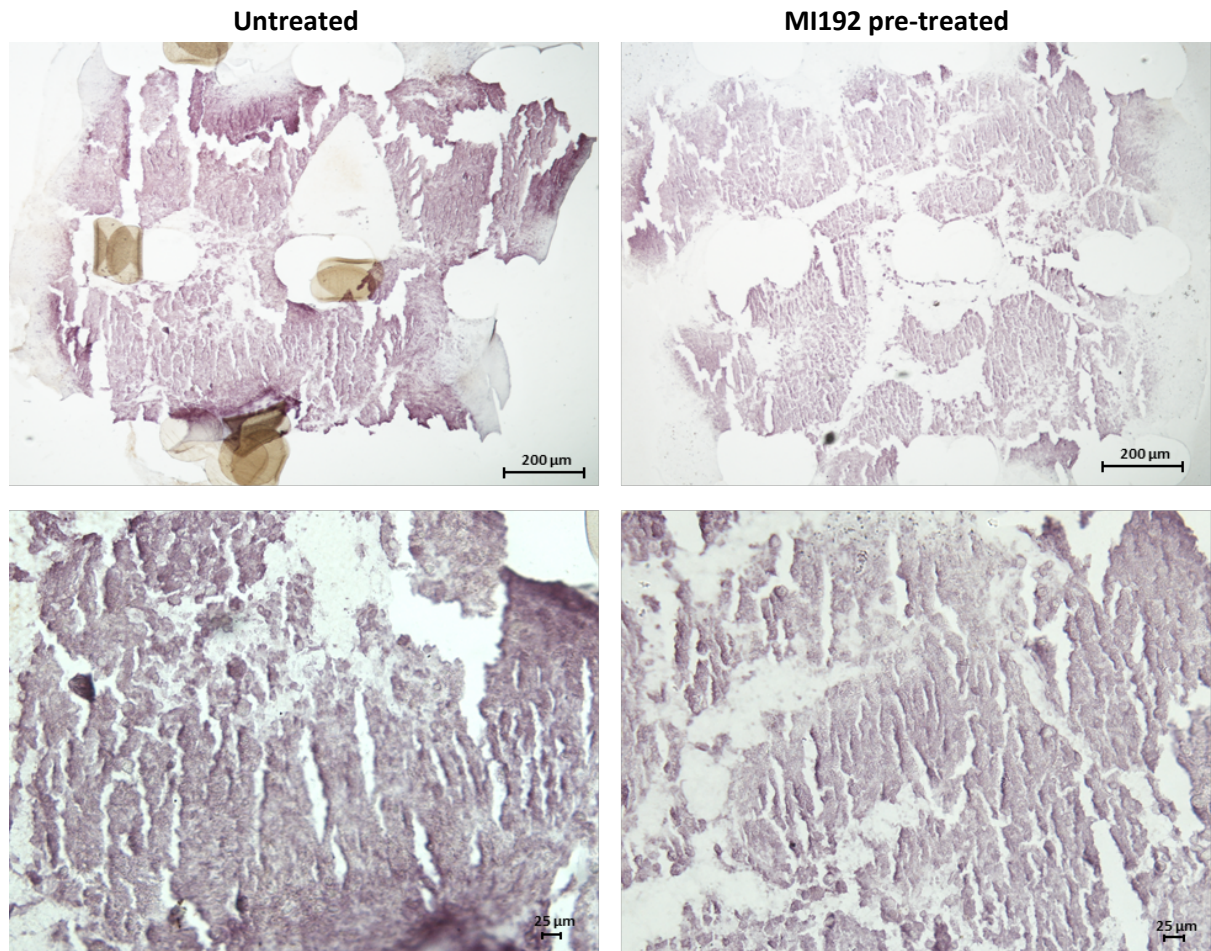


Figure 3.50 - Negative immunohistochemical staining of untreated/MI192 pre-treated hDPSC BMTs after 8 weeks *in vivo* implantation. Scale bars = 200 (top row) and 25 μm (bottom row), respectively.

3.3.4.5 - The effect of MI192 on hDPSCs calcium deposition and mineralisation during BMT *in vivo* implantation

Calcium deposition of MI192 pre-treated and untreated hDPSC BMT constructs was assessed following Alizarin red staining (Fig 3.51). The MI192 pre-treated group possessed strong Alizarin red staining intensity distributed uniformly throughout the construct. Within the untreated BMT, calcium deposition was observed throughout the construct at a much-reduced staining intensity compared to the MI192 pre-treated group. Increased staining intensity was situated at the outer regions of individual microtissues in both groups.

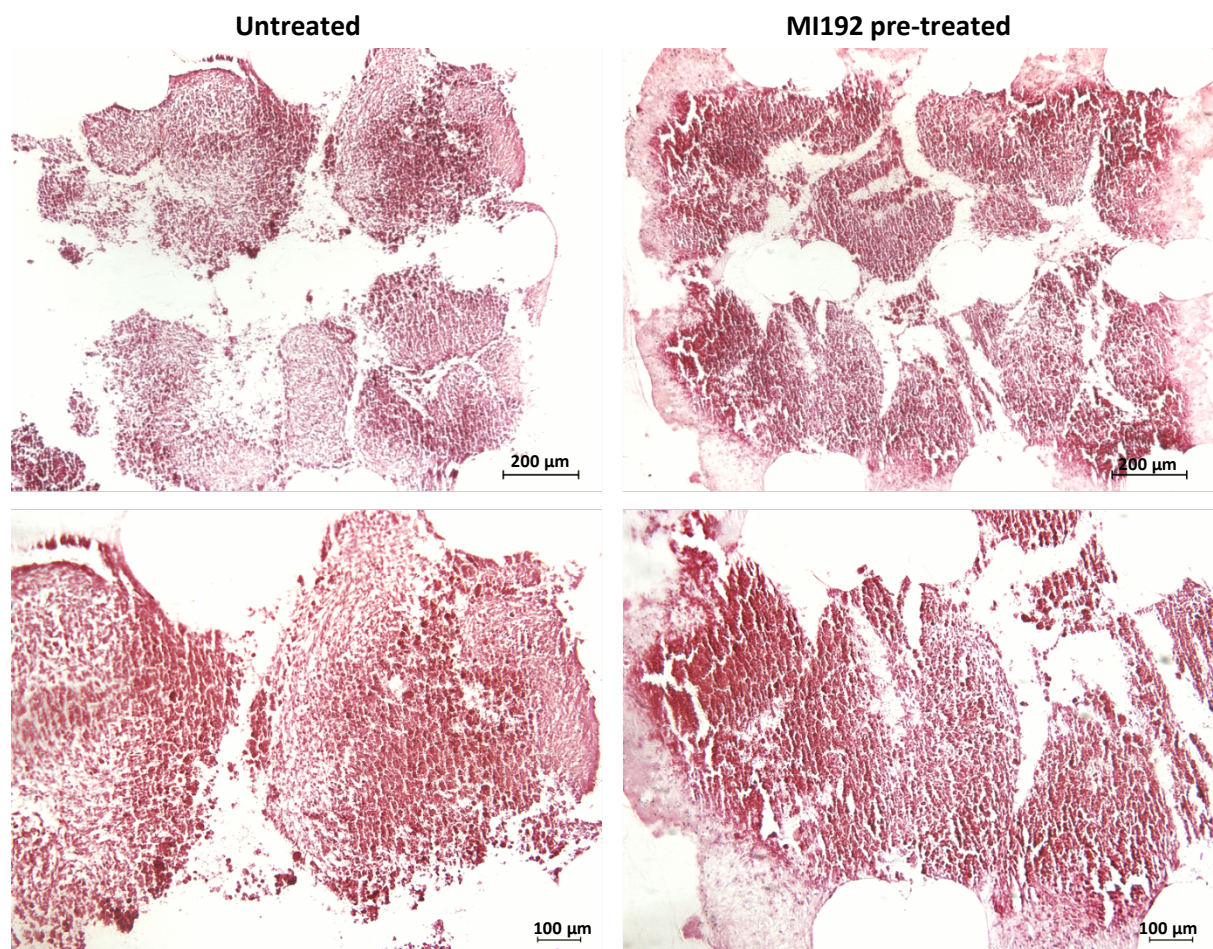


Figure 3.51 - Calcium deposition of untreated/MI192 pre-treated hDPSC BMT constructs after 8 weeks *in vivo* implantation observed by Alizarin red staining. Scale bars = 200 (top row) and 100 µm (bottom row), respectively.

Von Kossa staining on MI192 pre-treated and untreated hDPSC BMT constructs was performed to assess mineral nodule formation within the constructs (Fig 3.52). Within both groups, strong black staining was observed throughout the constructs, with particular increased intensity at the outer regions of the individual microtissues. However, the MI192 pre-treated group exhibited substantially increased black staining intensity throughout the BMT.

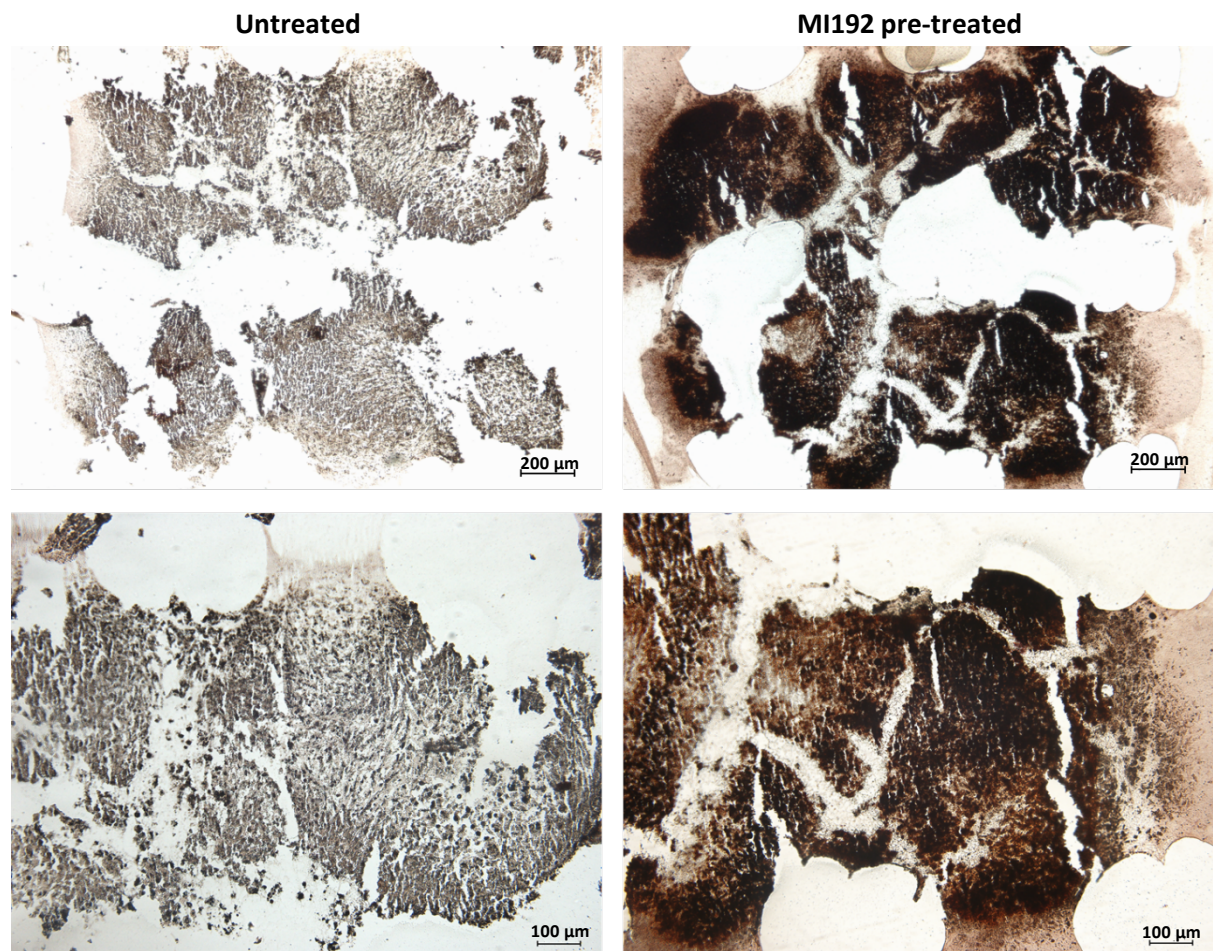


Figure 3.52 - Mineralisation of untreated/MI192 pre-treated hDPSC BMT constructs after 8 weeks *in vivo* implantation observed by Von Kossa staining. Scale bars = 200 (top row) and 100 μm (bottom row), respectively.

3.4 - Discussion

Within the bone tissue engineering field, a plethora of MSCs from different sources have been evaluated for bone augmentation strategies. In recent years, research has evaluated the use of alternative sources for MSCs such as DPSCs due to the ease of procurement, high rate of proliferation and osteogenic potential when compared to the gold standard BMSCs (261). Additionally, several studies have demonstrated cryopreservation does not affect the stem cell properties of DPSCs (231, 232), therefore providing considerable potential for tissue engineering applications, as extracted teeth are routinely discarded as medical waste. Although studies have reported successful utilisation of MSCs for bone tissue engineering, the development of clinically relevant bone tissue has not yet been achieved. Therefore, alternative methods to stimulate the osteogenic capacity of MSCs have been investigated. Epigenetic approaches for tissue engineering applications have garnered increasing attention due to their ability to alter MSCs transcriptional potential without altering the underlying DNA sequences. An increasing number of studies have demonstrated the potential of using HDACi compounds to stimulate MSCs osteogenic differentiation (74, 209), however, the majority of these studies have utilised panHDACis, which are associated with reduced differentiation efficacy and potential side-effects (213). Studies have demonstrated the importance of HDAC3 in osteogenesis due to its repression of the key osteogenic transcription factor Runx2 (140, 262). Previously, it was demonstrated that the selective HDAC2 and 3 inhibitor - MI192 stimulated the osteogenic potential of ADSCs when compared the panHDACi TSA (214). Therefore, the aim of this chapter was to determine the effects of MI192 on the behaviour and osteogenic capacity of hDPSCs on 2D and 3D *in vitro* and *in vivo*.

3.4.1 - The effects of MI192 on hDPSCs general behaviour in 2D culture

Various studies have shown that cancerous cells exhibit increased sensitivity to HDACi induced cell death compared to normal cells (129). For example, MS-275 and SAHA have been shown to halt the growth of normal human breast fibroblasts and embryonic lung fibroblasts but lead to rapid cell death of only the cancerous, transformed cells such as T-cell leukaemia and multiple myeloma (263). Therefore, to enhance the safety and efficacy of HDACi therapeutics, elucidating the effects of HDACis on normal cells (263), in particular MSCs is essential for potential clinical translation. In this study, the effects of MI192 treatment on hDPSCs morphology, metabolic activity, DNA content and cytotoxicity levels were evaluated.

From the morphological assessment, MI192 treatment induced a more flattened/elongated morphology, a phenotype associated with terminally differentiated osteogenic cells (209, 264). This

change in morphology correlated with similar findings by Lee *et al.* (2009) when human umbilical cord blood-derived MSCs (hUCSCs) and ADSCs were treated with VPA (264), while Paino *et al.* (2014) reported similar observations in VPA-treated hDPSCs (209). Moreover, Schroeder *et al.* (2005) demonstrated a flattened/elongated morphology of MC3T3-E1 osteoblast cell line treated with TSA, VPA and NaB (113). In this study, this morphological change was most evident in cells treated with lower concentrations of MI192 ($\leq 20 \mu\text{M}$), while higher concentrations altered the cells' appearance to a more condensed morphology. Moreover, within the higher MI192 groups ($\geq 20 \mu\text{M}$), an increased quantity of floating dead/detached cells in addition to decreasing attached cell density was observed, which was increasingly evident in a time-dose dependent manner. MI192 treatment of ADSCs showed similar effects on increasing quantity of floating dead/detached cells and reduced cell density, although no elongation in morphology was observed at low MI192 doses (214), likely due to the differences in the osteogenic capacity of ADSCs and hDPSCs (265). Together, the effects of MI192 on changing morphology, decreasing cell density and increasing quantity of floating dead/detached cells indicates the cytotoxicity of this HDACi.

The effects of MI192 on hDPSCs metabolic function and cell health were assessed. The AlamarBlue assay was utilised as it is regarded as a reliable, fast and high-throughput approach to assess viability (218). Additionally, this method has been utilised by studies investigating the effects of HDACis on the viability of cancer cell lines (TSA and SAHA on neuroblastoma BE (2)-C and MCF7 breast cancer cell lines, respectively) (266, 267). Upon MI192 treatment, a time-dose dependent reduction in the metabolic activity of hDPSCs was observed. Boissinot *et al.* (2012) reported a similar decrease in the metabolic activity of leukaemia cell lines following MI192 treatment (100). Moreover, the results in this study were consistent with those performed previously, where MI192 reduced the metabolic activity of ADSCs (214). This time-dose dependent decrease in metabolic function is likely an indication of the cytotoxic effects of MI192 as only viable cells are metabolically active, correlating with the morphological assessment results. However, the effects of HDACis on halting cell cycle progression (i.e. proliferation) may result in suspending/reducing the metabolic activity of the cells, with studies reporting close association of cell cycle and metabolic regulation (268, 269).

DNA quantification was undertaken to determine the effects of MI192 on hDPSCs proliferation and cell death, as indicated from the previous viability analysis (270). PicoGreen quantification of DNA content has been reported to provide a more accurate assessment of proliferation compared to metabolic assays (271). A time-dose dependent decrease in hDPSCs DNA content was observed following MI192 treatment, replicating the previous viability results in this study (morphological and metabolic assessment). The reduction in DNA content induced by MI192 is likely attributed

to halting cellular proliferation at lower MI192 doses/duration, while at higher MI192 doses/duration the cytotoxic effects of this HDACi are more prominent. It is important to note that these results do not take into consideration the number of detached viable cells which may recover and reattach, as these floating cells would be wash away prior to DNA quantification. Several studies have indicated the potential of HDACis in affecting the adhesion properties of cells (272, 273), therefore potentially resulting in the increased quantity of floating cells observed in the MI192 treatment groups from the morphological assessment.

The effect of MI192 on hDPSCs cytotoxicity was evaluated using the CytoTox-Fluor Cytotoxicity Assay. A time-dose dependent increase in the cytotoxicity marker was detected upon MI192 treatment, consistent with the other viability findings in this study. The data acquired from the cytotoxicity assay provides a more accurate indication of the cytotoxic effects of MI192, as this analysis measures the relative number of dead cells by assessing the release of protease activity (274). As this assay quantifies the release of protease from membrane permeable cells, if MI192 treatment caused damage to the cells, it may result in the release of protease into the medium. As with various studies utilising HDACis, these results clearly demonstrate that prolonged treatment with MI192 has a detrimental effect on cell viability; therefore, to investigate the effects of MI192 on stimulating osteogenesis, the exposure of this compound on hDPSCs must be tightly controlled.

The cell cycle is key in regulating normal cellular functions such as proliferation, differentiation and apoptosis (119). Numerous studies have reported that HDAC2 and 3 isoforms are involved in cell cycle regulation (119, 275), and HDACi compounds have been demonstrated to halt cells at various stages of the cell cycle (276, 277). In this study, 2 μ M MI192 was used to assess the effects on hDPSCs cell cycle progression due to the limited cytotoxicity induced and sufficiently enhancing H3K9 acetylation (Fig 3.7). Moreover, this treatment condition enhanced the osteogenic capacity of hDPSCs, as demonstrated in the ALPSA result (Fig 3.10). MI192 treatment was found to halt the accumulation of hDPSCs in the G₀/G₁ phase, increasing the percentage of cells in the S and G₂/M phase when compared to the untreated control. These findings indicate the role of MI192 in halting cell cycle progression through the G₂/M checkpoint. This checkpoint is where cells monitor for and repair DNA damage before cell division occurs. Therefore, the accumulation in this phase induced by MI192 may be due to the cell's response to DNA damage, where studies have demonstrated this effect with other HDACis (278, 279). DNA damage is often associated with cycle arrest, followed by induced apoptosis, particularly in cancer models. HDACi treatment on cancer cells has been shown to halt cell cycle progression at the G₂/M phase, allowing for the activation of the cell's apoptotic mechanisms (112). The effects of HDACis on normal cells are less pronounced compared to

cancerous cells, due to the intact cell cycle checkpoints (113). Therefore, the accumulation in the G₂/M phase is likely due to the effects of this HDACi in halting proliferation rather than inducing apoptosis, as the MI192 concentration utilised (2 µM) exhibited limited cytotoxicity. Jiang *et al.* (2014) reported similar findings where adult neural stem/progenitor's cells knockdown for HDAC3 were unable to pass the G₂/M phase, emphasising the role of HDAC3 in controlling the progression through this phase via stabilisation CDK1 (119). Xu *et al.* (2013) also reported that Vorinostat treatment halted BMSCs at the G₂/M phase (19). Moreover, the results of the present study were consistent with findings acquired previously with MI192 treated ADSCs (214). Zhang *et al.* (2017) showed a similar increase in the G₂/M phase following osteogenic induction of a hBMSC cell line (PTA-1058), indicating the increase in this phase induced by HDACis, may be linked to halting proliferation and preparing cells for differentiation (280). Therefore, the results of this study indicate MI192 synchronises hDPSCs cell cycle progression at the G₂/M phase, demonstrating the role of this HDACi in halting proliferation and priming cells for differentiation.

MSCs have been shown to be highly sensitive to epigenetic changes (281), indicating the potential of utilising HDACi compounds for enhancing MSCs efficacy for bone tissue engineering applications. Due to this, it is essential to acquire a deeper understanding of the possible mechanisms in which MI192 alters the epigenome of hDPSCs. In this study, MI192 treatment significantly reduced hDPSCs HDAC specific activity after 24 and 48 hours compared to the untreated cells, correlating with results acquired with this inhibitor on HeLa, PC3 and ADSCs (100, 282). In previous studies, it was demonstrated that 10 µM MI192 decreased HDAC activity by ~49% after 24 hours treatment in both HeLa and PC3 cells (100, 282), while the results of this study showed a ~83% reduction after 24 hours treatment. This indicates that MI192 exhibits increased potency in reducing HDAC activity in MSCs compared to HeLa and PC3 cells lines. Furthermore, 10 µM MI192 treatment for 24 and 48 hours reduced ADSCs HDAC activity by approximately 2.4- and 2.7-fold (214), while in this study HDAC activity was reduced by ~6- and ~6.8-fold in the same conditions, likely attributed to the differences in MSC phenotype. Following 1 week in basal culture, the MI192 pre-treated hDPSCs continued to exhibit a significant reduction in HDAC activity when compared to the untreated cells (~48% and ~55% reduction after 24 and 48 hours pre-treatment, respectively). The sustained inhibition of HDAC activity 1 week after the removal of MI192, demonstrates the slow binding kinetics of this HDACi on hDPSCs (100), which may be beneficial in augmenting the osteogenic capacity of MSCs. Additionally, in the literature, it has been demonstrated that HDACi incubation downregulates the expression of HDAC enzymes, correlating with the prolonged HDAC inhibition observed in this study (283, 284).

With MI192 demonstrated to inhibit HDAC activity in hDPSCs, the downstream effects of this inhibition on histone acetylation was assessed. H3K9 acetylation levels were evaluated as acetylation at these sites indicates a transcriptionally permissive chromatin structure (71). The findings in this study showed that only MI192 treatment for 48 hours significantly enhanced H3K9 acetylation levels when compared to untreated cells. This result is of particular importance as it confirms the HDAC inhibition induced by MI192 has a positive downstream effect on histone acetylation levels, demonstrating this HDACi is an effective epigenetic regulator for hDPSCs. More importantly, it has been suggested that the first and one of the most vital changes that occur in modifying the epigenome is altering the transcriptional potential of the cell, subsequently augmenting gene expression (209, 212, 285). It was demonstrated that MI192 was unable to increase H3K9 acetylation of cells after 24 hour treatment, therefore introducing osteogenic medium whilst the cell's chromatin remains condensed, will hinder the potency of osteoinductive growth factors. Boissinot *et al.* (2012) reported that MI192 exhibited a >250-fold selectivity for HDAC2/3 when compared to other HDAC isoforms (100). Therefore, due to this increased selectivity, within the MI192 pre-treated cells uninhibited HDAC enzymes could still remain and deacetylate the substrate at the 24 hour time point. MI192 treatment for 48 hours increased H3K9 acetylation levels, indicating this pre-treatment duration would enhance the efficacy of the introduced osteogenic growth factors, as confirmed by the ALPSA results (Fig 3.10).

3.4.2 - The effects of MI192 on hDPSCs osteogenic capacity in 2D culture

In the literature, panHDACis has been demonstrated to stimulate MSCs osteogenesis (209, 212), however, the use of these non-selective HDACis are associated with limitations (213). Consequently, there is a growing precedence to evaluate the efficacy of isoform-selective HDACis to stimulate MSCs osteogenic capacity. Therefore, in this study, the effects of MI192 on hDPSCs osteogenic differentiation was investigated via assessing ALPSA, osteoblast-related gene/protein expression, calcium deposition and mineralisation in 2D *in vitro* culture.

It was previously reported that prolonged culture with MI192 during osteogenic differentiation reduced the osteogenic capacity of ADSCs, in addition to having a detrimental effect on cell viability (214). Therefore, a pre-treatment strategy was adopted to limit the cytotoxic effects of this HDACi, consistent with studies in the literature (209, 286). In this study, a “safe range” of MI192 concentrations (5, 10, 20 μ M for 24 hours and 1, 2, 5 μ M for 48 hours) were utilised to evaluate the effect of MI192 on hDPSCs ALPSA, an early indicator of osteogenesis. MI192 pre-treatment for 24 hours (5, 10 and 20 μ M) significant reduced hDPSCs ALPSA in a dose-dependent manner compared to the untreated osteogenic control. After 48 hours pre-treatment, 2 and 5 μ M MI192 significantly

enhanced ALPSA when compared to the 1 μM MI192 group and the untreated controls. No significance was observed between the 2 and 5 μM groups, therefore the lower concentration was selected to minimise potential side-effects associated with HDACi exposure. Additionally, it was demonstrated that 2 μM MI192 pre-treatment increased hDPSCs ALP staining levels, with the MI192 pre-treated cells exhibiting a more flattened/elongated morphology, replicating the observations from the morphological assessment in this chapter (Fig 3.2). Interestingly, the ALPSA findings correlated with the acetylation results (Fig 3.7), where after 24 hours treatment a dose-dependent reduction in histone H3K9 acetylation was observed, while MI192 treatment for 48 hours significantly enhanced acetylation. The correlation of the acetylation and ALPSA profiles induced by MI192 indicates the importance of chromatin transcriptional permissiveness in stimulating the differentiation of hDPSCs. This indicates that after MI192 treatment for 48 hours, the induced hyperacetylation enhanced the transcriptional permissiveness of the chromatin, allowing for increased potency of introduced/intrinsic osteogenic growth factors. Moreover, this pre-treatment condition might be the dosage/duration necessary to selectively inhibit HDAC3 to a sufficient degree, resulting in the enhanced efficacy of the Runx2 transcription factor to stimulate downstream expression of osteoblast-related markers.

Several studies in the literature have demonstrated the effectiveness of HDACis in stimulating ALP activity. De Boer *et al.* (2006) reported enhanced ALP activity of human and goat BMSCs treated with TSA (74). Xu *et al.* (2013) showed that Vorinostat enhanced the ALP activity of BMSCs (19). Moreover, MI192 pre-treatment of 30 μM for 48 hours significantly increased ADSCs ALPSA (214). The differential MI192 treatment conditions required to stimulate ALPSA in ADSCs and DPSCs is likely attributed to the phenotypic differences between these MSCs. It has been demonstrated that DPSCs possesses a greater osteogenic potential than ADSCs (265), therefore requiring less stimulation to induced osteogenesis. The enhancement in ALPSA stimulated by MI192 within hDPSCs and ADSCs, indicate the efficacy of the pre-treatment strategy utilised, likely aided by the slow binding kinetics of this inhibitor demonstrated by the HDAC activity results in this chapter (Fig 3.6) and in the literature (100). Additionally, Xu *et al.* (2005) demonstrated the down-regulation in HDAC3 protein expression in SAHA treated BV-173 leukaemia cell lines (283). HDAC3 act as a co-repressor for the transcription factor Runx2, which is integral for initiating osteogenesis (140). In this study, it is likely a similar down-regulation in HDAC3 expression occurs within the HDACi treated hDPSCs, although due to MI192 selective inhibition of HDAC3, a greater reduction in HDAC3 expression may be observed compared to the use of panHDACis, although this would require further investigation. This could have contributed to the increased stimulation in ADSCs ALPSA induced by MI192 when compared to the panHDACi TSA reported previously (214).

Although confirming MI192 pre-treatment for 48 hours significantly increased hDPSCs ALPSA, donor variability is known to influence MSCs differentiation potential (287, 288). Therefore, the effects of MI192 pre-treatment (1, 2 and 5 μ M for 48 hours) on the ALPSA of hDPSCs acquired from three different donors were assessed, shown in the Appendix (Fig A1). The results of this study showed that 2 μ M MI192 for 48 hours significantly promoted ALPSA when compared to the 1 μ M MI192 group and the untreated cells in all three donors. 5 μ M MI192 significantly increased ALPSA compared to 1 μ M and the untreated osteogenic control, although was decreased compared to the 2 μ M MI192 in donor 1 and 2. The findings from this study clearly demonstrate that MI192 pre-treatment for 48 hours significantly increased hDPSCs ALPSA in all three donors, indicating MI192 stimulation of hDPSCs ALPSA was not donor-dependent. These findings were consistent with the effects of MI192 on promoting the ALPSA of ADSCs acquired from multiple donors (214), providing more substantial evidence in regards to the efficacy of MI192 in stimulating MSCs osteogenesis in the clinical setting. Due to the greater fold increase in ALPSA induced by 2 μ M MI192 pre-treatment acquired from donor 1 and for practicality reasons, cells from this donor was utilised to further investigate the effects of MI192 on hDPSCs in this chapter. The optimised MI192 pre-treatment condition of 2 μ M for 48 hours was subsequently utilised for the rest of this chapter.

Increasing evidence has suggested that MSCs multi-lineage potential is determined by developmental regulation of certain transcription factors and lineage-specific genes (289). The mRNA levels of osteoblast-related genes have been shown to be altered in the presence of HDACis due to their regulation of the cell's epigenetics (209, 212, 285). To acquire a better understanding of the mechanisms in which MI192 stimulates hDPSCs osteogenic differentiation, the effects of MI192 pre-treatment on hDPSCs osteoblast-related gene expression and the subsequent downstream protein production during osteogenic culture were assessed using RT-qPCR and ICW, respectively.

Runx2 is known to be the osteogenic lineage-specific transcription factor and has been shown to be key in promoting osteogenic differentiation and mineralisation via the stimulation of osteoblast-related markers (290). Immediately post-treatment, *RUNX2* mRNA levels were significantly reduced in the MI192 pre-treated cells compared to that in the untreated group. As MI192 is known to selectively inhibit HDAC3, the co-repressor of the Runx2 transcription factor (144), this may result in alleviating Runx2 inhibition, therefore causing negative feedback repression of *RUNX2* gene expression in the MI192 pre-treated cells. Interestingly, at day 21 and 28, *RUNX2* mRNA levels were significantly upregulated in the MI192 pre-treated cells. The initial downregulation and then delayed upregulation in *RUNX2* gene expression within the MI192 pre-treated hDPSCs replicated a similar profile observed in the MI192 pre-treated ADSCs (214), indicating a similar mechanism of action

induced by MI192 in these MSCs. The protein expression of this transcription factor after 7 days osteogenic culture was reduced in the MI192 pre-treated cells, while expression was significantly upregulated on day 14 and 28, consistent with the *RUNX2* gene expression profile. It is important to note that ICW measures total Runx2 protein within the cell, therefore, does not distinguish between HDAC3 bound/unbound transcription factors. Consequently, it is likely the MI192 pre-treated cells would possess an increased quantity of unbound, transcriptionally active Runx2, due to its selective inhibition of HDAC3. Moreover, hyperacetylation induced by HDACis is known to affect non-histone proteins such as transcription factors, in addition to its effect on chromatin remodelling (291). Jeon *et al.* (2006) reported that BMP2 increased p300 acetylation of Runx2 in Runx2-transfected HEK293 and C2C12 cells, inhibiting Smurf1-mediated degradation of Runx2, ultimately enhancing its stability and transcriptional activity (292). Hence, the hyperacetylation observed in the MI192 pre-treated cells may result in enhancing Runx2 transcriptional activity and stability, although this would require further investigation. Studies have also reported that HDACi treatment resulted in the downregulation of HDAC expression (283, 291), therefore it is possible MI192 inhibits HDAC3 expression within hPSCs, further increasing Runx2 transcriptional activity.

BMP2 is a potent osteogenic growth factor with a strong ability to induce ectopic bone formation (293). This bone associated growth factor acts to induce osteogenic differentiation via enhancing ATF6 transcription factor expression, which in turn promotes the expression of later osteogenic markers such as ALP (294). In this study, MI192 pre-treatment caused a significant upregulation of *BMP2* mRNA expression levels at all time points assessed compared to that in the untreated cells. It has been suggested that *RUNX2* is a downstream target of BMP2, therefore BMP2 may potentiate osteogenic differentiation in an autocrine and paracrine manner, as this growth factor is commonly used in osteogenic differentiation protocols (295, 296). This sustained upregulation in *BMP2* mRNA levels induced by MI192 likely promoted the expression of this growth factors' downstream targets, as confirmed by the enhanced expression of *RUNX2* and *ALP* in the MI192 pre-treated cells in this study. MI192 pre-treatment of ADSCs enhanced *BMP2* expression on day 3 alone which differed from the findings of this study, likely attributed to the differences in MSCs phenotype/osteogenic potential (265). ICW analysis showed MI192 pre-treatment increased BMP2 protein expression within hPSCs compared to the untreated cells throughout osteogenic culture, consistent with the mRNA expression results. Phimphilai *et al.* (2006) proposed that BMP signalling is an essential component to Runx2 dependent osteogenesis (296), and Hu *et al.* (2013) confirmed this in ADSCs with the addition of BMP antagonist, Noggin, resulting in a decrease in the *RUNX2* mRNA levels (290). The intimate coupling of *BMP2* and *RUNX2* during osteogenesis, correlated with the mRNA expression profiles observed in this study. In addition, there is evidence which suggests *RUNX2* and

BMP2 expression increases steadily throughout DPSCs osteogenic differentiation (209, 297), consistent with the mRNA and protein expression profiles acquired in this study.

The mRNA levels of the early osteogenic marker, *ALP*, was significantly upregulated in the MI192 pre-treated cells immediately post-treatment, likely contributing to the enhanced ALPSA and ALP staining observed in the MI192 pre-treated hDPSCs in this study. MI192 pre-treatment likely increased the potency of intrinsic osteogenic growth factors within hDPSCs via enhancing the transcriptional permissiveness of the chromatin, resulting in the enhanced *ALP* mRNA levels at this time point. The upregulation of *ALP* expression immediately post-treatment suggests MI192 is capable of directing osteogenic lineage-specific differentiation without the introduction of the osteogenic medium, likely due to inhibition of the bone-associated HDAC3 isoform (140). Additionally, the initial spike in *ALP* expression may be induced by the increased *BMP2* mRNA expression levels observed at the early time points. From day 3 to 14, *ALP* expression was at similar levels between the groups, likely caused by negative feedback repression induced by the previously elevated *ALP* levels within the MI192 pre-treated group. Moreover, MI192 increased expression on day 21 and 28 compared to the untreated cells, replicating a similar late upregulation with *RUNX2* and *BMP2* in this study. This late upregulation of these early markers indicates this pre-treatment condition is sufficient in potentiating the osteogenic phenotype of these cells, underlying the importance of the slow binding kinetics of this inhibitor (100). Additionally, Huynh *et al.* (2016) reported the downregulation in HDAC3 protein expression upon TSA treatment on hPDLCs (291). Therefore, a similar inhibition may occur within the MI192 pre-treated hDPSCs, resulting in the prolonged upregulation of these osteogenic markers after the removal of this HDACi. MI192 pre-treatment of ADSCs significantly upregulated *ALP* expression at early time points (day 5 and 7), while expression was significantly downregulated at later time points (day 14 and 21) compared to the untreated ADSCs (214). This expression profile did not correlate with the result acquired in this study, likely attributed to hDPSCs possessing a more advanced osteogenic phenotype compared to ADSCs (265). ICW analysis showed that ALP protein expression was significantly upregulated in the MI192 pre-treated cells compared to the untreated group at all times points assessed, consistent with the gene expression, ALPSA and ALP staining results acquired in this study.

The mRNA levels of *COL1A*, a key bone extracellular matrix protein (113), were significantly upregulated in the MI192 pre-treated cells immediately post-treatment. This indicates MI192 is capable of enhancing the expression of this marker prior to the introduction of the osteogenic medium, further supporting the lineage-specificity of this HDACi. It was previously reported that MI192 controlled the lineage-specific differentiation of ADSCs, by stimulating osteogenic

differentiation and inhibition of adipogenic differentiation (214). The increase in *COL1A* expression observed in this study is likely attributed to the basal phenotype of hDPSCs, as these cells are known to possess greater osteogenic capacity compared to other MSCs such as BMSCs (298). Therefore, hDPSCs would possess many of the required growth factors intrinsically to maintain this more advanced osteogenic phenotype. It is likely the hyperacetylation induced by MI192 increased the access of these intrinsic growth factors into the transcriptionally permissive chromatin, resulting in the upregulation of *ALP* and *COL1A* immediately post-treatment. Additionally, *COL1A* mRNA levels were significantly increased in the MI192 pre-treated cells on day 5 and 14, which is expected for this mid-late stage marker. A similar upregulation in *COL1A* gene expression was observed in TSA treated hPDLs (291). Moreover, MI192 pre-treated ADSCs displayed a significant down-regulation in mRNA levels at day 3, while at day 7 expression levels were significantly increased in the HDACi treated cells (214). The phenotypic difference between these MSCs, such as the basal phenotype and osteogenic potential (265), were likely responsible for the differential *COL1A* expression induced by MI192. At the protein level, a similar observation was observed where MI192 pre-treatment significantly increased Col1a protein expression throughout osteogenic culture, consistent with the gene expression finding in this study.

The mRNA levels of *OCN*, the noncollagenous extracellular matrix protein (33), was substantially enhanced in the MI192 pre-treated hDPSCs throughout the culture period assessed compared to that in the untreated cells, consistent with the observations from TSA treated hPDLs (291). *OCN* protein production was also significantly upregulated in the MI192 pre-treated cells, indicating the accelerated osteogenic maturation, consistent with the mRNA expression findings. Piano *et al.* (2014) pre-treated hDPSCs with VPA and showed a significant reduction in mRNA and protein expression of *OCN*, indicating this HDACi inhibited osteogenic maturation (209). Additionally, silencing of HDAC2 resulted in decreasing *OCN* expression in Saos-2M osteosarcoma cell line, indicating the importance of HDAC2 in regulating *OCN* mRNA expression (209). Although MI192 selectively inhibits HDAC2 and 3 isoforms (100), in this study, no downregulation in *OCN* expression was observed likely due to MI192 selective inhibition of HDAC3, which VPA does not possess. Due to the alleviation of Runx2 inhibition from HDAC3, the enhanced transcriptional activity of Runx2 in the MI192 pre-treated cells likely stimulated the transcription of several of its downstream target genes (299), such as *OCN*. Schroeder *et al.* (2004) used a transient transfection assay to show that HDAC3 suppressed the Runx2 mediated activation of the *OCN* promoter region, which reiterates the importance of the HDAC3-Runx2 interaction (140). Furthermore, these authors inhibited HDAC3 within MC3T3 preosteoblasts utilising small interfering RNAs (siRNA) and reported increased *OCN* expression, while the Runx2 mRNA levels remain unchanged (140), similar to the observations

acquired in this study. Interestingly, previous work showed that MI192 pre-treatment reduced *OCN* mRNA expression in ADSCs compared to the untreated cells throughout 21 days of osteogenic culture (214). As hDPSCs possess a greater osteogenic capacity compared to ADSCs (265), this likely has a significant role in promoting the expression of this maturation marker. Together, these results demonstrate MI192 pre-treatment is capable of enhancing the mRNA and protein expression of key osteoblast-related markers within hDPSCs.

Both Alizarin red and Von Kossa staining are often used for identifying calcium deposition and functional mineral nodule formation, respectively (300). The MI192 pre-treated hDPSCs exhibited increased calcium deposition and possessed extensively enhanced mineral nodule formation when compared to the untreated controls, indicating MI192 pre-treatment is able to not only accelerate the accumulation of calcium within the cells but stimulate the formation of functional mineral which is a key attribute for bone tissue engineering applications. The enhanced expression of key osteoblast-related matrix proteins (ALP, Col1a and *OCN*) observed in the MI192 pre-treated hDPSCs (Fig 3.13), likely promoted mineral nodule deposition within the more mature extracellular matrix, as these proteins are key in initiating the mineralisation process (301-303). This correlated with the enhanced Van Gieson's counterstaining for collagen deposition observed in the MI192 pre-treated group following Von Kossa staining. Similarly, numerous studies combining HDACis and MSCs for bone augmentation strategies have shown accelerated mineralisation compared to untreated controls (19, 286). Additionally, the results of this study replicated the effects of MI192 pre-treatment on ADSCs (214), indicating the capability of this HDACi in enhancing the mineralisation capacity of MSCs acquired from multiple tissue sources. Together, the findings of this study clearly demonstrate the capability of MI192 in promoting the osteogenic capacity of hDPSCs in 2D culture.

3.4.3 - The effects of MI192 on hDPSCs osteogenic differentiation in the lyophilised silk scaffold

Numerous studies have demonstrated the ability of HDACis to enhance MSCs osteogenic capacity in 2D culture (290, 291), however, the use of 3D *in vitro* models have been limited. Paino *et al.* (2014) demonstrated VPA pre-treatment enhanced hDPSCs osteogenesis within collagen scaffolds (209), which as of writing, is the only study to date combining HDACi treated hDPSCs with a scaffold system. This emphasises the current lack of knowledge in the literature of how HDACi treated hDPSCs behave in the 3D environment for bone augmentation strategies. Studies have evaluated the effects of HDACis in enhancing MSCs bone formation *in vivo* after 2D *in vitro* assessment, avoiding the 3D *in vitro* validation step (215, 286). The importance of 3D *in vitro* validation was demonstrated by de Boer *et al.* (2006), where the effects of NaB and TSA on hBMSCs bone formation within a calcium phosphate scaffold were assessed *in vivo* (74). The

results acquired were inconclusive and did not correlate with prior 2D *in vitro* investigation with these HDACis (74, 113, 212), underlining the importance of evaluating the effects of MI192 on hDPSCs within 3D *in vitro* culture as a pre-clinical validation step.

To investigate MI192 pre-treated hDPSCs osteogenic capacity in the 3D environment, *BM* silk scaffolds were chosen as this biomaterial possesses several desirable properties for tissue engineering applications such as their biocompatibility, biodegradability and ease of manufacture (304). Primarily silk scaffolds have been utilised for soft tissue engineering applications (237, 305); however, the use of these scaffolds may provide insufficient mechanical strength to support the bone defect. Therefore, silk scaffolds exhibiting enhanced mechanical properties may promote its clinical potential for load-bearing tissues. Lyophilised silk scaffolds, 2 wt%, which has previously been characterised for soft tissue engineering applications (260) and a 5 wt% scaffold were utilised in this study. Therefore, in this study, the lyophilised silk scaffolds were characterised and the effects of MI192 pre-treatment on hDPSCs osteogenic differentiation within this 3D culture environment were investigated.

Characterisation of silk scaffolds was undertaken by assessing the effects of silk concentration on surface topography, mechanical properties, degradation and swelling rate. The SEM micrographs showed the silk scaffolds displayed a highly porous surface topography. This reflects the biocompatible nature of this biomaterial, where possessing a highly porous surface topography favours cell attachment (169, 306). Additionally, the porous structure indicates the scaffold allows for the subsequent migration and proliferation of the cells within the scaffold but also suggests sufficient nutrient/waste diffusion within the construct. The 5 wt% scaffold possessed thicker internal sheet-like lamellae compared to the 2 wt% scaffold due to increased silk concentration, consistent with the work performed previously (169, 260).

Although increasing silk concentration is expected to enhance the mechanical properties of the scaffold, it is important to quantify the differences between the two wt% sponges. Moreover, altering silk concentration may impact other scaffold properties such as degradation and swelling characteristics. From the swelling analysis, it was clear that increasing silk concentration reduced the swelling capacity of the scaffold. This indicates increasing the concentration of silk, likely reduced the internal void volume/porosity of the scaffold. Another important scaffold characteristic for bone tissue engineering is their degradation rate (150, 151). Following Protease XIV incubation, the results demonstrated that the 2 wt% scaffold exhibited a significantly faster degradation rate compared to the 5 wt% scaffold. Although the use of Protease XIV *in vitro* is not exactly a physiologically relevant condition, it provides an indication

of the effects of silk concentration on the degradation of the scaffold *in vivo*. The degradation rate of the scaffold should be similar to the *de novo* tissue formation (238), therefore evaluating the effects of cell-laden silk constructs *in vivo* would provide a more accurate assessment of degradation rate of these scaffolds. Following mechanical testing, the 5 wt% scaffolds exhibited substantially increased compressive modulus compared to the 2 wt% construct (4.28-fold). The effect of silk concentration on degradation and mechanical properties were consistent with the data acquired in the literature (260). Therefore, these results indicate the higher wt% scaffold would provide enhanced mechanical strength which is desirable for load-bearing tissues; however, it is important to evaluate the effects of MI192 on hDPSCs behaviour and osteogenic capacity within these scaffold systems.

Distribution of cells within the silk scaffolds was assessed by fluorescent labelling. Visualisation of dead cells was not undertaken due to the scaffolds ability to absorb the dead dye. Following CLSM, viable cells are distributed throughout both wt% scaffolds after 24 hours post seeding. Cells within these scaffolds possessed two distinct morphologies, a rounded and a fibroblast-like morphology. These exist as cells which migrated into the scaffold the fastest attach to the pores within the scaffold and spread into the fibroblastic morphology associated with hDPSCs (168). The cellular interactions observed within the scaffolds were consistent with numerous studies utilising silk (169, 214). The MI192 pre-treated cells exhibited a slightly flattened/elongated morphology when compared to the untreated counterparts. This morphology observed within the HDACi treated cells, indicates a more mature osteogenic phenotype, correlating with similar findings acquired from the monolayer study (Fig 3.2 and 3.11) and the literature (168, 209). The 5 wt% scaffold possessed a higher quantity of cells exhibiting the rounded morphology compared to cells within the 2 wt% scaffold, indicating the increased material volume in the higher wt% group restricted cellular attachment, spreading and migration through the scaffold at this time point. The 2 wt% scaffolds possessed an increased cell density compared to the 5 wt% scaffolds. This is likely due to the reduced scaffold volume and increased porosity within the 2 wt% scaffold, indicated from the SEM micrographs and swelling analysis (Fig 3.16 and 3.17), allowing for increased cell migration and proliferation compared to the higher wt% group. Rnjak-Kovacina *et al.* (2015) reported similar findings with hBMSCs within lower silk concentration scaffolds exhibited increased cell proliferation compared to higher wt% scaffolds (260).

After 6 weeks in osteogenic culture, a greater difference in cell density was observed in the 5 wt% scaffold between the time points compared to the lower wt% group. It is probable the increased material volume within this scaffold, indicated by the increased lamellae thickness and enhanced mechanical strength (Fig 3.16 and 3.18), restricted migration and proliferation to a greater degree compared to the 2 wt% scaffold at the earlier time point. The MI192 pre-treated cells on both wt% scaffolds exhibited a more flattened/elongated morphology when compared to the untreated cells, correlating with the observation at the 24 hour time point. This change in morphology indicates the MI192 pre-treated cells possessed a more advanced osteogenic phenotype compared to the untreated group (209, 291). This did not correlate with the morphology observed in MI192 pre-treated ADSCs on *AM* silk scaffold (214), possibly due to differences in MSCs and scaffold utilised. Interestingly, the MI192 pre-treated cells appeared to exhibit a larger/elongated morphology when compared to the same cells on the 2 wt% scaffold at this time point. This may indicate the influence of the increased scaffold stiffness in stimulating the osteogenic phenotype of the MI192 pre-treated hDPSCs within the silk sponge.

The effects of MI192 on stimulating hDPSCs osteogenic capacity within the silk scaffolds were initially evaluated by quantifying ALPSA after 2 weeks osteogenic culture. In both wt% scaffolds, MI192 pre-treatment enhanced hDPSCs ALPSA compared to the untreated cells (~2-fold), clearly demonstrating the efficacy of this HDACi in stimulating the osteogenic capacity of hDPSCs in this 3D environment, consistent with the ALPSA findings in the monolayer study (Fig 3.10). Interestingly, these results showed that the ALPSA of the MI192 pre-treated and untreated cells within the 5 wt% scaffolds were significantly higher compared to their corresponding cells in the 2 wt% scaffolds, 1.27- and 1.43-fold, respectively. This implies that the increased mechanical properties exerted by the 5 wt% scaffold were integral in promoting the osteogenic capacity of hDPSCs, correlating with the CLSM observations. Numerous studies have investigated the effects of scaffold mechanical properties, more specifically scaffold stiffness in affecting lineage-specific differentiation of MSCs (307-309). The behaviour of MSCs is tightly regulated by the environment in which they exist, where the external microenvironment/scaffold stiffness affects key cellular processes such as proliferation and differentiation (310, 311). This indicates the importance of scaffold mechanical properties not only for supporting the macroscopic defect site but also at the microscale affecting mechanotransductive interactions with MSCs (312). Having demonstrated that both MI192 pre-treated and untreated cells exhibited significantly enhanced ALPSA on the 5 wt% scaffold, the higher wt% silk was utilised to further analyse the effects of MI192 pre-treated hDPSCs osteogenic differentiation within the silk scaffold.

The effects of MI192 pre-treatment on hDPSCs mRNA expression levels of key osteoblast-related genes was assessed within the 5 wt% silk scaffolds during osteogenic culture. The expression of early osteoblast-related genes (*RUNX2*, *BMP2* and *ALP*) was accelerated within the MI192 pre-treated cells when compared to that in the untreated group throughout osteogenic culture. This indicates that MI192 pre-treatment shifts the expression peaks for these markers earlier compared to that in the untreated cells within this 3D environment. The enhancement observed in *ALP* expression correlated with the increased ALPSA within the MI192 pre-treated silk constructs in this study. The expression profiles of these markers did not replicate the findings in the monolayer study (Fig 3.12), likely due to the differences in cell culture environments.

The effects of MI192 pre-treatment on the gene expression of late osteogenic markers (*COL1A* and *OCN*) were also analysed. The mRNA expression levels of *COL1A* was substantially upregulated within the MI192 pre-treated cells throughout the osteogenic culture period assessed, likely aided by the accelerated expression of the earlier markers within the HDACi treated cells. The upregulation in hDPSCs *COL1A* mRNA levels induced by MI192 pre-treatment was observed in both monolayer and silk scaffolds, however, the degree of enhancement was substantially higher in this 3D culture system. The increased upregulation in *COL1A* expression was likely stimulated by culturing these cells within this 3D microenvironment (313). It has been reported that cells within a 2D system experience a number of “artificial” stimuli such as apical-basal polarity, unrestricted spreading/migration and lack of soluble factor gradients (181), resulting in reduced differentiation capacity. A similar enhancement in osteogenic gene expression has been reported in 3D culture compared to the expression acquired from culturing cells in monolayer (314, 315). Additionally, it was observed that *OCN* mRNA expression levels were significantly upregulated in the MI192 pre-treated cells compared to that in the untreated cells throughout osteogenic. In both the monolayer and the silk study, MI192 pre-treatment substantially enhanced *OCN* mRNA expression, while the expression of its key activator, *RUNX2*, was not substantially altered throughout the culture periods assessed. Therefore, this emphasises the importance of MI192 isoform selectivity for stimulating hDPSCs osteogenic differentiation, similar to the observations in the literature (140).

Histological analysis was undertaken to assess the effects of MI192 pre-treatment on hDPSCs tissue formation within the silk scaffold. H&E staining demonstrated cells in both groups were distributed thoroughly within the scaffolds after 6 weeks osteogenic induction, correlating with the CLSM observations in this study. Cells were observed occupying the internal porous structure of the scaffold, while at the periphery cells possessed a slightly flattened/elongated

morphology, replicating studies performed previously with MI192 pre-treated ADSCs on AM silk scaffolds (214) and VPA pre-treated hDPSCs within a collagen sponge (209). Picrosirius red/Alcian blue staining was performed to evaluate the effects of MI192 pre-treatment on hDPSCs expression of collagens (type I/III collagen) and GAGs, respectively. Within the scaffolds, the strongest Picrosirius red staining was situated towards the edges of the constructs in both groups. Picrosirius red staining in the MI192 pre-treated group appeared more uniformly expressed throughout the scaffold when compared to the untreated control, indicating the capability of MI192 pre-treatment in stimulating hDPSCs collagen expression within the scaffold. This replicated the staining pattern acquired with MI192 pre-treated ADSCs on AM silk scaffolds (214) and with the enhanced *COL1A* gene expression induced by MI192 in this study. Paino *et al.* (2014) similarly reported enhanced collagen deposition within VPA pre-treated hDPSCs within a collagen sponge (209). In this present study, undetectable levels of GAGs were observed in both groups, indicating successful hDPSCs osteogenesis within this 3D environment, likely aided by the highly porous nature of this silk construct and the influence of scaffold stiffness on MSCs differentiation.

The effect of MI192 pre-treatment on hDPSCs extracellular matrix deposition within the silk scaffold was assessed via immunohistochemical staining. Both groups exhibited positive ALP protein expression throughout the scaffolds, with increased intensity located at the periphery of the construct. The MI192 pre-treated group exhibited enhanced global ALP expression throughout the scaffold, which correlated with the accelerated *ALP* mRNA expression and enhanced ALPSA observed in this study (Fig 3.20 and 3.21). A similar pattern was observed for Col1a protein expression, where the MI192 pre-treated group exhibited a global increase in protein expression throughout the scaffold, with enhanced intensity situated at the outer regions of the construct. This enhanced Col1a protein expression induced by MI192 pre-treatment correlated with the increased *COL1A* mRNA expression and Picrosirius red staining acquired in this study (Fig 3.21 and 3.23). Additionally, the enhancement in Col1a protein expression observed in the MI192 pre-treated group replicated work performed previously with MI192 pre-treated ADSCs on AM silk scaffolds (214), although protein expression was at a much-increased intensity in this present study. Positive OCN expression was observed in both groups, with the strongest staining situated at the outer regions of the scaffold, replicating the previously assessed osteogenic markers. MI192 pre-treatment stimulated enhanced global expression for OCN throughout the scaffold compared to the untreated cells, consistent with the mRNA expression results and the ALP and Col1a protein deposition in this study. The increased expression of these osteogenic proteins (ALP, Col1a and OCN) situated at the

periphery of the construct is likely due to the increased density of cells at the outer regions, in addition to enhanced exposure to osteogenic medium. Similarly, MI192 pre-treated ADSCs within the *AM* silk scaffolds exhibited increased extracellular matrix deposition at the outer regions of the construct (214). Additionally, the shear stress exerted to the scaffold at the periphery of the construct by the incubation medium likely potentiates the differentiation capacity of cells situated at the outer regions (316, 317). The increased deposition of these extracellular matrix proteins observed in this study, correlated with similar enhancements induced by MI192 in the monolayer study in this chapter (Fig 3.11 and 3.13).

In previous studies, MI192 pre-treatment of ADSCs enhanced the protein expression of Col1a within *AM* silk scaffolds, however, did not upregulate the expression of Runx2 or OCN within those constructs (214). This differed from protein expression profile acquired in this study likely attributed to the MSCs utilised, as hDPSCs are known to possess a greater osteogenic capacity compared to ADSCs (265), indicating the potential utility of this MSCs source for bone augmentation strategies (298, 318, 319). Additionally, Saha *et al.* (2013) reported that *BM* silk scaffolds are more osteoinductive when compared to *AM* silk (169), possibly contributing to the differences in osteogenic protein expression observed within the MI192 pre-treated hDPSCs and ADSCs within their respective scaffold systems. In the literature, Paino *et al.* (2014) seeded VPA pre-treated hDPSCs on a lyophilised collagen type I sponge (Gingistat) (209), which is a similar scaffold design used in this study. It was demonstrated that VPA pre-treated constructs exhibited increased collagen deposition compared to the untreated group confirmed via Mallory's Trichrome staining, consistent with the Picosirius red and Col1a immunostaining results in this study. Although reporting enhanced collagen deposition within the VPA pre-treated constructs, Mallory's Trichrome does not specifically target collagens. Additionally, these authors reported a reduction in OCN protein expression in the VPA pre-treated constructs (209), indicating the effect of VPA in reducing the osteogenic maturation of hDPSCs within the Gingistat sponge. This did not correlate with the findings of this study, probably attributed to the differences in HDAC isoform selectivity between VPA and MI192.

Having demonstrated that MI192 pre-treatment enhanced hDPSCs osteogenic protein expression within the silk scaffolds, it was important to determine MI192 effect on hDPSCs calcium deposition and mineralisation via Alizarin red and Von Kossa staining, respectively. Within both groups, calcium deposition was primarily situated at the periphery of the construct, with greater deposition observed in the MI192 pre-treated hDPSCs. Semi-quantitative analysis of the Alizarin red stained entire constructs confirmed the MI192 pre-treated group exhibited

significantly increased calcium accumulation compared to the untreated group. Paino *et al.* (2014) reported a similar increase in calcium deposition in VPA pre-treated hDPSCs within the Gingistat sponge (209). Following Von Kossa staining, an enhanced quantity of functional mineral nodules was observed in the MI192 pre-treated constructs. The location of increased calcium deposition and mineral nodule formation within the scaffold replicated the areas of increased osteogenic protein expression from the immunostaining in this study. This indicates that cells at the periphery of the construct exhibited a more advanced osteogenic phenotype, consistent with observations acquired from previous studies (214). The increased expression of bone-related osteogenic proteins in the MI192 pre-treated group likely promoted mineralisation within the scaffolds, as extracellular matrix deposition is an important precursor for mineralisation (301, 303). It is clear that the MI192 pre-treatment strategy was sufficient in promoting the osteogenic capacity of hDPSCs within the silk scaffold, resulting in the enhanced expression of osteogenic proteins and mineral nodules, which are key attributes for developing functional bone tissue. The effect of MI192 pre-treatment on hDPSCs mineralisation within silk scaffolds resembled the enhanced mineralisation induced by MI192 pre-treatment of ADSCs cultured within *AM* silk scaffolds (214), in addition to TSA pre-treated hPDLs on Polycaprolactone (PCL)/PEG co-polymer scaffold (320).

Together, the findings of this study demonstrate the effects of MI192 pre-treatment on hDPSCs osteogenic capacity in monolayer successfully translates into this 3D culture environment. Moreover, the findings of this study, in addition to the effects of MI192 pre-treated ADSCs within *AM* silk, demonstrates the capability of this selective HDACi in enhancing the osteogenic potential of MSCs acquired from two different tissue sources on a conventional 3D scaffold system such as the silk scaffold. Moreover, this study provides an essential 3D *in vitro* pre-clinical validation step for HDACi-based therapies, which has been lacking in the literature, providing greater evidence on the potential effectiveness of this epigenetic approach in stimulating bone formation in the clinical setting.

3.4.4 - The effects of MI192 on hDPSCs osteogenic differentiation within the BMT construct

Several 3D *in vitro* models have been utilised to investigate the formation of functional bone tissue in the literature, with each possessing their own advantages and disadvantages. Regarding the use of HDACis, a limited number of studies have assessed the effects of these compounds to stimulate MSCs osteogenesis in 3D *in vitro* models (209, 214). Although results have been promising, there are discrepancies regarding the use of HDACis, cell type and scaffold systems. Therefore, a lack of knowledge exists in the literature regarding the efficacy of HDACi-

based therapies to stimulate MSCs osteogenic differentiation in different culture systems. Of the scaffold systems utilised to evaluate HDACi induced bone formation, low cell density constructs have been assessed in the literature (209, 215) and also in this chapter with lyophilised silk sponges. Researchers have reported that a high-density culture environment is beneficial for stimulating bone formation (245). In particular, several studies have shown the potential of using microtissues (spheroidal pellets) culture to enhance the osteogenic potential of MSCs (245, 300, 321). Additionally, it has been reported that high-density culture promotes hDPSCs osteogenic differentiation (251, 252), therefore the microtissues model may provide a suitable platform to assess MI192 induced hDPSCs bone formation. However, the use of these microtissues for the repair of critical-sized bone defects are associated with limitations such as requiring high cell numbers, lack of spatial-temporal control of cells and low mechanical properties (254, 322).

Tatsuhiro *et al.* (2018) reported the development of hDPSC-derived tissue-engineered constructs as an alternative to the use of microtissues for bone tissue engineering. This approached cultured hDPSCs within a well plate for 4 weeks in basal conditions, following which 3D constructs were formed via cell sheet detachment and subsequent culture in osteogenic conditions (228). This method created tissue modules of irregular shape, size and tissue formation, therefore lacking the reproducibility of tissue modules create via microtissue culture, which is important in creating a function bone tissue. Thus, combining microtissues with a 3D scaffold will alleviate the issues regarding mechanical properties and spatial orientation. Langenbach *et al.* (2012) combined microtissues created with hUCSCs into an insoluble collagenous bone matrix (ICBM) scaffold and demonstrated successful osteogenesis; however, these cell pellets were incorporated into the scaffold irregularly due to the random ICBM porosity (300). Therefore, the biofabrication of a scaffold with regular porosity would allow for the spatial-temporal control of cellular components. Schon *et al.* (2012) developed a high throughput method of creating microtissues of regular size/shape, following which these microtissues were assembled within a 3D printed scaffold with regular porosity to create the BMT construct (253). This composite construct alleviates issues regarding spatial-temporal control of tissue modules and mechanical strength. Additionally, it increases the total size of tissue formed compared to the use of microtissues alone. Therefore, in this study, we characterised the 3D printed PEGT/PBT scaffolds and investigated the effect of MI192 pre-treatment on the osteogenic capacity of hDPSCs in the BMT model.

Since the formation of the BMT construct requires a suitable 3D printed scaffold, in this study the 3D printed scaffold acquired from Dr Tim Woodfield's CReaTE group was characterised. The scaffold utilised was the thermoplastic PEGT/PBT block copolymers possessing properties such as elasticity, strength and toughness which are advantageous for load-bearing tissues (323). Altering the molecular weight ratio between the PBT and PEGT segments allows for degradation to occur at a higher (>PEGT content) or lower rate (>PBT content), providing a method of controlling the degradation rate and mechanical properties of this material (324-326). Compared to the commonly utilised biomaterial PCL which has been used extensively for biofabrication applications (327, 328), the use of PEGT/PBT block copolymers for the creation of the scaffold would allow for more controllable mechanical properties and degradation rate. PCL is known to remain *in vivo* for up to 24 months due to its hydrophobicity and crystallinity, therefore may not be ideal for bone tissue engineering applications (329, 330). Although numerous studies have reported the use of osteoinductive biomaterials for bone tissue engineering applications (235, 331, 332), the PEGT/PBT scaffold which does not possess inherent osteoinductivity was utilised in this study to minimise the influence of the material in evaluating the effects of MI192 on stimulating hDPSCs osteogenesis in the BMT model.

Initially, in this study, the dimensions and surface topography of the 3D printed scaffold were characterised. As the printing of this scaffold is well optimised (253, 333), the scaffolds possessed an even fibre spacing (~1 mm) and width (~250 μm) with a smooth fibre surface topography, consistent with previous studies (334, 335). The pore size of these scaffolds was approximately 750 μm , which is suitable for press-fit incorporation of microtissues (~ \varnothing 1 mm). These observations demonstrate the reproducibility and accuracy of additive manufacturing techniques in creating scaffolds, emphasising the potential of biofabrication methods to create patient-specific scaffolds and the scale-up feasibility of these approaches (244).

The BMT constructs were formed by manually transferring pre-cultured microtissues into the pores of the 3D printed scaffold. Initially, the BMT was designed to be assembled via a singularisation device attached to the 3D printing head developed by the CReaTE group in order to automate this labour-intensive process (335). However, the manual transfer of these pre-cultured microtissues was a suitable alternative due to the lack of the singularisation device in Leeds. During optimisation, it was noted that microtissues formed using hDPSCs were of a reduced size than what was required for press-fit into the scaffold pore (~ \varnothing 1 mm). DPSCs are known to exhibit an accelerated proliferation rate and grow to an increased cell density compared to BMSCs *in vitro* (298); therefore, it is likely within the microtissue environment

these cells have much closer cell-cell/cell-matrix interactions, resulting in the reduced tissue module size. Additionally, the increased metabolic activity exhibited by hDPSCs, compared to MSCs such as BMSCs (298), may prevent the formation of appropriately sized pellets due to increased requirements for nutrient/waste exchange (333, 336). Moreover, increasing the number of cells to create larger microtissues resulted in enhanced pellet degradation likely due to breaching the threshold of nutrient diffusion (336), limiting the maximum size of hDPSC microtissues. Incorporating two microtissues per pore, was sufficient to effectively occupy the internal void volume of the 3D printed scaffold in this study.

Following construct assembly, hDPSCs viability within the BMT model was assessed via CLSM. Both groups possessed a high proportion of viable cells throughout the construct, with a small number of dead cells visible 24 hours after BMT formation. These dead cells may be due to hDPSCs at the surface of the microtissues prone to physical or mechanical deformation during transfer into the scaffold. This observation was consistent with findings in the literature with microtissues created using human articular chondrocytes (HAC) and human nasal chondrocytes (HNC) (253, 335). The fact that the pellets within the scaffold remained highly viable, even with twice the quantity of cells the BMT was initially designed for, indicates sufficient nutrient/waste exchange throughout the construct. Additionally, as these microtissues were <1 mm in diameter, this likely aided the viability of cells during the pre-culture incubation period. Moreover, as microtissues were incorporated into a pore which was cuboidal in shape, the corners of each pore would allow for the flow of nutrients/waste throughout the BMT, therefore, maintaining the viability of cells in this system. The CLSM observations correlated within the histological analysis of the BMT constructs with no necrotic cores observed within the construct.

Several studies have shown that culturing MSCs as pellets accelerate osteogenesis due to increased cell-cell/cell-matrix interactions, closely mimicking the *in vivo* environment (228, 254, 300). The enhanced cellular interactions induced by microtissue culture likely stimulate the expression of key osteoblast-related markers within MSCs. Therefore, the effect of MI192 pre-treatment on hDPSCs osteoblast-related gene expression during microtissue culture was investigated. *RUNX2* mRNA levels were elevated in the MI192 pre-treated hDPSCs compared to that in the untreated group, however, not significantly throughout the time points assessed. As MI192 is selective for HDAC3, it is likely the MI192 pre-treated cells would possess increased levels of transcriptionally active Runx2 transcription factor. Consequently, these cells may not need to stimulate *RUNX2* mRNA expression in the MI192 pre-treated cells, similar to the trend

observed in the monolayer study in this chapter (Fig 3.12). MI192 pre-treatment significantly upregulated *ALP* mRNA levels during osteogenic culture compared to that in the untreated cells. When compared to the expression observed in the monolayer study, *ALP* mRNA levels within MI192 pre-treated hDPSCs was substantially enhanced in microtissue culture, indicating the role of this 3D culture environment in accelerating hDPSCs osteogenesis compared to 2D culture, consistent with observations in the literature (228, 313). The expression of *BMP2* was significantly upregulated in the MI192 pre-treated cells in all time points evaluated, replicating the upregulation observed in the monolayer study. As *BMP2* is known to be a potent activator for osteogenesis, it is likely the enhancement in *BMP2* played a significant role in promoting *RUNX2* gene expression, as *BMP2* signalling is essential for Runx2 dependent osteogenesis (296). Moreover, *BMP2* is known to enhance *ATF6* expression, which promotes the expression of downstream markers such as *ALP* (294), as observed in this study. From the time points assessed, mRNA expression of these early osteoblast-related markers exhibited a time-dependent reduction. This is likely due to the accelerated osteogenesis caused by the 3D culture environment compared to 2D culture, consistent with observations in the literature (314, 315).

The effects of MI192 pre-treatment on the expression of later osteogenic markers (*COL1A* and *OCN*) were also evaluated. The mRNA levels of *COL1A* were significantly elevated in the MI192 pre-treated microtissues during osteogenic culture compared to that in the untreated cells. This enhancement was likely promoted by the increased expression of the early markers (*RUNX2*, *ALP* and *BMP2*) discussed previously. Moreover, MI192 significantly upregulated the expression of *OCN*, the marker associated with osteogenic maturation (303), in all time points assessed compared to that in the untreated group. As with the monolayer gene expression results, there was significantly elevated *OCN* expression levels, without the prior “significant” enhancement in *RUNX2* mRNA expression within the MI192 pre-treated cells (Fig 3.12), which emphasises the importance of MI192 in uncoupling HDAC3-Runx2 complex. Similar findings were reported by Schroeder *et al.* (2004), where siRNAs were utilised to inhibit HDAC3 within MC3T3 preosteoblasts, resulting in increased *OCN* expression, while the *RUNX2* mRNA levels remain unchanged (140). Additionally, studies have demonstrated the capability of HDACi treatment in reducing the expression of HDAC enzymes (283, 291). Therefore, it is probable the MI192 pre-treated cells exhibited reduced HDAC3 levels, resulting in increased transcriptional activity of Runx2. The increased transcriptional activity of Runx2 may downregulate the mRNA expression of *RUNX2*, although this would require further investigation. Together, these results demonstrate that MI192 is capable of stimulating the expression of key osteoblast-related genes in hDPSCs during osteogenic microtissue culture.

A similar increase in the mRNA expression of osteoblast-related markers was observed in the silk study (Fig 3.21), with particular differences observed in the expression of the early markers. For the early osteogenic markers (*RUNX2*, *ALP* and *BMP2*), MI192 pre-treatment upregulated gene expression compared to that in the untreated cells throughout the culture period assessed in this study, while only accelerating the expression peaks of these genes within the silk constructs. This may signify the role in which high-density 3D culture plays in promoting the osteogenic capacity of MSCs compared to lower cell density *in vitro* systems (321, 337). Nonetheless, the expression of key osteoblast-related genes was significantly upregulated in the MI192 pre-treated hDPSCs within both 3D *in vitro* models used in this chapter.

Several studies have shown that HDACi compounds are capable of promoting osteogenic protein expression within 3D environments (209, 214). To initially evaluate the effects of MI192 pre-treatment on hDPSCs osteogenic protein expression during BMT culture, ALPSA was quantified after 2 weeks osteogenic culture. The results of the study showed that the MI192 pre-treated hDPSCs exhibited a significantly enhanced ALPSA when compared to the untreated cells in this model. The 2.3-fold increase in ALPSA was similar to that observed in the monolayer study in this chapter (Fig 3.10). These findings also correlated with the enhancement in *ALP* mRNA expression observed in this study. Moreover, the enhanced ALPSA observed in this study replicated a similar enhancement observed within the silk scaffolds (1.9-fold) (Fig 3.20). A greater fold stimulation in ALPSA was observed in the BMT study, likely due to the advantageous environment high-density culture provides in stimulating MI192 pre-treated hDPSCs osteogenesis. These findings confirm the capability of MI192 in stimulating the early phase of hDPSCs osteogenesis in both low and high-density 3D cell culture environments.

Histological analysis was undertaken to evaluate the effects of MI192 pre-treatment on hDPSCs tissue formation within the BMT construct after 6 weeks osteogenic culture. The results of this analysis showed that the incorporated microtissues in both groups were able to combine together within the 3D scaffold framework and occupy the internal scaffold volume, including fusing around the internal scaffold fibres. The fusing of the microtissues around the internal scaffold fibres indicates the 3D printed scaffold was not toxic to the introduced tissue modules, replicating the CLSM analysis in this study and work performed previously (253). Moreover, these findings showed that the incorporation of two microtissues per pore was sufficient to effectively fill the internal volume of the 3D printed scaffold. Tissue formation within the constructs differed between the groups, where the MI192 pre-treated construct exhibited a more uniformly tissue formation distributed throughout the BMT, while within the untreated

group tissue formation replicated a typical pellet morphology in each incorporated tissue module, replicating the Picrosirius red/Alcian blue staining in this study. This observation indicates the role of MI192 pre-treatment in controlling the extracellular matrix production of all hDPSCs within the BMT construct during osteogenic culture.

Following Picrosirius red/Alcian blue staining for collagen and GAG expression respectively, the untreated group exhibited the strongest expression for collagens at the periphery of each individual microtissues, with weaker staining observed within the centre of the tissue modules. This gradient collagen distribution observed may be due to the increased exposure to osteogenic medium at the surface of the microtissue during pre-culture incubation. The MI192 pre-treated group possessed similar collagen expression intensity within the construct compared to untreated control; however, protein expression was more uniformly distributed throughout the BMT. This indicates MI192 pre-treatment is able to promote the osteogenic phenotype of all hDPSCs within the BMT, resulting in enhanced bone extracellular matrix deposition within the construct. Moreover, the MI192 pre-treated constructs exhibited an increased quantity of large circular nodules compared to the untreated control, with these regions displaying the strongest staining intensity for Picrosirius red. As extracellular collagen deposition is important for mineralisation (301), the increased quantity of the Picrosirius red positive circular nodules indicates enhanced mineralisation in the MI192 pre-treated group. The untreated BMT exhibited increased GAG accumulation within the core of each microtissue when compared to the MI192 pre-treated group. Although microtissue culture has been extensively utilised for chondrogenic differentiation studies (338, 339), the findings of this study showed that MI192 pre-treatment prior to microtissue formation was sufficient to inhibit chondrogenic differentiation. Lee and Im (2017) reported that TSA, an inhibitor shown to stimulate osteogenic differentiation (233), prevented the formation of cartilaginous tissues of MSC pellets compared to untreated controls (340), consistent with the findings in this study. The differential tissue formation observed from the histological analysis clearly indicates the capability of MI192 to control the lineage-specific differentiation of hDPSCs in this model.

The effects of MI192 pre-treatment on hDPSCs extracellular matrix deposition within the BMT model after 6 weeks osteogenic culture was further assessed using immunohistochemical staining. Positive ALP expression was observed throughout the entire constructs; however, the MI192 pre-treated group exhibited increased global expression throughout the BMT. The enhanced global ALP expression observed in the MI192 pre-treated group correlates with the increased *ALP* mRNA expression and ALPSA acquired in this study (Fig 3.34 and 3.35). As with the

Picrosirius red staining, the strongest ALP expression was located in the large circular nodules observed throughout the construct, which was much more prevalent in the MI192 pre-treated group. This may represent cells of a more advanced osteogenic phenotype, resulting in increased expression of osteogenic markers in these areas. ALP is known to be involved in the mineralisation of the extracellular matrix, due to promoting local inorganic phosphate concentration and decreasing extracellular pyrophosphate (a promoter and inhibitor of mineral formation, respectively)(302, 341). Therefore, the enhanced expression for ALP and collagens located at these nodule-like formations indicates a greater degree of mineralisation within the MI192 pre-treated BMT.

Positive Col1a protein expression was observed in both groups, however, the staining intensity was substantially enhanced in the MI192 pre-treated BMT construct. Within the untreated construct, Col1a protein fibres were situated between the cells within the core of the microtissue and also at the outer regions at a slightly increased intensity. The MI192 pre-treated group displayed enhanced expression intensity uniformly throughout the construct when compared to the untreated group. Additionally, strong Col1a expression was situated in the large nodule-like formations within the construct, correlating with the previous analysis (Picrosirius red and ALP immunostaining), therefore, corroborating the evidence of increased mineralisation within the MI192 pre-treated group. The differential Col1a expression observed between the groups correlates with the Picrosirius red staining distribution and expression intensity. The stark differences observed in protein expression within the BMTs were consistent with the mRNA and protein expression analysis in the monolayer study (Fig 3.12 and 3.13) and the *COL1A* gene expression in this study. VPA pre-treatment of hDPSCs similarly increased collagen deposition within the Gingistat scaffold (209). In addition, MI192 pre-treated ADSCs displayed increased Col1a expression within AM silk scaffolds (214), similar to the observations in this study, although protein expression was at an increased intensity in this BMT study.

OCN was positively expressed in both groups, indicating the osteogenic maturation of hDPSCs in this culture system. Within the untreated group, as with the Col1a protein expression, a similar pattern of differential OCN distribution was observed with enhanced expression located at the outer regions of the microtissues. This differed from the MI192 pre-treated group where OCN was uniformly expressed throughout the microtissues at a similar intensity to the outer regions of the untreated group. The expression pattern observed was consistent with the Picrosirius red and Col1a immunostaining results in these constructs. The more uniform protein deposition observed in the MI192 pre-treated BMTs indicates MI192 pre-treatment is able to “prime” all

hDPSCs with enhanced osteogenic capacity resulted in uniform tissue formation, while the untreated cells were heavily dependent on access to the osteogenic medium to induced osteogenesis, resulting in the gradient protein distribution observed in the microtissues (Picrosirius red, Col1a and OCN immunostaining). The MI192 pre-treated BMT exhibited an increased quantity of OCN-positive nodule-like formations when compared to the untreated group. This correlated with the enhanced deposition of ALP and Col1a-positive nodule-like formations observed in the MI192 pre-treated construct. As with the previously discussed markers (ALP and Col1a), it is well known that OCN mediates the mineralisation process during the osteogenic maturation of cells. Tsao *et al.* (2017) reported that after OCN was knocked down in MSCs, mineralisation was delayed, and total hydroxyapatite accumulation was inhibited (303). Therefore, the enhanced global expression of OCN observed in the MI192 pre-treated group, indicates increased mineralisation within the HDACi treated BMT, consistent with the findings from the previous histological analysis. As with the previously discussed markers, the enhanced OCN protein expression induced by MI192 treatment correlated with the mRNA expression results in this study. Previously, it was reported that MI192 pre-treatment reduced ADSCs OCN deposition within AM silk scaffolds (214), differing from the observations in this study. This is likely due to the different MSCs and 3D cell culture environments utilised in these studies. Together, these findings demonstrate that MI192 pre-treatment of hDPSCs is capable of enhancing the expression of key osteogenic extracellular matrix proteins in this 3D *in vitro* model, consistent with the ICW results in the monolayer study (Fig 3.13).

Mineralisation is a key attribute in the development of functional bone engineered constructs and several studies have demonstrated culturing MSCs as microtissues accelerate mineral deposition (254, 342). Therefore, the effect of MI192 pre-treatment on hDPSCs mineralisation within the BMT construct was assessed using Von Kossa staining. The MI192 pre-treated group exhibited more extensive black staining for functional mineral nodules throughout the entire construct when compared to the untreated BMT, replicating the effects of MI192 pre-treated hDPSCs on silk scaffolds assessed in this chapter (Fig 3.29). Additionally, the strongest Von Kossa staining intensity was located in the large nodule-like formations within the construct, where an enhanced quantity of these nodules was observed in the MI192 pre-treated group. The increased Von Kossa staining situated in these locations, corroborated with the observation from the Picrosirius red and immunohistochemical staining. This indicates the enhanced expression of these bone extracellular matrix proteins induced by MI192 pre-treatment, increased the mineralisation capacity of hDPSCs in the BMT construct. The increased number of these functional mineral nodules clearly demonstrates the capability of MI192 in enhancing

hDPSCs osteogenic maturation within this 3D model, ultimately resulting in enhancing bone-like tissue formation. This enhanced mineralisation capacity induced by MI192 in this model, replicated similar observations with MI192 pre-treated ADSCs within AM silk scaffolds, in addition to TSA pre-treated hPDLCs on PCL/PEG scaffold (320).

The substantial enhancement in the MI192 pre-treated hDPSCs osteogenic protein expression and mineralisation observed within the BMT, replicated a similar enhancement observed in the silk study in this chapter. Although the increase in hDPSCs osteogenic capacity induced by MI192 is clear in both scaffold systems, more extensive osteogenic extracellular matrix deposition and mineralisation was observed in the MI192 pre-treated BMT compared to the silk constructs, probably attributed to the inherent advantages high-density culture provides for bone tissue engineering (321, 337). Therefore, from the two 3D models assessed, the BMT model would provide the most appropriate platform to evaluate the effects of MI192 pre-treatment on stimulating hDPSCs bone formation *in vivo*.

3.4.5 - The effects of MI192 on hDPSCs BMT *in vivo* bone formation

To date, the effects of HDACi therapies for bone tissue engineering have primarily been investigated within the *in vitro* environment in the literature. Due to the limited number of *in vivo* studies, there is a lack of knowledge in how these epigenetic-based approaches behave in a physiologically relevant environment. Lee *et al.* (2011) demonstrated that Largazole soaked collagen scaffolds were able to enhance calvarial defect bone formation in mice (215). Similarly, PCL/PEG scaffolds combined with TSA pre-treated hPDLCs enhanced bone regeneration of mouse calvarial defects (320). However, the importance of evaluating the use of HDACis for bone tissue engineering *in vivo* was demonstrated by de Boer *et al.* (2006), where they could not replicate the enhancement in MSCs osteogenic differentiation upon TSA and NaB treatment which was previously demonstrated *in vitro* (74). Moreover, the studies in the literature have evaluated the efficacy of panHDACis to stimulate bone formation *in vivo*, which are associated with their limitations (213). From the 3D *in vitro* studies in this chapter, it was demonstrated that MI192 pre-treatment promoted hDPSCs osteogenesis within the lyophilised BM silk scaffold and the BMT model. Due to the substantially enhanced bone-like tissue formation induced by MI192 within the BMT model compared to the silk scaffolds, this model was utilised to investigate the effects of MI192 pre-treated hDPSCs bone-like tissue formation *in vivo*.

A diffusion chamber model was employed to investigate the effects of MI192 pre-treatment on hDPSCs osteogenesis within the BMT in a physiologically relevant environment. Numerous

studies have successfully demonstrated the use of this culture system for assessing bone engineered constructs *in vivo* (257, 258). MI192 pre-treated and untreated hDPSCs were cultured as microtissues in osteogenic conditions *in vitro* and formed into BMTs, following which these constructs were placed into diffusion chambers for intraperitoneal implantation within CD1 nude mice for 8 weeks. After chamber extraction, the macroscopic analysis showed that the incorporated tissue modules remained within the 3D scaffold framework, indicating successful microtissue fusion during *in vivo* incubation, correlating with the *in vitro* observations in this chapter (Fig 3.36). In addition, the 3D printed scaffold remained intact and did not completely degrade, indicating its suitability for supporting incorporated tissue modules during long-term *in vivo* implantation. X-ray scanning of the samples was undertaken to evaluate tissue density within the constructs. Following X-ray analysis, dense tissue formation was observed within the microtissue regions of the constructs. This indicates the osteogenic microtissue culture prior to BMT assembly and the inherent advantages high-density culture provides to mineralisation (254), promoted the deposition of mineral nodules within the construct *in vivo*. No clear differences in the radio-opacity intensity and distribution were observed between the groups.

To assess the effects of MI192 pre-treatment on hDPSCs bone-like tissue formation during BMT *in vivo* implantation, histological analysis was undertaken. Following H&E staining, it was observed that the incorporated microtissues were able to fuse together and fill the internal void volume of the scaffold, correlating with the macroscopic assessment, BMT *in vitro* results (Fig 3.36) and findings in the literature (253, 335). The complete occupation of the 3D printed scaffold by the incorporated microtissues is important as it would provide increased cellular contact with the surrounding host bone defect, thus promoting cell migration and enhanced tissue integration. Denser tissue formation was observed towards the edges of each individual microtissue within both constructs, likely due to the pre-culture incubation in osteogenic conditions prior to BMT formation. Much denser tissue formation was observed throughout the MI192 pre-treated construct when compared to the untreated group, indicated by the enhanced accumulation of the Eosin stain, which stains proteins non-specifically (343). The negative immunohistochemical staining images, counterstained with haematoxylin alone (Fig 3.50), confirmed this observation. Moreover, the tissue formation within the MI192 pre-treated group exhibited a greater degree of structural organisation throughout the construct when compared to the untreated BMT. The stratified tissue formation within the MI192 pre-treated group, in addition to the increased dense tissue formation observed, replicated the morphology of tissues within the zones of calcification/ossification during late-stage endochondral ossification (39, 344). The differential tissue formation observed clearly indicates the effects of MI192 in

stimulating hDPSCs extracellular matrix deposition within the BMT model *in vivo*. The *in vitro* results did not show this clear difference in tissue formation between the groups, likely due to the lack of osteogenic culture within the *in vivo* study, therefore, the effects of MI192 is much more prominent in this study. Additionally, the *in vivo* constructs were incubated for a longer duration than *in vitro* samples (8 vs 6 weeks, respectively) and were exposed to increased shear stress conditions within the diffusion chamber compared to the static conditions in the *in vitro* study. Several studies have indicated the influence on fluid shear stress on stimulating bone formation (316, 317). These factors may stimulate the greater degree of dense tissue formation observed in the MI192 pre-treated construct in this study.

The deposition of collagens and GAGs within these constructs was evaluated via Picrosirius red/Alcian blue staining, respectively. The MI192 pre-treated group exhibited stronger Picrosirius red staining intensity within the construct and also at the periphery when compared to the untreated control. This indicates that MI192 pre-treatment prior to osteogenic microtissue culture was sufficient to stimulate differentiation down the osteogenic lineage and maintain this osteogenic phenotype during *in vivo* implantation to a greater degree when compared to the untreated control. The untreated group exhibited increased global GAGs expression when compared to the MI192 pre-treated group. Although these MI192 pre-treated and untreated cells were cultured in osteogenic conditions prior to BMT assembly, the subsequent *in vivo* implantation may have directed differentiation into mixed lineages (chondrogenic/osteogenic), indicated by the increased GAG accumulation particularly in the untreated BMTs. This reduced culture in osteogenic inductive medium likely attributed to the greater GAG accumulation observed in this study when compared to the *in vitro* BMT constructs (Fig 3.37). The differential staining acquired for the collagens and GAGs between the groups demonstrates the capability of MI192 in controlling the lineage-specific differentiation of hDPSCs in the BMT model during *in vivo* implantation. It is important to note that within the diffusion chamber model, the BMTs would be exposed to passive diffusion of nutrients into the chamber via the filter membranes, which replicates the shear stresses conditions which are favourable for chondrogenic differentiation. Additionally, the prevention of vascular invasion by the chamber membrane, which may lead to calcification/bone formation, was avoided by the use of this model (345, 346). Therefore, it is likely that the diffusion chamber model is more favourable for chondrogenic differentiation, where it has been used for many studies (347, 348), possibly resulting in the increased accumulation of GAGs in this study compared to the *in vitro* BMT constructs. Nonetheless, it is clear that MI192 pre-treatment was capable of controlling the

lineage-specific differentiation of hDPSCs within this model, resulting in increased collagen deposition during *in vivo* implantation.

To further investigate the effects of MI192 pre-treatment on hDPSCs expression of osteoblast-related extracellular proteins within the BMT *in vivo*, immunohistochemical staining was undertaken. Col1a was positively expressed within the untreated group primarily situated at the periphery of individual microtissues and the entire construct. However, the MI192 pre-treated BMT exhibited substantially increased expression intensity distributed throughout the construct, with the strongest staining located in similar regions to the control group. The enhanced protein deposition situated at the outer regions of individual microtissues in both groups is likely attributed to microtissues pre-culture in osteogenic conditions; therefore, cells at the periphery would possess the most mature osteogenic phenotype. The differential expression observed between the groups correlates with dense tissue formation observed following H&E staining and the Picosirius red staining for collagens in this study. MI192 treatment enhanced hDPSCs Col1a protein expression to a much greater degree within the *in vivo* construct compared to the *in vitro* study (Fig 3.39), which may indicate the reliance of the untreated construct on osteogenic inductive medium to stimulate the expression of this protein during *in vitro* culture. Additionally, the passive nutrient/waste diffusion that occurs within diffusion chamber incubation, may further potentiate the expression of collagens from the MI192 pre-treated hDPSC BMT when compared to static *in vitro* culture conditions (349).

OCN was weakly expressed in the untreated group and was distributed in an aberrant nature within the construct. Within the MI192 pre-treated BMT, OCN was exhibited at a much-increased intensity and protein expression was distributed more uniformly throughout the BMT construct. These findings clearly demonstrate the effect of MI192 on enhancing the osteogenic maturation of hDPSCs in the BMT during *in vivo* implantation. The difference in OCN staining between the groups was much more evident within the *in vivo* constructs compared to the *in vitro* results (Fig 3.40). This likely indicates the ability of MI192 in enhancing the osteogenic capacity of cells *in vivo* with the lack of osteogenic induction medium, consistent with the observations from the Col1a protein staining in this study. Moreover, the OCN expression intensities observed between the groups were much closer within the *in vitro* BMT study, indicating the dependence of the untreated cells on osteogenic medium to stimulate hDPSCs osteogenic maturation, similar to the observations from the Col1a immunostaining in this study. As discussed previously, Col1a and OCN expression in the extracellular matrix are key in providing a template for mineralisation to occur (301, 303). Therefore, these findings indicate

MI192 pre-treatment accelerated the extracellular matrix deposition of hDPSCs within the BMT model *in vivo*, likely resulting in enhanced mineralisation in the HDACi treated group.

The effects of MI192 pre-treatment on the expression of chondrogenic proteins were also evaluated due to the accumulation of GAGs within the constructs and the chondrogenic favourable environment inferred by the BMT model (253). AGG, a key cartilage-specific proteoglycan (350), was expressed at an increased intensity throughout the untreated construct when compared to the MI192 pre-treated group, consistent with the Alcian blue staining for GAGs in this study. In addition to AGG, positive expression of Col2a, a key chondrogenic extracellular matrix protein (351), was observed within the untreated group at an increased expression intensity compared to the MI192 pre-treated group. These chondrogenic immunostaining results in conjunction with the Alcian blue staining indicates that MI192 pre-treatment was capable of inhibiting chondrogenic protein expression, consistent with the observations from the *in vitro* study and also in the literature (340). The lack of osteogenic culture as an assembled BMT construct prior to diffusion chamber implantation may have resulted in the enhanced accumulation of chondrogenic proteins observed in the *in vivo* constructs; therefore, increased *in vitro* osteogenic incubation prior to *in vivo* implantation may be beneficial. Additionally, the BMT system was initially designed for the incorporation of one microtissue per pore to create the construct; however, due to issues regarding hDPSC microtissue size, twice the number of tissue modules were required to create the BMT construct. This may contribute to reducing the nutrient diffusion through the construct, resulting in areas within the construct possessing a more favourable chondrogenic environment.

The differential expression of osteogenic/chondrogenic proteins between the groups may indicate MI192 pre-treatment directing bone formation via the intramembranous ossification route. Conversely, these findings may suggest MI192 accelerated endochondral ossification of hDPSCs within this model; therefore, in the time point assessed in this study, the HDACi treated group may have surpassed the cartilaginous template phase of endochondral bone formation (38). Although there is evidence of chondrogenic/osteogenic differentiation which may be indicative of bone formation via the endochondral ossification route, if these studies were repeated within a more physiologically relevant pre-clinical model with the influence of other cell types, similar to the environment within fracture healing, this could provide greater insights into the route of bone formation induced by MI192 within these constructs. Nonetheless, these findings clearly demonstrate MI192 pre-treatment is capable of controlling hDPSCs lineage-specific differentiation within the BMT model *in vivo*, consistent with observations from the

BMT *in vitro* study in this chapter (Fig 3.37). MI192 selectivity for the bone-associated HDAC3 isoform (100) (140), likely has a significant role in controlling hDPSCs lineage-specific differentiation in this model *in vivo*.

The effects of MI192 pre-treatment on hDPSCs calcium deposition and mineralisation within the BMT after 8 weeks *in vivo* implantation were assessed via Alizarin red and Von Kossa staining, respectively. Within the untreated group, positive calcium deposition was observed throughout the construct, however, areas of intense staining were observed aberrantly within the construct. The MI192 pre-treated group exhibited much stronger calcium deposition intensity, distributed more uniformly throughout the construct. This was consistent with the dense tissue formation observed from H&E staining and with the expression of osteogenic proteins (Col1a and OCN) in this study. The more homogeneous calcium deposition observed in the MI192 pre-treated group suggests that HDACi pre-treatment was able to enhance the osteogenic differentiation of all hDPSCs throughout the construct and not solely dependent on access to osteogenic medium during microtissue culture, as observed in the untreated group.

Following Von Kossa staining, both groups exhibited strong black staining throughout the construct indicating the formation of functional mineral nodules, with the increased deposition of nodules located at the edges of incorporated microtissues. However, the MI192 pre-treated group exhibited substantially enhanced mineralisation compared to the untreated BMT throughout the construct, consistent with the findings acquired for calcium deposition in this study. This clearly demonstrates that MI192 pre-treatment was able to substantially enhance the accumulation of functional mineral nodules in the construct compared to the untreated control, consistent with the dense tissue formation observed from the H&E staining analysis in this study. The increased Von Kossa staining observed in the MI192 pre-treated construct, correlated with the enhanced expression of late bone markers (Col1a and OCN immunostaining) in this study, further corroborating the role of these extracellular matrix proteins in stimulating mineralisation. These findings indicate that MI192 pre-treatment was able to stimulate the calcification of the more mature extracellular matrix, resulting in the greater degree of ossification. The much-reduced mineralisation observed within the untreated group indicates the weaker expression of bone-related matrix proteins were unable to stimulate mineral nodule formation at this time point, resulting in the unmineralised osteoid-like tissue formation observed (141). When compared to the mineralisation observed in the *in vitro* findings (Fig 3.42), a greater degree of mineralisation was observed in this study, likely due to the role of shear fluid stress in promoting bone formation (316, 317), in addition to the increase culture

period for the *in vivo* constructs. Moreover, a larger difference in mineralisation was observed between the groups in this study, indicating the untreated cells were heavily dependent on access to osteogenic medium to promote nodule formation in the *in vitro* study, consistent with the protein expression observations between the *in vitro* and *in vivo* BMT. The fact that both groups possessed strong calcium deposition and mineralisation following *in vivo* implantation despite the lack of osteogenic medium incubation, is likely attributed to the underlying hDPSCs phenotype which possesses an increased osteogenic capacity compared to other MSCs such as BMSCs (298), in addition to the osteogenic favourable environment this high cell density 3D model provides.

Together, the findings of this study demonstrate the potential of utilising epigenetic approaches, particularly selective HDACi compounds, to stimulate the osteogenic capacity of hDPSCs *in vivo* resulting in the enhanced formation of bone-like tissue. Currently, only one study has investigated the effects of HDACi compounds on hDPSCs *in vivo*, however, this study injected TSA within embryos and observed enhanced dentin thickness and odontoblast numbers (233), which is a more developmental perspective into the effects of HDACis on bone formation. However, Huynh *et al.* (2017) did report enhanced bone regeneration of mouse calvarial defects following implantation of TSA pre-treated hPDLs combined with PCL/PEG scaffolds (320). This demonstrates the successful utilisation of HDACis *in vivo* in stimulating the osteogenic capacity of MSCs acquired from dental tissues, correlating with the finding in this study. Therefore, as of writing, currently no studies have investigated the use of HDACis, particularly selective HDACis, on enhancing the osteogenic capacity of hDPSCs for promoting bone formation *in vivo*. Consequently, the findings of this study and its potential impact in the tissue engineering field, support the need for further *in vivo* examination into this potential therapeutic approach in creating clinically relevant bone tissue.

To summarise, the effects of the selective HDAC2 & 3 inhibitor - MI192 on hDPSCs behaviour and osteogenic capacity in 2D and 3D *in vitro* and *in vivo* was investigated in this chapter. In monolayer culture, it was found that MI192 caused a time-dose dependent reduction in hDPSCs viability. Additionally, MI192 halted cell cycle progression in the G₂/M phase and altered hDPSCs epigenetic functionality confirmed via HDAC inhibition and increased histone H3K9 acetylation. The effect of MI192 pre-treatment on stimulating hDPSCs osteogenic capacity in 2D culture was confirmed by enhanced ALPSA, osteoblast-related gene/protein expression and calcium deposition/ mineralisation. Within 3D *in vitro* culture (silk scaffolds and BMT model), MI192 pre-treatment enhanced hDPSCs osteoblast-related gene/protein expression, ALPSA and

mineralisation. However, substantially increased bone-like tissue formation was observed within the MI192 pre-treated hDPSCs within the BMT model. Following diffusion chamber intraperitoneal implantation within CD1 nude mice, MI192 pre-treatment substantially increased hDPSCs osteoblast-related extracellular matrix protein expression and calcium deposition/mineralisation within the BMT model, while inhibiting the expression chondrogenic proteins in this model. Together, these findings demonstrate the potential of utilising epigenetic approaches for enhancing hDPSCs efficacy for bone regeneration.

Chapter 4 - The Effects of MI192 on the Behaviour and Osteogenic capacity of Human Bone Marrow-Derived Stromal Cells *in vitro* and *In vivo*

The aim of this chapter was to investigate the effects of MI192 on hBMSCs behaviour and osteogenic capacity *in vitro* and *in vivo*. Initially, the effects of MI192 on the general properties of hBMSCs were assessed (morphology, viability, HDAC activity, H3K9 acetylation and cell cycle). Following this, the effects of MI192 on hBMSCs osteogenic capacity was evaluated by ALPSA, osteogenic gene/protein expression, calcium deposition and mineralisation. These were investigated in both 2D and 3D *in vitro* culture environments (GelMA hydrogel and BMT model). Finally, the effects of MI192 on hBMSCs bone formation were evaluated in a physiologically relevant *in vivo* model (diffusion chamber).

4.1 - Background

BMSCs have been the gold standard MSCs source used in stem cell research and tissue engineering applications for many decades, due to their well-characterised properties and proven differentiation down the mesoderm lineages (352). Friedenstein *et al.* (1968) were the first to describe the isolation of these MSCs from the bone marrow with the now established characteristics of adherence to plastic and fibroblastic-like morphology in culture (353). Since then, in the literature BMSCs have been extensively utilised for bone tissue engineering applications in numerous *in vitro* and *in vivo* studies (331, 354, 355). Additionally, it has been demonstrated that BMSCs exhibit an increased osteogenic capacity compared to other sources of MSCs such as ADSCs (318, 319). Although a promising MSCs source for bone augmentation strategies, BMSCs are associated with numerous drawbacks including their low procurement yield, the extensive *in vitro* expansion required and the heterogeneity of the multilineage differentiation potential they display (153, 319). Therefore, numerous methods have been investigated to enhance the efficacy of utilising this MSC source for bone augmentation strategies such as gene therapy, although these technologies are associated with their own limitations in regards to clinical safety and cost (356). The use of epigenetic approaches, particularly HDACis to enhance MSCs osteogenesis has been growing in the field. Numerous studies have proven the effects of HDACi treatment on stimulating the osteogenic capacity of BMSCs. De Boer *et al.* (2006) reported that TSA enhanced the osteogenic potential of hBMSCs (74). Similarly, it was demonstrated that VPA and SAHA were capable of accelerating hBMSCs osteogenesis *in vitro* (19, 286). Although these approaches have shown promise in the literature, the majority of these studies have focussed on the use of panHDACis which target a broad range of HDAC isoforms. These non-specific bindings may result in unwanted side-effects and reduced differentiation potential (213). Therefore, HDACis exhibiting selective binding affinities to

specific HDAC isoforms is becoming increasingly prevalent particularly in the cancer therapeutic arena (357). With the effects of the selective HDAC2 and 3 inhibitor - MI192 on the behaviour and osteogenic capacity previously evaluated with ADSCs (214) and DPSCs in this thesis, it is important to determine the effects of MI192 in promoting the osteogenic capacity of hBMSCs, broadening the potential clinical application of this epigenetic-based approach for creating functional bone tissue.

A plethora of studies have demonstrated the potential of utilising HDACis to enhance MSCs osteogenesis in 2D culture (204, 212), however, monolayer culture does not replicate the complex 3D microenvironment which exists within the human body (181). Hence, there is growing precedence to evaluate the effects of HDACi treatment on stimulating MSCs osteogenesis within a 3D microenvironment by utilising a scaffold system. With the growth of the tissue engineering field and the advancement in numerous technologies, there are an overwhelming variety of scaffolds which have been assessed for bone augmentation applications. These scaffolds vary in their material composition, biocompatibility, cost, ease of manufacture etc. As it is near impossible to find an ideal scaffold system to assess the effects of HDACi treated MSCs, utilising scaffold systems which have been demonstrated to support HDACi-treated MSCs osteogenesis is beneficial. In the previous chapter, it was demonstrated that MI192 pre-treatment enhanced the osteogenic capacity of hDPSCs within a conventional 3D scaffold such as *BM* lyophilised silk sponges, but also in the BMT model. In comparison, the BMT construct was capable of inducing more extensive bone-like tissue formation when compared to the use of lyophilised silk sponges. As with other scaffold systems, the BMT construct is associated with its own limitations, such as the large cell numbers required to create the construct. To overcome this issue, an alternative method of delivering cells at a lower cell density into this 3D scaffold framework should be investigated.

It is well known that hydrogels are an ideal biomaterial for tissue engineering applications as they possess properties such as high biocompatibility, porosity, water content and the ability to replicate the host tissue environment (327). In addition, this biomaterial is highly flexible in terms of controlling the introduction of cells and formation into complex shapes. Hydrogels are derived from either natural or synthetic sources. These naturally derived hydrogels are able to closely replicate the extracellular matrix found in the host tissues, with the potential to direct the migration, growth and organisation of cells during tissue regeneration (358). Synthetically made hydrogels have superior mechanical properties, however, lack the biocompatible properties compared to their natural counterparts. These biomaterials can be polymerised by numerous processes, either by an enzymatic, thermo-responsive or photopolymerisable reactions (327, 359, 360). The disadvantage of enzymatic polymerisation is that they are difficult to control *in situ* and may lead to the uncontrolled

degradation of the hydrogel. For thermoresponsive hydrogels, they must be tailored to their specific environment for implantation, but for bone tissue engineering this may differ depending on the defect site. In terms of photopolymerisable hydrogels, these materials are crosslinked with exposure to various wavelengths of light *in situ*; therefore, it overcomes the particular disadvantages described for the other polymerisation methods.

Gelatin methacrylate (GelMA) has become an extremely attractive biomaterial for use in tissue engineering due to its biocompatibility, biodegradability, low cost and photo-crosslinkable properties (361). Gelatin is a denatured form of collagen that can be acquired from numerous sources, is relatively inexpensive compared to other collagen-based materials (collagen type 1), while containing the natural cell binding motifs, such as RGD (362, 363). The functionalisation of gelatin by the addition of the methacrylate groups to the amine-containing side groups allows for the photopolymerisation of the hydrogel, which is stable at 37°C (Fig 4.1). Several studies have utilised GelMA for various tissue engineering applications (364-366). The majority of studies in the literature have utilised UV light-induced polymerisation, which may have a detrimental effect on the production of free radicals and also may cause genomic instability of encapsulated cells (367) (Fig 4.1). Moreover, if cells are introduced to the hydrogels which have already been polymerised, issues arise in regard to cellular distribution within the hydrogel. Consequently, there are several groups who have started to move towards the use of visible light photoinitiators in order to avoid the detrimental effects associated with UV irradiation (360).

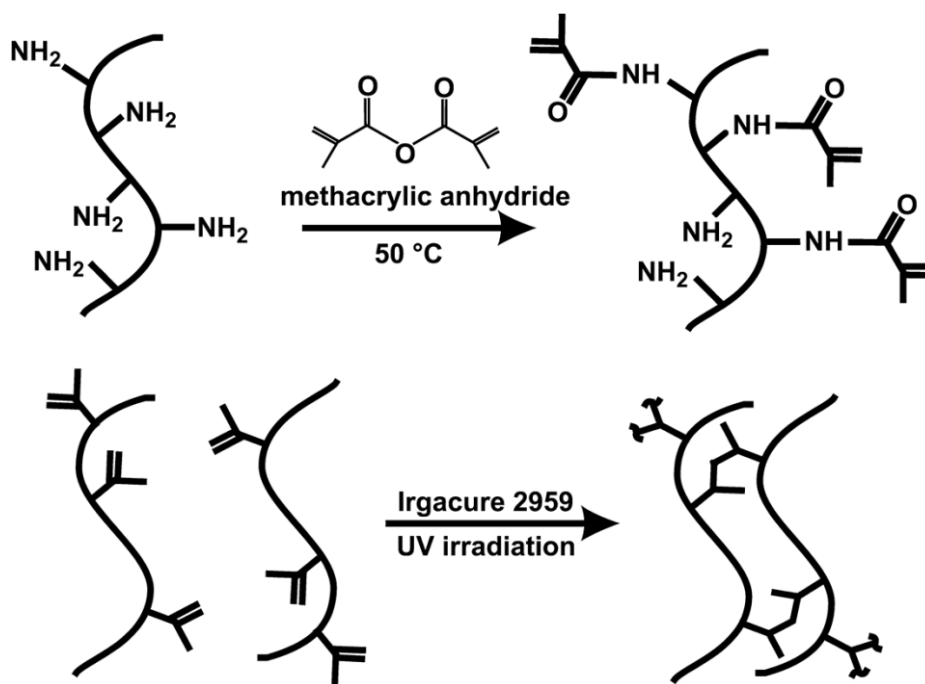


Figure 4.1 - Representation of methacrylate gelatin synthesis and crosslinking. Macromers of Gelatin containing amine groups were reacted with methacrylic anhydride which added methacrylate pendant groups. Methacrylate gelatin crosslinked with UV light in the presence of Irgacure 2959 initiator. Reprinted with permission (368).

Although a number of studies have shown the potential of utilising GelMA for bone tissue engineering applications (369, 370), the inherent lack of mechanical strength limits the materials clinical potential for bone augmentation strategies (327). To overcome this limitation, the combination of GelMA with an external scaffold framework to create a composite scaffold system would enhance the mechanical properties of this hydrogel. Various studies have shown that the GelMA hydrogel could be micropatterned into a variety of shapes and configurations for tissue engineering and microfluidic applications while retaining its high encapsulated cell viability and cell-responsive elements (368, 371). Therefore, incorporating hydrogels microspheres formed using a microfluidic system within a 3D plotted scaffold, similar to the BMT system created utilising microtissues in the previous chapter, would overcome the inherent lack of mechanical strength of hydrogels. This approach can accomplish a similarly sized construct as the BMT model, however requiring far fewer cells which subsequently reduces the *in vitro* expansion period, the cost and is more clinically relevant. In this chapter, the fabrication of GelMA microspheres of regular size and shape was investigated for assembly within the 3D printed scaffold (during collaborative research visit, at the University of Otago). Following which, the effects of MI192 in stimulating hBMSCs osteogenic capacity would be initially evaluated within the GelMA hydrogel alone, then within the GelMA hydrogel combined with the 3D printed scaffold (GelMA-PEBT/PBT) in Leeds. As this is an

example of a low cell density construct and having demonstrated the effective use of the BMT model in the hDPSCs chapter in this thesis, the effects of MI192 on hBMSCs osteogenic differentiation within the BMT will also be evaluated in this chapter.

In addition to evaluating the effects of MI192 on hBMSCs osteogenic differentiation *in vitro*, it is important to determine whether these effects successfully translate within a more physiologically relevant environment. To date, limited studies have investigated the effects of HDACis to stimulate MSCs osteogenic differentiation in 3D *in vivo* culture (208, 215, 320), therefore in the literature, there is a lack of knowledge on how HDACi therapies behave in physiological conditions. Moreover, the research performed *in vivo* have utilised panHDACis, which are associated with their limitations (213). The diffusion chamber model provides an ideal environment to investigate the effects of tissue engineered constructs *in vivo* while ensuring tissue growth within the chamber originates from the implanted cells. A number of studies have reported the successful use of this *in vivo* model for assessed bone engineered constructs (257, 258).

Therefore, the aim of this chapter was to investigate the effects of the HDAC2 & 3 selective inhibitor - MI192 on hBMSCs behaviour and osteogenic capacity on 2D and 3D *in vitro* and *in vivo*.

The main objectives of this chapter:

- To investigate the effects of MI192 on the behaviour and osteogenic capacity of hBMSCs in 2D *in vitro* culture (section 4.3.1).
- To evaluate the effects of MI192 on hBMSCs *in vitro* bone formation within 3D scaffold systems:
 - GelMA hydrogel (GelMA alone and GelMA-PEBT/PBT construct) (section 4.3.2).
 - BMT model (section 4.3.3).
- To investigate the effects of MI192 on hBMSCs bone formation *in vivo* (section 4.3.4).

4.2 - Materials and Methods

4.2.1 - Effect of MI192 on ALPSA in hBMSCs

Cells were seeded in two 24-well plates (5×10^4 cells per well) in basal medium. After 24 hours, the medium was replaced, and cells were pre-treated with a range of MI192 doses (10, 20, 30, 50, 70 μM) for 24 or 48 hours. Following pre-treatment, cells were cultured in osteogenic medium for 2 weeks. Untreated cells in basal or osteogenic medium were used as controls. The sample size was three for each group ($n=3$). After culture, cells were prepared for ALPSA as described in Chapter 2.

4.2.2 - Effect of MI192 on the expression of osteogenic genes in hBMSCs

Cells were seeded at 5×10^4 cells per well in four 24-well plates in basal medium. After 24 hours, the medium was replaced with fresh basal medium supplemented with MI192 (50 μM). Untreated cells in basal medium used as control. Following 48 hours pre-treatment, the medium was then replaced with osteogenic medium and plates were cultured for 3, 7, 14, 21 days. The sample size was three for each group ($n=3$). At each time point, one of the plates was stopped for RNA isolation, cDNA conversion and RT-qPCR as described in Chapter 2.

4.2.3 - GelMA macromer preparation

GelMA utilised in this chapter were provided by Dr Khoon Lim at the CReaTE group, at the University of Otago. GelMA was synthesised following methods described previously (372). Briefly, type A porcine skin gelatin (Sigma-Aldrich, G2500) was mixed at 5, 10 and 15% (w/v) into PBS at 50°C until fully dissolved. Methacrylic anhydride (MA) (Sigma-Aldrich, 276685) was added (0.6 ml MA/1 g Gelatin) to gelatin solution under stirred conditions at 50°C and incubated for 1 hour. The mixture was dialyzed against dH₂O using 12 - 14 kDa cut off dialyses tubing for 2 - 3 days at 40°C to remove salts and methacrylic acid. Solution pH at 7.4 and then sterile filtered. The solution was stored at -80°C for 24 hours then freeze-dried for 4 days. The visible light photo-polymerisation system previously developed by the CReaTE group was used in this chapter (371). Freeze-dried GelMA macromer was then mixed with PBS containing visible light initiators (0.2 mM Tris (2,2'-bipyridyl) dichlororuthenium (II) hexahydrate (Ru)) (Sigma-Aldrich, 544981) and 2 mM Sodium persulfate (SPS) (Sigma-Aldrich, 216232) until fully dissolved.

4.2.4 - Production of GelMA microspheres using microfluidics

Hydrogel microspheres of appropriate size and shape were prepared by utilising a microfluidic oil-emulsion system based on work in the literature (373). The microfluidic methods utilise an outer

continuous phase (sunflower oil) to focus the flow of an inner pre-polymer phase (GelMA) from which spheres are fabricated (374). The work involving the cell-laden microspheres was undertaken at the CReaTE group at the University of Otago, during a collaborative research visit. Assistance was provided by Catherine Chia an intern in the CReaTE group (experimental planning and preparation).

4.2.5 - Microfluidic device

The microfluidic device (Fig 4.2) consists of Polytetrafluoroethylene (PTFE) tubing, T-junctions and a fused silica capillary (internal diameter (ID) 530 μm , outer diameter (OD) 660 μm) (Postnova, Z-FSS-530660). The macromer and its shearing solution, sunflower oil, were loaded into separate syringes and placed into syringe pumps. A long coil of transparent Tygon R-3603 PTFE tubing (ID 1.6 mm, OD 3.2 mm) (Tygon, 2375 AJK00002) was connected to the outlet of the microfluidic device and this was positioned under a UV light source (Omniculture Series 1500) which is situated above a light filter, allowing only visible light wavelengths through, at 30 - 50 mW/dm^2 . This allows enough time for polymerisation of microspheres while flowing through the coiled tubing.

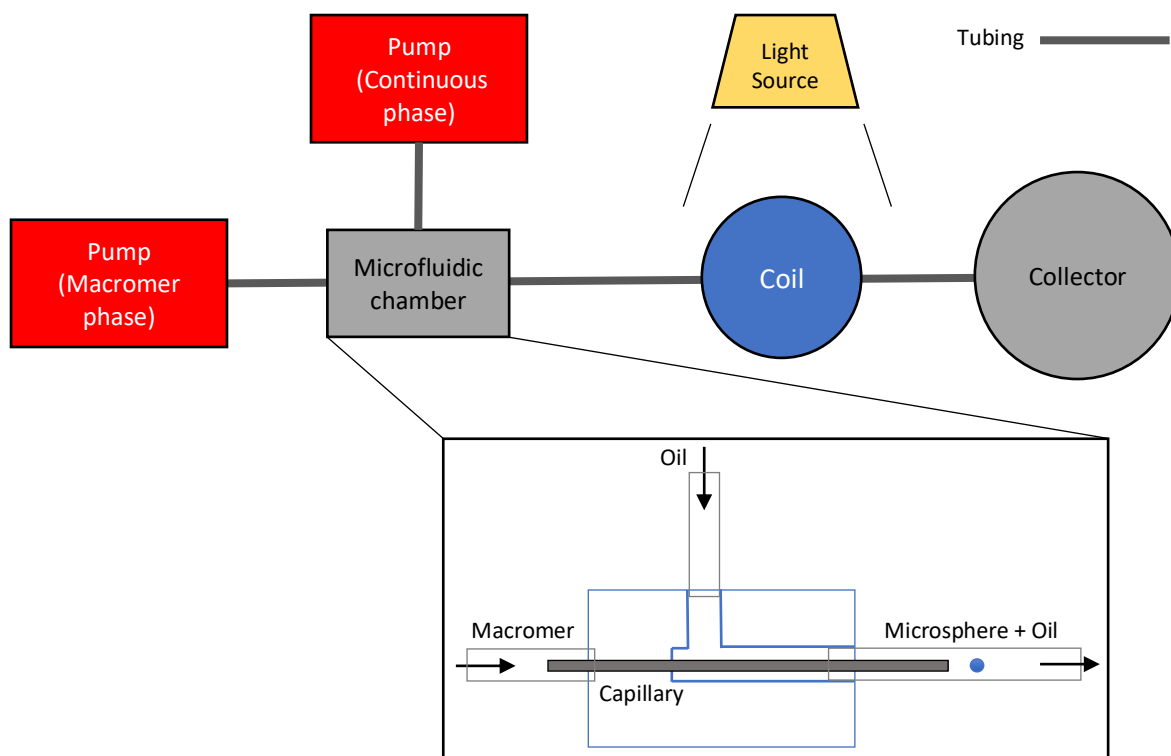


Figure 4.2 - Schematic representation of the microfluidic apparatus to form hydrogel microspheres. The continuous phase and macromer phase are delivered into the T-junction by syringe pumps. The macromer is injected along the main axis of the T-junction via a capillary needle, while the continuous phase is injected into the chamber perpendicularly. Microspheres exiting the T-junction are photo-polymerised within the coil then deposited in the collector.

4.2.6 - GelMA microsphere formation and characterisation

The production of microspheres requires a simultaneous flow of both the dispersed (GelMA) and the continuous phase (sunflower oil), which allows these to reach equilibrium (at least 5 minutes) to ensure flow pattern and droplet size stabilized. The UV light source was turned on ($50 \pm 5 \text{ mW/dm}^2$) and microspheres collected in centrifuge tubes containing PBS allowing separation from the oil phase. Microspheres were washed by centrifugation at 1000 RPM for 3 minutes and transfer into a fresh falcon tube to remove residual oil. The morphology and size of the microspheres produced were characterised before and after 24 hours swelling in different culture conditions, such as; room temperature in PBS, at 37°C in PBS and at 37°C in Dulbecco's Modified Eagle's Medium (DMEM) (Gibco, 10567014). The sample size was three for each group (n=3). Microspheres were imaged using a Zeiss Axioimager X1 microscope.

4.2.7 - Optimisation of cell encapsulation and BMT assembly using cell-laden GelMA microspheres

L929 murine fibroblasts were cultured in Minimum Essential Medium Eagle (Sigma-Aldrich, M2279) supplemented with P/S (100 units/ml, 100 µg/ml) and 10% FCS. Cells were collected by centrifugation at a density of 1×10^7 cells. GelMA was dissolved in sterile PBS at 5 and 10 wt% and the macromer solution (1 ml) was used to re-suspend the cell pellet. Sterile photo-initiators Ru and SPS were added to a final concentration of 0.2 mM and 2 mM respectively and the solution was gently mixed to ensure even cell distribution. Cell/macromer solution was transferred into a sterile syringe and microsphere formation was performed utilising sunflower oil with 0.5% Span 80 and a continuous flow rate of 1000 µl/min and polymer flow rate of 40 µl/min. Microspheres were separated from the oil as previously described, re-suspended in complete DMEM and incubated at 37°C in 5% CO₂. The viability of cells within the microspheres was assessed after 24 hours post-encapsulation by live/dead staining. Cell-laden microspheres were incubated in the staining solution in the dark for 30 minutes, washed with PBS and assessed immediately by fluorescence microscopy.

After 3 days post-encapsulation, cell-laden microspheres were incorporated within a 3D plotted PEGT/PBT polymer scaffolds (1-mm fibre spacing) utilising an automated BMT assembly system consisting of a fluidic-based singularisation and injection modules incorporated into a commercial 3D bioprinter (SYS-ENG Germany). The singularisation module delivers individual microspheres to an injection module for high throughput insertion into specific locations in a 3D plotted scaffold (335). Live/dead staining was performed and assessed as described previously.

4.2.8 - Encapsulation of MI192 pre-treated hBMSCs within GelMA hydrogel

Untreated and MI192 pre-treated hBMSCs ($50 \mu\text{M}$ MI192 for 48 hours) were collected by centrifugation at a density of 5×10^6 cells. 5 wt% GelMA solution (1 ml) was used to resuspend the cell pellet. Photoinitiators were added to cell/macromer solution as described previously. Cell/macromer solution was transferred into a sterile silicone mould ($\varnothing 5 \times 1 \text{ mm}$) placed on a glass slide. The slide was placed under the light source for 10 minutes at $50 \pm 5 \text{ mW}/\text{dm}^2$ (Fig 4.3A). Once crosslinked, cell-laden hydrogels were carefully transferred into low adherent 48 well plates and cultured in osteogenic medium for 6 weeks. The medium was changed every 3 - 4 days. The sample size was three for each group ($n=3$)

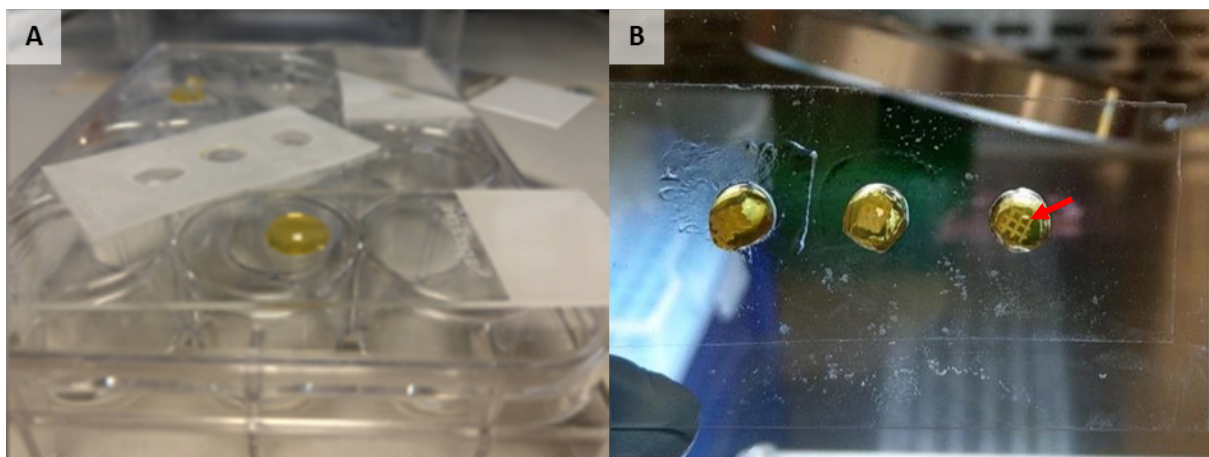


Figure 4.3 - *In situ* representation of A) GelMA hydrogels and B) GelMA-PEBT/PBT constructs. Cell-laden GelMA hydrogels placed within silicone moulds with/without 3D printed PEGT/PBT scaffold (red arrow) prior to photo-polymerisation.

4.2.9 - Fabrication of hBMSCs encapsulated GelMA-PEBT/PBT constructs

GelMA-PEBT/PBT construct was created by casting the PEBT/PBT scaffold into the cell-laden hydrogel during crosslinking (Fig 4.3B). This method was undertaken due to lack of 3D Bio-plotter, singularisation device and microfluidic apparatus at Leeds to create cell-laden microspheres. Untreated and MI192 pre-treated hBMSCs were encapsulated within GelMA (5×10^6 cells/ml) and placed into a sterile silicone mould ($\varnothing 5 \times 2 \text{ mm}$) on a glass slide. The sterilised 3D printed PEBT/PBT scaffold ($3 \times 3 \times 2 \text{ mm}$) was placed into the centre of the cell-laden macromer solution and crosslinked following the previous protocol. GelMA-PEBT/PBT constructs were transferred into low adherent 48-well plates and cultured in osteogenic medium for 6 weeks. The medium was changed every 3 - 4 days. The sample size was three for each group ($n=3$).

4.2.10 - Microtissue culture and BMT assembly

Untreated and MI192 pre-treated hBMSCs (50 μ M MI192 for 48 hours) (2.5×10^5 cells), were suspended in 250 μ l of osteogenic medium in a v-shaped bottom 96-well plate. Microtissues formed utilising the procedure described in Chapter 2. Following 1 week culture, microtissues were manually transferred into the scaffold (1 microtissue per pore) using a 1-ml pipette tip to form the BMT construct. A total of 8 microtissues were incorporated into the scaffold in a bi-layer configuration (4 microtissues per layer). BMTs were cultured in osteogenic conditions for a subsequent 6 weeks and the medium was changed every 3 - 4 days. The sample size was three for each group (n=3).

4.2.11 - 3D construct preparation for ALPSA assay

Following osteogenic culture for 2 weeks, the cell-laden GelMA hydrogel and BMT constructs were processed for ALPSA assay. Samples were washed twice with PBS and placed in Eppendorf tubes. 500 μ l 0.1% Triton X-100 in PBS was added and tubes were vortexed and sonicated for 5 minutes. Samples were frozen at -80°C then thawed in a 37°C oven, and the freeze/thaw process was repeated 5 times. Samples were homogenised by passing through a 20-gauge needle between freeze/thaw steps. Following this, samples were centrifuged at 10000g for 10 minutes at 4°C, then the lysate was collected and utilised for ALPSA assay described in Chapter 2. The sample size was three for each group (n=3).

4.3 - Results

4.3.1 - The Effects of MI192 on the Behaviour and Osteogenic capacity of hBMSCs in 2D culture

4.3.1.1 - Effect of MI192 on hBMSCs morphology

After 24 hours of culturing in basal medium supplemented with/without MI192, the images show that untreated cells in the basal group possessed the typical fibroblast-like morphology associated with stromal cells (Fig 4.4). Following treatment with 1 μM MI192, cells possessed a similar appearance with the untreated group. In the cells treated with 10 μM and greater concentrations, the morphology of the cells became less fibroblastic in shape, with decreasing cellular density. This also correlated with the increased quantity of floating dead/detached cells observed in the higher MI192 concentration groups.

At 48 hours, cells within the basal medium showed a slight increase in cell density with a continuation of the fibroblastic-like morphology as seen in the same group at the previous time point (Fig 4.4). In the MI192 treated groups, a similar pattern from the previous time point was observed, where the groups containing the highest MI192 concentrations exhibited the greatest reduction in cell density, loss of fibroblastic-like morphology and increased number of floating dead/detached cells. These observations were much more prevalent at the 48 hour time point compared to 24 hours.

After 72 hours of MI192 treatment, cells in the basal group continued to exhibit the fibroblastic-like morphology as seen in the earlier time points, with a slight increase in cell density (Fig 4.4). Following treatment with 1 μM MI192, there was an increased quantity of floating dead/detached cells visible when compared to the cells in the same group at the previous time points. Following treatment with higher MI192 concentrations (10 to 100 μM), there was a substantial increase in the quantity of visible floating dead/detached cells with a decrease in the density of attached cells compared to the lower MI192 dose and the same conditions at the previous time points.

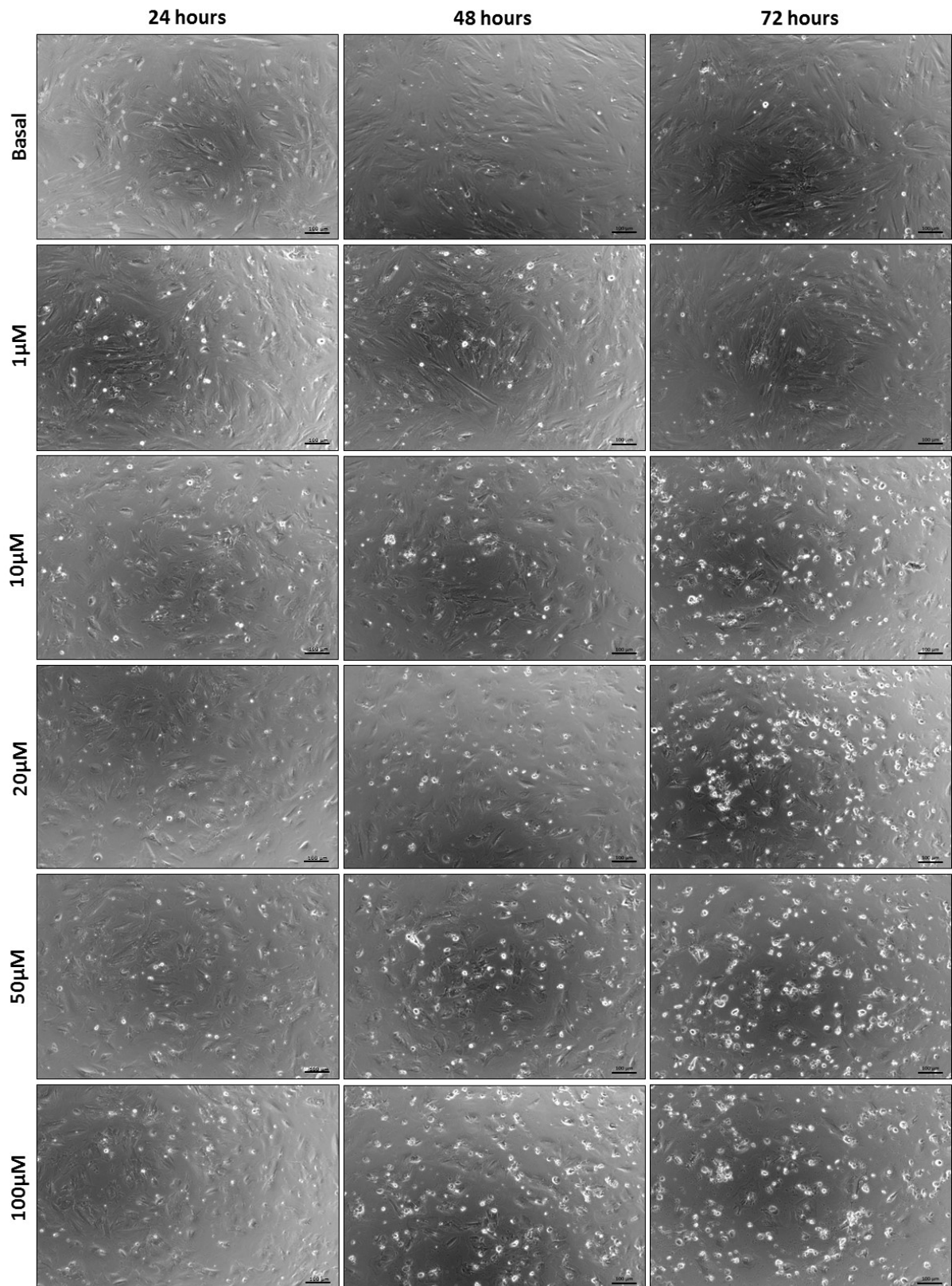


Figure 4.4 - Phase contrast images of hBMSCs treated with/without a range of MI192 dose (1, 10, 20, 50, 100 μ M) for 24, 48 and 72 hours. Scale bar = 100 μ m.

4.3.1.2 - Effect of MI192 on hBMSCs metabolic activity

Cells were treated with/without MI192 (1 - 100 μM) for up to 72 hours and the effects on hBMSCs metabolic activity were assessed. Following AlamarBlue analysis, results showed that MI192 treatment caused a time-dose dependent decrease in the metabolic activity of the cells when compared to the untreated controls (Fig 4.5). After 24 hours, MI192 concentrations of 20 μM and greater caused a significant decrease in the metabolic activity compared to the untreated control ($P \leq 0.01$). MI192 treatment for 48 hours exhibited a similar dose-dependent reduction in metabolic activity, where MI192 concentrations of 10 μM and above significantly decreased the metabolic activity compared to untreated control ($P \leq 0.001$). Following 72 hours treatment, MI192 concentrations of 1 μM and above significantly reduced the metabolic activity compared to the untreated control at that time point ($P \leq 0.001$).

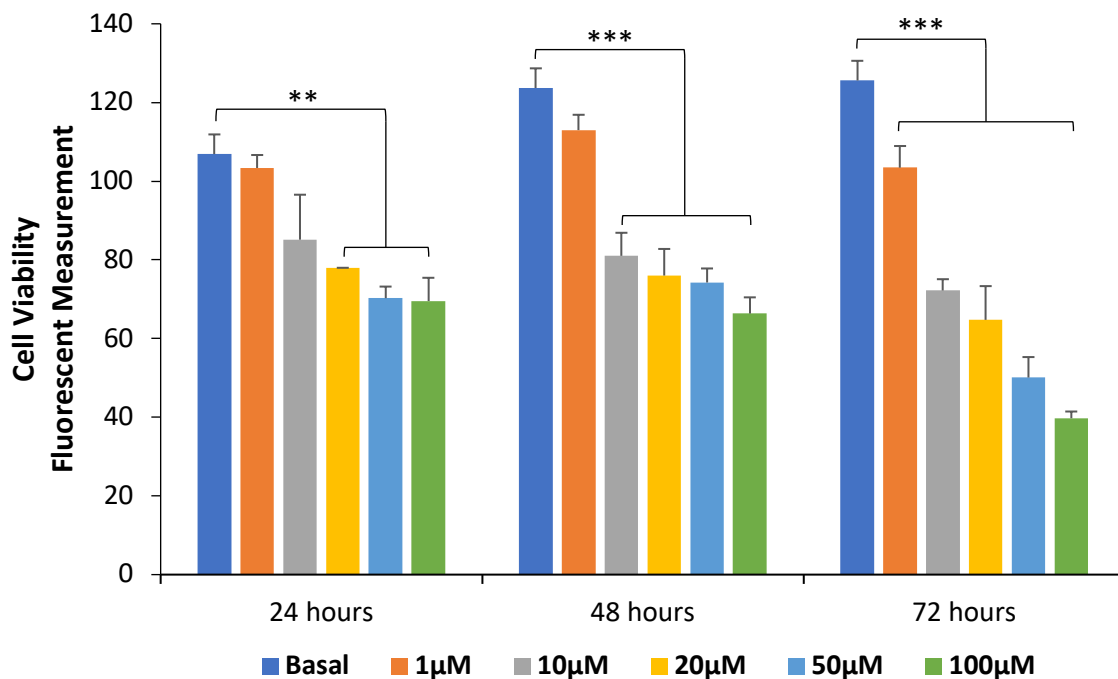


Figure 4.5 - AlamarBlue analysis of hBMSCs metabolic activity treated with/without a range of MI192 doses (1, 10, 20, 50, 100 μM) for 24, 48 and 72 hours. Data expressed as mean \pm SD (n=3). Significance levels shown are the test groups compared to the basal control for that time point. ** $P \leq 0.01$ and *** $P \leq 0.001$.

4.3.1.3 - Effect of MI192 on hBMSCs DNA quantity

Figure 4.6 shows the effects of MI192 treatment (1 - 100 μ M) on hBMSCs DNA content for up to 72 hours, quantified by PicoGreen assay. Following 24 hours of MI192 incubation, hBMSCs exhibited a dose-dependent decrease in the DNA quantity, where MI192 concentrations of 10 μ M and greater significantly reduced the DNA content compared to the untreated control group ($P \leq 0.05$). A similar dose-dependent decrease was observed after 48 hours treatment, where MI192 concentrations of 10 μ M and greater significantly reduced the DNA quantity ($P \leq 0.001$). At 72 hours, MI192 concentrations of 1 μ M and above significantly decreased the DNA content compared to the untreated control for that time point ($P \leq 0.001$). A time-dependent decrease in DNA content was observed for each MI192 concentration.

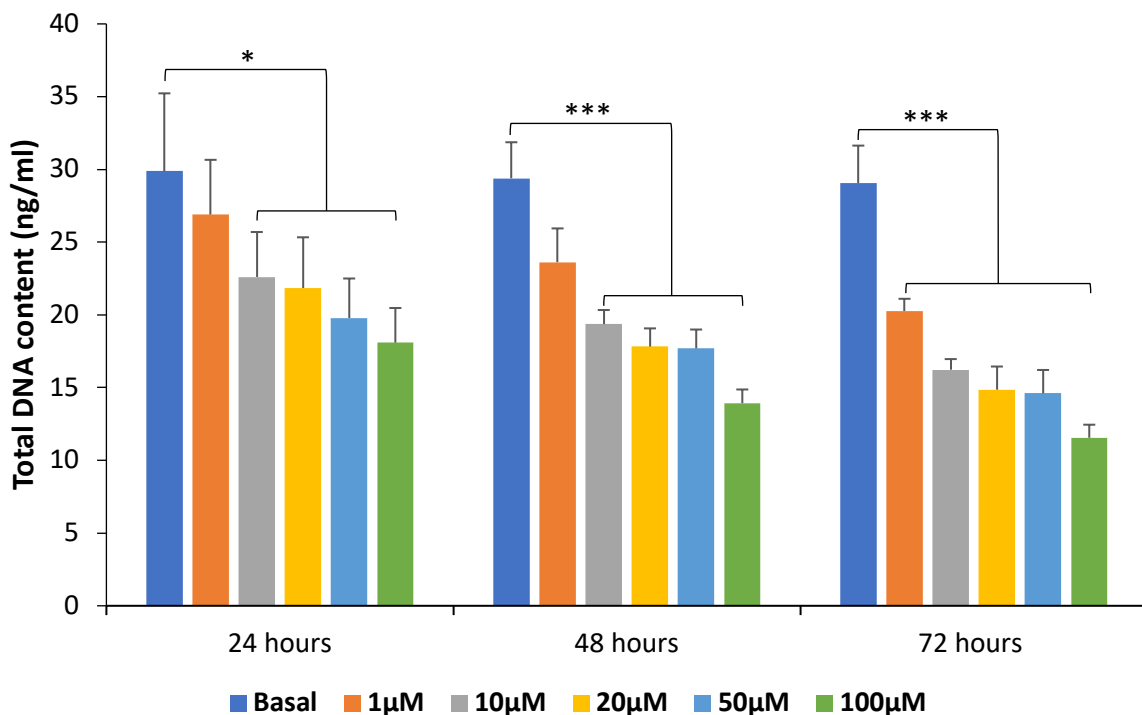


Figure 4.6 - DNA quantification of hBMSCs treated with/without a range of MI192 doses (1, 10, 20, 50, 100 μ M) for 24, 48 and 72 hours. Data expressed as mean \pm SD (n=3). Significance levels shown are the test groups compared to the basal control for that time point. * $P \leq 0.05$ and *** $P \leq 0.001$.

4.3.1.4 - Effect of MI192 on HDAC specific activity in hBMSCs

Cells were treated with/without a range of MI192 concentrations (1 - 50 μ M) for 24 and 48 hours to determine the effects of MI192 treatment on hBMSCs HDAC specific activity. MI192 treatment caused a dose-dependent reduction in hBMSCs HDAC specific activity when compared to the untreated cells, where MI192 at 1 μ M and greater concentrations significantly reduced HDAC activity (≥ 2.1 & ≥ 2.36 -fold) compared to the untreated cells after 24 and 48 hours treatment ($P \leq 0.001$) (Fig 4.7). Between treatment with different MI192 doses, significant reduction in HDAC specific activity was observed between MI192 concentrations of 1 - 5 μ M ($P \leq 0.001$), 5 - 10 μ M ($P \leq 0.01$), and 20 - 50 μ M ($P \leq 0.001$) at 24 hours, and between 1 - 5 μ M ($P \leq 0.001$), 5 - 10 μ M ($P \leq 0.05$) and 10 - 20 μ M ($P \leq 0.05$) at 48 hours.

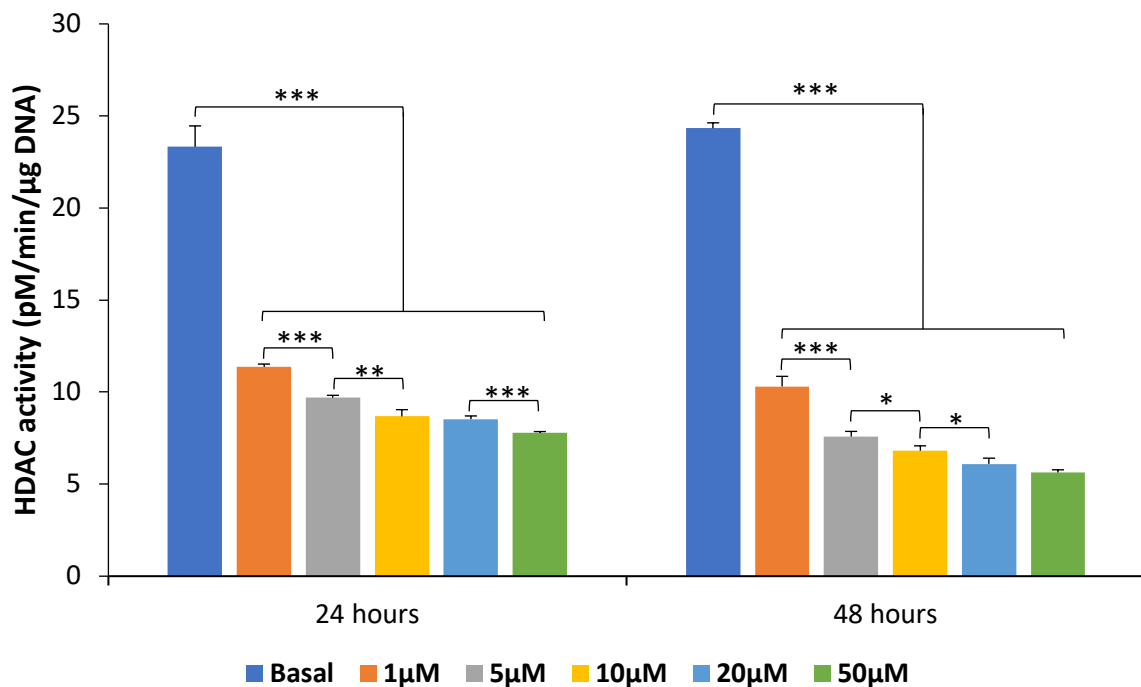


Figure 4.7 - HDAC specific activity in hBMSCs following MI192 treatment for 24 and 48 hours. Data expressed as mean \pm SD (n=3). Significance levels shown are the test groups compared to the basal control or between adjacent MI192 concentrations at that time point. * $P \leq 0.05$, ** $P \leq 0.01$ and *** $P \leq 0.001$.

4.3.1.5 - Effect of MI192 on the histone H3K9 specific acetylation in hBMSCs

Figure 4.8 shows the effects of MI192 treatment (1 - 50 μM) on hBMSCs histone H3K9 specific acetylation for up to 48 hours, quantified by *in situ* histone H3-K9 acetylation assay kit. A time-dose dependent increased in the H3K9 acetylation levels was observed at both time points assessed. MI192 treatments for 24 hours (1 - 50 μM), significantly downregulated the histone H3K9 specific acetylation levels when compared to the untreated cells (≥ 1.22 -fold) ($P \leq 0.01$). However, after 48 hours of MI192 treatment, concentrations of 20 μM and greater significantly enhanced the histone H3K9 specific acetylation levels in cells immediately after treatment compared to that in the untreated cells (≥ 1.28 -fold) ($P \leq 0.001$) (Fig 4.8). Between the different MI192 concentrations, a significant increase in acetylation was observed between MI192 doses of 1 - 20 μM ($P \leq 0.05$) and 20 - 50 μM ($P \leq 0.05$) at 24 hours, and between 5 - 10 μM ($P \leq 0.01$), 10 - 20 μM ($P \leq 0.05$) and 10 - 50 μM ($P \leq 0.01$) at 48 hours.

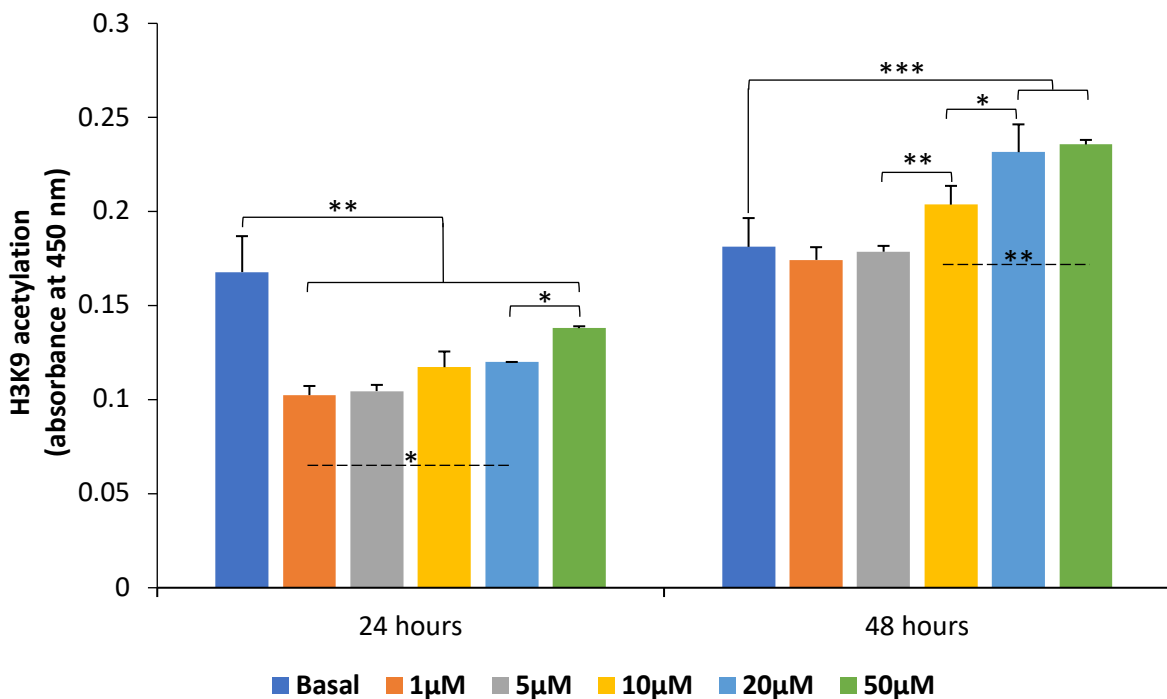


Figure 4.8 - H3K9 histone-specific acetylation levels in hBMSCs after treatment with five doses of MI192 for 24 and 48 hours. Data expressed as mean \pm SD (n=3). Significance levels shown are the test groups compared to the basal control or between adjacent MI192 concentrations at that time point. * $P \leq 0.05$, ** $P \leq 0.01$ and *** $P \leq 0.001$.

4.3.1.6 - Effect of MI192 on hBMSCs cell cycle progression

hBMSCs were cultured with/without 50 μ M MI192 for 24, 48 and 72 hours. The percentage of cells distributed in the phases of the cell cycle is shown in Table 4.1 and Figure 4.9. The representative FACS histograms show the number of cells at different stages of the cell cycle (Fig 4.10).

Table 4.1 - The effect of MI192 treatment on the distribution of hBMSCs at different phases of the cell cycle. Cells dosed with/without 50 μ M MI192, for 24, 48 and 72 hours. The table shows the average percentage of cells in each phase of the cell cycle, with the standard deviation (SD).

		G₀/G₁		G₂/M		S	
		Phase	SD	Phase	SD	Phase	SD
		Mean %		Mean %		Mean %	
24 hours	Untreated	73.03	3.59	11.02	2.18	15.95	1.62
	MI192	70.34	7.73	21.11	2.42	8.55	1.45
48 hours	Untreated	73.05	6.22	9.90	1.24	17.05	4.27
	MI192	72.84	1.06	21.14	1.44	6.02	1.77
72 hours	Untreated	77.54	2.91	8.33	0.68	14.13	1.48
	MI192	78.67	3.14	15.61	0.89	5.72	1.09

G₀/G₁ Phase

The percentage of cells within the MI192 treated group was at similar levels to the untreated group, approximately 70% at the 24 hour time point ($P > 0.05$) (Fig 4.9). At 48 hours, the percentage of cells within the G_0/G_1 phase between the groups was again at similar levels and this pattern was replicated at the 72 hour time point ($P > 0.05$). The percentage of cells in this phase remained at a constant level (~70 %) throughout the 72 hour culture period for both the untreated and MI192 treated cells.

G₂/M phase

At 24 hours, MI192 treatment significantly enhanced the percentage of cells in the G_2/M phase (21.11%) when compared to the untreated group (11.02%) ($P \leq 0.05$). At the 48 and 72 hour time points, the MI192 treated group maintained the significantly elevated number of cells in the G_2/M phase (21.14 & 15.61%) compared to the untreated group (9.90 & 8.33%) ($P \leq 0.01$ and $P \leq 0.05$, respectively). Both the untreated and MI192 treated G_2/M phase cell percentage decreased over time.

S Phase

At 24 hours, MI192 treatment causes a significant reduction in the cells within the S phase (8.55%) compared to the untreated control (15.95%) ($P \leq 0.05$). A similar significant decrease in S phase percentage induced by MI192 treatment (6.02 & 5.72%) was observed compared to the untreated cells (17.05 & 14.13%) at 48 and 72 hour time points ($P \leq 0.05$).

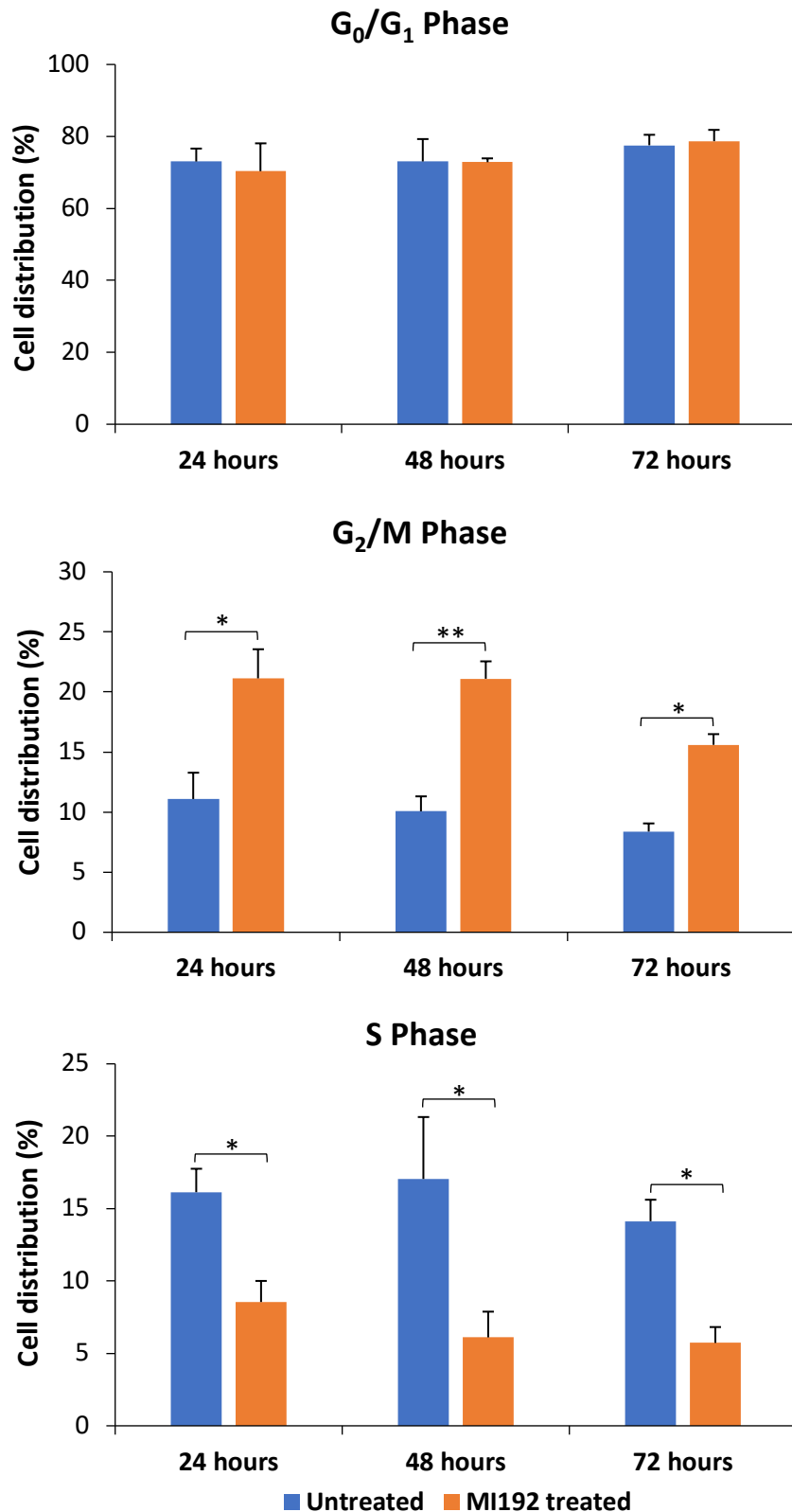


Figure 4.9 - The percentage of hBMSCs in the G₀/G₁, G₂/M and S phase after treatment with/without 50 μ M MI192 for 24, 48 and 72 hours. Data expressed as mean \pm SD (n=3). Significance levels shown are the test group compared to the basal control for that time point. *P \leq 0.05 and **P \leq 0.01.

4.3.1.7 - Effect of MI192 on ALPSA in hBMSCs

Following MI192 pre-treatment for 24 or 48 hours (10 - 70 μ M), hBMSCs were then cultured in osteogenic condition for 2 weeks, following which ALPSA was quantified (Fig 4.11). At both time points, untreated cells cultured in osteogenic conditions exhibited a significantly higher ALPSA compared to the same cells cultured in basal medium ($P \leq 0.001$). MI192 pre-treatment for 24 hours significantly reduced ALPSA of hBMSCs when compared to untreated cells cultured in osteogenic medium (≥ 1.38 -fold) ($P \leq 0.05$). After pre-treatment for 48 hours, MI192 dose of 50 μ M significantly enhanced the ALPSA of hBMSCs compared to the other MI192 concentrations and the untreated cells cultured in both basal and osteogenic medium (≥ 1.43 -fold) ($P \leq 0.001$). 50 μ M MI192 pre-treatment for 48 hours was shown to stimulate hBMSCs ALPSA in different donors shown in the Appendix (Fig A2). This optimised MI192 pre-treatment condition (50 μ M MI192 for 48 hours) was utilised in the subsequent experiments in this chapter.

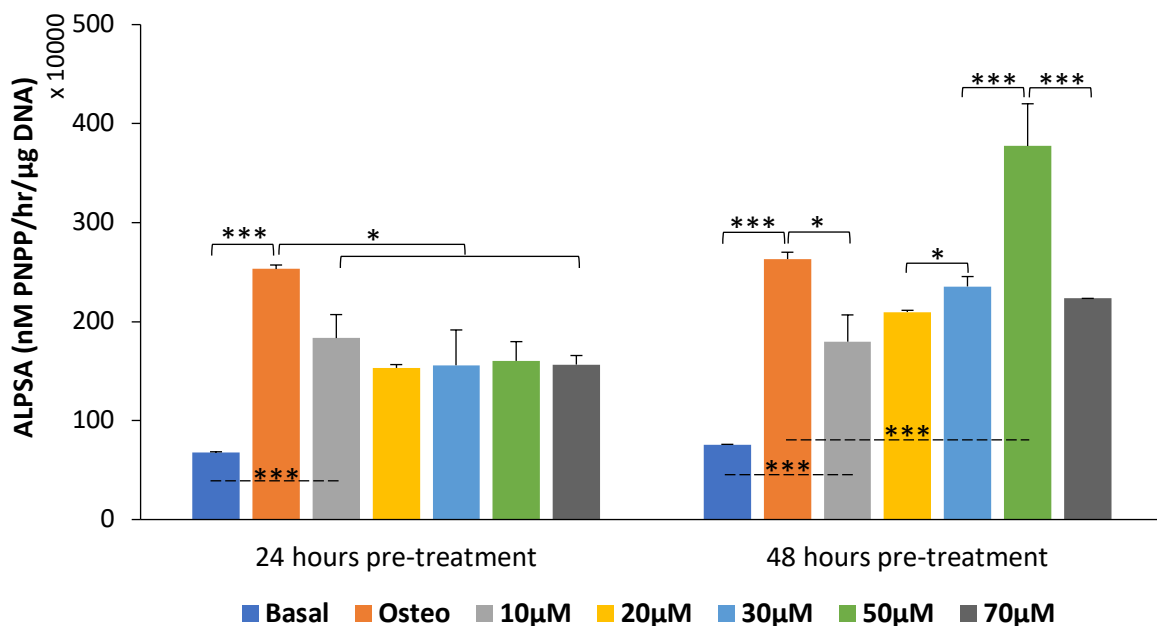


Figure 4.11 - ALPSA in hBMSCs pre-treated with/without MI192 for 24 and 48 hours then cultured in osteogenic medium. Cells were pre-treated with MI192 doses (10 - 70 μ M) for 24 or 48 hours, following which cells were cultured in osteogenic medium for 2 weeks, with untreated cells cultured in basal and osteogenic medium used as the controls. Data expressed as mean \pm SD (n=3). Significance levels shown are the test groups compared to the basal/osteogenic control or between adjacent MI192 concentrations at that time point. * $P \leq 0.05$ and *** $P \leq 0.001$.

4.3.1.8 - Effect of MI192 on the expression of osteogenic genes in hBMSCs

After pre-treatment with/without 50 μ M MI192 for 48 hours, hBMSCs were cultured in osteogenic conditions for up to 21 days and mRNA levels of key osteoblast-related genes (*RUNX2*, *ALP*, *BMP2*, *COL1A* and *OCN*) was assessed using RT-qPCR (Fig 4.12).

RUNX2

MI192 pre-treatment significantly increased hBMSCs *RUNX2* mRNA levels when compared to that in the untreated cells after 3 days osteogenic culture (1.12-fold) ($P \leq 0.05$). A similar pattern was observed throughout the remaining time points (7, 14 and 21 days) where the MI192 pre-treated group exhibited significantly higher *RUNX2* mRNA levels (1.2-, 1.17- and 1.09-fold, respectively) compared to that in the untreated cells at each time point ($P \leq 0.05$, $P \leq 0.01$ and $P \leq 0.01$, respectively). Within both cells, the peak expression was observed on day 7, following which mRNA expression declined on day 14 and 21.

ALP

After 3 and 7 days in osteogenic medium, the *ALP* mRNA levels were significantly enhanced within the MI192 pre-treated cells compared to that in the untreated cells (1.13- and 1.09-fold) ($P \leq 0.05$). On day 14, the *ALP* mRNA expression was significantly upregulated in the MI192 pre-treated cells (1.22-fold) ($P \leq 0.01$). On day 21, the *ALP* expression was upregulated compared to that in the untreated cells, although not significantly ($P > 0.05$). When compared across the time points, a time-dependent increase in *ALP* expression was observed in both cells, with the MI192 pre-treated group exhibiting higher expression levels compared to that in the untreated cells at each time point.

BMP2

The *BMP2* mRNA levels were significantly elevated in the MI192 pre-treated cells (1.03-, 1.2- and 1.06-fold, respectively) compared to that in the untreated group on day 3, 7 and 21 time points ($P \leq 0.01$, $P \leq 0.01$ and $P \leq 0.05$, respectively), with no significant difference observed between the groups on day 14 ($P > 0.05$). When compared across the time points, the MI192 pre-treated cells exhibited a time-dependent increase in mRNA expression to day 7, following which expression levels decreased in a time-dependent manner. Within the untreated cells, expression levels remained at similar levels where a peak in expression was observed on day 14, however, expression was downregulated following this time point.

COL1A

After 3 days osteogenic culture, the mRNA levels of *COL1A* was reduced in the MI192 pre-treated cells compared to that in the untreated group, although not significantly ($P > 0.05$). The *COL1A* mRNA levels were significantly upregulated within the MI192 pre-treated cells when compared to that in the untreated group on day 7 and 14 (1.16- and 1.69-fold) ($P \leq 0.05$ and $P \leq 0.01$). The expression levels were similar between the groups on day 21 ($P > 0.05$). Within both cells, a time-dependent increase in expression levels was observed, where mRNA expression peaked on day 14.

OCN

MI192 pre-treatment downregulated hBMSCs *OCN* mRNA levels when compared to that in the untreated cells on day 3, however not significantly ($P > 0.05$). After 7 and 14 days osteogenic culture, *OCN* mRNA levels were significantly enhanced in the MI192 pre-treated cells compared to that in the untreated cells at those time points (1.06- and 1.02-fold) ($P \leq 0.05$). On day 21, there was a slight increase in *OCN* expression exhibited in the MI192 pre-treated cells compared to that in the untreated control, however not significantly ($P > 0.05$). Both cells expression peaked on day 7, following which a time-dependent downregulation in mRNA expression levels was observed.

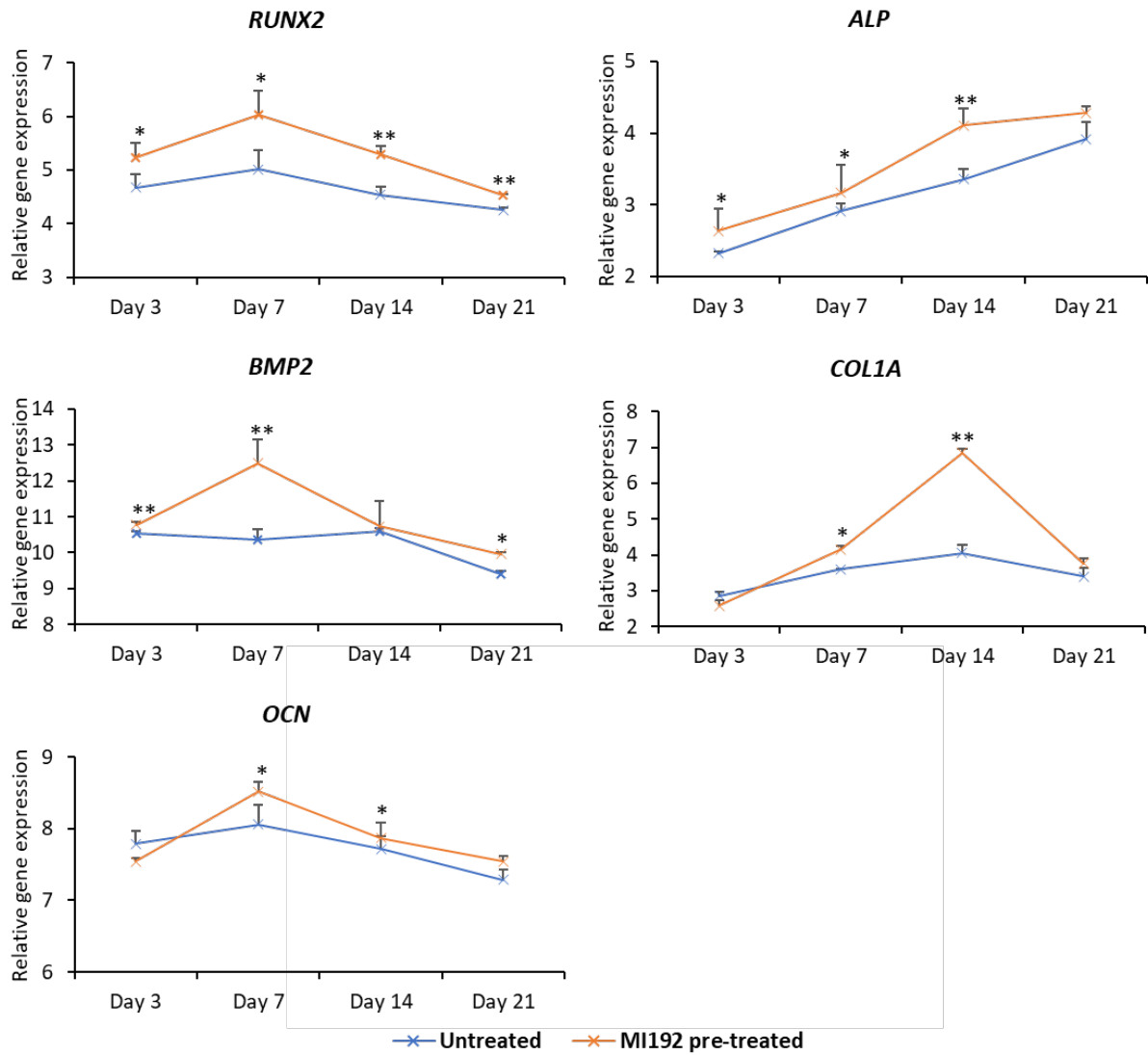


Figure 4.12 - Relative expression of osteoblast-related genes in untreated/MI192 pre-treated hBMSCs after culture in osteogenic conditions. Gene expression analysed on day 3, 7, 14 and 21. Data expressed as mean \pm SD (n=3). Significance levels shown are the test group compared to the untreated control at the same time point. *P \leq 0.05 and **P \leq 0.01.

4.3.1.9 - Effect of MI192 on the expression of osteogenic proteins in hBMSCs

Cells were pre-treated with/without 50 μ M MI192 for 48 hours, then cultured in osteogenic conditions for up to 28 days. The expression of key osteoblast-related markers (Runx2, ALP, BMP2, Col1a and OCN) was also assessed at the protein level using ICW (Fig 4.13).

Runx2

The Runx2 protein levels were significantly increased in the MI192 pre-treated cells compared to that in the untreated group on day 7 and 14 (2.6- and 1.21-fold) ($P \leq 0.05$). On day 21 and 28, expression levels remained significantly upregulated in the MI192 pre-treated cells compared to that in the control group (2.55- and 2.01-fold) ($P \leq 0.001$ and $P \leq 0.01$). Within both cells, a time-dependent increase in protein expression was observed until day 21, following which expression levels declined.

ALP

The ALP protein expression levels were similar between the groups on day 7, while on day 14 protein expression was significantly increased in the MI192 pre-treated cells compared to that in the untreated cells (1.35-fold) ($P \leq 0.05$). A similar significant upregulation was observed in the MI192 pre-treated cells on both day 21 and 28 compared to that in the untreated control group (1.56- and 1.3-fold) ($P \leq 0.01$). A time-dependent increase in ALP protein expression levels was observed, which peaked on day 21 within both groups.

BMP2

MI192 pre-treatment significantly enhanced the BMP2 protein levels when compared to that in the untreated cells after 7 days culture (4.64-fold) ($P \leq 0.01$). On day 14, 21 and 28, BMP2 expression levels remained significantly increased in the MI192 pre-treated group compared to that in the untreated cells (2.37-, 3- and 3.37-fold, respectively) ($P \leq 0.001$). Within both cells, expression levels increased in a time-dependent manner.

Col1a

The Col1a protein expression was significantly increased in the MI192 pre-treated cells on day 7 and 14 compared to that in the untreated group (1.44- and 1.56-fold) ($P \leq 0.05 - 0.01$). On day 21, expression levels were slightly higher in the untreated group ($P > 0.05$), however, the MI192 pre-treated cells exhibited significantly enhanced protein levels compared to that in the untreated cells on day 28 (1.05-fold) ($P \leq 0.05$). Col1a protein expression peaked on day 21 within both groups.

OCN

OCN protein levels were slightly increased in the MI192 pre-treated group after 7 days osteogenic culture, however not significantly ($P > 0.05$). On day 14, 21 and 28, protein expression levels were significantly upregulated in the MI192 pre-treated cells compared to that in the untreated cells (1.92-, 3.08- and 3.04-fold, respectively) ($P \leq 0.001$). Within both cells, a time-dependent increase in OCN protein expression was observed.

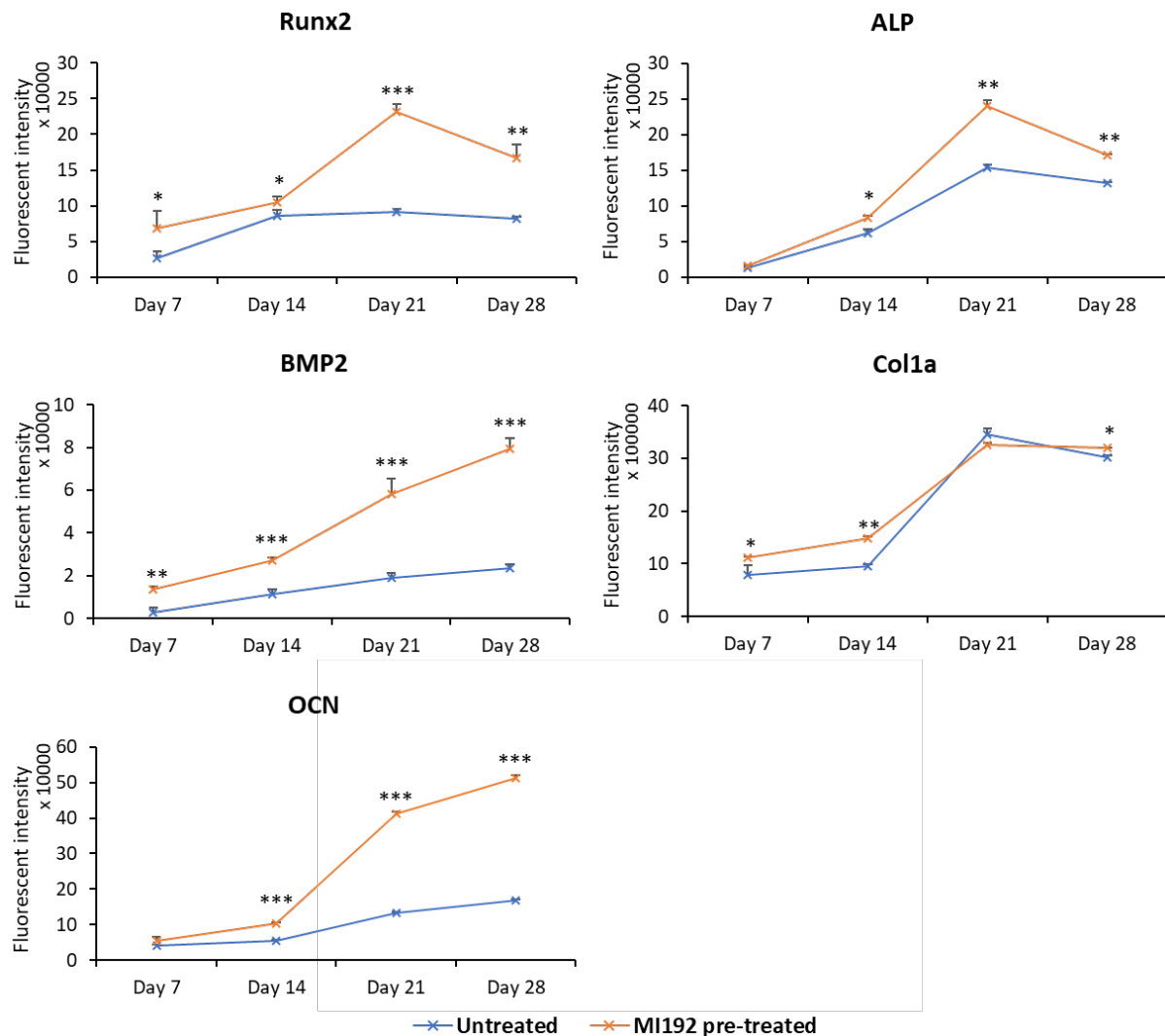


Figure 4.13 - Protein expression of osteoblast-related markers in untreated/MI192 pre-treated hBMSCs after culture in osteogenic conditions. Protein expression levels assessed on day 7, 14, 21 and 28. Data expressed as mean \pm SD (n=3). Significance levels shown are the test group compared to the untreated control at the same time point. * $P \leq 0.05$, ** $P \leq 0.01$ and *** $P \leq 0.001$.

4.3.1.10 - Effect of MI192 on hBMSCs calcium deposition and mineralisation

Figure 4.14A shows the calcium deposition of MI192 pre-treated and untreated hBMSCs after 28 days osteoinductive culture. Extensive Alizarin red staining was observed in both groups, however staining intensity was much greater in the MI192 pre-treated cells. Additionally, the MI192 pre-treated group exhibited increased accumulation of nodules compared to the untreated control group. Semi-quantitative analysis of the Alizarin red staining showed a significantly higher calcium deposition in the MI192 pre-treated cells compared to the untreated control (1.4-fold) ($P \leq 0.001$) (Fig 4.14B).

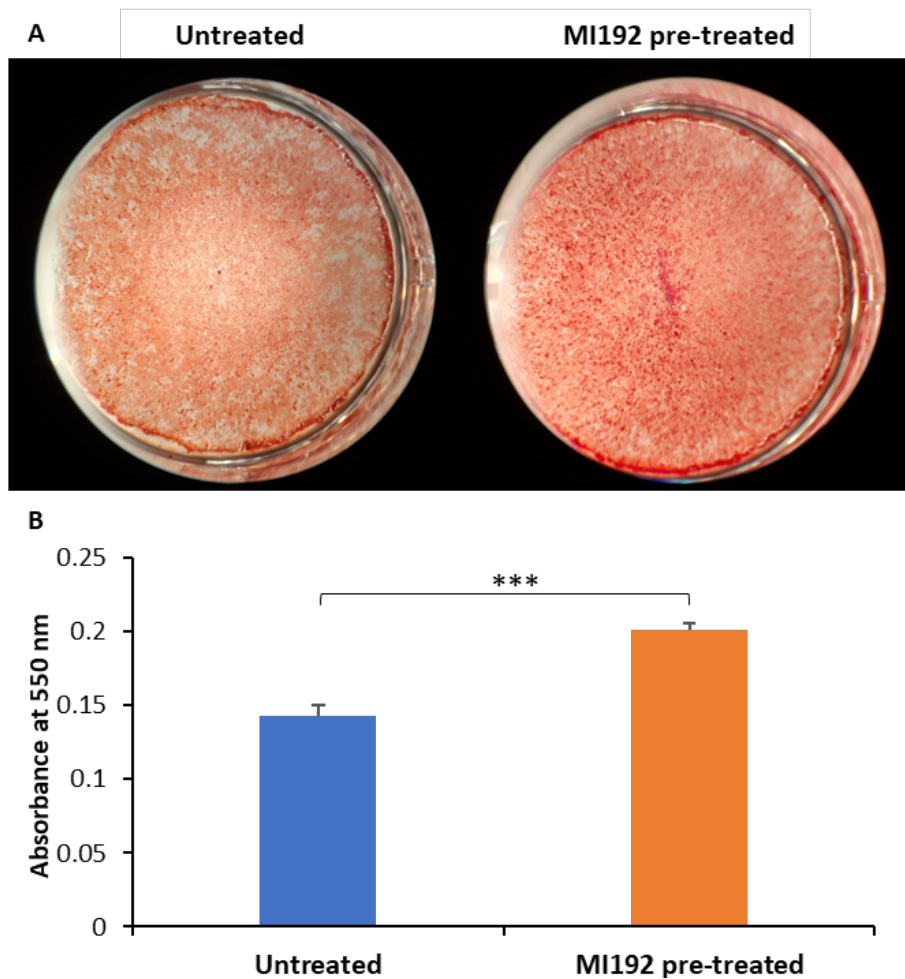


Figure 4.14 - Effects of MI192 pre-treatment on hBMSCs calcium deposition. A) Alizarin Red stained images. Microscopic image x100. B) Semi-quantification analysis of Alizarin red staining in untreated/MI192 pre-treated hBMSCs after 28 days osteogenic culture. Data expressed as mean \pm SD (n=3). *** $P \leq 0.001$.

Figure 4.15 shows mineral nodule formation within MI192 pre-treated and untreated hBMSCs after 28 days osteogenic culture observed by Von Kossa staining. A substantial increase in black staining within the MI192 pre-treated group was observed when compared to the untreated control, with an increased number on nodule-like formations (red arrows) in the HDACi treated group. Additionally, enhanced Van Gieson's staining (pink) for collagen deposition was observed in the MI192 pre-treated group, located in close proximity to the large nodule-like formations.

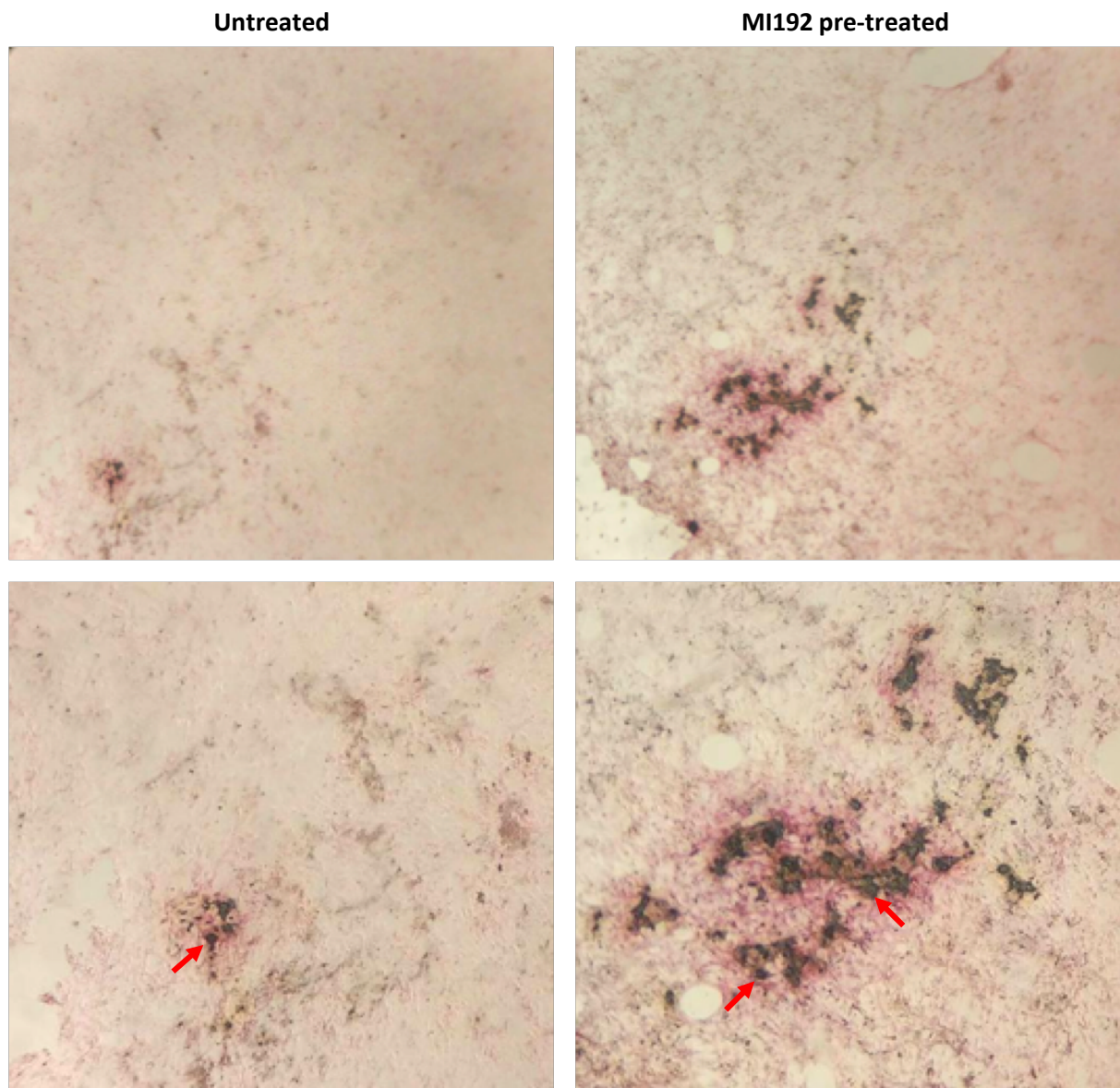


Figure 4.15 - Effect of MI192 pre-treatment on hBMSCs mineral nodule formation. Von Kossa staining (black) for functional mineral nodules (red arrows) of untreated/MI192 pre-treated hBMSCs after 28 days osteogenic culture. Van Gieson's counter staining undertaken to identify collagen deposition (pink). Microscopic images at x200 (top row) and x400 (bottom row).

4.3.2 - The Effects of MI192 on hBMSCs Osteogenic Differentiation within the GelMA hydrogel

4.3.2.1 - Effect of GelMA concentration on microsphere morphology and size

The GelMA microspheres created exhibited a smooth, spherical morphology in all wt% macromer concentrations used as shown in Figure 4.16A. Additionally, no noticeable differences in the morphology of the microspheres in the different culture conditions were observed.

The diameter of the GelMA microspheres immediately after formation was consistently above 1000 μm across the different wt% macromer (Fig 4.16B). The size of the 5 wt% GelMA microspheres after 24 hours incubation in PBS at room temperature slightly decreased compared to before incubation. Microspheres incubated in PBS at 37°C possessed the greatest shrinkage in microsphere diameter compared to other swelling conditions, while incubation in DMEM at 37°C produced microspheres of similar diameter compared to PBS RT. At 10 wt%, 24 hours incubation in PBS at room temperature caused an increase in microsphere diameter. Incubation at 37°C in both PBS and DMEM caused shrinkage in diameter compared to before swelling. A similar trend was observed in the 15 wt% microspheres.

4.3.2.2 - Effect of GelMA concentration on L929 cell-laden GelMA microsphere size and viability

L929 fibroblasts encapsulated in the 10 wt% GelMA microspheres were significantly larger than the cell-laden 5 wt% group immediately post-formation (Fig 4.17) ($P \leq 0.05$). After 24 hours swelling in medium, the diameters of both wt% increased approximately by 1.5% compared to that before swelling, although not significantly ($P > 0.05$). The 10 wt% group continued to exhibit an increased diameter when compared to the 5 wt% cell-laden microspheres, although not significant ($P > 0.05$).

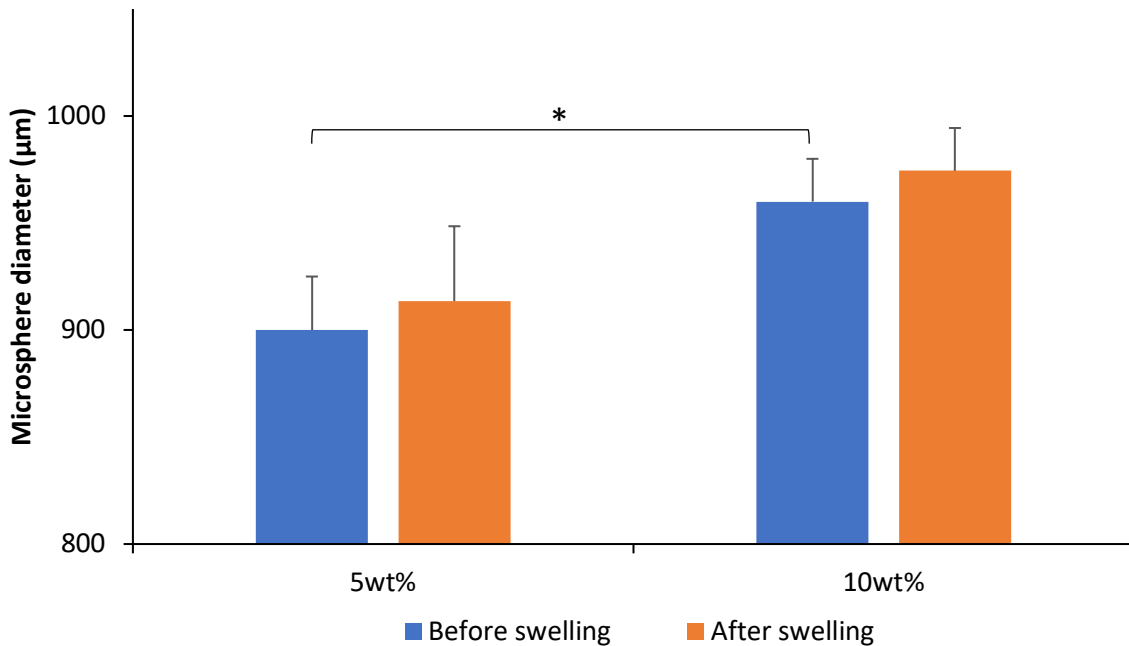


Figure 4.17 - Diameters of 5 and 10 wt% L929 cell-laden GelMA microspheres before and after 24 hours swelling in the medium. Data expressed as mean \pm SD ($n=3$). * $P \leq 0.05$.

After 24 hours post-encapsulation, live/dead staining of cell-laden GelMA microspheres was undertaken, and viability assessed using fluorescent microscopy. L929 cell-laden GelMA microspheres exhibited high cell viability, where cells were distributed thoroughly throughout the 10 wt% hydrogel (Fig 4.18A). Using the automated assembly device, microspheres were placed into the pores of the 3D printed PEGT/PBT scaffold 3 days post-encapsulation (Fig 4.18B). Cell-laden GelMA microspheres remained highly viable, although evidence of dead cells within the hydrogel was observed.

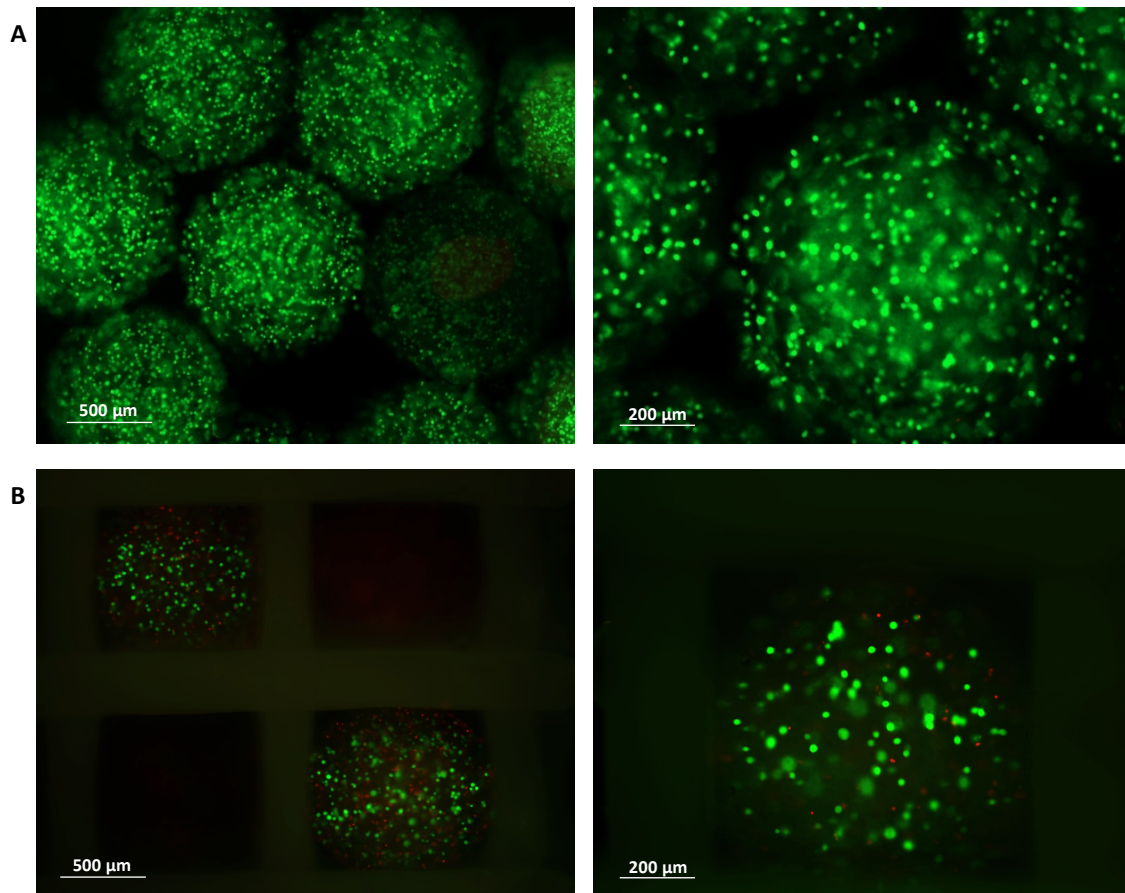


Figure 4.18 - Merged Live/Dead fluorescent image of L929 cells encapsulated in 10 wt% GelMA microspheres (live cells green, dead cells red). A) Cell-laden GelMA microspheres 24 hours after encapsulation. B) Cell-laden microspheres placed within a 3D PEGT/PBT scaffold using an automated assembly device 3 days after encapsulation. Scale bars = 500 (left column) and 200 μm (right column), respectively.

4.3.2.3 - Viability of MI192 pre-treated hBMSCs encapsulated within the GelMA hydrogel

Live/dead staining was undertaken on MI192 pre-treated and untreated hBMSCs encapsulated within the 5 wt% GelMA hydrogels after 24 hours post polymerisation. Figure 4.19A shows cells were distributed throughout the construct possessing a spherical morphology, with a large number of viable cells (green) and a low number of dead cells (red) in both groups. The cell density between the groups were similar at this time point. After 6 weeks culture in osteogenic conditions, cells in both groups remained highly viable throughout the hydrogel, with little evidence of dead cells (Fig 4.19B). Cells in both groups exhibited a fibroblastic-like spread morphology, however within the MI192 pre-treated group, cells displayed a more flattened/elongated morphology compared to the untreated cells at this time point.

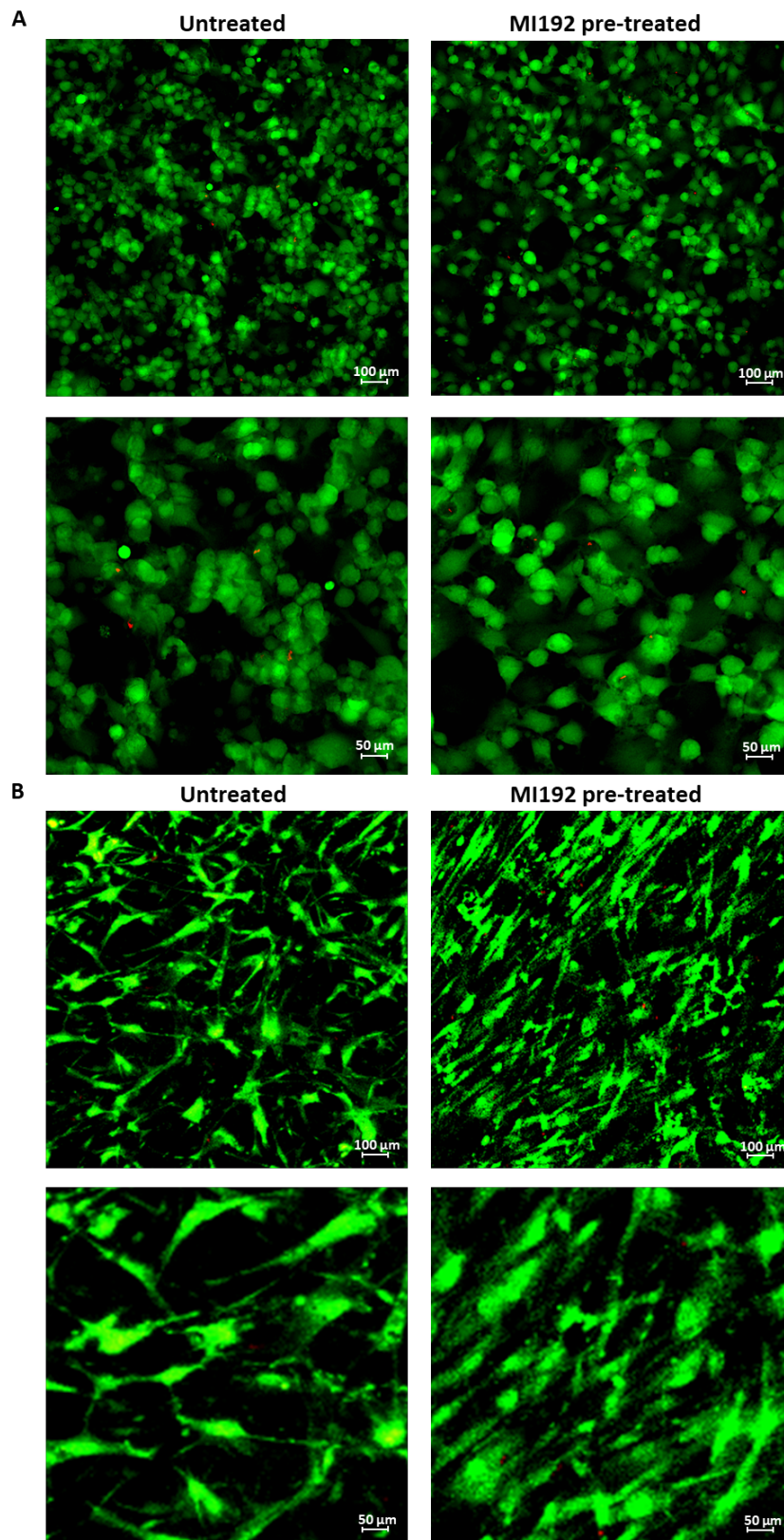


Figure 4.19 - Merged Live/Dead fluorescent image of untreated/MI192 pre-treated hBMSCs encapsulated in 5 wt% GelMA (live cells green, dead cells red). A) 24 hours after encapsulation. B) After 6 weeks osteogenic culture. Scale bars = 100 (top row) and 50 μm (bottom row), respectively.

4.3.2.4 - The effect of MI192 on hBMSCs ALPSA within the GelMA hydrogel

Figure 4.20 shows ALPSA of MI192 pre-treated and untreated hBMSCs encapsulated within 5 wt% GelMA hydrogels after cultured in osteogenic conditions for 2 weeks. The results show that ALPSA was significantly enhanced in the MI192 pre-treated cells (1.32-fold) when compared to that in the untreated hBMSCs within the GelMA hydrogel ($P \leq 0.001$).

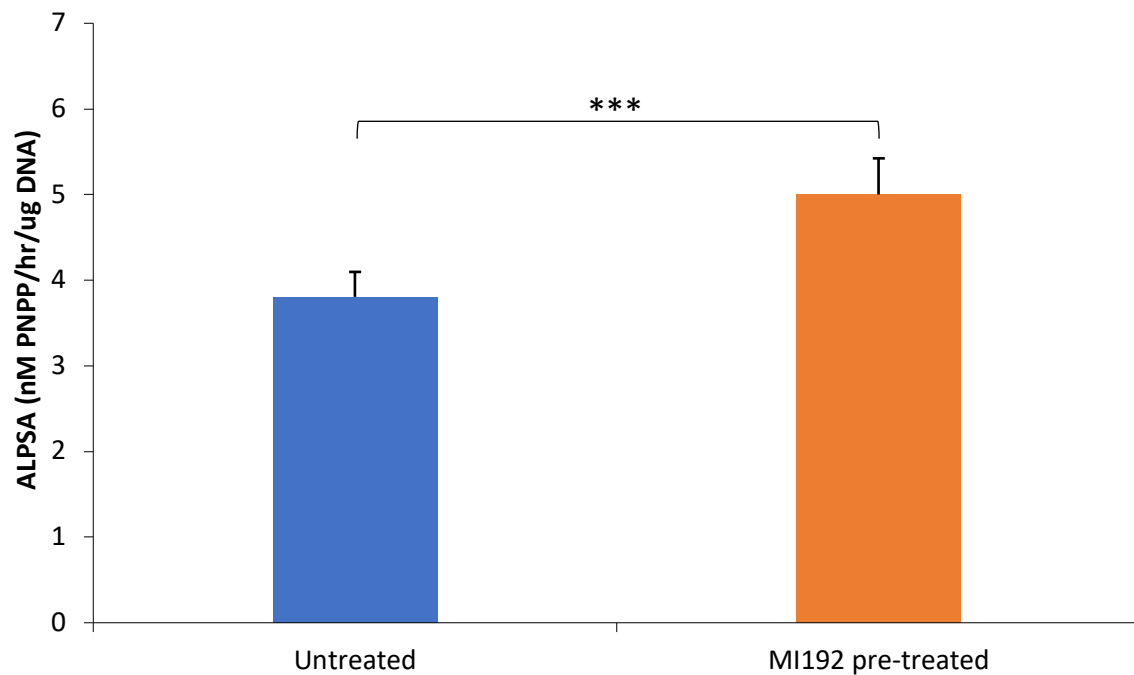


Figure 4.20 - ALPSA in untreated/MI192 pre-treated hBMSCs encapsulated in the GelMA hydrogel. ALPSA assessed after cell-laden GelMA hydrogels cultured in osteogenic conditions for 2 weeks. Data expressed as mean \pm SD (n=3). *** $P \leq 0.001$.

4.3.2.5 - The effect of MI192 on hBMSCs tissue formation within the GelMA hydrogel

Histological analysis was undertaken to assess the effects of MI192 pre-treatment on hBMSCs tissue formation within the 5 wt% GelMA hydrogel after 6 weeks osteogenic culture. Following H&E staining, both MI192 pre-treated and untreated hBMSCs were well distributed throughout the hydrogels, with a slightly increased number of cells at the periphery of the construct (Fig 4.21).

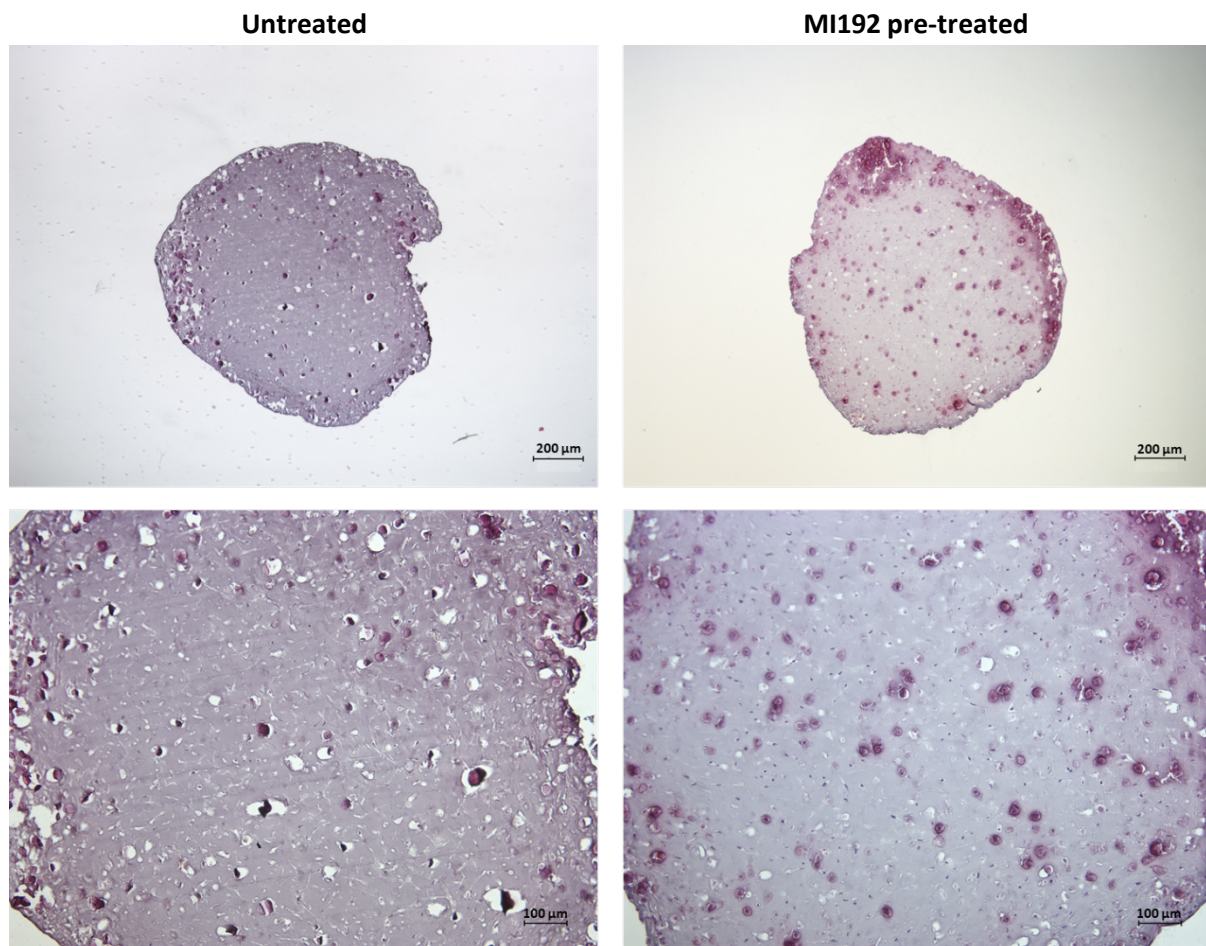


Figure 4.21 - H&E staining of untreated/MI192 pre-treated hBMSCs encapsulated within the GelMA hydrogel after 6 weeks osteogenic culture. Scale bars = 200 (top row) and 100 μm (bottom row), respectively.

Picrosirius red/Alcian blue staining was undertaken to assess the effects of MI192 pre-treatment on hBMSCs collagen and GAG expression within the GelMA hydrogel after 6 weeks osteogenic culture (Fig 4.22). Both groups exhibited positive Picrosirius red staining for collagens throughout the hydrogels, with the MI192 pre-treated group displaying stronger global staining intensity compared to the untreated group. There was little Alcian blue staining for GAG expression in both constructs. A greater quantity of cells was observed at the periphery in both groups, with an increased quantity of black/blue staining in these regions.

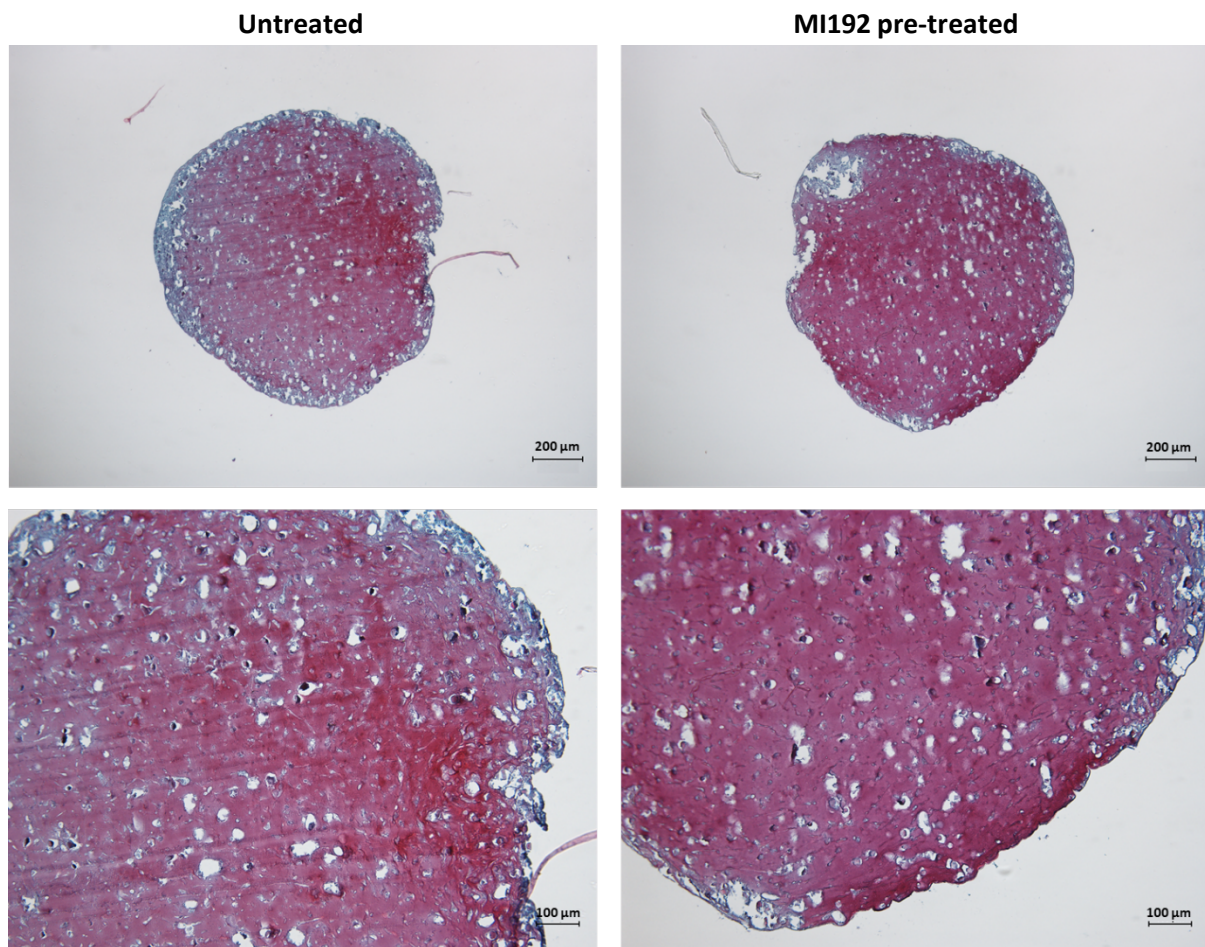


Figure 4.22 - Picrosirius red/Alcian blue staining of untreated/MI192 pre-treated hBMSCs encapsulated within the GelMA hydrogel after 6 weeks osteogenic culture. Collagens and GAGs stained with Picrosirius red and Alcian blue, respectively. Scale bars = 200 (top row) and 100 μm (bottom row), respectively.

4.3.2.6 - The effect of MI192 on hBMSCs osteogenic protein expression within the GelMA hydrogel

ALP

Positive ALP protein expression was observed in both MI192 pre-treated and untreated hBMSCs GelMA constructs, where the greatest staining intensity is located within cellular regions (Fig 4.23). In both groups, the strongest ALP staining was located at the outer regions of the scaffold. No clear difference in ALP expression intensity was observed between the groups.

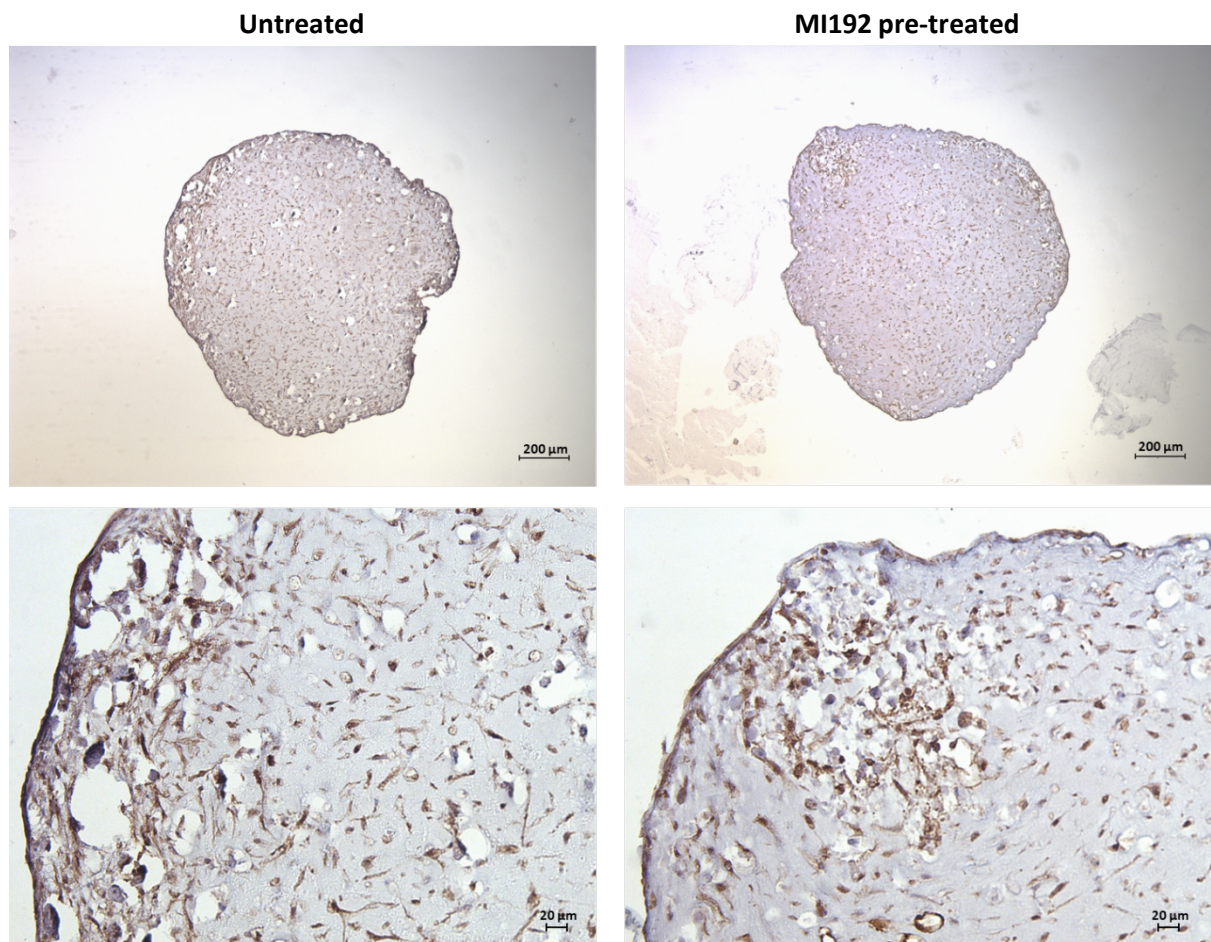


Figure 4.23 - ALP immunohistochemical staining of untreated/MI192 pre-treated hBMSCs encapsulated within the GelMA hydrogel after 6 weeks osteogenic culture. Positive ALP immunohistochemical staining (brown), with a weak Harris haematoxylin counterstain (purple). Scale bars = 200 (top row) and 20 μm (bottom row), respectively.

Col1a

Both MI192 pre-treated and untreated hBMSCs GelMA constructs exhibited positive Col1a expression throughout the hydrogel (Fig 4.24), with the strongest staining intensity located at the periphery. The MI192 pre-treated group exhibited a much stronger global staining intensity for this protein compared to the untreated control group.

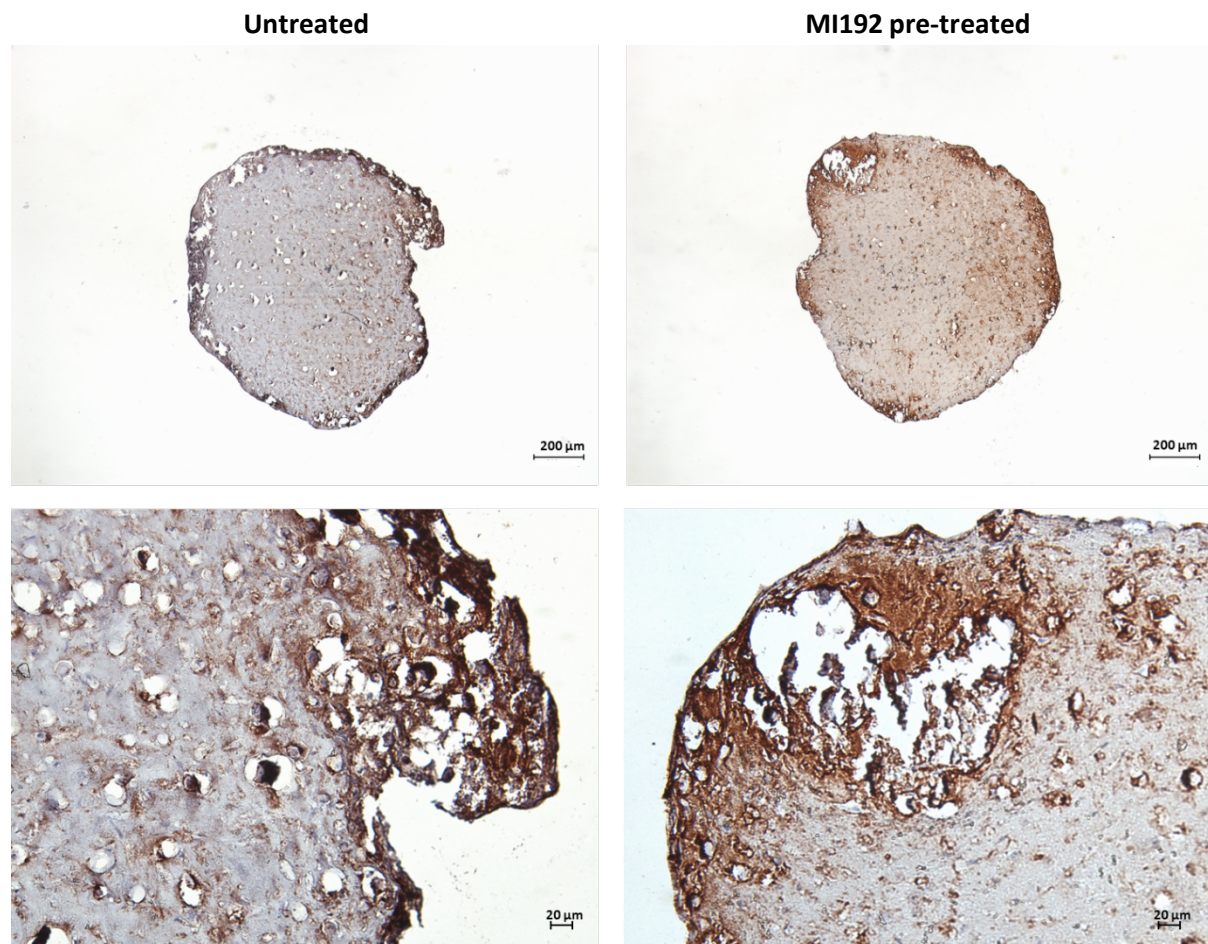


Figure 4.24 - Col1a immunohistochemical staining of untreated/MI192 pre-treated hBMSCs encapsulated within the GelMA hydrogel after 6 weeks osteogenic culture. Positive Col1a immunohistochemical staining (brown), with a weak Harris haematoxylin counterstain (purple). Scale bars = 200 (top row) and 20 μm (bottom row), respectively.

OCN

Positive OCN deposition was observed within both MI192 pre-treated and untreated groups, with the strongest staining located in cells at the periphery of the construct (Fig 4.25). The MI192 pre-treated group exhibited much stronger OCN protein staining throughout the construct, both in cellular regions and the surrounding hydrogel, while OCN staining within the untreated group was expressed at a much-reduced staining intensity primarily located in the cellular regions. The negative immunohistochemical staining of MI192 pre-treated and untreated constructs are shown in figure 4.26.

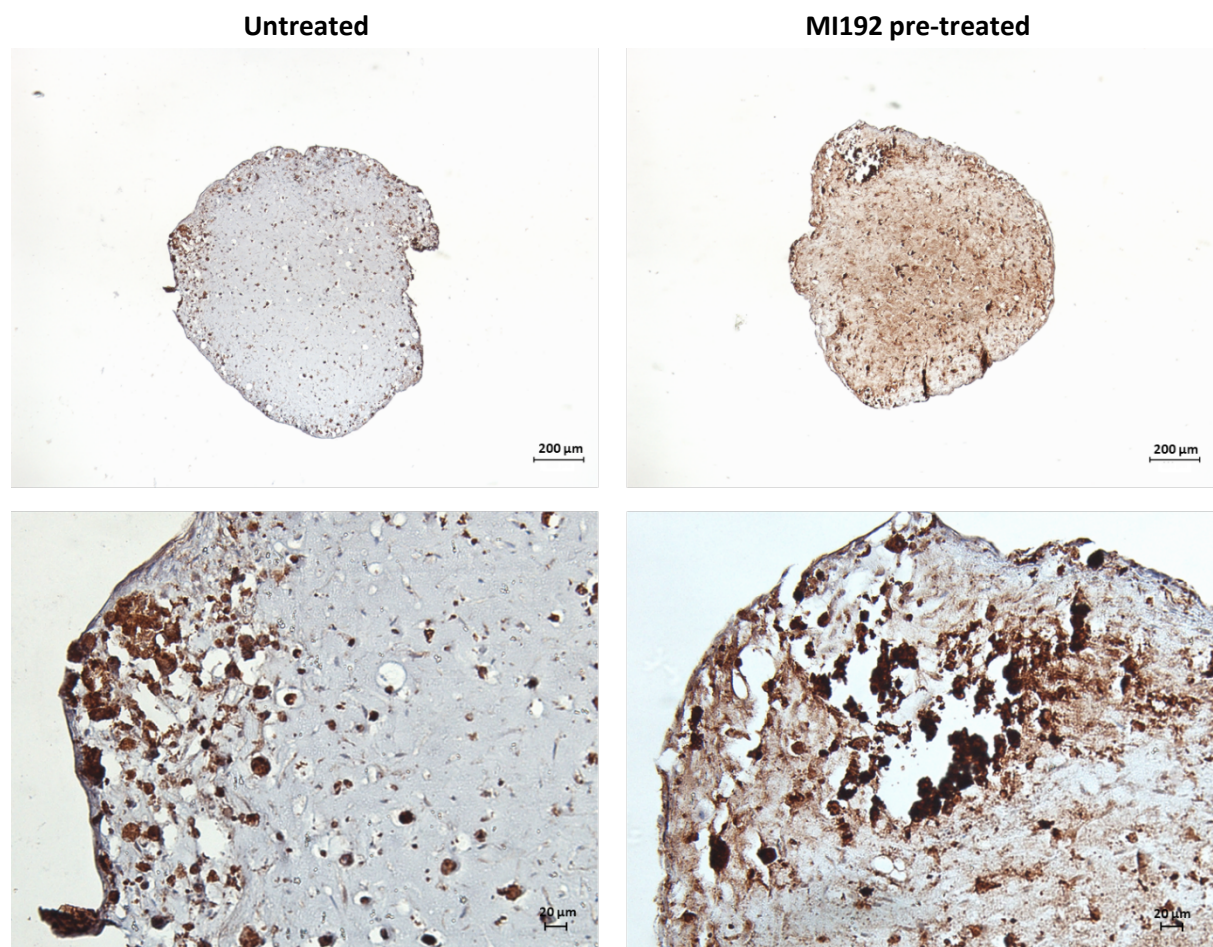


Figure 4.25 - OCN immunohistochemical staining of untreated/MI192 pre-treated hBMSCs encapsulated within the GelMA hydrogel after 6 weeks osteogenic culture. Positive OCN immunohistochemical staining (brown), with a weak Harris haematoxylin counterstain (purple). Scale bars = 200 (top row) and 20 μ m (bottom row), respectively.

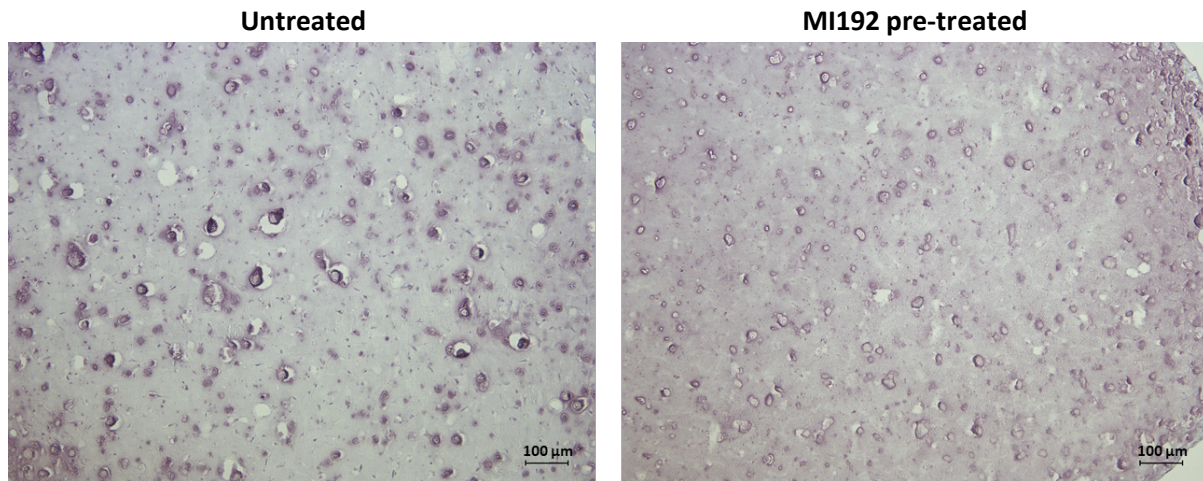


Figure 4.26 - Negative immunohistochemical staining of untreated/MI192 pre-treated hBMSCs encapsulated within the GelMA hydrogel after 6 weeks osteogenic culture. Scale bars = 100 μ m.

4.3.2.7 - The effect of MI192 on hBMSCs calcium deposition and mineralisation within the GelMA hydrogel

Alizarin red staining was undertaken on entire MI192 pre-treated and untreated hBMSCs GelMA constructs after 6 weeks osteogenic culture. Following staining, semi-quantitative analysis of the Alizarin red stained samples showed that the MI192 pre-treated constructs exhibited significantly enhanced calcium accumulation compared to untreated groups (1.3-fold) ($P \leq 0.001$) (Fig 4.27A).

Alizarin red staining of histological sections is shown in Figure 4.27B. Both groups exhibited strong red staining, particularly located within the cells in the construct. The MI192 pre-treated group exhibited much stronger staining throughout the entire hydrogel compared to the untreated control, located in the cellular regions and in the surrounding hydrogel. Moreover, the MI192 pre-treated group displayed an increased quantity of nodule-like formations (black arrows), which exhibited the strongest Alizarin red staining intensity in the construct.

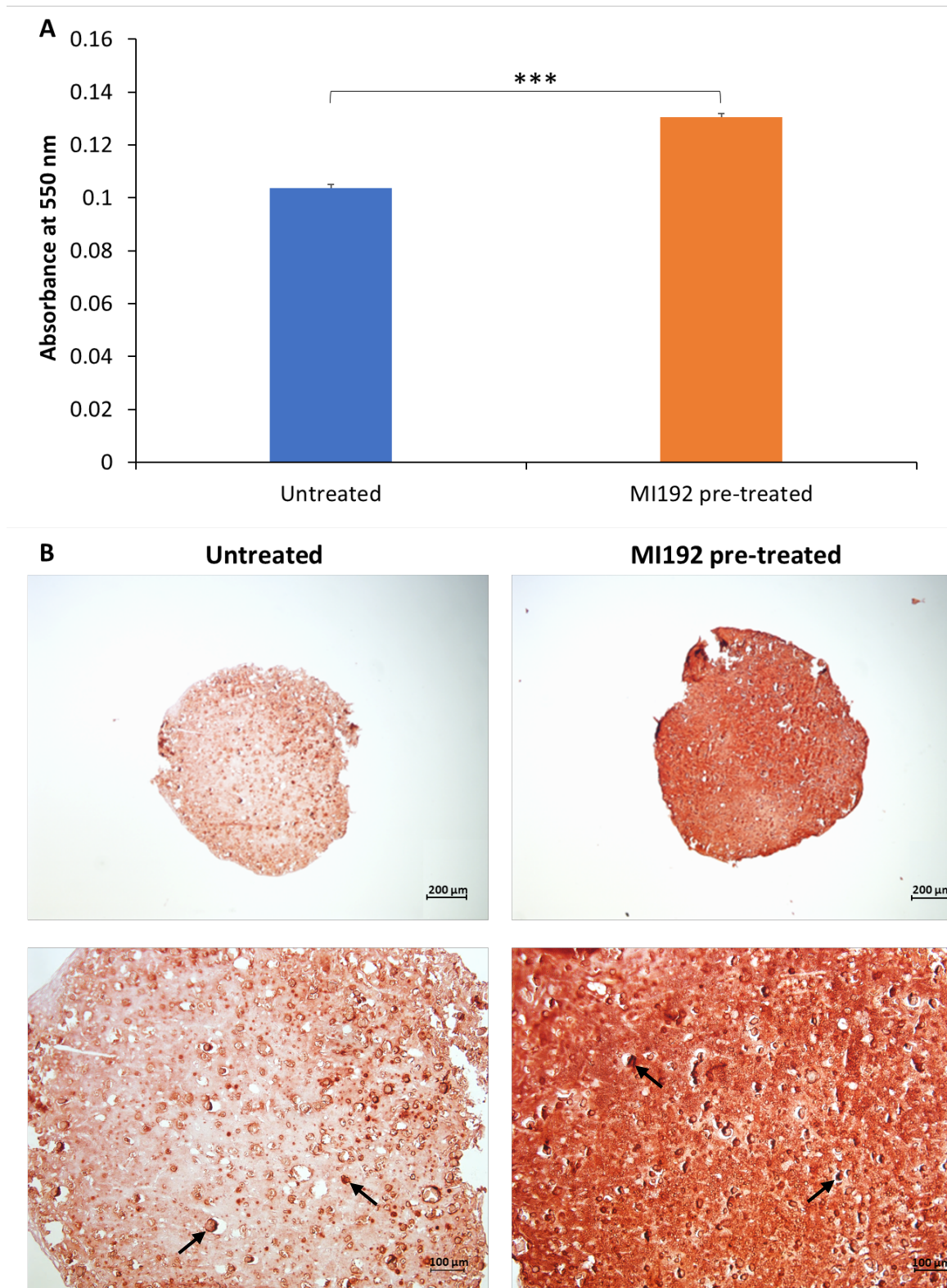


Figure 4.27 - Calcium deposition of untreated/MI192 pre-treated hBMSCs encapsulated within the GelMA hydrogel after 6 weeks osteogenic culture observed by Alizarin red staining. A) Semi-quantitative analysis of Alizarin red staining in the entire constructs. Data expressed as mean \pm SD (n=3). *P \leq 0.001. B) Alizarin red staining of histological sections. Nodule-like formations highlighted by black arrows. Scale bars = 200 (top row) and 100 μ m (bottom row), respectively.**

Von Kossa staining was undertaken to assess mineralisation within the constructs (Fig 4.28). Both the MI192 pre-treated and untreated groups exhibited positive Von Kossa staining, where the strongest black staining was located within the cellular regions and weaker staining situated in the surrounding hydrogel. Moreover, increased Von Kossa staining intensity was located at the periphery of the cell-laden hydrogel constructs. The MI192 pre-treated group contained substantially stronger black staining, with an increased quantity of functional mineral nodules (red arrows) compared to the untreated control throughout the hydrogel.

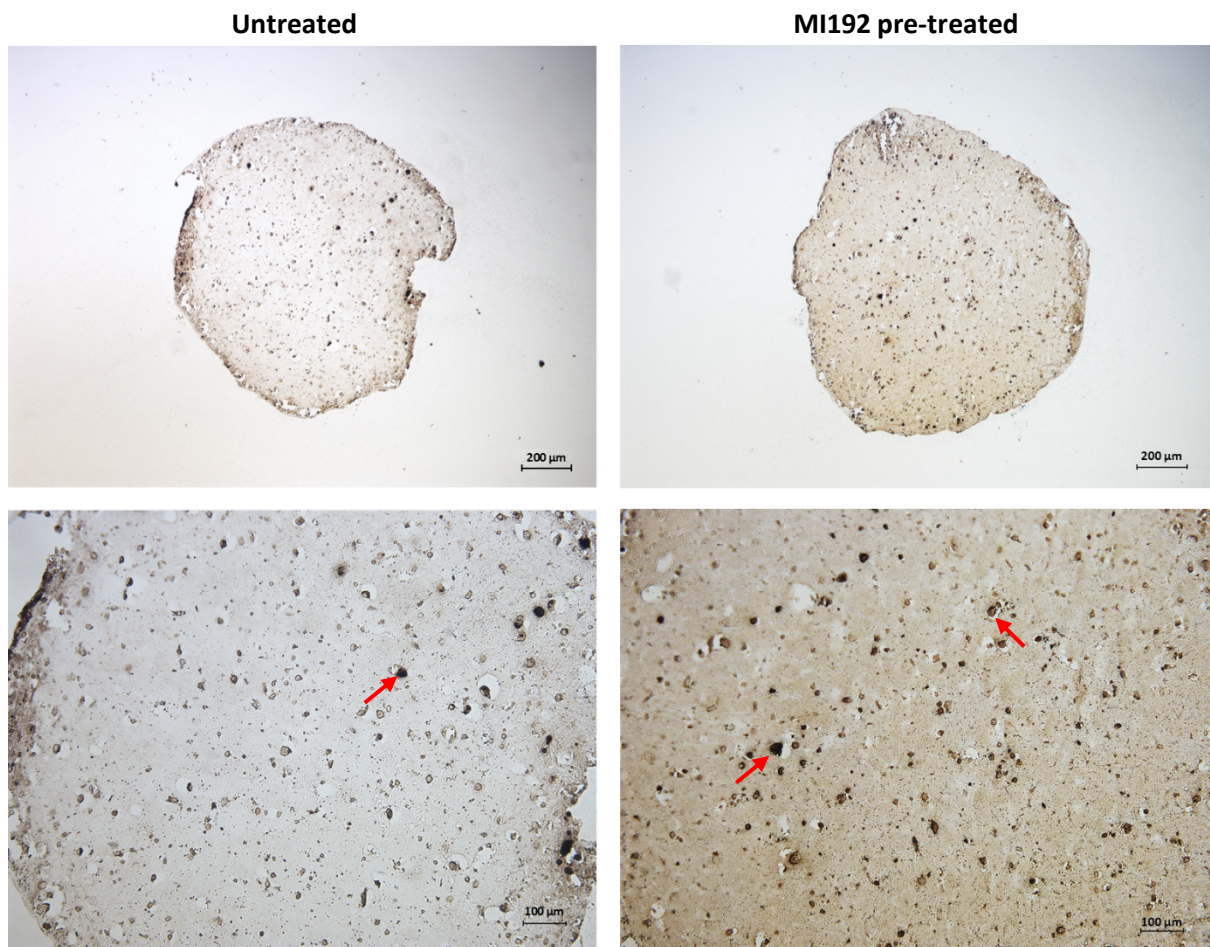


Figure 4.28 - Mineral nodule formation of untreated/MI192 pre-treated hBMSCs encapsulated within the GelMA hydrogel after 6 weeks osteogenic culture observed by Von Kossa staining. Mineral nodule formation highlighted by red arrows. Scale bars = 200 (top row) and 100 µm (bottom row), respectively.

4.3.2.8 - The effect of MI192 on hBMSCs tissue formation within the GelMA-PEBT/PBT construct

Figure 4.29 shows H&E staining of MI192 pre-treated and untreated hBMSCs encapsulated in the GelMA-PEBT/PBT constructs after 6 weeks osteogenic culture. The 3D printed scaffold was successfully incorporated into the hydrogel system during the crosslinking process (scaffold fibres dislodged during histological analysis). Cells were well distributed throughout the construct, with a slight increase in cell numbers at the periphery.

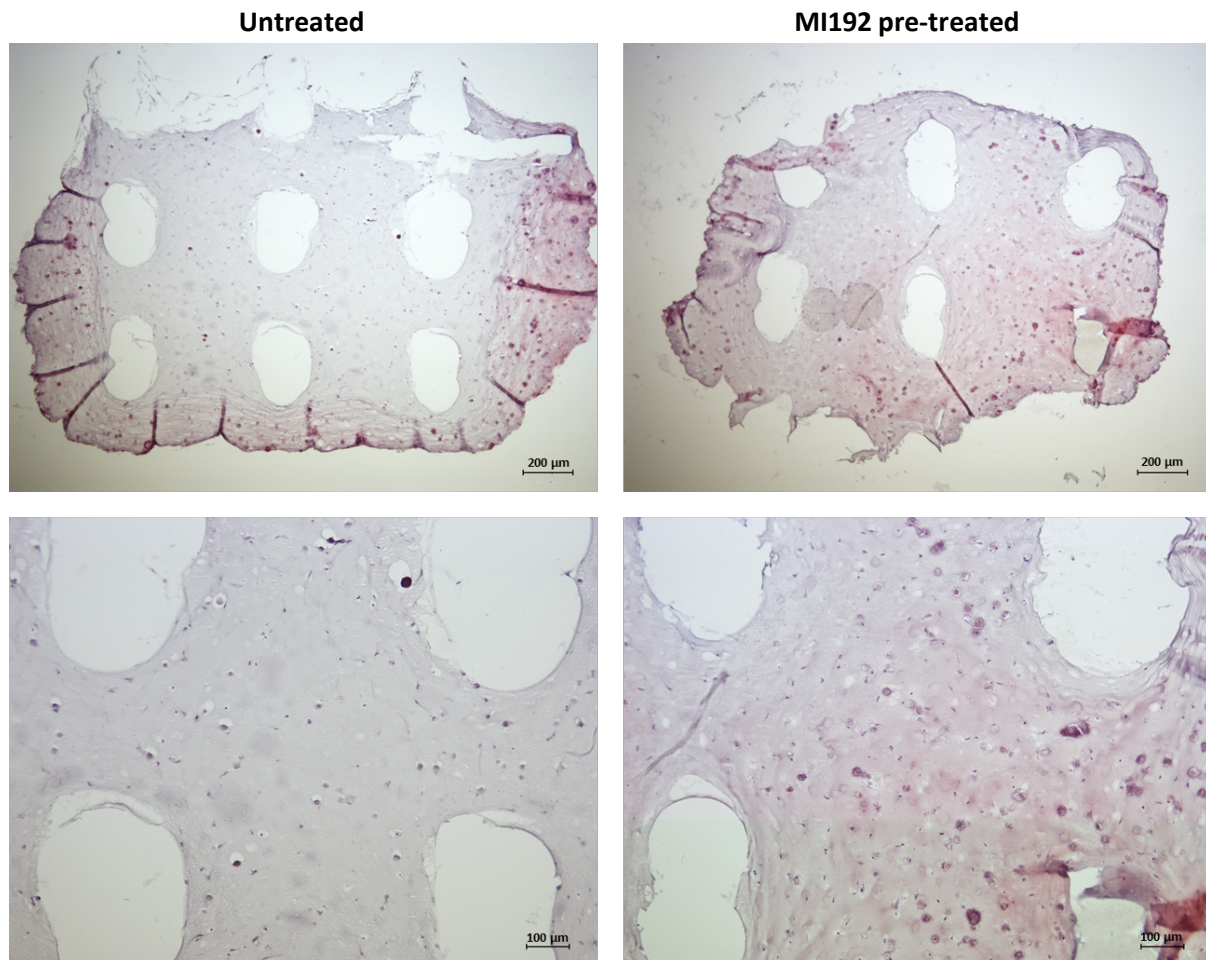


Figure 4.29 - H&E staining of untreated/MI192 pre-treated hBMSCs encapsulated within the GelMA-PEBT/PBT construct after 6 weeks osteogenic culture. Scale bars = 200 (top row) and 100 μm (bottom row), respectively.

Picrosirius red/Alcian blue staining was undertaken to investigate the effects of MI192 pre-treatment on hBMSCs collagen and GAG expression within the GelMA-PEBT/PBT constructs after 6 weeks osteogenic culture (Fig 4.30). Both groups exhibited strong Picrosirius red staining for collagens throughout the construct, particularly at the outer regions and at the hydrogel/scaffold interface. The MI192 pre-treated construct possessed substantially increased staining intensity for Picrosirius red compared to the untreated group. There was little Alcian blue staining for GAG expression in both groups.

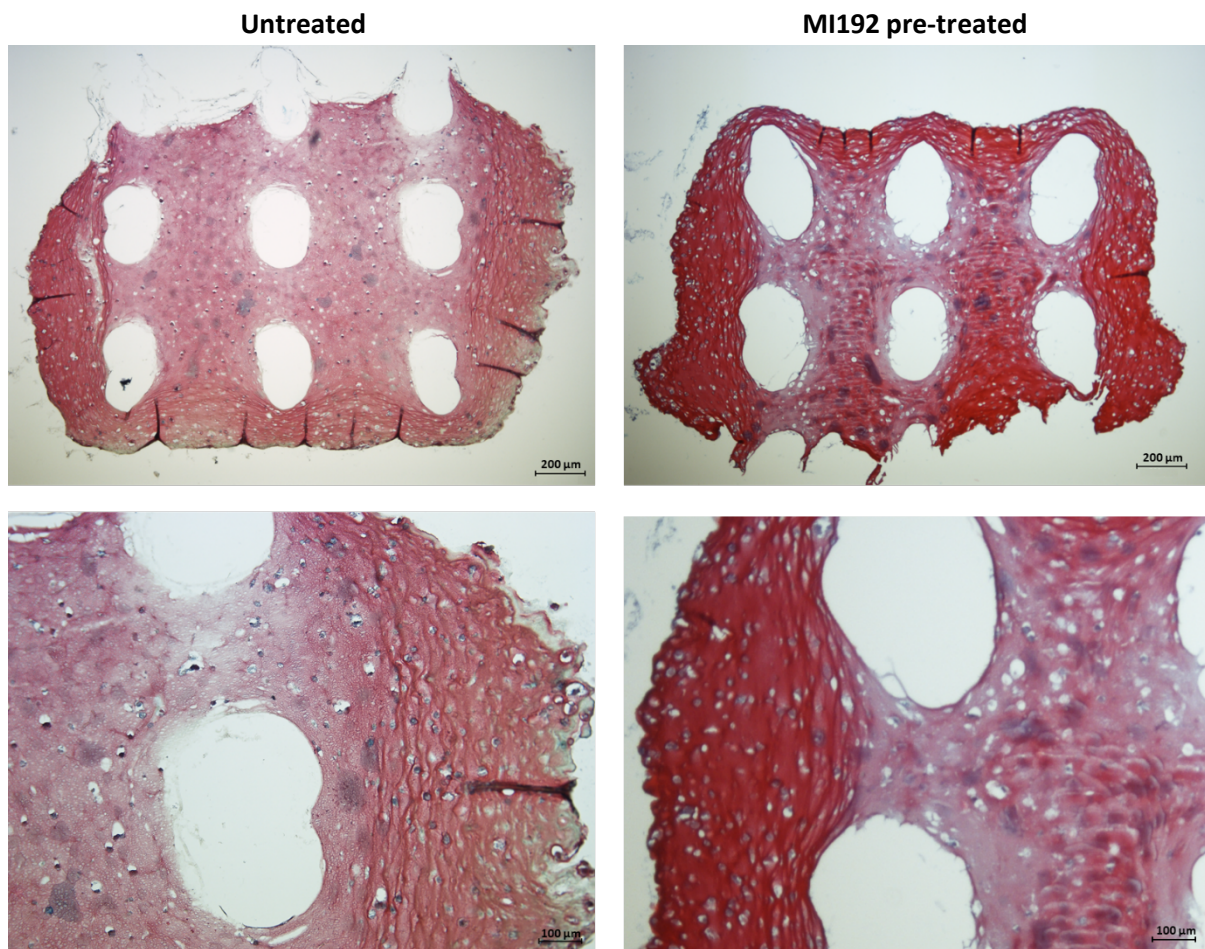


Figure 4.30 - Picrosirius red/Alcian blue of untreated/MI192 pre-treated hBMSCs encapsulated within the GelMA-PEBT/PBT construct after 6 weeks osteogenic culture. Collagens and GAGs stained with Picrosirius red and Alcian blue, respectively. Scale bars = 200 (top row) and 100 μm (bottom row), respectively.

4.3.2.9 - The effect of MI192 on hBMSCs osteogenic protein expression within the GelMA-PEBT/PBT construct

ALP

Both MI192 pre-treated and untreated groups exhibited positive ALP protein expression throughout the construct, particularly located at the cellular regions (Fig 4.31). The MI192 pre-treated group exhibited a greater quantity of ALP-positive cells compared to the untreated control group.

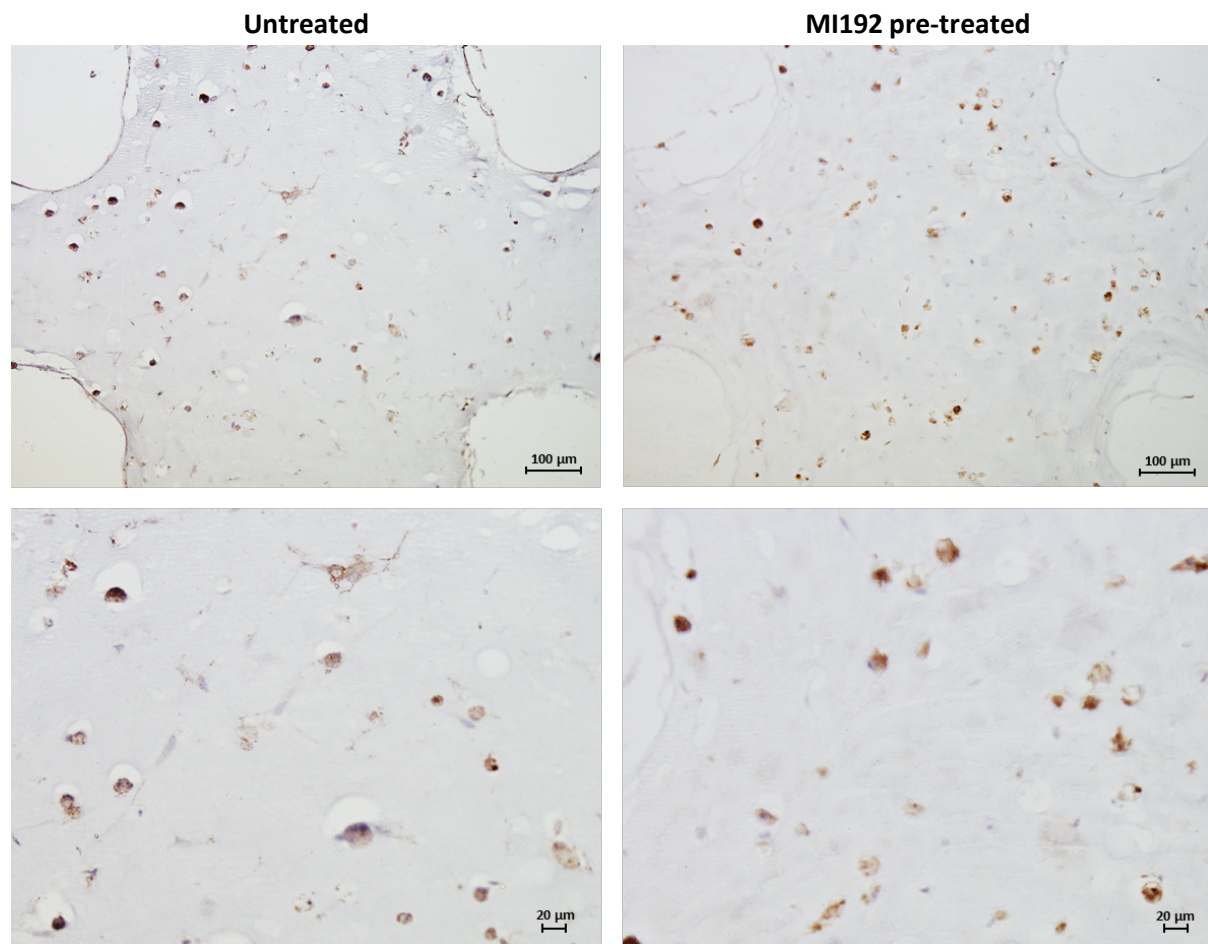


Figure 4.31 - ALP immunohistochemical staining of untreated/MI192 pre-treated hBMSCs encapsulated within the GelMA-PEBT/PBT construct after 6 weeks osteogenic culture. Positive ALP immunohistochemical staining (brown), with a weak Harris haematoxylin counterstain (purple). Scale bars = 100 (top row) and 20 μm (bottom row), respectively.

Col1a

Positive Col1a protein deposition was observed in both MI192 pre-treated and untreated groups located throughout the hydrogel, with particular strong staining situated at the hydrogel/scaffold interface (Fig 4.32). The MI192 pre-treated group displayed substantially greater global Col1a protein expression when compared to the untreated control.

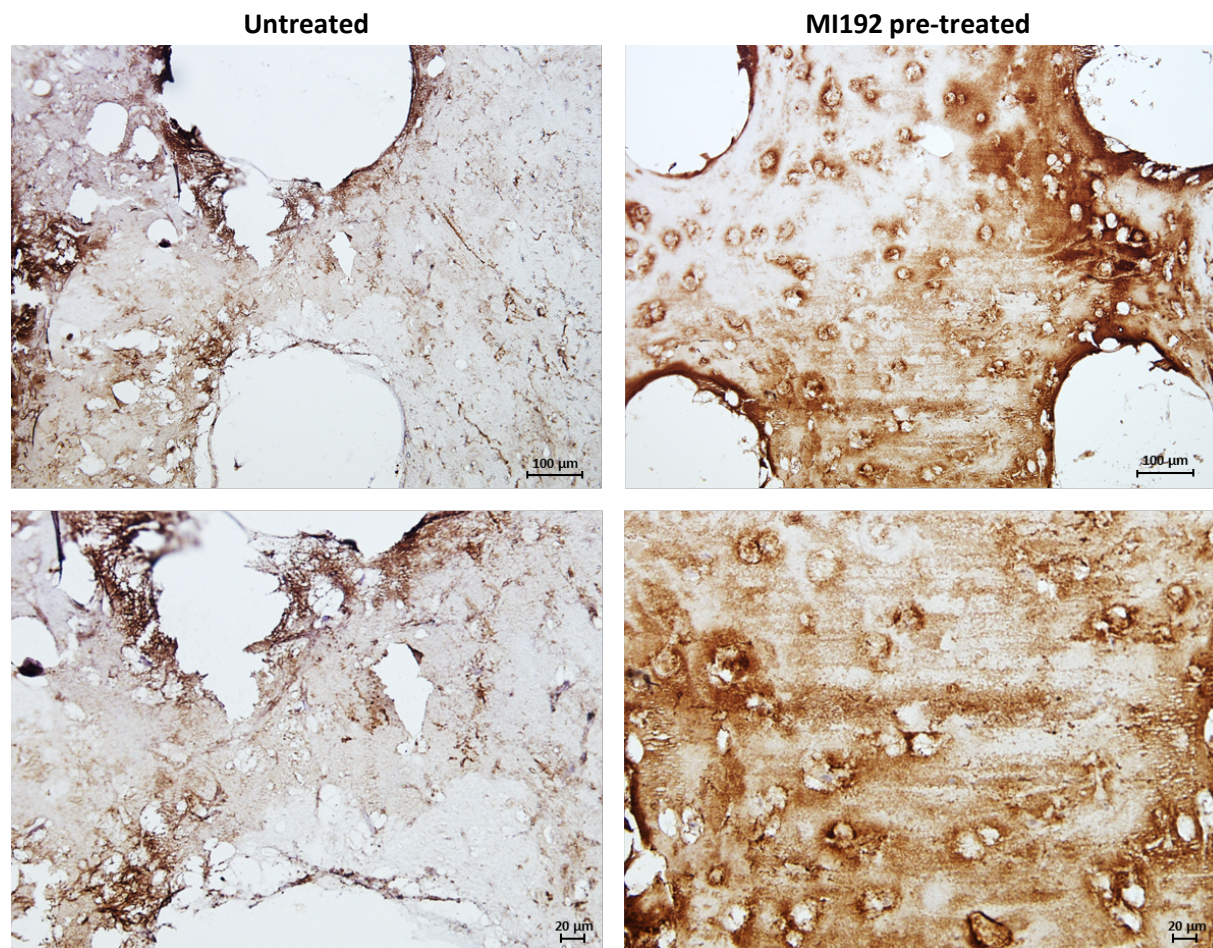


Figure 4.32 - Col1a immunohistochemical staining of untreated/MI192 pre-treated hBMSCs encapsulated within the GelMA-PEBT/PBT construct after 6 weeks osteogenic culture. Positive Col1a immunohistochemical staining (brown), with a weak Harris haematoxylin counterstain (purple). Scale bars = 100 (top row) and 20 μm (bottom row), respectively.

OCN

Both MI192 pre-treated and untreated groups exhibited positive OCN protein expression throughout the GelMA-PEBT/PBT construct (Fig 4.33). The MI192 pre-treated construct exhibited a higher quantity of OCN-positive hBMSCs compared to the untreated group. Negative immunohistochemical staining of both MI192 pre-treated and untreated GelMA-PEBT/PBT constructs is shown in Figure 4.34.

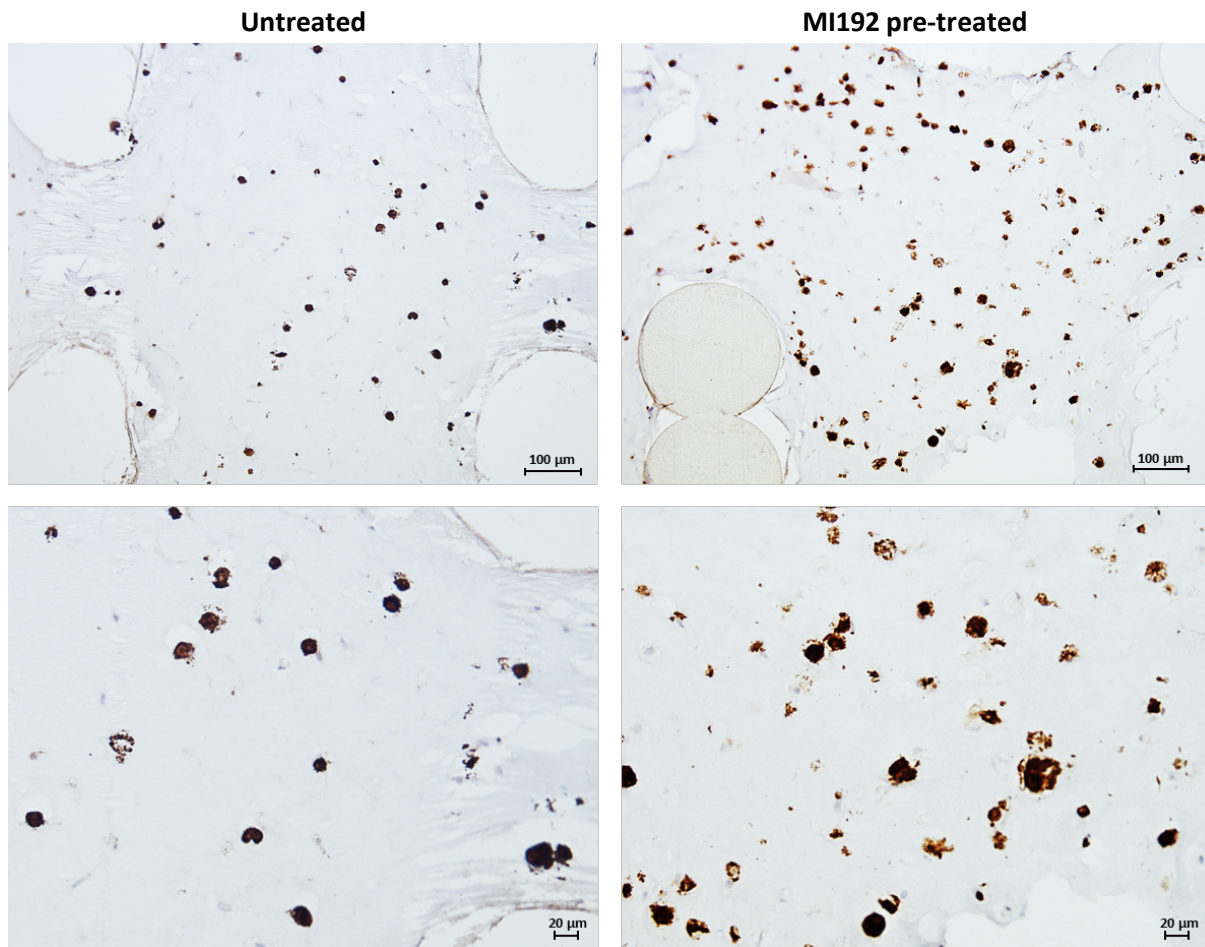


Figure 4.33 - OCN immunohistochemical staining of untreated/MI192 pre-treated hBMSCs encapsulated within the GelMA-PEBT/PBT construct after 6 weeks osteogenic culture. Positive OCN immunohistochemical staining (brown), with a weak Harris haematoxylin counterstain (purple). Scale bars = 100 (top row) and 20 μm (bottom row), respectively.

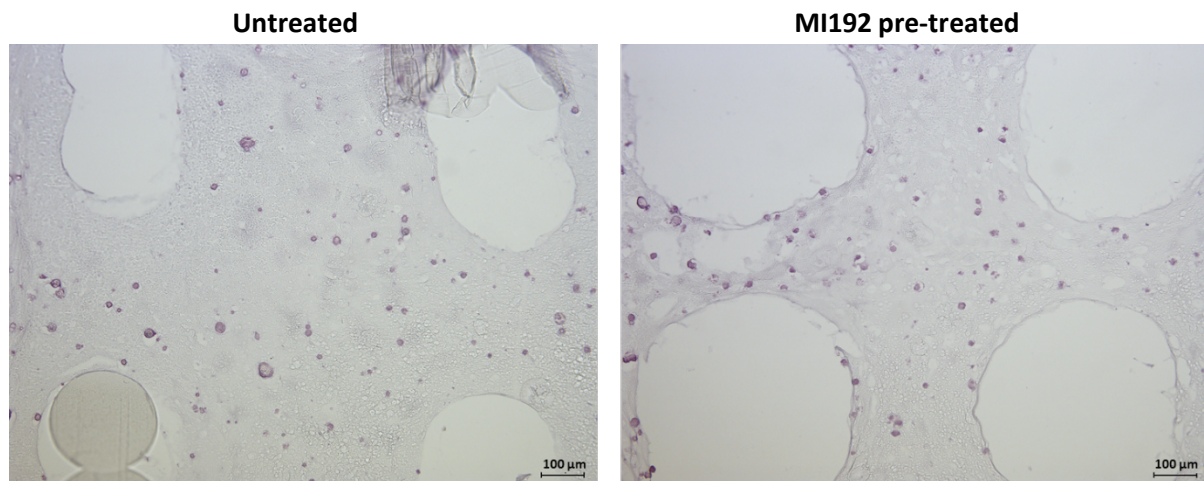


Figure 4.34 - Negative immunohistochemical staining of untreated/MI192 pre-treated hBMSCs encapsulated within the GelMA-PEBT/PBT construct after 6 weeks osteogenic culture. Scale bars = 100 µm.

4.3.2.10 - The effects of MI192 on hBMSCs calcium deposition and mineralisation within the GelMA-PEBT/PBT construct

Calcium deposition within the MI192 pre-treated and untreated GelMA-PEBT/PBT constructs was assessed via Alizarin red staining (Fig 4.35). Positive Alizarin red staining was observed in both groups within the cellular regions, with the strongest staining situated at the periphery of the constructs. The MI192 pre-treated group exhibited slightly stronger staining for calcium deposition when compared to that of the untreated group, particularly at the outer regions of the construct.

The effect of MI192 pre-treatment on hBMSCs mineral nodule formation within the construct was assessed using Von Kossa staining (Fig 4.36). Positive black staining was observed in both groups, predominantly in the cellular regions of the construct. The MI192 pre-treated group displayed substantially increased quantity of mineral nodules throughout when compared to the untreated construct.

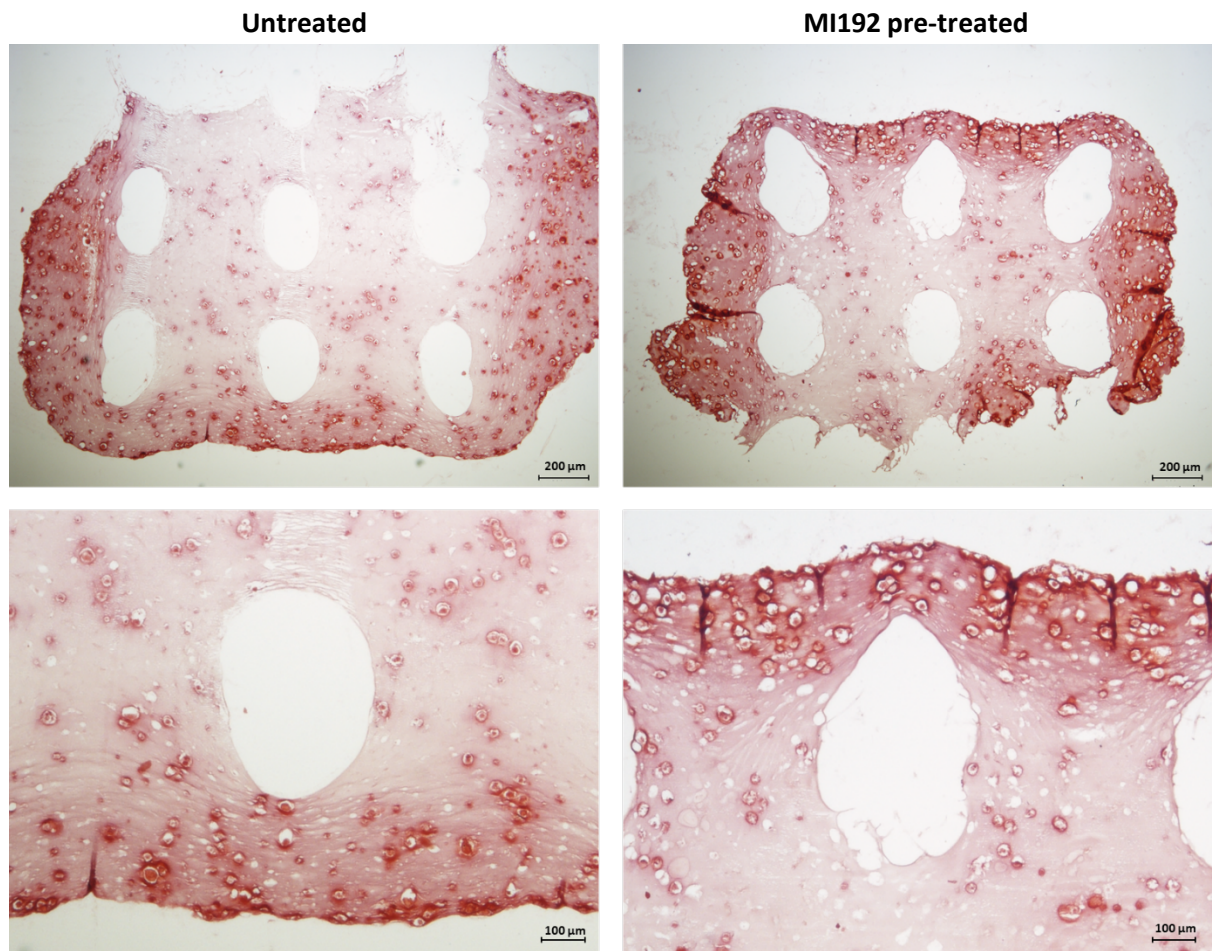


Figure 4.35 - Calcium deposition of untreated/MI192 pre-treated hBMSCs encapsulated within the GelMA-PEBT/PBT construct after 6 weeks osteogenic culture observed by Alizarin red staining. Scale bars = 200 (top row) and 100 μm (bottom row), respectively.

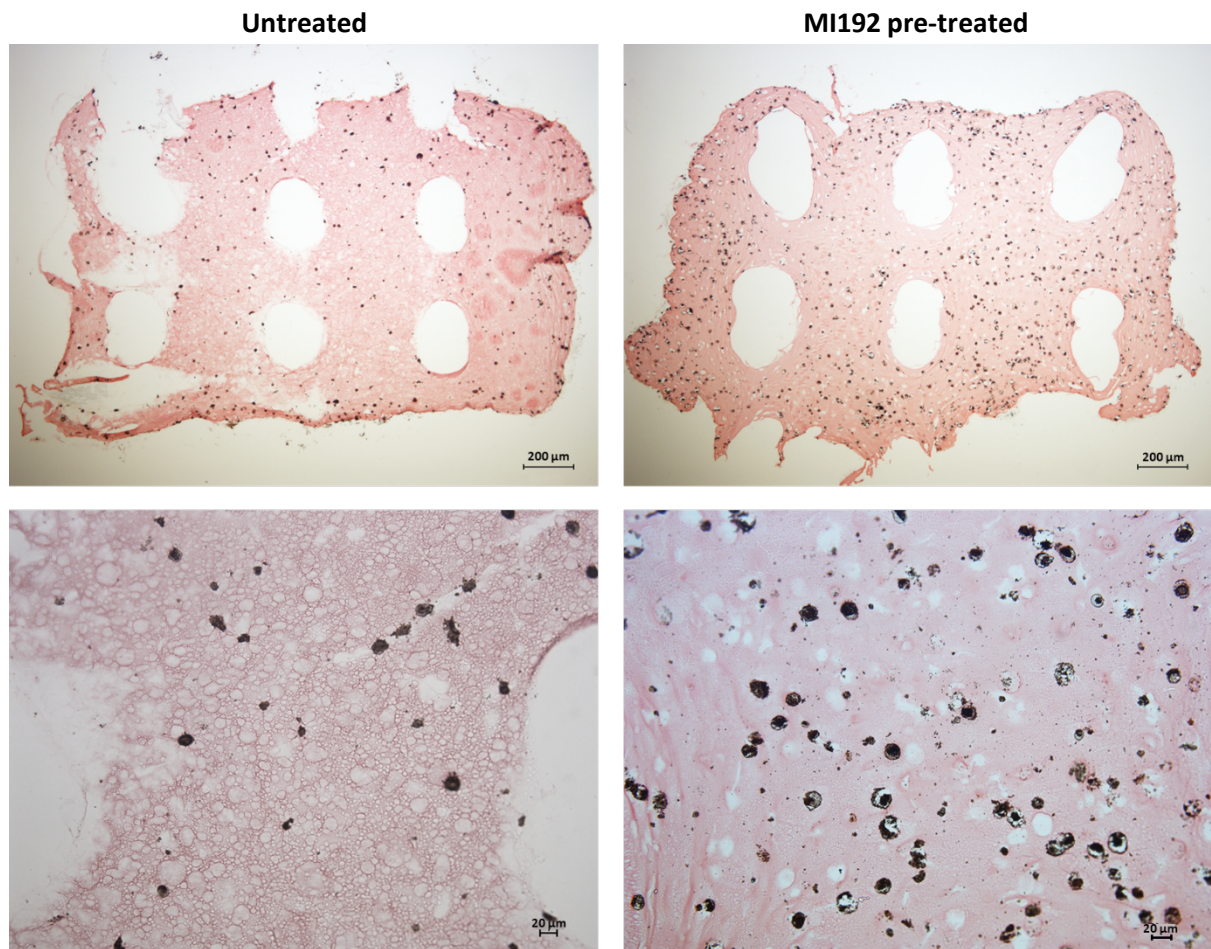


Figure 4.36 - Mineral nodule formation of untreated/MI192 pre-treated hBMSCs encapsulated within the GelMA-PEBT/PBT construct after 6 weeks osteogenic culture observed by Von Kossa staining. Sample counterstained with Van Gieson's solution (pink). Scale bars = 200 (top row) and 20 μm (bottom row), respectively.

4.3.3 - The Effects of MI192 on hBMSCs Osteogenic Differentiation within the BMT construct

4.3.3.1 - The effect of MI192 on hBMSCs osteogenic gene expression in microtissue culture

After pre-treatment with/without 50 μ M MI192 for 48 hours, hBMSCs were cultured as microtissues in osteogenic conditions for up to 21 days and the mRNA levels of key osteoblast-related genes (*RUNX2*, *ALP*, *BMP2*, *COL1A* and *OCN*) were assessed (Fig 4.37).

RUNX2

After 7 days culture, the *RUNX2* mRNA levels were increased in the MI192 pre-treated group compared to that in the untreated cells, however not significantly ($P > 0.05$). On day 14 and 21, the expression levels in the MI192 pre-treated cells was slightly reduced compared to that in the control group ($P > 0.05$). The Peak mRNA expression was observed on day 14 in both groups.

ALP

The *ALP* mRNA expression levels were similar between the groups on day 7 ($P > 0.05$), however, the expression was substantially upregulated within the MI192 pre-treated cells when compared to that in the untreated cells on day 14 and 21 (1.42- and 1.12-fold) ($P \leq 0.01$, $P \leq 0.05$). In both groups, the peak *ALP* expression was observed on day 7.

BMP2

The *BMP2* mRNA levels were significantly upregulated in the MI192 pre-treated cells after 7 days osteogenic culture compared to that in the untreated group (1.28-fold) ($P \leq 0.01$). On day 14, mRNA levels remained increased in the MI192 pre-treated group, although not significantly ($P > 0.05$). The MI192 pre-treated cells exhibited significantly elevated expression on day 21 (1.2-fold) ($P \leq 0.05$). A time-dependent reduction in *BMP2* mRNA expression was observed in both groups.

COL1A

In the MI192 pre-treated cells, the *COL1A* mRNA levels were significantly increased on day 7 compared to that in the untreated cells (2.11-fold) ($P \leq 0.05$). On day 14 and 21, the mRNA expression levels were similar between the groups ($P > 0.05$). Peak *COL1A* expression was observed on day 7, following which a reduction in expression was observed at day 14. On day 21, expression levels increased compared to that on day 14.

OCN

The *OCN* mRNA levels were significantly increased in the MI192 pre-treated cells compared to that in the untreated group after 7 days osteoinductive culture (1.15-fold) ($P \leq 0.01$). On day 14, expression levels between the groups were similar ($P > 0.05$), while on day 21, the *mRNA* levels were significantly reduced in the MI192 pre-treated group compared to that in the untreated cells (1.09-fold) ($P \leq 0.05$). Peak *OCN* expression was observed on day 7, following which a time-dependent downregulation in expression was observed.

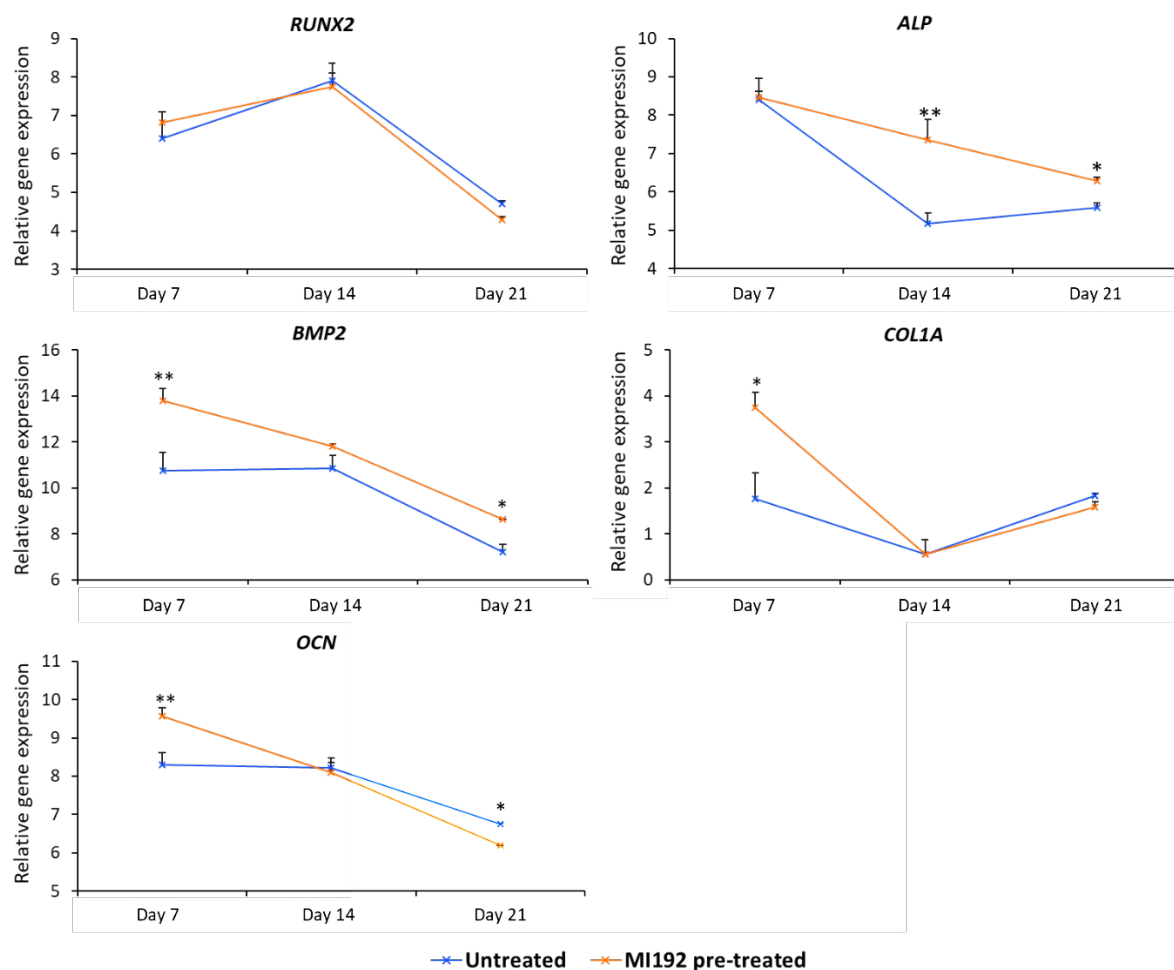


Figure 4.37 - Relative expression of osteoblast-related genes in untreated/MI192 pre-treated hBMSC microtissues in osteogenic conditions. Gene expression assessed on day 7, 14 and 21. Data expressed as mean \pm SD ($n=3$). Significance levels shown are the test group compared to the untreated control at the same time point. * $P \leq 0.05$ and ** $P \leq 0.01$.

4.3.3.2 - The effect of MI192 on hBMSCs ALPSA in BMT culture

The effect of MI192 pre-treatment on hBMSCs ALPSA during BMT culture was assessed after 2 weeks in osteogenic conditions (Fig 4.38). The MI192 pre-treated BMT exhibited a significantly higher (2.3-fold) ALPSA when compared to that of the untreated group ($P \leq 0.001$).

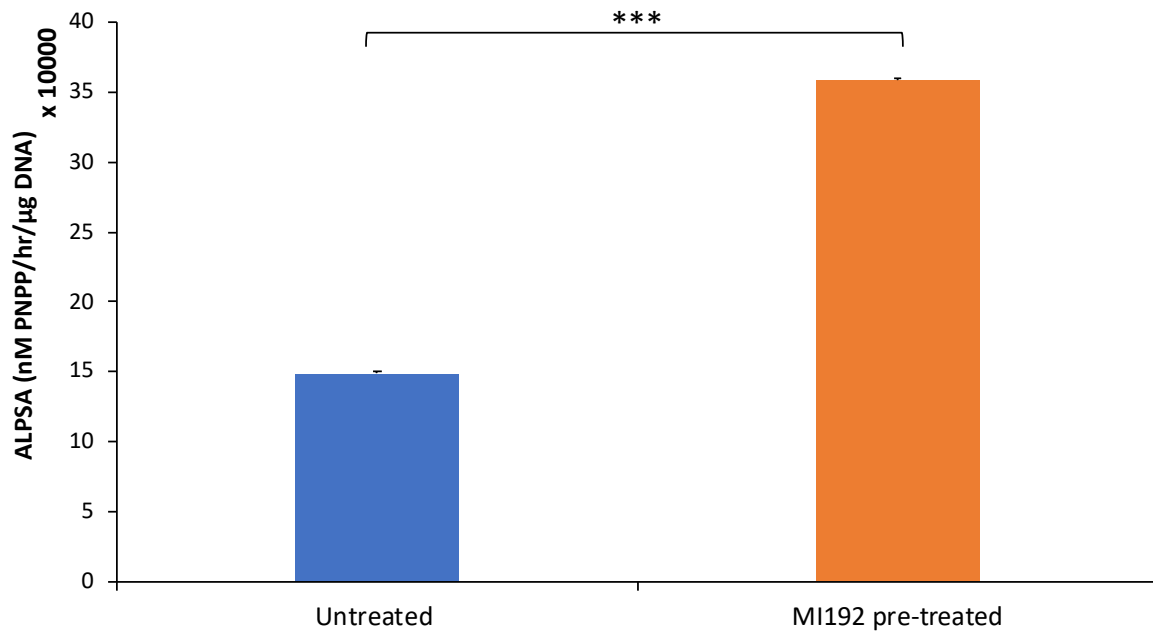


Figure 4.38 - ALPSA of untreated/MI192 pre-treated hBMSCs BMTs. ALPSA of BMT constructs were assessed after 2 weeks in osteogenic conditions. Data expressed as mean \pm SD (n=3). *** $P \leq 0.001$.

4.3.3.3 - The effect of MI192 on hBMSCs tissue formation within the BMT construct

Histological analysis was utilised to assess the effects of MI192 pre-treatment on hBMSCs tissue formation within the BMT construct after 6 weeks osteogenic culture. Following H&E staining, the incorporated microtissues occupied the entire internal void volume of the 3D printed scaffold (scaffold fibres dislodged during histological analysis), where microtissue fusion was observed (Fig 4.39). Within the MI192 pre-treated group, extensive dense tissue formation was observed throughout the construct, with increased intensity situated at the periphery. The untreated group exhibited similar dense tissue formation, however, this was distributed more aberrantly in the construct, primarily at the outer regions. Moreover, within the MI192 pre-treated BMT, tissue formation was aligned in a unidirectional fashion within the construct.

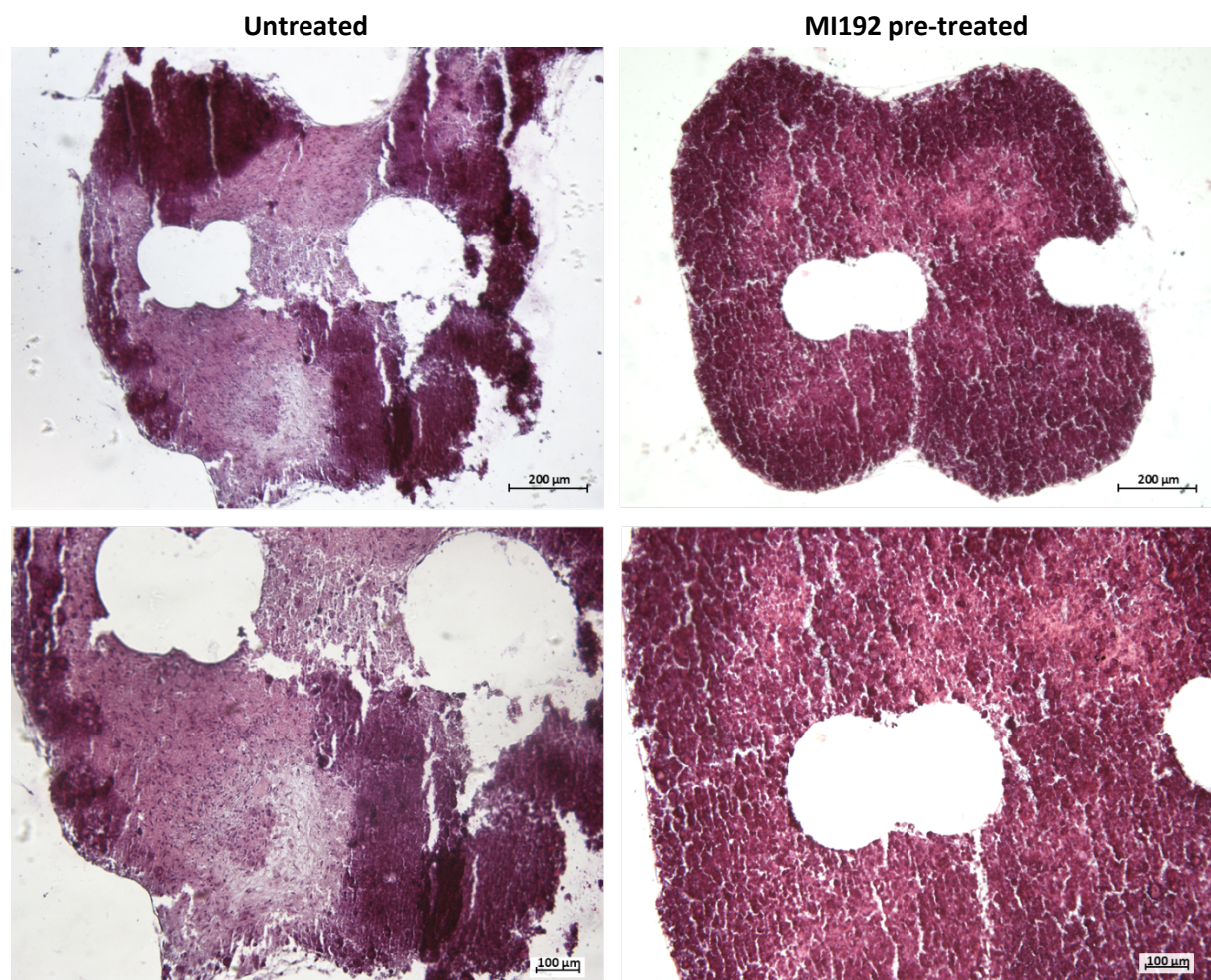


Figure 4.39 - H&E staining of untreated/MI192 pre-treated hBMSC BMT constructs after 6 weeks osteogenic culture. Incorporated microtissues (stained pink/purple) fused with neighbouring tissue modules around internal scaffold fibres. Scale bars = 200 (top row) and 100 µm (bottom row), respectively.

Following Picosirius red/Alcian blue staining, both the MI192 pre-treated and untreated groups exhibited positive Picosirius red staining for collagen deposition (Fig 4.40). Collagen expression was more uniformly distributed within the MI192 pre-treated BMT when compared to the aberrant distribution observed in the untreated group. Moreover, the MI192 pre-treated group possessed an enhanced quantity of nodule-like formations (black arrows) exhibiting strong Picosirius red staining intensity, while more fibrous tissue formation was observed within the untreated group. Additionally, the untreated constructs possessed a more extensive global Alcian blue staining when compared to the MI192 pre-treated group, with areas of intense GAG expression observed (blue arrows).

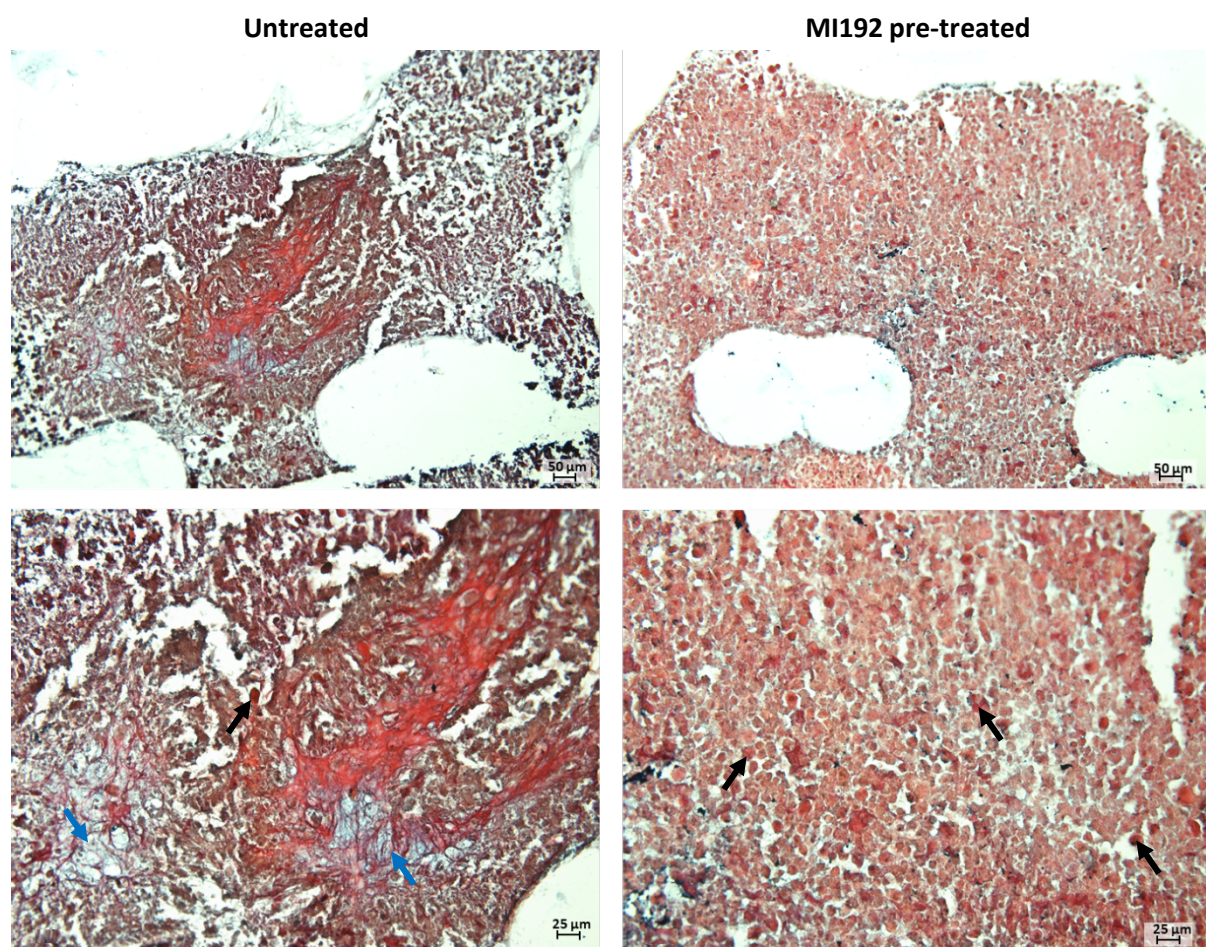


Figure 4.40 - Picosirius red/Alcian blue staining of untreated/MI192 pre-treated hBMSC BMT constructs after 6 weeks osteogenic culture. Collagens and GAGs stained with Picosirius red and Alcian blue, respectively. Strong Picosirius red staining located in circular nodules highlighted with black arrows. Strong Alcian blue staining highlighted with blue arrows. Scale bars = 50 (top row) and 25 μm (bottom row), respectively.

4.3.3.4 - The effect of MI192 on hBMSCs osteogenic protein expression within the BMT construct

ALP

The MI192 pre-treated group displayed strong ALP protein expression throughout the BMT, with the strongest staining situated at the periphery of the construct and at the microtissue/scaffold interface (Fig 4.41). The untreated group also exhibited positive ALP expression; however, the majority of the staining appeared in the outer regions of the individual microtissues and at the microtissue/scaffold interface. Areas of negative ALP expression were observed within the centre of certain microtissues within the untreated construct. Additionally, the MI192 pre-treated construct exhibited an increased quantity of nodule-like formations (red arrows) throughout the BMT which expressed the strongest ALP staining intensity. The untreated group possessed these nodule-like formations at the outer regions of the microtissues.

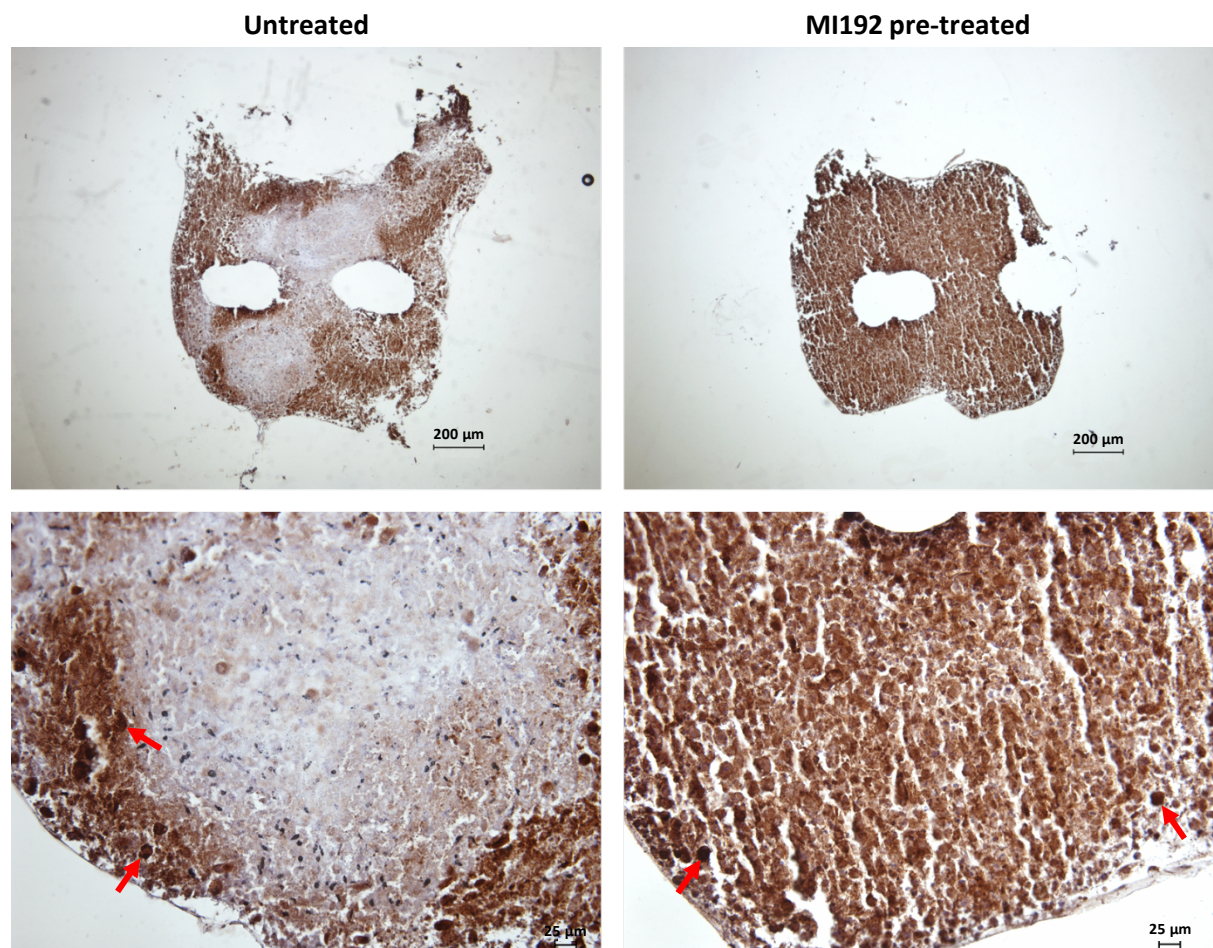


Figure 4.41 - ALP immunohistochemical staining of untreated/MI192 pre-treated hBMSC BMT constructs after 6 weeks osteogenic culture. Positive ALP immunohistochemical staining (brown), with a weak Harris haematoxylin counterstain (purple). Nodule-like formations highlighted with red arrows. Scale bars = 200 (top row) and 25 µm (bottom row), respectively.

BMP2

The MI192 pre-treated group exhibited positive BMP2 protein expression distributed throughout the construct, with the strongest intensity located towards the outer regions and at the microtissue/scaffold interface (Fig 4.42). In comparison, the untreated group exhibited little evidence of BMP2 protein staining, however weak protein expression was observed at the edges of the BMT construct and at the microtissue/scaffold interface.

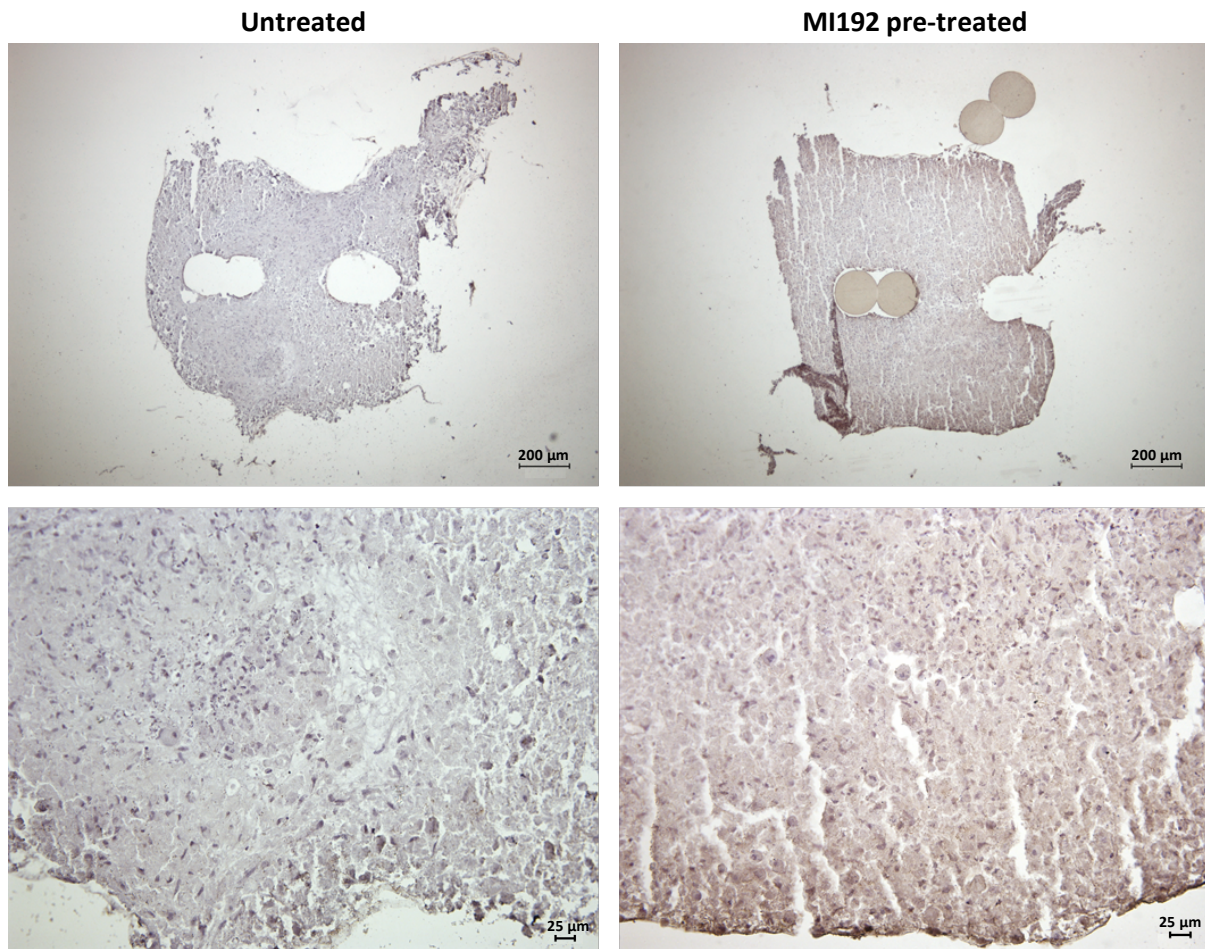


Figure 4.42 - BMP2 immunohistochemical staining of untreated/MI192 pre-treated hBMSC BMT constructs after 6 weeks osteogenic culture. Positive BMP2 immunohistochemical staining (brown), with a weak Harris haematoxylin counterstain (purple). Scale bars = 200 (top row) and 25 μm (bottom row), respectively.

Col1a

The MI192 pre-treated group exhibited positive Col1a protein expression throughout the BMT, with the strongest staining intensity located towards the outer regions of the construct and also at the microtissue/scaffold interface (Fig 4.43). Positive Col1a protein expression was present within the untreated hBMSC BMT, however at a much-reduced staining intensity situated aberrantly in the construct when compared to the MI192 pre-treated group. With both constructs, nodule-like formations were observed which exhibited increased Col1a staining intensity (black arrows). These Col1a-positive nodule-like formations were expression at a higher quantity in the MI192 pre-treated group, and more homogenously distributed throughout the construct.

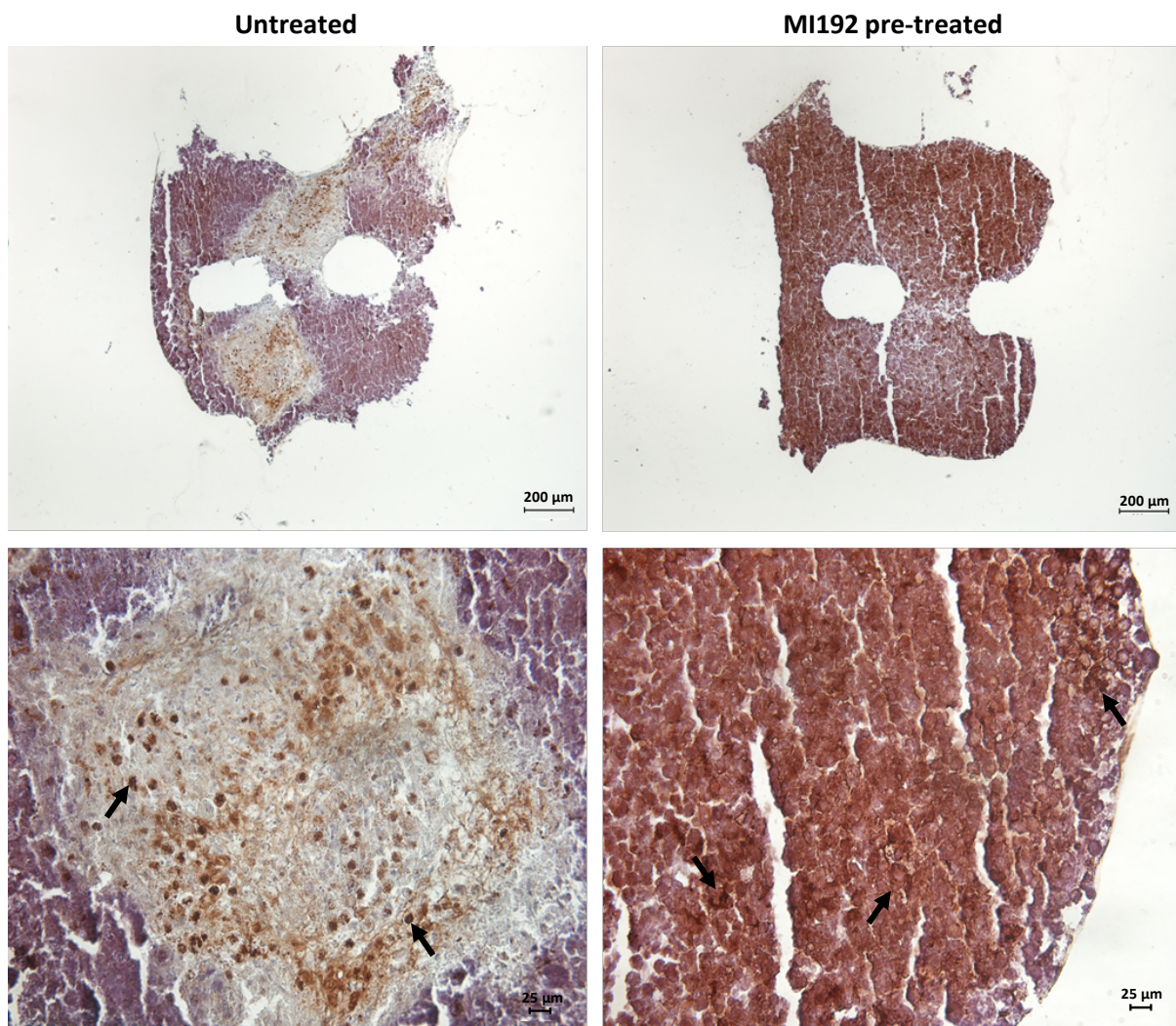


Figure 4.43 - Col1a immunohistochemical staining of untreated/MI192 pre-treated hBMSC BMT constructs after 6 weeks osteogenic culture. Positive Col1a immunohistochemical staining (brown), with a weak Harris haematoxylin counterstain (purple). Nodule-like formations highlighted with black arrows. Scale bars = 200 (top row) and 25 μm (bottom row), respectively.

OCN

The MI192 pre-treated group exhibited positive OCN protein expression throughout the construct at a much-increased staining intensity when compared to the untreated control (Fig 4.44). Within both groups, increased OCN expression was observed towards the periphery of the BMT construct and at the microtissue/scaffold interface. Both groups exhibited the strongest protein expression situated in the nodule-like formations (red arrows), which were of increased quantity in the MI192 pre-treated group.

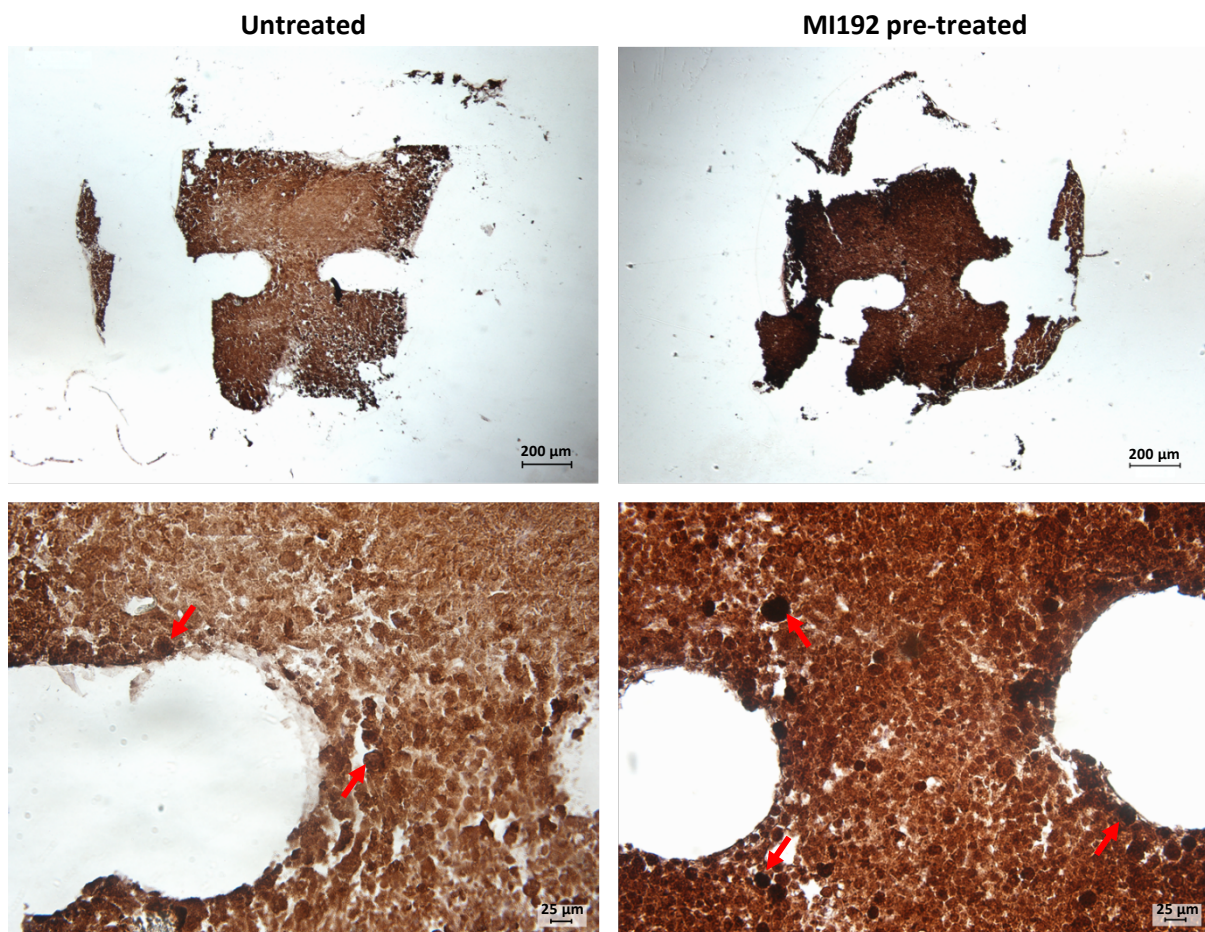


Figure 4.44 - OCN immunohistochemical staining of untreated/MI192 pre-treated hBMSC BMT constructs after 6 weeks osteogenic culture. Positive OCN immunohistochemical staining (brown), with a weak Harris haematoxylin counterstain (purple). Nodule-like formations highlighted with red arrows. Scale bars = 200 (top row) and 25 µm (bottom row), respectively.

4.3.3.5 - The effect of MI192 on hBMSCs chondrogenic protein expression within the BMT construct

AGG

AGG immunohistochemical staining was undertaken to determine the effects of MI192 pre-treatment on hBMSCs chondrogenic protein expression within this 3D *in vitro* model (Fig 4.45). Within the MI192 pre-treated group, the AGG protein expression was at a much-reduced staining intensity when compared to the untreated control group, where AGG expression was observed throughout the construct.

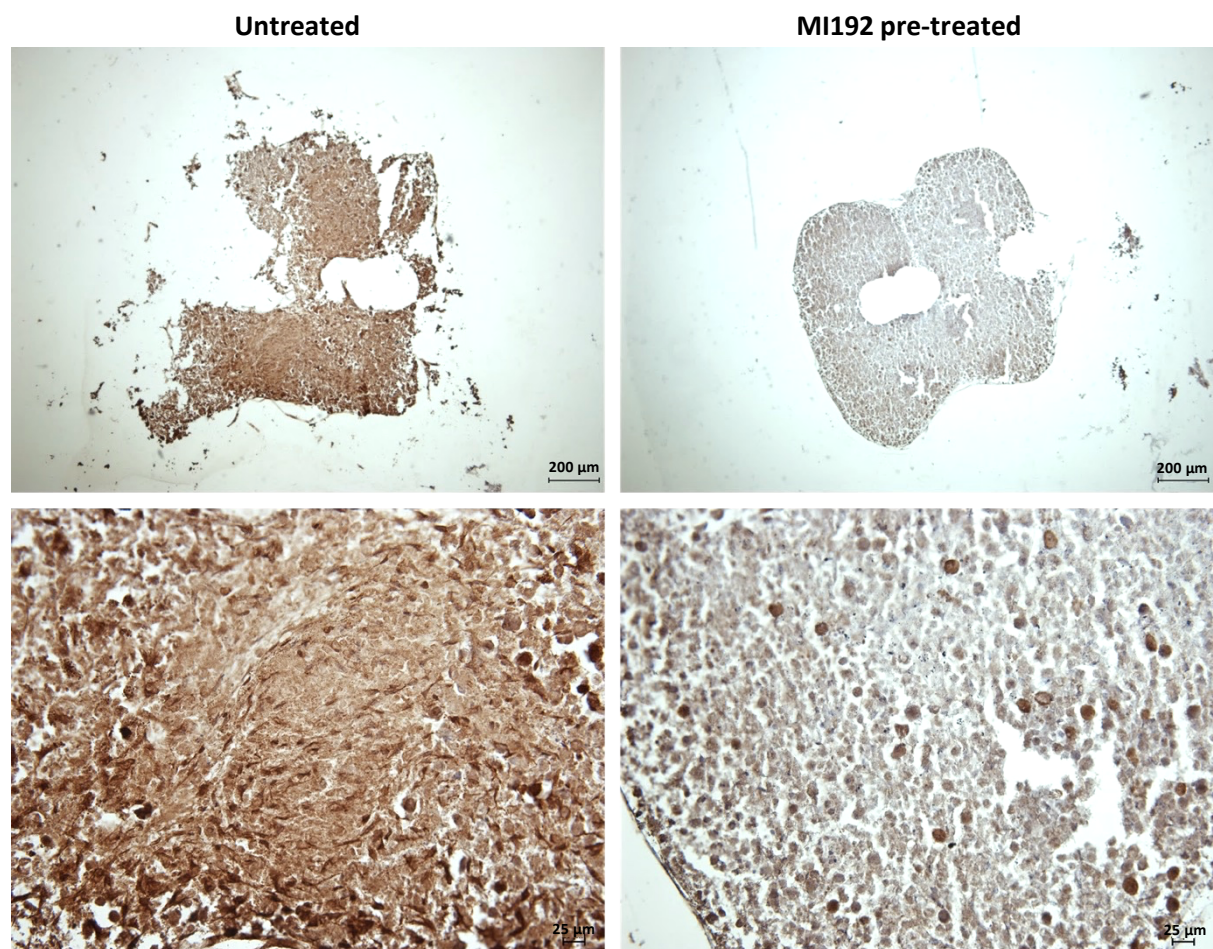


Figure 4.45 - AGG immunohistochemical staining of untreated/MI192 pre-treated hBMSC BMT constructs after 6 weeks osteogenic culture. Positive AGG immunohistochemical staining (brown), with a weak Harris haematoxylin counterstain (purple). Scale bars = 200 (top row) and 25 μm (bottom row), respectively.

Col2a

The MI192 pre-treated group exhibited weak Col2a protein expression within the construct, primarily located at the outer regions of the construct (Fig 4.46). In comparison, positive Col2a staining was observed within the untreated group at a higher staining intensity throughout the construct, particularly at the microtissue/scaffold interface and at the periphery of the construct. The negative immunohistochemical staining of MI192 pre-treated and untreated hBMSC BMTs is shown in Figure 4.47.

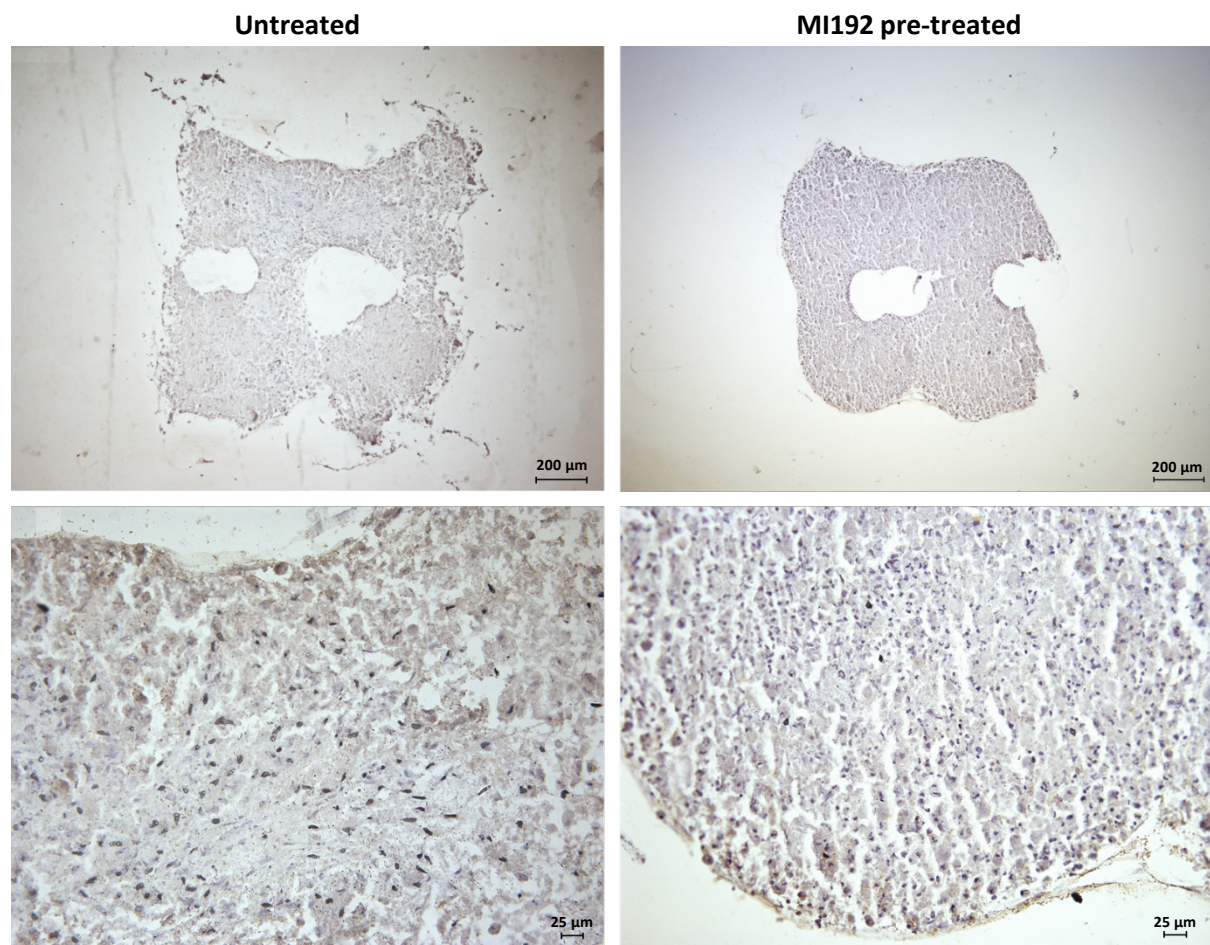


Figure 4.46 - Col2a immunohistochemical staining of untreated/MI192 pre-treated hBMSC BMT constructs after 6 weeks osteogenic culture. Positive Col2a immunohistochemical staining (brown), with a weak Harris haematoxylin counterstain (purple). Scale bars = 200 (top row) and 25 μm (bottom row), respectively.

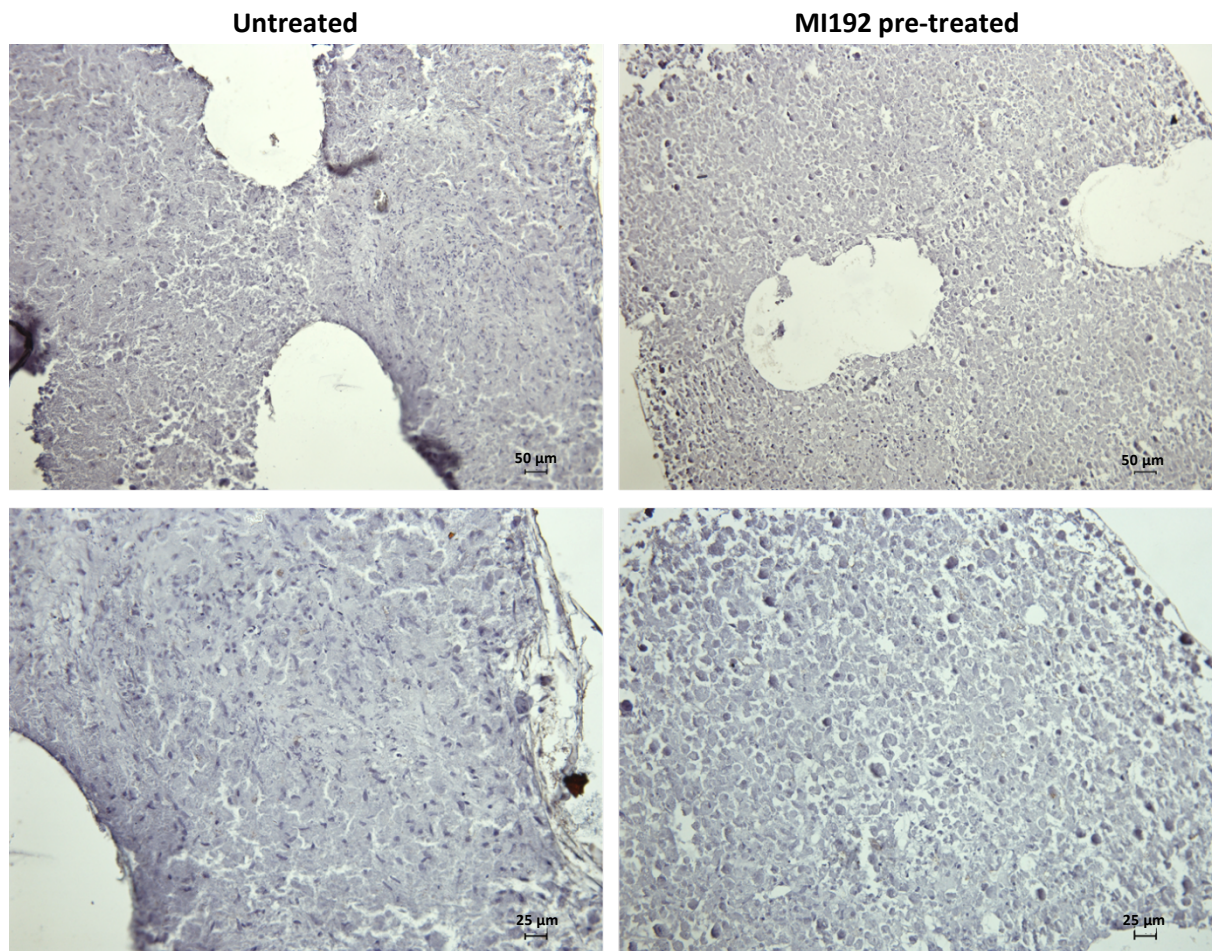


Figure 4.47 - Negative immunohistochemical staining of untreated/MI192 pre-treated hBMSC BMT constructs after 6 weeks osteogenic culture. Scale bar = 50 (top row) and 25 μm (bottom row), respectively.

4.3.3.6 - The effect of MI192 on hBMSCs calcium deposition and mineralisation within the BMT construct

The MI192 pre-treated and untreated BMTs exhibited extensive Alizarin Red staining for calcium deposition throughout the constructs (Fig 4.48). Positive Alizarin red staining within the MI192 pre-treated group was uniformly distributed throughout the BMT, while the control group possessed enhanced staining towards the periphery of the construct and at the microtissue/scaffold interface. Moreover, the untreated group exhibited areas of weak Alizarin red staining within the core of some microtissues. Increased quantity of large circular nodules (black arrows) was observed throughout the MI192 pre-treated group when compared to the untreated BMT which exhibited these nodules at the microtissue/scaffold interface and at the periphery of the construct.

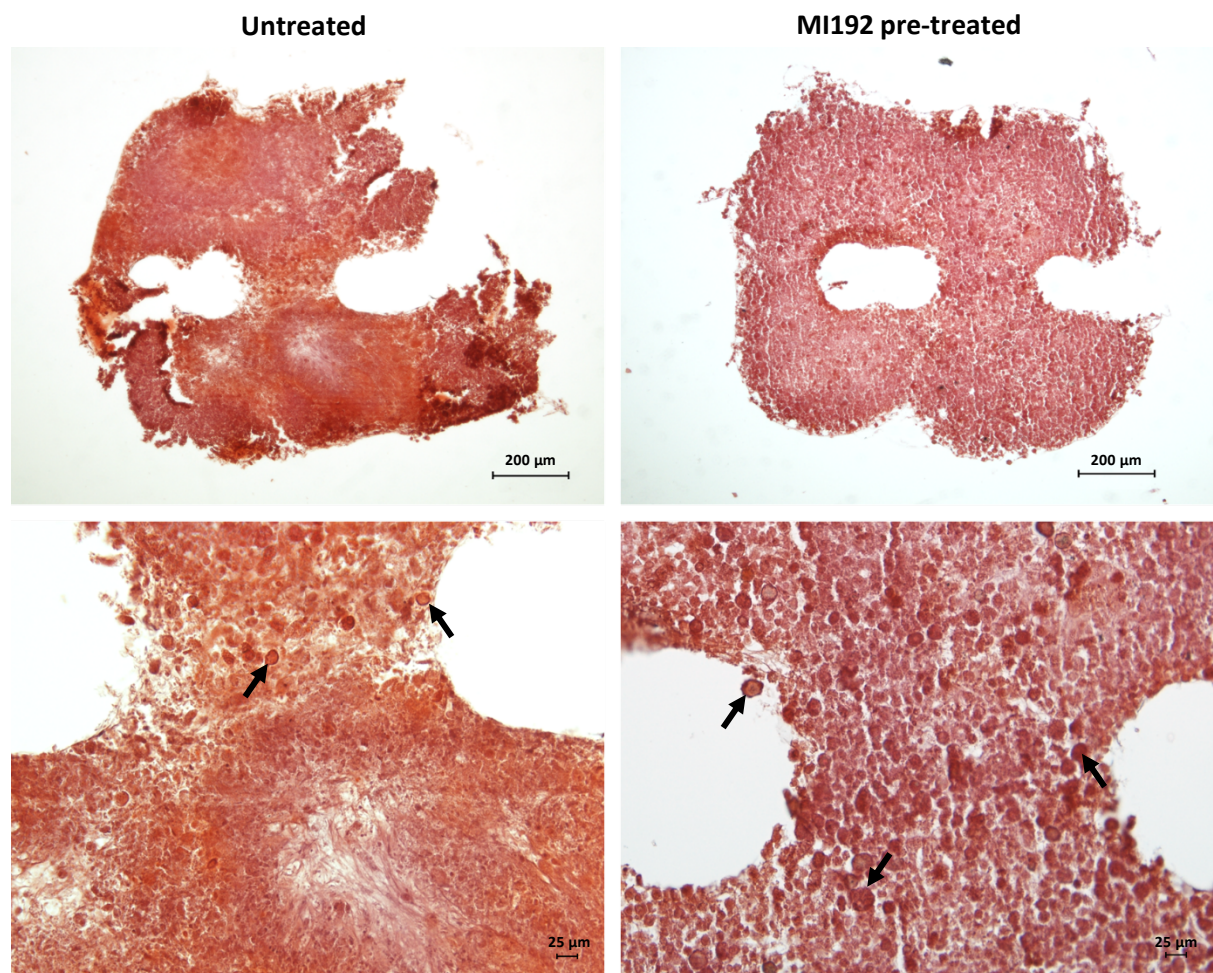


Figure 4.48 - Calcium deposition of untreated/MI192 pre-treated hBMSC BMT constructs after 6 weeks osteogenic culture observed by Alizarin red staining. Nodule-like formations highlighted with black arrows. Scale bars = 200 (top row) and 25 µm (bottom row), respectively.

To assess the effect of MI192 pre-treatment on hBMSCs mineralisation within the BMT constructs, Von Kossa staining was undertaken. Figure 4.49 shows both the MI192 pre-treated and untreated groups exhibited extensive black staining indication the formation of functional mineral nodules within the construct. In the MI192 pre-treated group, extensive black staining was uniformly distributed throughout the BMT, however, positive mineral nodule formation in the untreated group was situated at the microtissue/scaffold interface and at the periphery of the construct, with areas within the core of the microtissues exhibiting negative nodule formation.

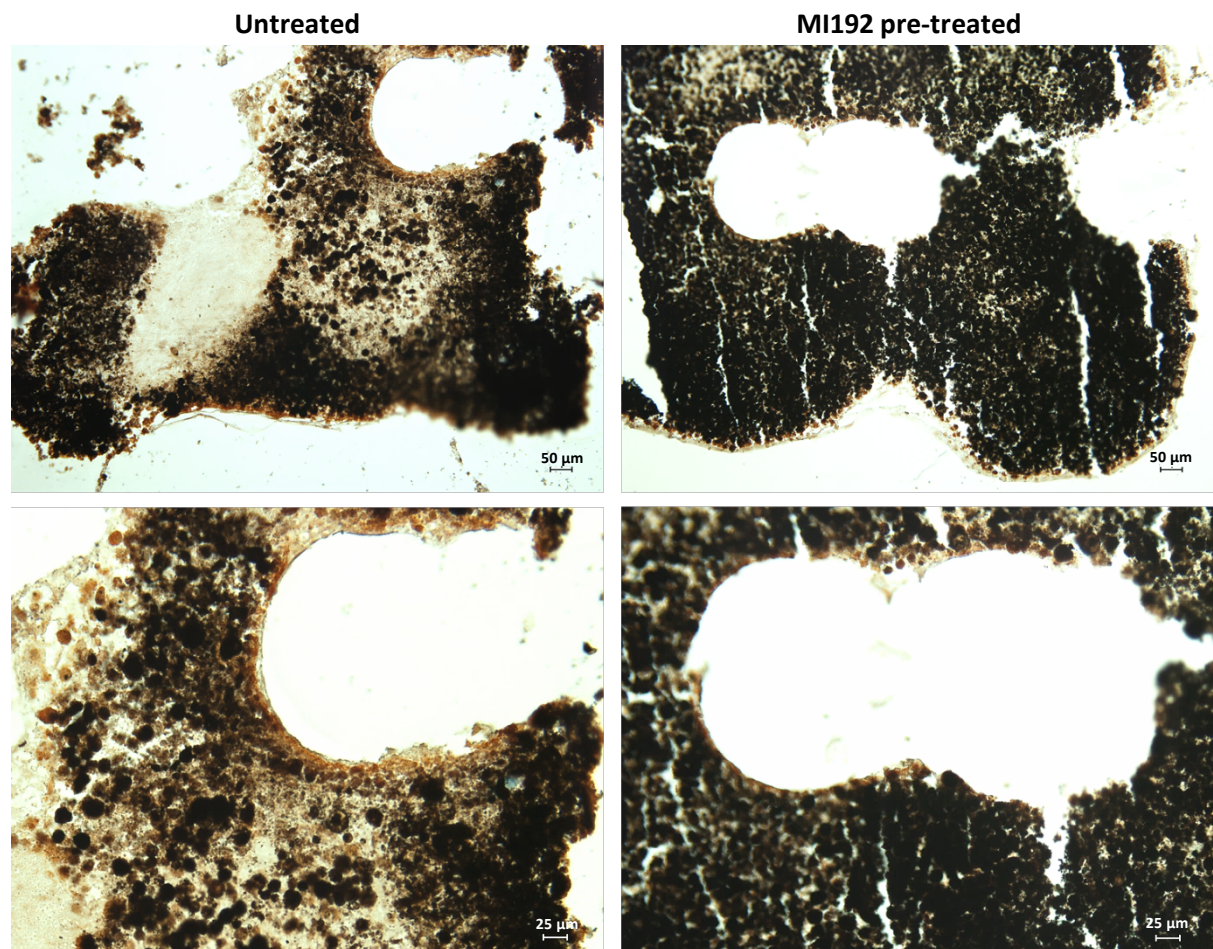


Figure 4.49 - Mineral nodule formation of untreated/MI192 pre-treated hBMSC BMT constructs after 6 weeks osteogenic culture observed by Von Kossa staining. Scale bar = 50 (top row) and 25 μm (bottom row), respectively.

4.3.4 - The Effects of MI192 on hBMSC BMT *in vivo* bone formation

4.3.4.1 - Macroscopic and X-ray analysis of hBMSC BMT constructs

Following the extraction of diffusion chambers from 8 weeks *in vivo* implantation, macroscopic assessment of hBMSC BMT constructs was undertaken. Within the chambers, the 3D printed scaffold remained intact containing the microtissues which were incorporated prior to placement within the chambers (Fig 4.50A). No tissue formation was detected in the regions surrounding the BMT construct within the chamber. Following X-ray analysis, strong radio-opacity was observed within the BMTs particularly in the microtissue regions of the construct (Fig 4.50B). The MI192 pre-treated group displayed strong radio-opacity throughout all visible microtissues in the construct. In comparison, the untreated group exhibited weaker radio-opacity within the BMT, with stronger intensity primarily located towards one face of the construct.

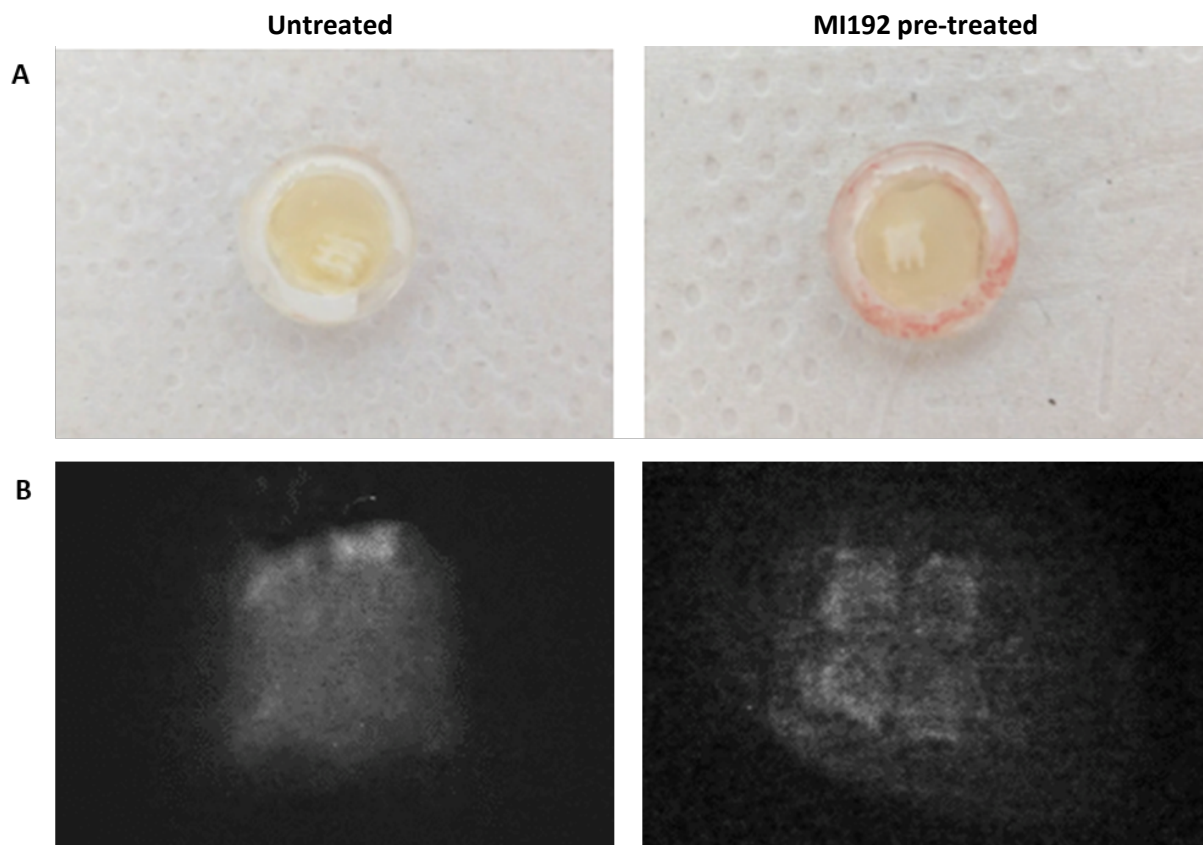


Figure 4.50 - Macroscopic and X-ray images of untreated/MI192 pre-treated hBMSC BMT constructs after 8 weeks *in vivo* implantation. A) Macroscopic images immediately post extraction. B) X-ray radiographs of BMT following extraction.

4.3.4.2 - The effect of MI192 on hBMSCs tissue formation during BMT *in vivo* implantation

Histological analysis was undertaken to assess the effects of MI192 pre-treatment on hBMSCs tissue formation within the BMT construct following 8 weeks *in vivo* implantation (Fig 4.51). Within both groups, incorporated microtissues were seen occupying the internal void volume of the 3D printed scaffold confirmed via H&E staining (some scaffold fibres dislodged during histological analysis). Within the MI192 pre-treated group, areas of denser tissue formation (dark purple) were observed at the periphery of each microtissue, while within the untreated group dense tissue formation was situated towards the right face of the construct.

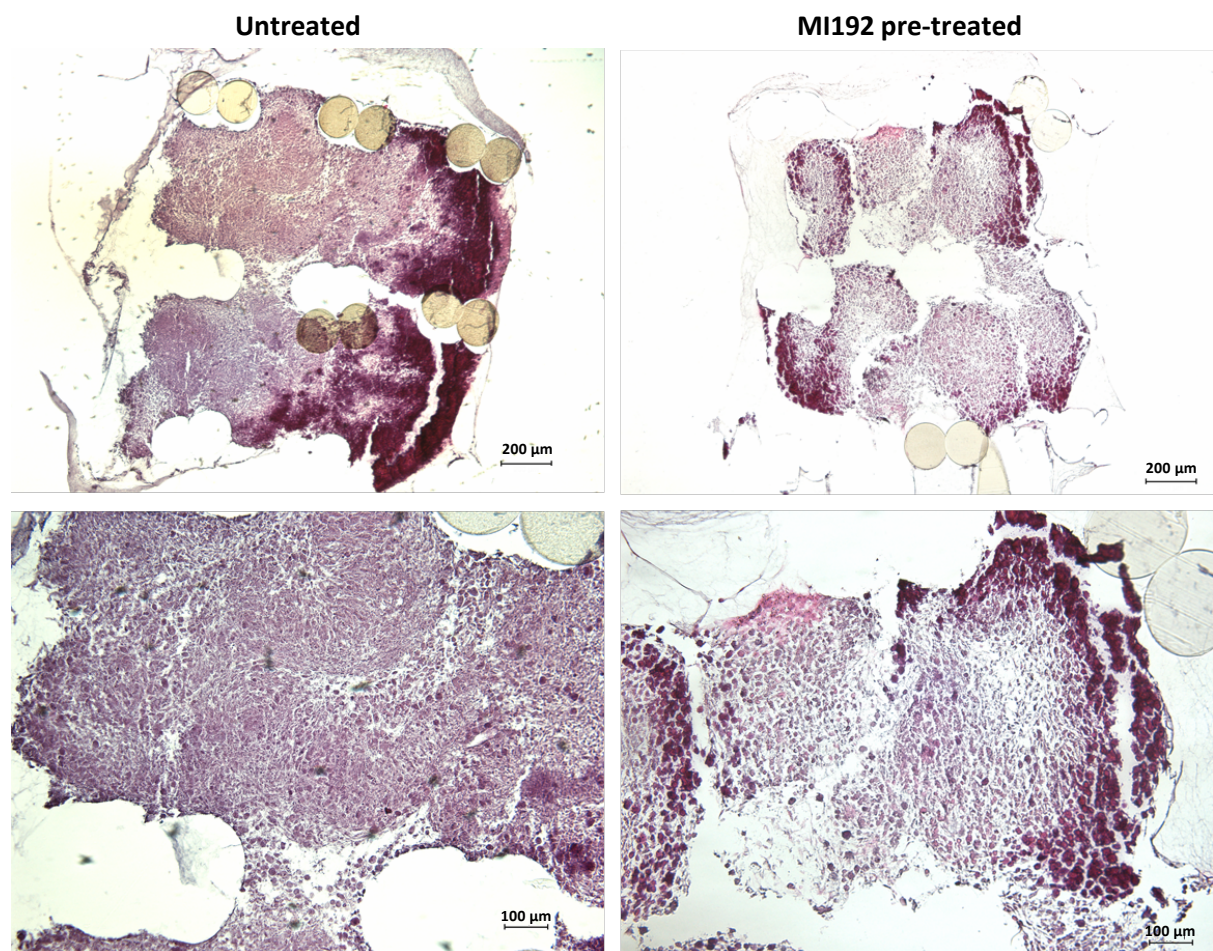


Figure 4.51 - H&E staining of untreated/MI192 pre-treated hBMSC BMT constructs after 8 weeks *in vivo* implantation. Scale bars = 200 (top row) and 100 μm (bottom row), respectively.

The MI192 pre-treated group exhibited positive Picrosirius red staining throughout the scaffold, with the strongest expression for collagens located at the edges of individual microtissues and at the periphery of the construct. In comparison, the untreated group exhibited positive collagen deposition located primarily towards the left half of the construct, although positive expression was also observed at the right face of the construct. The strongest expression for Picrosirius red was situated in the nodule-like formations within the constructs (black arrows), where an increased quantity was observed within the MI192 pre-treated group. The MI192 pre-treated group exhibited little Alcian blue staining for GAG accumulation, while the untreated group displayed increased GAG expression, primarily situated in the right half of the construct.

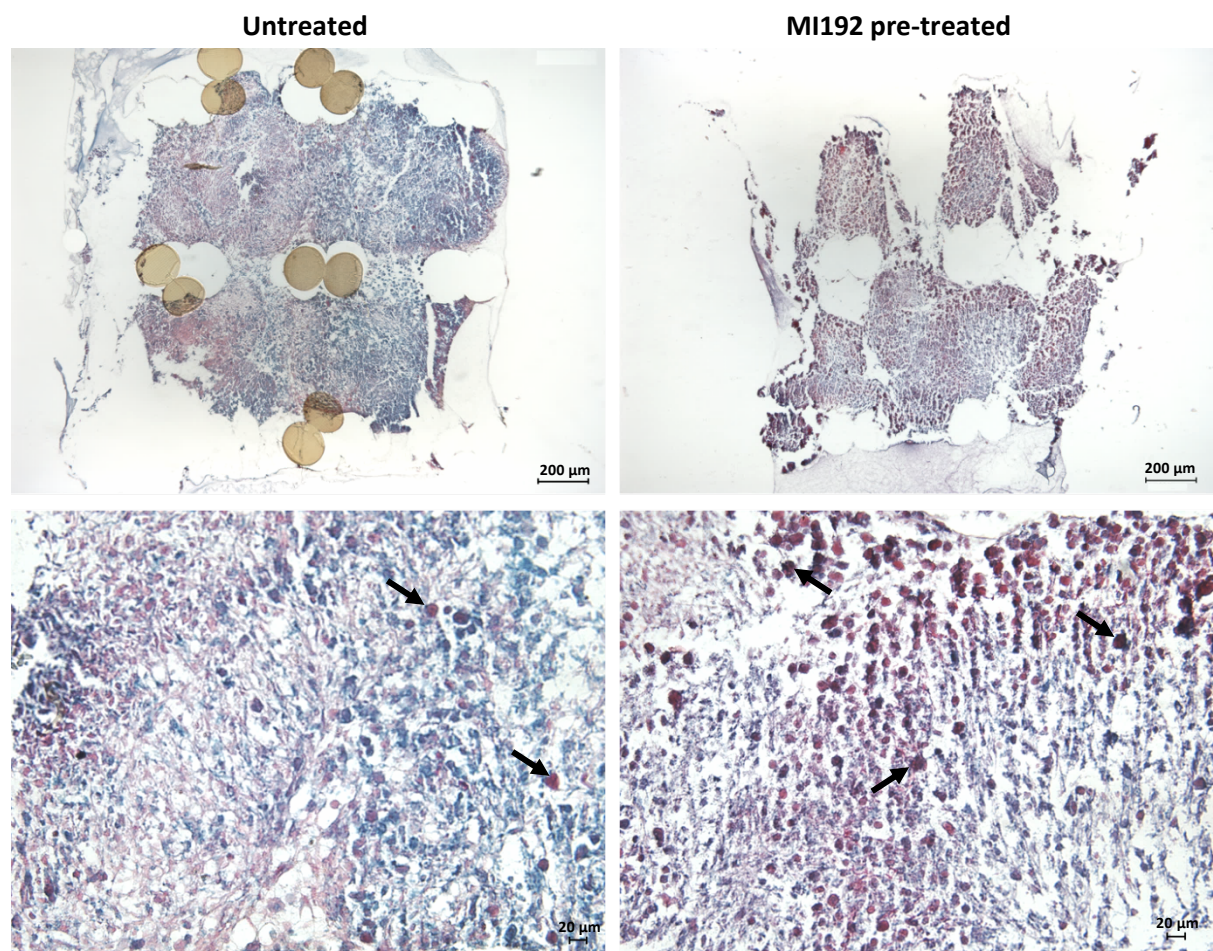


Figure 4.52 - Picrosirius red/Alcian blue staining of untreated/MI192 pre-treated hBMSC BMT constructs after 8 weeks *in vivo* implantation. Collagens and GAGs stained with Picrosirius red and Alcian blue, respectively. Strong Picrosirius red staining located in circular nodules highlighted by black arrows Scale bars = 200 (top row) and 20 µm (bottom row), respectively.

4.3.4.3 - The effect of MI192 on hBMSCs osteogenic protein expression during BMT *in vivo* implantation

Col1a

Positive Col1a protein expression was exhibited in both MI192 pre-treated and untreated constructs (Fig 4.53). The MI192 pre-treated group displayed increased Col1a deposition intensity within each microtissue in the construct compared to the untreated group which exhibited weak expression throughout.

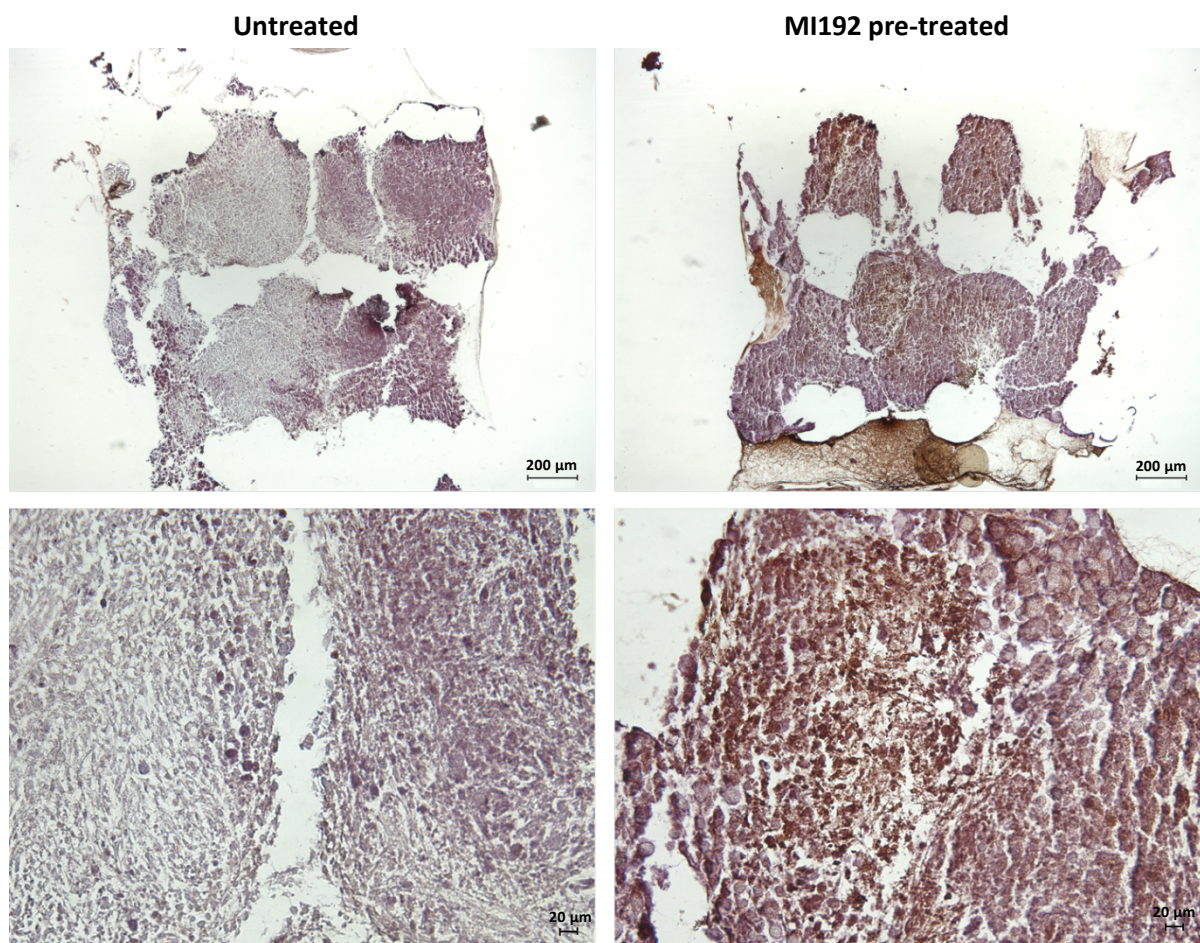


Figure 4.53 - Col1a immunohistochemical staining of untreated/MI192 pre-treated hBMSC BMT constructs after 8 weeks *in vivo* implantation. Positive Col1a immunohistochemical staining (brown), with a weak Harris haematoxylin counterstain (purple). Scale bars = 200 (top row) and 20 μm (bottom row), respectively.

OCN

Both the MI192 pre-treated and untreated groups displayed positive expression for OCN which was distributed throughout the constructs (Fig 4.54). The global OCN staining intensity was slightly stronger in the MI192 pre-treated construct when compared to the untreated group. The untreated group exhibited increased OCN expression intensity primarily towards the right face of the construct, while the greatest OCN staining intensity was located within each incorporated microtissue in the MI192 pre-treated BMT group.

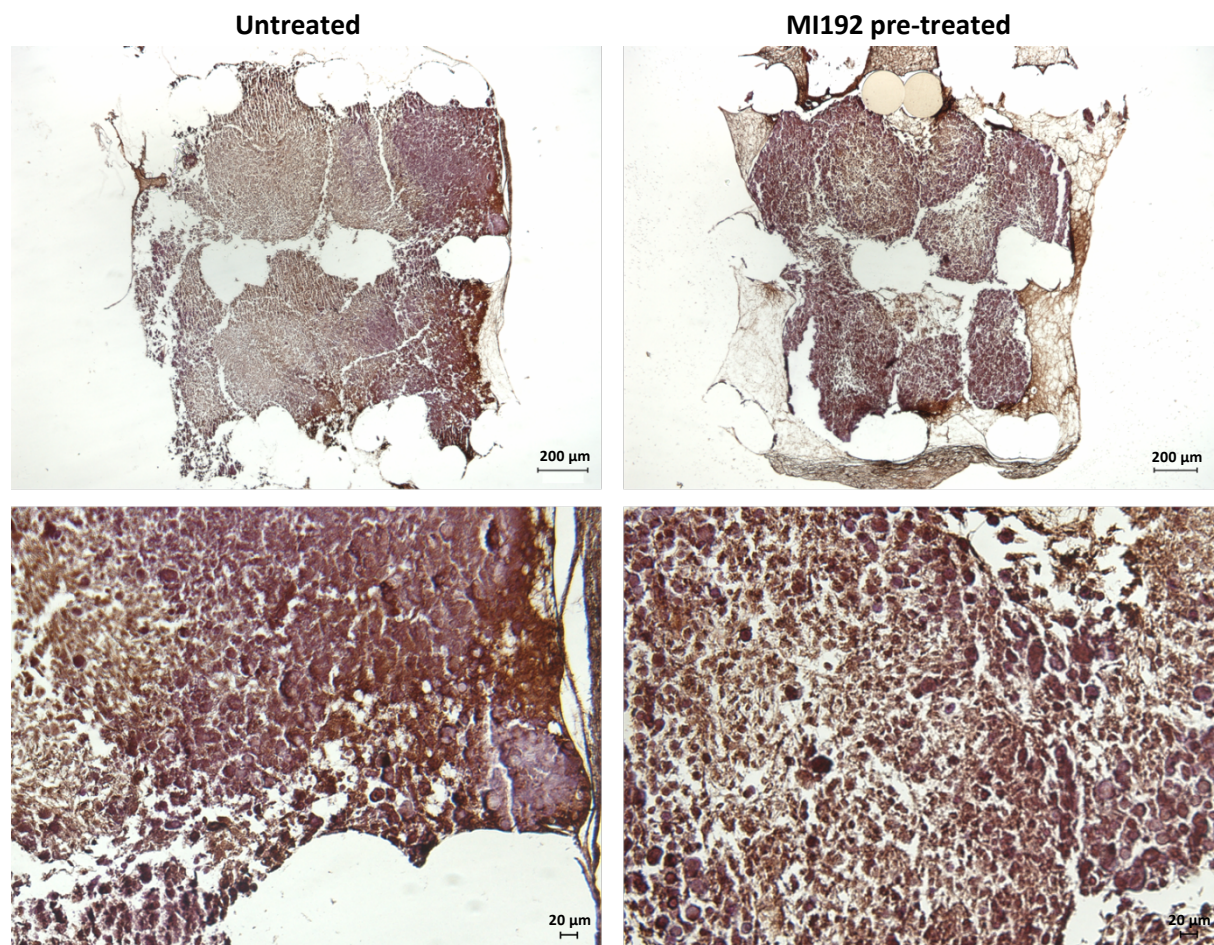


Figure 4.54 - OCN immunohistochemical staining of untreated/MI192 pre-treated hBMSC BMT constructs after 8 weeks *in vivo* implantation. Positive OCN immunohistochemical staining (brown), with a weak Harris haematoxylin counterstain (purple). Scale bars = 200 (top row) and 20 µm (bottom row), respectively.

4.3.4.4 - The effect of MI192 on hBMSCs chondrogenic protein expression during BMT *in vivo* implantation

AGG

The MI192 pre-treated group exhibited little AGG protein expression throughout the construct (Fig 4.55). In comparison, the untreated group displayed substantially increased AGG staining intensity compared to the MI192 pre-treated group, which was distributed throughout the construct with a slightly increased intensity situated at the right face of the BMT.

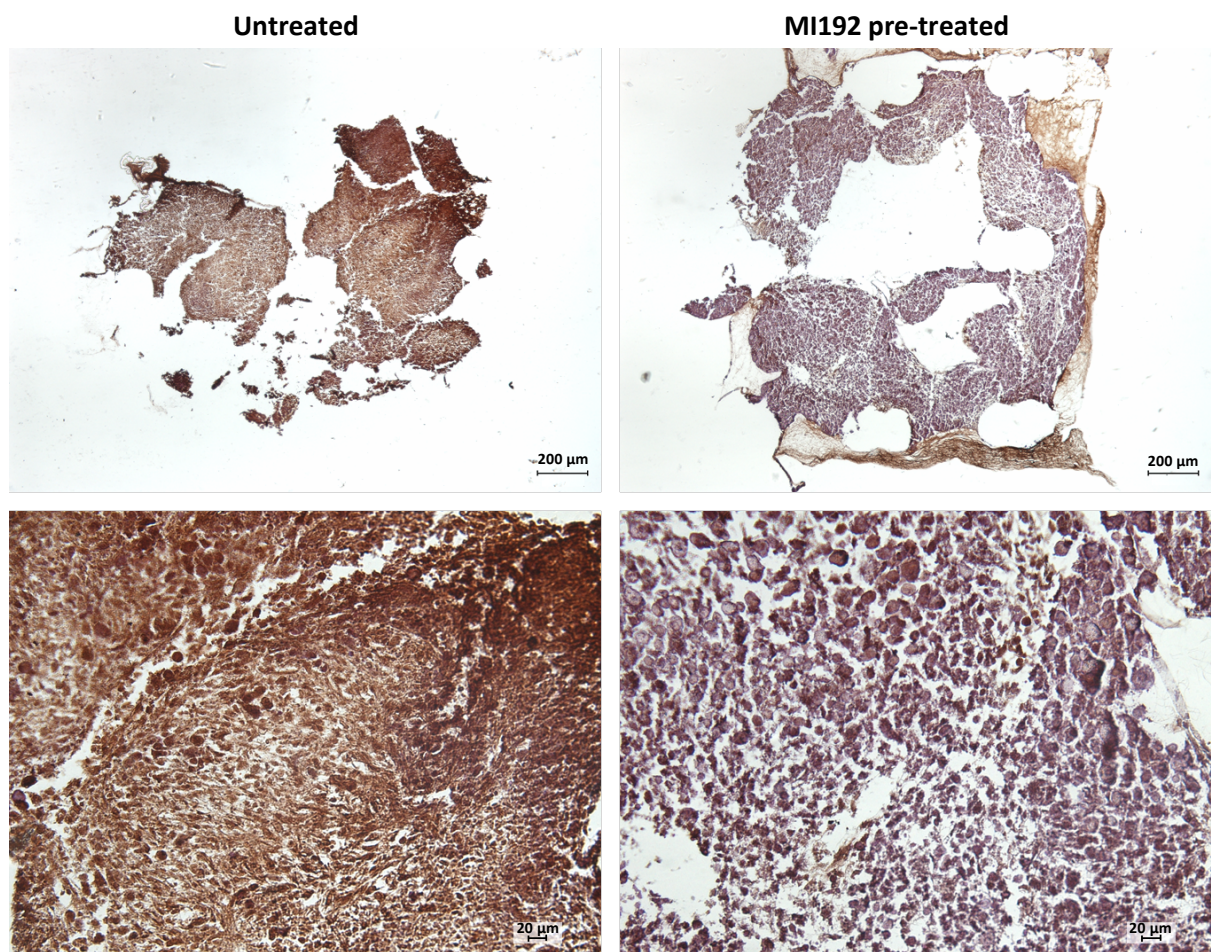


Figure 4.55 - AGG immunohistochemical staining of untreated/MI192 pre-treated hBMSC BMT constructs after 8 weeks *in vivo* implantation. Positive AGG immunohistochemical staining (brown), with a weak Harris haematoxylin counterstain (purple). Scale bars = 200 (top row) and 20 μm (bottom row), respectively.

Col2a

The MI192 pre-treated construct exhibited weak Col2a protein deposition when compared to the untreated group, which possessed strong protein expression distributed uniformly throughout the construct, with particular enhanced intensity located towards the right face of the construct (Fig 4.56). Negative immunohistochemical staining was undertaken on the MI192 pre-treated and untreated hBMSC BMT constructs (Fig 4.57).

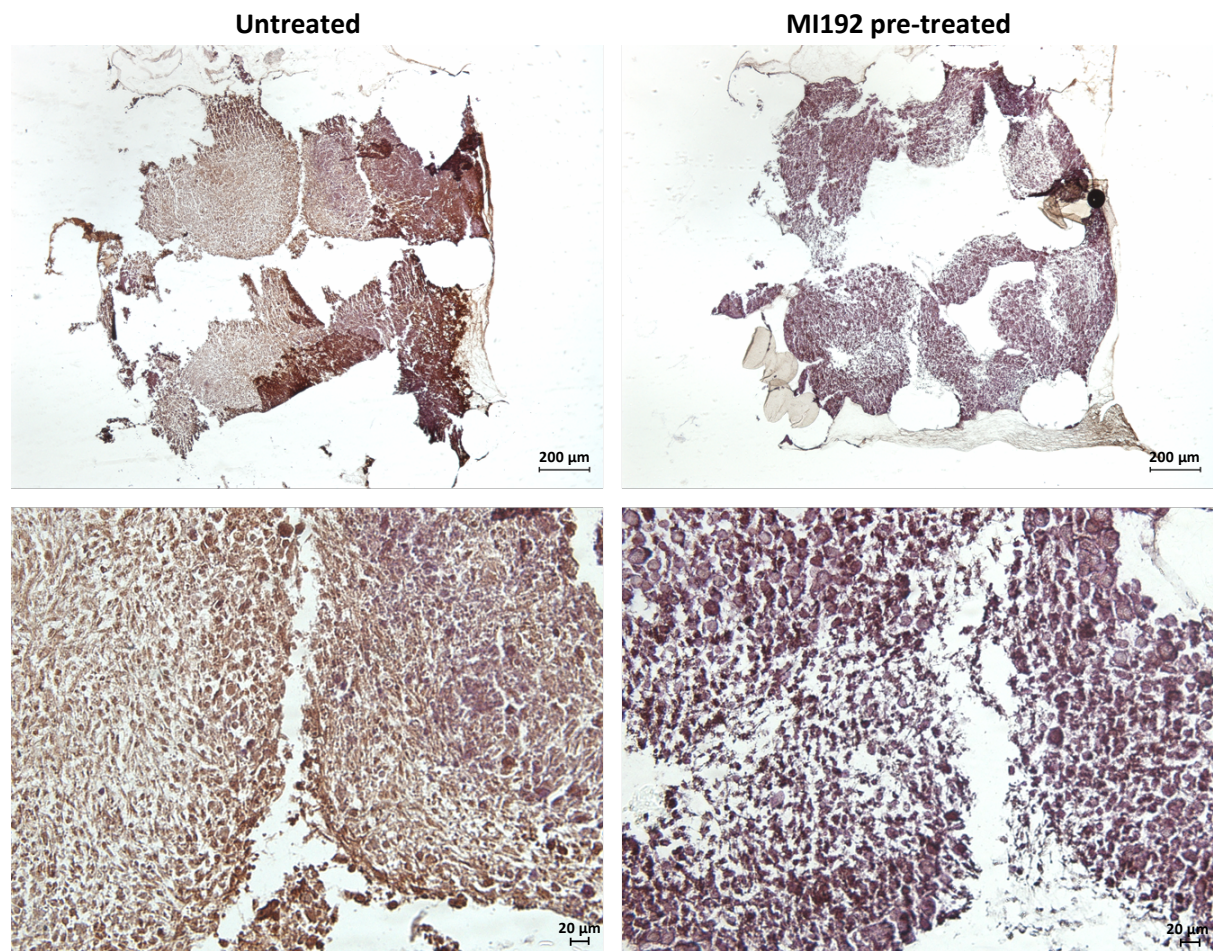


Figure 4.56 - Col2a immunohistochemical staining of untreated/MI192 pre-treated hBMSC BMT constructs after 8 weeks *in vivo* implantation. Positive Col2a immunohistochemical staining (brown), with a weak Harris haematoxylin counterstain (purple). Scale bars = 200 (top row) and 20 μm (bottom row), respectively.

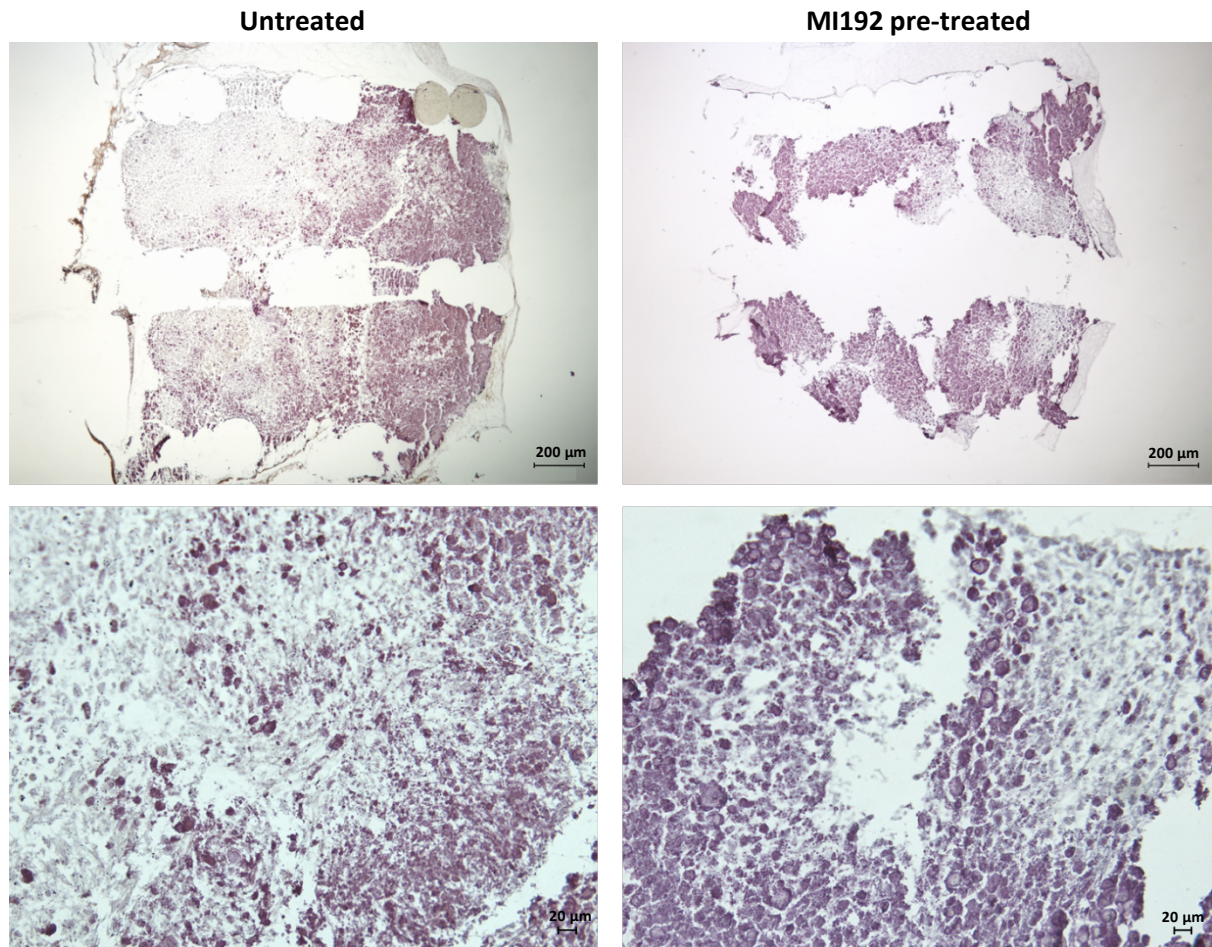


Figure 4.57 - Negative immunohistochemical staining of untreated/MI192 pre-treated hBMSC BMT constructs after 8 weeks *in vivo* implantation. Scale bars = 200 (top row) and 20 μm (bottom row), respectively.

4.3.4.5 - The effect of MI192 on hBMSCs calcium deposition and mineralisation during BMT *in vivo* implantation

Calcium deposition within the MI192 pre-treated and untreated hBMSC BMTs are shown in Figure 4.58 following Alizarin red staining. The MI192 pre-treated group possessed slighter stronger Alizarin red staining located at the periphery of the individual microtissues. Within the untreated BMT, calcium deposition was observed throughout the construct at a similar intensity as the MI192 pre-treated group, with increased calcium deposition observed towards the right face of the construct.

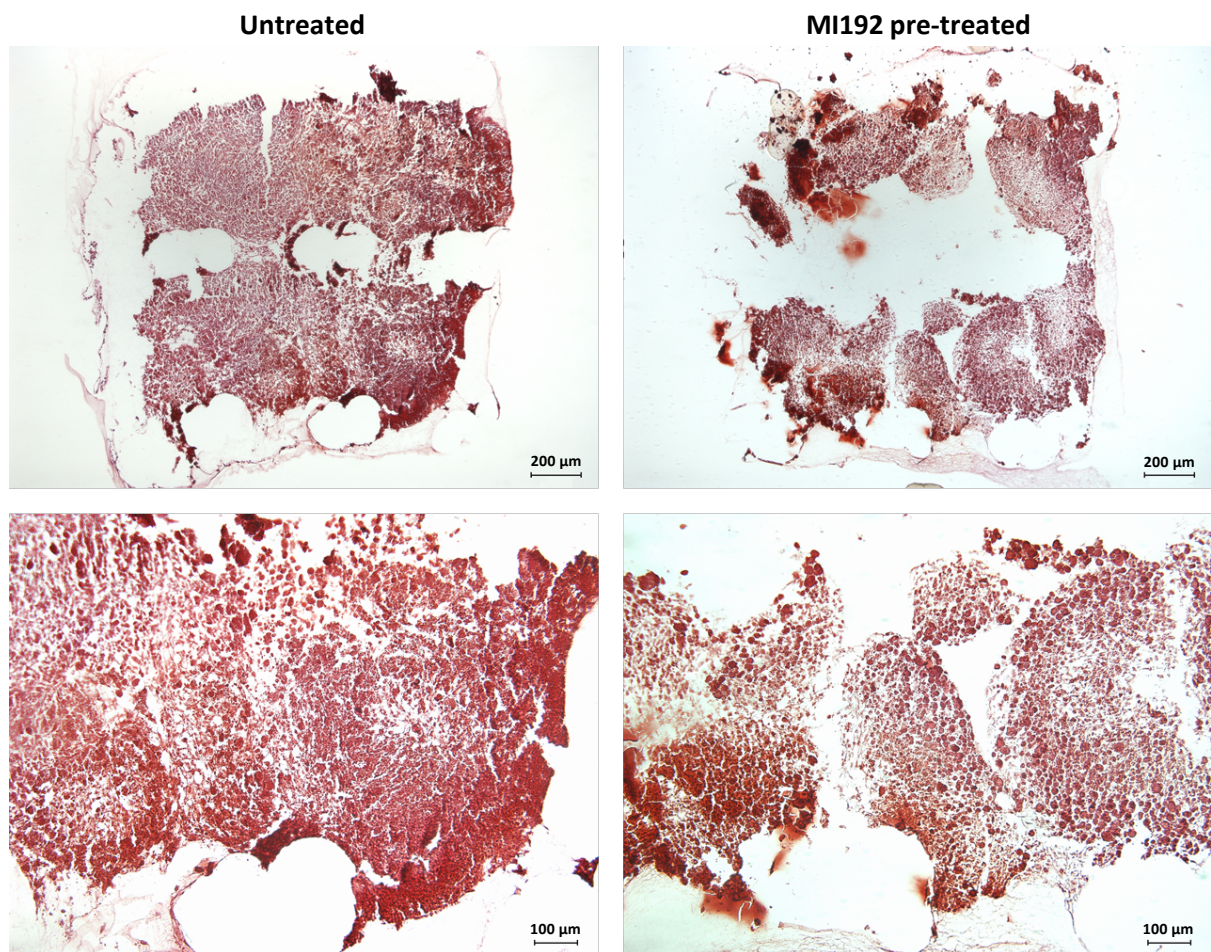


Figure 4.58 - Calcium deposition of untreated/MI192 pre-treated hBMSC BMT constructs after 8 weeks *in vivo* implantation observed by Alizarin red staining. Scale bars = 200 (top row) and 100 μm (bottom row), respectively.

Mineralisation within the MI192 pre-treated and untreated hBMSC BMT constructs was analysed via Von Kossa staining (Fig 4.59). The MI192 pre-treated group exhibited extensive black staining intensity for mineral nodule deposition primarily situated at the edges of the individual microtissues and at the periphery of the construct. Within the untreated group, mineral nodules were observed throughout the construct, with increased mineralisation located at the right face of the construct.

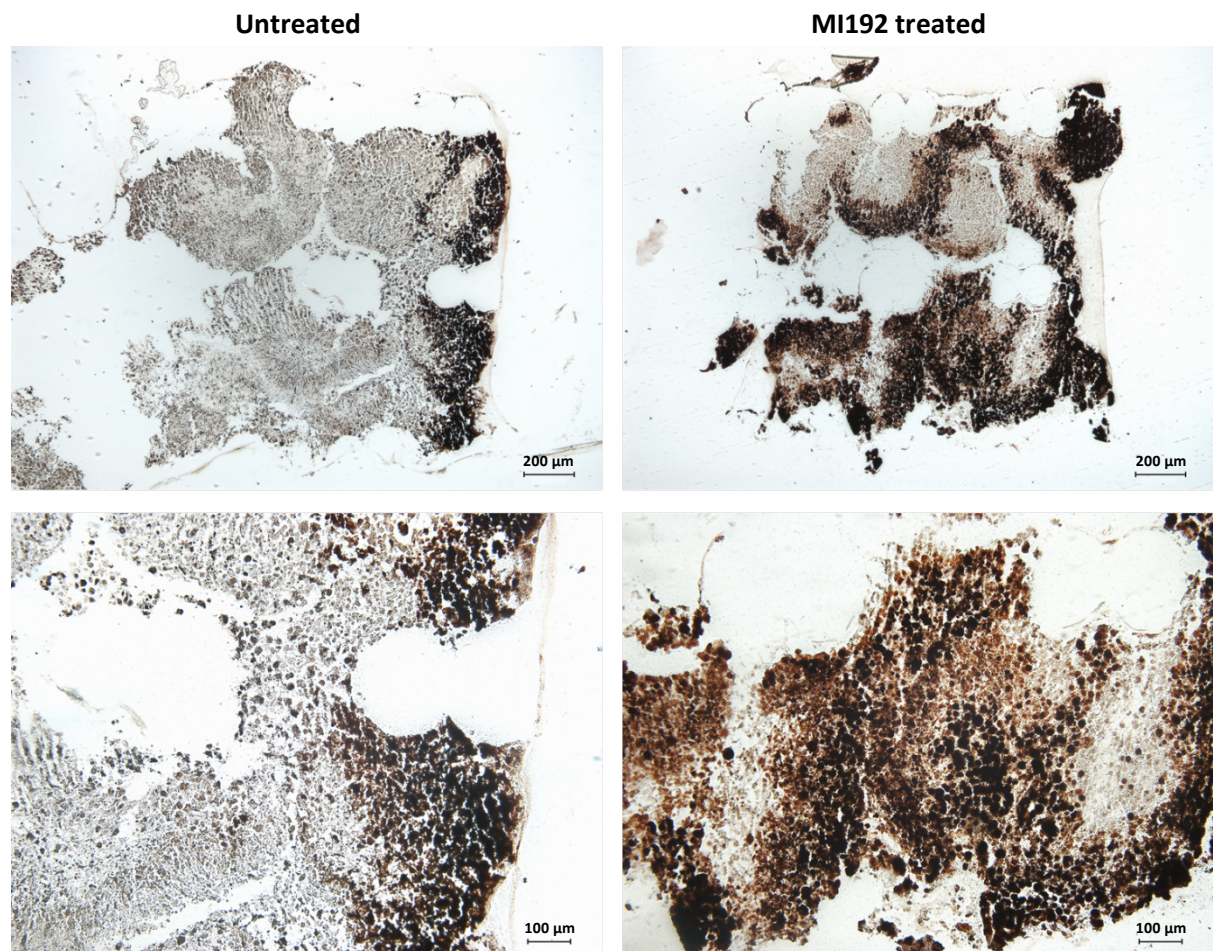


Figure 4.59 - Mineralisation of untreated/MI192 pre-treated hBMSC BMT constructs after 8 weeks *in vivo* implantation observed by Von Kossa staining. Scale bars = 200 (top row) and 100 μm (bottom row), respectively.

4.4 - Discussion

For bone tissue engineering applications, BMSCs have been the gold standard MSC source utilised for many decades due to their well-characterised properties, established isolation methods and proven differentiation down the mesoderm lineages (153). Although BMSCs have been extensively utilised, researchers have found limited clinical success due to drawbacks including low procurement yield, invasive acquisition, extensive *in vitro* expansion required and their inherent heterogeneity (222). Alternative MSCs have been investigated for bone tissue engineering applications such as ADSCs and DPSCs (375, 376), however, BMSCs still remains the preferred cell type for bone augmentation strategies. Recent technologies have looked to enhance the potency of these cells for bone regeneration via gene therapy, however, results have been inconsistent and there are safety concerns associated with their clinical translation (15). Modifications to the epigenome for tissue engineering purposes have recently gained notoriety due to their ability to affect cellular functions without inherently altering the genome. The use of HDACis has shown promise for enhancing MSCs osteogenic potential with an increasing number of reports demonstrating the feasibility of this epigenetic approach (204, 291). Although the potential of these compounds has been demonstrated, the majority of research has utilised non-selective panHDACis which are associated with reduced differentiation efficacy and unwanted side-effects (213). Several studies have demonstrated that HDAC3 is linked to osteogenic differentiation (140, 262). Previously, the selective HDAC2 and 3 inhibitor - MI192 substantially enhanced the osteogenic potential of ADSCs when compared to non-selective panHDACi TSA (214). Additionally, MI192 was shown to promote the osteogenic capacity of hDPSCs in Chapter 3 in this thesis. Therefore, the aim of this chapter was to investigate the effects of the HDAC2 & 3 selective inhibitor - MI192 on the behaviour and osteogenic capacity of hBMSCs on 2D and 3D *in vitro* and *in vivo*.

4.4.1 - The effects of MI192 on hBMSCs general behaviour in 2D culture

HDAC enzymes are known to target numerous histone and non-histone proteins which are involved in several cellular processes such as proliferation, differentiation, cell cycle regulation and apoptosis (83, 91). Therefore, it is clear inhibiting the activity of these enzymes will likely dysregulate these key cellular processes. Numerous studies have demonstrated the potential of HDACi compounds for initiating cell death, particularly against cancerous cells which possess increased sensitivity to these compounds compared to non-transformed cells (129, 377, 378). Due to the potential side-effects of utilising HDACis, it is important to investigate the effects of MI192 on hBMSCs viability in order to enhance MI192 clinical safety and efficacy. In this study, the effects of MI192 treatment on hBMSCs morphology, metabolic activity and DNA content were evaluated.

From the morphological assessment, it is clear that MI192 treatment caused a time-dose dependent reduction in the viability of the hBMSCs with increased numbers of floating dead/detached cells visible at higher MI192 concentrations and at the longer time points. Studies performed previously showed a similar effect on the morphology of ADSCs following MI192 treatment (214), indicating lower MI192 concentrations halts proliferation, while higher concentrations caused cell detachment/death. This time-dose dependent reduction in cell density upon MI192 treatment correlated with findings in the literature with TSA treated hDPLCs (291). Therefore, the reduced cell density and increased quantity of floating dead/detached cells induced by MI192 indicate the cytotoxic effects of this HDACi.

In addition, the effects of MI192 on hBMSCs metabolic function and cell health were also evaluated as an indication of its impact on cell viability. From the AlamarBlue assay, a time-dose dependent reduction in the metabolic activity was observed, correlating with the morphological assessment in this study. Previous research utilising this selective HDACi on leukaemia cell lines and ADSCs demonstrated a similar time-dose dependent reduction in the metabolic function of the treated cells (100, 214). The effect of MI192 on the metabolic activity of hBMSCs may be indicative of its cytotoxic properties particular at higher concentrations, as only viable cells possess metabolic activity. However, the ability of this HDACi in altering cell cycle progression, as confirmed from the cell cycle analysis in this chapter, may have an effect on the metabolic activity of these cells, as cell cycle and metabolic activity is closely linked (268).

To assess the effects of MI192 on hBMSCs proliferation and cell death, DNA content was quantified via the PicoGreen assay. From the results, MI192 induced a time-dose dependent reduction in DNA content, consistent with the effects of this HDACi on hBMSCs morphology and metabolic activity observed in this study. This result indicates the effect of MI192 in halting the proliferation of cells at lower concentrations and the cytotoxic effects of this HDACi at higher concentrations, consistent with the findings from MI192 treated ADSCs (214). As this assay quantifies the DNA content of attached cells, the floating dead/detached cells observed in the morphological assessment (which may contain viable cells) would have been removed and not included in the quantification.

Several studies have reported that HDACi compounds have the potential to affect cellular adhesion by blocking the expression of key adhesion proteins (272, 273). In a time-dose dependent manner, a large quantity of floating dead/detached cells was observed in the MI192 treated groups (Fig 4.4), which are presumed dead but may contain unattached viable cells. To confirm whether the unattached cells from the morphological assessment were viable, the MI192 treatment medium which contained the floating dead/detached cells was collected and the metabolic activity was

assessed, shown in the Appendix (Fig A5). From the results, the untreated group (basal medium supernatant), possessed significantly higher metabolic activity compared to the MI192 treatment groups for all time points assessed. This suggests that the untreated group, which possessed a low number of floating dead/detached cells from the morphological assessment, exhibited significantly higher metabolic activity from the few viable cells washed off/collected compared to the enhanced number of floating dead/detached cells observed in the MI192 treated groups. These findings indicate that the increased quantity of floating dead/detached cells induced by MI192 treatment were non-viable. Together, these results demonstrate that MI192 caused a time-dose dependent reduction in the viability of hBMSCs; therefore, the exposure of this HDACi on hBMSCs to enhance osteogenesis must be tightly controlled.

Normal cellular functions such as proliferation, differentiation and apoptosis are tightly controlled by the cell cycle (379). Studies have demonstrated that HDACis have the ability to disrupt the cell cycle at various stages (39, 40). In this study, 50 μ M MI192 was utilised as this concentration was found to enhance hBMSCs histone H3K9 acetylation levels and osteogenic capacity from the ALPSA results in this chapter (Fig 4.8 and 4.11). MI192 treatment decreased the percentage of cells in the S phase, and simultaneously increased the number of cells in the G₂/M phase of the cell cycle. This replicated the work performed previously with MI192 treated ADSCs (214). The G₂/M checkpoint is where the cell checks for DNA damage and undergoes repair prior to cellular division. Studies have demonstrated the ability of HDACis to induce DNA damage which resulted in the similar accumulation of cells in the G₂/M phase (278, 279). Therefore, the enhanced accumulation in this phase may be due to an increased response to DNA damage induced by MI192 resulting in cell cycle arrest. This may be linked to the reduction in proliferation and high cell death observed in the MI192 treated hBMSCs in the cell viability analysis. VPA and NaB were demonstrated to block cell cycle progression of ADSCs and hUCSCs, similar to the observations in this study (264). Jiang *et al.* (2014) demonstrated the importance of HDAC3 in controlling cell cycle progression, where HDAC3 knockdown neural stem cells were unable to progress through the G₂/M phase due to the dysregulation of CDK1 activity (119). These authors postulated HDAC3 involvement in the post-translational stabilisation of CDK1, preventing its degradation via ubiquitination. Similarly, Vidal-Laliena *et al.* (2013) reported the role of HDAC3 in deacetylating cyclin A, the cyclin partner of CDK1, preventing its ubiquitination and subsequent degradation within HeLa cells (380). These studies suggest HDACis dysregulates HDAC3 non-histone substrates which are integral in controlling cell cycle progression, particularly through the G₂/M checkpoint. The results of the present study demonstrated that MI192 halted hBMSCs cell cycle progression at the G₂/M phase, indicating the

role of this inhibitor in halting proliferation and synchronising cell cycle progression. This synchronisation of the cell cycle may be beneficial in inducing differentiation (381).

HDACi compounds have shown the potential in stimulating differentiation of MSCs, as they are highly receptive to epigenetic changes (281). Therefore, it is important to acquire a deeper understanding of the possible mechanisms in which MI192 alters hBMSCs epigenome. Previous reports have demonstrated that MI192 was able to inhibit the HDAC activity in HeLa, PC3 and ADSCs (100, 282). The result of this study showed that MI192 treatment for 24 and 48 hours significantly reduced HDAC specific activity in hBMSCs immediately after treatment (>51 and 58% reduction compared to untreated cells, respectively), where increasing MI192 concentrations further reduced HDAC activity in a time-dose dependant manner. These findings were consistent with previous studies assessing the effect of MI192 on ADSCs HDAC activity (214). Compared to the HDAC activity results acquired in the MI192 treated ADSCs, a greater fold reduction was observed in the MI192 treated hBMSCs (10 μ M MI192 reduced HDAC activity 2.4- and 2.7-fold (ADSCs) vs 2.7- and 3.6-fold (hBMSCs) after 24 and 48 hours, respectively).

Following HDAC activity analysis, it is important to evaluate the downstream effects of HDAC inhibition on histone H3K9 acetylation levels within the cell. Acetylation at these sites is associated with a transcriptionally permissive chromatin structure (71). After 48 hours treatment, MI192 concentrations of ≥ 20 μ M significantly enhanced histone H3K9 acetylation compared to the untreated cells, while MI192 treatment for 24 hours was unable to enhance H3K9 acetylation when compared to the untreated control. Although concentrations as low as 1 μ M MI192 significantly reduced HDAC activity at both time points, a higher concentration was required (for 48 hours) to significantly upregulate H3K9 acetylation immediately after treatment, where osteogenic medium would be introduced. Although a dose-dependent increase in acetylation was observed after 24 hours treatment, H3K9 acetylation was significantly reduced in the MI192 treated cells compared to the untreated control. Previously it has been reported that MI192 exhibits a >250-fold selectivity for HDAC2/3 when compared to other HDAC isoforms (100). Therefore, within the MI192 pre-treated hBMSCs at this time point, uninhibited HDAC enzymes could still remain and deacetylate the H3K9 site. In addition to acetylation at the histone H3K9 site, histone locations such as H3K14, H3K27 and H4K5, H4K8, H4K12, H4K16 are also involved in the regulating the transcriptional permissiveness of the chromatin (61, 62). Therefore, the acetylation profile at these sites induced by MI192 may differ from the results acquired for H3K9 acetylation in this study, although this would require further investigation. Moreover, having demonstrated the MI192 treatment condition of ≥ 20 μ M for 48 hours significantly enhanced H3K9 acetylation, this likely induced the conformational change in the

chromatin (heterochromatin to euchromatin). The increased transcriptional permissiveness of the chromatin likely enhanced the efficacy of introduced osteogenic growth factors, confirmed from the ALPSA results in this chapter (Fig 4.11).

4.4.2 - The effects of MI192 on hBMSCs osteogenic capacity in 2D culture

Numerous panHDACis have been demonstrated to enhance the osteogenic potential of MSCs in the literature (209, 212). Although showing promise, the use of non-selective HDACis are associated with limitations (213). Therefore, the use of isoform-selective HDACis have garnered increasing interest to stimulate the efficacy of MSCs for tissue engineering applications. Previously it was demonstrated that the HDAC2 and 3 selective inhibitor - MI192 enhanced ADSCs osteogenic capacity when compared to the use of the panHDACi TSA (214). Consequently, in this study, the effects of MI192 on hBMSCs osteogenic capacity was investigated by assessing ALPSA, osteoblast-related gene/protein expression, calcium deposition and mineralisation in 2D *in vitro* culture.

To determine the optimal treatment condition for promoting hBMSCs osteogenic differentiation, the effects of MI192 on hBMSCs ALPSA was evaluated. A pre-treatment strategy was adopted due to the effects of prolonged exposure of MI192 on hBMSCs viability (Fig 4.4 - 4.6) and this approach has been similarly employed in the literature (210, 214). Moreover, it was previously demonstrated that prolonged exposure with MI192 had a detrimental effect on the osteogenic capacity of ADSCs (214). From the results of this present study, pre-treatment with 50 μ M MI192 for 48 hours significantly enhanced ALPSA compared to the other MI192 pre-treatment doses and the untreated controls. A similar stimulation in ALP activity was demonstrated in the literature with TSA and Vorinostat treated hBMSCs (19, 74). Moreover, this replicated studies performed previously, where MI192 pre-treatment of 30 μ M for 48 hours significantly enhanced ALPSA of ADSCs, while these concentrations significantly reduced cell viability (214), similar to this study. These higher “toxic” concentrations required to initiate lineage-specific differentiation may be due to the basal phenotype of the cells, as hBMSCs exhibit reduced osteogenic potential compared to MSCs such as hDPSCs (265, 382); therefore, a greater “push” is required to stimulate hBMSCs osteogenic differentiation. In addition, from the acetylation results, MI192 incubation for 24 hours downregulated H3K9 specific acetylation immediately post HDACi treatment (Fig 4.8), indicating this treatment condition was unable to open the chromatin structure to a sufficient degree to enhance osteogenesis at this time point. This emphasises the importance of chromatin transcriptional permissiveness in controlling MSCs differentiation. MI192 concentrations of ≥ 20 μ M for 48 hours significantly upregulated histone H3K9 acetylation levels prior to the introduction of the osteogenic medium, indicating these concentrations increased the transcriptional permissiveness of the chromatin. This likely enhanced

the accessibility of osteogenic growth factors to their targets of interest, such as the promoter regions of key osteogenic genes. Moreover, this pre-treatment condition might be the dosage/duration necessary to selectively inhibit HDAC3 to a sufficient degree, resulting in the enhanced efficacy of the Runx2 transcription factor. Interestingly, several studies have reported the reduction on HDAC3 expression following HDACi treatment (283, 291), therefore, this may potentiate the effects of MI192 on stimulating hBMSCs osteogenesis after the removal of the pre-treatment medium.

It is well known that MSC properties such as differentiation are affected by the donor in which they are sourced (287, 288). To assess the effects of donor variability and to ensure the increase in ALPSA induced by MI192 was not donor-dependent, the effects of MI192 pre-treatment on hBMSCs ALPSA was analysed in two different donors, shown in the Appendix (Fig A2). From the donors assessed, it was confirmed that MI192 pre-treatment of 50 μ M for 48 hours significantly increased ALPSA when compared to the other MI192 doses (30 and 70 μ M) and the untreated controls. The findings of this study confirm that MI192 stimulation of hBMSCs osteogenic capacity was not donor-dependent, providing greater evidence for the effective use of this HDACi in the clinical setting. Due to the greater fold increase in ALPSA observed in cells acquired from donor 1 and for practicality reason, these cells were utilised to further investigate the effects of MI192 on hBMSCs in this chapter. The capability of MI192 to stimulate hBMSCs osteogenesis from multiple donors were consistent with similar findings acquired with MI192 pre-treated ADSCs (214). The optimised MI192 pre-treatment condition of 50 μ M MI192 for 48 hours was used for the subsequent studies in this chapter.

It has been reported in the literature that HDACis are able to modify gene expression due to their ability to alter epigenetics (209, 212, 285). In order to acquire a deeper understanding into the mechanism in which MI192 enhances hBMSCs osteogenic capacity, the effects of MI192 pre-treatment in stimulating hBMSCs osteoblast-related gene expression and the subsequent downstream protein expression were evaluated by RT-qPCR and ICW, respectively.

The role of Runx2 in osteoblast differentiation was demonstrated by Komori *et al.* (1997), where homozygous and heterozygous Runx2 knockout mice possessed a lack of mineralisation and impaired calvaria osteogenesis, respectively (383). Additionally, it has been shown that this transcription factor mediates the expression of numerous osteogenic genes such as bone sialoprotein, osteopontin, RANKL and OCN (384). In the present study, *RUNX2* mRNA levels were significantly upregulated in the MI192 pre-treated hBMSCs compared to that in the untreated cells throughout the culture period assessed. This correlated with work performed previously with ADSCs, however, expression was only significantly increased in the MI192 pre-treated ADSCs on day 7 and

14 (214). The difference in the stimulation of *RUNX2* expression is likely due to BMSCs exhibiting an increased osteogenic potential compared to ADSCs (318, 319). Relative expression of *RUNX2* peaked in the earlier time point which is expected as a transcription factor. The increased transcriptional permissiveness of the chromatin stimulated by hyperacetylation likely upregulated the expression of this key osteogenic transcription factor upon the introduction of osteoinductive medium. From the ICW results, Runx2 protein expression was significantly enhanced in the MI192 pre-treated cells throughout 28 days culture, consistent with the mRNA expression in this study. Additionally, this correlated with findings acquired from TSA pre-treated hPDLCs in the literature (291). The hyperacetylation induced by HDACis not only affect chromatin conformation but also affects non-histone proteins such as transcription factors. Jeon *et al.* (2006) reported that increased acetylation of Runx2 enhanced its transcriptional activity and stability via protection from Smurf-1 mediated degradation (292). In addition, MI192 possesses selective inhibition against HDAC3, the co-repressor of Runx2 (along with the ZFP521) (144); therefore, MI192 may not only enhance *RUNX2* mRNA levels but also increased its transcriptional activity and stability. Moreover, studies have demonstrated HDACi treatment reduces HDAC expression (283, 291), therefore, reduction in HDAC3 expression in this study may further increase the transcriptional activity of Runx2, although this would require further investigation. The enhanced upregulation of Runx2 gene and protein expression is significant as this transcription factor plays an important role in early and late osteogenesis for enhancing gene expression and osteoblast maturation, respectively (385).

BMP2 is a key osteogenic growth factor known to play a substantial role in stimulating osteogenesis (382, 386, 387). The results from this study showed that MI192 pre-treatment significantly upregulated *BMP2* mRNA levels compared to that in the untreated cells throughout the osteogenic culture period assessed. Additionally, MI192 accelerated the peak expression of *BMP2* compared to the untreated hBMSCs. It was previously reported that MI192 pre-treatment significant upregulated *BMP2* expression within ADSCs after 3 days osteogenic culture alone (214), differing from the expression profile acquired in this study. This may be due to differences in MSCs assessed, with BMSCs shown to possess increased osteogenic capacity compared to ADSCs in the literature (318, 319). Following ICW analysis, BMP2 protein expression was significantly increased in the MI192 pre-treated cells compared to the untreated group throughout 28 days osteogenic culture, correlating with the upregulation observed in the MI192 pre-treated cells at the gene level. The prolonged increase in BMP2 protein expression in the MI192 pre-treated group likely plays a significant role in stimulating the expression of Runx2, as BMP2 binds to cell surface receptors and trigger the SMAD pathways resulting in regulating *RUNX2* gene expression (292, 296).

The mRNA levels of the early osteogenic marker, *ALP*, was significantly upregulated in the MI192 pre-treated cells compared to that in the untreated controls throughout 21 days of osteogenic culture. This enhancement in *ALP* mRNA levels was consistent with studies utilising panHDACis to enhance MSCs osteogenesis (19, 286), in addition to research performed previously with MI192 pre-treated ADSCs (214). The prolonged upregulation in *Runx2* and *BMP2* gene and protein expression observed in the MI192 pre-treated hBMSCs is expected to promote hBMSCs osteogenic capacity, resulting in the enhancement of their downstream targets such as *ALP*, *Col1a* and *OCN* in this study (388, 389). Although studies have also demonstrated the capacity of panHDACis to stimulate *ALP* expression (286), it is probable the upregulation in *ALP* expression observed was heavily dependent on modifications to the chromatin structure, compared to MI192 additional mechanism of enhancing *Runx2* transcriptional activity via selective HDAC3 inhibition. The effects on enhancing *Runx2* transcriptional activity likely resulted in the increased ALPSA induced by MI192 compared to TSA in ADSCs (214). The protein expression of *ALP* was significantly upregulated in the MI192 pre-treated group after 14 days of culture compared to the untreated cells. This correlated with both the enhancement in *ALP* mRNA levels and ALPSA observed in this study.

Following the assessment of early osteogenic markers, the expression of late osteoblast-related genes such as *Col1a* and *OCN* was subsequently analysed. *Col1a* is an important component of the bone extracellular matrix and plays a significant role in providing the mechanical properties of bone tissue (113). The results of this study showed that MI192 pre-treatment significantly enhanced *COL1A* mRNA levels on day 7 and 14 when compared to that in the untreated cells. This demonstrates the upregulation in early osteogenic markers within the MI192 pre-treated cells, stimulated the downstream expression of this mid-late stage osteogenic marker (390), which is a key attribute for bone tissue engineering strategies. *COL1A* upregulation induced by MI192 pre-treatment was similar to findings observed in the literature. Huynh *et al.* (2016) demonstrated an increase in *COL1A* expression in TSA treated hPDLCs (291), while Nab and VPA similarly enhanced *COL1A* expression in ADSCs (286). MI192 pre-treated ADSCs exhibited an increase in *COL1A* mRNA expression compared to osteogenic controls, however only on day 7 (214), which did not reflect the results in this study. A similar enhancement was observed in *Col1a* protein expression in the MI192 pre-treated hBMSCs confirmed via ICW analysis. Peaks in protein expression were observed on day 21, consistent with the expected expression of this mid-late stage osteogenic marker and correlated with the mRNA expression results acquired in this study.

The mRNA levels of *OCN*, a marker associated with osteogenic maturation (113), was significantly upregulated in the MI192 pre-treated cells on day 7 and 14 when compared to that in the untreated

cells. Xu *et al.* (2009) reported similar findings in VPA and NaB treated murine ADSCs (286). However, it was previously reported that MI192 pre-treatment significantly reduced *OCN* gene expression in ADSCs (214), which did not reflect the findings in this study. This is probably due to differences in MSCs type utilised, as BMSCs have been reported to exhibit an enhanced osteogenic potential compared to ADSCs (391, 392). Paino *et al.* (2014) knocked out HDAC2 in hDPSCs, resulting in the downregulation of *OCN* gene expression (209). As MI192 is selective for both HDAC2 and 3, it was found that MI192 pre-treatment stimulated *OCN* gene expression in this study, likely due to MI192 activity in uncoupling the Runx2-HDAC3 complex. The role of HDAC3 in controlling *OCN* transcription has been demonstrated in the literature, where NFAT type c mediates HDAC3 binding to the proximal region of the *OCN* promoter, resulting in hypoacetylation of histone H3 and H4, thereby suppressing osteoblast maturation (142). Moreover, utilising a transient transfection assay, Schroeder *et al.* (2004) reported that HDAC3 suppressed Runx2 mediated activation of the *OCN* promoter region, which reiterates the importance of Runx2-HDAC3 complex (140). *OCN* protein expression was significantly increased in MI192 pre-treated cells compared to the untreated group, correlating with the mRNA expression data. This upregulation in *OCN* protein levels was expected as higher levels of transcriptionally active Runx2 in the MI192 pre-treated cells, would result in enhanced binding to the *OCN* promoter regions (393). The increased expression of these late osteogenic markers in the MI192 pre-treated cells is of particular importance, as it implies that the MI192 pre-treatment condition was sufficient to promote the osteogenic phenotype of hBMSCs throughout osteogenic culture. The sustained enhancement in osteogenesis observed after the removal of the HDACi treatment medium is likely attributed due to the slow binding kinetics of MI192 (100). Moreover, the prolonged enhancement of osteogenic proteins in this study may also indicate the effects of MI192 in down-regulating the expression of HDAC enzymes, particularly HDAC3, as demonstrated in the literature (291). Together, the upregulated expression of key osteoblast-related genes and proteins induced by MI192 pre-treatment indicates the capability of this selective HDACi in promoting the osteogenic phenotype of hBMSCs.

From assessing the expression of osteoblast-related proteins, it was demonstrated that MI192 enhanced the osteogenic phenotype of hBMSCs; however, mineralisation of the newly formed extracellular matrix is a key attribute for the development of functionally relevant bone tissue. Therefore, the effects of MI192 pre-treatment on calcium deposition and mineralisation were evaluated via Alizarin red and Von Kossa staining, respectively. It was demonstrated that MI192 pre-treatment significantly increased calcium deposition within hBMSCs after 28 days of osteoinductive culture compared to the untreated cells. Additionally, more extensive mineralisation was observed in the MI192 pre-treated hBMSCs, where an increased number and size of functional mineral

nodules were detected. Within the MI192 pre-treated group a greater degree of Van Gieson's staining for collagen deposition was situated in the regions of mineral nodule formation, indicating the role the enhanced extracellular collagen deposition in stimulating mineralisation (301-303). The increased deposition of collagens in the MI192 pre-treated group, correlated with the enhanced Col1a protein expression observed following ICW analysis. In the literature, HDACi treatment of MSCs has similarly resulted in enhancing mineralisation. De Boer *et al.* (2006) reported that TSA treatment increased hBMSCs mineralisation (74), while Cho *et al.* (2005) reported similar findings with VPA treated hBMSCs (212). Moreover, results in this study replicated those performed previously on MI192 pre-treated ADSCs (214). The importance of HDAC3 in osteogenic differentiation was demonstrated by Schroeder *et al.* (2004), where HDAC3 was inhibited with siRNA resulting in accelerated mineralisation within MC3T3 preosteoblasts (140). The enhanced mineralisation observed in the MI192 pre-treated hBMSCs, correlated with the upregulated expression of extracellular matrix proteins (ALP, Col1a and OCN) observed in this study, as these proteins are important for stimulating mineralisation (301-303). Together, the enhanced calcium deposition and mineralisation observed in the MI192 pre-treated hBMSCs are key attributes for bone formation, providing greater evidence for the potential use of this epigenetic approach to enhance the efficacy of hBMSCs for bone tissue engineering.

4.4.3 - The effects of MI192 on hBMSCs osteogenic differentiation within the GelMA hydrogel

In the literature, the capacity of HDACis to stimulate MSCs osteogenic capacity in 2D culture has been demonstrated extensively (290, 291), however, limited research has investigated the potential of HDACis to stimulate bone formation in the 3D culture environment. It is well known that 2D culture infers an "artificial" condition which does not replicate the complex 3D microenvironment that occurs *in vivo* (177, 178). Therefore, it is essential to evaluate the effects of MI192 on hBMSCs osteogenic capacity in 3D culture. Numerous studies have demonstrated that high cell density culture systems such as microtissues could be advantageous for bone augmentation strategies, as demonstrated in the previous chapter in this thesis and in the literature (254, 300). Although these approaches possess high potential for bone tissue engineering, the use of microtissues are associated with limitations such as requiring a large number of cells, fabrication is time-consuming/labour intensive and lacking mechanical strength/spatial orientation (253).

Hydrogels have been extensively utilised by researchers' due to their biocompatibility, porosity, water content and the ability to replicate the host tissue environment (327). Due to these favourable attributes, these biomaterials have been investigated for many tissue engineering

applications; however, the lack of mechanical strength has hindered their use for bone tissue engineering (327). Several studies have used gelatin as this material possess a number of desirable properties associated with hydrogels (394, 395). Gelatin is a denatured and partly hydrolysed native collagen, typically type 1, however, due to the denaturing process there is limited antigenicity (396). This material retains several biological sequences such as the natural cell binding motifs, RGD, required for cellular attachment via integrin-mediated adhesion and allows for cell-mediated degradation (362, 363, 397). Moreover, gelatin has been approved by the FDA for food processing and is routinely used as a stabiliser in vaccines and as plasma expanders (398). Modification of gelatin with methacrylic anhydride allows for the crosslinking of this hydrogel and this biomaterial has been investigated for numerous tissue engineering applications (399, 400). This study evaluated utilising GelMA as an alternative delivery system to incorporate cells into the 3D printed PEBT/PBT scaffold, therefore recreating the BMT model at a lower cell density compared to the use of microtissues. Following which it was investigated whether GelMA is capable of supporting MI192 pre-treated hBMSCs osteogenic differentiation within the GelMA hydrogel alone and the GelMA-PEBT/PBT composite construct in this study.

In this study, it was investigated whether GelMA microspheres of regular size and shape could be fabricated to replicate the use of microtissues within the BMT construct. Conventionally hydrogel microspheres have been fabricated using techniques such as droplet extrusion and electro-spray methods (401, 402), however, these techniques produce spheres of suboptimal quality where polydispersity is observed. Polydispersity has implications for cell encapsulation studies as size uniformity supports the controlled diffusion mechanism, vital for supporting cellular maintenance (403). Microfluidic technologies have been increasingly utilised due to advances in knowledge of microscale fluid flow and the enhancements in microfabrication processes (374). Droplet microfluidic techniques have been used for a variety of applications such as for cell and drug delivery, high throughput screening, diagnostic methods and as microreactors (404-406). This microfluidic fabrication process has shown to produce spheres of monodispersity (244). UV light has been extensively utilised due to the effective and convenient application of this crosslinking method (373, 407), however, UV irradiation has shown to have detrimental effects on cell viability and genomic instability (367). Thus, this study investigated the formation of GelMA microspheres of appropriate size/shape created using microfluidics in combination with a visible light photo-crosslinking system.

The findings of this study showed that the GelMA microspheres that were created exhibited a smooth surface morphology and were of similar size with each wt% GelMA (5, 10 and 15 wt%).

This was expected as the emulsion of aqueous droplets in an oil phase relies on surface tension to pull droplets into a spherical shape, consistent with studies in the literature (374, 408). The polymerisation mechanism did not disrupt droplet shape like some extrusion methods such as simple dripping extrusion (409), and the microspheres were completely polymerised within the coil of tubing. Microspheres of regular spherical morphology are important as the formation of irregular microspheres has been shown to create thicker fibrotic tissue, hindering proper nutrient/waste diffusion (410, 411). In this study, it was additionally demonstrated that all GelMA wt% assessed created microspheres of approximately 1000 μM in diameter, the size required for press-fit into the scaffold pore. The uniformity in the size of microspheres created from different wt% GelMA demonstrates the feasibility of using microfluidic approaches to create appropriately sized tissue modules for assembly into the 3D printed PEBT/PBT scaffold.

Using a photocrosslinkable hydrogel is advantageous as it allows for the encapsulation of cells while the macromer is in the liquid form, resulting in accurate cell seeding efficiency and homogenous cell distribution within the hydrogel (368, 412). L929 cells were used in combination with 5 and 10 wt% GelMA and the microfluidics system to optimise the formation of cell-laden microspheres of appropriate size and shape. The 10 wt% GelMA created larger microspheres compared with 5 wt% group, likely due to the effects of porosity on the mechanical properties of the material, where higher porosity results in a lower Young's modulus (413). Celikkin *et al.* (2018) demonstrated that increasing macromer concentration resulted in scaffolds exhibiting enhanced mechanical properties with lower porosity and smaller pores (414). Therefore, the 5 wt% hydrogel formed smaller microspheres due to the reduced stiffness compared to the 10 wt% group, likely due to the increased resistance to the shearing force in the higher wt% GelMA during microsphere formation. Although the stiffness of these hydrogels were not assessed, studies have shown that increasing macromer wt% results in a higher Young's modulus (368, 414). The incorporation of cells reduced the diameter when compared to acellular microspheres. This might be due to the incorporated cells occupying the pores within the hydrogel and forming cellular attachments between the internal scaffold structures. Additionally, the presence of cells reduces the occupation of pores by the medium resulting in a more compact sphere. After 24 hours incubation, both groups swelled although not significantly, still possessing the appropriate size/shape required to incorporate into the 3D printed scaffold.

Live/dead fluorescent labelling was utilised to assess the distribution and viability of cells within the 10 wt% GelMA microspheres. These findings showed that the addition of the L929 cells did not disrupt microsphere formation as they retained the smooth spherical surface, replicating

the morphology of acellular spheres acquired in this study (Fig 4.16). The microfluidic system did not affect the viability of the cells 24 hours post-encapsulation due to the relatively low flow rates used. Numerous studies have employed microfluidic approaches for cell encapsulation and have demonstrated high cell viability with materials such as alginate and PEG (415-417). Studies have looked to enhance the mechanical properties of hydrogels by creating composite materials, resulting in enhanced mechanical reinforcement for load-bearing applications such as bone and cartilage tissue engineering (418, 419). Having determined cell-laden hydrogels could be formed into microspheres of regular size and shape, an automated assembly system created in-house (CReaTE group, University of Otago) was utilised to incorporate these cell-laden GelMA microspheres into the 3D PEGT/PBT scaffold (335). The use of this method allows for the high throughput, scalable and accurate assembly of either microtissues or cell-laden hydrogel microspheres within the pores of a 3D printed scaffold (253, 335), increasing the potential clinical application of these approaches.

Compared to 24 hours post-encapsulation, there was an observable number of dead cells within the cell-laden microspheres after 3 days post-encapsulation. This may be due to the use of the singularisation device which is known to affect the viability of the cells due to microsphere physical or mechanical deformation (333). Incorporation of these microspheres by manual transference could eliminate this potential cause. Several studies using cell-laden hydrogels have demonstrated a decrease in cell viability correlated with increasing macromer concentration (368, 420, 421). Though hydrogels possess a porous interconnected structure which facilitates nutrient/waste diffusion, microspheres of this size ($\varnothing >1000 \mu\text{M}$) may have compromised diffusion which would be directly impacted by the cell density and porosity of the hydrogel (422). Together, these findings validate the use of microfluidics to create cell-laden GelMA microspheres for the assembly within the 3D printed scaffold, demonstrating the feasibility of this approach for incorporating cells at a lower cell density within an external scaffold framework.

Having determined cell-laden GelMA microspheres of regular size and shape could be fabricated as an alternative to microtissues, it is important to evaluate whether the GelMA hydrogel would provide a suitable environment to support MI192 pre-treated hBMSCs osteogenic differentiation. The 5 wt% GelMA was chosen for this study as the higher wt% concentrations have been routinely used for chondrogenic studies, where higher macromer concentrations supported the limited cell-cell contact and the spherical cell morphology replicating native chondrocytes (335). Additionally, higher macromer concentrations have shown to decrease cell

viability in the literature (420, 421) and in this study with L929 cell-laden microspheres. The use of lower macromer concentrations will promote cell migration, growth and cellular contact, which are essential for promoting osteogenesis (414). Moreover, similar GelMA concentrations and seeding density (5×10^6 cell/ml) have been successfully employed in the literature for bone tissue engineering applications (423).

The effects of MI192 pre-treatment on hBMSCs behaviour and osteogenic differentiation within the GelMA hydrogel were investigated in this study. Initially, live/dead fluorescent labelling was utilised to assess the effects of MI192 pre-treatment on hBMSCs behaviour within the GelMA hydrogel. After 24 hours post-encapsulation, CLSM images showed that cells in both groups were uniformly distributed throughout the hydrogel possessing a spherical morphology, indicating thorough crosslinking of the hydrogel. At this time point, cells remained highly viable in both groups, indicating the cross-linking procedure did not adversely affect cell viability. These observations replicated the live/dead visualisation of L929 cell-laden microspheres in this study (Fig 4.18) and in the literature with ADSCs encapsulated within GelMA (369). Following 6 weeks in osteogenic culture, cells in both groups changed from the spherical morphology observed 24 hours post-encapsulation, to a fibroblast-like spread morphology; indicating cells were able to attach, spread and migrate within the hydrogel during culture. This was likely aided by the use of the 5 wt% macromer concentration, which has shown to promote cell migration, growth and cellular contact, essential for promoting osteogenesis (414). This morphological observation replicated live/dead images of MG63 cells encapsulated within GelMA-Hydroxyapatite scaffolds (370). Additionally, the spread/elongated morphology observed resembles the morphology of mature osteogenic cells (209, 264). The MI192 pre-treated cells exhibited a more spread/elongated morphology compared to the untreated cells, replicating numerous studies investigating the effects of HDACis on MSCs (113, 209). This indicates the effects of MI192 in promoting the osteogenic maturation of hBMSCs within the GelMA environment. As with the previous time point, both groups remained highly viable demonstrating this scaffold supports hBMSCs viability over long-term culture.

To date, currently no studies have assessed the effects of HDACis to stimulate MSCs osteogenic differentiation within hydrogel systems. Therefore, to initially assess the effects of MI192 pre-treatment on hBMSCs osteogenic capacity within the GelMA hydrogel, ALPSA levels were quantified after 2 weeks in osteogenic culture. ALP is an early marker of osteogenesis and is involved in extracellular matrix mineralisation (424). The results of this study showed that the MI192 pre-treated hBMSCs exhibited a significantly enhanced ALPSA (~1.3-fold) when compared

to the untreated group. This indicates that the GelMA microenvironment was capable of supporting hBMSCs osteogenesis, similar to the findings reported by Arakawa *et al.* (2014) and Celikkin *et al.* (2018), with BMSCs encapsulated within a photopolymerisable chitosan-collagen and GelMA hydrogel, respectively (414, 425). This enhancement in ALPSA observed within the MI192 pre-treated hBMSCs in GelMA, correlated with a similar increase observed in the monolayer study in this chapter (ALP gene/protein expression and ALPSA (~1.4-fold)) (Fig 4.11-13).

Histological analysis was utilised to evaluate the effects of MI192 pre-treatment on hBMSCs tissue formation within the GelMA hydrogel after 6 weeks osteogenic culture. The findings of this study showed that cells were thoroughly distributed throughout the construct with slightly increased cell numbers at the periphery of the hydrogel. Cell morphology was spherical in shape which did not correlate with the spread morphology observed in the CLSM images, likely attributed to differences in histological and CLSM analysis of the hydrogel. Picrosirius red/Alcian blue staining was utilised to identify the formation of collagens and GAGs, respectively. The results showed both groups displayed strong Picrosirius red staining for collagens throughout the hydrogel, with little evidence of GAGs. The MI192 pre-treated group exhibited substantially enhanced global Picrosirius red staining, indicating MI192 enhanced hBMSCs collagen deposition in the constructs when compared to the untreated cells. This correlated with the Col1a gene and protein expression induced by MI192 within the monolayer study in this chapter (Fig 4.12 and 4.13). The lack of GAG accumulation in both groups indicates this macromer concentration sufficiently supported the differentiation down the osteogenic lineage and not the chondrogenic lineage, where higher wt% GelMA has been used in the literature (426). As with the H&E staining, a greater quantity of cells was observed at the periphery of the constructs. This may be due to the slight shrinkage observed in these constructs during culture/histological processing, resulting in increased density of cells at the periphery. Additionally, the increased exposure to medium at these locations may accelerate the proliferation of these cells compared to those at the core of the construct.

The deposition of hBMSCs osteoblast-related extracellular matrix proteins induced by MI192 pre-treatment within the GelMA hydrogel was investigated via immunohistochemical analysis. After 6 weeks osteogenic culture, ALP was positively expressed in both groups situated within the cellular regions of the construct. The strongest expression was located towards the outer regions of the hydrogel, likely due to the increased number of cells at these sites. These cells may possess the most advanced osteogenic phenotype due to increased exposure to osteogenic

medium and enhanced cell-cell/cell-matrix interactions compared to cells within the core of the hydrogel. The ALP expression intensities between the groups did not correlate with the previously acquired ALPSA results of these cell-laden hydrogels (Fig 4.20), probably attributed to the differences in the time points assessed. Positive expression of Col1a was observed in both groups throughout the hydrogel. The MI192 pre-treated group displayed substantially increased global Col1a protein expression compared to the untreated group, with enhanced expression intensity located towards the periphery. This enhancement in Col1a protein expression induced by MI192, correlated with the increased global Picrosirius red staining observed in the HDACi treated construct (Fig 4.22). Additionally, this correlated with the increased collagen deposition observed within VPA-pre-treated hDPSCs on a collagen scaffold (Gingostat) (209). The protein deposition of OCN was present in both groups; however, expression was substantially enhanced in the MI192 pre-treated group.

The substantial increase observed in the MI192 pre-treated group for these late osteogenic markers (Col1a and OCN) indicates that HDACi pre-treatment is capable of accelerating differentiation of hBMSCs into a mature osteogenic phenotype within this 3D culture environment. Much stronger global expression was observed within the MI192 pre-treated group throughout the hydrogel, not only isolated to cellular regions as observed in the untreated group. This indicates the MI192 pre-treated hBMSCs were able to secrete these extracellular matrix proteins into the surrounding hydrogel environment to a greater degree compared to the untreated cells. The enhanced expression for these key bone extracellular matrix proteins induced by MI192, correlated with a similar increase observed in the monolayer study in this chapter (Fig 4.12 and 4.13), demonstrating this HDACi is capable of enhancing hBMSCs osteogenic protein expression in both 2D and 3D cell culture environments. This increased expression of extracellular matrix proteins likely enhances the mineralisation potential of the MI192 pre-treated cells in this scaffold system (301, 303). Previously it was demonstrated that MI192 pre-treated ADSCs on AM silk scaffolds exhibited increased Col1a protein expression similar to this study, however, expression of OCN was reduced, which did not replicate the findings of this study (214). The differential osteogenic protein expression induced by MI192 was likely due to the differences in the MSCs and 3D scaffolds systems utilised.

The effects of MI192 pre-treatment on hBMSCs calcium deposition and mineralisation within the GelMA hydrogel were assessed via Alizarin red and Von Kossa staining, respectively. After 6 weeks osteogenic culture, the MI192 pre-treated group displayed substantially enhanced calcium deposition compared to the untreated group. The deposition of calcium was primarily

located within the cells in the untreated group, while in the MI192 pre-treated group, calcium deposition was also situated in the extracellular space between the cells. The differential calcium deposition observed between the groups was replicated by Von Kossa staining, where the MI192 pre-treated group exhibited an enhanced formation of functional mineral nodules, consistent with the monolayer findings (Fig 4.14 and 4.15). The increase in calcium deposition and mineralisation observed in the MI192 pre-treated group, replicated the enhanced expression of osteogenic proteins observed from immunohistochemical analysis (Fig 4.24 and Fig 4.25), indicating the role of these extracellular matrix proteins in stimulating hBMSCs mineralisation within GelMA (301, 303). Additionally, the increased mineralisation observed in the MI192 pre-treated group replicated the effects of MI192 on ADSCs cultured within AM silk constructs (214). Moreover, the results of this study correlated with studies performed in the literature, with VPA pre-treated hDPSCs on Gingistat scaffold and TSA pre-treated hDPLCs in PCL/PEG scaffold (209, 320). Together, these results clearly demonstrate that MI192 pre-treatment accelerates the differentiation of hBMSCs into a more advanced osteogenic phenotype within the GelMA hydrogel, resulting in enhanced bone-like tissue formation.

Numerous studies have demonstrated hydrogels are capable of supporting the osteogenic differentiation of MSCs (369, 370), however, their clinical potential is limited due to the inherent lack of mechanical strength for load-bearing tissues. As GelMA has been demonstrated to support the osteogenesis of MI192 pre-treated hBMSCs in this study, a composite construct combining cell-laden GelMA and the 3D printed scaffold was created. Although the fabrication of cell-laden GelMA microspheres of appropriate size and shape was demonstrated in this chapter (during a collaborative research visit at the University of Otago), due to the lack of appropriate microfluidic and microsphere equipment in Leeds, the 3D printed scaffold was cast within the cell-laden hydrogel during cross-linking, providing an alternative method in creating a GelMA-PEBT/PBT composite construct. Employing this method, the effects of MI192 pre-treatment on hBMSCs osteogenic differentiation within the GelMA-PEBT/PBT construct was subsequently assessed.

From the initial histological analysis, the cell-laden hydrogel occupied the entire void volume of the 3D printed scaffold, similar to the observations acquired from BMT created using microtissues in the literature (253). This may be advantageous compared to the fusion demonstrated in chondrocyte-laden GelMA microspheres within a 3D printed scaffold (335), as it may provide enhanced mechanical integrity to the construct which is important for load-bearing tissues. Additionally, this approach guarantees GelMA fusion within the scaffolds, where

incorporated cell-laden microspheres may disassociate from the scaffold prior to the fusion. Moreover, the complete occupation of the 3D printed scaffold void volume with the cell-laden hydrogel would enhance the cellular contact between the construct and the host bone tissue. This increased construct/defect site interaction will likely promote tissue integration. Cells exhibited a spherical morphology and were distributed uniformly throughout the construct in both groups, with a slight increase in the number of cells at the periphery, observations consistent with the GelMA alone study (Fig 4.21). Additionally, the MI192 pre-treated constructs exhibiting increased Eosin stain, which stains proteins non-specifically (343), therefore indicating increased extracellular matrix deposition in the MI192 pre-treated group.

Extracellular collagens were positively expressed in both groups, with the MI192 pre-treated constructs exhibiting increased global staining intensity, correlating with the increased accumulation of Eosin observed from the H&E staining, in addition to the findings from the GelMA alone study (Fig 4.22). The strongest Picrosirius red staining was observed at the periphery of the constructs and at the hydrogel/scaffold interface, likely due to the increased exposure to osteogenic medium in these locations. Due to increased fluid flow stresses and scaffold stiffness at the periphery and the hydrogel/scaffold interface respectively, these factors likely promoted MSC osteogenesis at these locations. An increased quantity of cells were located at the periphery of the construct caused by construct shrinkage, consistent with the H&E analysis, likely contributing to the enhanced collagen expression in these areas. This slight shrinkage in the construct during culture/histological processing replicated similar observations from the GelMA alone study. Picrosirius red staining in the GelMA alone study was much more uniformly expressed compared to GelMA-PEBT/PBT construct, indicating cells within the GelMA alone study possessed a more advanced osteogenic phenotype resulting in increased collagen expression throughout the hydrogel. This may be due to enhanced access to osteogenic medium in the GelMA alone construct. Little evidence of GAG accumulation was observed in both groups, similar to the findings in the GelMA alone study. This suggests the incorporated 3D printed scaffold did not restrict the diffusion of nutrients/waste within the GelMA-PEBT/PBT construct, resulting in successful lineage-specific differentiation of encapsulated hBMSCs.

The expression of osteoblast-related extracellular matrix proteins within the GelMA-PEBT/PBT construct was assessed via immunohistochemical staining. Both groups expressed positive staining for the osteogenic markers assessed (ALP, Col1a and OCN); however, the deposition was substantially enhanced within the MI192 pre-treated group, consistent with the protein expression observed within GelMA alone study (Fig 4.24 and 4.25). The MI192 pre-treated group

exhibited an increased number of ALP-positive cells when compared to the untreated construct, while no difference was observed between the groups in the GelMA alone study (Fig 4.23). This may indicate cells within the GelMA-PEBT/PBT construct possessed a less mature osteogenic phenotype; therefore, the increase in ALP expression, an early osteogenic marker, induced by MI192 was much more prominent in this study, while no difference was observed for this early marker in the GelMA alone constructs at this time point. Within the MI192 pre-treated construct, an increased Col1a expression was located throughout the GelMA-PEBT/PBT construct in both groups, particularly at the hydrogel/scaffold interface, correlating with the Picrosirius red staining in this study and GelMA alone results (Fig 4.24). A greater number of OCN-positive cells were observed in the MI192 pre-treated group, which differed from more uniform OCN expression observed throughout the GelMA alone study (Fig 4.25). This suggests that the cells within the GelMA alone study exhibited a more advanced osteogenic phenotype when compared to the GelMA-PEBT/PBT construct, consistent with similar observations from the Picrosirius red staining and ALP immunostaining between these studies.

The difference in the extent of osteogenic protein expression between these studies may be attributed to the cells increased access to osteogenic growth factors within the GelMA alone constructs. Moreover, the GelMA hydrogel exhibited increased construct shrinkage during osteogenic culture/histological processing when compared to the GelMA-PEBT/PBT construct, where the incorporation of the 3D printed scaffold in the latter restricted this effect. Studies have reported the incorporation of additional biomaterials to create composite constructs results in reducing scaffold shrinkage (427, 428). The reduction in construct size would enhance growth factors exposure to cells and increase cellular interactions in the GelMA alone scaffold, possibly contributing to the differences in the osteogenic protein expression observed in these studies. Pre-culturing cell-laden microspheres prior to combination with the 3D printed scaffold, similar to the pre-culture of microtissues for the BMT, could possibly further enhance hBMSCs expression of these osteogenic proteins, although this would require further investigation. Nonetheless, it is clear that MI192 pre-treatment is capable of stimulating hBMSCs extracellular matrix depositions within the GelMA hydrogel with/without the 3D printed PEPT/PBT scaffold.

In addition to assessing extracellular matrix protein expression within the GelMA-PEBT/PBT construct, the effects of MI192 pre-treatment on hBMSCs calcium deposition and mineralisation was evaluated by Alizarin red and Von Kossa staining, respectively. Both groups expressed strong calcium deposition throughout the construct, with the greatest accumulation situated at the periphery, correlating with the previous staining results in the GelMA-PEBT/PBT study

(histological analysis/immunostaining). Due to the increased access to osteogenic medium and enhanced cell density within these locations, it is likely cells secreted osteoblast-related proteins and deposited calcium at an accelerated rate compared to cells within the core of the GelMA-PEBT/PBT construct. However, following Von Kossa staining for mineralisation, it was observed that the MI192 pre-treated group exhibited an increased quantity of functional mineral nodules, correlating with similar observations from the protein expression analysis of the GelMA-PEBT/PBT construct. Additionally, a similar increase in functional mineral nodule formation was observed within the MI192 pre-treated group in the GelMA alone study (Fig 4.28). This enhanced mineralisation induced by HDACi treatment replicated similar findings acquired previously with MI192 pre-treated ADSCs on AM silk scaffolds (214) and in the literature with TSA pre-treated hDPLCs in PCL/PEG scaffold and VPA pre-treated hDPSCs in a collagen scaffold (209, 320). These findings indicate that MI192 pre-treatment is capable of promoting the differentiation of hBMSCs into a more advanced osteogenic phenotype, resulting in the enhanced expression of key osteoblast-related proteins and increased mineral deposition within the GelMA-PEBT/PBT composite construct.

Together, the work undertaken in this study demonstrated the fabrication of cell-laden GelMA microspheres of appropriate size/shape as an alternative cell delivery vehicle compared to the use of microtissues for assembly within the 3D printed scaffold. MI192 pre-treatment of hBMSCs was shown to enhance ALPSA, osteogenic protein expression and calcium deposition/mineralisation in the GelMA hydrogel, indicating this scaffold system is capable of supporting the osteogenic capacity of MI192 pre-treated hBMSCs, correlating with the effects observed in monolayer. Moreover, MI192 pre-treatment stimulated the osteogenic differentiation of hBMSCs encapsulated with the GelMA hydrogel reinforced with the 3D printed PEBT/PBT scaffold, increasing the potential clinical application of this hydrogel system for bone tissue engineering. These findings demonstrate the potential of combining MI192 pre-treated hBMSCs within a 3D printed scaffold at a much-reduced cell density compared to the use of microtissues, therefore, providing clinicians with greater options in applying this epigenetic-based approach for bone augmentation strategies.

4.4.4 - The effects of MI192 on hBMSCs osteogenic differentiation within the BMT construct

There are several limitations with investigating the effects of HDACi compounds for bone tissue engineering in 2D culture as this does not replicate the complex microenvironment found within the body (429). Therefore, several 3D *in vitro* models have been developed to mimic the *in vivo* environment for tissue engineering applications. Microtissues has been utilised for many years

particularly for cartilage tissue engineering and are associated with enhanced cell-cell and cell-matrix interactions replicating *in vivo*-like conditions (253). Moreover, it has been demonstrated that the high-density environment within the microtissue is advantageous for bone formation (245, 254). However, the use of these tissue modules for the repair of load-bearing tissues is associated with limitations such as their low mechanical properties, lack of spatial orientation and reduced size to repair bone defects (322), therefore, combining these microtissues within a scaffold system will potentially alleviate these issues (253). In the literature, the combination of microtissues with a scaffold system has been investigated for bone augmentation strategies. Pellets created from hUCSCs were combined with an ICBM scaffold and successful osteogenesis was observed; however, as the scaffold possessed random porosity, microtissues were incorporated within the construct irregularly (300). The controlled spatial-temporal placement of cellular components within a scaffold is key in engineering functional bone tissue. The CReaTE group at the University of Otago developed a high-density culture system (BMT model) which incorporated microtissues within the pores of the 3D printed scaffold with regular pore size and shape (253), alleviating issues such as lack of mechanical strength and spatial-temporal control associated with the use of microtissues for bone tissue engineering. Therefore, the aim of this study is to investigate the effects of MI192 pre-treatment on hBMSCs osteogenic differentiation within the BMT model for bone tissue engineering applications.

It has been demonstrated in the literature that microtissue culture accelerates MSCs osteogenesis due to increased cell-cell/cell-matrix interactions that occur due to the high-density culture environment (245, 254). These enhanced interactions likely alter the gene expression profiles within the cells compared to 2D culture. Having reported that MI192 pre-treatment upregulated the mRNA levels of osteoblast-related genes in the monolayer study in this chapter (Fig 4.12), the effects of MI192 pre-treatment on hBMSCs osteoblast-related gene expression within the microtissue was investigated. The mRNA levels of *RUNX2* was increased in the MI192 pre-treated cells on day 7, however, was reduced on day 21 compared to that in the untreated group, with no significance observed between the groups throughout. Expression profiles for *RUNX2* acquired in both monolayer and BMT studies were similar, however, a significant upregulation in expression was observed in the MI192 pre-treated cells in the monolayer study (Fig 4.12), likely due to the differences in the culture systems utilised. It has been demonstrated that osteogenic culture reduces the expression of HDAC enzymes, with HDACi treatment further inhibiting the expression of these proteins (283, 291), indicating enhanced levels of transcriptionally active Runx2 in the MI192 pre-treated cells. Moreover, as microtissue culture has been demonstrated to accelerate osteogenic differentiation compared to 2D culture (321), a greater enhancement

in Runx2 transcriptional activity may occur compared to monolayer culture, due to enhanced down-regulation in HDAC expression induced by accelerated osteogenesis and HDACi treatment. Hence, these factors may result in negative feedback repression of *RUNX2* gene expression in the MI192 pre-treated hBMSCs in this study. The expression of *ALP* was significantly enhanced within the MI192 pre-treated cells on day 14 and 21 compared to that in the untreated group, correlating with the observations in monolayer study and with the increased ALPSA (Fig 4.38) and *ALP* protein deposition (Fig 4.41) in this study. The mRNA expression profiles for *ALP* differed between the monolayer and microtissue culture, where a dose-dependent increase and decrease was observed in these studies, respectively. The differing expression profiles observed possibly indicates the role of microtissue culture in accelerating MSCs osteogenesis compared to 2D culture. The mRNA levels of *BMP2* was significantly elevated in the MI192 pre-treated cells on day 7 and 21 when compared to that in the untreated cells, replicating the time-dependent reduction in expression levels with the other early osteogenic markers assessed in this study. The close correlation in the expression profiles of these early osteogenic genes is likely due to their role in concurrently stimulating the expression of their downstream targets (i.e *BMP2* stimulates Runx2 expression, which promotes *ALP* expression) (296, 430). This increase in *BMP2* mRNA levels replicated a similar enhancement induced by MI192 pre-treatment in the monolayer study in this chapter, in addition to the enhanced *BMP2* protein deposition observed within the BMT construct (Fig 4.42).

Following the evaluation of early osteogenic markers, the expression of later bone markers such as *Col1a* and *OCN* were subsequently assessed. The mRNA levels of *COL1A* was substantially increased within the MI192 pre-treated cells on day 7 compared to that in the untreated group. The MI192 pre-treated group also exhibited a significant enhancement in *OCN* expression on day 7, however, on day 21, expression was significantly reduced in the MI192 pre-treated cells compared to that in the untreated group. The main activator of *OCN* expression is the transcription factor Runx2 (140) and the findings of this study showed a slight increase in Runx2 expression at the early time point (Day 7), although not significant. Therefore, MI192 selective inhibition for HDAC3 possibly plays an important role in increasing the transcriptional activity of Runx2, resulting in the enhanced *OCN* expression observed at the early time point. The upregulation in *COL1A* and *OCN* mRNA levels correlated with similar observations acquired from the monolayer study (Fig 4.12) and the BMT immunostaining (Fig 4.43 and 4.44) in this study. From the assessment of late osteogenic markers, the expression peaks observed were on day 7, further confirming the accelerated expression of osteogenic markers induced within the microtissue culture environment compared to 2D culture, consistent with the observations in

the literature (228, 313). Together, these findings demonstrate that MI192 pre-treatment is capable of enhancing the expression of key osteoblast-related genes in hBMSCs during microtissue culture, indicating the plasticity of MI192 induced osteogenesis in different cell culture environments.

In the literature, it has been reported that HDACis are capable of enhancing MSCs expression of osteogenic proteins in 3D culture environments (209, 214). To initially evaluate the effects of MI192 on hBMSCs osteogenic protein expression within the BMT, ALPSA was quantified after 2 weeks in osteogenic culture. The results of this study showed that ALPSA, an early indicator of osteogenic differentiation, was significantly enhanced in the MI192 pre-treated hBMSCs BMT constructs (2.3-fold) compared to the untreated group, consistent with the *ALP* mRNA expression results acquired in this study. Additionally, the enhanced ALPSA in the MI192 pre-treated BMT, correlated with the findings in the monolayer study in this chapter (Fig 4.11). A greater fold increase in ALPSA induced by MI192 was observed in the BMT (2.3-fold) when compared to the monolayer study (1.4-fold), indicating the role of this high-density culture environment in potentiating the osteogenic capacity of these cells, consistent with reports in the literature (431, 432). In this chapter, it was demonstrated that MI192 pre-treatment significantly increased hBMSCs ALPSA in both the GelMA hydrogel (Fig 4.20) and the BMT model, indicating the efficacy of this HDACi in stimulating the osteogenic capacity of hBMSCs in two different 3D culture environments. Although MI192 pre-treatment stimulated ALPSA of hBMSCs in both models, a greater fold increase was observed in the BMT model compared to the GelMA hydrogel (2.3- vs. 1.3-fold, respectively), emphasising the role of high-density culture in promoting MI192 pre-treated hBMSCs osteogenesis (254), when compared to the lower cell density environment of GelMA.

The high-density culture environment has been demonstrated to enhance MSCs osteogenesis in the literature (228, 245). From the increased osteoblast-related gene expression and ALPSA induced by MI192 in this study, it is expected MI192 pre-treatment would stimulate bone-like tissue formation within the BMT construct. Consequently, histological analysis was utilised to evaluate the effects of MI192 pre-treatment on hBMSCs bone-like tissue formation during BMT *in vitro* culture. After 6 weeks osteogenic culture, histological analysis showed that both untreated and MI192 pre-treated microtissues occupied the entire internal volume of the scaffold pore they were placed within. This resulted in the successful fusion of microtissues in the *x-y-z* planes of the construct to effectively fill the entire internal structure of the 3D printed scaffold, which is important as it enhances the mechanical integrity of the construct. Moreover,

successfully occupying the void volume of the scaffold increases the chances for successful integration of the implanted construct with the host tissue, due to increased cellular contact with the surrounding host bone tissue. These findings replicated studies in the literature where BMT constructs were created by placing HNC and HAC microtissues into the pores of a 3D printed PEBT/PBT scaffold (253, 335). From the H&E staining, the untreated group exhibited areas of dense tissue formation distributed in an aberrant nature, primarily located at the outer regions of the construct and the individual microtissues; while similar dense tissue formation was observed in the MI192 pre-treated group distributed more homogeneously throughout the BMT construct. The differential tissue distribution observed indicates the capability of MI192 pre-treatment to control hBMSCs bone-like tissue formation within the BMT during osteogenic culture. Moreover, a greater degree of tissue organisation was observed in the MI192 pre-treated group. The stratified tissue formations observed throughout the MI192 pre-treated BMT, replicated the types of tissues within the zones of calcification/ossification during late-stage endochondral ossification (39, 344). Therefore, the enhanced dense tissue formation observed within the MI192 pre-treated BMT, indicates increased mineralisation within the HDACi treated group.

Picrosirius red/Alcian blue staining was utilised to investigate the effects of MI192 pre-treatment on hBMSCs collagen and GAG expression within the BMT construct, respectively. Positive Picrosirius red staining was located in areas of aberrant tissue formation in the untreated group, while the MI192 pre-treated group possessed strong expression for collagens distributed uniformly throughout the construct. A similar enhancement on collagen expression was observed in the literature with VPA pre-treated hDPSCs in collagen scaffolds (209) and within the MI192 pre-treated ADSCs in the *AM* silk scaffolds (214). The differential distribution of collagens within the BMT constructs, correlated with the areas of dense tissue formation observed in the H&E staining. Additionally, the MI192 pre-treated BMT displayed an increased quantity of nodule-like formations, which possessed the strongest intensity of collagens. This may indicate enhanced mineralisation, as extracellular collagen deposition is important for stimulating mineral nodule formation (301). The untreated constructs exhibited increased Alcian blue staining for GAG accumulation when compared to the MI192 pre-treated BMT. Within the untreated group, areas of intense GAG expression were observed in tissues which replicate calcified cartilage during endochondral ossification (39, 344). Therefore, indicating the delayed progression from the cartilage to the bone phase of endochondral ossification when compared to the MI192 pre-treated group.

The differential deposition of bone/chondrogenic-related extracellular matrix proteins between these groups are likely attributed to MI192 pre-treatment priming all cells within the BMT to differentiation down the osteogenic lineage. While the untreated cells cultured in the BMT model, a culture system which has been favourable for chondrogenic differentiation (253), may be exposed to multiple competing differentiation signals (osteogenic and chondrogenic). This may not only inhibit differentiation down the osteogenic lineage but may direct differentiation down other mesodermal lineages, such as chondrogenic indicated by the increased GAG accumulation within the untreated group. The size of the microtissues formed ($\sim\varnothing$ 1 mm), may have compromised osteogenic differentiation of cells within the core of these tissue modules due to reduced nutrient/waste diffusion, in addition to the chondrogenic favourable environments provided by high-density culture (253). These observations suggest the capability of MI192 in controlling all hBMSCs lineage-specific differentiation within the construct. Similar observations were observed in previous studies, where MI192 enhanced ADSCs osteogenic lineage-specific differentiation while inhibiting adipogenic differentiation (214). Due to the differential protein expression observed, MI192 pre-treatment may have directed hBMSCs bone formation down the intramembranous ossification route, while tissue formation resembled endochondral ossification the untreated group. Conversely, these results may indicate MI192 pre-treatment accelerated hBMSCs endochondral bone formation compared to the untreated group at this time point, therefore surpassing the cartilaginous template phase of this ossification process (38).

To more accurately identify the deposition of extracellular matrix proteins stimulated by MI192 within the BMT model, immunohistochemical analysis was undertaken. After 6 weeks *in vitro* osteogenic culture, ALP protein expression in the untreated group was located at the edges of individual microtissues and at the outer regions of the entire construct, probably due to its increased access to the osteogenic medium. There were large areas within the core of some microtissues which exhibited negative ALP expression. The MI192 pre-treated group displayed a more homogeneous ALP expression throughout the entire construct, with the strongest intensity situated at the periphery of the construct. This result correlated with a similar enhancement in ALP expression observed in the monolayer study in this chapter (ALPSA (Fig 4.11) and ICW results (Fig 4.13)), in addition to the *ALP* mRNA expression and ALPSA acquired in this study. The differential expression of this osteogenic marker indicates the role of MI192 pre-treatment in promoting and maintaining the osteogenic phenotype of all cells within the construct when compared to the untreated group. Moreover, positive ALP expression was located at the edges of individual microtissues and at the periphery, this may indicate the

reliance of the untreated hBMSC microtissues on osteogenic medium to induced/maintain osteogenic lineage-specific differentiation in this 3D model. The differential ALP protein distribution observed in these constructs, correlated closely with the dense tissue formation observed in the H&E staining. Moreover, the strongest expression for ALP was observed within nodule-like formations within the constructs, which were of increased quantity and uniformly distributed in the MI192 pre-treated group. This likely indicates the enhanced mineralisation within these regions, as ALP protein deposition is an important precursor to extracellular matrix mineralisation (302).

Within the untreated BMT construct, areas of weak BMP2 expression were located towards the edges of the construct and also at the microtissue/scaffold interface. In comparison, BMP2 protein expression was observed throughout the MI192 pre-treated group, at an increased expression intensity compared to the untreated control. The strongest expression intensity was situated in areas that are in close proximity to osteogenic medium (periphery of the construct and microtissue/scaffold interface). The differences in BMP2 protein expression between the groups is of significance as this indicates MI192 is capable of promoting and maintaining the osteogenic phenotype of hBMSCs throughout the construct, even cells located within the core of the construct/microtissues. With positive BMP2 expression within the centre of each microtissue in the MI192 group, this indicates these HDACi-treated cells are committed to differentiate down the osteogenic lineage, without immediate access to osteogenic medium. High-density culture systems are advantageous for bone formation due to increased cellular interactions (245, 300, 321), therefore this emphasises the significance of the enhanced BMP2 expression which acts in an autocrine/paracrine manner within this high-density model to further promote the osteogenic phenotype of hBMSCs (433), correlating with increased ALP immunostaining observed in this study. Therefore, it is likely the increased cellular interactions inferred by this model, further potentiate the efficacy of BMP2 to stimulate hBMSCs osteogenesis. The weak BMP2 expression at the outer regions of the untreated group indicates the dependence of cells on access to osteogenic medium to promote the osteogenic phenotype at these locations. The negative BMP2 expression located in the core of the untreated construct indicates these regions possess a much weaker osteogenic phenotype, correlating with the previous analysis (histological staining and ALP immunostaining). Additionally, the increased global BMP2 expression induced by MI192 pre-treatment was consistent with the findings observed for this marker in the monolayer study (mRNA and ICW analysis) (Fig 4.11 and 4.12) and in this study (mRNA analysis).

Col1a deposition in the untreated group was observed in similar areas of aberrant fibrous tissue formation observed in the Picosirius red/Alcian blue staining and also at the outer regions of the construct. In the MI192 pre-treated group, Col1a protein expression was located throughout the BMT, towards the periphery and also at the core of the individual microtissues. The increase in global Col1a protein expression observed in the MI192 pre-treated group replicated the enhancements in the *COL1A* mRNA expression and Picosirius red staining acquired in this study. Moreover, a similar increase in Col1a protein expression was induced by MI192 pre-treatment of ADSCs cultured within *AM* silk scaffolds (214), in addition to VPA pre-treated hDPSCs within a collagen scaffold (209). The strongest protein expression was located at the periphery of both BMTs, likely attributed to cells at these regions possessing the most mature osteogenic phenotype induced by increased exposure to the osteoinductive medium, replicating the ALP and BMP2 immunostaining in this study. The strongest intensity deposition was observed within nodule-like formations within the constructs. The increased quantity and uniform distribution of these Col1a-positive nodules in the MI192 pre-treated BMT, correlated with the previous histological analysis (H&E and Picosirius red staining) and the ALP immunostaining results in this study. The increased quantity of these ALP/Col1a-positive nodules indicates enhanced mineralisation within the MI192 pre-treated BMT, as extracellular ALP and Col1a deposition are important in stimulating mineral nodule formation (301-303).

Positive OCN deposition was observed throughout the BMT constructs, with the strongest expression located at the periphery, consistent with the previous immunostaining in this study. The positive expression of this marker indicates successful osteogenic maturation of hBMSCs cultured within this model (303), correlating with studies in the literature using high cell density strategies for bone tissue engineering (228, 254). Substantially increased OCN expression intensity was observed in the MI192 pre-treated group, indicating MI192 pre-treatment promoted the differentiation of these hBMSCs, resulting in cells possessing a more mature osteogenic phenotype. Moreover, the MI192 pre-treated group exhibited an increased quantity of OCN-positive nodule-like formations, indicating enhanced mineralisation within the HDACi treated group (303), consistent with the previous immunostaining observations. The extensive enhancement in OCN deposition in the MI192 pre-treated group mirrors the mRNA expression results in this study, in addition to the results acquired in the monolayer study in this chapter (mRNA and ICW analysis (Fig 4.11 and 4.12)). VPA was shown to reduce the OCN expression in hDPSCs with a collagen scaffold (209), likely attributed to the differential isoform selectivity between VPA and MI192. Moreover, MI192 pre-treated ADSCs within the *AM* silk scaffold exhibited reduced expression of OCN compared to the untreated control (214), which did not

correlate with the findings of the present study. The difference in OCN expression is likely attributed to the differential osteogenic potential between these two MSCs (318, 319), in addition to the advantageous properties high-density culture provides in stimulating osteogenic differentiation compared to a lower density 3D model such as silk scaffold.

Together, these findings demonstrate that MI192 pre-treatment is able to enhance hBMSCs expression of key osteoblast-related proteins within the BMT model, replicating enhancements observed in the GelMA study in this chapter. Therefore, this emphasises the plasticity of MI192 to stimulate the expression of key-osteoblast related proteins in two different 3D culture environments. From the osteogenic protein expression observed within these 3D *in vitro* models, it is clear that the high-density culture environment of the BMT model promoted MSCs bone-like tissue formation to a greater degree when compared to the lower density GelMA environment. With the enhanced osteogenic protein deposition stimulated by MI192, this provides an indication into the effects of this HDACi in stimulating hBMSCs mineral deposition within this model, as extracellular matrix deposition is an important precursor for mineralisation (301, 303).

The effects of MI192 on hBMSCs expression of chondrogenic proteins were evaluated due to the chondrogenic favourable conditions known to be induced by microtissue and BMT culture (253, 335), in addition to the increased GAG accumulation observed in the untreated construct in this study. AGG, a key structural proteoglycan found within cartilage tissue (434), was positively expressed throughout the untreated BMT at an increased staining intensity compared to the MI192 pre-treated group. The reduction in AGG expression in the MI192 pre-treated group correlated with the Alcian blue staining for GAG expression (Fig 4.40) observed in this study. Col2a is a key extracellular matrix protein which is the basis of articular and hyaline cartilage (435). The untreated group expressed positive Col2a expression throughout the construct, at a greater intensity compared to the MI192 pre-treated BMT. The increased accumulation of these chondrogenic proteins in the untreated group indicates that MI192 pre-treatment is capable of controlling the lineage-specific differentiation of hBMSCs within this culture model. It was previously demonstrated that MI192 controlled the lineage-specific differentiation of ADSCs by stimulating osteogenic differentiation, while inhibition adipogenic differentiation (214). In the literature, Lee and Im (2017) demonstrated that TSA inhibited the formation of cartilaginous tissue of hBMSCs cultured in chondrogenic pellet conditions (340), similar to the observation of this study. This emphasises the importance of HDAC isoform selectivity in controlling MSCs differentiation in addition to chromatin remodelling effects of these epigenetic compounds. The

increased expression of osteogenic proteins/absence of chondrogenic proteins within the MI192 pre-treated group, indicates bone formation either via intramembranous ossification or a much-accelerated endochondral ossification route when compared to the untreated constructs (39, 344).

The effects of MI192 on hBMSCs calcium deposition and mineralisation within the BMT construct was assessed using Alizarin red and Von Kossa staining respectively, as these are key attributes for functional bone-like tissue. Both BMT constructs exhibited strong Alizarin red staining, indicating enhanced levels of calcium deposition in this model. This was expected as microtissue culture is known to accelerate MSCs mineralisation (321). In both groups, the strongest calcium deposition was situated towards the edges of the construct and at the microtissue/scaffold interface, replicating the location of enhanced protein expression from the immunostaining results in this study. Within the untreated group, areas of weak calcium deposition was observed within the core of some microtissues, correlating with the aberrant tissue formation observed from the H&E staining and immunohistochemical analysis (ALP, Col1a) in this study. The MI192 pre-treated group exhibited an increased quantity of large nodule-like formations throughout the construct, while these were situated towards the outer regions of the microtissues in the untreated group. These nodule-like formations exhibited intense Alizarin red staining, which may indicate the deposition of functional mineral nodules within the BMT, which was evaluated by Von Kossa staining.

Following Von Kossa staining for functional mineral nodules, it was observed that both groups exhibited extensive black staining throughout the construct. Within the untreated construct, nodule formation was primarily located towards the outer regions of the individual microtissues and the entire BMT; however, there were large areas within the core of the construct which lacked mineral nodules. It is likely increased access to osteogenic medium at the outer regions of the construct accelerated the deposition of mineral nodules; while within the microtissues the absence of mineral nodules indicates cells are still in the cartilaginous template phase of endochondral ossification (39, 344). Within the MI192 pre-treated group, functional nodule formation was observed throughout the construct, with almost the entire BMT exhibiting positive Von Kossa staining. These findings indicate the role of this HDACi in enhancing the mineralisation of the more mature extracellular matrix exhibited by the MI192 pre-treated hBMSCs within the construct, replicating the effects of HDACis on mineralisation in the literature (209, 320). Although both groups displayed positive calcium accumulation throughout the BMT, this only correlated with mineral nodule formation in the MI192 pre-treated group.

These mineralisation findings closely correlated with the observations following histological analysis (H&E and Picrosirius red staining) and the immunostaining results (ALP, Col1a and OCN) in this study. The enhanced deposition of bone-related matrix proteins within the MI192 pre-treated group, likely stimulated the increased mineral nodule deposition observed, as extracellular matrix deposition is known to be an important precursor for mineralisation (301, 303). The matrix mineralisation induced by MI192 correlated with the monolayer findings in this chapter (Fig. 4.14 and 4.15) and the effects of MI192 pre-treatment on the mineralisation capacity ADSCs within the *AM* silk scaffold (214). In comparison, a substantially increased mineral nodule deposition was observed in this study, likely attributed to the enhanced osteogenic potential of BMSCs compared to ADSCs (318, 319) and the advantages high-density microtissue culture provides for stimulating mineralisation (245, 248-250).

The findings from the histological/immunohistochemical analysis clearly demonstrate MI192 pre-treatment of hBMSCs is able to promote the deposition of key osteogenic proteins and functional mineral nodules within the BMT construct, not only to cells with immediate access to the osteoinductive medium, as observed in the untreated construct. The untreated group positively expressed the majority of the osteogenic markers assessed; however, the aberrant nature of the tissue formation observed within the construct indicates untreated hBMSCs osteogenesis was heavily dependent on access to the osteogenic medium. The regions of enhanced tissue formation located in the construct were likely induced by proximity to osteogenic medium, indicating that the scaffold fibres within the core of the construct allow for the diffusion of osteogenic factors into the centre of BMT. Without this increased access to the osteogenic medium, it is likely tissue formation within the core of the construct would favour the chondrogenic lineage or due to lack of nutrient exchange, may result in cell death. In addition, the environmental/mechanical stresses exerted to cells at the microtissue/scaffold interface, may have accelerated hBMSCs osteogenic differentiation in these locations, as MSCs interaction with stiffer substrates has been shown to promote MSCs osteogenesis (307, 436).

As with the osteoblast-related extracellular matrix proteins, MI192 substantially enhanced hBMSCs mineralisation within the GelMA hydrogel (GelMA alone and GelMA-PEBT/PBT), however, a greater degree of mineralisation was observed in the BMT study. This is probably attributed to the advantages of high-density culture for accelerating osteogenic differentiation (228, 254). Therefore, from the two 3D scaffold systems evaluated in this chapter, the BMT model would provide the most appropriate platform to evaluate the effects of MI192 pre-treatment on stimulating hBMSCs bone formation *in vivo*.

4.4.5 - The effects of MI192 on hBMSCs BMT *in vivo* bone formation

HDACi therapies for bone tissue engineering have primarily been evaluated *in vitro*; therefore, it is important to further investigate how these potential therapies would behave in a more physiologically relevant environment. In the literature, there have been limited studies investigating the effects of HDACis on stimulating bone formation *in vivo*. Jung *et al.* (2010) reported that NaB and TSA loaded α -calcium scaffolds enhanced bone defect formation within a rat calvarial model (208), while Lee *et al.* (2011) demonstrated Largazole combined with a collagen scaffold enhanced bone formation within a mouse calvarial defect (215). The importance of evaluating the use of HDACis *in vivo* was demonstrated by de Boer *et al.* (2006), where they could not replicate the stimulation of MSCs osteogenic differentiation upon TSA and NaB treatment *in vivo*, which was previously demonstrated *in vitro* (74). Additionally, the *in vivo* studies utilising this epigenetic approach for bone tissue engineering have employed panHDACis, with their associated limitations (213). Therefore, it is essential to determine the effects of MI192 pre-treated hBMSCs bone-like tissue formation *in vivo*. From the 3D *in vitro* studies in this chapter, MI192 pre-treatment was capable of promoting the osteogenic capacity of hBMSCs within the GelMA hydrogel (GelMA alone and GelMA-PEBT/PBT) and the BMT construct. However, it was observed that the BMT model exhibited substantially enhanced bone-like tissue formation when compared to the hydrogel system, likely influenced by the advantages of high-density culture on stimulating osteogenesis (254, 437). Therefore, the BMT system was utilised to investigate the effects of MI192 pre-treatment on hBMSCs bone-like tissue formation *in vivo*.

Several studies have demonstrated the successful use of diffusion chambers to assess bone engineered constructs *in vivo* (257, 258); therefore, this model was employed to evaluate the effects of MI192 in stimulating hBMSCs bone-like tissue formation in a physiologically relevant environment. Untreated and MI192 pre-treated hBMSCs were cultured as microtissues and formed into BMT constructs, following which they were placed into diffusion chambers for intraperitoneal implantation within CD1 mice for 8 weeks. Following extraction, macroscopic evaluation of the constructs was undertaken. The incorporated tissue modules remained within the scaffold framework throughout the *in vivo* implantation period, indicating successful microtissue fusion consistent with the *in vitro* observations in this chapter (Fig 4.39). X-ray analysis demonstrated dense tissue formation within the microtissue regions of the construct. The MI192 pre-treated group possessed strong radio-opacity in each microtissue region, while the untreated BMT exhibited a similar radio-opacity observed in an aberrant nature, primarily towards one face of the construct. These observations from the radio-graphs indicate MI192 pre-treatment enhanced the

dense tissue formation within the BMT construct during *in vivo* implantation when compared to the untreated group, inferring enhanced mineralisation in the HDACi treated BMT.

Histological analysis was undertaken to evaluate the effects of MI192 pre-treatment on hBMSCs *in vivo* bone-like tissue formation within the BMT. Following H&E staining, it was observed that the incorporated microtissues were able to fuse together and occupy the entire internal void volume of the 3D printed scaffold, similar to the *in vitro* findings acquired in this chapter (Fig 4.39) and consistent with findings in the literature (253, 335). The complete occupation of the scaffold void volume by the microtissues is important, as it would provide increased cellular contact with the surrounding host tissue, thus promoting cell migration and enhanced tissue integration. Dense tissue formation was observed towards one face of the untreated construct; however, in the MI192 pre-treated group, similar dense tissue formation was distributed more uniformly throughout the construct towards the edges of the individual microtissues. The dense tissue formation observed within the groups correlated with the radio-opacity observed following X-ray analysis, indicating mineralisation within these regions. Within the *in vitro* BMT study, a similar pattern of aberrant and uniform dense tissue formation was observed in the untreated and MI192 pre-treated groups, respectively (Fig 4.39). However, a greater degree of dense tissue formation was observed in both groups *in vitro* compared to the *in vivo* constructs, probably due to increased access to osteogenic medium.

Picrosirius red/Alcian blue staining was utilised to identify the formation of collagens and GAGs within these BMT constructs following *in vivo* implantation. The untreated group exhibited weak collagen expression throughout the construct, primarily located in the left half of the BMT. In comparison, the MI192 pre-treated group displayed increased Picrosirius red staining distributed more uniformly throughout the construct, with enhanced collagen expression located at the outer regions of each microtissue. The strongest expression for these collagens was situated within the nodule-like formations which were of greater quantity in the MI192 pre-treated group. Additionally, these nodules were located in similar regions of dense tissue formation observed from the H&E analysis, indicating enhanced mineralisation in these regions, as extracellular collagen deposition is important for mineralisation (301). A global increase in GAG accumulation was observed within the untreated group when compared to the MI192 pre-treated construct, with enhanced Alcian blue staining primarily situated towards the right half of the untreated BMT. The side which exhibited the strongest GAG expression also possessed the densest tissue formation observed from the H&E staining. This may indicate the bone formation within the untreated construct is a combination of endochondral ossification (GAG accumulation and dense tissue formation) and intramembranous

ossification (collagen expression); while the MI192 pre-treated group exhibited greater evidence of uniform bone like-tissue formation (either intramembranous or accelerated endochondral ossification) at the time point assessed (38). The differential expression of collagens/GAGs observed between the groups, clearly demonstrates the capability of MI192 to control the lineage-specific differentiation of hBMSCs in the BMT construct during *in vivo* implantation, consistent with the findings in the BMT *in vitro* study in this chapter (Fig 4.40). Untreated BMTs in both the *in vitro* and *in vivo* studies in this chapter, exhibited enhanced GAGs accumulation when compared to the MI192 pre-treated groups. However, GAG expression was much more prominent within the *in vivo* study, likely due to the reduced exposure to the osteoinductive medium. Additionally, the diffusion chamber model is known to create a chondrogenic favourable condition due to the passive diffusion of nutrients/waste and preventing the influence of angiogenesis with the construct. Therefore, the evidence of chondrogenic protein expression observed may be influenced by this *in vivo* model (345, 346). Nonetheless, these results clearly demonstrate that MI192 pre-treatment is able to control and accelerate osteogenic lineage-specific differentiation of hBMSCs within the BMT construct during *in vivo* implantation.

The effects of MI192 pre-treatment on hBMSCs extracellular matrix deposition within the BMT was analysed via immunohistochemical staining. Positive deposition of Col1a was observed in both groups; however, the MI192 pre-treated group exhibited a substantially increased expression intensity for Col1a located within each incorporated microtissue. The differential Col1a protein expression observed between the groups correlated with the Picosirius red staining results, further confirming the role of MI192 pre-treatment in enhancing the osteogenic phenotype of hBMSCs within the BMT *in vivo*, resulting in the increased expression of this key bone extracellular matrix protein (113). The weak Col1a expression in the untreated group following *in vivo* implantation did not correlate with the *in vitro* results (Fig 4.43), indicating the untreated BMT in the *in vitro* study were heavily dependent on access to the osteogenic medium to stimulate the expression of this bone matrix protein. Due to the reduced exposure to osteogenic medium for the *in vivo* constructs, the effects of MI192 on stimulating hBMSCs collagen expression is much more prominent in this study compared to the *in vitro* constructs. The correlating Picosirius red and Col1a expression acquired in this study were consistent with the dense tissue formation observed following H&E staining. This indicates enhanced mineral nodule formation in these areas as extracellular collagen deposition plays a significant role in providing a template for mineralisation to occur (438).

The MI192 pre-treated group exhibited increased OCN expression intensity throughout the construct when compared to the untreated control. This indicates MI192 pre-treatment promoted the

osteogenic maturation of hBMSCs within the BMT during *in vivo* incubation. The greatest expression for OCN was situated in similar regions to the dense tissue formation highlighted by H&E staining and the areas of enhanced Picrosirius red and Col1a expression within the constructs, indicating the role of these extracellular matrix proteins in stimulating hBMSCs mineralisation within this model *in vivo* (301, 303). OCN expression observed in these constructs was at a much-reduced staining intensity compared to the *in vitro* results, which is expected due to the lack of osteogenic inductive culture for the *in vivo* samples. Although OCN expression intensity was much stronger in the BMT constructs *in vitro*, the difference in expression intensity between the groups was similar within the *in vitro* and *in vivo* study. This indicates the ability of MI192 in stimulating the osteogenic maturation of hBMSCs within the BMT model with the lack of osteogenic medium, likely due to MI192 selectivity for the bone-associated HDAC3 isoform (140). This enhanced protein expression for OCN and Col1a correlated with similar observations observed in the *in vitro* study in this chapter (Fig 4.43 and 4.44). Together, these findings demonstrate the capability of MI192 in promoting hBMSCs osteogenic maturation within the BMT construct during *in vivo* implantation.

The effects of MI192 pre-treatment on hBMSCs chondrogenic protein expression was further evaluated due to the increased accumulation of GAGs observed in the untreated constructs (Fig 4.52) and the chondrogenic favourable environment provided by the BMT model and the diffusion chamber system (333, 345, 346). The MI192 pre-treated BMT exhibited little evidence of AGG accumulation, while within the untreated group, strong AGG expression was located throughout the construct. The strongest protein expression was observed in similar areas exhibiting enhanced GAG accumulation. The untreated group also exhibited increased Col2a protein expression distributed throughout the construct, with enhanced intensity situated in similar areas to the increased AGG and GAG accumulation. The differential chondrogenic protein expression acquired between the groups clearly demonstrates that MI192 pre-treatment controlled the lineage-specific differentiation of hBMSCs within the BMT during *in vivo* implantation, consistent with the findings acquired in the *in vitro* study (Fig 4.45 and 4.46). Lee and Im (2017) reported similar observations where TSA inhibited chondrogenic differentiation of BMSC pellets during chondrogenic culture (340). Moreover, the increased expression of these chondrogenic proteins observed within the untreated group provides more substantial evidence into the stage of bone formation within the untreated/MI192 pre-treated BMT at this time point. The increased expression of chondrogenic proteins in the untreated group provides evidence of the cartilaginous template phase of endochondral ossification. While the enhanced expression of osteogenic proteins in the MI192 pre-treated group indicates bone formation via intramembranous or accelerated endochondral ossification (38). To acquire a clearer understanding of whether the differential chondrogenic/osteogenic differentiation observed within

these constructs follow the endochondral ossification route, these constructs should be implanted within a more physiologically relevant pre-clinical model which would allow the influence of other cells types to modulate bone formation. From the differential protein expression observed in the *in vitro* and *in vivo* BMT study, this clearly demonstrates MI192 pre-treatment is capable of controlling lineage-specific differentiation of all hBMSCs within the BMT construct, resulting in the accelerated bone-like tissue formation.

The effects of MI192 pre-treatment on hBMSCs calcium deposition and mineralisation within the BMT following *in vivo* implantation were assessed via Alizarin red and Von Kossa staining respectively, as these are important attributes for the formation of clinically relevant bone tissue. Both groups exhibited strong Alizarin red staining throughout the constructs, indicating successful calcium deposition within this model. The positive accumulation of calcium observed within the BMT constructs was expected as the pellet culture environment is known to stimulate MSCs calcium deposition due to the increased cell-cell/cell-matrix interactions within this high-density environment (228, 321). Within the untreated group, increased calcium deposition was located towards one face of the construct, while within the MI192 pre-treated group, strong calcium deposition was situated at the edges of the individual microtissues. The increased calcium accumulation within these groups replicated the areas of dense tissue formation observed following X-ray analysis and H&E staining. The enhanced calcium deposition observed within the *in vitro* study (Fig 4.48) did not correlate with the findings in this study, likely attributed to the lack of osteogenic inductive culture for the *in vivo* samples.

Following Von Kossa staining, both groups exhibited extensive black staining throughout the constructs indicating the formation of functional mineral nodules. The mineral deposition was situated at the outer regions of the individual microtissues in the MI192 pre-treated group, while mineral nodules were located towards the right face of the untreated construct. The mineral deposition observed within these groups correlated with the regions of increased calcium deposition following Alizarin red staining. In addition, the enhanced mineralisation induced by MI192, correlated with the dense tissue formation observed following H&E staining and the increased osteogenic protein expression observed in this study. The fact that both groups exhibited positive mineral deposition within the BMT indicates microtissue culture was sufficient to induce mineralisation, consistent with findings in the literature (254). It is likely nodule formation was stimulated during osteogenic microtissues culture prior to BMT assembly and was maintained to differing degrees in the untreated and MI192 pre-treated groups during *in vivo* implantation. As with the Alizarin red staining, much-increased mineralisation was observed within the *in vitro* samples

(Fig 4.49) compared to this *in vivo* study, likely due to the prolonged incubation in osteogenic medium. Additionally, in this study, the untreated group possessed mineral nodules even at the core of each microtissue, which was absent in the *in vitro* BMT samples. This likely indicates the role of shear fluid flow of nutrients that occurs within the diffusion chamber in stimulating osteogenic differentiation and maturation, as studies have reported the influence of fluid shear stresses on bone formation (316, 317). Moreover, the increased culture period for the *in vivo* constructs compared to the *in vitro* BMT (8 weeks vs 6 weeks, respectively), may contribute to the observations of mineral deposition within the core of untreated microtissues *in vivo*. The difference in nodule formation between the groups is much greater in this study compared to that observed in the *in vitro* constructs, indicating the untreated hBMSCs were heavily dependent on access to osteogenic medium to promote mineral nodule formation in the *in vitro* study. This correlated with the observations from the osteogenic protein expression acquired between the *in vitro* and *in vivo* BMT constructs. The enhanced mineralisation stimulated by MI192 pre-treatment in this study replicated similar findings in the literature with TSA pre-treated hDPLCs combined with PCL/PEG scaffolds shown to repair mouse calvarial defects (320).

Together, the findings of this study demonstrate that MI192 pre-treatment was capable of promoting the osteogenic capacity of hBMSCs during BMT *in vivo* implantation, resulting in the enhanced formation of bone-like tissue. Moreover, these results clearly showed that MI192 controlled the lineage-specific differentiation of hBMSCs within this model *in vivo*. The majority of *in vivo* studies in the literature have investigated the potential of panHDACis for stimulating bone regeneration (208, 215). To date, Huynh *et al.* (2017) is the only study to demonstrate enhanced bone formation *in vivo* utilising a pre-treatment strategy similar to this study, with TSA pre-treated hDPLCs in PCL/PEG scaffolds repairing mouse calvarial bone defects (320). Therefore, as of writing, currently no studies have investigated the use of HDACis, particularly selective HDACis, to stimulate hBMSCs bone-like tissue formation *in vivo*. The findings of this study support the need for further *in vivo* examination into the potential of this epigenetic approach to stimulating bone repair.

To summarise, the effects of MI192 on hBMSCs behaviour and osteogenic capacity in 2D and 3D *in vitro* and *in vivo* culture was investigated in this chapter. In monolayer culture, it was demonstrated that MI192 caused a time-dose dependent reduction in hBMSCs viability. Additionally, MI192 halted cell cycle progression in the G₂/M phase and altered hBMSCs epigenetic functionality confirmed via HDAC inhibition and increased histone H3K9 acetylation. MI192 pre-treatment enhanced hBMSCs osteogenic capacity in 2D culture confirmed by

increased osteoblast-related gene/protein expression, ALPSA, calcium deposition and mineralisation. Within the 3D culture environment (GelMA hydrogel (GelMA alone and GelMA-PEBT/PBT construct) and BMT model), MI192 pre-treatment stimulated hBMSCs osteoblast-related gene/protein expression, ALPSA, calcium deposition and mineralisation. Bone-like tissue formation induced by MI192 was substantially increased within the BMT construct when compared to the GelMA hydrogel. Following diffusion chamber intraperitoneal implantation within CD1 nude mice, MI192 pre-treatment substantially enhanced hBMSCs expression of osteoblast-related extracellular matrix proteins and increased calcium deposition/mineralisation within the BMT, while inhibiting the expression of chondrogenic proteins within the construct. Together, the findings presented in this chapter demonstrate the potential of utilising this epigenetic approach for enhancing the efficacy of hBMSCs for bone tissue engineering applications.

Chapter 5 - General discussion

In this chapter, the findings of the thesis are collated together and placed into context within the literature. Conclusions from the findings are made, and potential future studies are discussed.

5.1 - General discussion

The aim of the research undertaken within this thesis was to evaluate the potential of a selective HDAC2 and 3 inhibitor - MI192 to enhance the efficacy of clinically relevant MSCs (hDPSCs and hBMSCs) for bone regeneration.

Tissue engineering has been seen as the potential solution to meet the rising clinical demand for bone tissue, although current approaches have garnered limited clinical success. Researchers have looked to enhance the osteogenic capacity of MSCs for bone regeneration via methods such as gene therapy, however, these technologies are associated with safety concerns which hinder their clinical translation (197, 356). Epigenetic regulators such as HDACi compounds have demonstrated the ability to stimulate MSCs differentiation (209, 212), which was extensively discussed in the literature review, therefore providing a possibly safer method of controlling MSCs differentiation compared to gene modifying techniques. The majority of studies in the literature have utilised panHDACis to stimulate MSCs osteogenic capacity, which due to their inhibition of a broad spectrum of HDAC isoforms may result in reduced differentiation efficacy and increased potential side-effects (213). The research undertaken in this thesis builds on the findings in the literature, however with the use of a selective HDACi which has not been extensively investigated for tissue engineering applications. Previously, it was demonstrated the selective HDAC2 & 3 inhibitor - MI192 enhanced the osteogenic capacity of ADSCs when compared to the use of the panHDACi TSA (214). Therefore, in this thesis, the effects of MI192 on stimulating the osteogenic differentiation of other clinically relevant MSCs for bone tissue engineering, such as DPSCs and BMSCs were evaluated. DPSCs have garnered increasing interest in the field due to their ease of procurement with limited donor site morbidity, high proliferation rate and osteogenic potential (168, 209). However, the use of these MSCs are associated with drawbacks such as low procurement yield and lack of consistent isolation/purification methods (439). Additionally, the effects of MI192 on BMSCs was evaluated in this thesis as these MSCs remain the gold standard MSCs source used for bone augmentation strategies, due to their well-characterised properties and proven differentiation down the mesoderm lineages (352). Similar to DPSCs, the use of BMSCs is associated with limitations such as invasive acquisition, low procurement yield and proliferation rate (153). Moreover, in this thesis, the effects of MI192 treatment on MSCs bone formation were investigated within 3D scaffolds systems

in vitro and *in vivo*, where the assessment of HDACi-based therapies in these environments have been lacking in the literature.

To enhance stem cell-based therapies for tissue engineering, stem cell enrichment protocols have been developed to isolate and acquire cells exhibiting the greatest differentiation potential. Although utilised within the tissue engineering field, the removal of these sorting methods maintains cells as minimally manipulated as possible, overcoming increasing regulatory issues regarding the use of cell-based therapies (440). The use of enrichment procedures are influenced by donor variability, as the majority of patients who require bone constructs tend to be older, where it has been reported that stem cell markers expression alters with age (441). Moreover, due to the low yield numbers of BMSC and DPSC progenitors procured from bone marrow aspirates and dental pulp tissues respectively (~0.01 – 0.001%) (153, 222), these enriched cells would require an extensive *in vitro* expansion which is time and cost-intensive. These issues would be further exacerbated with the use of stem cells acquired from older patients, as the quantity and quality of MSCs are known to decrease with age (442, 443). The prolonged expansion required to procure the necessary quantity of cells for clinical use will heavily impact the use of BMSCs due to their reduced proliferation rate compared to DPSCs (444). Although DPSCs exhibits an increased proliferation rate compared to BMSCs (223, 298), the low quantity of cells procured from the pulp tissue is a potential limitation for the clinical application of these cells (445), which would be further exacerbated by enrichment procedures. Additionally, DPSCs lack the specific isolation markers which prevent the accurate and consistent isolation of MSC populations (229, 446). The process of MSCs isolation results in the removal of cells which do not possess self-renewal and multipotency characteristics, however, in the niche environment these cells play a significant role in directing and maintaining MSCs proliferation and differentiation into bone-forming cells *in situ* (447), therefore their removal may be detrimental and further exacerbate the artificial environment provided by *in vitro* culture (177, 178). It has been reported in the literature that extensional and hydrodynamic forces that MSCs are exposed to during FACS, has a negative effect on cellular signalling and differentiation capacity of sorted MSCs (265, 448, 449). Therefore, minimally manipulated primary hDPSCs and hBMSCs were utilised in this thesis. The multipotency of MSCs acquired was confirmed by tri-lineage differentiation shown in the Appendix (Fig A3 & A4). Although the research in this thesis is not directly comparing the effects of MI192 on these MSCs populations, relative comparisons can still be made.

5.1.1 - The effects of MI192 on MSCs general behaviour in 2D culture

The objective of these studies was to evaluate the effects of MI192 on the general behaviour of MSCs during 2D *in vitro* culture. HDAC enzymes are known to target numerous histone and non-histone substrates which are involved in several key cellular processes such as proliferation, differentiation, cell cycle regulation and apoptosis (83, 91). Therefore, it is clear inhibiting the activity of these enzymes will likely dysregulate these cellular functions, which could impact the therapeutic use of HDACis for bone tissue engineering. In these studies, the effects of MI192 on MSCs morphology, viability, HDAC activity, histone acetylation and cell cycle progression were evaluated in the respective MSC chapters.

It was demonstrated that MI192 treatment caused a time-dose dependent decrease in the viability of both MSCs assessed in this thesis (morphology, metabolic activity, DNA content), consistent with the effects of MI192 on ADSCs and panHDACis utilised in the literature (209, 214, 264). As MI192 was shown to halt MSCs cell cycle progression at the G₂/M phase, this likely resulting in MI192 reducing the proliferation capacity of MSCs at lower concentrations and at higher concentrations was cytotoxic. As MI192 has been shown to be cytotoxic at high concentrations and increased exposure periods, it does not disregard the use of this HDACi for cell-based therapies if utilised correctly. This resulted in the adoption of a pre-treatment strategy in this thesis, which minimises the exposure of MI192 on MSCs while allowing further investigation into its effects in stimulating osteogenesis. The utilisation of a pre-treatment strategy was similarly adopted in the literature and in previous studies using MI192 (209, 214, 264).

MSCs have been shown to be highly sensitive to epigenetic modifications (281), indicating the potential efficacy of HDACi compounds for enhancing MSCs for bone augmentation strategies. Therefore, it is important to acquire a deeper understanding of the mechanisms in which these compounds alter MSCs epigenome. In this study, MI192 treatment successfully inhibited the HDAC activity in these MSCs, replicating the effects of this inhibitor on ADSCs, HeLa and PC3 cells (100, 214, 282). It was important to determine the effect of this inhibition on downstream acetylation within these MSCs, as the process of acetylation is associated with enhancing the transcriptional potential of the cell (71). Moreover, the effect of MI192 on MSCs acetylation has not been previously assessed, underlining the importance of this analysis undertaken within this thesis. MI192 treatment for 48 hours enhanced histone H3K9 acetylation levels in both MSCs assessed when compared to their respective untreated control groups, indicating this HDACi successfully altered MSCs epigenetic functionality. Interestingly, histone acetylation was significantly enhanced with MI192 concentrations of $\geq 1 \mu\text{M}$ and $\geq 20 \mu\text{M}$ in hDPSCs and hBMSCs after 48 hours, respectively.

The difference in the concentrations required to significantly alter histone H3K9 acetylation levels is possibly attributed to the variances between these MSCs. It is likely the MI192 concentration thresholds identified to substantially increase histone acetylation, indicates a transcriptionally permissive chromatin (71), therefore highlighting treatment conditions which are capable of augmenting MSCs differentiation.

Several studies have demonstrated that HDACis have the ability to disrupt the cell cycle at various stages (39, 40). It has been reported that HDAC3 inhibition results in cell cycle arrest in the G₂/M phase, due to dysregulation of its non-histone substrate CDK1 which is responsible for regulating G₂/M checkpoint progression (119). As MI192 selectively inhibits HDAC3, it would follow that this HDACi altered the cell cycle progression of both MSCs, with a particular accumulation observed in the G₂/M phase, consistent with the observations acquired for MI192 treated ADSCs (214). These findings replicated numerous studies investigating the effects of HDACi treatment on controlling cell cycle progression (19, 264), where differences in cycle arrest are attributed to the differential HDAC isoforms inhibited. It is likely the enhanced accumulation in this phase is linked to the increased response to DNA damage induced by HDACi treatment (122, 124), preventing the passage through the G₂/M checkpoint, resulting in either sufficient DNA repair (halting proliferation) or insufficient DNA repair (controlled apoptosis). Therefore, within hPSCs, the accumulation in the G₂/M phase is probably due to the effects of this HDACi in halting proliferation rather than inducing apoptosis, as the MI192 concentration utilised (2 µM) exhibited limited cytotoxicity. However, due to the increased MI192 dose utilised for hBMSCs (50 µM), it is likely a greater degree of DNA damage occurred resulting in increased apoptosis, replicating the effects with MI192 treated ADSCs (214). The differential MI192 concentrations utilised between the MSCs was due to the dose required to substantially alter hyperacetylation and ALPSA in the respective MSCs chapter. Future studies should look to fully elucidate the link between cell cycle progression and HDAC inhibition. Additionally, it would be interesting to evaluate the effects of a range of MI192 doses and different time points on MSCs cell cycle progression.

5.1.2 - The effects of MI192 on MSCs osteogenic capacity in 2D culture

The objective of these studies was to investigate the effects of MI192 on MSCs osteogenic capacity in 2D *in vitro* culture. Several panHDACis have been reported to enhance the osteogenic potential of MSCs in the literature (209, 212), however, limited studies have demonstrated the efficacy of selective HDACis in stimulating MSCs osteogenic differentiation (214). Therefore, in these studies, the effects of MI192 pre-treatment on MSCs osteoblast-related gene and protein expression, ALPSA, calcium deposition and mineralisation were analysed in the respective MSC chapters.

Initially, ALPSA levels were quantified to determine the effects of MI192 on the osteogenic capacity of these MSCs. The optimal MI192 pre-treatment conditions identified to significantly enhance ALPSA were 2 and 50 μM for 48 hours in hDPSCs and hBMSCs, respectively. These conditions which promoted MSCs osteogenic capacity correlated with a similar increase in H3K9 acetylation in the respective MSCs, indicating MI192 treatment promoting the transcriptional permissiveness of the chromatin (71), resulting in increased potency of introduced/intrinsic osteogenic factors (38, (291). Additionally, the hyperacetylation induced by MI192 treatment will affect non-histone substrates, such as altering the transcriptional activity of Runx2 (262), therefore resulting in enhancing downstream ALP expression. Moreover, these treatment conditions may be the threshold required to sufficiently inhibit HDAC3, resulting in alleviating Runx2 repression. The difference in the treatment conditions required to increase ALPSA between these MSCs is likely attributed to their underlying phenotypes. It has been reported that hDPSCs possess a greater osteogenic potential compared to hBMSCs (265, 298), therefore, the former requires a lower MI192 dose to stimulate osteogenesis. Previously it was reported that MI192 pre-treatment of 30 μM for 48 hours enhanced ALPSA in ADSCs, further confirming the influence of MSCs osteogenic capacity in determining MI192 pre-treatment condition required to stimulate osteogenesis. In the literature, Paino *et al.* (2014) reported a pre-treatment condition of 1 mM VPA for 48 hours increased osteogenic differentiation of hDPSCs (209), while Cho *et al.* (2005) reported a similar enhancement in hBMSCs and hADSCs osteogenic capacity following VPA pre-treatment condition of 1 mM for 96 hours (212), correlating with the observations made above. To thoroughly assess this, a donor-matched comparison study utilising MI192 or other HDACis on appropriate MSCs would be the most appropriate approach.

Although MSCs were not acquired from the same patient, ALPSA was significantly higher in the hDPSCs when compared hBMSCs in basal conditions, indicating hDPSCs exhibited an increased osteogenic phenotype, consistent with observations in the literature (265, 298). Moreover, it was observed that the MI192 pre-treatment conditions optimised in the respective MSC chapters, enhanced hDPSCs ALPSA to a greater degree (2.2-fold, 2 μM for 48 hours) when compared to the that in hBMSCs (1.4-fold, 50 μM for 48 hours). This indicates MSCs osteogenic capacity influences the efficacy of osteogenic stimulation induced by MI192. The optimised pre-treatment conditions were confirmed to similarly stimulate ALPSA of MSCs acquired from different donors in this thesis. It is worth noting the age and sex of the donors acquired is not representative of all possible donors in the clinical setting, therefore it would be interesting to assess the effects of MI192 on a broader range of donors. The optimised pre-treatment conditions (2 and 50 μM for 48 hours in hDPSCs and hBMSCs, respectively) was utilised for the rest of the respective MSCs chapters.

Following optimisation of the treatment condition, the effects of MI192 pre-treatment on the osteoblast-related gene and protein expression were assessed in these MSCs. It was determined that MI192 pre-treatment upregulated the expression of osteoblast-related genes (*RUNX2*, *ALP*, *BMP2*, *COL1A* and *OCN*) when compared to the untreated group in both hDPSCs and hBMSCs chapters; although differences in the expression profiles were observed particularly for the early markers (*RUNX2*, *ALP* and *BMP2*), likely attributed to the phenotypic differences between these MSCs. For these early markers, a greater degree of enhancement was observed in the hBMSCs upon MI192 pre-treatment when compared to hDPSCs. This may be indicative of the mechanisms in which MI192 stimulates the early phase of osteogenesis in these MSCs, by either enhancing the transcriptional permissiveness of the chromatin (increasing gene expression) and/or by inhibiting HDAC3 repression of Runx2 (enhancing Runx2 transcriptional activity). With hDPSCs possessing an increased osteogenic potential compared to hBMSCs (265, 298), these cells likely express higher levels of intrinsic osteogenic factors such as Runx2 in basal conditions; therefore, MI192 inhibition of HDAC3 results in increasing the transcriptional activity of Runx2 in hDPSCs, negatively repressing Runx2 gene expression. As hBMSCs exhibit a weaker osteogenic capacity compared to hDPSCs (265, 298), these cells must first rely on the chromatin conformation effect induced by HDACis to enhance the mRNA levels of early osteogenic markers. Once hBMSCs possess sufficient levels of early markers such as Runx2, the mechanism of alleviating HDAC3 repression of Runx2 comes into effect. Therefore, the differences in expression profiles observed for the early markers in these MSCs may be indicative of which mechanism of action MI192 most effectively stimulates early phase osteogenesis. Additionally, as MI192 was shown to stimulate hDPSCs H3K9 acetylation to an enhanced degree compared hBMSCs, it is probable that the increased hyperacetylation enhanced the transcriptional activity of Runx2 compared to that in hBMSCs, therefore influencing the *RUNX2* mRNA expression profile observed between these MSCs. It would be interesting to assess the effects of MI192 pre-treatment on the acetylation of Runx2 in these MSCs, as this would provide superior mechanistic knowledge on how MI192 enhances MSCs osteogenic capacity.

It was previously demonstrated that MI192 pre-treatment stimulated ADSCs osteoblast-related gene expression similar to the findings presented in this thesis, however, *OCN* expression was down-regulated within the MI192 pre-treated ADSCs, which did not correlate with the results in this thesis (214). It is likely the MSCs utilised (hDPSCS and hBMSCs) exhibits a greater osteogenic potential compared to ADSCs (298, 318, 319), therefore MI192 is capable of potentiating the maturation of these MSCs into a more mature osteogenic phenotype compared to ADSCs. Moreover, ADSCs utilised in the previous studies were sorted with stem cell markers, which has been demonstrated in the literature to have a negative effect on MSCs differentiation capacity (265, 449). ICW confirmed

MI192 pre-treatment increased the protein expression of key osteogenic markers within both MSCs, indicating the upregulation in gene expression successfully translated into enhanced production of osteogenic proteins. These findings replicated work in the literature with panHDACis and with MI192 pre-treated ADSCs on MSCs osteogenic gene and protein expression (209, 214).

From the findings in both MSCs chapters, this has provided insights into the potential mechanism of action in which MI192 stimulates osteogenic differentiation. It was demonstrated that a pre-treatment condition was capable of stimulating these MSCs long-term osteogenic capacity after the removal of the compound. This is likely due to MI192 histone and non-histone related effects. Previously it was shown that MI192 possess slow binding kinetics compared to conventional panHDACis (100), therefore the enhanced binding likely influenced the prolonged effects observed in altering chromatin remodelling. Additionally, studies have reported that HDAC inhibition causes a downregulation in the expression of HDAC enzymes, therefore potentially resulting in a more transcriptionally permissive chromatin throughout osteogenic differentiation. The effects of MI192 on non-histone proteins possibly plays a key role in stimulating MSCs osteogenesis. The selective inhibition of HDAC3 would alleviate its repression of the Runx2 transcription factor, therefore increasing its transcriptional activity. Future studies could look to utilise the FRET assay to determine the effects of MI192 in uncoupling HDAC3-Runx2 complex within these MSCs. Additionally, the hyperacetylation induced by inhibiting HDAC enzymes have been reported to enhance the transcriptional activity and stability of Runx2 and prevents its smurf1-mediated degradation. The hyperacetylation observed following the pre-treatment conditions likely resulted in enhanced Runx2 activity and stability, however future work assessing the acetylation state of Runx2 following MI192 pre-treatment and during osteogenic culture would provide greater insights into this HDACis mechanism of action.

In terms of the effects of MI192 on the MSCs assessed, there is increasing evidence which suggests the cells inherent basal phenotype and osteogenic potential affects the use of MI192 to stimulate their osteogenic differentiation. The pre-treatment conditions optimised in this thesis and previously in our group have demonstrated the dose required to stimulate the osteogenic capacity of MSCs is heavily dependent on their osteogenic potential, with a lower MI192 concentration required to stimulate DPSCs ALPSA compared to that used for ADSCs and BMSCs (2 μ M: DPSCs, 50 μ M: BMSCs and 30 μ M: ADSCs) (214).

In this thesis, it was observed that MI192 pre-treatment enhanced MSCs calcium deposition and mineralisation, correlating with the increased osteogenic protein expression induced by MI192 pre-treatment in both MSCs. Additionally, these results were consistent with the effects of MI192 pre-

treatment on ADSCs mineralisation, and also with panHDACis utilised in the literature (19, 214, 286). These findings are of great importance as calcium deposition and mineralisation are key attributes for the development of functional bone constructs. It would be interesting to assess the effects of MI192 pre-treatment on MSCs mineralisation during the osteogenic culture period assessed. Together, the findings from these studies clearly demonstrate that MI192 is capable of stimulating MSCs differentiation into a more mature osteogenic phenotype. Importantly, when put in a clinical context, these findings demonstrate the capability of this selective HDACi in promoting the osteogenic capacity of MSCs acquired from three different sources, providing clinicians with broader options for employing this epigenetic-based approach to repair patient-specific bone defects.

5.1.3 - The effects of MI192 on MSCs osteogenic capacity in 3D culture

The objective of these studies was to investigate the effects of MI192 pre-treatment on the osteogenic capacity of MSCs within different 3D *in vitro* culture systems. In the literature, limited studies have investigated the effects of HDACi treated MSCs osteogenic differentiation within 3D scaffold systems (209, 320). This has resulted in the lack of knowledge on how these HDACi treated MSCs behave in a more physiologically relevant environment compared to the greater “artificial” environment provided by 2D culture (177). The importance in validating HDACi-based therapies in 3D *in vitro* culture was demonstrated by de Boer *et al.* (2006), where the effects of NaB and TSA on stimulating hBMSCs osteogenesis within a calcium phosphate scaffold were assessed *in vivo* (74). The findings of this study were inconclusive and differed from results acquired following 2D *in vitro* assessment with these HDACis (74, 113, 212), emphasising the importance of evaluating MI192 treatment within 3D *in vitro* culture as a pre-clinical validation step. Advances in material science have provided biomaterials which are capable of providing a framework to help bridge the defect space and facilitate bone regeneration. Additionally, as 3D scaffolds are known to possess their own inherent advantages/disadvantages for bone tissue engineering, it is important to determine the effects of MI192 pre-treated MSCs osteogenic differentiation in different scaffold systems, providing clinicians with greater options to apply this epigenetic-based approach to repair bone defects. Therefore, the effects of MI192 pre-treatment on hDPSCs and hBMSCs osteogenic differentiation in different 3D *in vitro* models were evaluated (hDPSCs within silk scaffold and BMT model, hBMSCs within GelMA hydrogel and BMT model). Within the respective scaffold systems, the effects of MI192 pre-treatment on MSCs osteogenesis were assessed via ALPSA, osteoblast-related gene expression, extracellular matrix expression and calcium deposition/mineralisation.

Initially, MI192 pre-treated hDPSCs were combined with lyophilised *BM* silk sponges due to their well-established properties and proven potential for tissue engineering applications in the literature

(169, 237). The results of this study showed that increasing silk concentration enhanced scaffold compressive modulus while decreasing swelling and degradation rate. Silk concentration played a significant role in enhancing the osteogenic capacity of both untreated and MI192 pre-treated hDPSCs confirmed by ALPSA. MI192 pre-treatment increased hDPSCs ALPSA ~2-fold compared to the untreated cells in both 2 wt% and 5 wt% scaffolds, however, ALPSA was substantially increased in the 5 wt% scaffolds compared to the respective cells within the lower wt% group. Utilising the higher wt% silk sponge, it was observed that the MI192 pre-treated hDPSCs exhibited increased osteoblast-related gene expression (*RUNX2*, *ALP*, *BMP2*, *COL1A* and *OCN*), extracellular matrix protein deposition (*ALP*, *COL1A* and *OCN*) and calcium deposition/mineralisation within these constructs, replicating the monolayer findings and work performed with MI192 pre-treated ADSCs on AM silk scaffolds (214). Paino *et al.* (2014) reported a similar enhancement in VPA pre-treated hDPSCs within collagen scaffolds, although a reduction in *OCN* expression was observed in that study (209), emphasising the importance of HDACi selectivity on controlling MSCs differentiation. Future studies should investigate MI192 pre-treated cell-laden silk constructs *in vivo*.

It has been demonstrated in the literature that high-density environments are highly advantageous for MSCs osteogenesis (228, 254). Culturing cells as microtissues holds great clinical potential, however, due to their inherent lack of mechanical strength and spatial orientation to repair bone defects, limits their translational potential. Due to advances in additive manufacturing and biofabrication techniques in recent years, this has allowed for the reproducible creation of biologically functional products, which combine the structural organization of living cells, biomaterials, or hybrid cell-material constructs, through bioprinting or bioassembly (243), resulting in closer biomimicry of the *in vivo* environment (244). The assembly of microtissues within a 3D printed PEGT/PBT scaffold (BMT model) was utilised to overcome issues regarding the use of cell aggregates for bone repair (253). The BMT model allowed for the investigation into the effects of MI192 on hDPSCs osteogenesis in a high-density 3D culture system. The MI192 pre-treated hDPSCs exhibited a substantially increased osteogenic gene expression (*RUNX2*, *ALP*, *BMP2*, *COL1A* and *OCN*) and ALPSA within the BMT construct compared to the untreated group. Moreover, within the BMT constructs, a greater deposition of osteogenic extracellular matrix proteins (*ALP*, *COL1A* and *OCN*) and functional mineral nodules were observed in the MI192 pre-treated hDPSCs, consistent with the monolayer results. Although these studies evaluating the effects of MI192 on hDPSCs osteogenesis within silk and the BMT model were not carried out at the same time, therefore not a direct comparison between these 3D culture systems, the conclusions from these studies are clear. The marked enhancement in the MI192 pre-treated hDPSCs bone-like tissue formation within the BMT

model compared to the silk scaffold is likely promoted by the high-density culture environment, which has shown to promote MSCs osteogenic differentiation in the literature (228, 254).

High-density culture systems seemed favourable for enhancing the osteogenic capacity of HDACi treated BMSCs; however, this approach requires a high quantity of cells which is a potential limiting factor for translation, particularly regarding the slow proliferation rate associated with BMSCs (153). Due to these issues, the potential of using a hydrogel system as an alternative cell delivery vehicle to combine HDACi treated hBMSCs at a lower cell density with a 3D printed scaffold was evaluated. The combination of GelMA with a 3D printed scaffold will enhance the clinical feasibility of hydrogel systems for the repair of bone defects, due to their inherent lack of mechanical strength. The findings of this study demonstrated the creation of cell-laden GelMA microspheres of appropriate size and shape to replace the use of microtissues within the BMT construct; therefore, demonstrating the feasibility of utilising a hydrogel system as an alternative delivery vehicle to incorporate cells within a 3D printed scaffold. MI192 pre-treatment promoted hBMSCs ALPSA, osteogenic extracellular matrix proteins (ALP, COL1A and OCN) and calcium deposition/mineralisation within the GelMA hydrogel, consistent with the enhancement observed in monolayer. Similarly, MI192 pre-treatment promoted the osteogenic capacity (osteogenic extracellular matrix proteins and mineralisation) of hBMSCs encapsulated within the GelMA hydrogel reinforced with the 3D printed PEBT/PBT scaffold, enhancing the potential clinical application of GelMA for bone tissue engineering. These findings demonstrate the potential of combining MI192 pre-treated hBMSCs within a 3D printed scaffold at a much-reduced cell density compared to the use of microtissues; therefore, providing clinicians with greater options in applying this epigenetic-based approach for bone augmentation strategies. Future studies should investigate the assembly of MI192 pre-treated cell-laden microspheres into the 3D printed PEGT/PBT scaffold, as this will create closer comparisons to the BMT construct. Additionally, the effects of MI192 pre-treatment on hBMSCs bone-like tissue formation within the GelMA hydrogel should be assessed in the *in vivo* environment.

The effects of MI192 pre-treatment on hBMSCs osteogenic differentiation were additionally evaluated within the BMT model, due to the substantial enhancement in bone-like tissue formation observed in the hDPSCs BMT study. MI192 pre-treatment substantially enhanced hBMSCs ALPSA, osteoblast-related gene expression (*RUNX2*, *ALP*, *BMP2*, *COL1A* and *OCN*), protein expression (ALP, BMP2, COL1A and OCN) and calcium deposition/mineralisation when compared to the untreated BMT. This increase in bone-like tissue formation induced by MI192 replicated the findings from the hDPSCs BMT study, although a greater degree of enhancement induced by MI192 was observed in

the hBMSC constructs. This is likely due to DPSCs exhibiting an increased osteogenic phenotype and differentiation capacity when compared to BMSCs (298); therefore, the effects of MI192 on stimulating osteogenesis are more prominent in the hBMSCs study. Moreover, in this study MI192 inhibited the expression of chondrogenic proteins in the hBMSC BMTs compared to untreated constructs, indicating the capability of this HDACi in controlling the lineage-specific differentiation of MSCs in this culture system. This is likely due to MI192 selective inhibition of the bone-associated HDAC3 isoform (140). This correlated with work in the literature, where TSA inhibited the chondrogenic differentiation of MSCs during chondrogenic pellet culture (340, 450). A greater expression of GAGs was observed in the untreated hBMSCs BMT compared to the untreated hDPSCs BMT construct, likely attributed to the increased osteogenic/decreased chondrogenic potential DPSCs possesses compared to BMSCs (298). From the two 3D *in vitro* models utilised to assess MI192 pre-treated hBMSCs osteogenesis, it is clear that the BMT model substantially increased the formation of bone-like tissue of MI192 pre-treated hBMSCs compared to the GelMA hydrogel, consistent with reports demonstrating the accelerated MSCs osteogenesis within high-density environments (245). These findings correlated with those acquired in the hDPSCs chapter in this thesis, further confirming the effective use of the BMT model in combination with MI192 pre-treated MSCs to form more mature bone-like tissue. Although a limitation of this model is the high cell numbers required, as minimally manipulated primary MSCs were utilised in this thesis, this increases the number of cells, therefore enhancing the feasibility of utilising the BMT in combination with MI192 pre-treated MSCs to create function bone-like tissue.

Together, the findings of these studies demonstrate that MI192 pre-treatment is capable of stimulating MSCs osteogenic differentiation within different 3D systems (silk scaffold, GelMA hydrogel and BMT model) resulting in the enhanced formation of bone-like tissue, consistent with findings in the literature (209, 214). Additionally, these results correlated with the enhancement in MSCs osteogenic capacity observed in the monolayer studies in this thesis. MI192 pre-treated hDPSCs and hBMSCs exhibited increased osteogenic differentiation within the respective scaffold systems assessed, however a greater degree of bone-like tissue formation was observed in the BMT model. The evaluation into the efficacy of MI192 to stimulate MSCs osteogenesis in 3D culture systems is an important pre-clinical validation step that has been limited in the literature. These findings build on the only study as of writing to assess the efficacy of selective HDACis for bone tissue engineering (214). Moreover, having demonstrated the plasticity of MI192 pre-treatment in stimulating MSCs osteogenic capacity in different scaffold environments, this provides clinicians with greater options in applying this epigenetic-based approach depending on patient-specific characteristics (i.e. tissue source availability, patient age, size and defect location etc). Therefore, the

research undertaken within these 3D *in vitro* studies provides greater evidence into the potential efficacy of this epigenetic-based strategy on stimulating MSCs bone formation in the clinical setting.

5.1.4 - The effects of MI192 on MSCs bone formation *in vivo*

It is important to evaluate the effectiveness of HDACi-based therapies in promoting the osteogenic capacity of MSCs in physiologically relevant conditions, as this provides superior evidence of its potential efficacy in the clinical setting. In the literature, limited studies have investigated the efficacy of HDACi-based therapies to stimulate MSCs osteogenesis *in vivo* (74, 320), with those studies using panHDACis. Therefore, it was essential to evaluate the capability of MI192 in stimulating MSCs bone-like tissue formation in physiologically relevant conditions. From the *in vitro* studies in this thesis, MI192 pre-treatment substantially increased the osteogenic capacity of hDPSCs and hBMSCs in the respective scaffold systems investigated; however, it was clear that the BMT model accelerated bone-like tissue formation when compared to the lower cell density 3D systems assessed. Therefore, the BMT model was employed to further investigate the effects of MI192 pre-treatment on promoting MSCs bone-like tissue formation *in vivo* using the diffusion chamber model.

The findings from the *in vivo* studies showed that MI192 pre-treatment substantially increased bone-like tissue formation of both hDPSCs and hBMSCs BMT constructs, where a substantial increase in extracellular matrix deposition and calcium deposition/mineralisation was observed in the MI192 pre-treated constructs, consistent with the findings acquired in the BMT *in vitro* studies in the respective MSC chapters. In comparison, the MI192 pre-treated hDPSCs BMTs exhibited more extensive mineralisation when compared to MI192 pre-treated hBMSCs constructs, likely attributed to DPSCs possessing an advanced osteogenic phenotype when compared to BMSCs (298), therefore less reliant on osteogenic induction culture. Additionally, it is important to note that the DPSC BMT constructs possessed twice the quantity of cells compared to the BMSCs BMTs. This increased cell density may play a significant role in promoting the osteogenic capacity of MI192 pre-treated hDPSCs *in vivo* with the lack of osteogenic induction culture when compared to the hBMSCs constructs (251, 252). When comparing the bone-like tissue formation induced by MI192 pre-treatment within the BMT construct *in vitro* and *in vivo*, a greater degree of enhancement was observed compared to the respective untreated controls within the *in vivo* constructs. This indicates the untreated MSCs within this model were heavily reliant on osteoinductive medium to stimulate bone-like tissue formation *in vitro*, resulting in the greater disparity in the bone-like tissue formation observed between the groups in the *in vivo* studies. This clearly indicates that MI192 pre-treatment is able to stimulate the osteogenic phenotype of MSCs in this model *in vivo*, likely due to MI192 selectivity for the bone-associated isoform HDAC3 (100, 113). These findings provide more

substantial evidence into the potential efficacy of this epigenetic-based approach in stimulating bone-like tissue formation in the clinical setting.

The effects of MI192 on MSCs chondrogenic protein expression during BMT *in vivo* implantation was assessed, due to the favourable conditions exerted by the BMT model for chondrogenic differentiation (253, 335). From the results of these studies, the untreated constructs in both MSCs chapters expressed increased chondrogenic proteins (GAGs, AGG and Col2a) when compared to the MI192 pre-treated group, indicating the capability of MI192 pre-treatment in controlling the lineage-specific differentiation of MSCs during BMT *in vivo* implantation. This is likely due to MI192 selective inhibition of the bone-associated isoform HDAC3 (140). This differential expression of osteogenic/chondrogenic proteins in the untreated and MI192 pre-treated groups in both MSCs may indicate the route of bone formation within this model (endochondral or intramembranous ossification). Future *in vivo* studies within more physiologically relevant pre-clinical models should assess the effects of MI192 pre-treatment on bone like-tissue formation at several time points such as 4 and 8 weeks, as this would provide a better understanding of the effects of MI192 on MSCs bone formation. The effect of MI192 treatment inhibiting MSCs chondrogenic protein expression within the BMT constructs correlated with similar findings observed in the *in vitro* studies in this thesis and in the literature where TSA inhibited the chondrogenic differentiation of MSCs (340, 450). This further emphasises the importance of HDAC isoform selectivity, in addition to the chromatin remodelling capabilities of HDACi compounds in directing lineage-specific differentiation of MSCs.

Together, the findings of these studies demonstrate the potential of using this epigenetic-based approach to stimulate the osteogenic capacity of clinically relevant MSCs within the BMT model *in vivo*, resulting in the enhanced formation of bone-like tissue. Currently to date, no studies have investigated the use of selective HDACis on enhancing MSCs bone-like tissue formation *in vivo*. Therefore, these findings support the need for further *in vivo* examination into the potential of this epigenetic-based approach to stimulating bone repair.

Summary

The aim of this thesis was to investigate the effects of a selective HDAC2 and 3 inhibitor - MI192 on the behaviour and osteogenic capacity of clinically relevant MSCs (hDPSCs and hBMSCs) as a novel therapeutic approach for bone repair. The effects of MI192 on the general properties of MSCs such as morphology, viability, HDAC activity, H3K9 histone acetylation and cell cycle were evaluated. Following this, the effects of MI192 on MSCs osteogenic differentiation were assessed via ALPSA, osteoblast-related gene/protein expression, calcium deposition and mineralisation. These were investigated in both 2D and 3D *in vitro* culture environments (hDPSCs: silk scaffold and BMT model, hBMSCs: GelMA hydrogel and BMT model). Finally, the effects of MI192 on MSCs bone formation were evaluated in a physiologically relevant *in vivo* model (diffusion chamber).

Summary of key findings:

– 2D *in vitro* culture

- MI192 treatment induced a time-dose dependent reduction in MSCs viability.
- MI192 halted MSCs cell cycle progression, particularly in the G₂/M phase.
- MI192 treatment inhibited MSCs HDAC activity.
- MI192 enhanced MSCs histone H3K9 hyperacetylation.
- MI192 pre-treatment enhanced the ALPSA of MSCs.
- MI192 pre-treatment upregulated MSCs mRNA expression of key osteoblast-related genes (*RUNX2*, *ALP*, *BMP2*, *COL1A* and *OCN*).
- MI192 pre-treatment increased MSCs expression of key osteoblast-related proteins (Runx2, ALP, BMP2, COL1A and OCN).
- MI192 pre-treatment enhanced MSCs mineralisation, increasing calcium deposition and mineral nodule formation.

– 3D *in vitro* culture

- Increasing silk concentration enhanced scaffold compressive modulus, while decreased swelling and degradation rate.
- MI192 pre-treated hDPSCs exhibited enhanced osteogenic gene expression (*RUNX2*, *ALP*, *BMP2*, *COL1A* and *OCN*), ALPSA, osteogenic extracellular matrix expression (ALP, Col1a and OCN) and calcium deposition/mineralisation within the lyophilised *BM* silk sponges and the BMT 3D *in vitro* systems, however, a greater degree of bone-like tissue formation was observed in the MI192 pre-treated hDPSCs within the BMT model after 6 weeks in osteogenic culture.

- Cell-laden GelMA microspheres of appropriate size/shape were fabricated using microfluidics and a visible light polymerisation system.
- MI192 pre-treatment enhanced hBMSCs ALP, osteogenic extracellular matrix expression (ALP, Col1a and OCN) and calcium deposition/mineralisation within the GelMA hydrogel (GelMA alone and GelMA-PEBT/PBT construct) and the BMT model, however, the MI192 pre-treated hBMSCs displayed substantially increased bone-like tissue formation within the BMT model after 6 weeks in osteogenic culture.
- **3D *in vivo* culture**
 - MI192 pre-treated MSCs exhibited substantially enhanced osteogenic extracellular matrix expression (Col1a and OCN) and calcium deposition/mineralisation within the BMT constructs following *in vivo* intraperitoneal implantation within CD1 mice.
 - MI192 pre-treatment inhibited chondrogenic protein expression (GAGs, AGG and Col2a) of MSCs within the BMT model following *in vivo* intraperitoneal implantation.

As discussed in this thesis, MSCs acquired from both bone marrow and dental pulp tissues possess several advantages/disadvantages for use in bone tissue engineering applications. BMSCs are seen as the “gold standard” MSC source for bone regeneration due to their well-characterised properties and proven differentiation potential (352), however, they are associated with limitations such as invasive acquisition, low procurement yield and proliferation rate (153). DPSCs have garnered increasing interest due to the non-invasive acquisition, ease of procurement, proliferation rate and multilineage potential (168, 209). Additionally, studies have reported the significant potential of DPSCs for tissue engineering applications due to their ability to be cryopreserved without affecting key MSC properties (231, 232). By assessing the effects of MI192 on both MSC types, this demonstrates the considerable utility of this epigenetic approach to enhance MSCs osteogenic capacity for bone augmentation strategies. Additionally, when comparing the effects of MI192 on the general and osteogenic properties of DPSCs and BMSCs (Table 5.1), it is clear that MI192 is capable of effectively altering both MSCs epigenetic functionality, resulting in enhancing osteogenic differentiation. However, from the findings presented in this thesis, it was observed that DPSCs are more sensitive to MI192 induced alterations to epigenetic functionality, which resulted in greater enhancements in osteogenic differentiation when compared to BMSCs. This is likely due to the inherent differences in the MSC types and their osteogenic potential. Together, these findings demonstrate the considerable utility of utilising DPSCs in combination with MI192 for bone augmentation strategies.

Table 5.1 - Summary of the effects of MI192 on the general and osteogenic properties of DPSCs and BMSCs in this thesis.

Effects of MI192 on:	DPSCs	BMSCs
<i>2D culture</i>		
Reduced metabolic activity	≥ 20, 5, 1 μM for 24, 48, 72 hrs, respectively.	≥ 20, 10, 1 μM for 24, 48, 72 hrs, respectively.
Decreased DNA content	≥ 5, 1, 1 μM for 24, 48, 72 hrs, respectively.	≥ 10, 10, 1 μM for 24, 48, 72 hrs, respectively.
Halt cell cycle progression	> S, G ₂ M phase < G ₀ /G ₁ phase	> G ₂ M phase < S phase
Reduced HDAC activity	≥1 μM for 24 and 48 hrs (≥3.4- and 4.1-fold)	≥1 μM for 24 and 48 hrs (≥2.1- and 2.23-fold)
Enhanced H3K9 histone acetylation	≥1 μM 48 hrs (1.38-fold)	≥20 μM 48 hrs (1.28-fold)
Increased ALPSA	2 μM 48 hrs pre-treatment (2.2-fold)	50 μM 48 hrs pre-treatment (1.4-fold)
Enhanced calcium deposition	>4.75-fold	>1.4-fold
<i>3D culture</i>		
Increased ALPSA	Silk: 1.93-fold	GelMA: 1.32-fold
	BMT: 2.35-fold	BMT: 2.3-fold
Enhanced calcium deposition	Silk: 1.73-fold	GelMA: 1.3-fold

5.2 - Conclusion

In conclusion, the research presented in this thesis aims to investigate the effects of the novel selective HDAC2 and 3 inhibitor - MI192 on the behaviour and osteogenic capacity of clinically relevant MSCs (hDPSCs and hBMSCs), to enhance their efficacy for bone augmentation strategies. In 2D culture, MI192 caused a reduction in the viability of MSCs, while additionally halting cell cycle progression in the G₂/M phase. MI192 treatment altered the epigenetic functionality of treated MSCs, via altering HDAC activity resulting in enhanced histone H3K9 acetylation. MI192 pre-treatment enhanced the osteogenic gene/protein expression and ALPSA in both MSCs assessed. Moreover, substantial enhancement in calcium deposition and mineralisation was also observed in the MI192 pre-treated MSCs. In 3D *in vitro* culture, MI192 pre-treated hDPSCs exhibited increased osteogenic gene expression, protein deposition, ALPSA and mineralisation within the lyophilised *BM* silk scaffold and the BMT model, however, a greater degree of bone-like tissue formation was observed in the BMT model. A similar increase in hBMSCs ALPSA, osteogenic protein deposition and mineralisation was induced by MI192 pre-treatment within the GelMA hydrogel (GelMA alone and GelMA-PEBT/PBT construct) and the BMT model, however, the MI192 pre-treated hBMSCs within the BMT model exhibited substantially increased bone-like tissue formation. Following *in vivo* implantation, the MI192 pre-treated MSCs within the BMT model exhibited increased bone-like tissue formation, while inhibiting chondrogenic protein expression. Together, the research presented in this thesis provides greater evidence into the potential of utilising this epigenetic-based approach to enhance the efficacy of MSCs for bone augmentation strategies.

5.3 - Future work

The work undertaken in this thesis demonstrated the potential of MI192 to stimulate the osteogenic capacity of clinically relevant MSCs in 2D and 3D *in vitro* and *in vivo*, however, future work should look to further elucidate the exact mechanism in which MI192 stimulates MSCs osteogenic differentiation, in particular, its effects on the HDAC3-Runx2 complex. As mentioned in the general discussion, the effect of MI192 on both chromatin conformation and HDAC3 repression likely has a significant role in initiating differentiation in the MSCs assessed, therefore investigating the impact of each mechanism in different MSCs may provide greater mechanistic knowledge of how this HDACi behaves. Additionally, it would be interesting to assess the effects of MI192 treatment on up/downregulating key signalling pathways associated with osteogenic differentiation, enhancing the mechanistic knowledge into the behaviour of this HDACi within MSCs.

It would be interesting to investigate the effects of MI192 on MSCs chondrogenic differentiation, to confirm the lineage-specific specificity of this HDACis as indicated from the research presented in this thesis and previous studies with ADSCs (214).

Having demonstrated that MI192 caused a reduction in cell viability and halted the cell cycle possibly due to HDAC induced DNA damage, it would be interesting to further explore how MI192 induces cell death within these MSCs. Assessment of DNA fragmentation, stress markers and cytokines could provide indications of the pathways induced by MI192 treatment.

As stated in the general discussion, hDPSCs and hBMSCs were acquired from three and two different donors, respectively. Evaluating the efficacy of this inhibitor on a greater number and diversity of donors (sex, age etc) would provide a superior clinical representation of the potential patients this novel therapeutic approach would be targeted for.

Having assessed the effects of MI192 treatment on MSCs BMT *in vivo* bone formation within diffusion chambers, further evaluation within more physiologically relevant *in vivo* models such as subcutaneous implantation and critical-sized (calvarial and long bone) defects should be undertaken. This will provide a more thorough investigation into the ability of MI192 to promote MSCs bone formation within a more physiologically relevant condition, including the influence of host cell interactions, vascularisation and mechanical loading on MI192 treated MSCs bone formation. If conclusions acquired from these *in vivo* studies are that MI192 improves bone healing, this would provide more concrete evidence of the potential effectiveness of this epigenetic-based strategy in the clinical setting. Additionally, it would be interesting to investigate the effects of MI192 in stimulating MSCs bone like-tissue formation *in vivo* with the GelMA hydrogel and/or the silk scaffold.

Although it was demonstrated that MI192 pre-treatment enhanced hBMSCs osteogenic capacity within GelMA hydrogel (GelMA alone and GelMA-PEGT/PBT construct), the fabrication of cell-laden microspheres for assembly within the 3D printed scaffold could not be undertaken due to lack of appropriate equipment in Leeds. Due to this, the casting of the 3D printed scaffold within the cell-laden GelMA was employed as an alternative approach, thereby recreating the BMT model at a much-reduced cell density. With access to appropriate microfluidic and microsphere devices, the effects of MI192 pre-treatment on MSCs bone-like tissue formation should be assessed within cell-laden hydrogel microspheres assembled within the 3D printed scaffold, as this provides a closer comparison to the BMT model.

Within the BMT and GelMA studies in this thesis, the PEGT/PBT composite scaffolds were utilised as they have been well established by the collaborators of this research project for load-bearing tissues and fabrication optimised to hold incorporated microtissues/hydrogel microspheres. The primary function of the 3D printed scaffold utilised in this thesis was to control the spatial orientation of tissue modules, allowing for the investigation of MI192 pre-treated MSCs differentiation within low and high-density models (GelMA and microtissues). Therefore, it would be interesting for future studies to investigate the use of alternative scaffolds materials which possess either stronger mechanical characteristics and/or inherent osteoinductive properties which has the potential to further promote the osteogenic differentiation of incorporated MSCs. If scaffolds possessing these inherent osteoinductive properties are utilised, this may reduce or eliminate the *in vitro* osteogenic culture period utilised for MI192 pre-treated MSCs in this thesis, therefore enhancing the time and cost-effectiveness of these epigenetic-based therapies. Similarly, combining MI192 pre-treated MSCs within osteoinductive hydrogels may be beneficial for bone formation. Together, these approaches may be valuable in promoting MI192 pre-treated MSCs bone-like tissue formation during *in vivo* implantation.

Since the development of MI192, a plethora of other HDACi compounds has been created which may possess greater efficacy in stimulating MSCs osteogenic differentiation. Particularly, the use of a HDAC3 selective HDACis should be evaluated in terms of its ability to reduce potential side-effects and further increase the osteogenic capacity of MSCs compared to MI192.

In recent years, there has been growing research utilising epigenetic approaches for tissue engineering applications, with an increasing number of studies investigating the potential of microRNA (miRNA)-based therapies for bone tissue engineering (451, 452). These studies have demonstrated that miRNAs are easily combined within scaffolds systems and do not induce adverse side-effects. However, issues remain in terms of the therapeutic dosages as these miRNAs are easily

degraded (453). Similarly, as HDACis are known to affect acetylation resulting in increased transcriptional activity of the chromatin, these compounds are associated with side-effects such as cytotoxicity. The combination of this with HAT compounds may further enhance the transcriptional permissiveness of the chromatin, while potentially reducing HDACi induced side-effects. Therefore, future work could look to evaluate the potential of combining different epigenetic approaches (miRNAs, HATs and HDACis) which could eliminate the potential limitations of each approach and increase the stimulation of MSCs osteogenic differentiation.

It would be interesting to investigate the trophic properties of MSCs such as their immunomodulatory capability and the role in which MI192 affects this to ultimately enhance the therapeutic potential of the cells.

Having demonstrated that MI192 pre-treatment in monolayer was capable of promoting MSCs osteogenesis, the effects of combining this HDACi within a scaffold system for implantation would be an interesting advancement of this HDACi-based therapy. The development of an acellular HDACi-instructive biomaterial possesses a high translational potential as it overcomes many of the limitation associated with the cell-based approaches (i.e. regulatory, ethical and cost issues). Lee *et al.* (2011) reported the potential of this approach by soaking collagen scaffolds with Largazole and demonstrating repair of critical-sized calvarial defects (215). Although this approach seems ideal, the controlled exposure of HDACis to MSCs is known to be important from the literature and in this thesis. Therefore, approaches which can control the release profile of this inhibitor from the scaffold *in vivo* would potentially reduce possible side-effects and enhance MSCs differentiation potential, ultimately enhancing the therapeutic potential of HDACi-based therapies for bone augmentation strategies.

Finally, the commercialisation potential of MI192 would need to be explored. As it has been demonstrated that MI192 promotes the osteogenic potential of MSCs from three different tissue sources, MI192 could be sold as a pre-treatment medium to be utilised prior to the induction of differentiation with osteogenic medium. Additionally, MSCs could be pre-treated with MI192 then frozen and stored, ready to be sold as a source of MSCs with enhanced osteogenic potential. For these potential commercialisation routes for MI192 to be explored, full characterisation of the MI192 treated MSCs and protocol standardisation needs to be undertaken, to meet regulations.

References

1. Chen, X.P., Song, F.Y., Jhamb, D., Li, J.L., Bottino, M.C., Palakal, M.J. and Stocum, D.L. The Axolotl Fibula as a Model for the Induction of Regeneration across Large Segment Defects in Long Bones of the Extremities. *Plos One*. 2015, **10**(6).
2. McKee, M.D. Management of segmental bony defects: the role of osteoconductive orthobiologics. *J Am Acad Orthop Surg*. 2006, **14**(10 Spec No.), pp.S163-167.
3. NICE. Falls in older people: assessing risk and prevention 2016.
4. Dimitriou, R., Jones, E., McGonagle, D. and Giannoudis, P.V. Bone regeneration: current concepts and future directions. *Bmc Medicine*. 2011, **9**.
5. Mathoulin, C., Gras, M. and Roukos, S. Vascularized bone grafting from the volar distal radius for carpal bones reconstruction. *Chirurgie De La Main*. 2010, **29**, pp.S65-S76.
6. Solheim, E., Pinholt, E.M., Talsnes, O., Larsen, T.B. and Kirkeby, O.J. Revascularisation of fresh compared with demineralised bone grafts in rats. *Scandinavian Journal of Plastic and Reconstructive Surgery and Hand Surgery*. 2001, **35**(2), pp.113-116.
7. Calori, G.M., Mazza, E., Colombo, M. and Ripamonti, C. The use of bone-graft substitutes in large bone defects: Any specific needs? *Injury-International Journal of the Care of the Injured*. 2011, **42**, pp.S56-S63.
8. Djouad, F., Guerit, D., Marie, M., Toupet, K., Jorgensen, C. and Noel, D. Mesenchymal Stem Cells: New Insights into Bone Regenerative Applications. *Journal of Biomaterials and Tissue Engineering*. 2012, **2**(1), pp.14-28.
9. Campana, V., Milano, G., Pagano, E., Barba, M., Cicione, C., Salonna, G., Lattanzi, W. and Logroscino, G. Bone substitutes in orthopaedic surgery: from basic science to clinical practice. *Journal of Materials Science-Materials in Medicine*. 2014, **25**(10), pp.2445-2461.
10. Keating, J.F. and McQueen, M.M. Substitutes for autologous bone graft in orthopaedic trauma. *Journal of Bone and Joint Surgery-British Volume*. 2001, **83B**(1), pp.3-8.
11. Kessler, M.W. and Grande, D.A. Tissue engineering and cartilage. *Organogenesis*. 2008, **4**(1), pp.28-32.
12. Giannoudis, P.V., Einhorn, T.A. and Marsh, D. Fracture healing: the diamond concept. *Injury-International Journal of the Care of the Injured*. 2007, **38 Suppl 4**, pp.S3-6.
13. Amini, A.R., Laurencin, C.T. and Nukavarapu, S.P. Bone tissue engineering: recent advances and challenges. *Crit Rev Biomed Eng*. 2012, **40**(5), pp.363-408.
14. Ko, J.Y., Park, S. and Im, G.I. Osteogenesis from Human Induced Pluripotent Stem Cells: An In Vitro and In Vivo Comparison with Mesenchymal Stem Cells. *Stem Cells and Development*. 2014, **23**(15), pp.1788-1797.
15. Moschidou, D., Mukherjee, S., Blundell, M.P., Drews, K., Jones, G.N., Abdulrazzak, H., Nowakowska, B., Phoolchund, A., Lay, K., Ramasamy, T.S., Cananzi, M., Nettersheim, D., Sullivan, M., Frost, J., Moore, G., Vermeesch, J.R., Fisk, N.M., Thrasher, A.J., Atala, A., Adjaye,

- J., Schorle, H., De Coppi, P. and Guillot, P.V. Valproic Acid Confers Functional Pluripotency to Human Amniotic Fluid Stem Cells in a Transgene-free Approach. *Molecular Therapy*. 2012, **20**(10), pp.1953-1967.
16. Tollervey, J.R. and Lunyak, V.V. Epigenetics Judge, jury and executioner of stem cell fate. *Epigenetics*. 2012, **7**(8), pp.823-840.
 17. Bertino, E.M. and Otterson, G.A. Romidepsin: a novel histone deacetylase inhibitor for cancer. *Expert Opinion on Investigational Drugs*. 2011, **20**(8), pp.1151-1158.
 18. Prince, H.M., Bishton, M.J. and Johnstone, R.W. Panobinostat (LBH589): a potent pan-deacetylase inhibitor with promising activity against hematologic and solid tumors. *Future Oncology*. 2009, **5**(5), pp.601-612.
 19. Xu, S., De Veirman, K., Evans, H., Santini, G.C., Vande Broek, I., Leleu, X., De Becker, A., Van Camp, B., Croucher, P., Vanderkerken, K. and Van Riet, I. Effect of the HDAC inhibitor vorinostat on the osteogenic differentiation of mesenchymal stem cells in vitro and bone formation in vivo. *Acta Pharmacologica Sinica*. 2013, **34**(5), pp.699-709.
 20. Jonsson, K.L., Tolstrup, M., Vad-Nielsen, J., Kjaer, K., Laustsen, A., Andersen, M.N., Rasmussen, T.A., Sogaard, O.S., Ostergaard, L., Denton, P.W. and Jakobsen, M.R. Histone Deacetylase Inhibitor Romidepsin Inhibits De Novo HIV-1 Infections. *Antimicrobial Agents and Chemotherapy*. 2015, **59**(7), pp.3984-3994.
 21. Gillespie, J., Savic, S., Wong, C., Hempshall, A., Inman, M., Emery, P., Grigg, R. and McDermott, M.F. Histone deacetylases are dysregulated in rheumatoid arthritis and a novel histone deacetylase 3-selective inhibitor reduces interleukin-6 production by peripheral blood mononuclear cells from rheumatoid arthritis patients. *Arthritis and Rheumatism*. 2012, **64**(2), pp.418-422.
 22. McKinsey, T.A. Isoform-selective HDAC inhibitors: Closing in on translational medicine for the heart. *Journal of Molecular and Cellular Cardiology*. 2011, **51**(4), pp.491-496.
 23. De Boer, J., Licht, R., Bongers, M., Van Der Klundert, T., Arends, R. and Van Blitterswijk, C. Inhibition of histone acetylation as a tool in bone tissue engineering. *Tissue Eng*. 2006, **12**(10), pp.2927-2937.
 24. Taichman, R.S. Blood and bone: two tissues whose fates are intertwined to create the hematopoietic stem-cell niche. *Blood*. 2005, **105**(7), pp.2631-2639.
 25. Pocock, G. and Richards, C.D. *Human physiology : the basis of medicine*. 3rd ed. Oxford: Oxford University Press, 2006.
 26. Frohlich, M., Grayson, W.L., Wan, L.Q., Marolt, D., Drobnic, M. and Vunjak-Novakovic, G. Tissue Engineered Bone Grafts: Biological Requirements, Tissue Culture and Clinical Relevance. *Current Stem Cell Research & Therapy*. 2008, **3**(4), pp.254-264.
 27. Hench LL, W.J. An Introduction to Bioceramics. *World Scientific*. 1993, **1**.
 28. Orlovskij, V.P., Komlev, V.S. and Barinov, S.M. Hydroxyapatite and hydroxyapatite-based ceramics. *Inorganic Materials*. 2002, **38**(10), pp.973-984.

29. Jakob, M., Saxer, F., Scotti, C., Schreiner, S., Studer, P., Scherberich, A., Heberer, M. and Martin, I. Perspective on the Evolution of Cell-Based Bone Tissue Engineering Strategies. *European Surgical Research*. 2012, **49**(1), pp.1-7.
30. Eliaz, N. and Metoki, N. Calcium Phosphate Bioceramics: A Review of Their History, Structure, Properties, Coating Technologies and Biomedical Applications. *Materials*. 2017, **10**(4).
31. Sheng, G.J. The developmental basis of mesenchymal stem/stromal cells (MSCs). *Bmc Developmental Biology*. 2015, **15**.
32. Heino, T.J. and Hentunen, T.A. Differentiation of Osteoblasts and Osteocytes from Mesenchymal Stem Cells. *Current Stem Cell Research & Therapy*. 2008, **3**(2), pp.131-145.
33. Florencio-Silva, R., Sasso, G.R.D., Sasso-Cerri, E., Simoes, M.J. and Cerri, P.S. Biology of Bone Tissue: Structure, Function, and Factors That Influence Bone Cells. *Biomed Research International*. 2015.
34. Glimcher, M.J. The nature of the mineral component of bone and the mechanism of calcification. *Instr Course Lect*. 1987, **36**, pp.49-69.
35. Fernandez-Yague, M.A., Abbah, S.A., McNamara, L., Zeugolis, D.I., Pandit, A. and Biggs, M.J. Biomimetic approaches in bone tissue engineering: Integrating biological and physicommechanical strategies. *Advanced Drug Delivery Reviews*. 2015, **84**, pp.1-29.
36. Tanaka, Y., Nakayamada, S. and Okada, Y. Osteoblasts and osteoclasts in bone remodeling and inflammation. *Curr Drug Targets Inflamm Allergy*. 2005, **4**(3), pp.325-328.
37. Bradley, E.W., Carpio, L.R., van Wijnen, A.J., McGee-Lawrence, M.E. and Westendorf, J.J. Histone Deacetylases in Bone Development and Skeletal Disorders. *Physiol Rev*. 2015, **95**(4), pp.1359-1381.
38. Chen, G., Deng, C. and Li, Y.P. TGF-beta and BMP signaling in osteoblast differentiation and bone formation. *Int J Biol Sci*. 2012, **8**(2), pp.272-288.
39. Mackie, E.J., Ahmed, Y.A., Tatarczuch, L., Chen, K.S. and Mirams, M. Endochondral ossification: How cartilage is converted into bone in the developing skeleton. *International Journal of Biochemistry & Cell Biology*. 2008, **40**(1), pp.46-62.
40. Zhang, R.R., Oyajobi, B.O., Harris, S.E., Chen, D., Tsao, C., Deng, H.W. and Zhao, M. Wnt/beta-catenin signaling activates bone morphogenetic protein 2 expression in osteoblasts. *Bone*. 2013, **52**(1), pp.145-156.
41. Levi, G., Geoffroy, V., Palmisano, G. and de Vernejoul, M.C. Bones, genes and fractures - Workshop on the genetics of osteoporosis: from basic to clinical research. *Embo Reports*. 2002, **3**(1), pp.22-26.
42. Travers, A. and Muskhelishvili, G. DNA structure and function. *FEBS J*. 2015, **282**(12), pp.2279-2295.

43. Hondele, M. and Ladurner, A.G. The chaperone-histone partnership: for the greater good of histone traffic and chromatin plasticity. *Current Opinion in Structural Biology*. 2011, **21**(6), pp.698-708.
44. Jansen, A. and Verstrepen, K.J. Nucleosome Positioning in *Saccharomyces cerevisiae*. *Microbiology and Molecular Biology Reviews*. 2011, **75**(2), pp.301-+.
45. Luger, K., Mader, A.W., Richmond, R.K., Sargent, D.F. and Richmond, T.J. Crystal structure of the nucleosome core particle at 2.8 angstrom resolution. *Nature*. 1997, **389**(6648), pp.251-260.
46. Shahbazian, M.D. and Grunstein, M. Functions of site-specific histone acetylation and deacetylation. *Annual Review of Biochemistry*. 2007, **76**, pp.75-100.
47. Margueron, R., Trojer, P. and Reinberg, D. The key to development: interpreting the histone code? *Current Opinion in Genetics & Development*. 2005, **15**(2), pp.163-176.
48. Downs, J.A., Nussenzweig, M.C. and Nussenzweig, A. Chromatin dynamics and the preservation of genetic information. *Nature*. 2007, **447**(7147), pp.951-958.
49. Spivakov, M. and Fisher, A.G. Epigenetic signatures of stem-cell identity. *Nature Reviews Genetics*. 2007, **8**(4), pp.263-271.
50. Simara, P., Motl, J.A. and Kaufman, D.S. Pluripotent stem cells and gene therapy. *Translational Research*. 2013, **161**(4), pp.284-292.
51. Minarovits, J. Microbe-Induced Epigenetic Alterations in Host Cells: The Coming Era of Patho-Epigenetics of Microbial Infections a Review. *Acta Microbiologica Et Immunologica Hungarica*. 2009, **56**(1), pp.1-19.
52. Hillemacher, T., Frieling, H., Moskau, S., Muschler, M.A.N., Semmler, A., Kornhuber, J., Klockgether, T., Bleich, S. and Linnebank, M. Global DNA methylation is influenced by smoking behaviour. *European Neuropsychopharmacology*. 2008, **18**(4), pp.295-298.
53. Agudelo, M., Yoo, C. and Nair, M.P. Alcohol-induced serotonergic modulation: The role of histone deacetylases. *Alcohol*. 2012, **46**(7), pp.635-642.
54. Burdge, G.C., Hoile, S.P. and Lillycrop, K.A. Epigenetics: are there implications for personalised nutrition? *Current Opinion in Clinical Nutrition and Metabolic Care*. 2012, **15**(5), pp.442-447.
55. Shakespear, M.R., Halili, M.A., Irvine, K.M., Fairlie, D.P. and Sweet, M.J. Histone deacetylases as regulators of inflammation and immunity. *Trends in Immunology*. 2011, **32**(7), pp.335-343.
56. Ropero, S. and Esteller, M. The role of histone deacetylases (HDACs) in human cancer. *Molecular Oncology*. 2007, **1**(1), pp.19-25.
57. Filippakopoulos, P. and Knapp, S. The bromodomain interaction module. *Febs Letters*. 2012, **586**(17), pp.2692-2704.
58. Kretsovali, A., Hadjimichael, C. and Charmpilas, N. Histone Deacetylase Inhibitors in Cell Pluripotency, Differentiation, and Reprogramming. *Stem Cells International*. 2012.

59. Schemies, J., Uciechowska, U., Sippl, W. and Jung, M. NAD(+)-Dependent Histone Deacetylases (Sirtuins) as Novel Therapeutic Targets. *Medicinal Research Reviews*. 2010, **30**(6), pp.861-889.
60. Sadoul, K., Boyault, C., Pabion, M. and Khochbin, S. Regulation of protein turnover by acetyltransferases and deacetylases. *Biochimie*. 2008, **90**(2), pp.306-312.
61. Bjerling, P., Silverstein, R.A., Thon, G., Caudy, A., Grewal, S. and Ekwall, K. Functional divergence between histone deacetylases in fission yeast by distinct cellular localization and in vivo specificity (vol 22, pg 2170, 2002). *Molecular and Cellular Biology*. 2002, **22**(14), pp.5257-5258.
62. Yan, C. and Boyd, D.D. Histone H3 acetylation and H3 K4 methylation define distinct chromatin regions permissive for transgene expression. *Molecular and Cellular Biology*. 2006, **26**(17), pp.6357-6371.
63. Reichert, N., Choukrallah, M.A. and Matthias, P. Multiple roles of class I HDACs in proliferation, differentiation, and development. *Cellular and Molecular Life Sciences*. 2012, **69**(13), pp.2173-2187.
64. Zeng, L. and Zhou, M.M. Bromodomain: an acetyl-lysine binding domain. *Febs Letters*. 2002, **513**(1), pp.124-128.
65. Shukla, V., Vaissiere, T. and Herceg, Z. Histone acetylation and chromatin signature in stem cell identity and cancer. *Mutat Res*. 2008, **637**(1-2), pp.1-15.
66. Duncan, H.F., Smith, A.J., Fleming, G.J.P. and Cooper, P.R. HDACi: Cellular Effects, Opportunities for Restorative Dentistry. *Journal of Dental Research*. 2011, **90**(12), pp.1377-1388.
67. Roth, S.Y., Denu, J.M. and Allis, C.D. Histone acetyltransferases. *Annual Review of Biochemistry*. 2001, **70**, pp.81-120.
68. Grewal, S.I.S. and Moazed, D. Heterochromatin and epigenetic control of gene expression. *Science*. 2003, **301**(5634), pp.798-802.
69. Hake, S.B., Xiao, A. and Allis, C.D. Linking the epigenetic 'language' of covalent histone modifications to cancer. *British Journal of Cancer*. 2004, **90**(4), pp.761-769.
70. Yang, X.J. and Seto, E. HATs and HDACs: from structure, function and regulation to novel strategies for therapy and prevention. *Oncogene*. 2007, **26**(37), pp.5310-5318.
71. Huynh, N.C., Everts, V. and Ampornaramveth, R.S. Histone deacetylases and their roles in mineralized tissue regeneration. *Bone Rep*. 2017, **7**, pp.33-40.
72. Bertrand, P. Inside HDAC with HDAC inhibitors. *European Journal of Medicinal Chemistry*. 2010, **45**(6), pp.2095-2116.
73. Xu, W.S., Parmigiani, R.B. and Marks, P.A. Histone deacetylase inhibitors: molecular mechanisms of action. *Oncogene*. 2007, **26**(37), pp.5541-5552.

74. de Boer, J., Licht, R., Bongers, M., van der Klundert, T., Arends, R. and van Blitterswijk, C. Inhibition of histone acetylation as a tool in bone tissue engineering. *Tissue Eng.* 2006, **12**(10), pp.2927-2937.
75. Hochedlinger, K. and Plath, K. Epigenetic reprogramming and induced pluripotency. *Development.* 2009, **136**(4), pp.509-523.
76. Elizalde, C., Fernandez-Rueda, J., Salcedo, J.M., Dorronsoro, A., Ferrin, I., Jakobsson, E. and Trigueros, C. Histone Deacetylase 3 Modulates the Expansion of Human Hematopoietic Stem Cells. *Stem Cells and Development.* 2012, **21**(14), pp.2581-2591.
77. Martinez-Balbas, M.A., Bauer, U.M., Nielsen, S.J., Brehm, A. and Kouzarides, T. Regulation of E2F1 activity by acetylation. *EMBO J.* 2000, **19**(4), pp.662-671.
78. Spange, S., Wagner, T., Heinzl, T. and Kramer, O.H. Acetylation of non-histone proteins modulates cellular signalling at multiple levels. *International Journal of Biochemistry & Cell Biology.* 2009, **41**(1), pp.185-198.
79. Glozak, M.A., Sengupta, N., Zhang, X. and Seto, E. Acetylation and deacetylation of non-histone proteins. *Gene.* 2005, **363**, pp.15-23.
80. Gregoret, I.V., Lee, Y.M. and Goodson, H.V. Molecular evolution of the histone deacetylase family: functional implications of phylogenetic analysis. *J Mol Biol.* 2004, **338**(1), pp.17-31.
81. Haberland, M., Montgomery, R.L. and Olson, E.N. The many roles of histone deacetylases in development and physiology: implications for disease and therapy. *Nature Reviews Genetics.* 2009, **10**(1), pp.32-42.
82. Juan, L.J., Shia, W.J., Chen, M.H., Yang, W.M., Seto, E., Lin, Y.S. and Wu, C.W. Histone deacetylases specifically down-regulate p53-dependent gene activation. *Journal of Biological Chemistry.* 2000, **275**(27), pp.20436-20443.
83. Choudhary, C., Kumar, C., Gnad, F., Nielsen, M.L., Rehman, M., Walther, T.C., Olsen, J.V. and Mann, M. Lysine Acetylation Targets Protein Complexes and Co-Regulates Major Cellular Functions. *Science.* 2009, **325**(5942), pp.834-840.
84. Buchwald, M., Kramer, O.H. and Heinzl, T. HDACi--targets beyond chromatin. *Cancer Letters.* 2009, **280**(2), pp.160-167.
85. Bradner, J.E., West, N., Grachan, M.L., Greenberg, E.F., Haggarty, S.J., Warnow, T. and Mazitschek, R. Chemical phylogenetics of histone deacetylases. *Nature Chemical Biology.* 2010, **6**(3), pp.238-243.
86. Montgomery, R.L., Davis, C.A., Potthoff, M.J., Haberland, M., Fielitz, J., Qi, X.X., Hill, J.A., Richardson, J.A. and Olson, E.N. Histone deacetylases 1 and 2 redundantly regulate cardiac morphogenesis, growth, and contractility. *Genes & Development.* 2007, **21**(14), pp.1790-1802.
87. De Ruijter, A.J.M., Van Gennip, A.H., Caron, H.N., Kemp, S. and Van Kuilenburg, A.B.P. Histone deacetylases (HDACs): characterization of the classical HDAC family. *Biochemical Journal.* 2003, **370**, pp.737-749.

88. Elaut, G., Rogiers, V. and Vanhaecke, T. The pharmaceutical potential of histone deacetylase inhibitors. *Current Pharmaceutical Design*. 2007, **13**(25), pp.2584-2620.
89. Marks, P.A. and Xu, W.S. Histone Deacetylase Inhibitors: Potential in Cancer Therapy. *Journal of Cellular Biochemistry*. 2009, **107**(4), pp.600-608.
90. Suzuki, T. Explorative study on isoform-selective histone deacetylase inhibitors. *Chem Pharm Bull (Tokyo)*. 2009, **57**(9), pp.897-906.
91. Marks, P.A. Histone deacetylase inhibitors: a chemical genetics approach to understanding cellular functions. *Biochim Biophys Acta*. 2010, **1799**(10-12), pp.717-725.
92. Wagner, F.F., Weiwer, M., Lewis, M.C. and Holson, E.B. Small Molecule Inhibitors of Zinc-dependent Histone Deacetylases. *Neurotherapeutics*. 2013, **10**(4), pp.589-604.
93. Marks, P.A., Rifkind, R.A., Richon, V.M., Breslow, R., Miller, T. and Kelly, W.K. Histone deacetylases and cancer: Causes and therapies. *Nature Reviews Cancer*. 2001, **1**(3), pp.194-202.
94. Finnin, M.S., Donigian, J.R., Cohen, A., Richon, V.M., Rifkind, R.A., Marks, P.A., Breslow, R. and Pavletich, N.P. Structures of a histone deacetylase homologue bound to the TSA and SAHA inhibitors. *Nature*. 1999, **401**(6749), pp.188-193.
95. Wang, D.F., Wiest, O., Helquist, P., Lan-Hargest, H.Y. and Wiech, N.L. On the function of the 14 angstrom long internal cavity of histone deacetylase-like protein: Implications for the design of histone deacetylase inhibitors. *Journal of Medicinal Chemistry*. 2004, **47**(13), pp.3409-3417.
96. Hahnen, E., Hauke, J., Trankle, C., Eyupoglu, I.Y., Wirth, B. and Blumcke, I. Histone deacetylase inhibitors: possible implications for neurodegenerative disorders. *Expert Opinion on Investigational Drugs*. 2008, **17**(2), pp.169-184.
97. Estiu, G., Greenberg, E., Harrison, C.B., Kwiatkowski, N.P., Mazitschek, R., Bradner, J.E. and Wiest, O. Structural origin of selectivity in class II-selective histone deacetylase inhibitors. *Journal of Medicinal Chemistry*. 2008, **51**(10), pp.2898-2906.
98. Su, H., Altucci, L. and You, Q.D. Competitive or noncompetitive, that's the question: research toward histone deacetylase inhibitors. *Molecular Cancer Therapeutics*. 2008, **7**(5), pp.1007-1012.
99. Mottamal, M., Zheng, S.L., Huang, T.L. and Wang, G.D. Histone Deacetylase Inhibitors in Clinical Studies as Templates for New Anticancer Agents. *Molecules*. 2015, **20**(3), pp.3898-3941.
100. Boissinot, M., Inman, M., Hempshall, A., James, S.R., Gill, J.H., Selby, P., Bowen, D.T., Grigg, R. and Cockerill, P.N. Induction of differentiation and apoptosis in leukaemic cell lines by the novel benzamide family histone deacetylase 2 and 3 inhibitor MI-192. *Leukemia Research*. 2012, **36**(10), pp.1304-1310.
101. Shen, S. and Kozikowski, A.P. Why Hydroxamates May Not Be the Best Histone Deacetylase Inhibitors What Some May Have Forgotten or Would Rather Forget? *Chemmedchem*. 2016, **11**(1), pp.15-21.

102. Richardson, P., Mitsiades, C., Colson, K., Reilly, E., McBride, L., Chiao, J., Sun, L., Ricker, J., Rizvi, S., Oerth, C., Atkins, B., Fearen, I., Anderson, K. and Siegel, D. Phase I trial of oral vorinostat (suberoylanilide hydroxamic acid, SAHA) in patients with advanced multiple myeloma. *Leukemia & Lymphoma*. 2008, **49**(3), pp.502-507.
103. Christensen, D.P., Dahllof, M., Lundh, M., Rasmussen, D.N., Nielsen, M.D., Billestrup, N., Grunnet, L.G. and Mandrup-Poulsen, T. Histone Deacetylase (HDAC) Inhibition as a Novel Treatment for Diabetes Mellitus. *Molecular Medicine*. 2011, **17**(5-6), pp.378-390.
104. Bode, K.A. and Dalpke, A.H. HDAC inhibitors block innate immunity. *Blood*. 2011, **117**(4), pp.1102-1103.
105. Deschamps, N., Simoes-Pires, C.A., Carrupt, P.A. and Nurisso, A. How the flexibility of human histone deacetylases influences ligand binding: an overview. *Drug Discovery Today*. 2015, **20**(6), pp.736-742.
106. Bieliauskas, A.V. and Pflum, M.K.H. Isoform-selective histone deacetylase inhibitors. *Chemical Society Reviews*. 2008, **37**(7), pp.1402-1413.
107. Balasubramanian, S., Verner, E. and Buggy, J.J. Isoform-specific histone deacetylase inhibitors: The next step? *Cancer Letters*. 2009, **280**(2), pp.211-221.
108. Jones, P. Development of second generation epigenetic agents. *Medchemcomm*. 2012, **3**(2), pp.135-161.
109. Witt, O., Deubzer, H.E., Milde, T. and Oehme, I. HDAC family: What are the cancer relevant targets? *Cancer Letters*. 2009, **277**(1), pp.8-21.
110. Vermeulen, K., Van Bockstaele, D.R. and Berneman, Z.N. The cell cycle: a review of regulation, deregulation and therapeutic targets in cancer. *Cell Prolif*. 2003, **36**(3), pp.131-149.
111. Kastan, M.B. and Bartek, J. Cell-cycle checkpoints and cancer. *Nature*. 2004, **432**(7015), pp.316-323.
112. Johnstone, R.W. Histone-deacetylase inhibitors: novel drugs for the treatment of cancer. *Nat Rev Drug Discov*. 2002, **1**(4), pp.287-299.
113. Schroeder, T.M. and Westendorf, J.J. Histone deacetylase inhibitors promote osteoblast maturation. *Journal of Bone and Mineral Research*. 2005, **20**(12), pp.2254-2263.
114. Telles, E. and Seto, E. Modulation of cell cycle regulators by HDACs. *Front Biosci (Schol Ed)*. 2012, **4**, pp.831-839.
115. Zhou, Q., Dalgard, C.L., Wynder, C. and Doughty, M.L. Histone deacetylase inhibitors SAHA and sodium butyrate block G1-to-S cell cycle progression in neurosphere formation by adult subventricular cells. *BMC Neurosci*. 2011, **12**, p.50.
116. Zupkovitz, G., Grausenburger, R., Brunmeir, R., Senese, S., Tischler, J., Jurkin, J., Rembold, M., Meunier, D., Egger, G., Lagger, S., Chiocca, S., Propst, F., Weitzer, G. and Seiser, C. The Cyclin-Dependent Kinase Inhibitor p21 Is a Crucial Target for Histone Deacetylase 1 as a

- Regulator of Cellular Proliferation. *Molecular and Cellular Biology*. 2010, **30**(5), pp.1171-1181.
117. Kalucka, J., Missiaen, R., Georgiadou, M., Schoors, S., Lange, C., De Bock, K., Dewerchin, M. and Carmeliet, P. Metabolic control of the cell cycle. *Cell Cycle*. 2015, **14**(21), pp.3379-3388.
 118. Trivedi, C.M., Lu, M.M., Wang, Q. and Epstein, J.A. Transgenic overexpression of Hdac3 in the heart produces increased postnatal cardiac myocyte proliferation but does not induce hypertrophy. *Journal of Biological Chemistry*. 2008, **283**(39), pp.26484-26489.
 119. Jiang, Y.D. and Hsieh, J. HDAC3 controls gap 2/mitosis progression in adult neural stem/progenitor cells by regulating CDK1 levels. *Proceedings of the National Academy of Sciences of the United States of America*. 2014, **111**(37), pp.13541-13546.
 120. Richon, V.M., Sandhoff, T.W., Rifkind, R.A. and Marks, P.A. Histone deacetylase inhibitor selectively induces p21WAF1 expression and gene-associated histone acetylation. *Proc Natl Acad Sci U S A*. 2000, **97**(18), pp.10014-10019.
 121. Richon, V.M. Cancer biology: mechanism of antitumour action of vorinostat (suberoylanilide hydroxamic acid), a novel histone deacetylase inhibitor. *British Journal of Cancer*. 2006, **95**, pp.S2-S6.
 122. Eot-Houllier, G., Fulcrand, G., Magnaghi-Jaulin, L. and Jaulin, C. Histone deacetylase inhibitors and genomic instability. *Cancer Letters*. 2009, **274**(2), pp.169-176.
 123. Ma, X., Ezzeldin, H.H. and Diasio, R.B. Histone deacetylase inhibitors: current status and overview of recent clinical trials. *Drugs*. 2009, **69**(14), pp.1911-1934.
 124. Ruefli, A.A., Ausserlechner, M.J., Bernhard, D., Sutton, V.R., Tainton, K.M., Kofler, R., Smyth, M.J. and Johnstone, R.W. The histone deacetylase inhibitor and chemotherapeutic agent suberoylanilide hydroxamic acid (SAHA) induces a cell-death pathway characterized by cleavage of Bid and production of reactive oxygen species. *Proc Natl Acad Sci U S A*. 2001, **98**(19), pp.10833-10838.
 125. Kachhap, S.K., Rosmus, N., Collis, S.J., Kortenhorst, M.S., Wissing, M.D., Hedayati, M., Shabbeer, S., Mendonca, J., Deangelis, J., Marchionni, L., Lin, J., Hoti, N., Nortier, J.W., DeWeese, T.L., Hammers, H. and Carducci, M.A. Downregulation of homologous recombination DNA repair genes by HDAC inhibition in prostate cancer is mediated through the E2F1 transcription factor. *Plos One*. 2010, **5**(6), p.e11208.
 126. Munshi, A., Tanaka, T., Hobbs, M.L., Tucker, S.L., Richon, V.M. and Meyn, R.E. Vorinostat, a histone deacetylase inhibitor, enhances the response of human tumor cells to ionizing radiation through prolongation of gamma-H2AX foci. *Molecular Cancer Therapeutics*. 2006, **5**(8), pp.1967-1974.
 127. Rosato, R.R. and Grant, S. Histone deacetylase inhibitors: insights into mechanisms of lethality. *Expert Opinion on Therapeutic Targets*. 2005, **9**(4), pp.809-824.
 128. Xu, W.S., Ngo, L., Perez, G., Dokmanovic, M. and Marks, P.A. Intrinsic apoptotic and thioredoxin pathways in human prostate cancer cell response to histone deacetylase inhibitor. *Proceedings of the National Academy of Sciences of the United States of America*. 2006, **103**(42), pp.15540-15545.

129. Bolden, J.E., Shi, W., Jankowski, K., Kan, C.Y., Cluse, L., Martin, B.P., MacKenzie, K.L., Smyth, G.K. and Johnstone, R.W. HDAC inhibitors induce tumor-cell-selective pro-apoptotic transcriptional responses. *Cell Death & Disease*. 2013, **4**.
130. Locksley, R.M., Killeen, N. and Lenardo, M.J. The TNF and TNF receptor superfamilies: Integrating mammalian biology. *Cell*. 2001, **104**(4), pp.487-501.
131. Elmore, S. Apoptosis: A review of programmed cell death. *Toxicologic Pathology*. 2007, **35**(4), pp.495-516.
132. Borbone, E., Berlingieri, M.T., De Bellis, F., Nebbioso, A., Chiappetta, G., Mai, A., Altucci, L. and Fusco, A. Histone deacetylase inhibitors induce thyroid cancer-specific apoptosis through proteasome-dependent inhibition of TRAIL degradation. *Oncogene*. 2010, **29**(1), pp.105-116.
133. Coffey, D.C., Kutko, M.C., Glick, R.D., Butler, L.M., Heller, G., Rifkind, R.A., Marks, P.A., Richon, V.M. and La Quaglia, M.P. The histone deacetylase inhibitor, CBHA, inhibits growth of human neuroblastoma xenografts in vivo, alone and synergistically with all-trans retinoic acid. *Cancer Res*. 2001, **61**(9), pp.3591-3594.
134. Marks, P.A. The clinical development of histone deacetylase inhibitors as targeted anticancer drugs. *Expert Opinion on Investigational Drugs*. 2010, **19**(9), pp.1049-1066.
135. Ungerstedt, J.S., Sowa, Y., Xu, W.S., Shao, Y., Dokmanovic, M., Perez, G., Ngo, L., Holmgren, A., Jiang, X. and Marks, P.A. Role of thioredoxin in the response of normal and transformed cells to histone deacetylase inhibitors. *Proc Natl Acad Sci U S A*. 2005, **102**(3), pp.673-678.
136. Lillig, C.H. and Holmgren, A. Thioredoxin and related molecules--from biology to health and disease. *Antioxid Redox Signal*. 2007, **9**(1), pp.25-47.
137. Yokomizo, A., Ono, M., Nanri, H., Makino, Y., Ohga, T., Wada, M., Okamoto, T., Yodoi, J., Kuwano, M. and Kohno, K. Cellular levels of thioredoxin associated with drug sensitivity to cisplatin, mitomycin C, doxorubicin, and etoposide. *Cancer Res*. 1995, **55**(19), pp.4293-4296.
138. Westendorf, J.J., Zaidi, S.K., Cascino, J.E., Kahler, R., van Wijnen, A.J., Lian, J.B., Yoshida, M., Stein, G.S. and Li, X. Runx2 (Cbfa1, AML-3) interacts with histone deacetylase 6 and represses the p21(CIP1/WAF1) promoter. *Molecular and Cellular Biology*. 2002, **22**(22), pp.7982-7992.
139. Xu, S., De Veirman, K., Evans, H., Santini, G.C., Vande Broek, I., Leleu, X., De Becker, A., Van Camp, B., Croucher, P., Vanderkerken, K. and Van Riet, I. Effect of the HDAC inhibitor vorinostat on the osteogenic differentiation of mesenchymal stem cells in vitro and bone formation in vivo. *Acta Pharmacologica Sinica*. 2013, **34**(5), pp.699-709.
140. Schroeder, T.M., Kahler, R.A., Li, X.D. and Westendorf, J.J. Histone deacetylase 3 interacts with Runx2 to repress the osteocalcin promoter and regulate osteoblast differentiation. *Journal of Biological Chemistry*. 2004, **279**(40), pp.41998-42007.
141. Razidlo, D.F., Whitney, T.J., Casper, M.E., McGee-Lawrence, M.E., Stensgard, B.A., Li, X.D., Secreto, F.J., Knutson, S.K., Hiebert, S.W. and Westendorf, J.J. Histone Deacetylase 3 Depletion in Osteo/Chondroprogenitor Cells Decreases Bone Density and Increases Marrow Fat. *Plos One*. 2010, **5**(7).

142. Choo, M.K., Yeo, H. and Zayzafoon, M. NFATc1 mediates HDAC-dependent transcriptional repression of osteocalcin expression during osteoblast differentiation. *Bone*. 2009, **45**(3), pp.579-589.
143. Jensen, E.D., Gopalakrishnan, R. and Westendorf, J.J. Regulation of gene expression in osteoblasts. *Biofactors*. 2010, **36**(1), pp.25-32.
144. Hesse, E., Saito, H., Kiviranta, R., Correa, D., Yamana, K., Neff, L., Toben, D., Duda, G., Atfi, A., Geoffroy, V., Horne, W.C. and Baron, R. Zfp521 controls bone mass by HDAC3-dependent attenuation of Runx2 activity. *Journal of Cell Biology*. 2010, **191**(7), pp.1271-1283.
145. Lamour, V., Detry, C., Sanchez, C., Henrotin, Y., Castronovo, V. and Bellahcene, A. Runx2-and histone deacetylase 3-mediated repression is relieved in differentiating human osteoblast cells to allow high bone sialoprotein expression. *Journal of Biological Chemistry*. 2007, **282**(50), pp.36240-36249.
146. Singh, N., Gupta, M., Trivedi, C.M., Singh, M.K., Li, L. and Epstein, J.A. Murine craniofacial development requires Hdac3-mediated repression of Msx gene expression. *Developmental Biology*. 2013, **377**(2), pp.333-344.
147. Lee, H.W., Suh, J.H., Kim, A.Y., Lee, Y.S., Park, S.Y. and Kim, J.B. Histone deacetylase 1-mediated histone modification regulates osteoblast differentiation. *Mol Endocrinol*. 2006, **20**(10), pp.2432-2443.
148. Shen, J., Lian, J.B., Montecino, M., Stein, G.S., Stein, J.L. and van Wijnen, A.J. Histone acetylation in vivo at the osteocalcin locus is functionally coupled to chromatin remodeling and vitamin D dependent, bone tissue-specific gene activation. *Journal of Bone and Mineral Research*. 2001, **16**, pp.S232-S232.
149. Bauer, T.W. and Muschler, G.F. Bone graft materials - An overview of the basic science. *Clinical Orthopaedics and Related Research*. 2000, (371), pp.10-27.
150. Sabir, M.I., Xu, X.X. and Li, L. A review on biodegradable polymeric materials for bone tissue engineering applications. *Journal of Materials Science*. 2009, **44**(21), pp.5713-5724.
151. McMahon, R.E., Wang, L.N., Skoracki, R. and Mathur, A.B. Development of nanomaterials for bone repair and regeneration. *Journal of Biomedical Materials Research Part B-Applied Biomaterials*. 2013, **101B**(2), pp.387-397.
152. Athanasiou, K.A., Zhu, C.F., Lanctot, D.R., Agrawal, C.M. and Wang, X. Fundamentals of biomechanics in tissue engineering of bone. *Tissue Eng*. 2000, **6**(4), pp.361-381.
153. Asatrian, G., Pham, D., Hardy, W.R., James, A.W. and Peault, B. Stem cell technology for bone regeneration: current status and potential applications. *Stem Cells Cloning*. 2015, **8**, pp.39-48.
154. Finkemeier, C.G. Bone-grafting and bone-graft substitutes. *Journal of Bone and Joint Surgery-American Volume*. 2002, **84A**(3), pp.454-464.
155. Hammer, C., Linke, R., Wagner, F. and Diefenbeck, M. Organs from animals for man. *Int Arch Allergy Immunol*. 1998, **116**(1), pp.5-21.

156. Bach, F.H. Xenotransplantation: Problems and prospects. *Annual Review of Medicine*. 1998, **49**, pp.301-310.
157. Berthiaume, F., Maguire, T.J. and Yarmush, M.L. Tissue Engineering and Regenerative Medicine: History, Progress, and Challenges. *Annual Review of Chemical and Biomolecular Engineering, Vol 2*. 2011, **2**, pp.403-430.
158. Petrovic, V., Zivkovic, P., Petrovic, D. and Stefanovic, V. Craniofacial bone tissue engineering. *Oral Surgery Oral Medicine Oral Pathology Oral Radiology*. 2012, **114**(3), pp.E1-E9.
159. Nukavarapu, S.P. and Dorcemus, D.L. Osteochondral tissue engineering: Current strategies and challenges. *Biotechnol Adv*. 2013, **31**(5), pp.706-721.
160. Heng, B.C., Cao, T. and Lee, E.H. Directing stem cell differentiation into the chondrogenic lineage in vitro. *Stem Cells*. 2004, **22**(7), pp.1152-1167.
161. Gronthos, S., Brahim, J., Li, W., Fisher, L.W., Cherman, N., Boyde, A., DenBesten, P., Robey, P.G. and Shi, S. Stem cell properties of human dental pulp stem cells. *Journal of Dental Research*. 2002, **81**(8), pp.531-535.
162. Anker, P.S.I., Noort, W.A., Scherjon, S.A., Kleuburg-van der Keur, C., Kruisselbrink, A.B., van Bezoolien, R.L., Beekhuizen, W., Willemze, R., Kanhai, H.H.H. and Fibbe, W.E. Mesenchymal stem cells in human second-trimester bone marrow, liver, lung, and spleen exhibit a similar immunophenotype but a heterogeneous multilineage differentiation potential. *Haematologica*. 2003, **88**(8), pp.845-852.
163. Preynat-Seaube, O. and Krause, K.H. Stem cell sources for regenerative medicine: the immunological point of view. *Semin Immunopathol*. 2011, **33**(6), pp.519-524.
164. Nuti, N., Corallo, C., Chan, B.M.F., Ferrari, M. and Gerami-Naini, B. Multipotent Differentiation of Human Dental Pulp Stem Cells: a Literature Review. *Stem Cell Reviews and Reports*. 2016, **12**(5), pp.511-523.
165. Zuk, P.A., Zhu, M., Mizuno, H., Huang, J., Futrell, J.W., Katz, A.J., Benhaim, P., Lorenz, H.P. and Hedrick, M.H. Multilineage cells from human adipose tissue: implications for cell-based therapies. *Tissue Eng*. 2001, **7**(2), pp.211-228.
166. Young, H.E., Steele, T.A., Bray, R.A., Hudson, J., Floyd, J.A., Hawkins, K., Thomas, K., Austin, T., Edwards, C., Cuzzourt, J., Duenzl, M., Lucas, P.A. and Black, A.C., Jr. Human reserve pluripotent mesenchymal stem cells are present in the connective tissues of skeletal muscle and dermis derived from fetal, adult, and geriatric donors. *Anat Rec*. 2001, **264**(1), pp.51-62.
167. Drummond-Barbosa, D. Stem cells, their niches and the systemic environment: an aging network. *Genetics*. 2008, **180**(4), pp.1787-1797.
168. El-Gendy, R., Yang, X.B., Newby, P.J., Boccaccini, A.R. and Kirkham, J. Osteogenic differentiation of human dental pulp stromal cells on 45S5 Bioglass(R) based scaffolds in vitro and in vivo. *Tissue Eng Part A*. 2013, **19**(5-6), pp.707-715.
169. Saha, S., Kundu, B., Kirkham, J., Wood, D., Kundu, S.C. and Yang, X.B.B. Osteochondral Tissue Engineering In Vivo: A Comparative Study Using Layered Silk Fibroin Scaffolds from Mulberry and Nonmulberry Silkworms. *Plos One*. 2013, **8**(11).

170. Yang, X.B., Tare, R.S., Partridge, K.A., Roach, H.I., Clarke, N.M., Howdle, S.M., Shakesheff, K.M. and Oreffo, R.O. Induction of human osteoprogenitor chemotaxis, proliferation, differentiation, and bone formation by osteoblast stimulating factor-1/pleiotrophin: Osteoconductive biomimetic scaffolds for tissue engineering. *Journal of Bone and Mineral Research*. 2003, **18**(1), pp.47-57.
171. Liu, Y., Lim, J. and Teoh, S.H. Review: development of clinically relevant scaffolds for vascularised bone tissue engineering. *Biotechnol Adv*. 2013, **31**(5), pp.688-705.
172. Bueno, E.M. and Glowacki, J. *Biologic foundations for skeletal tissue engineering*. [Online]. San Rafael, Calif. (1537 Fourth Street, San Rafael, CA 94901 USA): Morgan & Claypool,, 2011. Available from: <http://0-www.morganclaypool.com.wam.leeds.ac.uk/doi/abs/10.2200/S00329ED1V01Y201101TIS007>
173. Bianco, P., Robey, P.G. and Simmons, P.J. Mesenchymal stem cells: Revisiting history, concepts, and assays. *Cell Stem Cell*. 2008, **2**(4), pp.313-319.
174. Murphy, M.B., Moncivais, K. and Caplan, A.I. Mesenchymal stem cells: environmentally responsive therapeutics for regenerative medicine. *Experimental and Molecular Medicine*. 2013, **45**.
175. Li, H.J., Shen, S., Fu, H.T., Wang, Z.Y., Li, X., Sui, X., Yuan, M., Liu, S.Y., Wang, G.Q. and Guo, Q.Y. Immunomodulatory Functions of Mesenchymal Stem Cells in Tissue Engineering. *Stem Cells International*. 2019.
176. Selmani, Z., Naji, A., Zidi, I., Favier, B., Gaiffe, E., Obert, L., Borg, C., Saas, P., Tiberghien, P., Rouas-Freiss, N., Carosella, E.D. and Deschaseaux, F. Human leukocyte antigen-G5 secretion by human mesenchymal stem cells is required to suppress T lymphocyte and natural killer function and to induce CD4(+)CD25(high)FOXP3(+) regulatory T cells. *Stem Cells*. 2008, **26**(1), pp.212-222.
177. Baker, B.M. and Chen, C.S. Deconstructing the third dimension - how 3D culture microenvironments alter cellular cues. *Journal of Cell Science*. 2012, **125**(13), pp.3015-3024.
178. Griffith, L.G. and Swartz, M.A. Capturing complex 3D tissue physiology in vitro. *Nat Rev Mol Cell Biol*. 2006, **7**(3), pp.211-224.
179. Jansen, K.A., Donato, D.M., Balcioglu, H.E., Schmidt, T., Danen, E.H. and Koenderink, G.H. A guide to mechanobiology: Where biology and physics meet. *Biochim Biophys Acta*. 2015, **1853**(11 Pt B), pp.3043-3052.
180. Meng, X., Leslie, P., Zhang, Y.P. and Dong, J.H. Stem cells in a three-dimensional scaffold environment. *Springerplus*. 2014, **3**.
181. Adjei, I.M. and Blanka, S. Modulation of the tumor microenvironment for cancer treatment: a biomaterials approach. *J Funct Biomater*. 2015, **6**(1), pp.81-103.
182. Vunjak-Novakovic G, G.S. Basic Orthopaedic Biomechanics and Mechano-biology. 2005, pp.343–408.
183. Langer, R. and Tirrell, D.A. Designing materials for biology and medicine. *Nature*. 2004, **428**(6982), pp.487-492.

184. Bose, S., Roy, M. and Bandyopadhyay, A. Recent advances in bone tissue engineering scaffolds. *Trends in Biotechnology*. 2012, **30**(10), pp.546-554.
185. Hersel, U., Dahmen, C. and Kessler, H. RGD modified polymers: biomaterials for stimulated cell adhesion and beyond. *Biomaterials*. 2003, **24**(24), pp.4385-4415.
186. Mizuno, M., Shindo, M., Kobayashi, D., Tsuruga, E., Amemiya, A. and Kuboki, Y. Osteogenesis by bone marrow stromal cells maintained on type I collagen matrix gels in vivo. *Bone*. 1997, **20**(2), pp.101-107.
187. O'Brien, F.J. Biomaterials & scaffolds for tissue engineering. *Materials Today*. 2011, **14**(3), pp.88-95.
188. Man, K., Jiang, L.H., Foster, R. and Yang, X.B.B. Immunological Responses to Total Hip Arthroplasty. *J Funct Biomater*. 2017, **8**(3).
189. Aida Elkayar, Y.E., Mariana Assaad. Properties of Hydroxyapatite from Bovine Teeth. *Bone and Tissue Regeneration Insights*. 2009, **2**, pp.31-36.
190. Dimitriou, R., Tsiridis, E. and Giannoudis, P.V. Current concepts of molecular aspects of bone healing. *Injury-International Journal of the Care of the Injured*. 2005, **36**(12), pp.1392-1404.
191. Tao, J., Sun, Y., Wang, Q.G. and Liu, C.W. Induced endothelial cells enhance osteogenesis and vascularization of mesenchymal stem cells. *Cells Tissues Organs*. 2010, **191**(5), p.430.
192. Nauth, A., Giannoudis, P.V., Einhorn, T.A., Hankenson, K.D., Friedlaender, G.E., Li, R. and Schemitsch, E.H. Growth Factors: Beyond Bone Morphogenetic Proteins. *Journal of Orthopaedic Trauma*. 2010, **24**(9), pp.543-546.
193. Simpson, A.H., Mills, L. and Noble, B. The role of growth factors and related agents in accelerating fracture healing. *J Bone Joint Surg Br*. 2006, **88**(6), pp.701-705.
194. Martin, I., Wendt, D. and Heberer, M. The role of bioreactors in tissue engineering. *Trends in Biotechnology*. 2004, **22**(2), pp.80-86.
195. Bleiziffer, O., Eriksson, E., Yao, F., Horch, R.E. and Kneser, U. Gene transfer strategies in tissue engineering. *Journal of Cellular and Molecular Medicine*. 2007, **11**(2), pp.206-223.
196. Baltzer, A.W., Lattermann, C., Whalen, J.D., Wooley, P., Weiss, K., Grimm, M., Ghivizzani, S.C., Robbins, P.D. and Evans, C.H. Genetic enhancement of fracture repair: healing of an experimental segmental defect by adenoviral transfer of the BMP-2 gene. *Gene Ther*. 2000, **7**(9), pp.734-739.
197. Evans, C.H. Gene therapy for bone healing. *Expert Reviews in Molecular Medicine*. 2010, **12**.
198. Worringer, K.A., Rand, T.A., Hayashi, Y., Sami, S., Takahashi, K., Tanabe, K., Narita, M., Srivastava, D. and Yamanaka, S. The let-7/LIN-41 pathway regulates reprogramming to human induced pluripotent stem cells by controlling expression of prodifferentiation genes. *Cell Stem Cell*. 2014, **14**(1), pp.40-52.
199. Takahashi, K. and Yamanaka, S. Induction of pluripotent stem cells from mouse embryonic and adult fibroblast cultures by defined factors. *Cell*. 2006, **126**(4), pp.663-676.

200. Ohradanova, A., Gradin, K., Barathova, M., Zatovicova, M., Holotnakova, T., Kopacek, J., Parkkila, S., Poellinger, L., Pastorekova, S. and Pastorek, J. Hypoxia upregulates expression of human endosialin gene via hypoxia-inducible factor 2. *Br J Cancer*. 2008, **99**(8), pp.1348-1356.
201. Kao, C.L., Tai, L.K., Chiou, S.H., Chen, Y.J., Lee, K.H., Chou, S.J., Chang, Y.L., Chang, C.M., Chen, S.J., Ku, H.H. and Li, H.Y. Resveratrol promotes osteogenic differentiation and protects against dexamethasone damage in murine induced pluripotent stem cells. *Stem Cells and Development*. 2010, **19**(2), pp.247-258.
202. Levi, B., Hyun, J.S., Montoro, D.T., Lo, D.D., Chan, C.K., Hu, S., Sun, N., Lee, M., Grova, M., Connolly, A.J., Wu, J.C., Gurtner, G.C., Weissman, I.L., Wan, D.C. and Longaker, M.T. In vivo directed differentiation of pluripotent stem cells for skeletal regeneration. *Proc Natl Acad Sci U S A*. 2012, **109**(50), pp.20379-20384.
203. Kumazaki, T., Kurata, S., Matsuo, T., Mitsui, Y. and Takahashi, T. Establishment of human induced pluripotent stem cell lines from normal fibroblast TIG-1. *Hum Cell*. 2011, **24**(2), pp.96-103.
204. Hu, X.Q., Fu, Y.T., Zhang, X., Dai, L.H., Zhu, J.X., Bi, Z.G., Ao, Y.F. and Zhou, C.Y. Histone deacetylase inhibitor sodium butyrate promotes the osteogenic differentiation of rat adipose- derived stem cells. *Development Growth & Differentiation*. 2014, **56**(3), pp.206-213.
205. Kim, T.I., Han, J.E., Jung, H.M., Oh, J.H. and Woo, K.M. Analysis of histone deacetylase inhibitor-induced responses in human periodontal ligament fibroblasts. *Biotechnology Letters*. 2013, **35**(1), pp.129-133.
206. Kim, H.N., Lee, J.H., Bae, S.C., Ryoo, H.M., Kim, H.H., Ha, H. and Lee, Z.H. Histone Deacetylase Inhibitor MS-275 Stimulates Bone Formation in Part by Enhancing Dlx36-Mediated TNAP Transcription. *Journal of Bone and Mineral Research*. 2011, **26**(9), pp.2161-2173.
207. Kim, H.N., Lee, J.H., Jin, W.J., Ko, S., Jung, K., Ha, H. and Lee, Z.H. MS-275, a benzamide histone deacetylase inhibitor, prevents osteoclastogenesis by down-regulating c-Fos expression and suppresses bone loss in mice. *Eur J Pharmacol*. 2012, **691**(1-3), pp.69-76.
208. Jung, H.M., Song, G.A., Lee, Y.K., Baek, J.H., Ryoo, H.M., Kim, G.S., Choung, P.H. and Woo, K.M. Modulation of the resorption and osteoconductivity of alpha-calcium sulfate by histone deacetylase inhibitors. *Biomaterials*. 2010, **31**(1), pp.29-37.
209. Paino, F., La Noce, M., Tirino, V., Naddeo, P., Desiderio, V., Pirozzi, G., De Rosa, A., Laino, L., Altucci, L. and Papaccio, G. Histone Deacetylase Inhibition with Valproic Acid Downregulates Osteocalcin Gene Expression in Human Dental Pulp Stem Cells and Osteoblasts: Evidence for HDAC2 Involvement. *Stem Cells*. 2014, **32**(1), pp.279-289.
210. Maroni, P., Brini, A.T., Arrigoni, E., de Girolamo, L., Niada, S., Matteucci, E., Bendinelli, P. and Desiderio, M.A. Chemical and genetic blockade of HDACs enhances osteogenic differentiation of human adipose tissue-derived stem cells by oppositely affecting osteogenic and adipogenic transcription factors. *Biochem Biophys Res Commun*. 2012, **428**(2), pp.271-277.

211. Xu, Y., Hammerick, K.E., James, A.W., Carre, A.L., Leucht, P., Giaccia, A.J. and Longaker, M.T. Inhibition of histone deacetylase activity in reduced oxygen environment enhances the osteogenesis of mouse adipose-derived stromal cells. *Tissue Eng Part A*. 2009, **15**(12), pp.3697-3707.
212. Cho, H.H., Park, H.T., Kim, Y.J., Bae, Y.C., Suh, K.T. and Jung, J.S. Induction of osteogenic differentiation of human mesenchymal stem cells by histone deacetylase inhibitors. *Journal of Cellular Biochemistry*. 2005, **96**(3), pp.533-542.
213. Yang, S.S., Zhang, R., Wang, G. and Zhang, Y.F. The development prospect of HDAC inhibitors as a potential therapeutic direction in Alzheimer's disease. *Translational Neurodegeneration*. 2017, **6**.
214. Lawlor, L.M. *The Effect of HDAC Inhibitor MI192 on Stem Cell Behaviour- The Potential of Utilising MI192 for Bone Tissue Engineering*. PhD thesis, University of Leeds, 2016.
215. Lee, S.U., Kwak, H.B., Pi, S.H., You, H.K., Byeon, S.R., Ying, Y., Luesch, H., Hong, J. and Kim, S.H. In Vitro and In Vivo Osteogenic Activity of Largazole. *ACS Med Chem Lett*. 2011, **2**(3), pp.248-251.
216. McGee-Lawrence, M.E., McCleary-Wheeler, A.L., Secreto, F.J., Razidlo, D.F., Zhang, M.Z., Stensgard, B.A., Li, X.D., Stein, G.S., Lian, J.B. and Westendorf, J.J. Suberoylanilide hydroxamic acid (SAHA; vorinostat) causes bone loss by inhibiting immature osteoblasts. *Bone*. 2011, **48**(5), pp.1117-1126.
217. Boluk, A., Guzelipek, M., Savli, H., Temel, I., Ozisik, H.I. and Kaygusuz, A. The effect of valproate on bone mineral density in adult epileptic patients. *Pharmacological Research*. 2004, **50**(1), pp.93-97.
218. Rampersad, S.N. Multiple Applications of Alamar Blue as an Indicator of Metabolic Function and Cellular Health in Cell Viability Bioassays. *Sensors*. 2012, **12**(9), pp.12347-12360.
219. Nociari, M.M., Shalev, A., Benias, P. and Russo, C. A novel one-step, highly sensitive fluorometric assay to evaluate cell-mediated cytotoxicity. *Journal of Immunological Methods*. 1998, **213**(2), pp.157-167.
220. Boveia, V. and Schutz-Geschwender, A. Quantitative Analysis of Signal Transduction with In-Cell Western Immunofluorescence Assays. *Methods Mol Biol*. 2015, **1314**, pp.115-130.
221. Hoffman, G.R., Moerke, N.J., Hsia, M., Shamu, C.E. and Blenis, J. A High-Throughput, Cell-Based Screening Method for siRNA and Small Molecule Inhibitors of mTORC1 Signaling Using the In Cell Western Technique. *Assay and Drug Development Technologies*. 2010, **8**(2), pp.186-199.
222. Izadpanah, R., Trygg, C., Patel, B., Kriedt, C., Dufour, J., Gimble, J.M. and Bunnell, B.A. Biologic properties of mesenchymal stem cells derived from bone marrow and adipose tissue. *Journal of Cellular Biochemistry*. 2006, **99**(5), pp.1285-1297.
223. Gronthos, S., Mankani, M., Brahimi, J., Robey, P.G. and Shi, S. Postnatal human dental pulp stem cells (DPSCs) in vitro and in vivo. *Proceedings of the National Academy of Sciences of the United States of America*. 2000, **97**(25), pp.13625-13630.

224. Seo, B.M., Miura, M. and Gronthos, S. Investigation of multipotent postnatal stem cells from human periodontal ligament. (vol 364, pg 149, 2004). *Lancet*. 2004, **364**(9447), pp.1756-1756.
225. Sonoyama, W., Liu, Y., Yamaza, T., Tuan, R.S., Wang, S., Shi, S. and Huang, G.T.J. Characterization of the apical papilla and its residing stem cells from human immature permanent teeth: A pilot study. *Journal of Endodontics*. 2008, **34**(2), pp.166-171.
226. Morsczeck, C., Gotz, W., Schierholz, J., Zellhofer, F., Kuhn, U., Mohl, C., Sippel, C. and Hoffmann, K.H. Isolation of precursor cells (PCs) from human dental follicle of wisdom teeth. *Matrix Biology*. 2005, **24**(2), pp.155-165.
227. Miura, M., Gronthos, S., Zhao, M., Lu, B., Fisher, L.W., Robey, P.G. and Shi, S. SHED - Stem cells from human exfoliated deciduous teeth. *Journal of Dental Research*. 2003, **82**, pp.B305-B305.
228. Tatsuhiro, F., Seiko, T., Yusuke, T., Reiko, T.T. and Kazuhito, S. Dental Pulp Stem Cell-Derived, Scaffold-Free Constructs for Bone Regeneration. *International Journal of Molecular Sciences*. 2018, **19**(7).
229. Teti, G., Salvatore, V., Focaroli, S., Durante, S., Mazzotti, A., Dicarlo, M., Mattioli-Belmonte, M. and Orsini, G. In vitro osteogenic and odontogenic differentiation of human dental pulp stem cells seeded on carboxymethyl cellulose-hydroxyapatite hybrid hydrogel. *Frontiers in Physiology*. 2015, **6**.
230. Fitzgerald, M., Chiego, D.J. and Heys, D.R. Autoradiographic Analysis of Odontoblast Replacement Following Pulp Exposure in Primate Teeth. *Archives of Oral Biology*. 1990, **35**(9), pp.707-715.
231. Lee, S.Y., Chiang, P.C., Tsai, Y.H., Tsai, S.Y., Jeng, J.H., Kawata, T. and Huang, H.M. Effects of Cryopreservation of Intact Teeth on the Isolated Dental Pulp Stem Cells. *Journal of Endodontics*. 2010, **36**(8), pp.1336-1340.
232. Zhang, W.B., Walboomers, X.F., Shi, S.T., Fan, M.W. and Jansen, J.A. Multilineage differentiation potential of stem cells derived from human dental pulp after cryopreservation. *Tissue Eng*. 2006, **12**(10), pp.2813-2823.
233. Jin, H., Park, J.Y., Choi, H. and Choung, P.H. HDAC Inhibitor Trichostatin A Promotes Proliferation and Odontoblast Differentiation of Human Dental Pulp Stem Cells. *Tissue Engineering Part A*. 2013, **19**(5-6), pp.613-624.
234. Duncan, H.F., Smith, A.J., Fleming, G.J.P. and Cooper, P.R. Histone deacetylase inhibitors epigenetically promote reparative events in primary dental pulp cells. *Experimental Cell Research*. 2013, **319**(10), pp.1534-1543.
235. Ghassemi, T., Shahroodi, A., Ebrahimzadeh, M.H., Mousavian, A., Movaffagh, J. and Moradi, A. Current Concepts in Scaffolding for Bone Tissue Engineering. *Archives of Bone and Joint Surgery-Abjs*. 2018, **6**(2), pp.90-99.
236. Stevens, M.M. Biomaterials for bone tissue engineering. *Materials Today*. 2008, **11**(5), pp.18-25.

237. Patra, C., Talukdar, S., Novoyatleva, T., Velagala, S.R., Muhlfeld, C., Kundu, B., Kundu, S.C. and Engel, F.B. Silk protein fibroin from *Antheraea mylitta* for cardiac tissue engineering. *Biomaterials*. 2012, **33**(9), pp.2673-2680.
238. Kundu, B., Rajkhowa, R., Kundu, S.C. and Wang, X.G. Silk fibroin biomaterials for tissue regenerations. *Advanced Drug Delivery Reviews*. 2013, **65**(4), pp.457-470.
239. Allmeling, C., Jokuszies, A., Reimers, K., Kall, S., Choi, C.Y., Brandes, G., Kasper, C., Scheper, T., Guggenheim, M. and Vogt, P.M. Spider silk fibres in artificial nerve constructs promote peripheral nerve regeneration. *Cell Proliferation*. 2008, **41**(3), pp.408-420.
240. Correia, C., Bhumiratana, S., Yan, L.P., Oliveira, A.L., Gimble, J.M., Rockwood, D., Kaplan, D.L., Sousa, R.A., Reis, R.L. and Vunjak-Novakovic, G. Development of silk-based scaffolds for tissue engineering of bone from human adipose-derived stem cells. *Acta Biomaterialia*. 2012, **8**(7), pp.2483-2492.
241. Zhao, J., Zhang, Z.Y., Wang, S.Y., Sun, X.J., Zhang, X.L., Chen, J., Kaplan, D.L. and Jiang, X.Q. Apatite-coated silk fibroin scaffolds to healing mandibular border defects in canines. *Bone*. 2009, **45**(3), pp.517-527.
242. Meinel, L., Fajardo, R., Hofmann, S., Langer, R., Chen, J., Snyder, B., Vunjak-Novakovic, G. and Kaplan, D. Silk implants for the healing of critical size bone defects. *Bone*. 2005, **37**(5), pp.688-698.
243. Groll, J., Boland, T., Blunk, T., Burdick, J.A., Cho, D.W., Dalton, P.D., Derby, B., Forgacs, G., Li, Q., Mironov, V.A., Moroni, L., Nakamura, M., Shu, W.M., Takeuchi, S., Vozzi, G., Woodfield, T.B.F., Xu, T., Yoo, J.J. and Malda, J. Biofabrication: reappraising the definition of an evolving field. *Biofabrication*. 2016, **8**(1).
244. Schon, B.S., Hooper, G.J. and Woodfield, T.B. Modular Tissue Assembly Strategies for Biofabrication of Engineered Cartilage. *Ann Biomed Eng*. 2016.
245. Langenbach, F., Berr, K., Naujoks, C., Hassel, A., Hentschel, M., Depprich, R., Kubler, N.R., Meyer, U., Wiesmann, H.P., Kogler, G. and Handschel, J. Generation and differentiation of microtissues from multipotent precursor cells for use in tissue engineering. *Nature Protocols*. 2011, **6**(11), pp.1726-1735.
246. Chambers, K.F., Mosaad, E.M.O., Russell, P.J., Clements, J.A. and Doran, M.R. 3D Cultures of Prostate Cancer Cells Cultured in a Novel High-Throughput Culture Platform Are More Resistant to Chemotherapeutics Compared to Cells Cultured in Monolayer. *Plos One*. 2014, **9**(11).
247. Mackay, A.M., Beck, S.C., Murphy, J.M., Barry, F.P., Chichester, C.O. and Pittenger, M.F. Chondrogenic differentiation of cultured human mesenchymal stem cells from marrow. *Tissue Eng*. 1998, **4**(4), pp.415-428.
248. Salaszyk, R.M., Williams, W.A., Boskey, A., Batorsky, A. and Plopper, G.E. Adhesion to vitronectin and collagen I promotes osteogenic differentiation of human mesenchymal stem cells. *Journal of Biomedicine and Biotechnology*. 2004, (1), pp.24-34.
249. Levi, B., Nelson, E.R., Brown, K., James, A.W., Xu, D., Dunlevie, R., Wu, J.C., Lee, M., Wu, B., Commons, G.W., Vistnes, D. and Longaker, M.T. Differences in Osteogenic Differentiation of

- Adipose-Derived Stromal Cells from Murine, Canine, and Human Sources In Vitro and In Vivo. *Plastic and Reconstructive Surgery*. 2011, **128**(2), pp.373-386.
250. Lammers, L., Naujoks, C., Berr, K., Depprich, R., Kubler, N., Meyer, U., Langenbach, F., Luttenberg, B., Kogler, G., Wiesmann, H.P. and Handschel, J. Impact of DAG stimulation on mineral synthesis, mineral structure and osteogenic differentiation of human cord blood stem cells. *Stem Cell Research*. 2012, **8**(2), pp.193-205.
 251. Tomlinson, M.J., Dennis, C., Yang, X.B.B. and Kirkham, J. Tissue non-specific alkaline phosphatase production by human dental pulp stromal cells is enhanced by high density cell culture. *Cell and Tissue Research*. 2015, **361**(2), pp.529-540.
 252. Noda, S., Kawashima, N., Yamamoto, M., Hashimoto, K., Nara, K., Sekiya, I. and Okiji, T. Effect of cell culture density on dental pulp-derived mesenchymal stem cells with reference to osteogenic differentiation. *Scientific Reports*. 2019, **9**.
 253. Schon, B.S., Schrobback, K., van der Ven, M., Stroebel, S., Hooper, G.J. and Woodfield, T.B.F. Validation of a high-throughput microtissue fabrication process for 3D assembly of tissue engineered cartilage constructs. *Cell and Tissue Research*. 2012, **347**(3), pp.629-642.
 254. Langenbach, F., Naujoks, C., Smeets, R., Berr, K., Depprich, R., Kubler, N. and Handschel, J. Scaffold-free microtissues: differences from monolayer cultures and their potential in bone tissue engineering. *Clinical Oral Investigations*. 2013, **17**(1), pp.9-17.
 255. Ashton, B.A., Allen, T.D., Howlett, C.R., Eaglesom, C.C., Hattori, A. and Owen, M. Formation of Bone and Cartilage by Marrow Stromal Cells in Diffusion-Chambers Invivo. *Clinical Orthopaedics and Related Research*. 1980, (151), pp.294-307.
 256. Partridge, K.A., Yang, X., Clarke, N.M.P., Okubo, Y., Bessho, K., Howdle, S.M., Shakesheff, K.M. and Oreffo, R.O.C. Adenoviral BMP-2 gene transfer in mesenchymal stem cells - In vitro and in vivo bone formation on biodegradable polymer scaffolds. *Journal of Bone and Mineral Research*. 2002, **17**(7), pp.1326-1326.
 257. Howard, D., Partridge, K., Yang, X.B., Clarke, N.M.P., Okubo, Y., Bessho, K., Howdle, S.M., Shakesheff, K.M. and Oreffo, R.O.C. Immunoselection and adenoviral genetic modulation of human osteoprogenitors: in vivo bone formation on PLA scaffold. *Biochem Biophys Res Commun*. 2002, **299**(2), pp.208-215.
 258. Yang, X.B.B., Whitaker, M.J., Sebald, W., Clarke, N., Howdle, S.M., Shakesheff, K.M. and Oreffo, R.O.C. Human osteoprogenitor bone formation using encapsulated bone morphogenetic protein 2 in porous polymer scaffolds. *Tissue Eng*. 2004, **10**(7-8), pp.1037-1045.
 259. Rockwood, D.N., Preda, R.C., Yucel, T., Wang, X.Q., Lovett, M.L. and Kaplan, D.L. Materials fabrication from Bombyx mori silk fibroin. *Nature Protocols*. 2011, **6**(10), pp.1612-1631.
 260. Rnjak-Kovacina, J., Wray, L.S., Burke, K.A., Torregrosa, T., Golinski, J.M., Huang, W.W. and Kaplan, D.L. Lyophilized Silk Sponges: A Versatile Biomaterial Platform for Soft Tissue Engineering. *Acs Biomaterials Science & Engineering*. 2015, **1**(4), pp.260-270.

261. La Noce, M., Pain, F., Spina, A., Naddeo, P., Montella, R., Desiderio, V., De Rosa, A., Papaccio, G., Tirino, V. and Laino, L. Dental pulp stem cells: State of the art and suggestions for a true translation of research into therapy. *Journal of Dentistry*. 2014, **42**(7), pp.761-768.
262. Jonason, J.H., Xiao, G., Zhang, M., Xing, L. and Chen, D. Post-translational Regulation of Runx2 in Bone and Cartilage. *Journal of Dental Research*. 2009, **88**(8), pp.693-703.
263. Di Bernardo, G., Squillaro, T., Dell'Aversana, C., Miceli, M., Cipollaro, M., Cascino, A., Altucci, L. and Galderisi, U. Histone Deacetylase Inhibitors Promote Apoptosis and Senescence in Human Mesenchymal Stem Cells. *Stem Cells and Development*. 2009, **18**(4), pp.573-581.
264. Lee, S., Park, J.R., Seo, M.S., Roh, K.H., Park, S.B., Hwang, J.W., Sun, B., Seo, K., Lee, Y.S., Kang, S.K., Jung, J.W. and Kang, K.S. Histone deacetylase inhibitors decrease proliferation potential and multilineage differentiation capability of human mesenchymal stem cells. *Cell Proliferation*. 2009, **42**(6), pp.711-720.
265. Davies, O.G., Cooper, P.R., Shelton, R.M., Smith, A.J. and Scheven, B.A. A comparison of the in vitro mineralisation and dentinogenic potential of mesenchymal stem cells derived from adipose tissue, bone marrow and dental pulp. *Journal of Bone and Mineral Metabolism*. 2015, **33**(4), pp.371-382.
266. Bellarosa, D., Bressan, A., Bigioni, M., Parlani, M., Maggi, C.A. and Binaschi, M. SAHA/Vorinostat induces the expression of the CD137 receptor/ligand system and enhances apoptosis mediated by soluble CD137 receptor in a human breast cancer cell line. *International Journal of Oncology*. 2012, **41**(4), pp.1486-1494.
267. Kuljaca, S., Liu, T., El Tee, A., Haber, M., Norris, M.D., Dwarte, T. and Marshall, G.M. Enhancing the anti-angiogenic action of histone deacetylase inhibitors. *Molecular Cancer*. 2007, **6**.
268. Fajas, L. Re-thinking cell cycle regulators: the cross-talk with metabolism. *Front Oncol*. 2013, **3**, p.4.
269. Lee, I.H. and Finkel, T. Metabolic regulation of the cell cycle. *Current Opinion in Cell Biology*. 2013, **25**(6), pp.724-729.
270. Ahn, S.J., Costa, J. and Emanuel, J.R. PicoGreen quantitation of DNA: Effective evaluation of samples pre- or post-PCR (vol 24, pg 2623, 1996). *Nucleic Acids Research*. 1996, **24**(16), pp.3282-3282.
271. Quent, V.M.C., Loessner, D., Friis, T., Reichert, J.C. and Hutmacher, D.W. Discrepancies between metabolic activity and DNA content as tool to assess cell proliferation in cancer research. *Journal of Cellular and Molecular Medicine*. 2010, **14**(4), pp.1003-1013.
272. Singh, B.N., Zhou, H.Y., Li, J.P., Tipton, T., Wang, B., Shao, G., Gilbert, E.N., Li, Q. and Jiang, S.W. Preclinical studies on histone deacetylase inhibitors as therapeutic reagents for endometrial and ovarian cancers. *Future Oncology*. 2011, **7**(12), pp.1415-1428.
273. Jones, J., Juengel, E., Mickuckyte, A., Hudak, L., Wedel, S., Jonas, D., Hintereder, G. and Blaheta, R.A. Valproic acid blocks adhesion of renal cell carcinoma cells to endothelium and extracellular matrix. *Journal of Cellular and Molecular Medicine*. 2009, **13**(8B), pp.2342-2352.

274. Niles, A.L., Moravec, R.A. and Riss, T.L. In vitro viability and cytotoxicity testing and same-well multi-parametric combinations for high throughput screening. *Curr Chem Genomics*. 2009, **3**, pp.33-41.
275. Yamaguchi, T., Cubizolles, F., Zhang, Y., Reichert, N., Kohler, H., Seiser, C. and Matthias, P. Histone deacetylases 1 and 2 act in concert to promote the G1-to-S progression. *Genes & Development*. 2010, **24**(5), pp.455-469.
276. Yoshida, M., Matsuyama, A., Komatsu, Y. and Nishino, N. From discovery to the coming generation of histone deacetylase inhibitors. *Current Medicinal Chemistry*. 2003, **10**(22), pp.2351-2358.
277. Zhu, J.X., Gu, J.H., Ma, J., Xu, Z.X. and Tao, H.R. Histone deacetylase inhibitors repress chondrosarcoma cell proliferation. *Journal of Buon*. 2015, **20**(1), pp.269-274.
278. McGee-Lawrence, M.E. and Westendorf, J.J. Histone deacetylases in skeletal development and bone mass maintenance. *Gene*. 2011, **474**(1-2), pp.1-11.
279. Petruccelli, L.A., Dupere-Richer, D., Pettersson, F., Retrouvey, H., Skoulikas, S. and Miller, W.H. Vorinostat Induces Reactive Oxygen Species and DNA Damage in Acute Myeloid Leukemia Cells. *Plos One*. 2011, **6**(6).
280. Zhang, J.L., Tao, Z.W. and Wang, Y.L. Long non-coding RNA DANCR regulates the proliferation and osteogenic differentiation of human bone-derived marrow mesenchymal stem cells via the p38 MAPK pathway. *International Journal of Molecular Medicine*. 2018, **41**(1), pp.213-219.
281. Shafa, M., Krawetz, R. and Rancourt, D.E. Returning to the stem state: Epigenetics of recapitulating pre-differentiation chromatin structure. *Bioessays*. 2010, **32**(9), pp.791-799.
282. Bacon, T., Seiler, C., Wolny, M., Hughes, R., Watson, P., Schwabe, J., Grigg, R. and Peckham, M. Histone deacetylase 3 indirectly modulates tubulin acetylation. *Biochemical Journal*. 2015, **472**, pp.367-377.
283. Xu, Y.X., Voelter-Mahlknecht, S. and Mahlknecht, U. The histone deacetylase inhibitor suberoylanilide hydroxamic acid down-regulates expression levels of Bcr-abl, c-Myc and HDAC3 in chronic myeloid leukemia cell lines. *International Journal of Molecular Medicine*. 2005, **15**(1), pp.169-172.
284. Seto, E. The Biology of HDAC3. In: Verdin, E. ed. *Histone Deacetylases: Transcriptional Regulation and Other Cellular Functions*. Totowa, NJ: Humana Press, 2006, pp.61-86.
285. Schroeder, T.M., Nair, A.K., Staggs, R., Lamblin, A.F. and Westendorf, J.J. Gene profile analysis of osteoblast genes differentially regulated by histone deacetylase inhibitors. *Bmc Genomics*. 2007, **8**.
286. Xu, Y., Hammerick, K.E., James, A.W., Carre, A.L., Leucht, P., Giaccia, A.J. and Longaker, M.T. Inhibition of Histone Deacetylase Activity in Reduced Oxygen Environment Enhances the Osteogenesis of Mouse Adipose-Derived Stromal Cells. *Tissue Engineering Part A*. 2009, **15**(12), pp.3697-3707.

287. Russell, A.L., Lefavor, R., Durand, N., Glover, L. and Zubair, A.C. Modifiers of mesenchymal stem cell quantity and quality. *Transfusion*. 2018, **58**(6), pp.1434-1440.
288. Siddappa, R., Licht, R., van Blitterswijk, C. and de Boer, J. Donor variation and loss of multipotency during in vitro expansion of human mesenchymal stem cells for bone tissue engineering. *Journal of Orthopaedic Research*. 2007, **25**(8), pp.1029-1041.
289. Collas, P., Noer, A. and Sorensen, A.L. Epigenetic Basis for the Differentiation Potential of Mesenchymal and Embryonic Stem Cells. *Transfus Med Hemother*. 2008, **35**(3), pp.205-215.
290. Hu, X.Q., Zhang, X., Dai, L.H., Zhu, J.X., Jia, Z.Q., Wang, W.P., Zhou, C.Y. and Ao, Y.F. Histone Deacetylase Inhibitor Trichostatin A Promotes the Osteogenic Differentiation of Rat Adipose-Derived Stem Cells by Altering the Epigenetic Modifications on Runx2 Promoter in a BMP Signaling-Dependent Manner. *Stem Cells and Development*. 2013, **22**(2), pp.248-255.
291. Huynh, N.C., Everts, V., Pavasant, P. and Ampornaramveth, R.S. Inhibition of Histone Deacetylases Enhances the Osteogenic Differentiation of Human Periodontal Ligament Cells. *Journal of Cellular Biochemistry*. 2016, **117**(6), pp.1384-1395.
292. Jeon, E.J., Lee, K.Y., Choi, N.S., Lee, M.H., Kim, H.N., Jin, Y.H., Ryoo, H.M., Choi, J.Y., Yoshida, M., Nishino, N., Oh, B.C., Lee, K.S., Lee, Y.H. and Bae, S.C. Bone morphogenetic protein-2 stimulates Runx2 acetylation. *Journal of Biological Chemistry*. 2006, **281**(24), pp.16502-16511.
293. Sasano, Y., Ohtani, E., Narita, K., Kagayama, M., Murata, M., Saito, T., Shigenobu, K., Takita, H., Mizuno, M. and Kuboki, Y. Bmps Induce Direct Bone-Formation in Ectopic Sites Independent of the Endochondral Ossification Invivo. *Anatomical Record*. 1993, **236**(2), pp.373-380.
294. Jang, W.G., Kim, E.J., Kim, D.K., Ryoo, H.M., Lee, K.B., Kim, S.H., Choi, H.S. and Koh, J.T. BMP2 protein regulates osteocalcin expression via Runx2-mediated Atf6 gene transcription. *Journal of Biological Chemistry*. 2012, **287**(2), pp.905-915.
295. Carragee, E.J., Hurwitz, E.L. and Weiner, B.K. A critical review of recombinant human bone morphogenetic protein-2 trials in spinal surgery: emerging safety concerns and lessons learned. *Spine Journal*. 2011, **11**(6), pp.471-491.
296. Phimphilai, M., Zhao, Z.R., Boules, H., Roca, H. and Franceschi, R.T. BMP signaling is required for RUNX2-dependent induction of the osteoblast phenotype. *Journal of Bone and Mineral Research*. 2006, **21**(4), pp.637-646.
297. Jin, H., Park, J.Y., Choi, H. and Choung, P.H. HDAC inhibitor trichostatin A promotes proliferation and odontoblast differentiation of human dental pulp stem cells. *Tissue Eng Part A*. 2013, **19**(5-6), pp.613-624.
298. Alge, D.L., Zhou, D., Adams, L.L., Wyss, B.K., Shadday, M.D., Woods, E.J., Chu, T.M.G. and Goebel, W.S. Donor-matched comparison of dental pulp stem cells and bone marrow-derived mesenchymal stem cells in a rat model. *Journal of Tissue Engineering and Regenerative Medicine*. 2010, **4**(1), pp.73-81.
299. Fu, Y., Zhang, P., Ge, J., Cheng, J., Dong, W.J., Yuan, H., Du, Y.F., Yang, M.F., Sun, R.X. and Jiang, H.B. Histone deacetylase 8 suppresses osteogenic differentiation of bone marrow

- stromal cells by inhibiting histone H3K9 acetylation and RUNX2 activity. *International Journal of Biochemistry & Cell Biology*. 2014, **54**, pp.68-77.
300. Langenbach, F., Naujoks, C., Laser, A., Kelz, M., Kersten-Thiele, P., Berr, K., Depprich, R., Kubler, N., Kogler, G. and Handschel, J. Improvement of the Cell-loading Efficiency of Biomaterials by Inoculation with Stem Cell-based Microspheres, in Osteogenesis. *Journal of Biomaterials Applications*. 2012, **26**(5), pp.549-564.
 301. Tomoiaia, G. and Pasca, R.D. On the Collagen Mineralization. A Review. *Clujul Med*. 2015, **88**(1), pp.15-22.
 302. Orimo, H. The mechanism of mineralization and the role of alkaline phosphatase in health and disease. *J Nippon Med Sch*. 2010, **77**(1), pp.4-12.
 303. Tsao, Y.T., Huang, Y.J., Wu, H.H., Liu, Y.A., Liu, Y.S. and Lee, O.K. Osteocalcin Mediates Biomineralization during Osteogenic Maturation in Human Mesenchymal Stromal Cells. *International Journal of Molecular Sciences*. 2017, **18**(1).
 304. Melke, J., Midha, S., Ghosh, S., Ito, K. and Hofmann, S. Silk fibroin as biomaterial for bone tissue engineering. *Acta Biomaterialia*. 2016, **31**, pp.1-16.
 305. Yang, Y., Ding, F., Wu, H., Hu, W., Liu, W., Liu, H. and Gu, X. Development and evaluation of silk fibroin-based nerve grafts used for peripheral nerve regeneration. *Biomaterials*. 2007, **28**(36), pp.5526-5535.
 306. Collado-Gonzalez, M., Pecci-Lloret, M.P., Garcia-Bernal, D., Aznar-Cervantes, S., Onate-Sanchez, R.E., Moraleda, J.M., Cenis, J.L. and Rodriguez-Lozano, F.J. Biological effects of silk fibroin 3D scaffolds on stem cells from human exfoliated deciduous teeth (SHEDs). *Odontology*. 2018, **106**(2), pp.125-134.
 307. Ghasemi-Mobarakeh, L., Prabhakaran, M.P., Tian, L.L., Shamirzaei-Jeshvaghani, E., Dehghani, L. and Ramakrishna, S. Structural properties of scaffolds: Crucial parameters towards stem cells differentiation. *World Journal of Stem Cells*. 2015, **7**(4), pp.728-744.
 308. Shih, Y.R.V., Tseng, K.F., Lai, H.Y., Lin, C.H. and Lee, O.K. Matrix Stiffness Regulation of Integrin-Mediated Mechanotransduction During Osteogenic Differentiation of Human Mesenchymal Stem Cells. *Journal of Bone and Mineral Research*. 2011, **26**(4), pp.730-738.
 309. Engler, A.J., Sen, S., Sweeney, H.L. and Discher, D.E. Matrix elasticity directs stem cell lineage specification. *Cell*. 2006, **126**(4), pp.677-689.
 310. Seib, F.P., Prewitz, M., Werner, C. and Bornhauser, M. Matrix elasticity regulates the secretory profile of human bone marrow-derived multipotent mesenchymal stromal cells (MSCs). *Biochem Biophys Res Commun*. 2009, **389**(4), pp.663-667.
 311. Patwari, P. and Lee, R.T. Mechanical control of tissue morphogenesis. *Circulation Research*. 2008, **103**(3), pp.234-243.
 312. Vining, K.H. and Mooney, D.J. Mechanical forces direct stem cell behaviour in development and regeneration. *Nature Reviews Molecular Cell Biology*. 2017, **18**(12), pp.728-742.

313. Persson, M., Lehenkari, P.P., Berglin, L., Turunen, S., Finnila, M.A.J., Risteli, J., Skrifvars, M. and Tuukkanen, J. Osteogenic Differentiation of Human Mesenchymal Stem cells in a 3D Woven Scaffold. *Scientific Reports*. 2018, **8**.
314. Shekaran, A., Sim, E., Tan, K.Y., Chan, J.K.Y., Choolani, M., Reuveny, S. and Oh, S. Enhanced in vitro osteogenic differentiation of human fetal MSCs attached to 3D microcarriers versus harvested from 2D monolayers. *Bmc Biotechnology*. 2015, **15**.
315. Hishikawa, K., Miura, S., Marumo, T., Yoshioka, H., Mori, Y., Takato, T. and Fujita, T. Gene expression profile of human mesenchymal stem cells during osteogenesis in three-dimensional thermoreversible gelation polymer. *Biochem Biophys Res Commun*. 2004, **317**(4), pp.1103-1107.
316. Bancroft, G.N., Sikavitsast, V.I., van den Dolder, J., Sheffield, T.L., Ambrose, C.G., Jansen, J.A. and Mikos, A.G. Fluid flow increases mineralized matrix deposition in 3D perfusion culture of marrow stromal osteoblasts in a dose-dependent manner. *Proceedings of the National Academy of Sciences of the United States of America*. 2002, **99**(20), pp.12600-12605.
317. Bilodeau, K. and Mantovani, D. Bioreactors for tissue engineering: Focus on mechanical constraints. A comparative review. *Tissue Eng*. 2006, **12**(8), pp.2367-2383.
318. Pizzute, T., Lynch, K. and Pei, M. Impact of Tissue-Specific Stem Cells on Lineage-Specific Differentiation: A Focus on the Musculoskeletal System. *Stem Cell Reviews and Reports*. 2015, **11**(1), pp.119-132.
319. Liao, H.T. and Chen, C.T. Osteogenic potential: Comparison between bone marrow and adipose-derived mesenchymal stem cells. *World Journal of Stem Cells*. 2014, **6**(3), pp.288-295.
320. Huynh, N.C.N., Everts, V., Nifuji, A., Pavasant, P. and Ampornaramveth, R.S. Histone deacetylase inhibition enhances in-vivo bone regeneration induced by human periodontal ligament cells. *Bone*. 2017, **95**, pp.76-84.
321. Hildebrandt, C., Buth, H. and Thielecke, H. A scaffold-free in vitro model for osteogenesis of human mesenchymal stem cells. *Tissue & Cell*. 2011, **43**(2), pp.91-100.
322. Lee, J.I., Sato, M., Kim, H.W. and Mochida, J. Transplantation of scaffold-free spheroids composed of synovium-derived cells and chondrocytes for the treatment of cartilage defects of the knee. *Eur Cell Mater*. 2011, **22**, pp.275-290; discussion 290.
323. Malda, J., Woodfield, T.B.F., van der Vloodt, F., Wilson, C., Martens, D.E., Tramper, J., van Blitterswijk, C.A. and Riesle, J. The effect of PEGT/PBT scaffold architecture on the composition of tissue engineered cartilage. *Biomaterials*. 2005, **26**(1), pp.63-72.
324. Sackers, R.J., de Wijn, J.R., Dalmeyer, R.A., van Blitterswijk, C.A. and Brand, R. Evaluation of copolymers of polyethylene oxide and polybutylene terephthalate (polyactive): mechanical behaviour. *J Mater Sci Mater Med*. 1998, **9**(7), pp.375-379.
325. Deschamps, A.A., Claase, M.B., Sleijsler, W.J., de Bruijn, J.D., Grijpma, D.W. and Feijen, J. Design of segmented poly(ether ester) materials and structures for the tissue engineering of bone. *Journal of Controlled Release*. 2002, **78**(1-3), pp.175-186.

326. Vanblitterswijk, C.A., Vanderbrink, J., Leenders, H. and Bakker, D. The Effect of Peo Ratio on Degradation, Calcification and Bone Bonding of Peo/Pbt Copolymer (Polyactive). *Cells and Materials*. 1993, **3**(1), pp.23-36.
327. Malda, J., Visser, J., Melchels, F.P., Jungst, T., Hennink, W.E., Dhert, W.J.A., Groll, J. and Hutmacher, D.W. 25th Anniversary Article: Engineering Hydrogels for Biofabrication. *Advanced Materials*. 2013, **25**(36), pp.5011-5028.
328. Hutmacher, D.W. Scaffolds in tissue engineering bone and cartilage. *Biomaterials*. 2000, **21**(24), pp.2529-2543.
329. Yilgor, P., Sousa, R.A., Reis, R.L., Hasirci, N. and Hasirci, V. 3D plotted PCL scaffolds for stem cell based bone tissue engineering. *Macromolecular Symposia*. 2008, **269**, pp.92-99.
330. Sun, M.Z. and Downes, S. Physicochemical characterisation of novel ultra-thin biodegradable scaffolds for peripheral nerve repair. *Journal of Materials Science-Materials in Medicine*. 2009, **20**(5), pp.1181-1192.
331. Totaro, A., Salerno, A., Imparato, G., Domingo, C., Urciuolo, F. and Netti, P.A. PCL-HA microscaffolds for in vitro modular bone tissue engineering. *Journal of Tissue Engineering and Regenerative Medicine*. 2015.
332. Lu, L., Zhang, Q.W., Wootton, D., Chiou, R., Li, D.C., Lu, B.H., Lelkes, P. and Zhou, J. Biocompatibility and biodegradation studies of PCL/beta-TCP bone tissue scaffold fabricated by structural porogen method. *Journal of Materials Science-Materials in Medicine*. 2012, **23**(9), pp.2217-2226.
333. Mekhileri, N., S.B., Lim, K., Hooper, G., Woodfield, T. Biofabrication of tissue engineered cartilage constructs via an automated 3D micro-tissue assembly system. *International Conference on Biofabrication*. 2015.
334. Woodfield, T.B.F., Malda, J., de Wijn, J., Peters, F., Riesle, J. and van Blitterswijk, C.A. Design of porous scaffolds for cartilage tissue engineering using a three-dimensional fiber-deposition technique. *Biomaterials*. 2004, **25**(18), pp.4149-4161.
335. Mekhileri, N.V., Lim, K.S., Brown, G.C.J., Mutreja, I., Schon, B.S., Hooper, G.J. and Woodfield, T.B.F. Automated 3D bioassembly of micro-tissues for biofabrication of hybrid tissue engineered constructs. *Biofabrication*. 2018, **10**(2).
336. Zhang, L.M., Su, P.Q., Xu, C.X., Yang, J.L., Yu, W.H. and Huang, D.S. Chondrogenic differentiation of human mesenchymal stem cells: a comparison between micromass and pellet culture systems. *Biotechnology Letters*. 2010, **32**(9), pp.1339-1346.
337. Handschel, J.G., Depprich, R.A., Kubler, N.R., Wiesmann, H.P., Ommerborn, M. and Meyer, U. Prospects of micromass culture technology in tissue engineering. *Head Face Med*. 2007, **3**, p.4.
338. Yoo, J.U., Barthel, T.S., Nishimura, K., Solchaga, L., Caplan, A.I., Goldberg, V.M. and Johnstone, B. The chondrogenic potential of human bone-marrow-derived mesenchymal progenitor cells. *Journal of Bone and Joint Surgery-American Volume*. 1998, **80A**(12), pp.1745-1757.

339. Johnstone, B., Hering, T.M., Caplan, A.I., Goldberg, V.M. and Yoo, J.U. In vitro chondrogenesis of bone marrow-derived mesenchymal progenitor cells. *Experimental Cell Research*. 1998, **238**(1), pp.265-272.
340. Lee, J. and Im, G.I. Effects of Trichostatin A on the Chondrogenesis from Human Mesenchymal Stem Cells. *Tissue Engineering and Regenerative Medicine*. 2017, **14**(4), pp.403-410.
341. Golub, E.E., Harrison, G., Taylor, A.G., Camper, S. and Shapiro, I.M. The Role of Alkaline-Phosphatase in Cartilage Mineralization. *Bone and Mineral*. 1992, **17**(2), pp.273-278.
342. Futrega, K., Mosaad, E., Chambers, K., Lott, W.B., Clements, J. and Doran, M.R. Bone marrow-derived stem/stromal cells (BMSC) 3D microtissues cultured in BMP-2 supplemented osteogenic induction medium are prone to adipogenesis. *Cell and Tissue Research*. 2018, **374**(3), pp.541-553.
343. Fischer, A.H., Jacobson, K.A., Rose, J. and Zeller, R. Hematoxylin and eosin staining of tissue and cell sections. *CSH Protoc*. 2008, **2008**, p.pdb prot4986.
344. White, A. and Wallis, G. Endochondral ossification: A delicate balance between growth and mineralisation. *Current Biology*. 2001, **11**(15), pp.R589-R591.
345. Zheng, L., Sun, J., Chen, X.N., Wang, G., Jiang, B., Fan, H.S. and Zhang, X.D. In Vivo Cartilage Engineering with Collagen Hydrogel and Allogeneous Chondrocytes After Diffusion Chamber Implantation in Immunocompetent Host. *Tissue Engineering Part A*. 2009, **15**(8), pp.2145-2153.
346. Nawata, M., Wakitani, S., Nakaya, H., Tanigami, A., Seki, T., Nakamura, Y., Saito, N., Sano, K., Hidaka, E. and Takaoka, K. Use of bone morphogenetic protein 2 and diffusion chambers to engineer cartilage tissue for the repair of defects in articular cartilage. *Arthritis and Rheumatism*. 2005, **52**(1), pp.155-163.
347. Zheng, L., Yang, J.S., Fan, H.S. and Zhang, X.D. Material-induced chondrogenic differentiation of mesenchymal stem cells is material-dependent. *Experimental and Therapeutic Medicine*. 2014, **7**(5), pp.1147-1150.
348. Zheng, L., Fan, H.S., Sun, J., Chen, X.N., Wang, G., Zhang, L., Fan, Y.J. and Zhang, X.D. Chondrogenic differentiation of mesenchymal stem cells induced by collagen-based hydrogel: An in vivo study. *Journal of Biomedical Materials Research Part A*. 2010, **93A**(2), pp.783-792.
349. Weyand, B., Reimers, K. and Vogt, P.M. Influences of Extracellular Matrix Properties and Flow Shear Stresses on Stem Cell Shape in a Three-Dimensional Dynamic Environment. *8th International Conference on Cell & Stem Cell Engineering (Icce)*. 2011, **30**, pp.47-+.
350. Kiani, C., Chen, L., Wu, Y.J., Yee, A.J. and Yang, B.B. Structure and function of aggrecan. *Cell Research*. 2002, **12**(1), pp.19-32.
351. Carballo, C.B., Nakagawa, Y., Sekiya, I. and Rodeo, S.A. Basic Science of Articular Cartilage. *Clin Sports Med*. 2017, **36**(3), pp.413-425.

352. Jo, I., Lee, J.M., Suh, H. and Kim, H. Bone tissue engineering using marrow stromal cells. *Biotechnology and Bioprocess Engineering*. 2007, **12**(1), pp.48-53.
353. Friedenstein, A.J., Petrakova, K.V., Kurolesova, A.I. and Frolova, G.P. Heterotopic Transplants of Bone Marrow - Analysis of Precursor Cells for Osteogenic and Hematopoietic Tissues. *Transplantation*. 1968, **6**(2), pp.230-+.
354. Zhao, J.J., Yang, C.B., Su, C., Yu, M., Zhang, X.M., Huang, S., Li, G., Yu, M.L. and Li, X.R. Reconstruction of orbital defects by implantation of antigen-free bovine cancellous bone scaffold combined with bone marrow mesenchymal stem cells in rats. *Graefes Archive for Clinical and Experimental Ophthalmology*. 2013, **251**(5), pp.1325-1333.
355. Gan, Y.K., Dai, K.R., Zhang, P., Tang, T.T., Zhu, Z.N. and Lu, J.X. The clinical use of enriched bone marrow stem cells combined with porous beta-tricalcium phosphate in posterior spinal fusion. *Biomaterials*. 2008, **29**(29), pp.3973-3982.
356. Balmayor, E.R. and van Griensven, M. Gene therapy for bone engineering. *Front Bioeng Biotechnol*. 2015, **3**, p.9.
357. Goessler, U.R., Riedel, K., Hormann, K. and Riedel, F. Perspectives of gene therapy in stem cell tissue engineering. *Cells Tissues Organs*. 2006, **183**(4), pp.169-179.
358. Lu, L., Qi, Y.S., Zhou, C.R. and Jiao, Y.P. Rapidly in situ forming biodegradable hydrogels by combining alginate and hydroxyapatite nanocrystal. *Science China-Technological Sciences*. 2010, **53**(1), pp.272-277.
359. Teixeira, L.S.M., Feijen, J., van Blitterswijk, C.A., Dijkstra, P.J. and Karperien, M. Enzyme-catalyzed crosslinkable hydrogels: Emerging strategies for tissue engineering. *Biomaterials*. 2012, **33**(5), pp.1281-1290.
360. Lim, K.S., Alves, M.H., Poole-Warren, L.A. and Martens, P.J. Covalent incorporation of non-chemically modified gelatin into degradable PVA-tyramine hydrogels. *Biomaterials*. 2013, **34**(29), pp.7097-7105.
361. Van den Bulcke, A.I., Bogdanov, B., De Rooze, N., Schacht, E.H., Cornelissen, M. and Berghmans, H. Structural and rheological properties of methacrylamide modified gelatin hydrogels. *Biomacromolecules*. 2000, **1**(1), pp.31-38.
362. Galis, Z.S. and Khatri, J.J. Matrix metalloproteinases in vascular remodeling and atherogenesis - The good, the bad, and the ugly. *Circulation Research*. 2002, **90**(3), pp.251-262.
363. Van den Steen, P.E., Dubois, B., Nelissen, I., Rudd, P.M., Dwek, R.A. and Opdenakker, G. Biochemistry and molecular biology of gelatinase B or matrix metalloproteinase-9 (MMP-9). *Critical Reviews in Biochemistry and Molecular Biology*. 2002, **37**(6), pp.375-536.
364. Gevaert, E., Dolle, L., Billiet, T., Dubrueel, P. and van Grunsven, L. High Throughput Micro-Well Generation of Hepatocyte Micro-Aggregates for Tissue Engineering (vol 9, e105171, 2014). *Plos One*. 2014, **9**(11).

365. Shin, S.R., Bae, H., Cha, J.M., Mun, J.Y., Chen, Y.C., Tekin, H., Shin, H., Farshchi, S., Dokmeci, M.R., Tang, S. and Khademhosseini, A. Carbon Nanotube Reinforced Hybrid Microgels as Scaffold Materials for Cell Encapsulation. *Acs Nano*. 2012, **6**(1), pp.362-372.
366. Schuurman, W., Levett, P.A., Pot, M.W., van Weeren, P.R., Dhert, W.J.A., Hutmacher, D.W., Melchels, F.P.W., Klein, T.J. and Malda, J. Gelatin-Methacrylamide Hydrogels as Potential Biomaterials for Fabrication of Tissue-Engineered Cartilage Constructs. *Macromolecular Bioscience*. 2013, **13**(5), pp.551-561.
367. Fedorovich, N.E., Oudshoorn, M.H., van Geemen, D., Hennink, W.E., Alblas, J. and Dhert, W.J.A. The effect of photopolymerization on stem cells embedded in hydrogels. *Biomaterials*. 2009, **30**(3), pp.344-353.
368. Nichol, J.W., Koshy, S.T., Bae, H., Hwang, C.M., Yamanlar, S. and Khademhosseini, A. Cell-laden microengineered gelatin methacrylate hydrogels. *Biomaterials*. 2010, **31**(21), pp.5536-5544.
369. Fang, X.X., Xie, J., Zhong, L.X., Li, J.R., Rong, D.M., Li, X.S. and Ouyang, J. Biomimetic gelatin methacrylamide hydrogel scaffolds for bone tissue engineering. *Journal of Materials Chemistry B*. 2016, **4**(6), pp.1070-1080.
370. Zuo, Y.C., Liu, X.L., Wei, D., Sun, J., Xiao, W.Q., Zhao, H., Guo, L.K., Wei, Q.R., Fan, H.S. and Zhang, X.D. Photo-Cross-Linkable Methacrylated Gelatin and Hydroxyapatite Hybrid Hydrogel for Modularly Engineering Biomimetic Osteon. *Acs Applied Materials & Interfaces*. 2015, **7**(19), pp.10386-10394.
371. Lim, K.S., Schon, B.S., Mekhileri, N.V., Brown, G.C.J., Chia, C.M., Prabakar, S., Hooper, G.J. and Woodfield, T.B.F. New Visible-Light Photoinitiating System for Improved Print Fidelity in Gelatin-Based Bioinks. *Acs Biomaterials Science & Engineering*. 2016, **2**(10), pp.1752-1762.
372. Brown, G.C.J., Lim, K.S., Farrugia, B.L., Hooper, G.J. and Woodfield, T.B.F. Covalent Incorporation of Heparin Improves Chondrogenesis in Photocurable Gelatin-Methacryloyl Hydrogels. *Macromolecular Bioscience*. 2017, **17**(12).
373. Serra, C., Berton, N., Bouquey, M., Prat, L. and Hadziioannou, G. A predictive approach of the influence of the operating parameters on the size of polymer particles synthesized in a simplified microfluidic system. *Langmuir*. 2007, **23**(14), pp.7745-7750.
374. Young, C., Rozario, K., Serra, C., Poole-Warren, L. and Martens, P. Poly(vinyl alcohol)-heparin biosynthetic microspheres produced by microfluidics and ultraviolet photopolymerisation. *Biomicrofluidics*. 2013, **7**(4).
375. Liao, H.T., Tsai, M.J., Brahmayya, M. and Chen, J.P. Bone Regeneration Using Adipose-Derived Stem Cells in Injectable Thermo-Gelling Hydrogel Scaffold Containing Platelet-Rich Plasma and Biphasic Calcium Phosphate. *International Journal of Molecular Sciences*. 2018, **19**(9).
376. Khanna-Jain, R., Mannerstrom, B., Vuorinen, A., Sandor, G.K., Suuronen, R. and Miettinen, S. Osteogenic differentiation of human dental pulp stem cells on beta-tricalcium phosphate/poly (l-lactic acid/caprolactone) three-dimensional scaffolds. *J Tissue Eng*. 2012, **3**(1), p.2041731412467998.

377. Insinga, A., Monestiroli, S., Ronzoni, S., Gelmetti, V., Marchesi, F., Viale, A., Altucci, L., Nervi, C., Minucci, S. and Pelicci, P.G. Inhibitors of histone deacetylases induce tumor-selective apoptosis through activation of the death receptor pathway. *Nature Medicine*. 2005, **11**(1), pp.71-76.
378. Ungerstedt, J.S., Sowa, Y., Xu, W.S., Shao, Y., Dokmanovic, M., Perez, G., Ngo, L., Holmgren, A., Jiang, X. and Marks, P.A. Role of thioredoxin in the response of normal and transformed cells to histone deacetylase inhibitors. *Proceedings of the National Academy of Sciences of the United States of America*. 2005, **102**(3), pp.673-678.
379. Ruijtenberg, S. and van den Heuvel, S. Coordinating cell proliferation and differentiation: Antagonism between cell cycle regulators and cell type-specific gene expression. *Cell Cycle*. 2016, **15**(2), pp.196-212.
380. Vidal-Laliena, M., Gallastegui, E., Mateo, F., Martinez-Balbas, M., Pujol, M.J. and Bachs, O. Histone Deacetylase 3 Regulates Cyclin A Stability. *Journal of Biological Chemistry*. 2013, **288**(29), pp.21096-21104.
381. Kwon, M., Kim, J.M., Lee, K., Park, S.Y., Lim, H.S., Kim, T. and Jeong, D. Synchronized Cell Cycle Arrest Promotes Osteoclast Differentiation. *International Journal of Molecular Sciences*. 2016, **17**(8).
382. Jones, E. and Yang, X.B. Mesenchymal stem cells and bone regeneration: Current status. *Injury-International Journal of the Care of the Injured*. 2011, **42**(6), pp.562-568.
383. Komori, T., Yagi, H., Nomura, S., Yamaguchi, A., Sasaki, K., Deguchi, K., Shimizu, Y., Bronson, R.T., Gao, Y.H., Inada, M., Sato, M., Okamoto, R., Kitamura, Y., Yoshiki, S. and Kishimoto, T. Targeted disruption of Cbfa1 results in a complete lack of bone formation owing to maturational arrest of osteoblasts. *Cell*. 1997, **89**(5), pp.755-764.
384. Li, Y., Ge, C.X., Long, J.P., Begun, D.L., Rodriguez, J.A., Goldstein, S.A. and Franceschi, R.T. Biomechanical stimulation of osteoblast gene expression requires phosphorylation of the RUNX2 transcription factor. *Journal of Bone and Mineral Research*. 2012, **27**(6), pp.1263-1274.
385. Stein, G.S., Lian, J.B., van Wijnen, A.J., Stein, J.L., Montecino, M., Javed, A., Zaidi, S.K., Young, D.W., Choi, J.Y. and Pockwinse, S.M. Runx2 control of organization, assembly and activity of the regulatory machinery for skeletal gene expression. *Oncogene*. 2004, **23**(24), pp.4315-4329.
386. Carbonare, L.D., Innamorati, G. and Valenti, M.T. Transcription Factor Runx2 and its Application to Bone Tissue Engineering. *Stem Cell Reviews and Reports*. 2012, **8**(3), pp.891-897.
387. Long, F.X. Building strong bones: molecular regulation of the osteoblast lineage. *Nature Reviews Molecular Cell Biology*. 2012, **13**(1), pp.27-38.
388. Sakano, S., Murata, Y., Miura, T., Iwata, H., Sato, K., Matsui, N. and Seo, H. Collagen and Alkaline-Phosphatase Gene-Expression during Bone Morphogenetic Protein (Bmp)-Induced Cartilage and Bone Differentiation. *Clinical Orthopaedics and Related Research*. 1993, (292), pp.337-344.

389. Takuwa, Y., Ohse, C., Wang, E.A., Wozney, J.M. and Yamashita, K. Bone Morphogenetic Protein-2 Stimulates Alkaline-Phosphatase Activity and Collagen-Synthesis in Cultured Osteoblastic Cells, Mc3t3-E1. *Biochem Biophys Res Commun.* 1991, **174**(1), pp.96-101.
390. Sun, J., Li, J.Y., Li, C.C. and Yu, Y.C. Role of bone morphogenetic protein-2 in osteogenic differentiation of mesenchymal stem cells. *Molecular Medicine Reports.* 2015, **12**(3), pp.4230-4237.
391. Peng, L.Y., Jia, Z.Q., Yin, X.H., Zhang, X., Liu, Y.A., Chen, P., Ma, K.T. and Zhou, C.Y. Comparative analysis of mesenchymal stem cells from bone marrow, cartilage, and adipose tissue. *Stem Cells and Development.* 2008, **17**(4), pp.761-773.
392. Lee, R.H., Kim, B., Choi, I., Kim, H., Choi, H.S., Suh, K., Bae, Y.C. and Jung, J.S. Characterization and expression analysis of mesenchymal stem cells from human bone marrow and adipose tissue. *Cellular Physiology and Biochemistry.* 2004, **14**(4-6), pp.311-324.
393. Roca, H. and Franceschi, R.T. Analysis of transcription factor interactions in osteoblasts using competitive chromatin immunoprecipitation. *Nucleic Acids Research.* 2008, **36**(5), pp.1723-1730.
394. Lai, J.Y. and Li, Y.T. Functional Assessment of Cross-Linked Porous Gelatin Hydrogels for Bioengineered Cell Sheet Carriers. *Biomacromolecules.* 2010, **11**(5), pp.1387-1397.
395. Echave, M.C., Burgo, L.S., Pedraz, J.L. and Orive, G. Gelatin as Biomaterial for Tissue Engineering. *Current Pharmaceutical Design.* 2017, **23**(24), pp.3567-3584.
396. S. Gorgieva, V.K. Collagen- vs. Gelatine-Based Biomaterials and Their Biocompatibility: Review and Perspectives. *Biomaterials Applications for Nanomedicine.* 2011.
397. Heino, J., Huhtala, M., Kapyla, J. and Johnson, M.S. Evolution of collagen-based adhesion systems. *International Journal of Biochemistry & Cell Biology.* 2009, **41**(2), pp.341-348.
398. Elzoghby, A.O. Gelatin-based nanoparticles as drug and gene delivery systems: Reviewing three decades of research. *Journal of Controlled Release.* 2013, **172**(3), pp.1075-1091.
399. Kessler, L., Gehrke, S., Winnefeld, M., Huber, B., Hoch, E., Walter, T., Wyrwa, R., Schnabelrauch, M., Schmidt, M., Kuckelhaus, M., Lehnhardt, M., Hirsch, T. and Jacobsen, F. Methacrylated gelatin/hyaluronan-based hydrogels for soft tissue engineering. *J Tissue Eng.* 2017, **8**, pp.1-14.
400. Klotz, B.J., Gawlitta, D., Rosenberg, A.J.W.P., Malda, J. and Melchels, F.P.W. Gelatin-Methacryloyl Hydrogels: Towards Biofabrication-Based Tissue Repair. *Trends in Biotechnology.* 2016, **34**(5), pp.394-407.
401. Watanabe, H., Matsuyama, T. and Yamamoto, H. Preparation of immobilized enzyme gel particles using an electrostatic atomization technique. *Biochemical Engineering Journal.* 2001, **8**(2), pp.171-174.
402. Young, C.J., Poole-Warren, L.A. and Martens, P.J. Combining submerged electrospray and UV photopolymerization for production of synthetic hydrogel microspheres for cell encapsulation. *Biotechnology and Bioengineering.* 2012, **109**(6), pp.1561-1570.

403. Orive, G., Tam, S.K., Pedraz, J.L. and Halle, J.P. Biocompatibility of alginate-poly-L-lysine microcapsules for cell therapy. *Biomaterials*. 2006, **27**(20), pp.3691-3700.
404. Teh, S.Y., Lin, R., Hung, L.H. and Lee, A.P. Droplet microfluidics. *Lab on a Chip*. 2008, **8**(2), pp.198-220.
405. Wheeler, A.R., Thronset, W.R., Whelan, R.J., Leach, A.M., Zare, R.N., Liao, Y.H., Farrell, K., Manger, I.D. and Daridon, A. Microfluidic device for single-cell analysis. *Analytical Chemistry*. 2003, **75**(14), pp.3581-3586.
406. Bernath, K., Hai, M.T., Mastrobattista, E., Griffiths, A.D., Magdassi, S. and Tawfik, D.S. In vitro compartmentalization by double emulsions: sorting and gene enrichment by fluorescence activated cell sorting. *Analytical Biochemistry*. 2004, **325**(1), pp.151-157.
407. Jeong, W.J., Kim, J.Y., Choo, J., Lee, E.K., Han, C.S., Beebe, D.J., Seong, G.H. and Lee, S.H. Continuous fabrication of biocatalyst immobilized microparticles using photopolymerization and immiscible liquids in microfluidic systems. *Langmuir*. 2005, **21**(9), pp.3738-3741.
408. Hong, J.S., Shin, S.J., Lee, S., Wong, E. and Cooper-White, J. Spherical and cylindrical microencapsulation of living cells using microfluidic devices. *Korea-Australia Rheology Journal*. 2007, **19**(3), pp.157-164.
409. Ching, S.H., Bansal, N. and Bhandari, B. Alginate gel particles-A review of production techniques and physical properties. *Critical Reviews in Food Science and Nutrition*. 2017, **57**(6), pp.1133-1152.
410. Fritschy, W.M., Devos, P., Groen, H., Klatter, F.A., Plasma, A., Wolter, G.H.J. and Vanschlifgaarde, R. The Capsular Overgrowth on Microencapsulated Pancreatic-Islet Grafts in Streptozotocin and Autoimmune Diabetic Rats. *Transplant International*. 1994, **7**(4), pp.264-271.
411. De Vos, P., Van Straaten, J.F.M., Nieuwenhuizen, A.G., de Groot, M., Ploeg, R.J., De Haan, P.J. and Van Schilfgaarde, R. Why do microencapsulated islet grafts fail in the absence of fibrotic overgrowth? *Diabetes*. 1999, **48**(7), pp.1381-1388.
412. Benton, J.A., DeForest, C.A., Vivekanandan, V. and Anseth, K.S. Photocrosslinking of Gelatin Macromers to Synthesize Porous Hydrogels That Promote Valvular Interstitial Cell Function. *Tissue Engineering Part A*. 2009, **15**(11), pp.3221-3230.
413. Gerecht, S., Townsend, S.A., Pressler, H., Zhu, H., Nijst, C.L.E., Bruggeman, J.P., Nichol, J.W. and Langer, R. A porous photocurable elastomer for cell encapsulation and culture. *Biomaterials*. 2007, **28**(32), pp.4826-4835.
414. Celikkin, N., Mastrogiacomo, S., Jaroszewicz, J., Walboomers, X.F. and Swieszkowski, W. Gelatin methacrylate scaffold for bone tissue engineering: The influence of polymer concentration. *Journal of Biomedical Materials Research Part A*. 2018, **106**(1), pp.201-209.
415. Kim, C., Chung, S., Kim, Y.E., Lee, K.S., Lee, S.H., Oh, K.W. and Kang, J.Y. Generation of core-shell microcapsules with three-dimensional focusing device for efficient formation of cell spheroid. *Lab on a Chip*. 2011, **11**(2), pp.246-252.

416. Choi, C.H., Jung, J.H., Rhee, Y.W., Kim, D.P., Shim, S.E. and Lee, C.S. Generation of monodisperse alginate microbeads and in situ encapsulation of cell in microfluidic device. *Biomedical Microdevices*. 2007, **9**(6), pp.855-862.
417. Rossow, T., Heyman, J.A., Ehrlicher, A.J., Langhoff, A., Weitz, D.A., Haag, R. and Seiffert, S. Controlled Synthesis of Cell-Laden Microgels by Radical-Free Gelation in Droplet Microfluidics. *Journal of the American Chemical Society*. 2012, **134**(10), pp.4983-4989.
418. Visser, J., Melchels, F.P.W., Jeon, J.E., van Bussel, E.M., Kimpton, L.S., Byrne, H.M., Dhert, W.J.A., Dalton, P.D., Huttmacher, D.W. and Malda, J. Reinforcement of hydrogels using three-dimensionally printed microfibrils. *Nature Communications*. 2015, **6**.
419. Schuurman, W., Khristov, V., Pot, M.W., van Weeren, P.R., Dhert, W.J.A. and Malda, J. Bioprinting of hybrid tissue constructs with tailorable mechanical properties. *Biofabrication*. 2011, **3**(2).
420. Du, Y.A., Lo, E., Ali, S. and Khademhosseini, A. Directed assembly of cell-laden microgels for fabrication of 3D tissue constructs. *Proceedings of the National Academy of Sciences of the United States of America*. 2008, **105**(28), pp.9522-9527.
421. Yeh, J., Ling, Y.B., Karp, J.M., Gantz, J., Chandawarkar, A., Eng, G., Blumling, J., Langer, R. and Khademhosseini, A. Micromolding of shape-controlled, harvestable cell-laden hydrogels. *Biomaterials*. 2006, **27**(31), pp.5391-5398.
422. de Vos, P., Faas, M.M., Strand, B. and Calafiore, R. Alginate-based microcapsules for immunoisolation of pancreatic islets. *Biomaterials*. 2006, **27**(32), pp.5603-5617.
423. Zuo, Y.C., He, X.H., Yang, Y., Wei, D., Sun, J., Zhong, M.L., Xie, R., Fan, H.S. and Zhang, X.D. Microfluidic-based generation of functional microfibrils for biomimetic complex tissue construction. *Acta Biomaterialia*. 2016, **38**, pp.153-162.
424. Marom, R., Shur, I., Solomon, R. and Benayahu, D. Characterization of adhesion and differentiation markers of osteogenic marrow stromal cells. *Journal of Cellular Physiology*. 2005, **202**(1), pp.41-48.
425. Arakawa, C., Ng, R., Tan, S., Kim, S., Wu, B. and Lee, M. Photopolymerizable chitosan-collagen hydrogels for bone tissue engineering. *J Tissue Eng Regen Med*. 2014.
426. Li, X.M., Zhang, J., Kawazoe, N. and Chen, G.P. Fabrication of Highly Crosslinked Gelatin Hydrogel and Its Influence on Chondrocyte Proliferation and Phenotype. *Polymers*. 2017, **9**(8).
427. Wang, J.B., Wu, D.Y., Zhang, Z.Z., Li, J., Shen, Y., Wang, Z.X., Li, Y., Zhang, Z.Y. and Sun, J. Biomimetically Ornamented Rapid Prototyping Fabrication of an Apatite-Collagen-Polycaprolactone Composite Construct with Nano-Micro-Macro Hierarchical Structure for Large Bone Defect Treatment. *Acs Applied Materials & Interfaces*. 2015, **7**(47), pp.26244-26256.
428. Misra, S.K., Mohn, D., Brunner, T.J., Stark, W.J., Philip, S.E., Roy, I., Salih, V., Knowles, J.C. and Boccaccini, A.R. Comparison of nanoscale and microscale bioactive glass on the properties of P(3HB)/Bioglass (R) composites. *Biomaterials*. 2008, **29**(12), pp.1750-1761.

429. Hong, J.K., Yun, J., Kim, H. and Kwon, S.M. Three-dimensional Culture of Mesenchymal Stem Cells. *Tissue Engineering and Regenerative Medicine*. 2015, **12**(4), pp.211-221.
430. Cho, Y.-E. and Kwun, I.-S. Zinc upregulates bone-specific transcription factor Runx2 expression via BMP-2 signaling and Smad-1 phosphorylation in osteoblasts. *J Nutr Health*. 2018, **51**(1), pp.23-30.
431. Tian, X.F., Heng, B.C., Ge, Z., Lu, K., Rufaihah, A.J., Fan, V.T.W., Yeo, J.F. and Cao, T. Comparison of osteogenesis of human embryonic stem cells within 2D and 3D culture systems. *Scandinavian Journal of Clinical & Laboratory Investigation*. 2008, **68**(1), pp.58-67.
432. Levenberg, S., Huang, N.F., Lavik, E., Rogers, A.B., Itskovitz-Eldor, J. and Langer, R. Differentiation of human embryonic stem cells on three-dimensional polymer scaffolds. *Proceedings of the National Academy of Sciences of the United States of America*. 2003, **100**(22), pp.12741-12746.
433. Carreira, A.C.O., Zambuzzi, W.F., Rossi, M.C., Astorino, R., Sogayar, M.C. and Granjeiro, J.M. Bone Morphogenetic Proteins: Promising Molecules for Bone Healing, Bioengineering, and Regenerative Medicine. *Bone Morphogenic Protein*. 2015, **99**, pp.293-322.
434. Bayliss, M.T., Howat, S., Davidson, C. and Dudhia, J. The organization of aggrecan in human articular cartilage - Evidence for age-related changes in the rate of aggregation of newly synthesized molecules. *Journal of Biological Chemistry*. 2000, **275**(9), pp.6321-6327.
435. Pulkkinen, H.J., Tiitu, V., Valonen, P., Hamalainen, E.R., Lammi, M.J. and Kiviranta, I. Recombinant human type II collagen as a material for cartilage tissue engineering. *International Journal of Artificial Organs*. 2008, **31**(11), pp.960-969.
436. Sun, M., Chi, G., Xu, J., Tan, Y., Xu, J., Lv, S., Xu, Z., Xia, Y., Li, L. and Li, Y. Extracellular matrix stiffness controls osteogenic differentiation of mesenchymal stem cells mediated by integrin alpha5. *Stem Cell Res Ther*. 2018, **9**(1), p.52.
437. Holy, C.E., Shoichet, M.S. and Davies, J.E. Engineering three-dimensional bone tissue in vitro using biodegradable scaffolds: Investigating initial cell-seeding density and culture period. *Journal of Biomedical Materials Research*. 2000, **51**(3), pp.376-382.
438. Lausch, A.J., Quan, B.D., Miklas, J.W. and Sone, E.D. Extracellular Matrix Control of Collagen Mineralization In Vitro. *Advanced Functional Materials*. 2013, **23**(39), pp.4906-4912.
439. Bansal, R. and Jain, A. Current overview on dental stem cells applications in regenerative dentistry. *J Nat Sci Biol Med*. 2015, **6**(1), pp.29-34.
440. Petricciani, J., Hayakawa, T., Stacey, G., Trouvin, J.H. and Knezevic, I. Scientific considerations for the regulatory evaluation of cell therapy products. *Biologicals*. 2017, **50**, pp.20-26.
441. Siegel, G., Kluba, T., Hermanutz-Klein, U., Bieback, K., Northoff, H. and Schafer, R. Phenotype, donor age and gender affect function of human bone marrow-derived mesenchymal stromal cells. *Bmc Medicine*. 2013, **11**.
442. Ganguly, P., El-Jawhari, J.J., Giannoudis, P.V., Burska, A.N., Ponchel, F. and Jones, E.A. Age-related Changes in Bone Marrow Mesenchymal Stromal Cells: A Potential Impact on

- Osteoporosis and Osteoarthritis Development. *Cell Transplantation*. 2017, **26**(9), pp.1520-1529.
443. Stolzing, A., Jones, E., McGonagle, D. and Scutt, A. Age-related changes in human bone marrow-derived mesenchymal stem cells: Consequences for cell therapies. *Mechanisms of Ageing and Development*. 2008, **129**(3), pp.163-173.
444. Stanko, P., Kaiserova, K., Altanerova, V. and Altaner, C. Comparison of human mesenchymal stem cells derived from dental pulp, bone marrow, adipose tissue, and umbilical cord tissue by gene expression. *Biomedical Papers-Olomouc*. 2014, **158**(3), pp.373-377.
445. Tatullo, M., Marrelli, M., Shakesheff, K.M. and White, L.J. Dental pulp stem cells: function, isolation and applications in regenerative medicine. *Journal of Tissue Engineering and Regenerative Medicine*. 2015, **9**(11), pp.1205-1216.
446. Ledesma-Martinez, E., Mendoza-Nunez, V.M. and Santiago-Osorio, E. Mesenchymal Stem Cells Derived from Dental Pulp: A Review. *Stem Cells International*. 2016.
447. Donnelly, H., Salmeron-Sanchez, M. and Dalby, M.J. Designing stem cell niches for differentiation and self-renewal. *Journal of the Royal Society Interface*. 2018, **15**(145).
448. Mollet, M., Godoy-Silva, R., Berdugo, C. and Chalmers, J.J. Computer Simulations of the energy dissipation rate in a fluorescence-activated cell sorter: Implications to cells. *Biotechnology and Bioengineering*. 2008, **100**(2), pp.260-272.
449. Herbertson, A. and Aubin, J.E. Cell sorting enriches osteogenic populations in rat bone marrow stromal cell cultures. *Bone*. 1997, **21**(6), pp.491-500.
450. Wang, J.P., Wen, M.H., Chen, Y.T., Lee, H.H., Chiang, E.R., Lee, Y.T., Liu, C.L., Chen, T.H. and Hung, S.C. Trichostatin A inhibits TGF-beta 1 induced in vitro chondrogenesis of hMSCs through Sp1 suppression. *Differentiation*. 2011, **81**(2), pp.119-126.
451. James, E.N., Delany, A.M. and Nair, L.S. Post-transcriptional regulation in osteoblasts using localized delivery of miR-29a inhibitor from nanofibers to enhance extracellular matrix deposition. *Acta Biomaterialia*. 2014, **10**(8), pp.3571-3580.
452. Deng, Y., Bi, X.P., Zhou, H.F., You, Z.W., Wang, Y.D., Gu, P. and Fan, X.Q. Repair of Critical-Sized Bone Defects with Anti-Mir-31-Expressing Bone Marrow Stromal Stem Cells and Poly(Glycerol Sebacate) Scaffolds. *European Cells & Materials*. 2014, **27**, pp.13-25.
453. Beavers, K.R., Nelson, C.E. and Duvall, C.L. MiRNA inhibition in tissue engineering and regenerative medicine. *Advanced Drug Delivery Reviews*. 2015, **88**, pp.123-137.

List of Abbreviations

2D	Two dimensional
3D	Three dimensional
α-MEM	Alpha
ADSCs	Adipose-derived stromal cells
ALP	Alkaline phosphatase
ALPSA	Alkaline phosphatase specific activity
ANOVA	Analysis of variance
aq.	Aqueous
BMP	Bone morphogenic protein
cDNA	Complimentary DNA
CFMDA	5-chloromethylfluorescein diacetate
Col1a	Collagen type 1
Ct	Cycle threshold
dH₂O	Distilled water
DMEM	Dulbecco's Modified Eagle's Medium
DMSO	Dimethyl sulfoxide
DNA	Deoxyribonucleic acid
DPX	Distyrene, plasticiser and xylene
EDTA	Ethylenediaminetetraacetic acid
ESCs	Embryonic stem cells
EthD-1	Ethidium Homodimer-1

EtOH	Ethanol
FACS	Fluorescence-activated cell sorting
FCS	Foetal calf serum
FDA	Food and Drug Administration
FGF	Fibroblast growth factor
GelMA	Gelatin methacrylate
GPa	Gigapascal
H&E	Haematoxylin and Eosin
HATs	Histone acetyltransferase
hBMSCs	Human bone marrow stromal cells
hDPSCs	Human dental pulp stromal cells
hUCSCs	Human umbilical cord stromal cells
HCL	Hydrochloric acid
HDAC	Histone deacetylase
HDACi	Histone deacetylase inhibitor
H₂O	Water
HSCs	Hematopoietic stem cells
IC₅₀	Half-maximal inhibitory concentration
ICBM	insoluble collagenous bone matrix
ID	Internal diameter
iPSCs	Induced pluripotent stem cells
kPa	Kilopascal

L	Litre
L-G	L-Glutamine
Lys	Lysine
mg	Milligram
ml	Millilitre
mm	Millimetre
mM	Millimolar
miRNA	MicroRNA
MPa	Megapascal
mRNA	Messenger RNA
MSCs	Mesenchymal stem/stromal cells
mW	Molecular weight
NaB	Sodium butyrate
NaOH	Sodium hydroxide
NBF	Neutral buffered formalin
nl	Nanolitre
nm	Nanomolar
OCN	Osteocalcin
OD	Outer diameter
PBS	Phosphate-buffered saline
PBT	Poly (butylene terephthalate)
PC3	Human prostate cancer cell line

PCL	Polycaprolactone
PCR	Polymerase chain reaction
PEGT	Poly (ethylene glycol)-terephthalate
PI	Propidium Iodide
psi	Pounds per square inch
P/S	Penicillin-Streptomycin
PTFE	Polytetrafluoroethylene
RGD	Arginine-glycine-aspartic acid
RNA	Ribonucleic acid
ROS	Reactive oxygen species
RPM	Rotations per minute
RT-qPCR	Quantitative real-time polymerase chain reaction
Ru	Tris (2,2'-bipyridyl) dichlororuthenium (II) hexahydrate
Runx2	Runt-related transcription factor 2
SAHA	Suberoylanilide hydroxamic acid
SD	Standard deviation
SEM	Scanning electron microscopy
siRNA	Small interfering RNAs
SPS	Sodium persulfate
T/E	Trypsin-EDTA
TGF	Transforming growth factor
TNF	Tumour necrosis factor

TSA	Trichostatin A
UV	Ultraviolet
VPA	Valproic acid
μg	Microgram
μl	Microlitre
μm	Micrometre
μM	Micromolar

Appendix A - Supplementary data

A1 - Comparison of MI192 pre-treatment on hDPSCs ALPSA from three donors

To evaluate donor variability, hDPSCs were acquired from three donors (Table A1), and the effect of MI192 pre-treatment on ALPSA was assessed after 2 weeks osteogenic culture (Fig A1). In all donors, untreated cells in osteogenic medium exhibited a significantly higher ALPSA compared to untreated cells in basal conditions ($P \geq 0.01 - 0.001$). After MI192 pre-treatment for 48 hours (1, 2 and 5 μM), 2 μM MI192 significantly increased ALPSA compared to the 1 μM group and the osteogenic control in all donors ($P \geq 0.01 - 0.001$). In all three donors, 5 μM MI192 decreased ALPSA compared to the 2 μM , although not significantly ($P > 0.05$). Within donor 1, 1 μM MI192 significantly increased ALPSA compared to the osteogenic control ($P \geq 0.01$), while 5 μM pre-treatment significantly enhanced ALPSA compared to that in the 1 μM group in both donor 1 and 2 ($P \geq 0.01$).

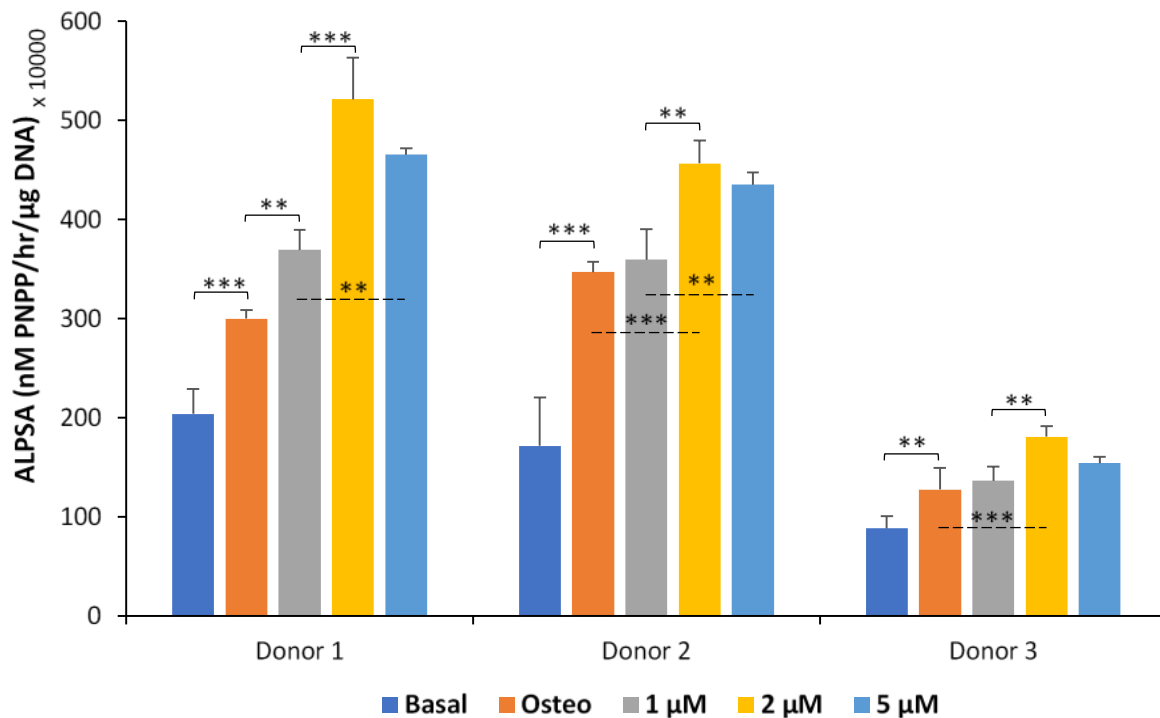


Figure A1 - ALPSA of hDPSCs from three different donors pre-treated with/without MI192. Cells pre-treated with MI192 (1, 2 and 5 μM) for 48 hours, following culture in osteogenic medium for 2 weeks, with untreated cells cultured in basal and osteogenic medium used as the controls. Data expressed as mean \pm SD ($n=3$). Significance levels shown are the test groups compared to the basal/osteogenic control or between adjacent MI192 concentrations for that time point. ** $P \leq 0.01$ and *** $P \leq 0.001$.

A2 - Comparison of MI192 pre-treatment on hBMSCs ALPSA from two donors

The effects of MI192 pre-treatment on hBMSCs ALPSA from two different donors (Table A1) were evaluated after 2 weeks osteogenic culture (Fig A2). In both donors, untreated cells exhibited significantly increased ALPSA when compared to the same cells in basal conditions ($P \geq 0.001$). MI192 pre-treatment with 50 μM MI192 for 48 hours significantly enhanced ALPSA when compared to the other MI192 pre-treatment conditions assessed (30 and 70 μM) and the untreated osteogenic control ($P \geq 0.001$).

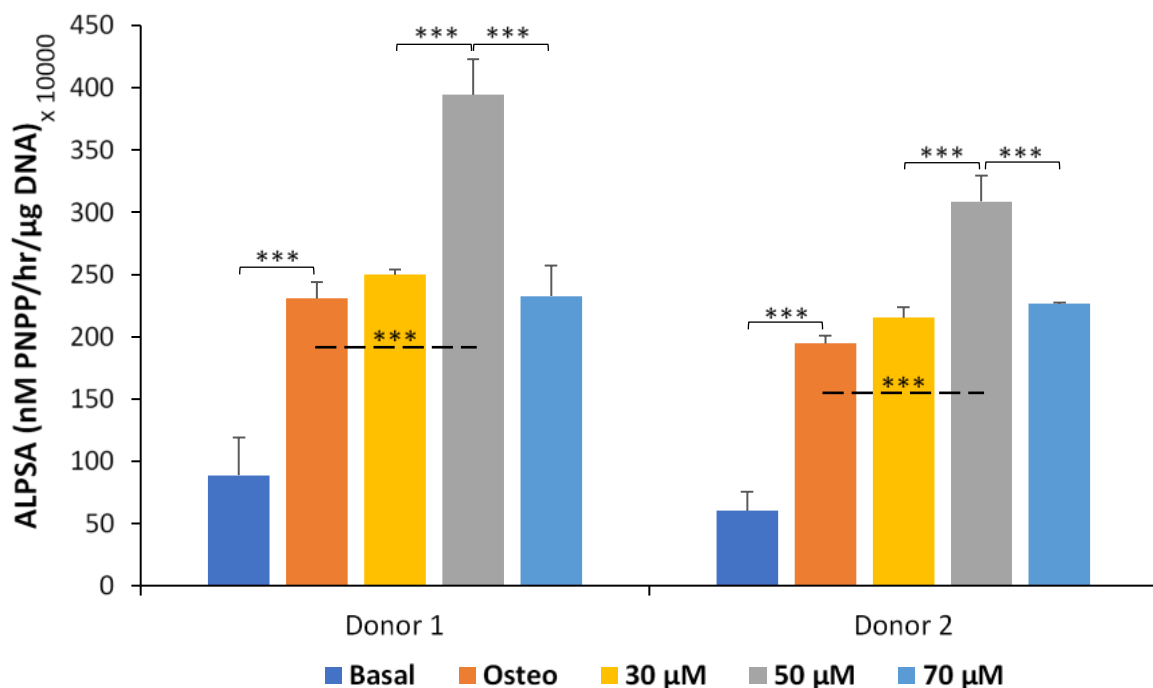


Figure A2 - ALPSA of hBMSCs from two different donors pre-treated with/without MI192. Cells pre-treated with MI192 (30, 50 and 70 μM) for 48 hours, following culture in osteogenic medium for 2 weeks, with untreated cells cultured in basal and osteogenic medium used as the controls. Data expressed as mean \pm SD ($n=3$). Significance levels shown are the test groups compared to the basal/osteogenic control or between adjacent MI192 concentrations for that time point. *** $P \leq 0.001$.

Table A1 - Donor information for hDPSCs and hBMSCs utilised in this thesis.

Donor	Donor age/sex
hDPSCs	
1	13/F
2	25/M
3	35/M
hBMSCs	
1	33/M
2	41/M

A3 - Confirmation of multi-lineage differentiation potential of hDPSCs

Tri-lineage differentiation of hDPSCs is shown in Figure A3. Positive calcium accumulation was observed in the hDPSCs cultured osteogenic induction medium following Alizarin red staining. No calcium accumulation staining was observed in the negative control cultured in the basal medium.

Adipogenic differentiation potential was determined via Oil red O staining. Positive lipid droplets accumulation was observed in hDPSCs cultured in adipogenic induction medium for 14 days. The hDPSCs cultured in basal medium exhibited negative staining for lipid droplet accumulation.

Chondrogenic potential of hBMSCs was assessed via Picrosirius red/Alcian blue staining. Positive GAG accumulation was observed in hDPSC pellets cultured in chondrogenic induction medium for 21 days. The negative control group exhibited weaker Alcian blue staining for GAGs while exhibiting increased staining for Picrosirius red (collagens) when compared to the positive induction culture control.

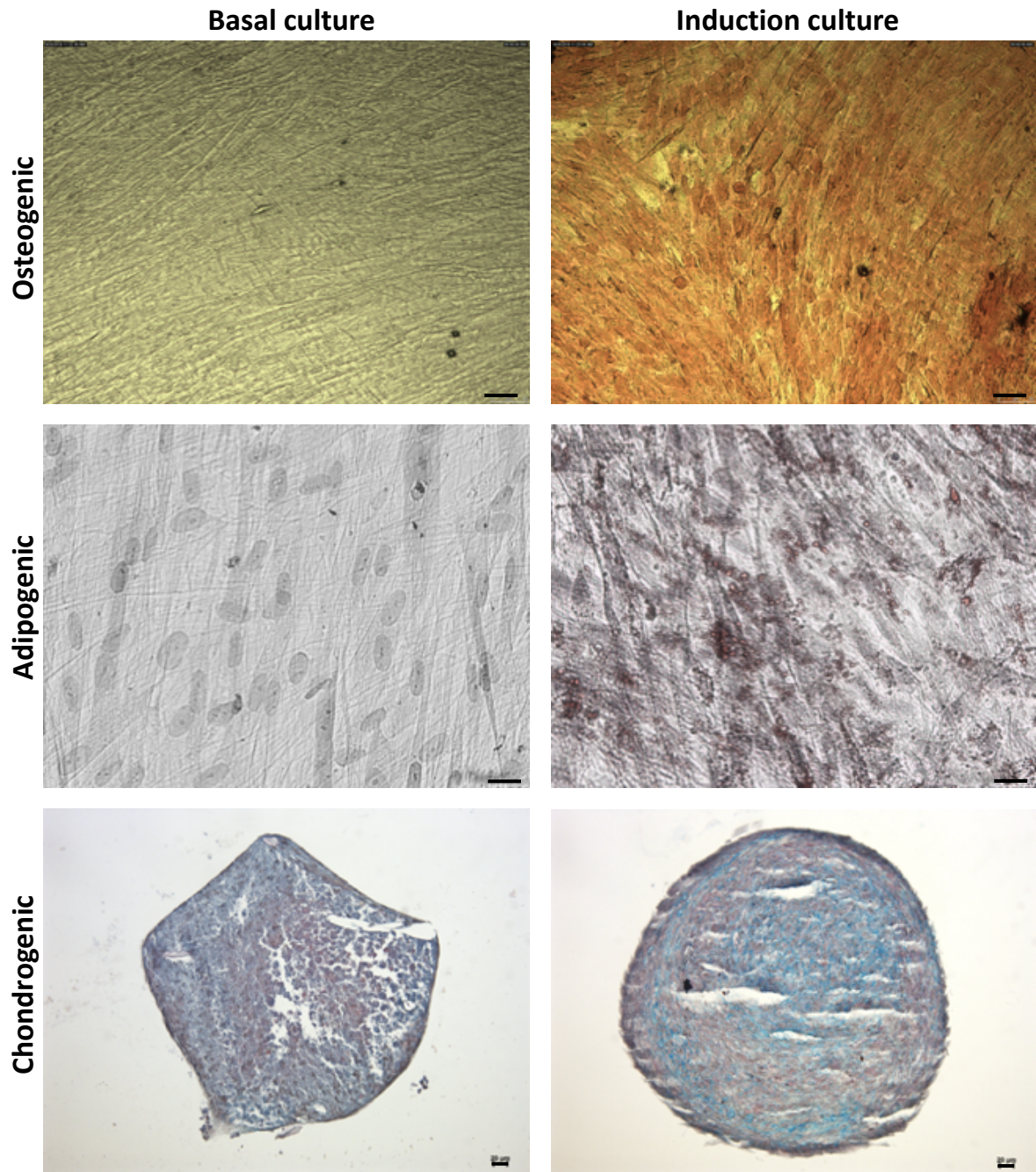


Figure A3 - Multi-lineage potential of hDPSCs. Osteogenic differentiation: Positive calcium accumulation was observed after 28 days cultured in osteogenic medium confirmed by Alizarin Red staining (Scale bar = 75 μm); Adipogenic differentiation: lipid droplet formation was observed in hDPSCs after 14 days culture in adipogenic induction medium after Oil red O staining (Scale bar = 75 μm); Chondrogenic differentiation: hDPSCs were capable of forming cartilage like pellets after 21 days cultured as pellets in chondrogenic induction medium, stained blue for GAGs (Alcian blue staining) and red for collagen (Picosirius red staining). Scale bar = 20 μm .

A4 - Confirmation of multi-lineage differentiation potential of hBMSCs

Figure A4 shows the tri-lineage differentiation of hBMSCs. Following 28 days culture in osteogenic induction medium, hBMSCs were capable of differentiation down the osteogenic lineage confirmed by positive calcium accumulation staining. Within the negative control, hBMSCs cultured in basal medium exhibited no staining for calcium accumulation.

Following 14 days of culture in adipogenic induction medium, positive accumulation of lipid droplets were observed in hBMSCs following Oil red O staining. The hBMSCs cultured in basal medium exhibited no positive staining for lipid droplet accumulation.

Positive Alcian blue staining for GAG accumulation was observed in the hBMSC pellets cultured in chondrogenic induction medium. GAG staining was at a greater intensity and more globally expressed through the pellet compared to hBMSC pellets cultured in basal medium. Additionally, the negative group possessed enhanced staining for Picrosirius red throughout the pellet compared to the group cultured in chondrogenic inductive medium.

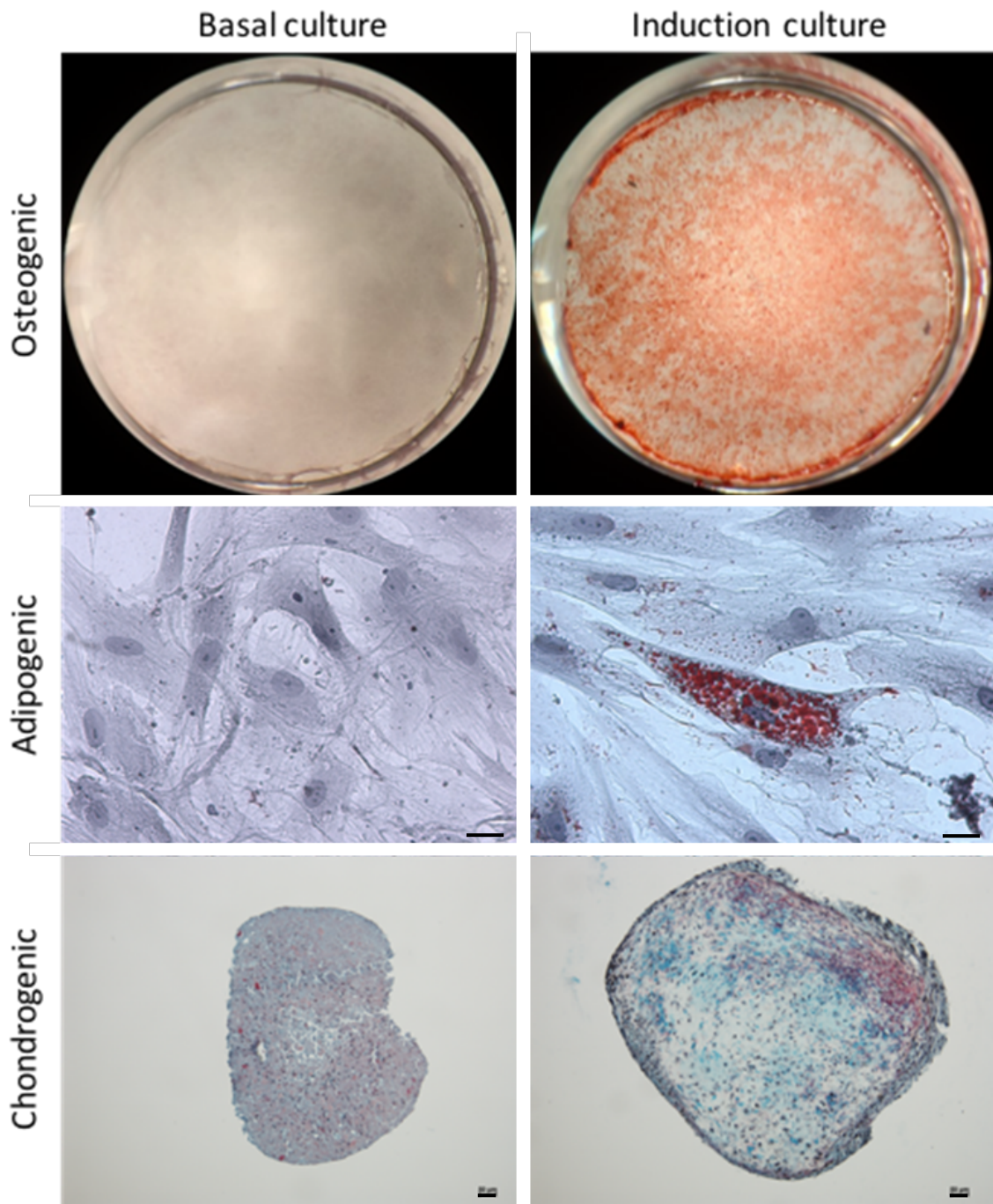


Figure A4 - Multi-lineage potential of hBMSCs. Osteogenic differentiation: Positive calcium accumulation was observed after 28 days cultured in osteogenic medium confirmed by Alizarin Red staining; Adipogenic differentiation: lipid droplet formation was observed in hBMSCs after 14 days culture in adipogenic induction medium after Oil red O staining (Scale bar = 50 μ m); Chondrogenic differentiation: hBMSCs were capable of forming cartilage like pellets after 21 days cultured as pellets in chondrogenic induction medium, stained blue for GAGs (Alcian blue staining) and red for collagen (Picosirius red staining). Scale bar = 20 μ m.

A5 - Viability of floating cell/debris induced by MI192 treatment on hBMSCs

To determine whether the increased quantity of floating cells/debris observed within the MI192 treatment groups was viable, the metabolic activity of those floating cells/debris were assessed via Alamarblue assay (Fig A5). Following treatment with/without MI192 for 24, 48 and 72 hours, the treatment medium was collected along with the floating cell/debris and AlamarBlue was added to assess the metabolic activity of unattached cells. Figure A5 shows that the metabolic activity was significantly lower in all MI192 treated groups when compared to the untreated cells in there respectively time points ($P \geq 0.05 - 0.01$).

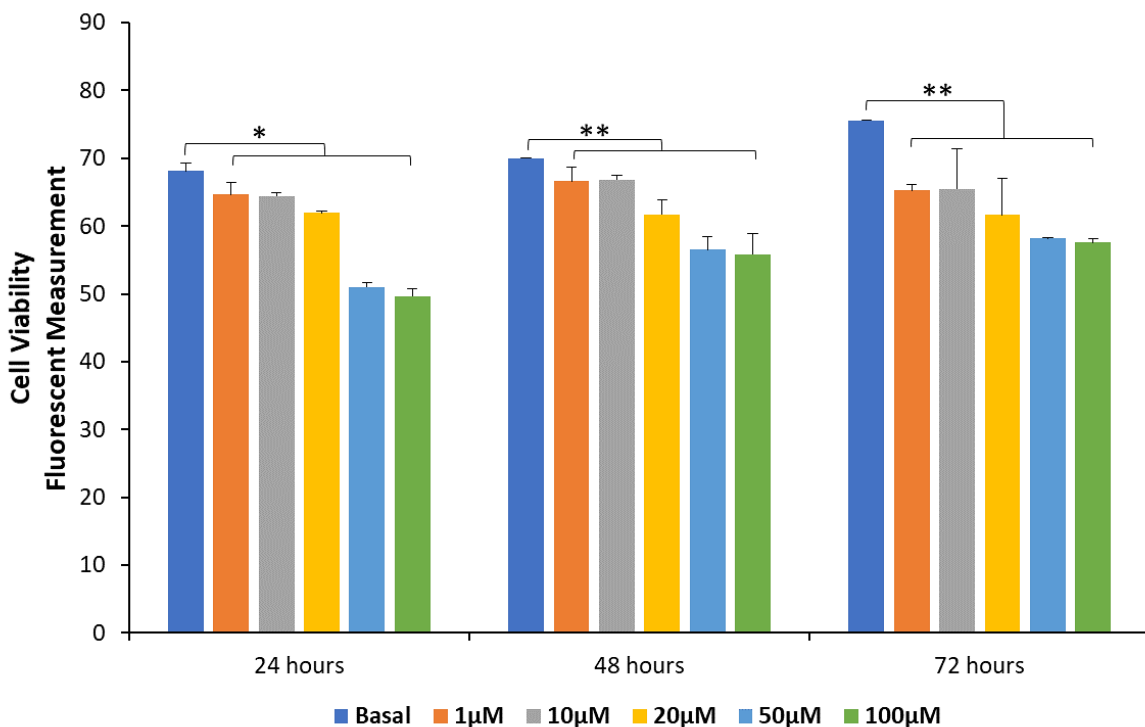


Figure A5 - AlamarBlue analysis of supernatant acquired from hBMSCs treated with/without MI192 (1, 10, 20, 50, 100 µM) for 24, 48 and 72 hours. Data expressed as mean \pm SD (n=3). Significance levels shown are the sample compared to the basal control for that time point. * $P \leq 0.05$ and ** $P \leq 0.01$.

Appendix B - List of conference presentations and publications

B1 - Oral presentations

- K. Man, N. Mekhileri, B. Schon, K. Lim, L.H. Jiang, R. Foster, T. Woodfield and X.B. Yang. *Utilising a Novel Histone Deacetylase Inhibitor to Enhance Human Bone Marrow Stromal Cell Osteogenic Differentiation*. Tissue Engineering and Regenerative Medicine International Society (TERMIS) World Congress. 3 - 7 Sept 2018. Kyoto, Japan.
- K. Man, N. Mekhileri, B. Schon, K. Lim L.H. Jiang, R. Foster, T. Woodfield and X.B. Yang. *Using a Novel Histone Deacetylase Inhibitor to Enhance Human Bone Marrow Stromal Cell Osteogenic Differentiation In Vitro*. UK - China Workshop: For Regenerative Dentistry - From Tooth Development to Regeneration. 22 - 24 July 2018. Leeds, UK.
- K. Man, L.H. Jiang, R. Foster, and X.B. Yang. *Using an Epigenetic Approach to Enhance Stem Cell Osteogenic differentiation*. School of Dentistry Research Day. 11 July 2018. Leeds, UK.
- K. Man, N. Mekhileri, B. Schon, L.H. Jiang, R. Foster, T. Woodfield and X.B. Yang. *Enhancing Human Dental Pulp Stem Cell Osteogenesis via an Epigenetic Approach*. TERMIS Asia - Pacific. 21 - 24 Sept 2017. Nantong, China.
- K. Man, L.H. Jiang, R. Foster, and X.B. Yang. *Using an Epigenetic Approach for Enhancing Human Dental Pulp Stem Cell Osteogenesis In vitro*. Tissue and Cell Engineering Society (TCES). 5 - 7 July 2017. Manchester, UK.
- K. Man, L.H. Jiang, R. Foster, and X.B. Yang. *Using an epigenetic approach for enhancing human dental pulp stem cell osteogenesis In Vitro*. CDT TERM Symposium 2017 (2nd prize). 10 July 2017. Leeds, UK.
- K. Man, L.H. Jiang, R. Grigg, and X.B. Yang. *The Utilisation of a Novel Histone Deacetylase Inhibitor for Bone Tissue Engineering*. SkelGEN Annual Meeting. 15 - 16 Sept 2015. Guimarães, Portugal.

B2 - Poster presentations

- K. Man, L.H. Jiang, R. Foster, X. Manz, J. Rnjak-Kovacina and X.B. Yang. *Epigenetic regulators enhance osteogenesis of human dental pulp stromal cells in 2D & 3D silk scaffolds*. TCES. 2 - 4 July 2018. Keele, UK.
- K. Man, N. Mekhileri, B. Schon, R. Foster, L.H. Jiang, T. Woodfield and X.B. Yang. School of Dentistry Research day. *Enhancing Human Dental Pulp Stem Cell Osteogenesis via an Epigenetic Approach*. 12 July 2017. Leeds, UK.
- K. Man, L.H. Jiang, R. Foster, and X.B. Yang. *Using an epigenetic approach for enhancing human dental pulp stem cell osteogenesis in vitro*. EPSRC Centres for Doctoral Training in Tissue Engineering and Regenerative Medicine Joint Conference. 9 Oct 2017. Leeds, UK.
- K. Man, B. Schon, R. Foster, L.H. Jiang, T. Woodfield and X.B. Yang. *Pre-treatment of Human Dental Pulp Stem Cells with Novel Histone Deacetylase Inhibitors to Enhance Bone Tissue Engineering Efficacy*. BORS. 5 - 6 Sept 2016. Glasgow, UK.
- K. Man, B. Schon, R. Grigg, R. Foster, L.H. Jiang, T. Woodfield and X.B. Yang. *Pre-treatment of human dental pulp stem cells with a selective histone deacetylase inhibitor to enhance bone tissue engineering efficacy*. 7th CDT Joint Conference in Regenerative Medicine. 8 July 2016. Manchester, UK.
- K. Man, L.H. Jiang, R. Grigg, and X.B. Yang. *Pre-treatment of stem cells with HDAC inhibitors to enhance bone tissue engineering efficacy*. EPSRC Centres for Doctoral Training in Tissue Engineering and Regenerative Medicine Joint Conference. 10 July 2015, Leeds, UK.

B3 - Publications

- J. Zhang, K. Man, D. Li, P. Gao, J. Kirkham and X.B. Yang (2019). *Resveratrol up-regulates SIRT1 expression and reverses oxidative stress in human dental pulp stromal cells.* (Manuscript submitted).

- Y. Guo, J. Zhang, Z. Qu, N. Zhang, K. Man and X.B. Yang (2017). *Effects of Resveratrol on Proliferation and Osteogenic Differentiation of Dental Pulp Stem Cells on Titanium Implants in Oxidative Stress.* *Oral biomedicine* 8 (3), 155 - 158.

- K. Man, L.H. Jiang, R. Foster, and X.B. Yang (2017). *Immunological Responses to Total Hip Arthroplasty.* *Journal of Functional Biomaterials* 8 (3), 33.

Appendix C - Rights for reprinting permission

License numbers for re-print permission:

Fig 1.4 -



The screenshot shows the RightsLink interface. At the top left is the Copyright Clearance Center logo. To its right is the RightsLink logo. Further right are navigation buttons for Home, Create Account, and Help, along with a chat icon. Below the navigation is a box with a LOGIN button and instructions for users. The main content area features the American Society for Microbiology logo and the following metadata:

Title: Nucleosome Positioning in *Saccharomyces cerevisiae*
Author: An Jansen, Kevin J. Verstrepen
Publication: Microbiology and Molecular Biology Reviews
Publisher: American Society for Microbiology
Date: Jun 6, 2011

Copyright © 2011, American Society for Microbiology

Permissions Request

ASM authorizes an advanced degree candidate to republish the requested material in his/her doctoral thesis or dissertation. If your thesis, or dissertation, is to be published commercially, then you must reapply for permission.

BACK

CLOSE WINDOW

Copyright © 2019 Copyright Clearance Center, Inc. All Rights Reserved. [Privacy statement](#), [Terms and Conditions](#).
Comments? We would like to hear from you. E-mail us at customer@copyright.com

Fig 1.5 - 4312641153407

Fig 1.8 - 4572511290934

Fig 3.1 - 4560291220524

Fig 4.1 - 4551990641436

